frontiers | Research Topics

The role of dimethylsulphide, and other sulphur substances, on the climate and ecology of coral reefs

Edited by
Graham Barry Jones, Gabrielle Nevitt and Rafel Simó

Published in
Frontiers in Marine Science

ISSN 1664-8714
ISBN 978-2-83251-479-5
DOI 10.3389/978-2-83251-479-5

About Frontiers

Frontiers is more than just an open access publisher of scholarly articles: it is a pioneering approach to the world of academia, radically improving the way scholarly research is managed. The grand vision of Frontiers is a world where all people have an equal opportunity to seek, share and generate knowledge. Frontiers provides immediate and permanent online open access to all its publications, but this alone is not enough to realize our grand goals.

Frontiers journal series

The Frontiers journal series is a multi-tier and interdisciplinary set of open-access, online journals, promising a paradigm shift from the current review, selection and dissemination processes in academic publishing. All Frontiers journals are driven by researchers for researchers; therefore, they constitute a service to the scholarly community. At the same time, the *Frontiers journal series* operates on a revolutionary invention, the tiered publishing system, initially addressing specific communities of scholars, and gradually climbing up to broader public understanding, thus serving the interests of the lay society, too.

Dedication to quality

Each Frontiers article is a landmark of the highest quality, thanks to genuinely collaborative interactions between authors and review editors, who include some of the world's best academicians. Research must be certified by peers before entering a stream of knowledge that may eventually reach the public - and shape society; therefore, Frontiers only applies the most rigorous and unbiased reviews. Frontiers revolutionizes research publishing by freely delivering the most outstanding research, evaluated with no bias from both the academic and social point of view. By applying the most advanced information technologies, Frontiers is catapulting scholarly publishing into a new generation.

What are Frontiers Research Topics?

Frontiers Research Topics are very popular trademarks of the *Frontiers journals series*: they are collections of at least ten articles, all centered on a particular subject. With their unique mix of varied contributions from Original Research to Review Articles, Frontiers Research Topics unify the most influential researchers, the latest key findings and historical advances in a hot research area.

Find out more on how to host your own Frontiers Research Topic or contribute to one as an author by contacting the Frontiers editorial office: frontiersin.org/about/contact

The role of dimethylsulphide, and other sulphur substances, on the climate and ecology of coral reefs

Topic editors

Graham Barry Jones — Southern Cross University, Australia
Gabrielle Nevitt – University of California, Davis, United States
Rafel Simó — Institut de Ciències del Mar (ICM-CSIC), Catalonia, Spain

Citation

Jones, G. B., Nevitt, G., Simó, R., eds. (2023). *The role of dimethylsulphide, and other sulphur substances, on the climate and ecology of coral reefs*. Lausanne: Frontiers Media SA. doi: 10.3389/978-2-83251-479-5

Table of contents

frontiers | Frontiers in Marine Science

TYPE Editorial
PUBLISHED 13 January 2023
DOI 10.3389/fmars.2023.1119817

OPEN ACCESS

Edited and Reviewed by:Raquel Peixoto, King Abdullah University of Science and Technology, Saudi Arabia

*CORRESPONDENCE
Graham Jones
graham.jones@scu.edu.au

†PRESENT ADDRESS
Graham Jones,
Faculty of Science and Engineering,
Southern Cross University, NSW, Australia

SPECIALTY SECTION
This article was submitted to Coral Reef Research, a section of the journal Frontiers in Marine Science

RECEIVED 09 December 2022
ACCEPTED 04 January 2023
PUBLISHED 13 January 2023

CITATION
Jones G, Nevitt G and Simó R (2023) Editorial: The role of dimethylsulfide and other sulfur substances on the climate and ecology of coral reefs.
Front. Mar. Sci. 10:1119817.
doi: 10.3389/fmars.2023.1119817

Editorial: The role of dimethylsulfide and other sulfur substances on the climate and ecology of coral reefs

Graham Jones[1*†], Gabrielle Nevitt[2] and Rafel Simó[3]

[1]Faculty of Science and Egineering, Southern Cross University, Lismore, NSW, Australia, [2]Department of Neurobiology, Physiology and Behaviour, University of California, Davis, CA, United States, [3]Department of Marine Biology and Oceanography, Institut de Ciències del Mar (ICM-CSIC), Barcelona, Catalonia, Spain

KEYWORDS

climate regulation, SST and ocean warming, DMS emission, methane emission, acrylate, DMSP catabolism, dsyB, betaines

Editorial on the Research Topic
The role of dimethylsulphide, and other sulphur substances, on the climate and ecology of coral reefs

Whilst ground-breaking research on dimethylsulfide (DMS) on coral reefs was published over 25 years ago (Jones et al., 1994; Hill et al., 1995), the goal of this special topic is to highlight more recent research on the climatic and ecological role of DMS, its biological precursor dimethylsulfoniopropionate (DMSP), and related compounds in tropical coral reef environments. Forty-three researchers contributed eleven high quality manuscripts from the Australian Great Barrier Reef (GBR), French Polynesia, and Okinawan reefs off Japan. Contributions include case studies and review articles covering atmospheric science, remote sensing, biogeochemistry, microbiology, coral physiology and ecology, and genetic research.

McGowan et al. compare observations of coral reef-atmospheric interactions during summer monsoon conditions on the Great Barrier Reef with those of a desert fringing coral reef in the Gulf of Eilat, Red Sea. While in the Gulf of Eilat the stability of the atmospheric boundary layer inhibits the impact of the reef on the overlying atmosphere, GBR reefs during the summer monsoon are characterized by convective exchange of heat and moisture, which may allow the vertical transport of DMS and other aerosol and cloud droplet precursors. In a mini review, Swan discusses the potential for coral reef-derived, atmospheric DMS oxidation products to regulate the regional climate of the GBR (Figure 1). He describes how low wind speeds over tidally exposed coral reefs cause plumes of atmospheric DMS and sulfate aerosols. Upon subsequent growth, these aerosols can affect cloud microphysics and regulate regional cloud albedo. Massive coral bleaching events may currently weaken such regulation. Jackson et al. investigated this further using an Australian Community Climate and Earth System Model. Incorporation in the model of the coral-to-air DMS emission, during aerial exposure at low tide, revealed that the GBR is an important regional source of atmospheric sulfur. However, no influence on sulfate aerosol mass or number concentration was detected, in contrast to observational studies that suggest otherwise. In a companion paper, Jackson

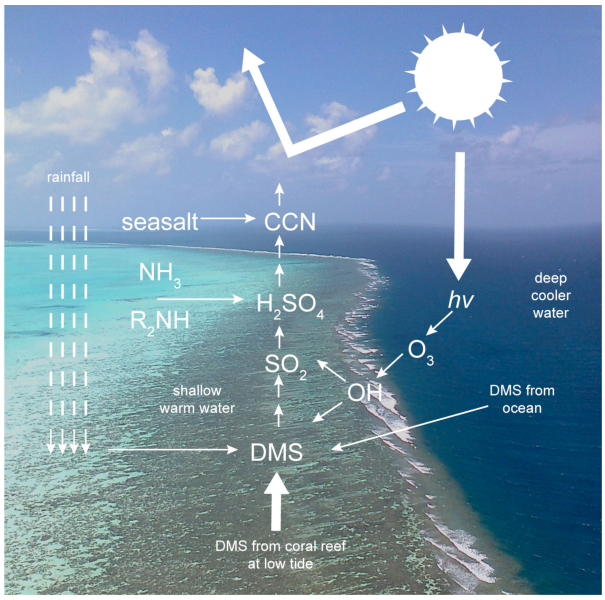

FIGURE 1
An aerial photograph of Wistari Reef near Heron Island in the Capricorn–Bunker group of coral reefs southern Great Barrier Reef, Australia (23.13° S, 151.85° E to 23.92° S, 152.60° E). Superimposed on this image is a conceptual model of factors controlling hygroscopic sulfate aerosol production (H_2SO_4) over the GBR. Ocean-derived atmospheric DMS and pulses of atmospheric DMS from the coral reef at low tide are oxidised by photochemically produced hydroxyl radical (OH) forming sulfate aerosol that can grow to cloud condensation nuclei (CCN). This process can assist formation of high-albedo low-level marine clouds that influence solar radiation over the GBR. Source: Hilton B. Swan, Graham B. Jones, Elisabeth S. M. Deschaseaux, and Bradley D. Eyre. Biogeosciences, 14, 229–239, 2017 www.biogeosciences.net/14/229/2017/doi:10.5194/bg-14-229-2017 © Authors 2017. CC Attribution 3.0 License.

et al. used a CMIP6 model to investigate the influence of predicted increases in sea surface temperature and photosynthetically active radiation on DMS emissions from the GBR by the end of the century. They conclude that the predicted 10-14% increase in DMS emission is unlikely to significantly influence the regional atmosphere of the GBR, though further research is needed. Whilst DMS is considered a climate-cooling gas, methane is a powerful greenhouse gas with warming effects. Deschaseaux et al. report a correlation of DMS emission fluxes with methane fluxes from the Heron Island Reef, GBR. DMS emissions were also positively correlated with the abundance of intermediate and large diameter aerosols, suggesting that DMS significantly contributes to the growth of existing atmospheric particles.

Xue et al. measured concentrations of DMSP and its breakdown product acrylate in a coral reef-open ocean transect in Mo'orea, French Polynesia. While concentrations showed little change along the transect, the microbial consumption of both compounds was much faster in the reef, suggesting that rapid biological turnover maintains the reef-borne dissolved concentrations of these two compounds at low levels similar to those of the open ocean. In the same Mo'orean reefs, Masdeu-Navarro et al. measured DMSP-related compounds (DMSPCs, i.e., DMSP, DMS, acrylate and DMSO) and volatile organic compounds (VOCs). Dominant corals were sources of DMSPCs, while a dominant seaweed was a source of DMSPCs and VOCs such as carbonyl sulfide and poly-halomethanes. The diel cycle of DMSPCs concentrations near the polyps of *Acropora pulchra* paralleled changes in sunlight intensity, and rDNA meta-barcoding and metagenomic analyses suggested that solar radiation-induced oxidative stress caused the release of DMSPCs by the coral holobiont, either directly or through symbiont expulsion. With similar ecophysiological objectives, Gardner et al. exposed *Acropora millepora* to thermal stress experiments and observed a large increase in coral DMSP concentrations. The distinct bacterial communities of the coral mucus showed increases in the abundance of two DMSP catabolic genes, *dmdA* (demethylation) and *dddP* (cleavage to DMS), under thermal stress, and a shift occurred to cleavage as the DMSP concentration increased. This helps explain why DMS emission is enhanced in heat-stressed corals.

Corals are holobionts where the distinct roles of each of the components (i.e., the cnidarian host and the symbiotic algae, as well as the other members of the associated microbiome) in the physiology of the entire coral are not easy to tease out. For instance, bacteria do not only catabolise DMSP but can also synthesize it. Kuek et al. confirmed this by finding the DMSP-synthesis gene *dsyB* in 9% of 157 isolates of bacteria associated with four common coral species. Genome sequencing of one of the isolates, *Shimia aestuarii* AMM-P-2, revealed the complete genetic machineries to assimilate sulfate and synthesise sulfur-containing aminoacids and DMSP, and demethylate and cleave DMSP, as well as utilise or detoxify acrylate. Intracellular DMSP increased two-fold under both hypersaline conditions and high UV exposure. Chiu and Schinzato carried out molecular identification of DMSP lyase-like genes in *Acropora digitifera* tissue, and saw that multiple variants were expressed. A comprehensive survey of available transcriptomic databases revealed that DMSP lyase-like genes occur across Cnidaria: in Hexacorallia and Octocorallia (Anthozoa), and even in a jellyfish (Hydrozoa), and evolved from a gene in the last common ancestor of Cnidaria, dating to the Precambrian. Given that DMSP lyase-like gene-harbouring cnidarians thrive in coral reefs and shallow, warm waters, these genes may be essential for animals to survive in such environments and adapt to environmental changes. Quaternary ammonium compounds (QACs) – e.g., betaines – have a chemical structure analogous to that of the tertiary sulfonium compounds such as DMSP. In coral tissues, QACs are suggested to protect the photosystem machinery of the algal symbiont against photon and thermal stresses by stabilizing photosystem proteins and scavenging reactive-oxygen-species. Hill reviews the available evidence on the roles of QACs, and calls for more studies of QAC-related ecophysiology in corals.

All in all, the contributions in this Research Topic provide further evidence for the critical role of DMSP, DMS and related compounds in the evolution of tropical corals and their adaptation to the conditions of high temperatures and irradiances that characterise their distribution. Most importantly, they highlight the need to look at the coral as a holobiont, where the different components all contribute to the ecophysiological aspects of sulfur cycling. A consequence of these ecophysiological aspects is the increased emission of DMS from reefs where high irradiances, high temperature and aerial exposure by

low tides converge. In combination with atmospheric convective uplifts, DMS emissions represent an important injection of sulfur up into the atmosphere where low level clouds form. Whether this injection has significant impact on regional climate is still controversial and requires further evaluation.

Author contributions

All authors listed have made a substantial, direct and intellectual contribution to the work, and approved it for publication.

Funding

GJ (SCU) was supported by an ARC Discovery Project grant (ARCDP) DP150101649 as part of the Reef to Rainforest (R2R) experiment in the Great Barrier Reef. RS is holder of a European Research Council Advanced Grant (ERC-2018-ADG-834162) of the EU Horizon H2020 Research and Innovation Programme.

Acknowledgments

We thank all the contributors and reviewers who made this Research Topic. We would also like to thank the Frontiers team for their support.

Conflict of interest

The authors declare that the research was conducted in the absence of any commercial or financial relationships that could be construed as a potential conflict of interest.

Publisher's note

References

Hill, R. W., Dacey, J. W. H., and Krupp, D. A. (1995). Dimethylsulphoniopropionate in reef corals. *Bull. Mar. Sci.* 57, 489–494.

Jones, G. B., Curran, M. A. J., and Broadbent, A. D. (1994). "Dimethylsulphide in the south pacific," in *6th South Pacific congress on marine science and technology* (Townsville, Queensland, Australia: Pacon International and James Cook University), 183–190.

frontiers | Frontiers in Marine Science

ORIGINAL RESEARCH
published: 04 May 2022
doi: 10.3389/fmars.2022.869574

DMSP Production by Coral-Associated Bacteria

Felicity W.I. Kuek[1,2,3,4,5], *Cherie A. Motti*[1,5†], *Jia Zhang*[3,4], *Ira R. Cooke*[3,4], *Jonathan D. Todd*[6], *David J. Miller*[2,3,4†], *David G. Bourne*[1,5,7†] *and Jean-Baptiste Raina*[8*†]

[1] AIMS@JCU, Division of Research and Innovation, James Cook University, Townsville, QLD, Australia, [2] Australian Research Council (ARC) Centre of Excellence for Coral Reef Studies, James Cook University, Townsville, QLD, Australia, [3] Centre for Tropical Bioinformatics and Molecular Biology, James Cook University, Townsville, QLD, Australia, [4] College of Public Health, Medical and Veterinary Sciences, James Cook University, Townsville, QLD, Australia, [5] Tropical Marine Water Quality and Impacts, Australian Institute of Marine Science, Townsville, QLD, Australia, [6] School of Biological Sciences, University of East Anglia, Norwich Research Park, Norwich, United Kingdom, [7] College of Science and Engineering, James Cook University, Townsville, QLD, Australia, [8] Climate Change Cluster (C3), University of Technology Sydney, Ultimo, NSW, Australia

OPEN ACCESS

Edited by:
Gabrielle Nevitt, University of California, Davis, CA, United States

Reviewed by:
Chuya Shinzato, The University of Tokyo, Japan
Kshitij Tandon, The University of Melbourne, Australia

***Correspondence:**
Jean-Baptiste Raina
Jean-Baptiste.Raina@uts.edu.au

[†]*These authors have contributed equally to this work*

Specialty section:
This article was submitted to Coral Reef Research, a section of the journal Frontiers in Marine Science

Received: *04 February 2022*
Accepted: *06 April 2022*
Published: *04 May 2022*

Citation:
Kuek FWI, Motti CA, Zhang J, Cooke IR, Todd JD, Miller DJ, Bourne DG and Raina J-B (2022) DMSP Production by Coral-Associated Bacteria. Front. Mar. Sci. 9:869574. doi: 10.3389/fmars.2022.869574

Dimethylsulfoniopropionate (DMSP) is an important molecule in the marine sulfur cycle, produced in large amounts by corals and their dinoflagellate endosymbionts, Symbiodiniaceae. Although corals are known to harbour bacteria that can catabolise DMSP, the recent discovery of bacteria capable of producing DMSP in coastal and deep-sea environments raises the possibility of a bacterial contribution to the DMSP output of corals. Here, 157 bacteria associated with four common coral species were isolated and screened for their ability to produce DMSP by targeting *dsyB*, a key gene involved in DMSP biosynthesis. Approximately 9% (14 out of 157) of the bacterial isolates harboured *dsyB*, all being members of the Alphaproteobacteria. The ability of these isolates to produce DMSP was confirmed by liquid chromatography-mass spectrometry (LC-MS) and nuclear magnetic resonance (NMR) measurements. A *dsyB*-harbouring strain, *Shimia aestuarii* AMM-P-2, was selected for genome sequencing. This strain harbours the complete genetic machinery to (i) assimilate sulfate and synthesise the DMSP precursors, cysteine and methionine; (ii) demethylate DMSP and generate methanethiol; (iii) cleave DMSP, generating dimethyl sulfide (DMS) and acrylate; and (iv) utilise or detoxify acrylate. The impacts of varied environmental factors (temperature, salinity, light and UV radiation) on *S. aestuarii* AMM-P-2 DMSP biosynthesis were characterised. DMSP levels in *S. aestuarii* AMM-P-2 increased almost two-fold under both hypersaline conditions (40 PSU) and high UV exposure. DMSP catabolism through the cleavage pathway also increased under these conditions, producing the antioxidants DMS and acrylate, a potential response to the oxidative stress generated. Overall, our results reveal that coral-associated bacteria can synthesize DMSP and may therefore contribute to DMSP production by the coral holobiont.

Keywords: DMSP, sulfur cycle, coral-associated bacteria, holobiont, acrylate

INTRODUCTION

Dimethylsulfoniopropionate (DMSP) is one of the most abundant organic sulfur compounds in the ocean (Sievert et al., 2007; Johnston et al., 2012), with global production estimates ranging between 12 and 103 Tmol of sulfur per year (Howard et al., 2006). Functionally speaking, this molecule is the chemical equivalent of a Swiss Army knife, being a key source of carbon and reduced-sulfur for marine microbes (Kiene et al., 2000), a potent chemoattractant affecting the behaviour of organisms ranging from bacteria to fish (DeBose et al., 2008; Seymour et al., 2010), an antioxidant (Sunda et al., 2002), a cryoprotectant (Karsten et al., 1996), a protectant against hydrostatic pressure (Zheng et al., 2020), and an osmolyte (Kirst, 1996; Stefels, 2000). In addition, its role as the main precursor of dimethyl sulfide (DMS) has received considerable attention because this highly abundant gaseous compound is released into the atmosphere where it ultimately plays a role in cloud formation, bridging marine and atmospheric sulfur cycles (Andreae et al., 1983; Bates et al., 1987; Ayers and Gras, 1991).

DMSP biosynthesis was long thought to be restricted to marine photosynthetic eukaryotes (Kiene et al., 1996). However, recent studies have demonstrated that photosynthesis is not a prerequisite for DMSP production with marine heterotrophic bacteria found in saltmarshes, the photic zone and even deep seafloor sediments producing this compound (Curson et al., 2017; Williams et al., 2019). Many marine Alphaproteobacteria belonging to the orders Rhodobacterales, Rhizobiales, and Rhodospirillales produce DMSP *via* the methionine transamination pathway (Curson et al., 2017). The *dysB* gene in these bacteria encodes the key *S*-adenosyl methionine-dependent methylthiohydroxybutryrate (MTHB) methyltransferase enzyme in this pathway. Furthermore, some Alphaproteobacteria and Actinobacteria have been shown to produce DMSP *via* a different methionine methylation pathway in which a methionine *S*-methyltransferase, termed MmtN, is an important enzyme (Williams et al., 2019). Approximately 0.3–0.6% of marine bacteria are predicted to produce DMSP, with the majority containing *dsyB* (Curson et al., 2017; Curson et al., 2018; Williams et al., 2019). Importantly, Alphaproteobacteria orders that are known to harbour *dsyB* can represent up to 50% of the bacterial communities associated with some reef-building coral species (Luo et al., 2021).

Coral reefs are recognised as DMSP hotspots (Jones and Trevena, 2005), thought to largely result from the photosynthetic endosymbionts of the family Symbiodiniaceae within the coral tissue that produce large amounts of the compound (Hill et al., 1995). However, the coral host itself can also produce DMSP and contain a DsyB-like MTHB *S*-methyltransferase, termed DSYB (Raina et al., 2013; Aguilar et al., 2017; Curson et al., 2018). Bacteria are also abundant in and around corals (Bourne et al., 2016; Pogoreutz et al., 2020) and, together with protists, fungi, archaea, and viruses, they form a metaorganism referred to as the coral holobiont (Rohwer et al., 2002). These microorganisms likely support central metabolic processes of the coral host and their microalgal partners through the fixation of carbon, cycling of nitrogen, synthesis of essential B-vitamins, and antimicrobial production (Rädecker et al., 2015; Robbins et al., 2019; Matthews et al., 2020; Ngugi et al., 2020). A large proportion of coral-associated bacteria can also catabolise DMSP, and this compound constitutes an important source of carbon and reduced sulfur for microorganisms in the holobiont (Raina et al., 2009; Raina et al., 2010; Frade et al., 2016; Tandon et al., 2020). Yet, the potential contribution of coral-associated bacteria to the production of the high DMSP concentrations measured in some reef-building corals has never been considered.

Here, bacteria associated with four common species of reef-building corals from the Great Barrier Reef (GBR) were investigated. We hypothesized that these corals harbour DMSP-producing bacteria that may contribute to DMSP concentrations measured in the holobiont. Bacterial isolates were screened for the presence of the *dsyB* gene, and their capacity to produce DMSP was investigated through chemical analyses. A representative DMSP-producing coral-associated bacterial isolate was exposed to abiotic stressors relevant for coral reefs and the role environmental factors may play in driving DMSP production characterised.

MATERIALS AND METHODS

Sample Collection

Coral-associated bacteria were isolated from four scleractinian coral species, *Acropora millepora*, *Acropora tenuis*, *Pocillopora acuta*, and *Stylophora pistillata*, all collected from Davies Reef (18°49'03.7"S, 147°38'39.6"E). Corals were maintained at the Australian Institute of Marine Science (AIMS) National Sea Simulator (SeaSim) and were healthy when the samples were collected, with no visual signs of bleaching or disease. Five coral fragments per colony were rinsed in sterile artificial sea water (ASW) prior to mucus collection using sterile 50 mL syringes fitted with 20-gauge hypodermic needles. Mucus samples were kept on ice and processed within an hour. In addition, two coral fragments per colony were placed in separate Whirl-Pak sterile sample bags (Nasco, United States) and immediately air-brushed with 5 mL of sterile ASW to remove coral tissue and their associated microorganisms from the coral skeleton. The tissue slurry was homogenised and transferred into sterile 50 mL centrifuge tubes, placed on ice, and processed within an hour.

Bacterial Isolation

To isolate coral-associated bacteria, each sample type (mucus and tissue slurry) was serially diluted in ASW (2-, 10-, 100-, and 1,000-fold; **Figure 1A**). Aliquots (50 μL) of each dilution were then spread onto Difco Marine Agar 2216 (MA; Becton Dickinson, United States) or modified minimal basal medium (MBM) agar enriched with mixed carbon sources [300 mM; details in **Table S1**; (Curson et al., 2017)], methionine ($C_5H_{11}NO_2S$; 0.5 mM), and ammonium chloride, (NH_4Cl; 20 mM) as nitrogen source. All agar plates were incubated at 28°C in the dark for one week and inspected daily for growth and the

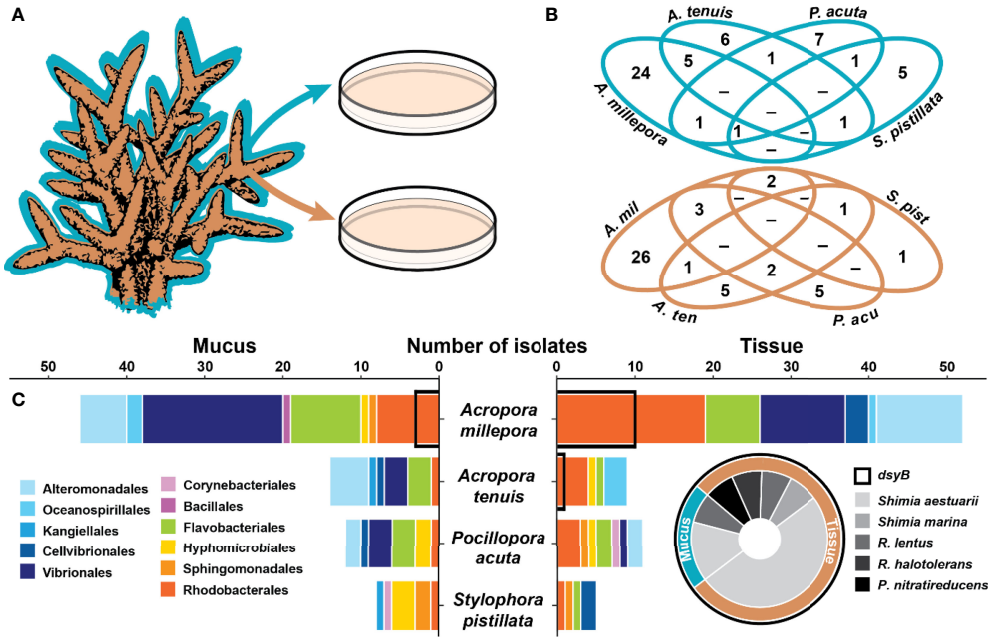

FIGURE 1 | Coral associated bacteria harbour the *dsyB* gene. **(A)** Isolation of 157 bacteria from the mucus (blue) and tissue (brown) of four coral species. **(B)** Venn diagrams for the mucus (blue) and tissue (brown) of the four species showing the overlap in the isolated bacterial species (identified by their 16S rRNA gene) between the four coral species. **(C)** Taxonomic composition of the isolates (order level) between the four coral species for the mucus (left panel) and the tissue (right panel). Isolates harbouring *dsyB* (14 of 157) are indicated by a black outline on the bar graph and their taxonomic composition is presented as a pie chart (for more information, see **Table S2**). The genera *Roseivivax* and *Pseudooceanicola* are abbreviated.

formation of morphologically distinct individual colonies. Colonies were picked using sterile 20 µL pipette tips and resuspended in 5 mL of Difco Marine Broth 2216 (MB; Becton Dickinson, United States). The isolates were incubated at 28°C and 180 RPM until growth was visible. These liquid cultures were replated on MA and this procedure repeated until pure isolates were obtained. Isolates were then cultured in MB and aliquots of each isolate stored in 20% v/v glycerol at -80°C.

Isolate Identification

A 5 mL liquid culture of each isolate was grown overnight in MB at 28°C with agitation (orbital shaker at 180 RPM) before being centrifuged for 5 min at 10,000 *g* and the supernatant decanted. DNA extraction was performed using the DNeasy UltraClean Microbial Kit (Qiagen, Germany) according to the manufacturer's instructions. Extracted DNA was resuspended in 20 µL of UltraPure DNase/RNase-Free Distilled Water (Invitrogen, United States) and quantified by spectrophotometry (NanoDrop ND-1000, ThermoFisher, United States). Aliquots of extracted DNA were diluted with sterile Milli-Q water to 10 ng μL^{-1} and stored at -20°C until required.

PCR Amplification of Bacterial 16S rRNA and *dsyB* Genes

Extracted DNA was used as template in PCR with the universal 16S rRNA genes primers 27F and 1492R (Lane, 1991), as well as the *dsyB* specific primers dsyB_deg1F and dsyB_deg2R that amplify a 246 bp region of the gene (Williams et al., 2019). Each PCR reaction mixture contained 1× reaction buffer, 2 mM of $MgCl_2$ solution, 1 mM of deoxyribonucleotide triphosphate (dNTP) mix, 0.4 µM of each primer, 0.5 µL of BIOTAQ DNA Polymerase (Bioline, United Kingdom), 1 ng μL^{-1} of template DNA, and adjusted to a final volume of 25 µL with UltraPure DNase/RNase-free distilled water (Thermo Fisher Scientific, United States). PCR amplifications were as follows: (i) dsyB_deg1F/dsyB_deg2R: initial step at 95°C for 5 min; 30 cycles at 95°C for 30 s, 61°C for 1 min and 72°C for 15 s; and a final extension step at 72°C for 5 min; (ii) 27F/1492R: as described by Bourne and Munn (2005). PCR products were purified with the Wizard SV Gel and PCR Clean-Up System (Promega, United States) and visualised *via* electrophoresis on a 1% agarose gel stained with ethidium bromide.

Sanger Sequencing and Phylogenetic Analysis

PCR products were sequenced at Macrogen Inc. (Seoul, South Korea). The forward and reverse 16S rRNA and *dsyB* amplicon sequences were paired and the overlapping fragments were merged using Geneious Prime 2019.2.3 (Biomatters, New Zealand). Some *dsyB* amplicon sequences were too short (or of poor quality) to be merged and only one sequence (forward or reverse) was used.

To identify the closest taxonomic-relative of each isolate, BLAST searches (Altschul et al., 1990) were conducted through the National Center for Biotechnology Information (NCBI). 16S rRNA gene sequences were then aligned using MAFFT (Multiple

Alignment using Fast Fourier Transform) v7 (Katoh et al., 2002; Katoh and Standley, 2013) with default settings, then trimmed using trimAl v1.4 (Capella-Gutiérrez et al., 2009) to remove sites with more than 50% missing or degraded data. Following the Bayesian Information Criterion (Schwarz, 1978), the maximum likelihood phylogeny for each sample niche was calculated. Phylogenetic trees were constructed using IQ-TREE v1.6.12, with 1,000 ultrafast bootstrap replicates (Minh et al., 2013), and formatted using the ggtree package (Yu et al., 2017) in R (R Core Team, 2020).

The *dsyB* amplicons were translated into protein sequences and searches to find regions of local similarity were performed using BLASTP. These translated sequences were also aligned with DsyB from *Labrenzia aggregata* (AOR83342) (Curson et al., 2017) to assess their similarity using the Needleman-Wunsch algorithm (Needleman and Wunsch, 1970). A multiple sequence alignment (MSA) of the prokaryotic DsyB protein sequences was visualised to show conserved residues, conservative mutations, and divergence between the different homologues. The MSA was conducted using T-Coffee v11.00 (Notredame et al., 2000; Di Tommaso et al., 2011) with default settings and formatted using Boxshade v3.21. Conserved domains within the predicted DsyB sequence were detected using CD-Search (Marchler-Bauer and Bryant, 2004) against the Conserved Domain Database (CDD) v3.18 (Lu et al., 2019).

Culture of *dsyB*-Positive Bacterial Strains

To confirm the DMSP biosynthesis capability of bacteria harbouring *dsyB*, each strain was cultured in 500 mL of either MB, yeast tryptone sea salts [YTSS; (González et al., 1996)], MBM broth or methionine-enriched MBM broth (final concentration 0.5 mM). The cultures were incubated at 28°C with agitation (orbital shaker at 180 RPM) for 24 hours before being harvested by centrifugation (3,000 *g* for 15 min at 4°C). The clarified medium was discarded and the remaining cell pellets snap-frozen with liquid nitrogen, lyophilised overnight (Dynavac freeze dryer, Massachusetts, United States; model FD12) and stored at -20°C until required.

Chemical Extraction

The freeze-dried cell pellets were resuspended in 1 mL of deuterated methanol (CD_3OD; Cambridge Isotope Laboratories, Massachusetts, United States), vortexed at maximum speed for 5 min, and sonicated for 5 min at room temperature. A further 1 mL of CD_3OD and 666 µL of deuterium oxide (D_2O; Cambridge Isotope Laboratories, Massachusetts, United States) were added into the mixture (for a final CD_3OD to D_2O ratio of 3:1), which were then vortexed at maximum speed for 5 min and sonicated for 10 min at room temperature. Bacterial extracts were subsequently centrifuged at 3,000 g for 5 min. The particulate-free extracts (final volume of ~2.6 mL) were then used for subsequent analyses on the LC-MS and NMR.

Liquid Chromatography-Mass Spectrometry

LC-MS was used to assess the presence of intracellular DMSP in *dsyB*-positive bacterial isolates. Particulate-free bacterial extracts were analysed on an Agilent 1100 series high performance liquid chromatograph coupled to a Bruker Esquire 3000 quadrupole ion trap mass spectrometer (LC-MS; Bruker Daltonics, Massachusetts, United States) equipped with an electrospray ionisation interface (ESI). Extracts (5 µL) were separated on a reverse-phase Luna 3 µm HILIC column (Phenomenex, California, United States; 150 × 3 mm, with a particle size of 3 µm) maintained at 25°C. Separation was achieved using a programmed step gradient consisting of solvent A: 0.1% formic acid (HCOOH) in Milli-Q water and solvent B: methanol (CH_3OH, HPLC grade OmniSolv), at a flow rate of 0.5 mL min^{-1}. The column was pre-equilibrated at 60% B for 10 min prior to injection. The programmed step gradient was t = 0 min, 60% B; t = 12 min, 10% B; t = 14 min, 10% B; t = 15 min, 60% B; t = 20 min, 60% B; t = 22 min, 60% B. The ESI was operated in positive mode and the target mass of *m/z* 135, corresponding to the $[M+H]^+$ of DMSP, monitored (established from a DMSP standard).

Nuclear Magnetic Resonance

The presence of intracellular DMSP in *dsyB*-positive bacterial isolates was also assessed using NMR. A 700 µL aliquot of each bacterial particulate-free extract was transferred into a 5 mm Norell 509-UP NMR tube (North Carolina, United States) and analysed immediately using quantitative NMR (qNMR) *via* the ERETIC method (Electronic REference To access *In vivo* Concentrations) (Akoka and Trierweiler, 2002) to measure the concentration of DMSP, as described in Tapiolas et al. (2013).

NMR spectra of the bacterial extracts were recorded on a Bruker Avance 600 MHz NMR spectrometer (Bruker BioSpin, United States) with a triple resonance cryoprobe (TXI), referenced using CD_3OD (δ_H 3.31). ^1H NMR spectra were acquired as outlined in Tapiolas et al., (2013) using a standard Bruker solvent suppression pulse sequence. 2D NMR spectra were also acquired to confirm the assignment of DMSP. All spectra were referenced to residual ^1H and ^{13}C resonances in CD_3OD. In addition, one extract was spiked with 14 µL of 50 mM DMSP to confirm the position of the methyl singlet, as NMR signals can shift as the sample matrix changes.

Genome Sequencing of Isolate AMM-P-2

A phenol:chloroform extraction method, outlined in detail in Raina et al. (2016), was used to extract high-molecular weight DNA from a representative bacterial isolate producing DMSP (called AMM-P-2 hereafter). Extracted DNA was sent to the Ramaciotti Centre for Genomics (Sydney, Australia) for library preparation using the Nextera XT DNA Library Preparation Kit (Illumina, United States) and sequenced on the Illumina MiSeq system using V2 with 2×250 bp paired-end reads.

Genome Assembly and Annotation

The MiSeq read set was trimmed, assembled, and error-corrected using Trimmomatic 0.38 (Bolger et al., 2014), SPAdes v3.13.0 (Bankevich et al., 2012), and Pilon v1.23 (Walker et al., 2014), respectively. All were implemented through Shovill v1.0.4 using default settings. Prediction of coding regions and annotation were performed with Prokka v1.14.6 (Seemann, 2014) using standard databases (i.e., ISfinder, NCBI Bacterial Antimicrobial

Resistance Reference Gene Database, and UniProtKB (SwissProt)) and default settings.

Bioinformatic Analyses

To confirm the presence of *dsyB* within the genome of AMM-P-2, we used a reciprocal BLAST approach between the protein sequence reported by Curson et al. (2017) and the AMM-P-2 genome (E-value ≥ 1 e^{-50}). Similarly, to explore the genomic potential of the bacterium to utilise and metabolise other sulfur compounds (e.g., sulfate, cysteine), target genes were obtained from KEGG (Kyoto Encyclopedia of Genes and Genomes) (Kanehisa et al., 2004) and compared against the AMM-P-2 genome. The orthology of the highest scoring match (E-value ≥ 1 e^{-50}) was confirmed by conducting BLASTP analyses against the NCBI NR (non-redundant) database, followed by BLASTP analyses of retrieved best match against the AMM-P-2 predicted proteins.

Stress Experiment

Isolate AMM-P-2 was grown in MBM broth with methionine (final concentration 0.5 mM) (Curson et al., 2017), and the culture incubated at 27°C, 180 RPM, ambient lighting, and 35 practical salinity units (PSU). After three days, a 1:10 dilution of this starter culture was inoculated into 60 mL replicate cultures and incubated under different environmental conditions simulating stress experienced by tropical corals: (i) high temperature (32°C; T_{32}), (ii) low temperature (22°C; T_{22}), (iii) high UV (through a combination of Deluxlite Black Light Blue (18W) and Reptile One UVB 5.0 (18W) with an average total radiation in the incubator of 1.328 mW cm^{-2} measured using a Solarmeter Model 5.0 UVA + UVB meter (Solar Technology, Pennsylvania, United States)), (iv) complete darkness, (v) high salinity (40 PSU), and (vi) low salinity (25 PSU). Three biological replicates were grown for each of the described conditions, including control conditions maintained at ambient lighting, and 35 PSU.

Culture density was monitored through time using spectrophotometry (2 µL was measured at 600 nm (OD_{600}) on a NanoDrop 1000 spectrophotometer; Thermo Fisher Scientific, United States). Cultures were sampled over four time points, corresponding to the mid-exponential (24 h), late exponential (28 h), early stationary (32 h), and late stationary (36 h) growth stages of the bacterium, as previously established by a standard growth curve. At each time point, one culture per treatment was removed and samples were taken for quantitative nuclear magnetic resonance (qNMR) analysis (50 mL; centrifuged for 5 min at 3,000 *g*, pellet snap frozen and stored at -20°C until analysis).

Bacterial Cell Counts

To convert the optical density data recorded with spectrophotometry into bacterial cell numbers, OD_{600} and flow cytometry counts were carried out simultaneously on isolate AMM-P-2 grown under standard conditions in triplicate (27°C at 180 RPM, ambient lighting, 35 PSU, in modified MBM). After each OD_{600} measurement, 100 µL of cells were fixed for 15 min in 2% glutaraldehyde for subsequent flow cytometry analysis. Samples were then stained with SYBR Green (1:10,000 final dilution; ThermoFisher, Massachusetts, United States), incubated for 15 min in the dark and analysed on a CytoFLEX S flow cytometer (Beckman Coulter, California, United States) with filtered MilliQ water as the sheath fluid. For each sample, forward scatter (FSC), side scatter (SSC), and green (SYBR) fluorescence were recorded. The samples were analysed at a flow rate of 25 µL min^{-1}. Microbial populations were characterized according to SSC and SYBR Green fluorescence (Marie et al., 1997) and cell abundances were calculated by running a standardized volume (50 µL) per sample.

Statistical Analyses

Statistics were performed using IBM SPSS Statistics v27.0.1. qNMR signals associated with DMSP and acrylate were normalised to cell density and tested for significance using repeated-measures ANOVA, with Greenhouse-Geisser correction applied (a correction for sphericity). A simple main effect test, applied following significant interactions between treatments, was used to determine the difference between treatments at each time point for both DMSP and acrylate. A Pearson product-moment correlation was used to determine the relationship between DMSP and acrylate concentrations in AMM-P-2.

RESULTS

Corals Harbour DMSP Producing Bacteria

A total of 157 isolates were recovered from coral mucus (51%) and tissue (49%) (**Figure 1B** and **Table S2**). The highest proportion of these were members of the Gammaproteobacteria (49%), followed by Alphaproteobacteria (32%) and Flavobacteriia (17%) (**Table S2**). The taxonomic composition of the isolates in each compartment was different (**Figure 1** and **Table S2**), and few isolates were shared between coral species (**Figure 1B**).

From the 157 bacterial isolates screened, 14 harboured the *dsyB* gene (9% of total isolates). These strains all belong to the Alphaproteobacteria class, specifically the family Rhodobacteraceae, and include members of the *Shimia* (n=10), *Roseivivax* (n=3), and *Pseudooceanicola* (n=1) genera (**Figure 1C** and **Table S2**). All of these *dsyB*-harbouring strains were isolated from *Acropora millepora* and *Acropora tenuis*, with 3 strains derived from the mucus and 11 from the tissue. More specifically, bacteria harbouring *dsyB* represented 19% (10 of 52) of the isolates from *A. millepora* tissue. The average sequence identity of the predicted (partial) DsyB amino acid sequences derived from the isolates to the protein from *Labrenzia aggregata* was ~65% (**Figure S1**) (Curson et al., 2017; Curson et al., 2018). Interestingly, three different *Labrenzia* strains were isolated from corals, including two strains with more than 98% 16S rRNA gene sequence identity to *L. aggregata*, but *dsyB* could not be amplified from these isolates.

The 14 *dsyB*-harbouring strains were assessed for their ability to produce DMSP. The isolates were initially grown in MB and YTSS, but DMSP could not be detected in any of the cultures using either LC-MS (**Figure S2**) or NMR (**Figure S3**). However,

LC-MS did detect a peak at *m/z* 135 and retention time of 5.9 min, consistent with DMSP, in all isolates grown in methionine-enriched MBM (**Figure S4**). ^{1}H NMR analysis established the presence of a well-resolved diagnostic singlet at δ_H 2.95 ppm (2 × CH_3) (Tapiolas et al., 2013) (**Figure 2**) and ^{1}H-^{1}H correlation spectroscopy (COSY) revealed two coupled methylene groups, S-CH_2- (δ_H 3.45, t) and -CH_2-CO_2H (δ_H 2.70, t) (**Figure S5**). In addition, a ^{1}H-^{13}C heteronuclear multiple bond correlation (HMBC) revealed long-range chemical shift correlations between: (i) the protons of the two methyl groups (S-CH_3) and the carbon of the S-methylene group (δ_H 2.94 - δ_C 43.21); (ii) the carboxyl-methylene protons of the carboxyl carbon (δ_H 2.69 - δ_C 172.03) and the S-methylene carbon (δ_H 2.69 - δ_C 43.21) (**Figure S6**). Together, these COSY and HMBC correlations confirmed the structure of DMSP, thus verifying the presence of DMSP in the bacterial extracts.

Sulfur Transformation Potential of the DMSP Producer *Shimia aestuarii* AMM-P-2

To further characterise the genomic underpinnings of DMSP production in coral-associated bacteria, isolate AMM-P-2 was selected for whole-genome sequencing (**Table 1**). This isolate belongs to the *Shimia* genus, which accounted for 71% (or 10 of 14) of *dsyB*-positive bacteria isolated. This strain exhibited >97% similarity with *Shimia aestuarii* based on its full 16S rRNA gene sequence.

Comparison of the predicted amino acid sequence of DsyB from *S. aestuarii* AMM-P-2 with previously characterised homologues representing the diversity of this protein family (n=14) revealed the presence of two conserved domains which are common to all *dsyB* orthologues (**Figure S7**): (i) an S-adenosylmethionine-dependent methyltransferase (AdoMet-MTase) class I superfamily domain (pfam00891; E-value 4.02 e^{-16}) and (ii) a dimerization2 superfamily domain (pfam16864; E-value 4.13 e^{-7}). As in several other Rhodobacterales strains (Curson et al., 2017), *isc* [iron sulfur cluster] or *suf* [sulfur formation] gene clusters were present 5' of *dsyB* in *S. aestuarii* AMM-P-2 (**Figure S8**). However, in the region 3' of *dsyB*, only limited synteny was observed between *S. aestuarii* AMM-P-2 and other Rhodobacterales.

To determine the source of sulfur used by *S. aestuarii* AMM-P-2 for DMSP biosynthesis, its sulfur metabolic potential was assessed. Distinct orthologues of all the enzymes in the sulfate reduction pathway were identified (**Figure 3** and **Table S3**), confirming *S. aestuarii* AMM-P-2 has the genetic machinery required to uptake and convert extracellular inorganic sulfate to sulfide (**Table S3**). Following sulfide production, *S. aestuarii*

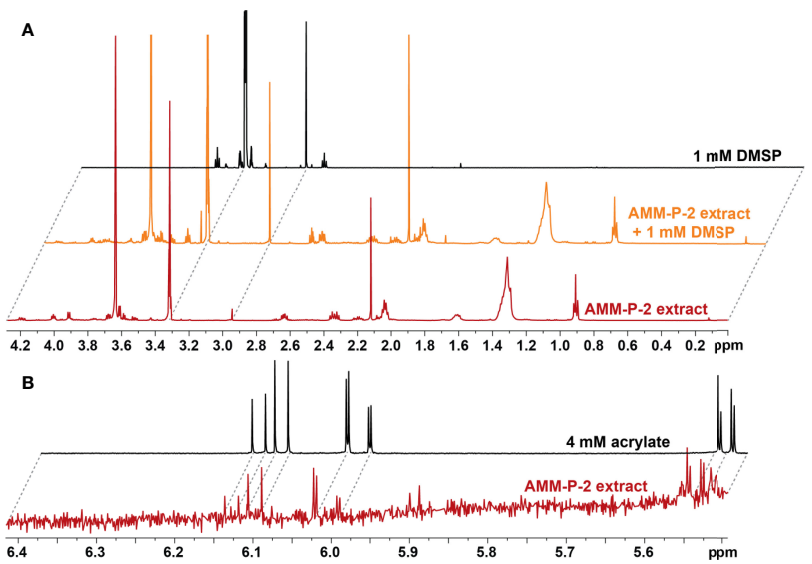

FIGURE 2 | Isolates harbouring *dsyB* produce dimethylsulfoniopropionate (DMSP). **(A)** ^{1}H NMR spectra of the DMSP region identifying diagnostic peaks (δ_H 2.95 ppm) in deuterated methanol (CD_3OD) extract of *Shimia* AMM-P-2 cultured in methionine-enriched minimal basal medium; the same *Shimia* AMM-P-2 cell extract spiked with 10 µl of 1 mM DMSP standard; and 1 mM DMSP standard in CD_3OD. **(B)** ^{1}H NMR spectra of the acrylate region identifying diagnostic peaks (δ_H 5.71, 6.13 and 6.20 ppm) in CD_3OD cell extracts of *Shimia* AMM-P-2 cultured in methionine-enriched minimal basal medium; 4 mM acrylate standard in CD_3OD.

TABLE 1 | Genome statistics for *Shimia aestuarii* AMM-P-2.

Attribute	Value
Estimated genome size (bp)	4,151,190
Assembly size (bp)	3,972,669
No. of sequences	75
GC content (%)	60.6
N50	181,193
Gap ratio (%)	0
Number of CDSs	3,906
Number of rRNA	3
Number of tRNA	46
Number of CRISPRs	0
Coding ratio (%)	89.7

AMM-P-2 can produce cysteine (through serine or homocysteine) and ultimately the DMSP precursor methionine (*via* aspartate; **Figure 3**).

Turning the attention to DMSP catabolism, *S. aestuarii* AMM-P-2 has the genetic potential to both demethylate and cleave this sulfur compound (**Figure 3** and **Table S3**). *S. aestuarii* AMM-P-2 has the entire *dmdABCD* suite of genes enabling conversion of DMSP to MeSH (Zhang et al., 2019). This bacterium also contains the DMSP lyase genes *dddP* and *dddW*, whose products liberate equimolar amounts of DMS and acrylate from DMSP (Zhang et al., 2019). It is also able to metabolise acrylate to propionyl-CoA through *acuI*, *acuH* and *prpE* genes (Wang et al., 2017). Significant matches to *dddA* and *dddC* (E-values ≥ 1.39 e^{-93}) which catabolise 3-hydroxypropionyl-CoA (3HP) to acetyl-CoA (Wang et al., 2017) (**Table S3**) were also identified.

DMSP Production by *Shimia aestuarii* AMM-P-2 Under Different Environmental Conditions

To assess the influence of environmental factors on DMSP production by *S. aestuarii* AMM-P-2, cultures were grown in methionine-enriched MBM under six different conditions and sampled four times over a 48-hour incubation period. The conditions tested are known to elicit stress responses in corals (high and low temperature, high and low salinity, high UV, and darkness), and were compared to controls. Intracellular DMSP levels per cell within each treatment were not statistically different through time (repeated-measure ANOVA, $p = 0.078$; see **Table S4**) and no significant interaction was identified between time and treatments (repeated-measure ANOVA, $p = 0.204$; **Table S4**).

Changes in salinity affected DMSP levels per cell (**Figure 4A**). Levels of DMSP in cultures grown under hyposaline conditions (25 PSU) were 63% lower than the controls (35 PSU) over all four time points. In contrast, the highest DMSP levels were recorded under hypersaline conditions (40 PSU), which were 80% higher than the controls. DMSP levels also increased when cells were grown under high UV (65% higher) or in complete darkness (43% higher) compared to control ambient light conditions. Finally, at higher temperature (32°C), DMSP levels were 42% lower than the controls, while the low temperature treatment (22°C) had no effect throughout the experiment.

Although it was not possible to quantify DMS with qNMR due to the volatility of this compound, DMSP lysis releases equimolar concentrations of acrylate, which was detected in every sample. Overall, the level of acrylate per cell was approximately one order of magnitude lower than that of DMSP (**Figure 4B**). These measurements confirm that a fraction of the synthesized DMSP is channelled through the cleavage pathway. A significant interaction between time and treatments was identified for acrylate levels per cell (ANOVA, $p = 0.047$; **Table S5**). However, the differences between control conditions and the different treatments were not as pronounced for acrylate compared to DMSP. The 32°C treatment exhibited the lowest levels of acrylate across all timepoints (with 68% less acrylate on average than the control), while the high salinity treatment gave rise to the highest concentrations (with 36% more acrylate).

The six treatments were divided into two categories: (i) those likely to elicit a stress response in bacteria (i.e., high UV, low and high salinity), and (ii) those unlikely to be stressors (i.e., darkness, 22 and 32°C), and the level of correlation of the intracellular levels of DMSP and acrylate between these assessed. No significant correlation was identified between DMSP and acrylate levels for the mild conditions (Pearson's R = 0.23, $p = 0.39$; **Figure 4D**). However, a strong positive correlation was identified for the stress treatments (Pearson's R = 0.87, $p < 0.001$; **Figure 4C**).

DISCUSSION

Coral-Associated Bacteria Can Produce DMSP

Of the 157 bacteria isolated from the mucus and tissues of four coral species, approximately 9% harboured the *dsyB* gene (14 out

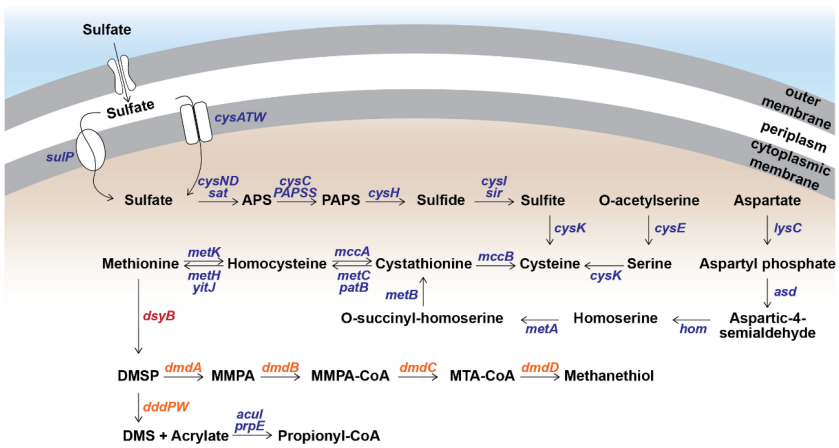

FIGURE 3 | Metabolism of methylated sulfur compounds in *Shimia aestuarii* AMM-P-2. Orthologous genes for each step are presented in blue. The DMSP production gene *dsyB* is presented in red, while the catabolism genes are in orange. E-values and additional information can be found in **Table S3**.

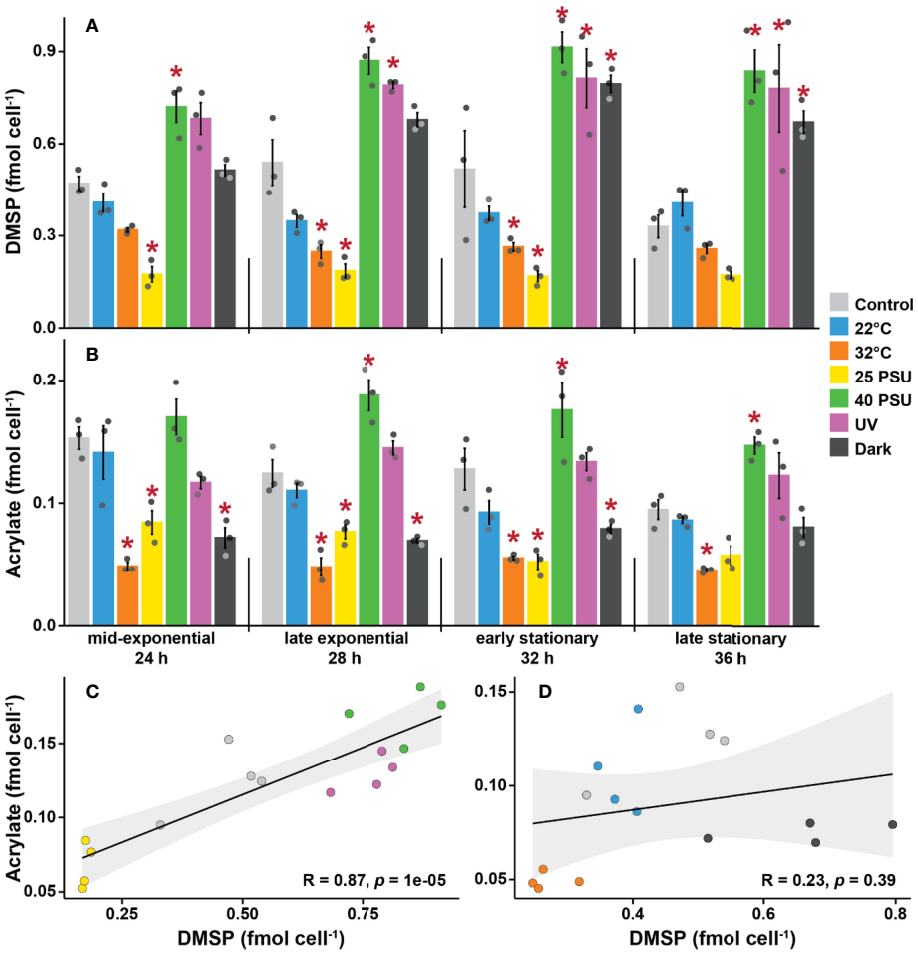

FIGURE 4 | Dimethylsulfoniopropionate (DMSP) and acrylate levels are strongly influenced by environmental stressors in *Shimia aestuarii* AMM-P-2. Levels of **(A)** DMSP and **(B)** acrylate in bacterial cells exposed to high and low temperatures (32 and 22°C), high and low salinity (40 and 25 PSU), constant darkness, and high UV. Controls were grown at 27°C under ambient light in a modified MBM media adjusted to 35 PSU and supplemented with 0.5 mM methionine. Error bars indicate standard error (n = 3). Experimental conditions marked with an asterisk are significantly different ($p < 0.05$) from the controls (Repeated-measure ANOVA). Correlation between DMSP and acrylate levels in *Shimia aestuarii* AMM-P-2 under conditions **(C)** likely to stress the cells (high-low salinity and high UV), **(D)** unlikely to stress the cells (22-32°C and darkness). Pearson correlation coefficient and associated p values are displayed on each graph.

of 157). Although three genera (four species) of corals were screened, *dysB*-positive bacteria were only isolated from the two *Acropora* species, which correlates with the high DMSP production by members of this genus (Tapiolas et al., 2013). Note, it is possible that other DMSP-producing bacteria were present in the corals sampled, potentially containing *mmtN* or other unknown DMSP synthesis genes (Williams et al., 2019). All bacteria with *dsyB* belonged to the Rhodobacterales order (Curson et al., 2017), with *Shimia* species representing 71% of these isolates (10 out of 14). *Shimia* are metabolically versatile members of the Roseobacter clade (Choi and Cho, 2006), and are abundant in the water column, marine sediments, and commonly associated with eukaryotic hosts (Lenk et al., 2012; Luo and Moran, 2014), particularly phytoplankton (Ajani et al., 2018; Behringer et al., 2018) and reef-building corals (Chen et al., 2011; Zhang et al., 2021). The other *dsyB*-harbouring bacteria isolated in our screen belonged to the genera *Pseudooceanicola* – which are common DMSP producers in the water column (Zheng et al., 2020) – and *Roseivivax* – which have been isolated from corals (Chen et al., 2012) and can induce coral larval settlement (Sharp et al., 2015).

DMSP was unambiguously identified in extracts of *dsyB*-harbouring bacteria when the cells were grown in methionine-supplemented MBM. In MBM lacking methionine, DMSP signal intensity was close to or below the detection limits of the LC-MS and NMR. Addition of pathway intermediates, including methionine, have been shown to enhance DMSP production in bacteria, but most *dsyB*-harbouring strains can also produce methionine *de novo* (through sulfate assimilation) (Curson et al., 2017). This study therefore reveals the presence of bacteria capable of DMSP production in corals and shows that these microorganisms are likely to contribute to the DMSP production by coral holobionts.

Three strains of *Labrenzia*, the bacterial genus from which the *dsyB* gene was initially identified (Curson et al., 2017), were

isolated from *Pocillopora acuta* and *Stylophora pistillata*. The 16S rRNA genes of one of the strains was 98.6% similar to *Labrenzia alba*, while of the other two were more than 98% similar to *L. aggregata*. However, the *dsyB* gene was not detected in any of the three strains. This is consistent with the previously-reported lack of *de novo* DMS production from a Symbiodiniaceae-associated *Labrenzia* strain (Lawson et al., 2020), suggesting that the ability to produce DMSP is not conserved across the *Labrenzia* genus.

Shimia aestuarii AMM-P-2 Can Produce DMSP *de novo*

To investigate the potential of a representative DMSP-producing bacterium from corals to metabolise sulfur compounds, the genome of *S. aestuarii* AMM-P-2 was fully sequenced. *S. aestuarii* is capable of assimilating sulfate from seawater to produce sulfide and sulfur-containing amino acids. Although all the genes required for methionine synthesis were present, its growth on methionine-enriched media indicates that it can also use exogenous methylated sulfur compounds, enhancing the pool of reduced sulfur intermediates available for the synthesis of DMSP. The *S. aestuarii* AMM-P-2 genome also encodes both the demethylation and the cleavage pathways, allowing it to produce the sulfurous gases methanethiol and DMS. Given that metabolic interdependencies between different partners are common in symbiotic systems, it is important to note that *S. aestuarii* AMM-P-2 has all the required genes to produce DMSP *de novo*.

As in other Rhodobacterales (Curson et al., 2017), *dsyB* in *S. aestuarii* AMM-P-2 is located downstream of multiple genes (*iscRS*, *sufBCDS*) encoding iron-sulfur cluster (Isc) proteins involved in the formation of Fe-S clusters and cellular defence against oxidative stress. Specifically, the cysteine desulfurase IscS provides the sulfur that is then incorporated into Fe-S clusters and its deletion renders the cells hypersensitive to oxidative stress (Ayala-Castro et al., 2008; Rybniker et al., 2014). In addition, the IscR protein is a transcriptional regulator of the *suf* operon (Yeo et al., 2006) and both the *suf* and *isc* operons are highly induced by oxidative stress (Yeo et al., 2006). Therefore, the tight linkage of *dsyB* to the *suf* and *isc* operons suggests that DMSP transcription may be directly affected by oxidants (Sunda et al., 2002; Curson et al., 2017).

DMSP Production by *Shimia aestuarii* AMM-P-2 Is Enhanced by Environmental Stress

DMSP levels in *S. aestuarii* cells were affected by changes in salinity. Fluctuations in salinity are known to affect DMSP levels in corals (Gardner et al., 2016; Aguilar et al., 2017), while also impacting DMSP degradation in bacteria (Salgado et al., 2014; Liu et al., 2018). The nearly 5-fold increase in intracellular DMSP under hypersaline compared to hyposaline conditions reported here is consistent with previous reports in algae (Vairavamurthy et al., 1985; Kirst et al., 1991; Trossat et al., 1998), and bacteria (Curson et al., 2017), and supports the proposed function of this molecule as an osmolyte (Kirst et al., 1991).

UV exposure and complete darkness both caused significant increases in DMSP levels in *S. aestuarii* cells. The level of UV radiation applied here was approximately 50% higher than values previously measured at 1 m depth on the Great Barrier Reef (Nordborg et al., 2018), and is therefore likely to cause oxidative stress in the *S. aestuarii* cells. Indeed, because of their lack of pigmentation and low internal self-shading due to small cell volume, heterotrophic bacteria are amongst the most UV-sensitive organisms (Ruiz-Gonzalez et al., 2013). Similar increases in DMSP levels triggered by UV exposure have been reported in phytoplankton (Sunda et al., 2002; Slezak and Herndl, 2003) and have been attributed to the antioxidant capacity of DMSP (Sunda et al., 2002). More surprising was the increase in DMSP levels in cells grown in darkness. Recent studies have revealed that bacteria in aphotic environments, such as the deep ocean as well as coastal and deep sediments, produce substantial amounts of DMSP (Williams et al., 2019; Zheng et al., 2020). Although the effect of sunlight on bacterioplankton has been extensively studied at the community level (Ruiz-Gonzalez et al., 2013), the impact of prolonged darkness on the physiology of heterotrophic bacteria has received little attention to date. Our results suggest that the absence of light influences sulfur metabolism in *S. aestuarii*, and further investigation should aim to identify the mechanism driving the production of DMSP in aphotic conditions.

Intracellular acrylate levels in *S. aestuarii* AMM-P-2 were almost one order of magnitude lower than those of DMSP and decreased significantly over time in all growth conditions. Acrylate and DMSP levels were strongly and positively correlated under conditions likely to stress the bacteria (e.g., salinity, UV), but were decoupled under conditions that are stressful for the coral host but not necessarily for the bacteria (e.g., small temperature variations, darkness). This suggests that under conditions stressful for the bacteria, more DMSP is channelled towards the DMSP cleavage pathway, which generates equal amounts of DMS and acrylate, rather than the demethylation pathway (Gao et al., 2020). DMS and acrylate are efficient scavengers of hydroxyl radicals produced by the cells during stress (Sunda et al., 2002), which may explain why the cleavage pathway is preferred during stressful conditions.

CONCLUSION

This study demonstrates that some coral-associated bacteria can produce the important organosulfur compound DMSP, implying that, along with the animal host and Symbiodiniaceae, bacterial communities may contribute to DMSP production by the coral holobiont. It has recently been shown that bacteria can also use a second (*dsyB*-independent) pathway to produce DMSP, involving the *mmtN* gene (Williams et al., 2019). Since this gene is also present in Gammaproteobacteria and Actinobacteria, it is likely that some DMSP-producing bacteria were overlooked by the *dsyB*-centric screening approach and thus that the proportion of DMSP-producing bacteria in corals might be greater than estimated here. Analysis of the genome of a *Shimia* strain, representing the most abundant *dsyB*-harbouring genus of those isolated from corals, revealed that this bacterium has the genetic machinery to

assimilate sulfate, to synthesise the sulfur-based amino acids cysteine and methionine, to catabolise DMSP to methanethiol, DMS and acrylate, and to utilise or detoxify acrylate. Furthermore, DMSP production in *S. aestuarii* AMM-P-2 is regulated by specific environmental conditions, some of which are not necessarily tied to coral stress. The capacity of coral-associated bacteria to produce DMSP not only adds this trait to the functional repertoire of prokaryotes associated with corals, but also indicates that bacteria may contribute to the large DMSP pool produced by this metaorganism.

DATA AVAILABILITY STATEMENT

The datasets presented in this study can be found in online repositories. The 16S rRNA gene amplicon sequences of the isolated bacteria have been deposited in GenBank (https://www.ncbi.nlm.nih.gov/genbank/) under the accession numbers MW828351 to MW828429 and MW828507 to MW828582. The assembled genome of isolate AMM-P-2 has been deposited in GenBank under the accession number PRJNA810763.

AUTHOR CONTRIBUTIONS

CM, DM, DB, FK and J-BR designed the experiments. FK collected the samples and performed all laboratory work and data analysis with the assistance of CM, DM, DB, JT and J-BR. FK, JZ, IC and DM analysed the genomic data. FK, CM, DM, DB and J-BR wrote the manuscript, with input from all authors before submission. All authors contributed to the article and approved the submitted version.

FUNDING

FWIK was supported through scholarships and funding from the AIMS@JCU Division of Research & Innovation and the College of Public Health, Medical and Veterinary Sciences at James Cook University. This research was funded in part by the Pilot Research Awards from AIMS@JCU.

ACKNOWLEDGMENTS

The coral colonies were collected under permit G14/36802 issued by the Great Barrier Reef Marine Park Authority. The authors thank the staff of AIMS SeaSim for providing coral samples as needed, and Aurélie Moya, Sara Bell, Peter Thomas-Hall, and Nahshon Siboni for discussions and assistance in the lab. The authors acknowledge the Traditional Owners of the land on which the research was conducted, the Wulgurukaba, Bindal and Gadigal people; we recognise their connection to land, sea, and community, and pay our respects to Elders past, present and emerging. Finally, a special thanks goes to Libby Evans-Illidge (AIMS@JCU) for her unwavering support throughout the project.

SUPPLEMENTARY MATERIAL

The Supplementary Material for this article can be found online at: https://www.frontiersin.org/articles/10.3389/fmars.2022.869574/full#supplementary-material

REFERENCES

Aguilar, C., Raina, J.-B., Motti, C. A., Fôret, S., Hayward, D. C., Lapeyre, B., et al. (2017). Transcriptomic Analysis of the Response of *Acropora Millepora* to Hypo-Osmotic Stress Provides Insights Into DMSP Biosynthesis by Corals. *BMC Genomics* 18, 612. doi: 10.1186/s12864-017-3959-0

Ajani, P. A., Kahlke, T., Siboni, N., Carney, R., Murray, S. A., and Seymour, J. R. (2018). The Microbiome of the Cosmopolitan Diatom Leptocylindrus Reveals Significant Spatial and Temporal Variability. *Front. Microbiol.* 9. doi: 10.3389/fmicb.2018.02758

Akoka, S., and Trierweiler, M. (2002). Improvement of the ERETIC Method by Digital Synthesis of the Signal and Addition of a Broadband Antenna Inside the NMR Probe. *Instrum. Sci. Technol.* 30, 21–29. doi: 10.1081/CI-100108768

Altschul, S. F., Gish, W., Miller, W., Myers, E. W., and Lipman, D. J. (1990). Basic Local Alignment Search Tool. *J. Mol. Biol.* 215, 403–410. doi: 10.1016/S0022-2836(05)80360-2

Andreae, M. O., Barnard, W. R., and Ammons, J. M. (1983). The Biological Production of Dimethylsulfide in the Ocean and Its Role in the Global Atmospheric Sulfur Budget. *Ecol. Bull.* 35, 167–177. doi: jstor.org/stable/20112852

Ayala-Castro, C., Saini, A., and Outten, F. W. (2008). Fe-S Cluster Assembly Pathways in Bacteria. *Microbiol. Mol. Biol. Rev.* 72, 110–125. doi: 10.1128/MMBR.00034-07

Ayers, G. P., and Gras, J. L. (1991). Seasonal Relationship Between Cloud Condensation Nuclei and Aerosol Methanesulphonate in Marine Air. *Nature* 353, 834–835. doi: 10.1038/353834a0

Bankevich, A., Nurk, S., Antipov, D., Gurevich, A. A., Dvorkin, M., Kulikov, A. S., et al. (2012). SPAdes: A New Genome Assembly Algorithm and Its Applications to Single-Cell Sequencing. *J. Comput. Biol.* 19, 455–477. doi: 10.1089/cmb.2012.0021

Bates, T. S., Charlson, R. J., and Gammon, R. H. (1987). Evidence for the Climatic Role of Marine Biogenic Sulphur. *Nature* 329, 319–321. doi: 10.1038/329319a0

Behringer, G., Ochsenkühn, M. A., Fei, C., Fanning, J., Koester, J. A., and Amin, S. A. (2018). Bacterial Communities of Diatoms Display Strong Conservation Across Strains and Time. *Front. Microbiol.* 9. doi: 10.3389/fmicb.2018.00659

Bolger, A. M., Lohse, M., and Usadel, B. (2014). Trimmomatic: A Flexible Trimmer for Illumina Sequence Data. *Bioinformatics* 30, 2114–2120. doi: 10.1093/bioinformatics/btu170

Bourne, D. G., Morrow, K. M., and Webster, N. S. (2016). Insights Into the Coral Microbiome: Underpinning the Health and Resilience of Reef Ecosystems. *Annu. Rev. Microbiol.* 70, 317–340. doi: 10.1146/annurev-micro-102215-095440

Bourne, D. G., and Munn, C. B. (2005). Diversity of Bacteria Associated With the Coral *Pocillopora Damicornis* From the Great Barrier Reef. *Environ. Microbiol.* 7, 1162–1174. doi: 10.1111/j.1462-2920.2005.00793.x

Capella-Gutiérrez, S., Silla-Martínez, J. M., and Gabaldón, T. (2009). trimAl: A Tool for Automated Alignment Trimming in Large-Scale Phylogenetic Analyses. *Bioinformatics* 25, 1972–1973. doi: 10.1093/bioinformatics/btp348

Chen, M.-H., Sheu, S.-Y., Chen, C. A., Wang, J.-T., and Chen, W.-M. (2011). *Shimia Isoporae* Sp. Nov., Isolated From the Reef-Building Coral *Isopora Palifera*. *Int. J. Syst. Evol. Microbiol.* 61, 823–827. doi: 10.1099/ijs.0.022848-0

Chen, M.-H., Sheu, S.-Y., Chen, C. A., Wang, J.-T., and Chen, W.-M. (2012). *Roseivivax Isoporae* Sp. Nov., Isolated From a Reef-Building Coral, and Emended Description of the Genus *Roseivivax*. *Int. J. Syst. Evol. Microbiol.* 62, 1259–1264. doi: 10.1099/ijs.0.032961-0

Choi, D. H., and Cho, B. C. (2006). *Shimia Marina* Gen. Nov., Sp. Nov., a Novel Bacterium of the *Roseobacter* Clade Isolated From Biofilm in a Coastal Fish Farm. *Int. J. Syst. Evol. Microbiol.* 56, 1869–1873. doi: 10.1099/ijs.0.64235-0

Curson, A. R. J., Liu, J., Bermejo Martínez, A., Green, R. T., Chan, Y., Carrión, O., et al. (2017). Dimethylsulfoniopropionate Biosynthesis in Marine Bacteria and Identification of the Key Gene in This Process. *Nat. Microbiol.* 2, 17009. doi: 10.1038/nmicrobiol.2017.9

Curson, A. R. J., Williams, B. T., Pinchbeck, B. J., Sims, L. P., Martínez, A. B., Rivera, P. P. L., et al. (2018). DSYB Catalyses the Key Step of Dimethylsulfoniopropionate Biosynthesis in Many Phytoplankton. *Nat. Microbiol.* 3, 430–439. doi: 10.1038/s41564-018-0119-5

DeBose, J. L., Lema, S. C., and Nevitt, G. A. (2008). Dimethylsulfoniopropionate as a Foraging Cue for Reef Fishes. *Science* 319, 1356–1356. doi: 10.1126/science.1151109

Di Tommaso, P., Moretti, S., Xenarios, I., Orobitg, M., Montanyola, A., Chang, J.-M., et al. (2011). T-Coffee: A Web Server for the Multiple Sequence Alignment of Protein and RNA Sequences Using Structural Information and Homology Extension. *Nucleic Acids Res.* 39, W13–W17. doi: 10.1093/nar/gkr245

Frade, P. R., Schwaninger, V., Glasl, B., Sintes, E., Hill, R. W., Simó, R., et al. (2016). Dimethylsulfoniopropionate in Corals and its Interrelations With Bacterial Assemblages in Coral Surface Mucus. *Environ. Chem.* 13, 252–265. doi: 10.1071/EN15023

Gao, C., Fernandez, V. I., Lee, K. S., Fenizia, S., Pohnert, G., Seymour, J. R., et al. (2020). Single-Cell Bacterial Transcription Measurements Reveal the Importance of Dimethylsulfoniopropionate (DMSP) Hotspots in Ocean Sulfur Cycling. *Nat. Commun.* 11, 1942. doi: 10.1038/s41467-020-15693-z

Gardner, S. G., Nielsen, D. A., Laczka, O., Shimmon, R., Beltran, V. H., Ralph, P. J., et al. (2016). Dimethylsulfoniopropionate, Superoxide Dismutase and Glutathione as Stress Response Indicators in Three Corals Under Short-Term Hyposalinity Stress. *Proc. R. Soc. B.: Biol. Sci.* 283, 20152418. doi: 10.1098/rspb.2015.2418

González, J. M., Whitman, W. B., Hodson, R. E., and Moran, M. A. (1996). Identifying Numerically Abundant Culturable Bacteria From Complex Communities: An Example From a Lignin Enrichment Culture. *Appl. Environ. Microbiol.* 62, 4433–4440. doi: 10.1128/aem.62.12.4433-4440.1996

Hill, R. W., Dacey, J. W. H., and Krupp, D. A. (1995). Dimethylsulfoniopropionate in Reef Corals. *Bull. Marine. Sci.* 57, 489–494.

Howard, E. C., Henriksen, J. R., Buchan, A., Reisch, C. R., Bürgmann, H., Welsh, R., et al. (2006). Bacterial Taxa That Limit Sulfur Flux From the Ocean. *Science* 314, 649–652. doi: 10.1126/science.1130657

Johnston, A., Todd, J., and Curson, A. (2012). Microbial Origins and Consequences of Dimethyl Sulfide. *Microbe* 7, 181–185. doi: 10.1128/microbe.7.181.1

Jones, G. B., and Trevena, A. J. (2005). The Influence of Coral Reefs on Atmospheric Dimethylsulphide Over the Great Barrier Reef, Coral Sea, Gulf of Papua and Solomon and Bismarck Seas. *Marine. Freshwater. Res.* 56, 85–93. doi: 10.1071/MF04097

Kanehisa, M., Goto, S., Kawashima, S., Okuno, Y., and Hattori, M. (2004). The KEGG Resource for Deciphering the Genome. *Nucleic Acids Res.* 32, D277–D280. doi: 10.1093/nar/gkh063

Karsten, U., Kück, K., Vogt, C., and Kirst, G. O. (1996). "Dimethylsulfoniopropionate Production in Phototrophic Organisms and its Physiological Functions as a Cryoprotectant," in *Biological and Environmental Chemistry of DMSP and Related Sulfonium Compounds*. Eds. R. P. Kiene, P. T. Visscher, M. D. Keller and G. O. Kirst (Boston, MA: Springer US), 143–153.

Katoh, K., Misawa, K., i. Kuma, K., and Miyata, T. (2002). MAFFT: A Novel Method for Rapid Multiple Sequence Alignment Based on Fast Fourier Transform. *Nucleic Acids Res.* 30, 3059–3066. doi: 10.1093/nar/gkf436

Katoh, K., and Standley, D. M. (2013). MAFFT Multiple Sequence Alignment Software Version 7: Improvements in Performance and Usability. *Mol. Biol. Evol.* 30, 772–780. doi: 10.1093/molbev/mst010

Kiene, R. P., Linn, L. J., and Bruton, J. A. (2000). New and Important Roles for DMSP in Marine Microbial Communities. *J. Sea. Res.* 43, 209–224. doi: 10.1016/S1385-1101(00)00023-X

Kiene, R. P., Visscher, P. T., Keller, M. D., and Kirst, G. O. (1996). *Biological and Environmental Chemistry of DMSP and Related Sulfonium Compounds* (Boston, MA: Springer).

Kirst, G. O. (1996). "Osmotic Adjustment in Phytoplankton and MacroAlgae," in *Biological and Environmental Chemistry of DMSP and Related Sulfonium Compounds*. Eds. R. P. Kiene, P. T. Visscher, M. D. Keller and G. O. Kirst (Boston, MA: Springer US), 121–129.

Kirst, G. O., Thiel, C., Wolff, H., Nothnagel, J., Wanzek, M., and Ulmke, R. (1991). Dimethylsulfoniopropionate (DMSP) in Icealgae and its Possible Biological Role. *Marine. Chem.* 35, 381–388. doi: 10.1016/S0304-4203(09)90030-5

Lane, D. (1991). "16s/23s rRNA Sequencing," in *Nucleic Acid Techniques in Bacterial Systematics*. Eds. E. Stackebrandt and M. Goodfellow (New York, NY, USA: John Wiley & Sons), 115–175.

Lawson, C. A., Seymour, J. R., Possell, M., Suggett, D. J., and Raina, J.-B. (2020). The Volatilomes of Symbiodiniaceae-Associated Bacteria Are Influenced by Chemicals Derived From Their Algal Partner. *Front. Marine. Sci.* 7. doi: 10.3389/fmars.2020.00106

Lenk, S., Moraru, C., Hahnke, S., Arnds, J., Richter, M., Kube, M., et al. (2012). *Roseobacter* Clade Bacteria are Abundant in Coastal Sediments and Encode a Novel Combination of Sulfur Oxidation Genes. *ISME. J.* 6, 2178–2187. doi: 10.1038/ismej.2012.66

Liu, J., Liu, J., Zhang, S.-H., Liang, J., Lin, H., Song, D., et al. (2018). Novel Insights Into Bacterial Dimethylsulfoniopropionate Catabolism in the East China Sea. *Front. Microbiol.* 9. doi: 10.3389/fmicb.2018.03206

Luo, H., and Moran, M. A. (2014). Evolutionary Ecology of the Marine *Roseobacter* Clade. *Microbiol. Mol. Biol. Rev.* 78, 573–587. doi: 10.1128/MMBR.00020-14

Luo, D., Wang, X., Feng, X., Tian, M., Wang, S., Tang, S.-L., et al. (2021). Population Differentiation of Rhodobacteraceae Along With Coral Compartments. *ISME. J.* 15, 3286–3302. doi: 10.1038/s41396-021-01009-6

Lu, S., Wang, J., Chitsaz, F., Derbyshire, M. K., Geer, R. C., Gonzales, N. R., et al. (2019). CDD/SPARCLE: The Conserved Domain Database in 2020. *Nucleic Acids Res.* 48, D265–D268. doi: 10.1093/nar/gkz991

Marchler-Bauer, A., and Bryant, S. H. (2004). CD-Search: Protein Domain Annotations on the Fly. *Nucleic Acids Res.* 32, W327–W331. doi: 10.1093/nar/gkh454

Marie, D., Partensky, F., Jacquet, S., and Vaulot, D. (1997). Enumeration and Cell Cycle Analysis of Natural Populations of Marine Picoplankton by Flow Cytometry Using the Nucleic Acid Stain SYBR Green I. *Appl. Environ. Microbiol.* 63, 186–193. doi: 10.1128/aem.63.1.186-193.1997

Matthews, J. L., Raina, J.-B., Kahlke, T., Seymour, J. R., van Oppen, M. J. H., and Suggett, D. J. (2020). Symbiodiniaceae-Bacteria Interactions: Rethinking Metabolite Exchange in Reef-Building Corals as Multi-Partner Metabolic Networks. *Environ. Microbiol.* 22, 1675–1687. doi: 10.1111/1462-2920.14918

Minh, B. Q., Nguyen, M. A. T., and von Haeseler, A. (2013). Ultrafast Approximation for Phylogenetic Bootstrap. *Mol. Biol. Evol.* 30, 1188–1195. doi: 10.1093/molbev/mst024

Needleman, S. B., and Wunsch, C. D. (1970). A General Method Applicable to the Search for Similarities in the Amino Acid Sequence of Two Proteins. *J. Mol. Biol.* 48, 443–453. doi: 10.1016/0022-2836(70)90057-4

Ngugi, D. K., Ziegler, M., Duarte, C. M., and Voolstra, C. R. (2020). Genomic Blueprint of Glycine Betaine Metabolism in Coral Metaorganisms and Their Contribution to Reef Nitrogen Budgets. *iScience* 23, 101120. doi: 10.1016/j.isci.2020.101120

Nordborg, F. M., Flores, F., Brinkman, D. L., Agustí, S., and Negri, A. P. (2018). Phototoxic Effects of Two Common Marine Fuels on the Settlement Success of the Coral *Acropora Tenuis*. *Sci. Rep.* 8, 8635. doi: 10.1038/s41598-018-26972-7

Notredame, C., Higgins, D. G., and Heringa, J. (2000). T-Coffee: A Novel Method for Fast and Accurate Multiple Sequence Alignment. *J. Mol. Biol.* 302, 205–217. doi: 10.1006/jmbi.2000.4042

Pogoreutz, C., Voolstra, C. R., Rädecker, N., Weis, V., Cardenas, A., and Raina, J.-B. (2020). "The Coral Holobiont Highlights the Dependence of Cnidarian Animal Hosts on Their Associated Microbes," in *Cellular Dialogues in the Holobiont*. Eds. T. C. G. Bosch and M. G. Hadfield (CRC Press: Taylor & Francis Group), 91–118.

Rädecker, N., Pogoreutz, C., Voolstra, C. R., Wiedenmann, J., and Wild, C. (2015). Nitrogen Cycling in Corals: The Key to Understanding Holobiont Functioning? *Trends Microbiol.* 23, 490–497. doi: 10.1016/j.tim.2015.03.008

Raina, J.-B., Dinsdale, E. A., Willis, B. L., and Bourne, D. G. (2010). Do the Organic Sulfur Compounds DMSP and DMS Drive Coral Microbial Associations? *Trends Microbiol.* 18, 101–108. doi: 10.1016/j.tim.2009.12.002

Raina, J.-B., Tapiolas, D. M., Foret, S., Lutz, A., Abrego, D., Ceh, J., et al. (2013). DMSP Biosynthesis by an Animal and its Role in Coral Thermal Stress Response. *Nature* 502, 677–680. doi: 10.1038/nature12677

Raina, J.-B., Tapiolas, D., Motti, C. A., Foret, S., Seemann, T., Tebben, J., et al. (2016). Isolation of an Antimicrobial Compound Produced by Bacteria Associated With Reef-Building Corals. *PeerJ* 4, e2275. doi: 10.7717/peerj.2275

Raina, J.-B., Tapiolas, D., Willis, B. L., and Bourne, D. G. (2009). Coral-Associated Bacteria and Their Role in the Biogeochemical Cycling of Sulfur. *Appl. Environ. Microbiol.* 75, 3492–3501. doi: 10.1128/AEM.02567-08

R Core Team (2020). *R: A Language and Environment for Statistical Computing* (Vienna, Austria: R Foundation for Statistical Computing).

Robbins, S. J., Singleton, C. M., Chan, C. X., Messer, L. F., Geers, A. U., Ying, H., et al. (2019). A Genomic View of the Reef-Building Coral *Porites Lutea* and its Microbial Symbionts. *Nat. Microbiol.* 4, 2090–2100. doi: 10.1038/s41564-019-0532-4

Rohwer, F., Seguritan, V., Azam, F., and Knowlton, N. (2002). Diversity and Distribution of Coral-Associated Bacteria. *Marine. Ecol. Prog. Ser.* 243, 1–10. doi: 10.3354/meps243001

Ruiz-Gonzalez, C., Simo, R., Sommaruga, R., and Gasol, J. M. (2013). Away From Darkness: A Review on the Effects of Solar Radiation on Heterotrophic Bacterioplankton Activity. *Front. Microbiol.* 4. doi: 10.3389/fmicb.2013.00131

Rybniker, J., Pojer, F., Marienhagen, J., Kolly, G. S., Chen, J. M., van Gumpel, E., et al. (2014). The Cysteine Desulfurase IscS of Mycobacterium Tuberculosis is Involved in Iron–Sulfur Cluster Biogenesis and Oxidative Stress Defence. *Biochem. J.* 459, 467–478. doi: 10.1042/BJ20130732

Salgado, P., Kiene, R., Wiebe, W., and Magalhães, C. (2014). Salinity as a Regulator of DMSP Degradation in Ruegeria Pomeroyi DSS-3. *J. Microbiol.* 52, 948–954. doi: 10.1007/s12275-014-4409-1

Schwarz, G. (1978). Estimating the Dimension of a Model. *Ann. Stat* 6, 461–464. doi: 10.1214/aos/1176344136

Seemann, T. (2014). Prokka: Rapid Prokaryotic Genome Annotation. *Bioinformatics* 30, 2068–2069. doi: 10.1093/bioinformatics/btu153

Seymour, J. R., Simó, R., Ahmed, T., and Stocker, R. (2010). Chemoattraction to Dimethylsulfoniopropionate Throughout the Marine Microbial Food Web. *Science* 329, 342–345. doi: 10.1126/science.1188418

Sharp, K. H., Sneed, J. M., Ritchie, K. B., McDaniel, L., and Paul, V. J. (2015). Induction of Larval Settlement in the Reef Coral *Porites Astreoides* by a Cultivated Marine *Roseobacter* Strain. *Biol. Bull.* 228, 98–107. doi: 10.1086/BBLv228n2p98

Sievert, S. M., Kiene, R. P., and Schulz-Vogt, H. N. (2007). The Sulfur Cycle. *Oceanography* 20, 117–123. doi: 10.5670/oceanog.2007.55

Slezak, D., and Herndl, G. J. (2003). Effects of Ultraviolet and Visible Radiation on the Cellular Concentrations of Dimethylsulfoniopropionate (DMSP) in Emiliania Huxleyi (Strain L). *Marine. Ecol. Prog. Ser.* 246, 61–71. doi: 10.3354/meps246061

Stefels, J. (2000). Physiological Aspects of the Production and Conversion of DMSP in Marine Algae and Higher Plants. *J. Sea. Res.* 43, 183–197. doi: 10.1016/S1385-1101(00)00030-7

Sunda, W., Kieber, D. J., Kiene, R. P., and Huntsman, S. (2002). An Antioxidant Function for DMSP and DMS in Marine Algae. *Nature* 418, 317–320. doi: 10.1038/nature00851

Tandon, K., Lu, C.-Y., Chiang, P.-W., Wada, N., Yang, S.-H., Chan, Y.-F., et al. (2020). Comparative Genomics: Dominant Coral-Bacterium Endozoicomonas Acroporae Metabolizes Dimethylsulfoniopropionate (DMSP). *ISME. J.* 14, 1290–1303. doi: 10.1038/s41396-020-0610-x

Tapiolas, D. M., Raina, J.-B., Lutz, A., Willis, B. L., and Motti, C. A. (2013). Direct Measurement of Dimethylsulfoniopropionate (DMSP) in Reef-Building Corals Using Quantitative Nuclear Magnetic Resonance (qNMR) Spectroscopy. *J. Exp. Marine. Biol. Ecol.* 443, 85–89. doi: 10.1016/j.jembe.2013.02.037

Trossat, C., Rathinasabapathi, B., Weretilnyk, E. A., Shen, T.-L., Huang, Z.-H., Gage, D. A., et al. (1998). Salinity Promotes Accumulation of 3-Dimethylsulfoniopropionate and Its Precursor *S*-Methylmethionine in Chloroplasts. *Plant Physiol.* 116, 165–171. doi: 10.1104/pp.116.1.165

Vairavamurthy, A., Andreae, M. O., and Iverson, R. L. (1985). Biosynthesis of Dimethylsulfide and Dimethylpropiothetin by *Hymenomonas Carterae* in Relation to Sulfur Source and Salinity Variations. *Limnol. Oceanogr.* 30, 59–70. doi: 10.4319/lo.1985.30.1.0059

Walker, B. J., Abeel, T., Shea, T., Priest, M., Abouelliel, A., Sakthikumar, S., et al. (2014). Pilon: An Integrated Tool for Comprehensive Microbial Variant Detection and Genome Assembly Improvement. *PloS One* 9, e112963. doi: 10.1371/journal.pone.0112963

Wang, P., Cao, H.-Y., Chen, X.-L., Li, C.-Y., Li, P.-Y., Zhang, X.-Y., et al. (2017). Mechanistic Insight Into Acrylate Metabolism and Detoxification in Marine Dimethylsulfoniopropionate-Catabolizing Bacteria. *Mol. Microbiol.* 105, 674–688. doi: 10.1111/mmi.13727

Williams, B. T., Cowles, K., Bermejo Martínez, A., Curson, A. R. J., Zheng, Y., Liu, J., et al. (2019). Bacteria are Important Dimethylsulfoniopropionate Producers in Coastal Sediments. *Nat. Microbiol.* 4, 1815–1825. doi: 10.1038/s41564-019-0527-1

Yeo, W.-S., Lee, J.-H., Lee, K.-C., and Roe, J.-H. (2006). IscR Acts as an Activator in Response to Oxidative Stress for the Suf Operon Encoding Fe-S Assembly Proteins. *Mol. Microbiol.* 61, 206–218. doi: 10.1111/j.1365-2958.2006.05220.x

Yu, G., Smith, D. K., Zhu, H., Guan, Y., and Lam, T. T.-Y. (2017). Ggtree: An R Package for Visualization and Annotation of Phylogenetic Trees With Their Covariates and Other Associated Data. *Methods Ecol. Evol.* 8, 28–36. doi: 10.1111/2041-210X.12628

Zhang, X.-H., Liu, J., Liu, J., Yang, G., Xue, C.-X., Curson, A. R. J., et al. (2019). Biogenic Production of DMSP and its Degradation to DMS—their Roles in the Global Sulfur Cycle. *Sci. China Life Sci.* 62, 1296–1319. doi: 10.1007/s11427-018-9524-y

Zhang, Y., Yang, Q., Zhang, Y., Ahmad, M., Ling, J., Tang, X., et al. (2021). Shifts in Abundance and Network Complexity of Coral Bacteria in Response to Elevated Ammonium Stress. *Sci. Total. Environ.* 768, 144631. doi: 10.1016/j.scitotenv.2020.144631

Zheng, Y., Wang, J., Zhou, S., Zhang, Y., Liu, J., Xue, C.-X., et al. (2020). Bacteria are Important Dimethylsulfoniopropionate Producers in Marine Aphotic and High-Pressure Environments. *Nat. Commun.* 11, 4658. doi: 10.1038/s41467-020-18434-4

Conflict of Interest: The authors declare that the research was conducted in the absence of any commercial or financial relationships that could be construed as a potential conflict of interest.

Publisher's Note: All claims expressed in this article are solely those of the authors and do not necessarily represent those of their affiliated organizations, or those of the publisher, the editors and the reviewers. Any product that may be evaluated in this article, or claim that may be made by its manufacturer, is not guaranteed or endorsed by the publisher.

frontiers | Frontiers in Marine Science

REVIEW
published: 24 May 2022
doi: 10.3389/fmars.2022.869739

Quaternary Ammonium Compounds as Candidate Photoprotective Compounds in Reef-Building Corals

*Richard W. Hill**

Department of Integrative Biology, Michigan State University, East Lansing, MI, United States

Quaternary ammonium compounds (QACs) – e.g., betaines – have a chemical structure related to that of the tertiary sulfonium compounds (TSCs) – e.g., dimethylsulfoniopropionate – explaining why these two classes of coral metabolites are often studied and interpreted together. Functionally, both QACs and TSCs play important roles in the photobiology of reef-building corals under stress, according to recent hypotheses. The TSC dimethylsulfoniopropionate (DMSP) is the principal precursor of the gas dimethylsulfide (DMS) which is hypothesized to affect, through influences on cloud formation, the photon and thermal fluxes to which corals are exposed. Simultaneously, QACs – e.g., glycine betaine – in coral tissues are hypothesized to protect the zooxanthellae photosystems against photon and thermal stresses by exerting stabilizing effects on photosystem proteins and by ameliorating reactive-oxygen-species perturbations. This review, which synthesizes the most current available evidence on the relevant actions of QACs, emphasizes the need for enhanced direct study of QAC physiology in corals to ascertain the degree to which coral QACs exert photoprotective effects paralleling their well-established protective effects in plants.

Keywords: abiotic stress, betaines, bleaching, glycine betaine, osmolytes, photon stress, photosynthesis, Tridacnidae

OPEN ACCESS

Edited by:
Graham Barry Jones,
Southern Cross University, Australia

Reviewed by:
Yandu Lu,
Hainan University, China
David R. Nelson,
New York University, United States

***Correspondence:**
Richard W. Hill
hillr@msu.edu

Specialty section:
This article was submitted to Coral Reef Research, a section of the journal Frontiers in Marine Science

Received: *04 February 2022*
Accepted: *30 March 2022*
Published: *24 May 2022*

Citation:
Hill RW (2022) Quaternary Ammonium Compounds as Candidate Photoprotective Compounds in Reef-Building Corals. Front. Mar. Sci. 9:869739. doi: 10.3389/fmars.2022.869739

INTRODUCTION

In a watershed paper, Rhodes and Hanson (1993) emphasized the logic and value of considering the tertiary sulfonium compounds (TSCs), notably dimethylsulfoniopropionate (DMSP), and the quaternary ammonium compounds (QACs) together because of their similarities in chemical structure and properties. Twenty-five years later, with far more data available, Somero et al. (2017) again affirmed the logic of emphasizing the shared properties of these two sets of small molecules, which they termed the methylsulfonium and methylammonium compounds – terms highlighting the key positions the compounds often occupy in methyl trafficking in cells. In this Special Issue on dimethylsulfide (DMS) in coral reefs, this paper on QACs is included not only because of the shared chemical properties of TSCs and QACs (**Figure 1**), but also because of important ways in which the two sets of compounds may interact in the ecological physiology of reef-building corals.

Glycine betaine is probably the most thoroughly studied QAC. Mäkelä et al. (2019) document that published research on glycine betaine has more than doubled in each successive decade over the past five decades, with more than 25,000 papers published in 2011-2020. Simultaneously, fewer than

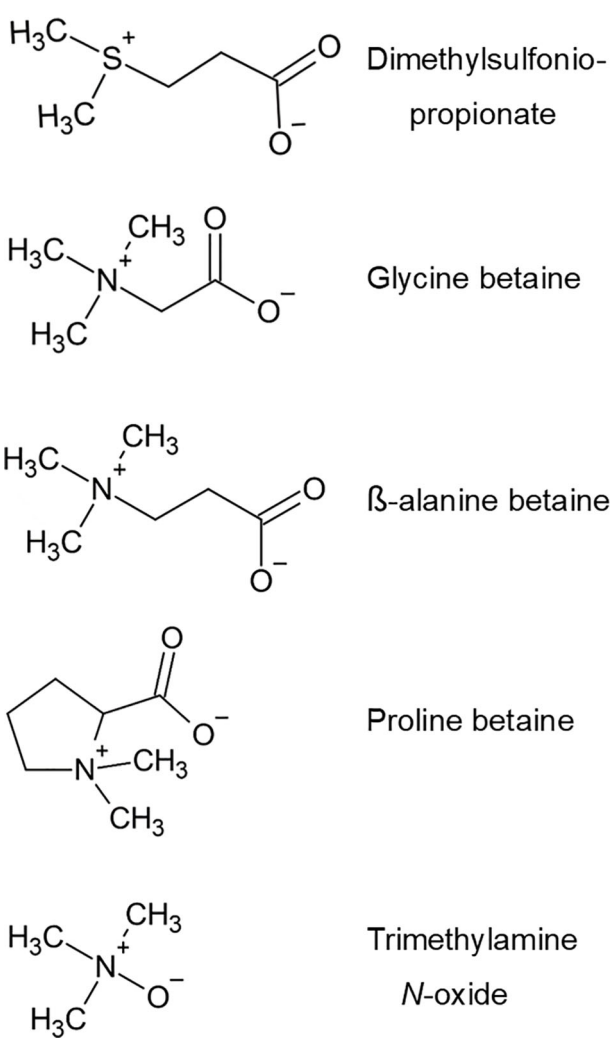

FIGURE 1 | Chemical structures of five compounds that are discussed in this manuscript: dimethylsulfoniopropionate (DMSP), glycine betaine (often called simply "betaine" in the older literature); ß-alanine betaine (trimethylammonium propionate); proline betaine (stachydrine), and trimethylamine *N*-oxide (TMAO).

20 papers have been published on glycine betaine or other QACs in reef-building corals over the entire five decades. In this paper, I argue that the near-total neglect of glycine betaine and other QACs in research on corals may represent a serious omission in the effort to conserve coral-reef ecosystems.

The betaines are one of the principal subsets of QACs. Structurally speaking, betaines are amino (or imino) acids fully methylated at the N position; there are in principle as many betaines as there are amino acids. Until a few decades ago, the most common betaine, glycine betaine, was typically called simply "betaine". However, in this paper – and usually in the current scientific literature – it is called "glycine betaine" to specify the molecule and distinguish it from other betaines (although it is still called "betaine" in nontechnical contexts, such as ingredient lists for consumer products). In addition to glycine betaine, a number of other betaines, such as proline betaine and ß-alanine betaine, are commonly detected in vascular plants and algae when looked for (Rhodes and Hanson, 1993; McNeil et al., 1999). Trimethylamine *N*-oxide (TMAO) is a chemically related compound, long known in animals but only recently identified in plants (Catalá et al., 2021). All these compounds are zwitterionic, with a permanent positive charge at the N position: a structure that, as emphasized by Rhodes and Hanson (1993), is analogous to that of the TSC dimethylsulfoniopropionate, which is fully methylated at the S position and bears a permanent positive charge at that position (**Figure 1**).

A principal reason for glycine betaine to be of interest to coral biologists is its potential importance for photosynthesis. Already in 1995, Papageorgiou and Murata (1995) stressed the "unusually strong stabilizing effects of glycine betaine" on photosystem II in vascular plants. Other papers – such as those by Sakamoto and Murata (2002) and Allakhverdiev et al. (2003) – soon reinforced that message, helping to thrust glycine betaine into the center of research on photosynthesis under abiotic stress in vascular plants.

For discussing betaines and other QACs today, it is instructive to recognize the ways in which knowledge of the roles played by these compounds in photosynthetic organisms has expanded over the last several decades. In the 1970s and 1980s, glycine betaine was recognized principally as a compatible solute: an osmolyte that tended not to disturb cellular function (Yancey et al., 1982). As years passed, investigators identified additional roles, including glycine betaine's stabilization of proteins in photosynthesis already alluded to (and addressed in detail later) and glycine betaine's favorable effects (Chen and Murata, 2011) on reactive oxygen species (ROS) (Lesser, 2006). In the last few years, investigators have increasingly emphasized evidence that glycine betaine in addition can play signaling roles, as by directly or indirectly controlling gene expression (Figueroa-Soto and Valenzuela-Soto, 2018; Dutta et al., 2019; Hossain et al., 2019; Mäkelä et al., 2019; Valenzuela-Soto and Figueroa-Soto, 2019), and glycine betaine can modulate heat-shock protein expression (Li et al., 2011; Zhang et al., 2020). Today, therefore, when we consider glycine betaine and other QACs, we recognize that they may have broad ranges of action and be multifunctional (Derakhshani et al., 2017).

BETAINES IN REEF-BUILDING CORALS

Only about a decade has passed since publication of the first definitive information on betaines in the tissues of reef-building corals. The very first information seems to have been a report in 1976 by Moore and Huxley (1976) that crown-of-thorns seastars (*Acanthaster planci*) exhibit aversive behavior when exposed to a compound, tentatively identified as glycine betaine, in the tissues of certain reef-building corals. In 2010, Hill et al. (2010) and Yancey et al. (2010) used rigorous chemical methods [liquid chromatography/mass spectrometry (LC/MS) with internal standards in the case of Hill et al.] to quantify multiple betaines in the tissues of wild-collected, reef-building corals in the Caribbean (Hill et al., 2010) and at Hawaii (Yancey et al., 2010). Later, Hill et al. (2017), working mostly with wild-collected specimens, quantified multiple betaines in coral

species in the western Pacific and also in five species of tridacnid clams (genera *Tridacna* and *Hippopus*), animals that inhabit Indo-Pacific coral-reef ecosystems and, like corals, live in symbioses with dinoflagellate symbionts. Swan et al. (2017a) also quantified multiple betaines in a set of wild-collected Great Barrier Reef branching corals.

The evidence shows that betaines, despite their relative obscurity in corals, are abundant metabolites in the tissues of reef-building corals in the wild. Among the 10 species of Caribbean corals (6 genera) and the 6 species of western Pacific corals (5 genera), collected from the wild, that Hill et al. (2010; 2017) analyzed using LC/MS with internal standards, total betaine concentration was estimated to be 12-204 mmole per liter of living tissue (mean: 60 m*M*), except in one species, *Acropora formosa*, in which the total concentration was much lower (1.5 m*M*). An important point to stress is that these concentrations were calculated assuming a homogeneous distribution of the betaines in tissue. The true, operative concentrations of betaines in living tissue are likely substantially higher because betaines are probably, in fact, more concentrated in some subcellular regions than others. This same consideration applies also to other values reported.

Yancey et al. (2010), using a somewhat less sensitive analytical method than Hill et al. (2010; 2017), measured two betaines, glycine betaine and proline betaine, in 6 wild-collected species (4 genera) of Hawaiian reef-building corals and found total concentrations of about 9-69 m*M* (mean: 37 m*M*). Swan et al. (2017a), using a high-sensitivity method, focused on a restricted part of the anatomy, the branch tips, in 6 species of *Acropora* and one of *Stylophora*. Most of their estimates of total betaine concentration were 12-52 m*M*, although in *A. valida*, their estimate was lower, 6 m*M*.

Considering all studied coral species as a set, the two most abundant betaines in reef-building corals are glycine betaine and proline betaine. In the three studies that attempted to measure all betaines present in wild-collected corals (Hill et al., 2010; Hill et al., 2017; Swan et al., 2017a), glycine betaine and proline betaine together accounted for ≥90% of all betaines (on a molar basis) in 14 species, 58-88% in 8 species, and <50% in 1 species. Multiple additional betaines (e.g., alanine betaine, ß-alanine betaine, and hydroxyproline betaine) are also typically present in reef-building corals, some at just low concentrations. Different coral taxa sometimes differ substantially in the particular suite of betaines they express.

Ngugi et al. (2020) recently completed a genomic survey of pathways for glycine betaine synthesis, transport, and degradation in a wide sample of invertebrates, including reef-building corals. According to the genomic evidence, corals have pathways for the *de novo* synthesis of glycine betaine and for transport of glycine betaine into their tissues from the seawater environment. The transporters in particular have a restricted phylogenetic distribution within the invertebrates, suggesting a specialized role in corals and/or coral relatives. Strikingly, Ngugi et al. (2020) calculated that corals worldwide store sufficient glycine betaine to account for 16% of their tissue nitrogen.

POTENTIAL PROTECTIVE EFFECTS OF BETAINES IN REEF-BUILDING CORALS: THE MESSAGE FROM PHYSIOLOGICAL DATA ON VASCULAR PLANTS AND ECOLOGICAL DATA ON CORALS

In corals, the biochemical and physiological actions of betaines have yet to be directly studied. However, the situation in vascular plants is quite opposite: By virtue of the massive effort to understand photosynthesis under abiotic stress in crop plants, a great deal is known about protective actions of glycine betaine. By applying the knowledge from vascular plants to reef-building corals, it seems highly reasonable to hypothesize that glycine betaine and other betaines are important photoprotective, protein- and membrane-stabilizing, compounds in corals. Should this hypothesis prove correct, manipulations of betaines (or other QACs) might be useful interventions for protecting reefs against threats of photoinhibition and bleaching (Gorbunov et al., 2001; Lesser, 2011; Frieler et al., 2013; Van Oppen and Lough, 2018), or for aiding recovery. Clearly, the tissue betaine concentrations measured in corals (reviewed in the previous section) are of sufficient magnitude for stabilization of protein and membrane functions, judging by studies in plants (e.g., Prasad and Saradhi, 2004; Shirasawa et al., 2006; Yang et al., 2007; Chen and Murata, 2011).

Before going further to explore these ideas, a few comments are appropriate regarding the fact that, at this time, although most research on the functions of betaines in photosynthetic organisms has been carried on one chemical species (glycine betaine), in the literature betaines are often discussed as a group: as a set of chemical species that, to a first approximation, have similar actions in protecting proteins and membranes. At the present time, there are two reasons for considering betaines as a group with common properties. First, several betaines in addition to glycine betaine, including ß-alanine betaine and proline betaine (**Figure 1**), have been demonstrated in at least limited ways to act as compatible solutes (Rhodes and Hanson, 1993; Bashir et al., 2014). Second, existing theories of betaine action emphasize molecular properties that are shared by betaines as a group rather than being highly specific to certain chemical species. Specifically, the protein- and membrane-stabilizing effects of betaines are attributed for the most part to influences that betaines noncovalently exert – by virtue of their fundamental chemical nature – on the structure of water in the immediate vicinity of protein molecules, enhancing thereby the extent to which native protein states are more favorable thermodynamically than nonnative states (McNeil et al., 1999; Bennion and Daggett, 2004; Street et al., 2006; Auton et al., 2011; Guinn et al., 2011; Bruździak et al., 2013; Roychoudhury et al., 2013). At the present state of knowledge, it seems parsimonious and reasonable to hypothesize that (1) all the principal betaines in corals exert, to a significant extent, similar protective actions in corals and (2) as a corollary, the total betaine concentration in tissues is likely a useful index of betaine functional significance. Of course, looking forward, a full functional understanding of

betaines in corals will ultimately require direct empirical study of each specific chemical species.

For discussing betaines as potential protective compounds for photosynthesis in reef-building corals, two interacting lines of investigation on photosynthesis in vascular plants deserve particular attention: first, studies of photosystem II (PSII) and, second, studies of reactive oxygen species (ROS). Regarding PSII, abundant evidence exists that when corals are exposed to heat and photon stress sufficient to cause bleaching or photoinhibition, damaging effects are directly or indirectly exerted on PSII and/or the pathways of electron flow downstream from PSII in the algal symbionts of the corals (Warner et al., 1999; Fitt et al., 2001; Gorbunov et al., 2001; Jones and Hoegh-Guldberg, 2001; Hill et al., 2004; Lesser and Farrell, 2004; Weis, 2008; Warner and Suggett, 2016). Possibly the D1 protein (PsbA) in the PSII reaction center in coral symbionts – sometimes termed the Achilles heel of PSII (Weis, 2008) – is particularly affected (Warner et al., 1999; Hill et al., 2011; Warner and Suggett, 2016). As already emphasized, potential protective actions of glycine betaine or other QACs have not yet been directly studied in corals. However, in vascular plants and free-living algae that have been studied, glycine betaine has been demonstrated by many studies to protect PSII against a number of abiotic stresses, including photon stress and heat stress (Papageorgiou and Murata, 1995; Yang et al., 1996; Schiller and Dau, 2000; Sakamoto and Murata, 2002; Allakhverdiev et al., 2003; Klimov et al., 2003; Prasad and Saradhi, 2004; Hema et al., 2007; Yang et al., 2007; Allakhverdiev et al., 2008; Chen and Murata, 2011; Li et al., 2014; Wang et al., 2014; Kurepin et al., 2015; Huang et al., 2020; Li et al., 2021).

Regarding ROS, when corals are exposed to heat and photon stress sufficient to cause bleaching or photoinhibition, abundant evidence points to accumulation in the coral tissues of ROS, which are generally judged to be principal agents of photodamage (Lesser, 2006; Weis, 2008; Lesser, 2011; Oakley and Davy, 2018). Again, potential protective actions of glycine betaine or other QACs have not yet been directly studied in corals. Glycine betaine, however, has repeatedly been demonstrated to increase photosystem defenses against ROS in vascular plants (Prasad and Saradhi, 2004; Yang et al., 2007; Chen and Murata, 2011; Fan et al., 2012; Li et al., 2014; Gómez et al., 2019; Zhang et al., 2020; Li et al., 2021).

The research on glycine betaine in vascular plants has often had a very practical goal: to enhance the productivity of crop plants by capitalizing on glycine betaine's beneficial properties. As part of this effort, glycine betaine has long occupied a focal position in the overall effort to employ genetic modification, or other deliberate manipulation, to offset the negative impacts on crop plants of a variety of abiotic stresses, including photon stress and heat stress (Alia et al., 1998; McNeil et al., 1999; Sakamoto and Murata, 2002; Prasad and Saradhi, 2004; Yang et al., 2007; Chen and Murata, 2011; Giri, 2011; Li et al., 2011; Li et al., 2014; Kurepin et al., 2015; Castiglioni et al., 2018; Annunziata et al., 2019; Dutta et al., 2019; Hasanuzzaman et al., 2019; Kido et al., 2019; Zhang et al., 2020; Niazian et al., 2021). Recent review papers provide overviews on the biology and manipulation of glycine betaine from this perspective (Kurepin et al., 2015; Annunziata et al., 2019; Hasanuzzaman et al., 2019; Huang et al., 2020; Zulfiqar et al., 2020).

Ecological studies on coral reefs bolster the hypothesis that glycine betaine and other betaines are important photoprotective compounds in reef-building corals. The ecological studies represent a second major line of investigation pointing in this direction, in addition to the extrapolations from physiological studies of vascular plants already discussed.

Hill et al. (2010) hypothesized that within a population of a species of reef-building corals subject to potential photon stress, if tissue betaines are in fact protective agents for algal symbiont function [by providing either direct protection to the algal cells or indirect protection (e.g., stabilization of the symbiosome membrane)], betaine concentrations would be expected to vary among individual coral colonies in direct relation to solar irradiance experienced. For testing this hypothesis, Hill et al. (2010) selected *Madracis* species in Curaçao reefs because the light relations of those species had previously been studied in exceptional detail (Vermeij and Bak, 2002). *M. mirabilis* occurs over a wide range of depths and almost always occupies fully exposed (unshaded) locations regardless of depth (Vermeij and Bak, 2002). With this information, Hill et al. (2010) hypothesized *a priori* that betaine concentrations in colonies of *M. mirabilis* vary inversely with depth of residence. In fact, when measured, the concentrations of glycine betaine and proline betaine (**Figure 2**) – and also alanine betaine and hydroxyproline betaine – were found to vary significantly with depth, being 37-94% higher in coral colonies at 5 m depth than ones at 20 m (Hill et al., 2010). Glycine betaine and proline betaine are the most abundant betaines in *M. mirabilis*. Another *Madracis* species, *M. pharensis*, occupies both fully exposed and highly shaded locations at most depths where it occurs (Vermeij and Bak, 2002). Hill et al. (2010) hypothesized *a priori* that, at any particular depth, betaine concentrations are higher in exposed colonies than in shaded ones. In fact, when *M. pharensis* colonies at a single depth (10 m) were studied (Hill et al., 2010), glycine betaine, proline betaine, and alanine betaine were found to be significantly higher in concentration (by 30-44%) in exposed colonies than in shaded ones. Glycine betaine and proline betaine are by far the most abundant betaines in *M. pharensis*.

Reinforcing the ecological evidence for a protective role for glycine betaine in *Madracis*, Swan et al. (2017a) studied osmolyte concentrations in the branch tips of three *Acropora* species (*A. aspera*, *A. millepora*, and *A. valida*) during summer (February) and winter (August) in the Great Barrier Reef. They observed a 3.7- to 7.8-fold increase in average glycine betaine concentration in summer, compared with winter, in all three species: the pattern predicted if glycine betaine is employed in photoprotection. Although proline betaine was also abundant in these species, it exhibited just relatively small, inconsistent differences in concentration between the summer and winter samplings.

In summary, existing physiological and ecological evidence justifies a hypothesis that betaines play interacting

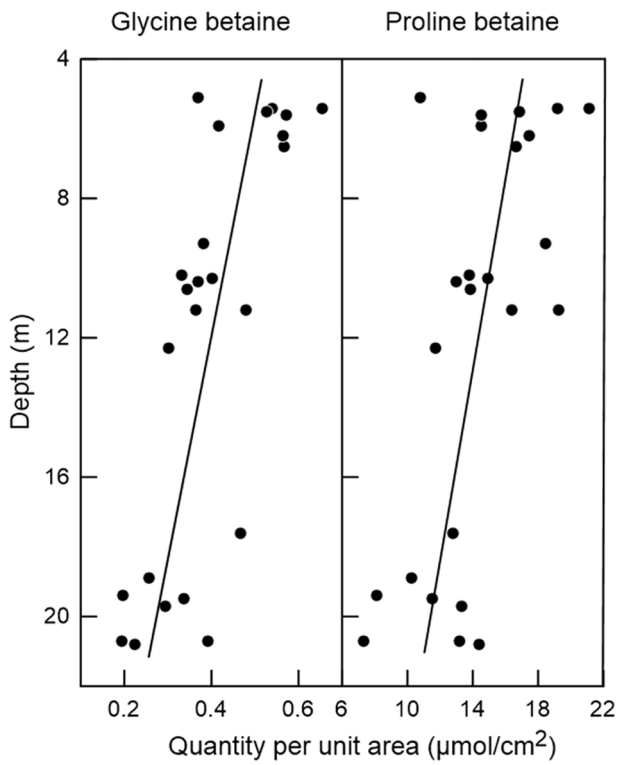

FIGURE 2 | Abundance of glycine betaine and proline betaine in the tissues of *Madracis mirabilis* as a function of depth of residence. Each symbol is for a single, separate coral colony. All colonies grew in fully exposed, unshaded locations. Lines were fitted by least-squares regression. Based on ANOVA, differences among depths are statistically significant ($p < 0.05$). Betaine abundance is expressed as a ratio of the coral surface area sampled. (Data from Hill et al., 2010).

photoprotective and ROS-protective roles in reef-building corals. In my view, recognizing the dire threats now faced by corals (Frieler et al., 2013), it would be logical to place a high priority on carrying out direct tests of this hypothesis in the near future (Hill et al., 2010; Hill et al., 2017). Lesser (2011) and others have emphasized that throughout the history of studies on photosynthesis in reef-building corals, investigators have made great progress by using prior studies on vascular plants and free-living algae as guides. Today, based on a large literature (Mäkelä et al., 2019), glycine betaine is well known in the study of vascular plants as a metabolite that exerts multiple effects – notably protein-stabilizing, membrane-stabilizing, and ROS-ameliorating effects – that help defend plants stressed by high irradiance, unusual temperatures, and other agents. Because this knowledge has been sought principally with the practical objective of defending crop plants against abiotic stress, many published attempts have been made – often with successful results – to manipulate glycine betaine to advantage, either by exogenous application or by genetic manipulation of endogenous synthesis (Alia et al., 1998; McNeil et al., 1999; Sakamoto and Murata, 2002; Prasad and Saradhi, 2004; Yang et al., 2007; Chen and Murata, 2011; Giri, 2011; Li et al., 2011; Li et al., 2014; Kurepin et al., 2015; Castiglioni et al., 2018; Annunziata et al., 2019; Dutta et al., 2019; Hasanuzzaman et al., 2019; Hossain et al., 2019; Huang et al., 2020; Zhang et al., 2020; Niazian et al., 2021). Perhaps this background of experience will prove useful for the protection of coral reefs confronted with photosystem and ROS stress (Van Oppen and Lough, 2018).

Just recently, trimethylamine *N*-oxide (TMAO; **Figure 1**) has been discovered to be widespread in vascular plants, and evidence from *Arabidopsis* and tomato indicates that TMAO, like betaines, plays roles in protein stabilization and tolerance of abiotic stress (Catalá et al., 2021). If TMAO proves to be present in reef-building corals, it also should be investigated along with betaines for actions that have potential to aid coral survival.

PHYSIOLOGICAL AND ECOLOGICAL INTERACTIONS BETWEEN THE TSC SYSTEM AND THE QAC SYSTEM

If we assume for the moment that glycine betaine and other QACs exert protective effects in reef-building corals – paralleling their demonstrated protective effects in vascular plants – important potential interactions between QACs and TSCs in corals become apparent. These interactions could be manifest at an ecosystem level and/or within the tissues of particular coral polyps.

At an ecosystem level, long-term monitoring has revealed that the atmospheric concentration of DMS varies significantly in coral-reef ecosystems on hourly, daily, and seasonal time scales; and as the atmospheric DMS concentration varies, the atmospheric concentration of aerosols and the solar irradiance at sea level sometimes vary in correlated ways (Jackson et al., 2020a). At times when the atmospheric DMS concentration falls and the irradiance at sea level accordingly increases, corals could offset the increased risk of photosystem stress by upregulating glycine betaine or other QACs in their tissues. To assess the likelihood of this type of response, more research will be required on the time scales on which corals are able to modulate betaine expression.

At the level of an individual coral polyp, tissue QACs and TSCs seem likely interact in ameliorating ROS damage, including ROS-mediated damage to photosystem components such as PSII. As earlier noted, tissue glycine betaine has repeatedly been demonstrated to enhance defenses against ROS in vascular plants and free-living algae (Prasad and Saradhi, 2004; Hema et al., 2007; Yang et al., 2007; Chen and Murata, 2011; Fan et al., 2012; Gómez et al., 2019; Li et al., 2021). Similarly, DMSP and DMS are recognized as ROS scavengers in corals (Sunda et al., 2002; Lesser, 2006; Deschaseaux et al., 2014; Jones and King, 2015; Oakley and Davy, 2018; Jackson et al., 2020b). Thus both tissue QACs and TSCs likely function in the amelioration of ROS damage in corals, and they may be coordinated in various ways. To illustrate, corals have been observed to outgas DMS during air exposure or other stresses of low tide, when exposed or nearly exposed corals are subject to relatively high solar irradiance (Swan et al., 2017b). The corals might upregulate tissue betaines to compensate for any reduction in tissue DMS.

These briefly described hypothetical scenarios help to articulate the potential ways in which the QAC and TSC systems interact in the lives of reef corals and other photosynthetic reef inhabitants such as the tridacnid clams (Hill et al., 2017).

CONCLUSION

In the study of photosynthesis, of all the focal topics receiving frequent attention in vascular plants, the actions of betaines and other QACs are among the most neglected in reef-building corals. This neglect in corals is regrettable because corals are existentially threatened by abiotic stresses, and betaines attract interest in the study of crop plants precisely because of evidence that they can reduce the impact of abiotic stresses.

Recent research demonstrates that betaines (particularly glycine betaine and proline betaine) are abundant metabolites in the tissues of reef-building corals. Their functions in corals have not yet been directly studied. However, two lines of investigation – physiological and ecological – point to a hypothesis that betaines are photoprotective in corals. The physiological evidence focuses on the fact that when corals are subjected to heat and photon stresses sufficient to cause bleaching or photoinhibition, they experience damage to photosystems (e.g., PSII) and they accumulate photodamaging ROS: exigencies known to be ameliorated by glycine betaine in vascular plants. The ecological evidence is that when free-living corals have been examined to detect correlations between betaine abundance and solar irradiance, glycine betaine and (in some cases) other betaines have been observed to be significantly more concentrated in the tissues of coral colonies exposed to high irradiance than in conspecific colonies exposed to lower irradiance.

Betaines are not simple to study, in part because of the complexity of technologies available for quantification (e.g., LC/MS) and the challenges of calibration (Hill et al., 2010; Swan et al., 2017a). Nonetheless, a large body of evidence exists on their manipulation (e.g., exogenous application and genetic manipulation) in crop plants to defend against abiotic stresses, and with this background of experience, it is reasonable to hypothesize that they could be manipulated to aid the survival of corals exposed to heat and photon stresses.

AUTHOR CONTRIBUTIONS

RH composed this paper in its entirety and prepared the figures.

FUNDING

No external funding was sought or provided for the preparation of this publication.

ACKNOWLEDGMENTS

This paper is dedicated to the memory of Ron Kiene in recognition of his personal encouragement and his prescient contributions to the science of QACs and TSCs. John Dacey, Douglas Gage, and Wayne Hicks provided insights without which I would never have become interested in the betaines. Special thanks to the following colleagues who have played important roles in my direct studies of coral betaines: Eric Armstrong, Rolf Bak, Ahser Edward, Aaron Florn, Pedro Frade, Dan Jones, Chao Li, and Mark Vermeij. Mark Hahn and his lab at Woods Hole Oceanographic Institution continue to provide much-appreciated intellectual support. Thanks to ACD/Labs for their generosity in providing the freeware version of ChemSketch.

REFERENCES

Alia, Hayashi, H., Sakamoto, A., and Murata, N. (1998). Enhancement of the tolerance of *Arabidopsis* to high temperatures by genetic engineering of the synthesis of glycinebetaine. *Plant J.* 16, 155–161. doi: 10.1046/j.1365-313x.1998.00284.x

Allakhverdiev, S. I., Hayashi, H., Nishiyama, Y., Ivanov, A. G., Aliev, J. A., Klimov, V. V., et al. (2003). Glycinebetaine protects the D1/D2/Cyt*b559* complex of photosystem II against photo-induced and heat-induced inactivation. *J. Plant Physiol.* 160, 41–49. doi: 10.1078/0176-1617-00845

Allakhverdiev, S. I., Kreslavski, V. D., Klimov, V. V., Los, D. A., Carpentier, R., and Mohanty, P. (2008). Heat stress: an overview of molecular responses in photosynthesis. *Photosynth. Res.* 98, 541–550. doi: 10.1007/s11120-008-9331-0

Annunziata, M. G., Ciarmiello, L. F., Woodrow, P., Dell'Aversana, E., and Carillo, P. (2019). Spatial and temporal profile of glycine betaine accumulation in plants under abiotic stress. *Front. Plant Sci.* 10, 230. doi: 10.3389/fpls.2019.00230

Auton, M., Rösgen, J., Sinev, M., Holthauzen, L. M. F., and Bolen, D. W. (2011). Osmolyte effects on protein stability and solubility: a balancing act between backbone and side-chains. *Biophys. Chem.* 159, 90–99. doi: 10.1016/j.bpc.2011.05.012

Bashir, A., Hoffmann, T., Kempf, B., Xie, X., Smits, S. H. J., and Bremer, E. (2014). Plant-derived compatible solutes proline betaine and betonicine confer enhanced osmotic and temperature stress tolerance to *Bacillus subtilis*. *Microbiology* 160, 2283–2294. doi: 10.1099/mic.0.079665-0

Bennion, B. J., and Daggett, V. (2004). Counteraction of urea-induced protein denaturation by trimethylamine *N*-oxide: a chemical chaperone at atomic resolution. *Proc. Natl. Acad. Sci. U. S. A.* 101, 6433–6438. doi: 10.1073/pnas.0308633101

Bruździak, P., Panuszko, A., and Stangret, J. (2013). Influence of osmolytes on protein and water structure: a step to understanding the mechanism of protein stabilization. *J. Phys. Chem. B* 117, 11502–11508. doi: 10.1021/jp404780c

Castiglioni, P., Bell, E., Lund, A., Rosenberg, A. F., Galligan, M., Hinchey, B. S., et al. (2018). Identification of *GB1*, a gene whose constitutive overexpression increases glycinebetaine content in maize and soybean. *Plant Direct* 2018, 1–7. doi: 10.1002/pld3.40

Catalá, R., López-Cobollo, R., Berbis, M. A., Jiménez-Barbero, J., and Salinas, J. (2021). Trimethylamine *N*-oxide is a new plant molecule that promotes abiotic stress tolerance. *Sci. Adv.* 7, eabd9296. doi: 10.1126/sciadv.abd9296

Chen, T. H. H., and Murata, N. (2011). Glycinebetaine protects plants against abiotic stress: mechanisms and biotechnological applications. *Plant Cell Environ.* 34, 1–20. doi: 10.1111/j.1365-3040.2010.02232.x

Derakhshani, Z., Malherbe, F., and Bhave, M. (2017). Multifunctional biomolecules with roles in abiotic stress tolerance as well as nutraceutical potential. *J. Plant Biochem. Biotechnol.* 26, 121–131. doi: 10.1007/s13562-016-0372-8

Deschaseaux, E. S. M., Jones, G. B., Deseo, M. A., Shepherd, K. M., Kiene, R. P., Swan, H. B., et al. (2014). Effects of environmental factors on dimethylated sulfur compounds and their potential role in the antioxidant system of the coral holobiont. *Limnol. Oceanogr.* 59, 758–768. doi: 10.4319/lo.2014.59.3.0758

Dutta, T., Neelapu, N. R. R., Wani, S. H., and Surekha, C. (2019). "Role and regulation of osmolytes as signaling molecules to abiotic stress tolerance," in *Plant Signaling Molecules. Role and Regulation Under Stressful Environments*. Eds. M. I. R. Khan, P. S. Reddy, A. Ferrante and N. A. Khan (Duxford: Elsevier), p. 459–477.

Fan, W., Zhang, M., Zhang, H., and Zhang, P. (2012). Improved tolerance to various abiotic stresses in transgenic sweet potato (*Ipomoea batatas*) expressing spinach betaine aldehyde dehydrogenase. *PloS One* 7, e37344. doi: 10.1371/journal.pone.0037344

Figueroa-Soto, C. G., and Valenzuela-Soto, E. M. (2018). Glycine betaine rather than acting only as an osmolyte also plays a role as regulator in cellular metabolism. *Biochimie* 147, 89–97. doi: 10.1016/j.biochi.2018.01.002

Fitt, W. K., Brown, B. E., Warner, M. E., and Dunne, R. P. (2001). Coral bleaching: interpretation of thermal tolerance limits and thermal thresholds in tropical corals. *Coral Reefs* 20, 51–65. doi: 10.1007/s003380100146

Frieler, K., Meinschausen, M., Golly, A., Mengel, M., Lebek, K., Donner, S. D., et al. (2013). Limiting global warming to 2°C is unlikely to save most coral reefs. *Nat. Climate Change* 3, 165–170. doi: 10.1038/nclimate1674

Giri, J. (2011). Glycinebetaine and abiotic stress tolerance in plants. *Plant Signal. Behav.* 6, 1746–1751. doi: 10.4161/psb.6.11.17801

Gómez, R., Vicino, P., Carrillo, N., and Lodeyro, A. F. (2019). Manipulation of oxidative stress responses as a strategy to generate stress-tolerant crops. From damage to signaling to tolerance. *Crit. Rev. Biotechnol.* 39, 693–708. doi: 10.1080/07388551.2019.1597829

Gorbunov, M. Y., Kolber, Z. S., Lesser, M. P., and Falkowski, P. G. (2001). Photosynthesis and photoprotection in symbiotic corals. *Limnol. Oceanogr.* 46, 75–85. doi: 10.4319/lo.2001.46.1.0075

Guinn, E. J., Pegram, L. M., Capp, M. W., Pollock, M. N., and Record, M. T., Jr. (2011). Quantifying why urea is a protein denaturant, whereas glycine betaine is a protein stabilizer. *Proc. Nat. Acad. Sci. U. S. A.* 108, 16932–16937. doi: 10.1073/pnas.1109372108

Hasanuzzaman, M., Banerjee, A., Bhuyan, M. H. M. B., Roychoudhury, A., Al Mahmud, J., and Fujita, M. (2019). Targeting glycinebetaine for abiotioc stress tolerance in crop plants: physiological mechanism, molecular interaction and signaling. *Phyton. Intl. J. Exp. Bot.* 88, 185–221. doi: 10.32604/phyton.2019.07559

Hema, R., Senthil-Kumar, M., Shivakumar, S., Reddy, P. C., and Udayakumar, M. (2007). *Chlamydomonas reinhardtii*, a model system for functional validation of abiotic stress responsive genes. *Planta* 226, 655–670. doi: 10.1007/s00425-007-0514-2

Hill, R. W., Armstrong, E. J., Flornm, A. M., Li, C., Walquist, R. W., and Edward, A. (2017). Abundant betaines in giant clams (Tridacnidae) and western Pacific reef corals, including study of coral betaine acclimatization. *Mar. Ecol. Progr. Ser.* 576, 27–41. doi: 10.3354/meps12181

Hill, R., Brown, C. M., DeZeeuw, K., Campbell, D. A., and Ralph, P. J. (2011). Increased rate of D1 repair in coral symbionts during bleaching is insufficient to counter accelerated photo-inactivation. *Limnol. Oceanogr.* 56, 139–146. doi: 10.4319/lo.2011.56.1.0139

Hill, R., Larkum, A. W. D., Frankart, C., Kühl, M., and Ralph, P. J. (2004). Loss of functional photosystem II reaction centres in zooxanthellae of corals exposed to bleaching conditions: Using fluorescence rise kinetics. *Photosynth. Res.* 82, 59–72. doi: 10.1023/B:PRES.0000040444.41179.09

Hill, R. W., Li, C., Jones, A. D., Gunn, J. P., and Frade, P. R. (2010). Abundant betaines in reef-building corals and ecological indicators of a photoprotective role. *Coral Reefs* 29, 869–880. doi: 10.1007/s00338-010-0662-x

Hossain, M. A., Kumar, V., Burritt, D. J., Fujita, M., and Mäkelä, P. S. A. Eds. (2019). *Osmoprotectant-Mediated Abiotic Stress Tolerance in Plants. Recent Advances and Future Perspectives. Recent advances and Future Perspectives* (Cham: Springer Nature Switzerland).

Huang, S., Zuo, T., and Ni, W. (2020). Important roles of glycinebetaine in stabilizing the structure and function of the photosystem II complex under abiotic stresses. *Planta* 251, 36. doi: 10.1007/s00425-019-0330-z

Jackson, R. L., Gabric, A. J., Woodhouse, M. T., Swan, H. B., Jones, G. B., Cropp, R., et al. (2020a). Coral reef emissions of atmospheric dimethylsulfide and the influence on marine aerosols in the southern Great Barrier Reef, Australia. *J. Geophys. Res. Atmos.* 125, e2019JD031837. doi: 10.1029/2019JD031837

Jackson, R. L., Gabric, A. J., Cropp, R., and Woodhouse, M. T. (2020b). Dimethylsulfide (DMS), marine biogenic aerosols and the ecophysiology of coral reefs. *Biogeosciences* 17, 2181–2204. doi: 10.5194/bg-17-2181-2020

Jones, R. J., and Hoegh-Guldberg, O. (2001). Diurnal changes in the photochemical efficiency of the symbiotic dinoflagellates (Dinophyceae) of corals: photoprotection, photoinactivation and the relationship to coral bleaching. *Plant Cell Environ.* 24, 89–99. doi: 10.1046/j.1365-3040.2001.00648.x

Jones, G. B., and King, S. (2015). Dimethylsulphoniopropionate (DMSP) as an indicator of bleaching tolerance in scleractinian corals. *J. Mar. Sci. Eng.* 3, 444–465. doi: 10.3390/jmse3020444

Kido, E. A., Ferreira-Neto, J. R. C., da Silva, M. D., Santos, V. E. P., Filho, J. L. B. S., and Benko-Iseppon, A. M. (2019). "Osmoprotectant-related genes in plants under abiotic stress: expression dynamics, in silico genome mapping, and biotechnology," in *Osmoprotectant-Mediated Abiotic Stress Tolerance in Plants*. Eds. M. A. Hossain, V. Kumar, D. J. Burritt, M. Fujita and P. S. A. Mäkelä (Cham: Springer Nature Switzerland), p. 1–40.

Klimov, V. V., Allakhverdiev, S. I., Nishiyama, Y., Khorobrykh, A. A., and Murata, N. (2003). Stabilization of the oxygen-evolving complex of photosystem II by bicarbonate and glycinebetaine in thylakoid and subthylakoid preparations. *Funct. Plant Biol.* 30, 797–803. doi: 10.1071/FP03068

Kurepin, L. V., Ivanov, A. G., Zaman, M., Pharis, R. P., Allakhverdiev, S. I., Hurry, V., et al. (2015). Stress-related hormones and glycinebetaine interplay in protection of photosynthesis under abiotic stress conditions. *Photosyn. Res.* 126, 221–235. doi: 10.1007/s11120-015-0125-x

Lesser, M. P. (2006). Oxidative stress in marine environments: biochemistry and physiological ecology. *Annu. Rev. Physiol.* 68, 253–278. doi: 10.1146/annurev.physiol.68.040104.110001

Lesser, M. P. (2011). "Coral bleaching: causes and mechanisms," in *Coral Reefs: An Ecosystem in Transition*. Eds. Z. Dubinsky and N. Stambler (New York: Springer), 405–419.

Lesser, M. P., and Farrell, J. H. (2004). Exposure to solar radiation increases damage to both host tissues and algal symbionts of corals during thermal stress. *Coral Reefs* 23, 367–377. doi: 10.1007/s00338-004-0392-z

Li, M., Li, Z., Li, S., Guo, S., Meng, Q., Li, G., et al. (2014). Genetic engineering of glycine betaine biosynthesis reduces heat-enhanced photoinhibition by enhancing antioxidative defense and alleviating lipid peroxidation in tomato. *Plant Mol. Biol. Rep.* 32, 42–51. doi: 10.1007/s11105-013-0594-z

Li, S., Li, F., Wang, J., Zhang, W., Meng, Q., Chen, T. H. H., et al. (2011). Glycinebetaine enhances the tolerance of tomato plants to high temperature during germination of seeds and growth of seedlings. *Plant Cell Environ.* 34, 1931–1943. doi: 10.1111/j.1365-3040.2011.02389.x

Li, D., Wang, M., Zhang, T., Chen, X., Li, C., Liu, Y., et al. (2021). Glycinebetaine mitigated the photoinhibition of photosystem II at high temperature in transgenic tomato plants. *Photosyn. Res.* 147, 301–315. doi: 10.1007/s11120-020-00810-2

Mäkelä, P. S. A., Jokinen, K., and Himanen, K. (2019). "Roles of endogenous glycinebetaine in plant abiotic stress responses", in *Osmoprotectant-Mediated Abiotic Stress Tolerance in Plants*. Eds. M. A. Hossain, V. Kumar, D. J. Burritt, M. Fujita and P. S. A. Mäkelä (Cham: Springer Nature Switzerland), 153–173.

McNeil, S. D., Nuccio, M. L., and Hanson, A. D. (1999). Betaines and related osmoprotectants. Targets for metabolic engineering of stress resistance. *Plant Physiol.* 120, 945–949. doi: 10.1104/pp.120.4.945

Moore, R. J., and Huxley, C. J. (1976). Aversive behaviour of crown-of-thorns starfish to coral evoked by food-related chemicals. *Nature* 263, 407–409. doi: 10.1038/263407a0

Ngugi, D. K., Ziegler, M., Duarte, C. M., and Voolstra, C. R. (2020). Genomic blueprint of glycine betaine metabolism in coral metaorganisms and their contribution to reef nitrogen budgets. *iScience* 23, 101120. doi: 10.1016/j.isci.2020.101120

Niazian, M., Sadat-Noori, S. A., Tohidfar, M., Mortazavian, S. M. M., and Sabbatini, P. (2021). Betaine aldehyde dehydrogenase (*BADH*) vs. flavodoxin (*Fld*): two important genes for enhancing plants stress tolerance and productivity. *Front. Plant Sci.* 12, 650215. doi: 10.3389/fpls.2021.650215

Oakley, C. A., and Davy, S. K. (2018). "Cell biology of coral bleaching," in *Coral Bleaching. Patterns, Processes, Causes and Consequences, 2nd ed*. Eds. M. J. H. Van Oppen and J. M. Lough (Cham: Springer International Publishing), 189–211.

Papageorgiou, G. C., and Murata, N. (1995). The unusually strong stabilizing effects of glycine betaine on the structure and function of the oxygen-evolving photosystem II complex. *Photosynth. Res.* 44, 243–252. doi: 10.1007/BF00048597

Prasad, K. V. S. K., and Saradhi, P. P. (2004). Enhanced tolerance to photoinhibition in transgenic plants through targeting of glycinebetaine biosynthesis into the chloroplasts. *Plant Sci.* 166, 1197–1212. doi: 10.1016/j.plantsci.2003.12.031

Rhodes, D., and Hanson, A. D. (1993). Quaternary ammonium and tertiary sulfonium compounds in higher plants. *Annu. Rev. Plant Physiol. Plant Mol. Biol.* 44, 357–384. doi: 10.1146/annurev.pp.44.060193.002041

Roychoudhury, A., Bieker, A., Häussinger, D., and Oesterhelt, F. (2013). Membrane protein stability depends on the concentration of compatible solutes –a single molecule force spectroscopic study. *Biol. Chem.* 394, 1465–1474. doi: 10.1515/hsz-2013-0173

Sakamoto, A., and Murata, N. (2002). The role of glycine betaine in the protection of plants from stress: clues from transgenic plants. *Plant Cell Environ.* 25, 163–171. doi: 10.1046/j.0016-8025.2001.00790.x

Schiller, H., and Dau, H. (2000). Preparation protocols for high-activity photosystem II membrane particles of green algae and higher plants, pH dependence of oxygen evolution and comparison of the S_2-state multiline signal by X-band EPR spectroscopy. *J. Photochem. Photobiol. B Biol.* 55, 138–144. doi: 10.1016/S1011-1344(00)00036-1

Shirasawa, K., Takabe, T., Takabe, T., and Kishitani, S. (2006). Accumulation of glycinebetaine in rice plants that overexpress choline monooxygenase from spinach and evaluation of their tolerance to abiotic stress. *Ann. Bot.* 98, 565–571. doi: 10.1093/aob/mcl126

Somero, G. N., Lockwood, B. L., and Tomanek, L. (2017). *Biochemical Adaptation. Response to Environmental Challenges From Life's Origins to the Anthropocene* (Sunderland, MA: Sinauer Associates).

Street, T. O., Bolen, D. W., and Rose, G. D. (2006). A molecular mechanism for osmolyte-induced protein stability. *Proc. Natl. Acad. Sci. USA* 17064, 13997–14002. doi: 10.1073/pnas.0606236103

Sunda, W., Kieber, D. J., Kiene, R. P., and Huntsman, S. (2002). An antioxidant function for DMSP and DMS in marine algae. *Nature* 418, 317–320. doi: 10.1038/nature00851

Swan, H. B., Deschaseaux, E. S. M., Jones, G. B., and Eyre, B. D. (2017a). The relative abundance of dimethylsulfoniopropionate (DMSP) among other zwitterions in branching coral at Heron Island, southern Great Barrier Reef. *Anal. Bioanal. Chem.* 409, 4409–4423. doi: 10.1007/s00216-017-0385-8

Swan, H. B., Jones, G. B., Deschaseaux, E. S. M., and Eyre, B. D. (2017b). Coral reef origins of atmospheric dimethylsulfide at Heron Island, southern Great Barrier Reef, Australia. *Biogeosciences* 14, 229–239. doi: 10.5194/bg-14-229-2017

Valenzuela-Soto, E. M., and Figueroa-Soto, C. G. (2019). "Biosynthesis and degradation of glycine betaine and its potential to control plant growth and development," in *Osmoprotectant-Mediated Abiotic Stress Tolerance in Plants*. Eds. M. A. Hossain, V. Kumar, D. J. Burritt, M. Fujita and P. S. A. Mäkelä (Cham: Springer Nature Switzerland), 123–140.

Van Oppen, M. J. H., and Lough, J. M. Eds (2018). *Coral Bleaching. Patterns, Processes, Causes and Consequences*. *2nd ed* (Cham: Springer International Publishing).

Vermeij, M. J. A., and Bak, R. P. M. (2002). How are coral populations structured by light? Marine light regimes and the distribution of *Madracis*. *Mar. Ecol. Prog. Ser.* 233, 105–116. doi: 10.3354/meps233105

Wang, Y., Liu, S., Zhang, H., Zhao, Y., Zhao, H., and Liu, H. (2014). Glycine betaine application in grain filling wheat plants alleviates heat and high light-induced photoinhibition by enhancing the *psbA* transcription and stomatal conductance. *Acta Physiol. Plant* 36, 2195–2202. doi: 10.1007/s11738-014-1596-7

Warner, M. E., Fitt, W. K., and Schmidt, G. W. (1999). Damage to photosystem II in symbiotic dinoflagellates: A determinant of coral bleaching. *Proc. Natl. Acad. Sci. U. S. A.* 96, 8007–8012. doi: 10.1073/pnas.96.14.8007

Warner, M. E., and Suggett, D. J. (2016). "The photobiology of *Symbiodinium* spp.: linking physiological diversity to the implications of stress and resilience," in *The Cnidaria, Past, Present and Future*. Eds. S. Goffredo and Z. Dubinsky (Cham: Springer Nature Switzerland), 489–509.

Weis, V. M. (2008). Cellular mechanisms of cnidarian bleaching: stress causes the collapse of symbiosis. *J. Exp. Biol.* 211, 3059–3066. doi: 10.1242/jeb.009597

Yancey, P. H., Clark, M. E., Hand, S. C., Bowlus, R. D., and Somero, G. N. (1982). Living with water stress: evolution of osmolyte systems. *Science* 217, 1214–1222. doi: 10.1126/science.7112124

Yancey, P. H., Heppenstall, M., Ly, S., Andrell, R. M., Gates, R. D., Carter, V. L., et al. (2010). Betaines and dimethysulfoniopropionate as major osmolytes in Cnidaria with endosymbiotic dinoflagellates. *Physiol. Biochem. Zool.* 83, 167–173. doi: 10.1086/644625

Yang, G., Rhodes, D., and Joly, R. J. (1996). Effects of high temperature on membrane stability and chlorophyll fluorescence in glycinebetaine-deficient and glycinebetaine-containing maize lines. *Aust. J. Plant Physiol.* 23, 437–443. doi: 10.1071/PP9960437

Yang, X., Wen, X., Gong, H., Lu, Q., Yang, Z., Tang, Y., et al. (2007). Genetic engineering of the biosynthesis of glycinebetaine enhances thermotolerance of photosystem II in tobacco plants. *Planta* 225, 719–733. doi: 10.1007/s00425-006-0380-3

Zhang, T., Li, Z., Li, D., Li, C., Wei, D., Li, S., et al. (2020). Comparative effects of glycinebetaine on the thermotolerance in *codA*- and *BADH*-transgenic tomato plants under high temperature stress. *Plant Cell Rep.* 39, 1525–1538. doi: 10.1007/s00299-020-02581-5

Zulfiqar, F., Akram, N. A., and Ashraf, M. (2020). Osmoprotection in plants under abiotic stresses: new insights into a classical phenomenon. *Planta* 251, 3. doi: 10.1007/s00425-019-03293-l

Conflict of Interest: The author declares that the research was conducted in the absence of any commercial or financial relationships that could be construed as a potential conflict of interest.

Publisher's Note: All claims expressed in this article are solely those of the authors and do not necessarily represent those of their affiliated organizations, or those of the publisher, the editors and the reviewers. Any product that may be evaluated in this article, or claim that may be made by its manufacturer, is not guaranteed or endorsed by the publisher.

frontiers | Frontiers in Marine Science

ORIGINAL RESEARCH
published: 13 June 2022
doi: 10.3389/fmars.2022.889866

Evolutionary History of *DMSP Lyase-Like* Genes in Animals and Their Possible Involvement in Evolution of the Scleractinian Coral Genus, *Acropora*

Yi-Ling Chiu and Chuya Shinzato *

Atmosphere and Ocean Research Institute, The University of Tokyo, Kashiwa, Japan

OPEN ACCESS

Edited by:
Rafel Simó,
Institut de Ciències del Mar (ICM-CSIC), Spain

Reviewed by:
Jean-Baptiste Raina,
University of Technology Sydney, Australia
Uria Alcolombri,
ETH Zürich, Switzerland
Michael Steinke,
University of Essex, United Kingdom

***Correspondence:**
Chuya Shinzato
c.shinzato@aori.u-tokyo.ac.jp

Specialty section:
This article was submitted to Coral Reef Research, a section of the journal Frontiers in Marine Science

Received: *04 March 2022*
Accepted: *19 May 2022*
Published: *13 June 2022*

Citation:
Chiu Y-L and Shinzato C (2022) Evolutionary History of DMSP Lyase-Like Genes in Animals and Their Possible Involvement in Evolution of the Scleractinian Coral Genus, Acropora. Front. Mar. Sci. 9:889866. doi: 10.3389/fmars.2022.889866

Dimethlysulfoniopropionate (DMSP) lyase is an enzyme that mediates cleavage of DMSP into dimethyl sulfide (DMS) and acrylate. DMS is an aerosol substance that may affect cloud formation, solar radiation and ocean temperatures. DMSP lyases in marine organisms, such as marine bacteria, release DMS, which might contribute to atmosphere-ocean feedback. Although DMSP lyases were first identified in marine bacteria, eukaryotic DMSP lyases or genes similar to DMSP lyase, *DMSP lyase-like* (*DL-L*) genes have been found not only in coccolithophores (*Emiliania huxleyi*) and symbiotic algae of the Family Symbiodiniaceae, but also in animals, including scleractinian corals (Cnidaria: Anthozoa: Hexacorallia). Comparative genomic analysis showed that gene expansion events of *DL-L* genes have occurred specifically in the scleractinian genus, *Acropora*. In the present study, we performed molecular identification of *DL-L* genes in *Acropora digitifera*. Thirteen full-length Open Reading Frames were isolated, confirming that these duplicated *DL-L* genes are likely expressed. A comprehensive survey of available transcriptomic databases revealed that *DL-L* genes have been identified not only in scleractinians (Hexacorallia), but also Octocorallia (Anthozoa) and even in a jellyfish (Cnidaria: Hydrozoa). Molecular phylogenetic analyses showed that although some sequences from cnidarian transcriptomic databases apparently originated with their symbiotic algae, cnidarian sequences from Anthozoa and Hydrozoa clustered together, indicating that these evolved from a gene in the last common ancestor of Cnidaria, dating to the Precambrian. Interestingly, cnidarian species possessing *DL-L* genes apparently occur only in coral reefs or shallow, warmer environments, suggesting that these genes may be essential for animals to survive in such environments. *Acropora*-specific duplicated *DL-L* genes, which originated during the past warm geological periods, may enable them to adapt to environmental changes.

Keywords: DMPS lyase, DMS, Cnidaria, Scleractinia, *Acropora*, evolution, gene duplication

INTRODUCTION

Coral reefs in tropical and subtropical waters harbor about 30% of all marine life, making them the most biodiverse habitats in marine ecosystems (Knowlton et al., 2010). In addition, coral reefs provide many fishery resources, protect coastlines, and fix carbon and nitrogen. Scleractinian or stony corals (Anthozoa, Cnidaria) are the main builders of coral reefs, forming massive calcium carbonate skeletons. Corals are metaorganisms or "holobionts" associated with a variety of microorganisms, such as dinoflagellates of the family Symbiodiniaceae and diverse communities of bacteria, archaea, fungi, viruses, and protists (Rohwer et al., 2002; Ainsworth et al., 2010). They rely mainly on symbiotic algae (Symbiodiniaceae) to trap solar energy for survival, growth, and calcification (Goreau and Goreau, 1959; Muscatine, 1990; Davy et al., 2012). In stony corals, dinoflagellate symbionts use the substrates (nitrogen and phosphorus) produced by their hosts for photosynthesis (Muscatine and Porter, 1977). Prokaryotic microorganisms provide sources of nitrogen, sulfur, and other elements to corals or release them into the water column (Ainsworth et al., 2010; Rädecker et al., 2015). These allow coral reefs to remain highly productive in oligotrophic waters, while also facilitating global biogeochemical cycles.

The sulfur cycle is one of the most important of these cycles, providing biosynthetic proteins and cofactors. Dimethylsulfoniopropionate (DMSP) is an organic sulfur compound that is abundant in marine surface waters. The majority of it is produced by phytoplankton and algae, but it has also been reported in some angiosperms and bacteria (Keller et al., 1989; Hanson et al., 1994; Paquet et al., 1994; Gage et al., 1997; Kocsis et al., 1998; Lyon et al., 2011; Kettles et al., 2014; Curson et al., 2017). Although functions of DMSP are not entirely understood, several physiological functions, such as osmoregulation, oxidative stress protection, and cryoprotection, have been demonstrated in phytoplankton and green algae (Kirst et al., 1991; Karsten et al., 1996; Sunda et al., 2002; Lesser, 2006; Husband et al., 2012; Curson et al., 2018). Biological functions such as chemoattraction, predator deterrence, and mediation of bacterial virulence have been identified (Wolfe and Steinke, 1996; Miller and Belas, 2004; Barak-Gavish et al., 2018). The most notable and important aspect of DMSP is that it is a precursor of dimethyl sulfide (DMS) (van Boeckel and Stefels, 1993), which is a major source of sulfur in the atmosphere, promoting cloud formation and combating greenhouse gasses. DMSP is cleaved by an enzyme called DMSP lyase (EC 4.4.1.3), which converts DMSP to DMS. Recently, studies reported that DMSP lyase products, DMS and acrylate, may have ecological roles such as chemical defenses against predation (Strom et al., 2003; Teng et al., 2021) and enhancing predation by grazers (Shemi et al., 2021). When DMS enters the atmosphere, it is oxidized into aerosol particles that can induce cloud formation and increase reflectivity. This may reduce light levels and water temperatures in marine environments, thus contributing to local climate regulation (**Figure 1**) (Ayers and Gras, 1991; Vallina and Simo, 2007), although some studies suggest that sea-air DMS flux is low, and that the role of DMS in climate regulation is likely insignificant (Woodhouse et al., 2010; Quinn and Bates, 2011).

Marine phytoplankton and macroalgae are considered the primary producers of DMSP, while marine bacteria are the primary degraders (Stefels et al., 2007; Reisch et al., 2011). DMSP is released from marine phytoplankton and macroalgae upon cellular lysis caused by zooplankton grazing, viral infection, and senescence (**Figure 1**) (van Boekel and Stefels, 1993; Wolfe et al., 1997; Hill et al., 1998). Bacteria acquire DMSP mainly from the ocean and demethylate it into methanethiol and acetaldehyde, turning DMSP into DMS *via* the lysis pathway (**Figure 1**). DMSP lyase was first identified in bacteria, and at least eight prokaryotic DMSP lyase genes have been identified to date (Li et al., 2021).

Some studies have reported that eukaryotic phytoplankton, including dinoflagellates and algae, possess DMSP lyase activity (Stefels et al., 1995; Steinke and Kirst, 1996; Steinke et al., 1998; Niki et al., 2000; Yoch, 2002), but the responsible gene was difficult to isolate. In 2015, a gene, Alma l, was identified from the eukaryotic coccolithophore, *Emiliania huxleyi*, and was shown to have high DMSP lyase activity (Alcolombri et al., 2015). It has been suggested that Alma 1 can directly lyse algal DMSP, releasing acrylate and DMS (**Figure 1**). Interestingly, sequences similar to Alma 1, *DMSP lyase-like* (*DL-L*) genes were also found in scleractinian corals and Symbiodiniaceae (Alcolombri et al., 2015). Furthermore, recent comparative genomic analysis of scleractinian and cnidarian genomes showed that numbers of *DL-L* genes in genomes of the scleractinian coral genus, *Acropora*, are significantly larger than in other cnidarian genomes and that gene expansion events specifically occurred in *Acropora* (Shinzato et al., 2021a).

Acropora is currently the most studied coral genus in the world (Maor-Landaw and Levy, 2016), as it includes the most widespread, abundant, and diverse scleractinian corals on Earth (Wallace and Rosen, 2006). Approximately 180 species have been recorded from the Red Sea to the Indo-Pacific Ocean and the Caribbean Ocean (Wallace, 1999; Veron, 2000; van Oppen et al., 2001). With the increase of research data, more genetic databases (genome and transcriptome databases) and molecular techniques (CRISPR/Cas9 and gene knockdown) have been developed (Yasuoka et al., 2016; Cleves et al., 2018; Ying et al., 2019; Shinzato et al., 2021a). Genetic analyses suggest that *Acropora* has been evolutionarily very successful and may have become a dominant genus through acquisition and expansion of gene families (Shinzato et al., 2011; Shinzato et al., 2021a). Examples of *Acropora*-specific gene duplication and expansion events have been reported (Hislop et al., 2005; Shinzato et al., 2021a). Symbiotic relationship with Symbiodiniaceae may also have contributed to rapid adaptation to changing environments (Qin et al., 2019). Interestingly, Shinzato et al. (2021a) showed that *DL-L* genes are the most diversified gene family in *Acropora* genomes and that possible coral- or cnidarian-specific stress response genes, including Caspase-X and SCRiPs, have also been tandemly duplicated in *Acropora* genomes. In this study, to better understand evolution of *DL-L* genes in animals and their possible involvement in *Acropora* evolution, we first confirmed

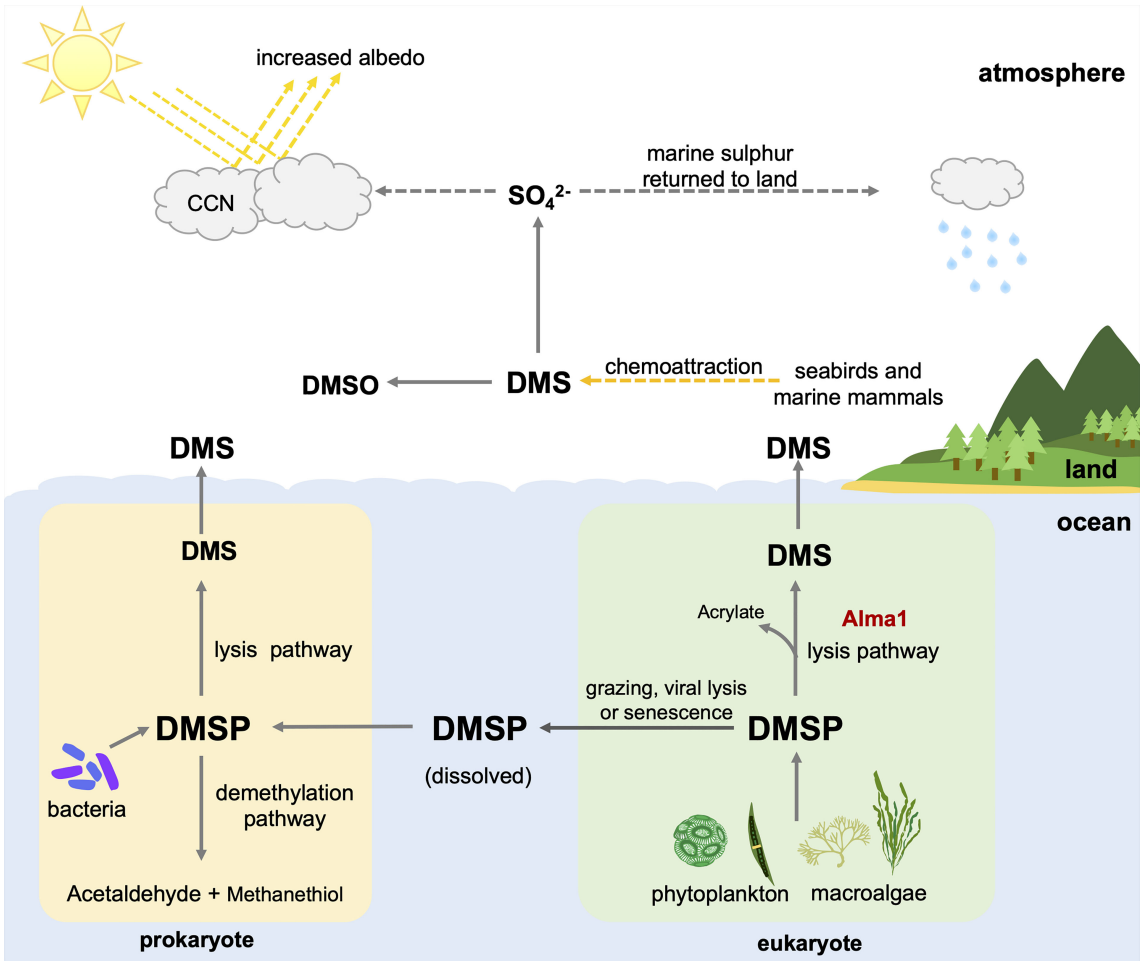

FIGURE 1 | Contributions of prokaryotes and eukaryotes to the biogeochemical cycle and possible functions of dimethylsulfoniopropionic acid (DMSP) and dimethyl sulfide (DMS). CCN, Cloud condensation nuclei; DMSO, dimethyl sulfoxide.

that *DL-L* genes are indeed expressed in *A. digitifera* as possible functional mRNAs without in-frame stop codons. Then, we performed a comprehensive database survey and molecular phylogenetic analyses to investigate the existence of *DL-L* genes in various eukaryotes, including scleractinian corals, cnidarians, and other animals, to gain insight into the evolutionary origin of *DL-L* genes in the animal kingdom.

MATERIALS AND METHODS

Cloning of *DL-L* Genes From *Acropora digitifera*

The same RNA samples used in previous studies including different developmental stages of *A. digitifera* (eggs, blastulae, gastrulae, planula larvae, early polyps, and adult branches) were used for cDNA synthesis (Shinzato et al., 2011; Shinzato et al., 2021a; Yoshioka et al., 2021). Samples were homogenized in TRIzol reagent (Invitrogen) on ice, and total RNA was extracted following the manufacturer's instruction and Chiu et al. (2020). Extracted total RNA was treated with recombinant DNase I (Roche) to remove contaminating genomic DNA. First-strand cDNA was synthesized from 5 μg of DNase-treated RNA using SuperScriptTM III reserve transcriptase (Thermo Fisher Scientific). Possible *DL-L* genes of *A. digitifera* were derived from predicted genes of *A. digitifera* (Shinzato et al., 2021a), and primers amplifying full length open reading frames (ORFs) were designed for each gene (**Supplementary Table 1**). PCR products were cloned into the pGEM-T Easy cloning vector (Promega), transformed into competent cells (*Escherichia coli*, DH5α strain), and plasmids were sequenced at a commercial laboratory (Eurofin Genomics, Tokyo, Japan).

Gene Expression Patterns of *Acropora digitifera DL-L* Genes Under Different Developmental Stages and Increased Sea Water Temperature

To investigate gene expression patterns of 18 *DL-L* genes predicted from the *A. digitifera* genome assembly (Shinzato et al., 2021a), we

used previously reported RNA-Seq transcriptome data of *A. digitifera* from different developmental stages (egg, blastula, gastrula, planula, polyp, Shinzato et al., 2021a), adult stages (Yoshioka et al., 2021), and increased seawater temperature treatments (25°C to 30°C, Shinzato et al., 2021b). Briefly, Illumina adaptor sequences and low-quality reads (Quality score < 20, length < 25 bp) in the RNA-Seq data were trimmed with CUTADAPT v1.16 (Martin, 2011), and cleaned reads were mapped to *A. digitifera* gene models (Shinzato et al., 2021a) using KALLISTO v0.44.0 (Bray et al., 2016) or MiniMap v2.9 (Li, 2018) with default settings. Mapping counts were normalized using the trimmed mean of M values (TMM) method, and then converted to counts per million (CPM) using EdgeR v3.28.1 (Robinson et al., 2010; McCarthy et al., 2012) in R v3.6.3 (team 2015).

Identification of DL-L Genes From Publicly Available Eukaryote and Cnidarian Transcriptomic Databases

Amino acid sequences were deduced from cloned cDNA sequences using the ExPASy translate tool (https://web.expasy.org/translate/; Gasteiger et al., 2003). To search for genes similar to DMSP lyase gene from transcriptomic databases, the deduced amino acid sequences of cloned *A. digitifera DL-L* genes, *Emiliania huxleyi* Alma1 (KR703620.1), and *Symbiodinium* A1 DMSP lyase (P0DN22) were used as query sequences in homology searches against the Transcriptome Shotgun Assembly (TSA) database at the National Center for Biotechnology Information (NCBI) using tBlastn (*A. digitifera DL-L* genes: e-value cutoff $1e^{-50}$, query coverage >80%, *Emiliania huxleyi* Alma1 and *Symbiodinium* A1 DMSP lyase: e-value cutoff $1e^{-5}$, query coverage >70%). Sequences satisfying these criteria were retrieved, and amino acid sequences were prepared using the ExPASy translate tool.

Sequence Alignment and Molecular Phylogenetic Analyses

Sequences downloaded from NCBI TSA databases, including cnidarians, animals, phytoplankton and macroalgae were used for phylogenetic analyses, with bacterial *DMSP lyase* genes (WP028324949.1, WP012448288.1, WP034745099.1, WP020674609.1, and WP006965703.1) as an outgroup. First, all amino acid sequences were aligned using MAFFT v7.310 (Katoh et al., 2002; Katoh and Standley, 2013), and poorly aligned sequences were removed manually. Gaps in alignments were removed using trimAl v1.2 (Capella-Gutiérrez et al., 2009) with the "gappyout" option. After removing gaps, maximum likelihood analyses were performed using RAxML v8.2.10 (Stamatakis, 2014) with the "bootstrap 100" and "protgammaauto" options.

RESULTS

DL-L Genes Isolated From *Acropora digitifera* RNAs and Their Gene Expression Patterns

Among 18 *DL-L* genes predicted from the *A. digitifera* genome (Shinzato at el., 2021a), we successfully obtained 13 *DL-L* gene sequences with full-length mRNA coding regions from cDNA (**Figure 2**; **Supplementary Figure 1**), demonstrating that multiple *DL-L* genes exist in the *A. digitifera* genome and that these are actually expressed as possible functional mRNAs without in-frame stop codons. The resultant 13 amino acid sequences had the same Asp/Glu/hydantoin racemase superfamily conserved domain as in Alma1 of *E. huxleyi* (**Figure 2**; **Supplementary Figure 1**) (Alcolombri et al., 2015). These 18 genes showed different levels and patterns of gene expression in different developmental stages (**Supplementary Table 2**) as shown by previous studies (Shinzato et al., 2021a; Shinzato et al., 2021b; Yoshioka et al., 2021). Gene expression of five genes was significantly changed (one upregulated and four downregulated) by increased sea water temperature (25°C to 30°C, $q < 0.05$, **Supplementary Table 2**).

DL-L Genes in Eukaryotes

Among the 6,258 eukaryotic TSA databases deposited in NCBI, we identified 123 gene sequences from 72 species that showed similarity to *A. digitifera DL-L* genes and satisfied the above criteria (tBlastn e-value cutoff $1e^{-50}$, query coverage >80%). Most sequences were identified from the Cnidaria (stony corals, sea anemones, jellyfish and hydra), phytoplankton (Phyla Haptophyta, Myzozoa, Ochrophyta) and macroalgae (Phyla Chlorophyta and Rhodophyta) (**Table 1**). Unexpectedly, four sequences were also identified from other animals, including a ctenophore (*Beroe forskalii*), a mollusk (*Limacina retroversa*) and arthropods (*Dendroctonus frontalis* and *Pleuromamma xiphias*) (**Table 1**). We further investigated the amino acid sequence similarity of these sequences with the only known DMSP lyases from eukaryotes to date (Alcolombri et al., 2015), *Emiliania huxleyi* Alma1 and *Symbiodinium* A1 DMSP lyase (**Supplementary Table 3**). Most eukaryote sequences similar to *A. digitifera DL-L* genes (**Table 1**) also showed sequence similarities to both DMSP lyases, but percent identities were lower than those to *A. digitifera DL-L* genes (**Supplementary Table 3**).

In order to infer evolutionary relationships of the identified sequences from eukaryotes and the four sequences from non-cnidarian animals, we performed molecular phylogenetic analyses with amino acid sequences of the 13 A. *digitifera DL-L* genes as representatives of Cnidaria and bacterial DMSP lyase genes from prokaryotes as an outgroup. Sequences from prokaryotes and eukaryotes separated into two distinct clusters, indicating that all of the sequences obtained from eukaryote TSA databases originated from eukaryotes, and were not contaminants from symbiotic bacteria (**Figure 3**; **Supplementary Figure 2**). All sequences from *A. digitifera* clustered, demonstrating that they originated from the host coral (**Figure 3**; **Supplementary Figure 2**). None of the sequences from non-cnidarian animals clustered with those from *A. digitifera*. Clustering of the *D. frontalis* sequence with dinoflagellate sequences displayed 100% bootstrap support, indicating that this sequence was derived from symbiotic or adhesive algae, not from the animal itself. However, the other three sequences from *B. forskalii*, *P. xiphias* and *L. retroversa* did not cluster with those of *A. digitifera* and other eukaryotes (**Figure 3**; **Supplementary Figure 2**); thus, the evolutionary origin (animals or other eukaryotes) are unclear.

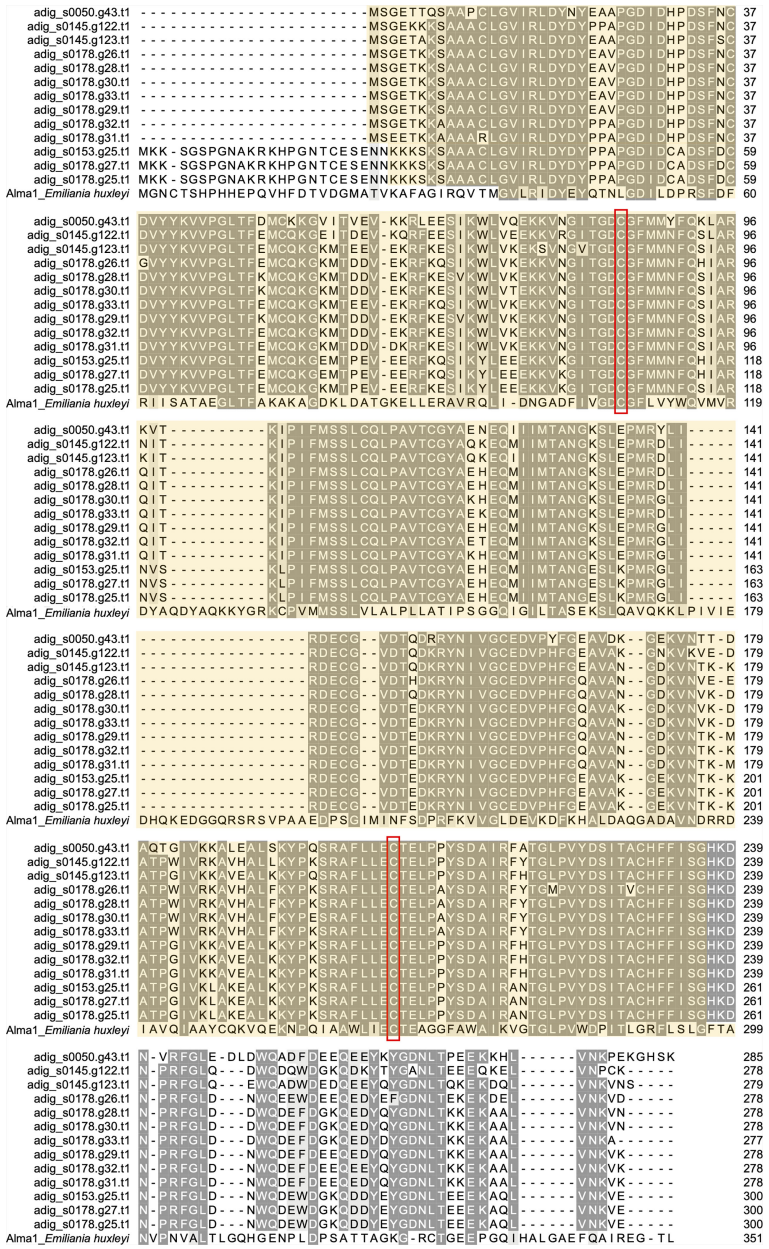

FIGURE 2 | Molecular characterization of *DL-L* genes in *Acropora digitifera*. Multiple sequence alignment of deduced amino acid sequences from 13 *DL-L* genes of *A. digitifera* and *Emiliania huxleyi*, Alma1 (KR703620.1). Identical residues are indicated in the same color. Lengths of amino acid sequences are shown at the right and positions of the Asp/Glu/hydantoin racemase superfamily conserved domain are shown in light yellow and the two putative active site residues are shown in red boxes.

DL-L Genes in Cnidaria

Among 137 Cnidarian TSA databases in NCBI, we found sequences similar to *DL-L* genes from 35 species (**Table 2**). Most of these sequences were from *Acropora millepora* and *A. tenuis* and had been previously identified (Alcolombri et al., 2015; Shinzato et al., 2021a). Interestingly, possible *DL-L* genes were found not only in the subclass Hexacorallia, including stony corals, sea anemones, and zoanthids, but also in the Octocorallia, including soft corals and blue corals, and even from Hydroidolina, including jellyfishes and fire corals (**Table 2**). We also investigated amino acid sequence similarity of these cnidarian sequences with known eukaryote DMSP lyases from *E. huxleyi* and *Symbiodinium* A1 (see above), and all sequences except one from *Seriatopora caliendrum* had significant similarities with these eukaryote DMSP lyases (**Supplementary Table 4**).

Coral and/or cnidarian transcriptomic databases often contain sequences originating with symbiotic algae, as well as associated microorganisms. In order to identify which sequences

TABLE 1 | *DL-L* genes in Eukaryotes, excluding those from cnidarians.

Kingdom	Phylum	Class	Species	Accession
Animalia	Ctenophora	Nuda	*Beroe forskalii**	GHXY01272785.1
Animalia	Mollusca	Gastropoda	*Limacina retroversa**	GBXC01047479.1
Animalia	Arthropoda	Insecta	*Dendroctonus frontalis**	GAFI01013939.1
Animalia	Arthropoda	Hexanauplia	*Pleuromamma xiphias**	GFCI01194001.1
Chromista	Foraminifera	Globothalamea	*Globobulimina* sp.	GGCD01090783.1
Chromista	Haptophyta	Prymnesiophyceae	*Emiliania huxleyi*	HBTT01010599.1
Chromista	Haptophyta	Prymnesiophyceae	*Gephyrocapsa muellerae*	HBRT01085803.1
Chromista	Haptophyta	Prymnesiophyceae	*Haptolina ericina*	HBHX01042533.1
Chromista	Haptophyta	Prymnesiophyceae	*Pelagophyceae* sp.	HBPV01017070.1
Chromista	Haptophyta	Prymnesiophyceae	*Phaeocystis antarctica*	HBQY01084461.1
Chromista	Haptophyta	Prymnesiophyceae	*Phaeocystis globosa*	HBRY01017421.1
Chromista	Haptophyta	Prymnesiophyceae	*Phaeocystis rex*	HBRF01010364.1
Chromista	Haptophyta	Prymnesiophyceae	*Phaeocystis* sp.	HBRH01022669.1
Chromista	Haptophyta	Prymnesiophyceae	*Prymnesium parvum*	HBJC01021087.1
Chromista	Myzozoa	Dinophyceae	*Apocalathium aciculiferum*	HBPP01113651.1
Chromista	Myzozoa	Dinophyceae	*Breviolum minutum*	GICE01003031.1
Chromista	Myzozoa	Dinophyceae	*Crypthecodinium cohnii*	HBOA01074003.1
Chromista	Myzozoa	Dinophyceae	*Dinophysis acuminata*	HBJU01034009.1
Chromista	Myzozoa	Dinophyceae	*Alexandrium andersonii*	HBGQ01027533.1
Chromista	Myzozoa	Dinophyceae	*Alexandrium catenella*	HBGE01066426.1
Chromista	Myzozoa	Dinophyceae	*Alexandrium monilatum*	HBNR01038033.1
Chromista	Myzozoa	Dinophyceae	*Alexandrium tamarense*	GAIU01003918.1
Chromista	Myzozoa	Dinophyceae	*Amphidinium carterae*	HBNO01025899.1
Chromista	Myzozoa	Dinophyceae	*Amphidinium massartii*	HBLR01031444.1
Chromista	Myzozoa	Dinophyceae	*Ansanella granifera*	GFBE01033504.1
Chromista	Myzozoa	Dinophyceae	*Brandtodinium nutricula*	HBGW01061089.1
Chromista	Myzozoa	Dinophyceae	*Durinskia baltica*	GAAT01001280.1
Chromista	Myzozoa	Dinophyceae	*Gambierdiscus australes*	HBLT01061594.1
Chromista	Myzozoa	Dinophyceae	*Gambierdiscus excentricus*	GETL01004569.1
Chromista	Myzozoa	Dinophyceae	*Gambierdiscus pacificus*	GIJQ01009298.1
Chromista	Myzozoa	Dinophyceae	*Gambierdiscus polynesiensis*	GETK01055910.1
Chromista	Myzozoa	Dinophyceae	*Gonyaulax spinifera*	HBNG01065451.1
Chromista	Myzozoa	Dinophyceae	*Gymnodinium catenatum*	HBLW01077801.1
Chromista	Myzozoa	Dinophyceae	*Gyrodiniellum shiwhaense*	GFHE01000685.1
Chromista	Myzozoa	Dinophyceae	*Heterocapsa arctica*	HBNJ01038395.1
Chromista	Myzozoa	Dinophyceae	*Heterocapsa rotundata*	HBLO01067633.1
Chromista	Myzozoa	Dinophyceae	*Heterocapsa triquetra*	HBLK01063662.1
Chromista	Myzozoa	Dinophyceae	*Karenia brevis*	GFLM01039285.1
Chromista	Myzozoa	Dinophyceae	*Karenia mikimotoi*	GISR01008935.1
Chromista	Myzozoa	Dinophyceae	*Lingulodinium polyedra*	HBOU01097259.1
Chromista	Myzozoa	Dinophyceae	*Lingulodinium polyedrum*	JO709806.1
Chromista	Myzozoa	Dinophyceae	*Noctiluca scintillans*	HBFQ01012472.1
Chromista	Myzozoa	Dinophyceae	*Pelagodinium beii*	HBNF01082217.1
Chromista	Myzozoa	Dinophyceae	*Prorocentrum minimum*	GHMX01159955.1
Chromista	Myzozoa	Dinophyceae	*Scrippsiella hangoei*	HBPM01101163.1
Chromista	Myzozoa	Dinophyceae	*Symbiodinium muscatinei*	GFDR03033769.1
Chromista	Myzozoa	Dinophyceae	*Symbiodinium* sp.	HBTG01057664.1
Chromista	Myzozoa	Dinophyceae	*Symbiodinium* sp. A1	GAKY01102437.1
Chromista	Myzozoa	Dinophyceae	*Symbiodinium* sp. A4	GFPM01010862.1
Chromista	Myzozoa	Dinophyceae	*Symbiodinium* sp. B2	GBRZ01003534.1
Chromista	Myzozoa	Dinophyceae	*Symbiodinium* sp. CCMP2430	*HBTH01081069.1*
Chromista	Myzozoa	Dinophyceae	*Symbiodinium* sp. clade A	HBSZ01019953.1
Chromista	Myzozoa	Dinophyceae	*Symbiodinium* sp. clade C	GBSC01004690.1
Chromista	Myzozoa	Dinophyceae	*Symbiodinium* sp. clade D	GAFP01017879.1
Chromista	Myzozoa	Dinophyceae	*Symbiodinium* sp. clade D	GBRR01002019.1
Chromista	Myzozoa	Dinophyceae	*Togula jolla*	HBKY01023746.1
Chromista	Ochrophyta	Pelagophyceae	*Chrysoreinhardia* sp.	HBSO01018369.1
Chromista	Ochrophyta	Bacillariophyceae	*Coscinodiscus wailesii*	HBJZ01008141.1
Chromista	Ochrophyta	Bacillariophyceae	*Navicula* sp.	HBQT01035211.1
Chromista	Ochrophyta	Pelagophyceae	*Pelagomonas calceolata*	HBQU01000605.1
Chromista	Ochrophyta	Bacillariophyceae	*Pleurosigma* sp.	HBRE01034425.1
Chromista	Ochrophyta	Bacillariophyceae	*Proboscia alata*	HBOX01003438.1
Chromista	Ochrophyta	Bacillariophyceae	*Pseudo-nitzschia fraudulenta*	HBPF01070060.1

(Continued)

TABLE 1 | Continued

Kingdom	Phylum	Class	Species	Accession
Chromista	Ochrophyta	Phaeophyceae	*Sargassum vulgare*	GEHA01001042.1
Chromista	Ochrophyta	Bacillariophyceae	*Synedra* sp.	HBQV01036945.1
Chromista	Ochrophyta	Bacillariophyceae	*Thalassiosira antarctica*	HBPL01059889.1
Plantae	Chlorophyta	Ulvophyceae	*Ulva lactuca*	GFUR01013571.1
Plantae	Chlorophyta	Chloropicophyceae	*Chloroparvula pacifica*	HBPX01006065.1
Plantae	Chlorophyta	Mamiellophyceae	*Crustomastix stigmatica*	HBLU01015603.1
Plantae	Rhodophyta	Florideophyceae	*Laurencia pacifica*	GFZU01073384.1
Plantae	Rhodophyta	Florideophyceae	*Lithophyllum* sp.	GHIV01139773.1
Plantae	Rhodophyta	Florideophyceae	*Porolithon* sp.	GHIO01088530.1

**The origin of sequence is unknown, and may represent contamination from symbiotic/adhesive algae.*

were from animal hosts, we further performed molecular phylogenetic analyses of sequences from cnidarian TSA databases together with *DL-L* genes from the Symbiodiniaceae, coccolithophores and prokaryotes (**Figure 4A**). Six distinct clades were supported by strong bootstrap probabilities (93 ~ 100%). Most of the sequences belonging to the Hexacorallia clustered together in Clade 1 with *A. digitifera DL-L* genes, indicating that these originated from hexacorallian hosts.

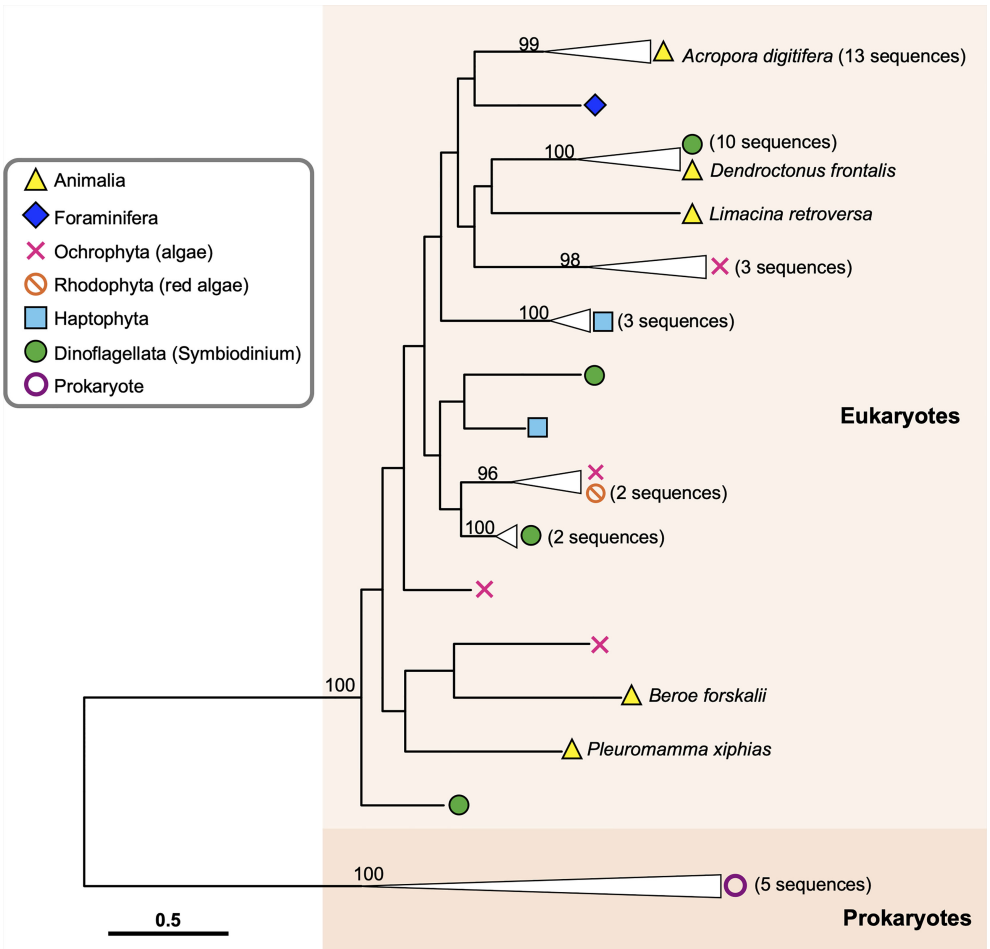

FIGURE 3 | Molecular phylogenetic analysis of *DL-L* genes identified from transcriptomic databases of eukaryotes. Possible *DL-L* genes from eukaryotic NCBI TSA databases were analyzed using the maximum likelihood method. 337 gap-trimmed aligned amino acids were used for phylogenetic analysis. Bootstrap support for representative nodes is shown. Eukaryotic and prokaryotic DMSP lyase genes clades are highlighted in different colors. *A. digitifera DL-L* genes cloned from cDNA are represented as animal genes in the analysis. *DL-L* genes from the Animalia, Foraminifera, Ochrophyta, Rhodophyta, Haptophyta, Dinoflagellata, and Prokaryota are colored in yellow (triangle), indigo (diamond), pink (cross), orange (prohibited), blue (square), green (circle), and purple (white circle), respectively. The bar indicates 0.5 substitutions per site in aligned regions. The complete phylogenetic tree is shown in **Supplementary Figure 2**.

TABLE 2 | *DL-L* genes in cnidarians excluding *Acropora*.

Class	Subclass	Order	Family	Genus	Species	Sequences originated from cnidarian hosts confirmed by molecular phylogenetic analysis (Figure 4)	Accession
Hydrozoa	Hydroidolina	Anthoathecata	Milleporidae	*Millepora*	*Millepora alcicornis*	No	GFAS01239487.1
Hydrozoa	Hydroidolina	Anthoathecata	Milleporidae	*Millepora*	*Millepora complanata*	No	GIXC01089652.1
Hydrozoa	Hydroidolina	Anthoathecata	Milleporidae	*Millepora*	*Millepora* sp.	No	GFGV01397967.1
Hydrozoa	Hydroidolina	Anthoathecata	Milleporidae	*Millepora*	*Millepora squarrosa*	No	GFGU01029924.1
Hydrozoa	Hydroidolina	Anthoathecata	Porpitidae	*Velella*	*Velella velella*	Yes	GHAZ01122917.1
Anthozoa	Octocorallia	Alcyonacea	Briareidae	*Briareum*	*Briareum asbestinum*	No	GHBD02057672.1
Anthozoa	Octocorallia	Alcyonacea	Clavulariidae	*Clavularia*	*Clavularia* sp.	Yes	GHAW01081527.1
Anthozoa	Octocorallia	Alcyonacea	Xeniidae	*Xenia*	*Xenia* sp.	No	GHBC01044802.1
Anthozoa	Octocorallia	Helioporacea	Helioporidae	*Heliopora*	*Heliopora coerulea*	No	IABP01030506.1
Anthozoa	Hexacorallia	Zoantharia	Sphenopidae	*Palythoa*	*Palythoa caribaeorum*	Yes	GESO01095871.1
Anthozoa	Hexacorallia	Zoantharia	Sphenopidae	*Palythoa*	*Palythoa* sp.	No	GGUI01140954.1
Anthozoa	Hexacorallia	Zoantharia	Sphenopidae	*Protopalythoa*	*Protopalythoa variabilis*	Yes	GCVI01065809.1
Anthozoa	Hexacorallia	Zoantharia	Zoanthidae	*Zoanthus*	*Zoanthus* sp.	No	GGTW01049612.1
Anthozoa	Hexacorallia	Actiniaria	Actiniidae	*Anemonia*	*Anemonia viridis*	No	GGLT01126584.1
Anthozoa	Hexacorallia	Actiniaria	Actiniidae	*Anthopleura*	*Anthopleura elegantissima*	No	GBXJ01017739.1
Anthozoa	Hexacorallia	Corallimorpharia	Discosomidae	*Rhodactis*	*Rhodactis indosinensis*	Yes	GELO01068433.1
Anthozoa	Hexacorallia	Scleractinia	Acroporidae	*Montipora*	*Montipora digitata*	Yes	GIVM01155846.1
Anthozoa	Hexacorallia	Scleractinia	Acroporidae	*Alveopora*	*Alveopora japonica*	Yes	GGJR01165973.1
Anthozoa	Hexacorallia	Scleractinia	Euphylliidae	*Fimbriaphyllia*	*Fimbriaphyllia ancora*	No	ICQS01038312.1
Anthozoa	Hexacorallia	Scleractinia	Agariciidae	*Agaricia*	*Agaricia lamarcki*	No	GGLC03011859.1
Anthozoa	Hexacorallia	Scleractinia	Siderastreidae	*Siderastrea*	*Siderastrea siderea*	Yes	GIYO011329375.1
Anthozoa	Hexacorallia	Scleractinia	Poritidae	*Porites*	*Porites astreoides*	Yes	GIYN01600157.1
Anthozoa	Hexacorallia	Scleractinia	Poritidae	*Porites*	*Porites australiensis*	Yes	FX437344.1
Anthozoa	Hexacorallia	Scleractinia	Poritidae	*Porites*	*Porites lutea*	Yes	GGER01067412.1
Anthozoa	Hexacorallia	Scleractinia	Merulinidae	*Cyphastrea*	*Cyphastrea serailia*	Yes	GETH01074762.1
Anthozoa	Hexacorallia	Scleractinia	Merulinidae	*Favites*	*Favites colemani*	Yes	GIVN01210226.1
Anthozoa	Hexacorallia	Scleractinia	Mussidae	*Favia*	*Favia lizardensis*	Yes	GDZU01025741.1
Anthozoa	Hexacorallia	Scleractinia	Pocilloporidae	*Pocillopora*	*Pocillopora acuta*	No	GJER01286462.1
Anthozoa	Hexacorallia	Scleractinia	Pocilloporidae	*Seriatopora*	*Seriatopora caliendrum*	Yes	GIAR01012305.1

Interestingly, *Clavularia* sp. of the Octocorallia and *Velella velella* of the Hydroidolina were also relegated to Clade 1, indicating that these share a common ancestral gene with hexacorallian species. The family Symbiodiniaceae is genetically diverse, and includes multiple genera (LaJeunesse et al., 2018). As expected, some Cnidarian sequences clustered with sequences of symbiotic algae (Symbiodiniaceae) and were assigned to Clades 3-5 (**Figure 4A**; **Supplementary Figure 3**), indicating that these were contaminant from symbiotic algae. Among them, a sequence from *Pocillopora acuta* was clustered into Clade 3, sequences from *Anthopleura elegantissima*, *Millepora squarrosa*, *Agaricia lamarcki*, *Heliopora coerulea*, *Zoanthus* sp., *Palythoa* sp., *M. alcicornis*, *Millepora* sp. were clustered in Clade 4, and sequences from *Fimbriaphyllia ancora*, *M. complanata*, and *Xenia* sp. were clustered in Clade 5 (**Figure 4A**; **Supplementary Figure 3**; **Table 2**). Different cnidarian species

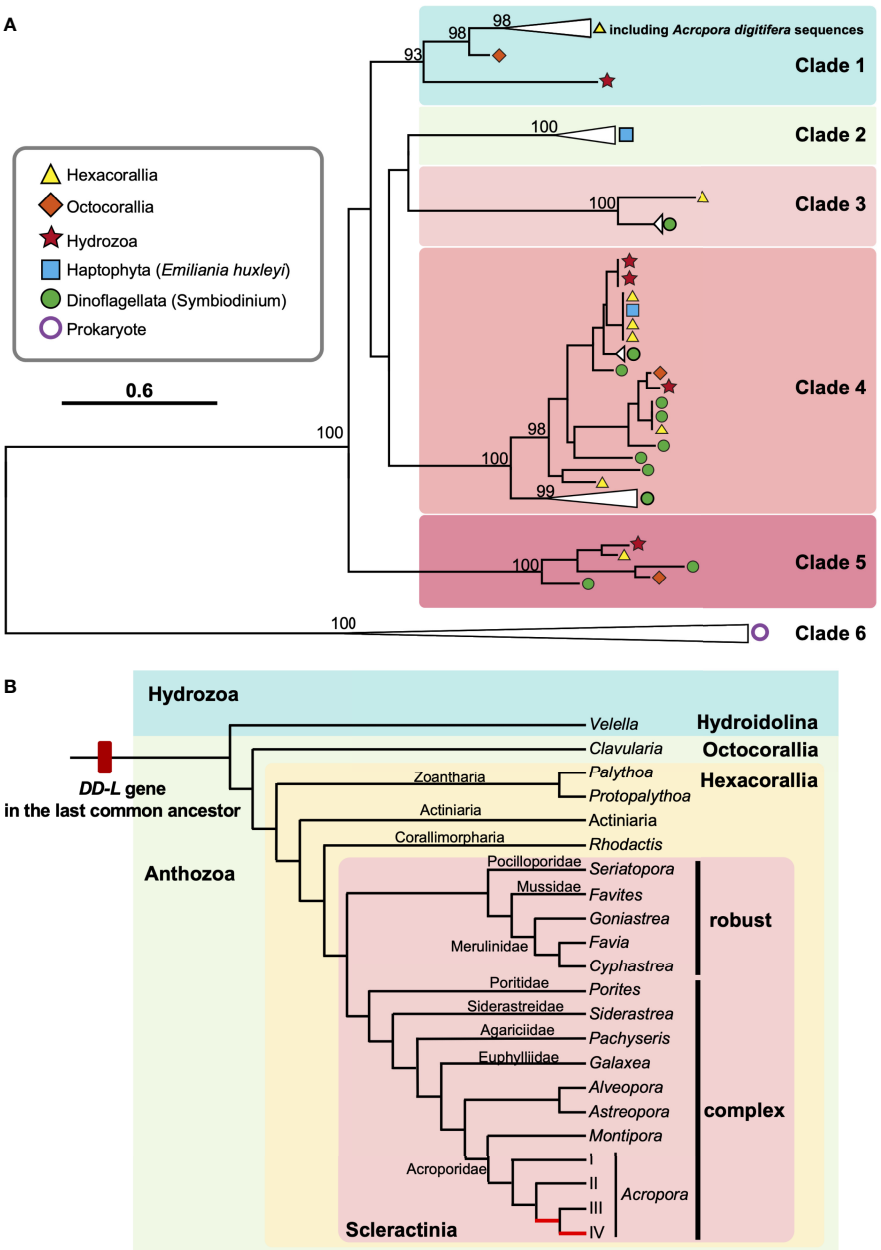

FIGURE 4 | Molecular phylogenetic analysis of *DL-L* genes identified from transcriptomic databases of Cnidaria. **(A)** Possible *DL-L* genes from cnidarian NCBI TSA databases were analyzed using the maximum likelihood method. 667 gap-trimmed aligned amino acids were used for phylogenetic analysis. Bootstrap support for representative nodes is shown. Clades 1-6 of *DL-L* genes of cnidarians, other eukaryotes and prokaryotes are highlighted in different colors. **(A)** *digitifera DL-L* genes identified from cDNA, which were all clustered in Clade 1, are also included. *DL-L* genes from Hexacorallia, Octocorallia, Hydrozoa, Haptophyta, Dinoflagellata, and Prokaryota are colored in yellow (triangle), orange (diamond), red (start), blue (square), green (circle), and purple (white circle), respectively. The bar indicates 0.6 substitutions per site in aligned regions. The complete phylogenetic tree is shown in **Supplementary Figure 3**. **(B)** Updated evolutionary history of *DL-L gene* in the Phylum Cnidaria. Only species of cnidarians possessing animal-type *DL-L* genes are shown. Two *Acropora*-specific gene expansion events proposed by Shinzato et al. (2021a) are shown in red in the phylogenetic tree. Phylogenetic relationships of cnidarians and scleractinian corals are derived from Kayal et al. (2018) and Kitahara et al. (2016).

harbor different types of symbiotic algae; thus, Clades 3-5, containing Symbiodiniaceae could reflect different types of symbiotic algae. All *DL-L* genes of the coccolithophore *E. huxleyi* within the Haptophyta clustered in Clade 2, and bacterial DMSP lyase genes clustered in Clade 6. Taken together, all *DL-L* genes of Cnidaria, including scleractinian corals, soft corals, and jellyfishes, evolved from an ancestral gene that already existed in the last common ancestor of

Anthozoa and Hydrozoa, and have completely different evolutionary backgrounds from those of coccolithophores, the Family Symbiodiniaceae, or prokaryotes.

DISCUSSION

A Variety of Scleractinian Corals Possess *DL-L* Genes

It has been reported that coral reefs are hotspots for DMSP, which have been attributed to symbiotic algae of corals (Broadbent et al., 2002; Broadbent and Jones, 2004; Broadbent and Jones, 2006; Swan et al., 2012). Recent studies have shown that adult and juvenile *A. tenuis* and *A. millepora* without symbiotic algae both produce DMSP (Raina et al., 2013). *DL-L* genes have also been discovered, not only in *Acropora* genomes (Alcolombri et al., 2015; Shinzato et al., 2021a), but also in genomes of *Montipora*, *Astreopora*, *Goniastrea*, and two corallimorpharians, *Amplexidiscus* and *Discosoma* (Shinzato et al., 2021a).

In this study, we successfully identified full-length ORFs of 13 *DL-L* genes, which are expressed in *A. digitifera*, and we identified *DL-L* genes from a variety of scleractinian lineages (**Figures 1**, **4A**; **Supplementary Figure 3**). The earliest coral fossil record of a Scleractinian dates to the middle Triassic (240 Ma) (Stanley, 2003). Most extant scleractinians are classified into two major clades, known as the Complexa (complex corals) and Robusta (robust corals), and are assumed to have diverged in the Late Carboniferous (300 Ma) (Romano and Palumbi, 1996; Romano and Cairns, 2000). In genomes of robust corals, a *DL-L* gene has been detected only in *Goniastrea aspera* to date (Shinzato et al., 2021a). However, in this study, we identified animal-type *DL-L* genes from four robust corals, including *Cyphastrea serailia*, *Favites colemani*, *Favia lizardensis*, and *Seriatopora caliendrum* (**Figure 4B**; **Table 2**), indicating that *DL-L* genes have been preserved in a variety of complex and robust corals, but were lost from some lineages.

Ancient Origin of DL-L Genes in Cnidarians

Although a large proportion of *DL-L* genes were identified in corals and cnidarians, we also identified similar sequences from non-cnidarian animals, *B. forskalii*, *P. xiphias* and *L. retroversa*. However, none of these share a common ancestry with coral *DL-L* genes (**Figure 3**). Although the origins of these sequences are not clear, we suggest that they may have come from symbiotic/adhesive algae, as in the case of a sequence from *D. frontalis* (**Figure 3**). Based on our phylogenetic analyses using currently available transcriptomic databases, we conclude that, to date, only cnidarians possess *DL-L* genes that are clearly of animal origin. Further addition of more phytoplankton *DL-L* genes may reveal the origins of these from non-cnidarian species.

The Phylum Cnidaria contains three clades (subphyla): Anthozoa (comprising the Octocorallia, Hexacorallia, and Ceriantharia), Endocnidozoa (a clade of parasites) and Medusozoa (consisting of the Cubozoa, Hydrozoa, Scyphozoa, and Staurozoa) (Collins, 2009; Kayal et al., 2018). In this study, we identified eukaryotic *DL-L* genes, not only in the Scleractinia and Corallimorpharia but also in the Zoantharia (Hexacorallia), Alcyonacea (Octocorallia), and Hydrozoa (Anthoathecata, Hydroidolina) (**Figure 4B**; **Table 2**). This indicates that the last common ancestor of Anthozoa and Hydrozoa possessed a *DL-L* gene and that this gene has been inherited in a wide range of cnidarian species. The earliest cnidarian fossils occur in strata of the Ediacaran (560 Ma, Liu et al., 2014), and together with molecular and paleontological analyses, suggest that the phylum Cnidaria probably originated during the Precambrian Eon from the Cryogenian to the Ediacaran (700-595 Ma, Peterson et al., 2004; Erwin et al., 2011). Divergence of 2 major taxa (Anthozoaria and Medusozoa) may have occurred before the Cambrian (543 Ma) (Cartwright et al., 2007; Park et al., 2012). Consequently, we hypothesize that the *DL-L* gene may be have originated from an ancient gene that already existed in the last common ancestor of Cnidaria in the pre-Cambrian (**Figure 4B**).

How did cnidarians, including corals, obtain *DL-L* genes? Shinzato et al. (2021a) hypothesized that *DL-L* genes may have been acquired by the common ancestor of scleractinians and corallimorpharians, both of which are hexacorallians (Anthozoa), *via* horizontal gene transfer from symbiotic Symbiodiniaceae or *Emiliania*. However, as mentioned above, a variety of anthozoans and hydrozoans possess these genes (**Figure 4A**). McFadden et al. (2021) suggested that the Anthozoa probably arose in the Cryogenian to Tonian periods (648-894 Ma) and lacked photosymbionts. In the Devonian (383 Ma) from the Palaeozoic Era, anthozoans of the Scleractinia first formed associations with photosymbionts, followed by alcyonacean octocorals (318 Ma) and corallimorpharians (312 Ma), and photosymbioses have been gained and lost repeatedly in all orders through the Jurassic (199-151 Ma, McFadden et al., 2021). In addition, the fossil record shows that scleractinian corals had photosymbionts in most of the upper Triassic since the Mesozoic Era (Stolarski et al., 2011; Frankowiak et al., 2016). Recent molecular dating estimates suggest that the earliest diversification of the Symbiodiniaceae occurred in the Jurassic (~160 Ma, LaJeunesse et al., 2018) and the first *E. huxleyi* appeared 270,000 years ago (Thierstein et al., 1977; Paasche, 2001), which were much later than the origin of the Anthozoa. Our phylogenetic analysis (**Figure 4**) confirms distinct ancestries of *DL-L* genes in Symbiodiniaceae and cnidarians, indicating that they have completely different evolutionary backgrounds. Therefore, acquisition of *DL-L* genes *via* horizontal gene transfer from symbiotic algae (Shinzato et al., 2021a) may not have occurred. Based on the present findings, we propose an updated hypothesis: *DL-L* genes in cnidarians are "ancient genes" in the animal kingdom, dating back to the pre-Cambrian.

DL-L Genes: Essential for Survival in Coral Reef or Shallow and Warm Water Environments?

As of 10th February 2022, 137 transcriptomic databases from 91 cnidarian species had been registered in NCBI TSA.

Interestingly, we realized that all cnidarian species, except *V. velella*, possessing animal type *DL-L* genes (15 species) are limited to coral reefs (**Table 1**). *V. velella* (**Figure 4**; **Table 2**), known as "by-the-wind sailor", is a cosmopolitan, free-floating, colonial hydrozoan that lives mainly at the water/air interface and floats in temperate and tropical seas (Araya and Aliaga, 2018). This implies that *DL-L* genes may be essential for animals to survive in coral reef or warm, shallow-water environments, although we acknowledge that publicly available transcriptomic databases of cnidarians to date may be limited to coral reef species.

Comparative genomic analysis using reported scleractinian coral genomes showed that *DL-L* genes are the most diversified gene family among gene families that significantly increased number of genes in the last common ancestor of *Acropora* (Shinzato et al., 2021a). Why did gene duplication events of *DL-L gene* specifically occur in the *Acropora* lineage? The earliest fossil records of *Acropora* are known from the late Paleocene (65-54 Ma) in Somalia and Austria (Carbone et al., 1993; Baron-Szabo, 2006), indicating that *Acropora* has existed for more than 50 million years. *Acropora* was the main reef builder in the Oligocene (28-23 Ma) of Greece and Early Miocene of Egypt (Schuster, 2002), and was widely distributed throughout the Miocene in different regions, including the Indo-Pacific and Caribbean (Budd, 2000). It is suggested that *Acropora* began to spread throughout the world in the Cenozoic and species diversification occurred in the Eocene and Oligocene (around 25-50 Ma). Molecular dating analysis using whole-genome data indicates that the *Acropora* ancestor survived warm periods without sea ice from the mid or late Cretaceous to the Early Eocene, when gene expansion of *DL-L* genes occurred specifically in the *Acropora* ancestor (Shinzato et al., 2021a). In addition, *Acropora* species also have high concentrations of DMSP compared to other corals (Broadbent et al., 2002; Guibert et al., 2020), suggesting that *Acropora* corals actively utilize DMSP and that high concentrations of DMSP may have triggered *Acropora*-specific duplication of *DL-L* genes. Several studies have shown that DMSP is involved in a wide range of coral stress responses, including responses to heat, sunlight, air exposure, and hyposalinity (Sunda et al., 2002; Raina et al., 2009; Deschaseaux et al., 2014; Aguilar et al., 2017). Not all *A. digitifera DL-L* genes (5 out of 18) responded to increased sea water temperature and response patterns of differentially expressed genes vary (1 upregulated and 4 downregulated, **Supplementary Table 2**), suggesting that the functions of the *DL-L* genes in *A. digitifera* have also diverged. Taken together, diversified *DL-L* genes in *Acropora* may have acquired new or different functions, not only mediating cleavage of DMSP into DMS, but that they may assist *Acropora* in adapting to environmental changes, for example from intense heat, light, and salinity (Shinzato et al., 2021a). Eventually *Acropora* may become the dominant coral genus in extant coral reefs.

The functions of *DL-L genes* in corals are completely undetermined at this stage. Interestingly, although overexpression of the Alma l genes from *E. huxleyi* and *Symbiodinium* A1 in *E. coli* cells had high DMSP lyase activities, an Alma1 homolog from *A. millepora* showed almost no DMSP lyase activity (Alcolombri et al., 2015), indicating that not all *DL-L* genes in eukaryotes retain their DMSP lyase function, and that acquisition of other functions or functional differentiation may have occurred during the process of gene duplication. In particular, duplicated *DL-L* genes in *Acropora* will need to be investigated to determine which genes have DMSP lyase activity. We identified expressed sequences of *DL-L* genes from *A. digitifera* RNA, and these could be used for molecular and functional characterization in DMSP lyase assays. We also found that expression levels of *DL-L* genes were indeed diverse in *A. digitifera*. Therefore, even if some *DL-L* genes in corals do not function as DMSP lyases, they may have other functions enabling adaptation to coral reef or warm, shallow-water environments. Identifying their actual biological functions in *Acropora* corals will be important to understand not only adaptation mechanisms to shallow and warmer environments, but also the impact of *Acropora* corals on the sulfur cycle in the oceans.

DATA AVAILABILITY STATEMENT

The datasets presented in this study can be found in online repositories. The names of the repository/repositories and accession number(s) can be found in the article/ **Supplementary Material**.

AUTHOR CONTRIBUTIONS

CS conceptualized, commenced and supervised the project. Y-LC performed the lab work, database searches and molecular phylogenetic analyses. Y-LC and CS analyzed the data and wrote the manuscript. All authors contributed to the article and approved the submitted version.

FUNDING

This research was supported with funding from the Japan Society for the Promotion of Science (JSPS) Grants-in-Aid for Scientific Research (KAKENHI) grants (20H03235 and 20K21860) to CS.

ACKNOWLEDGMENTS

This research was supported by a grant from Japan Society for the Promotion of Science (JSPS) Grants-in-Aid for Scientific Research (KAKENHI) grants (20H03235 and 20K21860) to CS.

SUPPLEMENTARY MATERIAL

The Supplementary Material for this article can be found online at: https://www.frontiersin.org/articles/10.3389/fmars.2022.889866/full#supplementary-material

Supplementary Figure 1 | Domain structure of the 13 deduced amino acid sequences of *A. digitifera* and *Emiliania huxleyi*, Alma1 (KR703620.1). Lengths of amino acid sequences are shown at the right and positions of the Asp/Glu/hydantoin racemase superfamily conserved domain are shown in gray boxes. Scale bar=20 aa, aa: the number of amino acids.

Supplementary Figure 2 | Maximum likelihood analysis of *DL-L* genes identified from transcriptomic databases of eukaryotes. A total of 65 *DL-L* genes from prokaryotes and eukaryotes, including *A. digitifera DL-L* genes, were aligned using MAFFT v7.310. Then, 337 gap-trimmed aligned amino acid sequences were used for the phylogenetic analysis. Each species name is followed by a different symbol indicating the taxonomy of the species. The bar indicates 0.5 substitutions per site in aligned regions.

Supplementary Figure 3 | Maximum likelihood analysis of *DL-L* genes identified from transcriptomic databases of cnidarians. A total of 65 *DL-L* genes from cnidaria and prokaryotes including, *A. digitifera DL-L* genes, were aligned using MAFFT v7.310. Then, 337 gap-trimmed aligned amino acid sequences were used for the phylogenetic analysis. Each species name is followed by a different symbol indicating the taxonomy of the species. The bar indicates 0.6 substitutions per site in aligned regions.

Supplementary Table 1 | List of the primers for cloning PCR analysis.

Supplementary Table 2 | Gene expression levels (counts per million) of *Acropora digitifera DL-L* genes in different developmental stages (Shinzato et al., 2021a and Yoshioka et al., 2021) and increased sea water temperature (Shinzato et al., 2021b).

Supplementary Table 3 | *DL-L* genes in Eukaryotes, excluding cnidarians. *Emiliania huxleyi* Alma1 (Accession: KR703620.1) and *Symbiodinium* A1 DMSP lyase (Accession: P0DN22) were used as query sequences in homology searches against the TSA at NCBI using tBlastn (e-value cutoff $1e^{-5}$, query range >70%).

Supplementary Table 4 | *DL-L* genes in cnidarians excluding *Acropora*. *Emiliania huxleyi* Alma1 (Accession: KR703620.1) and *Symbiodinium* A1 DMSP lyase (Accession: P0DN22) were used as query sequences in homology searches against the TSA at NCBI using tBlastn (e-value cutoff $1e^{-5}$, query range >70%).

REFERENCES

Aguilar, C., Raina, J. B., Motti, C. A., Fôret, S., Hayward, D. C., Lapeyre, B., et al. (2017). Transcriptomic Analysis of the Response of *Acropora Millepora* to Hypo-Osmotic Stress Provides Insights Into DMSP Biosynthesis by Corals. *BMC Genomics* 18 (1), 612. doi: 10.1186/s12864-017-3959-0

Ainsworth, T. D., Thurber, R. V., and Gates, R. D. (2010). The Future of Coral Reefs: A Microbial Perspective. *Trends Ecol. Evol.* 25, 233–240. doi: 10.1016/j.tree.2009.11.001

Alcolombri, U., Ben-Dor, S., Feldmesser, E., Levin, Y., Tawfik, D. S., and Vardi, A. (2015). Identification of the Algal Dimethyl Sulfide-Releasing Enzyme: A Missing Link in the Marine Sulfur Cycle. *Science* 348(6242), 1466–1469. doi: 10.1126/science.aab1586

Araya, J., and Aliaga, J. (2018). El Niño Invaders: The Occurrence of the by-the-Wind Sailor *Velella Velella* (Linnaeus 1758) in the Southeastern Pacific. *Spixiana* 14, 132. doi: 10.3800/pbr.14.206

Ayers, G. P., and Gras, J. L. (1991).). Seasonal Relationship Between Cloud Condensation Nuclei and Aerosol Methanesulphonate in Marine Air. *Nature* 353, 834–835. doi: 10.1038/353834a0

Barak-Gavish, N., Frada, M. J., Ku, C., Lee, P. A., DiTullio, G. R., Malitsky, S., et al. (2018). Bacterial Virulence Against an Oceanic Bloom-Forming Phytoplankter is Mediated by Algal DMSP. *Sci. Adv.* 4 (10) eaau5716. doi: 10.1126/sciadv.aau5716

Baron-Szabo, R. C. (2006). Corals of the K/T-Boundary: Scleractinian Corals of the Suborders Astrocoeniina, Faviina, Rhipidogyrina and Amphiastraeina. *J. Syst. Palaeontol.* 4, 1. doi: 10.1017/S1477201905001689

Bray, N. L., Pimentel, H., Melsted, P., and Pachter, L. (2016). Near-Optimal Probabilistic RNA-Seq Quantification. *Nat. Biotechnol.* 34 (5), 525–527. doi: 10.1038/nbt.3519

Broadbent, A. D., and Jones, G. B. (2004). DMS and DMSP in Mucus Ropes, Coral Mucus, Surface Films and Sediment Pore Waters From Coral Reefs in the Great Barrier Reef. *Mar. Freshw. Res.* 55, 849–855. doi: 10.1071/MF04114

Broadbent, A., and Jones, G. (2006). Seasonal and Diurnal Cycles of Dimethylsulfide, Dimethylsulfoniopropionate and Dimethylsulfoxide at One Tree Reef Lagoon. Environ. *Chem. Lett.* 3, 260–267. doi: 10.1071/EN06011

Broadbent, A. D., Jones, G. B., and Jones, R. J. (2002). DMSP in Corals and Benthic Algae From the Great Barrier Reef. *Estuar. Coast. Shelf. Sci.* 55, 547–555. doi: 10.1006/ecss.2002.1021

Budd, A. F. (2000). Diversity and Extinction in the Cenozoic History of Caribbean Reefs. *Coral. Reefs.* 19, 25–35. doi: 10.1007/s003380050222

Capella-Gutiérrez, S., Silla-Martínez, J. M., and Gabaldón, T. (2009). trimAl: A Tool for Automated Alignment Trimming in Large-Scale Phylogenetic Analyses. *Bioinformatics* 25, 1972–1973. doi: 10.1093/bioinformatics/btp348

Carbone, F., Matteucci, R., Pignatti, J. S., and Russo, A. (1993). Facies Analysis and Biostratigraphy of the Auradu Limestone Formation in the Berbera-Sheikh Area, Northwestern Somalia. *Geol. Rom.* 29, 213–235.

Cartwright, P., Halgedahl, S. L., Hendricks, J. R., Jarrard, R. D., Marques, A. C., Collins, A. G., et al. (2007). Exceptionally Preserved Jellyfishes From the Middle Cambrian. *PLoS One* 2, e1121. doi: 10.1371/journal.pone.0001121

Chiu, Y. L., Shikina, S., Yoshioka, Y., Shinzato, C., and Chang, C. F (2020). CDe Novo Transcriptome Assembly From The Gonads of a Scleractinian Coral, Euphyllia Ancora: Molecular Mechanisms Underlying Scleractinian Gametogenesis. *PBMC Genomics* 21 (1), 732. doi: 10.1186/s12864-020-07113-9

Cleves, P. A., Strader, M. E., Bay, L. K., Pringle, J. R., and Matz, M. V. (2018). CRISPR/Cas9-Mediated Genome Editing in a Reef-Building Coral. *Proc. Natl. Acad. Sci. U. S. A.* 115, 5235–5240. doi: 10.1073/pnas.1722151115

Collins, A. G. (2009). Recent Insights Into Cnidarian Phylogeny. *Smithson. Contrib. Mar. Sci.* 38, 139–149.

Curson, A. R., Liu, J., Bermejo Martínez, A., Green, R. T., Chan, Y., Carrión, O., et al. (2017). Dimethylsulfoniopropionate Biosynthesis in Marine Bacteria and Identification of the Key Gene in This Process. *Nat. Microbiol.* 2, 17009. doi: 10.1038/nmicrobiol.2017.9

Curson, A., Williams, B. T., Pinchbeck, B. J., Sims, L. P., Martínez, A. B., Rivera, P., et al. (2018). DSYB Catalyses the Key Step of Dimethylsulfoniopropionate Biosynthesis in Many Phytoplankton. *Nat. Microbiol.* 3, 430–439. doi: 10.1038/s41564-018-0119-5

Davy, S. K., Allemand, D., and Weis, V. M. (2012). Cell Biology of Cnidarian-Dinoflagellate Symbiosis. *Microbiol. Mol. Biol. Rev.* 76 (2), 229–261. doi: 10.1128/MMBR.05014-11

Deschaseaux, E. S., Jones, G. B., Deseo, M. A., Shepherd, K. M., Kiene, R. P., Swan, H. B., et al. (2014). Effects of Environmental Factors on Dimethylated Sulfur Compounds and Their Potential Role in the Antioxidant System of the Coral Holobiont. *Limnol. Oceanogr.* 59 (3), 758–768. doi: 10.4319/lo.2014.59.3.0758

Erwin, D. H., Laflamme, M., Tweedt, S. M., Sperling, E. A., Pisani, D., and Peterson, K. J. (2011). The Cambrian Conundrum: Early Divergence and Later Ecological Success in the Early History of Animals. *Science* 334, 1091–1097. doi: 10.1126/science.1206375

Frankowiak, K., Wang, X. T., Sigman, D. M., Gothmann, A. M., Kitahara, M. V., Mazur, M., et al. (2016). Photosymbiosis and the Expansion of Shallow-Water Corals. *Sci. Adv.* 2, e1601122. doi: 10.1126/sciadv.1601122

Gage, D. A., Rhodes, D., Nolte, K. D., Hicks, W. A., Leustek, T., Cooper, A. J., et al. (1997). A New Route for Synthesis of Dimethylsulphoniopropionate in Marine Algae. *Nature* 387 (6636), 891–894. doi: 10.1038/43160

Gasteiger, E., Gattiker, A., Hoogland, C., Ivanyi, I., Appel, R. D., and Bairoch, A. (2003). ExPASy: The Proteomics Server for In-Depth Protein Knowledge and Analysis. *Nucleic Acids Res.* 31, 3784–3788. doi: 10.1093/nar/gkg563

Goreau, T. F., and Goreau, N. I. (1959). The Physiology of Skeleton Formation in Corals. II. Calcium Deposition by Hermatypic Corals Under Various Conditions in the Reef. *Biol. Bull.* 117, 239–250. doi: 10.2307/1538903

Guibert, I., Bourdreux, F., Bonnard, I., Pochon, X., Dubousquet, V., Raharivelomanana, P., et al. (2020). Dimethylsulfoniopropionate Concentration in Coral Reef Invertebrates Varies According to Species Assemblages. *Sci. Rep.* 10, 9922. doi: 10.1038/s41598-020-66290-5

Hanson, A. D., Rivoal, J., Paquet, L., and Gage, D. A. (1994). Biosynthesis of 3-Dimethylsulfoniopropionate in *Wollastonia Biflora* (L.) DC. (Eevidence That S-Methylmethionine Is an Intermediate). *Plant Physiol.* 105, 103–110. doi: 10.1104/pp.105.1.103

Hill, R. W., White, B. A., Cottrell, M. T., and Dacey, J. W. (1998). Virus-Mediated Total Release of Dimethylsulfoniopropionate From Marine Phytoplankton: A Potential Climate Process. *Aquat. Microb. Ecol.* 14, 1–6. doi: 10.3354/ame014001

Hislop, N. R., de Jong, D., Hayward, D. C., Ball, E. E., and Miller, D. J. (2005). Tandem Organization of Independently Duplicated Homeobox Genes in the Basal Cnidarian *Acropora Millepora*. *Dev. Genes Evol.* 215, 268–273. doi: 10.1007/s00427-005-0468-y

Husband, J. D., Kiene, R. P., and Sherman, T. D. (2012). Oxidation of Dimethylsulfoniopropionate (DMSP) in Response to Oxidative Stress in Spartina Alterniflora and Protection of a Non-DMSP Producing Grass by Exogenous DMSP+ Acrylate. *Environ. Exp. Bot.* 79, 44–48. doi: 10.1016/j.envexpbot.2012.01.006

Karsten, U., Kück, K., Vogt, C., and Kirst, G. O. (1996). "Dimethylsulfoniopropionate Production in Phototrophic Organisms and its Physiological Functions as a Cryoprotectant," in *Biological and Environmental Chemistry of DMSP and Related Sulfonium Compounds*. Eds. M. D. Keller, R. P. Kiene, G. O. Kirst and P. T. Visscher (Boston, MA: Springer), 143–153.

Katoh, K., Misawa, K., Kuma, K. I., and Miyata, T. (2002). MAFFT: A Novel Method for Rapid Multiple Sequence Alignment Based on Fast Fourier Transform. *Nucleic Acids Res.* 30, 3059–3066. doi: 10.1093/nar/gkf436

Katoh, K., and Standley, D. M. (2013). MAFFT Multiple Sequence Alignment Software Version 7: Improvements in Performance and Usability. *Mol. Biol. Evol.* 30 (4), 772–780. doi: 10.1093/molbev/mst010

Kayal, E., Bentlage, B., Sabrina Pankey, M., Ohdera, A. H., Medina, M., Plachetzki, D. C., et al. (2018). Phylogenomics Provides a Robust Topology of the Major Cnidarian Lineages and Insights on the Origins of Key Organismal Traits. *BMC Evol. Biol.* 18, 1–18. doi: 10.1186/s12862-018-1142-0

Keller, M. D., Bellows, W. K., and Guillard, R. R. L. (1989). "Dimethylsulfide Production in Marine Phytoplankton," in *Biogenic Sulfur in the Environment*. Eds. E. S. Saltzman and W. J. Cooper (Washington, DC: American Chemical Society), 167–182.

Kettles, N. L., Kopriva, S., and Malin, G. (2014). Insights Into the Regulation of DMSP Synthesis in the Diatom *Thalassiosira Pseudonana* Through APR Activity, Proteomics and Gene Expression Analyses on Cells Acclimating to Changes in Salinity, Light and Nitrogen. *PLoS One* 9, e94795. doi: 10.1371/journal.pone.0094795

Kirst, G. O., Thiel, C., Wolff, H., Nothnagel, J., Wanzek, M., and Ulmke, R. (1991). Dimethylsulfoniopropionate (DMSP) in Icealgae and its Possible Biological Role. *Mar. Chem.* 35 (1-4), 381–388. doi: 10.1016/S0304-4203(09)90030-5

Kitahara, M. V., Fukami, H., Benzoni, F., and Huang, D. (2016). "The New Systematics of Scleractinia: Integrating Molecular and Morphological Evidence," in *The Cnidaria, Past, Present and Future*. Eds. S. Goffredo and Z. Dubinsky (Switzerland: Springer), 41–59.

Knowlton, N., Brainard, R. E., Fisher, R., Moews, M., Plaisance, L., and Caley, M. J. (2010). Coral Reef Biodiversity. *Life World's Oceans: Diversity Distribution Abundance*, editor A. McIntyre (Wiley-Blackwell: Oxford), 65–7465–74. doi: 10.1002/9781444325508.ch4

Kocsis, M. G., Nolte, K. D., Rhodes, D., Shen, T. L., Gage, D. A., and Hanson, A. D. (1998). Dimethylsulfoniopropionate Biosynthesis in Spartina Alterniflora1. Evidence That S-Methylmethionine and Dimethylsulfoniopropylamine Are Intermediates. *Plant Physiol.* 117, 273–281. doi: 10.1104/pp.117.1.273

LaJeunesse, T. C., Parkinson, J. E., Gabrielson, P. W., Jeong, H. J., Reimer, J. D., Voolstra, C. R., et al. (2018). Systematic Revision of Symbiodiniaceae Highlights the Antiquity and Diversity of Coral Endosymbionts. *Curr. Biol.* 28, 2570–2580. doi: 10.1016/j.cub.2018.07.008

Lesser, M. P. (2006). Oxidative Stress in Marine Environments: Biochemistry and Physiological Ecology. *Annu. Rev. Physiol.* 68, 253–278. doi: 10.1146/annurev.physiol.68.040104.110001

Li, H. (2018). Minimap2: Pairwise Alignment for Nucleotide Sequences. *Bioinformatics* 34 (18), 3094–3100. doi: 10.1093/bioinformatics/bty191

Liu, A. G., Matthews, J. J., Menon, L. R., McIlroy, D., and Brasier, M. D. (2014). Haootia Quadriformis N. Gen. N. sp. Interpreted Muscular Cnidarian Impression Late Ediacaran Period (Approx. 560 Ma). *Proc. R. Soc. B.: Biol. Sci.* 281 (1793), 20141202. doi: 10.1098/rspb.2014.1202

Li, C. Y., Wang, X. J., Chen, X. L., Sheng, Q., Zhang, S., Wang, P., et al. (2021). A Novel ATP Dependent Dimethylsulfoniopropionate Lyase in Bacteria That Releases Dimethyl Sulfide and Acryloyl-CoA. *eLife* 10, e64045. doi: 10.7554/eLife.64045

Lyon, B. R., Lee, P. A., Bennett, J. M., DiTullio, G. R., and Janech, M. G. (2011). Proteomic Analysis of a Sea-Ice Diatom: Salinity Acclimation Provides New Insight Into the Dimethylsulfoniopropionate Production Pathway. *Plant Physiol.* 157, 1926–1941. doi: 10.1104/pp.111.185025

Maor-Landaw, K., and Levy, O. (2016). "Survey of Cnidarian Gene Expression Profiles in Response to Environmental Stressors: Summarizing 20 Years of Research, What are We Heading for?," in *The Cnidaria, Past, Present and Future*. Eds. S. Goffredo and Z. Dubinsky (Switzerland: Springer), 523–543.

Martin, M. (2011). Cutadapt Removes Adapter Sequences From High-Throughput Sequencing Reads. *EMBnet. J.* 17 (1), 10–12. doi: 10.14806/ej.17.1.200

McCarthy, D. J., Chen, Y., and Smyth, G. K. (2012). Differential Expression Analysis of Multifactor RNA-Seq Experiments With Respect to Biological Variation. *Nucleic Acids Res.* 40 (10), 4288–4297. doi: 10.1093/nar/gks042

McFadden, C. S., Quattrini, A. M., Brugler, M. R., Cowman, P. F., Dueñas, L. F., Kitahara, M. V., et al. (2021). Phylogenomics, Origin, and Diversification of Anthozoans (Phylum Cnidaria). *Syst. Biol.* 70, 635–647. doi: 10.1093/sysbio/syaa103

Miller, T. R., and Belas, R. (2004). Dimethylsulfoniopropionate Metabolism by Pfiesteria-Associated *Roseobacter* Spp. *Appl. Environ. Microbiol.* 70, 3383–3391. doi: 10.1128/AEM.70.6.3383-3391.2004

Muscatine, L. (1990). The Role of Symbiotic Algae in Carbon and Energy Flux in Reef Corals. *Coral. Reefs.* 25, 1–29.

Muscatine, L. E. O. N. A. R. D., and Porter, J. W. (1977). Reef Corals: Mutualistic Symbioses Adapted to Nutrient-Poor Environments. *Bioscience* 27, 454–460. doi: 10.2307/1297526

Niki, T., Kunugi, M., and Otsuki, A. (2000). DMSP-Lyase Activity in Five Marine Phytoplankton Species: Its Potential Importance in DMS Production. *Mar. Biol.* 136, 759–764. doi: 10.1007/s002279900235

Paasche, E. (2001). A Review of the Coccolithophorid *Emiliania Huxleyi* (Prymnesiophyceae), With Particular Reference to Growth, Coccolith Formation, and Calcification-Photosynthesis Interactions. *Phycologia* 40 (6), 503–529. doi: 10.2216/i0031-8884-40-6-503.1

Paquet, L., Rathinasabapathi, B., Saini, H., Zamir, L., Gage, D. A., Huang, Z. H., et al. (1994). Accumulation of the Compatible Solute 3-Dimethylsulfoniopropionate in Sugarcane and its Relatives, But Not Other Gramineous Crops. *Funct. Plant Biol.* 21, 37–48. doi: 10.1071/PP9940037

Park, E., Hwang, D. S., Lee, J. S., Song, J. I., Seo, T. K., and Won, Y. J. (2012). Estimation of Divergence Times in Cnidarian Evolution Based on Mitochondrial Protein-Coding Genes and the Fossil Record. *Mol. Phylogenet. Evol.* 62 (1), 329–345. doi: 10.1016/j.ympev.2011.10.008

Peterson, K. J., Lyons, J. B., Nowak, K. S., Takacs, C. M., Wargo, M. J., and McPeek, M. A. (2004). Estimating Metazoan Divergence Times With a Molecular Clock. *Proc. Natl. Acad. Sci. U. S. A.* 101 (17), 6536–6541. doi: 10.1073/pnas.0401670101

Qin, Z., Yu, K., Chen, B., Wang, Y., Liang, J., Luo, W., et al. (2019). Diversity of Symbiodiniaceae in 15 Coral Species From the Southern South China Sea: Potential Relationship With Coral Thermal Adaptability. *Front. Microbiol.* 10, 2343. doi: 10.3389/fmicb.2019.02343

Quinn, P. K., and Bates, T. S. (2011). The Case Against Climate Regulation *via* Oceanic Phytoplankton Sulphur Emissions. *Nature* 480 (7375), 51–56. doi: 10.1038/nature10580

Rädecker, N., Pogoreutz, C., Voolstra, C. R., Wiedenmann, J., and Wild, C. (2015). Nitrogen Cycling in Corals: The Key to Understanding Holobiont Functioning? *Trends Microbiol.* 23, 490–497. doi: 10.1016/j.tim.2015.03.008

Raina, J. B., Tapiolas, D. M., Forêt, S., Lutz, A., Abrego, D., Ceh, J., et al. (2013). DMSP Biosynthesis by an Animal and its Role in Coral Thermal Stress Response. *Nature* 502 (7473), 677–680. doi: 10.1038/nature12677

Raina, J. B., Tapiolas, D., Willis, B. L., and Bourne, D. G. (2009). Coral-Associated Bacteria and Their Role in the Biogeochemical Cycling of Sulfur. *Appl. Environ.* 75, 3492–3501. doi: 10.1128/AEM.02567-08

Reisch, C. R., Moran, M. A., and Whitman, W. B. (2011). Bacterial Catabolism of Dimethylsulfoniopropionate (DMSP). *Front. Microbiol.* 2, 172. doi: 10.3389/fmicb.2011.00172

Robinson, M. D., McCarthy, D. J., and Smyth, G. K. (2010). Edger: A Bioconductor Package for Differential Expression Analysis of Digital Gene Expression Data. *Bioinformatics* 26 (1), 139–140. doi: 10.1093/bioinformatics/btp616

Rohwer, F., Seguritan, V., Azam, F., and Knowlton, N. (2002). Diversity and Distribution of Coral-Associated Bacteria. *Mar. Ecol. Prog. Ser.* 243, 1–10. doi: 10.3354/meps243001

Romano, S. L., and Cairns, S. D. (2000). Molecular Phylogenetic Hypotheses for the Evolution of Scleractinian Corals. *Bull. Mar. Sci.* 67 (3), 1043–1068.

Romano, S. L., and Palumbi, S. R. (1996). Evolution of Scleractinian Corals Inferred From Molecular Systematics. *Science* 271 (5249), 640–642. doi: 10.1126/science.271.5249.640

Schuster, F. (2002). *Taxonomy of Oligocene to Early Miocene Scleractinian Corals-From Iran, Egypt, Turkey and Greece*. Courier Forschungsinst: Senckenberg. 239, 1–3.

Shemi, A., Alcolombri, U., Schatz, D., Farstey, V., Vincent, F., Rotkopf, R., et al. (2021). Dimethyl Sulfide Mediates Microbial Predator-Prey Interactions Between Zooplankton and Algae in the Ocean. *Nat. Microbiol.* 6 (11), 1357–1366. doi: 10.1038/s41564-021-00971-3

Shinzato, C., Khalturin, K., Inoue, J., Zayasu, Y., Kanda, M., Kawamitsu, M., et al. (2021a). Eighteen Coral Genomes Reveal the Evolutionary Origin of *Acropora* Strategies to Accommodate Environmental Changes. *Mol. Biol. Evol.* 38, 16–30. doi: 10.1093/molbev/msaa216

Shinzato, C., Shoguchi, E., Kawashima, T., Hamada, M., Hisata, K., Tanaka, M., et al. (2011). Using the *Acropora Digitifera* Genome to Understand Coral Responses to Environmental Change. *Nature* 476, 320–323. doi: 10.1038/nature10249

Shinzato, C., Takeuchi, T., Yoshioka, Y., Tada, I., Kanda, M., Broussard, C., et al. (2021b). Whole-Genome Sequencing Highlights Conservative Genomic Strategies of a Stress-Tolerant, Long-Lived Scleractinian Coral, *Porites Australiensis* Vaughan 1918. *Genome Biol. Evol.* 13 (12), evab270. doi: 10.1093/gbe/evab270

Stamatakis, A. (2014). RAxML Version 8: A Tool for Phylogenetic Analysis and Post-Analysis of Large Phylogenies. *Bioinformatics* 30, 1312–1313. doi: 10.1093/bioinformatics/btu033

Stanley,G. D.Jr. (2003). The Evolution of Modern Corals and Their Early History. *Earth Sci. Rev.* 60, 195–225. doi: 10.1016/S0012-8252(02)00104-6

Stefels, J., Dijkhuizen, L., and Gieskes, W. W. C. (1995). DMSP-Lyase Activity in a Spring Phytoplankton Bloom Off the Dutch Coast, Related to *Phaeocystis* Sp. Abundance. *Mar. Ecol. Prog. Ser.* 123, 235–243. doi: 10.3354/meps123235

Stefels, J., Steinke, M., Turner, S., Malin, G., and Belviso, S. (2007). Environmental Constraints on the Production and Removal of the Climatically Active Gas Dimethylsulphide (DMS) and Implications for Ecosystem Modelling. *Biogeochemistry* 83 (1), 245–275. doi: 10.1007/s10533-007-9091-5

Steinke, M., and Kirst, G. O. (1996). Enzymatic Cleavage of Dimethylsulfoniopropionate (DMSP) in Cell-Free Extracts of the Marine Macroalga *Enteromorpha Clathrata* (Roth) Grev. (Ulvales, Chlorophyta). *J. Exp. Mar. Biol. Ecol.* 201 (1-2), 73–85. doi: 10.1016/0022-0981(95)00207-3

Steinke, M., Wolfe, G. V., and Kirst, G. O. (1998). Partial Characterisation of Dimethylsulfoniopropionate (DMSP) Lyase Isozymes in 6 Strains of *Emiliania Huxleyi*. *Mar. Ecol. Prog. Ser.* 175, 215–225. doi: 10.3354/meps175215

Stolarski, J., Kitahara, M. V., Miller, D. J., Cairns, S. D., Mazur, M., and Meibom, A. (2011). The Ancient Evolutionary Origins of Scleractinia Revealed by Azooxanthellate Corals. *BMC Evol. Biol.* 11, 1–11. doi: 10.1186/1471-2148-11-316

Strom, S., Wolfe, G., Holmes, J., Stecher, H., Shimeneck, C., and Sarah, L. (2003). Chemical Defense in the Microplankton I: Feeding and Growth Rates of Heterotrophic Protists on the DMS-Producing Phytoplankter *Emiliania Huxleyi*. *Limnol. Oceanogr.* 48 (1), 217–229. doi: 10.4319/lo.2003.48.1.0217

Sunda, W. K. D. J., Kieber, D. J., Kiene, R. P., and Huntsman, S. (2002). An Antioxidant Function for DMSP and DMS in Marine Algae. *Nature* 418, 317–320. doi: 10.1038/nature00851

Swan, H. B., Jones, G. B., and Deschaseaux, E. (2012). "Dimethylsulfide, Climate and Coral Reef Ecosystems," in *Proc. 12th Int. Coral Reef Symp*, 9–13. Townsville, Qld: James Cook University

Teng, Z. J., Wang, P., Chen, X. L., Guillonneau, R., Li, C. Y., Zou, S. B., et al. (2021). Acrylate Protects a Marine Bacterium From Grazing by a Ciliate Predator. *Nat. Microbiol.* 6 (11), 1351–1356. doi: 10.1038/s41564-021-00981-1

Thierstein, H. R., Geitzenauer, K. R., Molfino, B., and Shackleton, N. J. (1977). Global Synchroneity of Late Quaternary Coccolith Datum Levels Validation by Oxygen Isotopes. *Geology* 5 (7), 400–404. doi: 10.1130/0091-7613(1977)5<400:GSOLQC>2.0.CO;2

Vallina, S. M., and Simó, R. (2007). Strong Relationship Between DMS and the Solar Radiation Dose Over the Global Surface Ocean. *Science* 315 (5811), 506–508. doi: 10.1126/science.1133680

Van Boekel, J. S. W., and Stefels, W. H. M. (1993). Production of DMS From Dissolved DMSP in Axenic Cultures of the Marine Phytoplankton Species Phaeocystis Sp. *Mar. Ecol. Prog. Ser.* 97, 11–18. doi: 10.3354/meps097011

van Oppen, M. J., McDonald, B. J., Willis, B., and Miller, D. J. (2001). The Evolutionary History of the Coral Genus *Acropora* (Scleractinia, Cnidaria) Based on a Mitochondrial and a Nuclear Marker: Reticulation, Incomplete Lineage Sorting, or Morphological Convergence? *Mol. Biol. Evol.* 18, 1315–1329. doi: 10.1093/oxfordjournals.molbev.a003916

Veron, J. E. N. (2000). *Corals of the World*. Vol. 1-3. (Townsville Queensland: Australian Institute of Marine Science).

Wallace, C. C. (1999). "Staghorn Corals of the World: A Revision of the Coral Genus Acropora (Scleractinia; Astrocoeniina; Acroporidae) Worldwide," in *With Emphasis on Morphology, Phylogeny and Biogeography* (Melbourne: CSIRO Publishing).

Wallace, C. C., and Rosen, B. R. (2006). Diverse Staghorn Corals (*Acropora*) in High-Latitude Eocene Assemblages: Implications for the Evolution of Modern Diversity Patterns of Reef Corals. *Proc. Biol. Sci.* 273 (1589), 975–982. doi: 10.1098/rspb.2005.3307

Wolfe, G. V., and Steinke, M. (1996). Grazing-Activated Production of Dimethyl Sulfide (DMS) by Two Clones of Emiliania Huxleyi. *Limnol. Oceanogr.* 41 (6), 1151–1160. doi: 10.4319/lo.1996.41.6.1151

Wolfe, G. V., Steinke, M., and Kirst, G. O. (1997). Grazing-Activated Chemical Defence in a Unicellular Marine Alga. *Nature* 387 (6636), 894–897. doi: 10.1038/43168

Woodhouse, M. T., Carslaw, K. S., Mann, G. W., Vallina, S. M., Vogt, M., Halloran, P. R., et al. (2010). Low Sensitivity of Cloud Condensation Nuclei to Changes in the Sea-Air Flux of Dimethyl-Sulphide. *Atmos. Chem. Phys.* 10 (16), 7545–7559. doi: 10.5194/acp-10-7545-2010

Yasuoka, Y., Shinzato, C., and Satoh, N. (2016). The Mesoderm-Forming Gene Brachyury Regulates Ectoderm-Endoderm Demarcation in the Coral *Acropora Digitifera*. *Curr. Biol.* 26 (21), 2885–2892. doi: 10.1016/j.cub.2016.08.011

Ying, H., Hayward, D. C., Cooke, I., Wang, W., Moya, A., Siemering, K. R., et al. (2019). The Whole-Genome Sequence of the Coral *Acropora Millepora*. *Genome Biol. Evol* 11 (5), 1374–1379. doi: 10.1093/gbe/evz077

Yoch, D. C. (2002). Dimethylsulfoniopropionate: Its Sources, Role in the Marine Food Web, and Biological Degradation to Dimethylsulfide. *Appl. Environ. Microbiol.* 68 (12), 5804–5815. doi: 10.1128/AEM.68.12.5804-5815.2002

Yoshioka, Y., Yamashita, H., Suzuki, G., Zayasu, Y., Tada, I., Kanda, M., et al. (2021). Whole-Genome Transcriptome Analyses of Native Symbionts Reveal

Host Coral Genomic Novelties for Establishing Coral-Algae Symbioses. *Genome Biol. Evol.* 13 (1), evaa240. doi: 10.1093/gbe/evaa240

Conflict of Interest: The authors declare that the research was conducted in the absence of any commercial or financial relationships that could be construed as a potential conflict of interest.

Publisher's Note: All claims expressed in this article are solely those of the authors and do not necessarily represent those of their affiliated organizations, or those of the publisher, the editors and the reviewers. Any product that may be evaluated in this article, or claim that may be made by its manufacturer, is not guaranteed or endorsed by the publisher.

frontiers | Frontiers in Marine Science

ORIGINAL RESEARCH
published: 17 June 2022
doi: 10.3389/fmars.2022.900679

Coral Reef Coupling to the Atmospheric Boundary Layer Through Exchanges of Heat, Moisture, and Momentum: Case Studies From Tropical and Desert Fringing Coral Reefs

Hamish McGowan[1]*, *Nadav G. Lensky*[2,3], *Shai Abir*[2,3] *and Melissa Saunders*[1]

[1] Atmospheric Observations Research Group, The University of Queensland, Brisbane, QLD, Australia, [2] Geological Survey of Israel, Jerusalem, Israel, [3] Hebrew University of Jerusalem, Jerusalem, Israel

OPEN ACCESS

Edited by:
Graham Barry Jones,
Southern Cross University, Australia

Reviewed by:
Steven Siems,
Monash University, Australia
Małgorzata Kitowska,
Polish Academy of Sciences, Poland

***Correspondence:**
Hamish McGowan
h.mcgowan@uq.edu.au

Specialty section:
This article was submitted to Coral Reef Research, a section of the journal Frontiers in Marine Science

Received: 21 March 2022
Accepted: 19 May 2022
Published: 17 June 2022

Citation:
McGowan H, Lensky NG, Abir S and Saunders M (2022) Coral Reef Coupling to the Atmospheric Boundary Layer Through Exchanges of Heat, Moisture, and Momentum: Case Studies From Tropical and Desert Fringing Coral Reefs. Front. Mar. Sci. 9:900679. doi: 10.3389/fmars.2022.900679

Coral reefs represent abrupt changes in surface roughness, temperature, and humidity in oceanic and coastal locations. This leads to formation of internal atmospheric boundary layers that grow vertically in response to turbulent mixing which conveys changes in surface properties into the prevailing wind. As a result, coral reefs under favourable conditions couple to the overlying atmosphere. Here we present rare observations of coral reef – atmospheric interactions during summer monsoon conditions on the Great Barrier Reef, Australia, and a desert fringing coral reef in the Gulf of Eilat, Israel. We show that in the hyper-arid location of the Gulf of Eilat where air temperatures are greater than water temperatures, a stable atmospheric boundary inhibits coupling of the reef to the atmosphere. In contrast, under monsoon conditions on the Great Barrier Reef, the coral reef is shown to couple to the overlying atmosphere leading to the formation of a convective internal boundary layer in which convective exchange of heat and moisture influences cloud and possibly precipitation. We conclude that understanding these processes is essential for determining the role of coral reefs in coastal meteorology, and whether through coupling with the overlying atmosphere coral reefs may regulate their meteorology by triggering formation of cloud and/or vertical exchange on aerosols and their precursor gases such as Dimethyl sulphide.

Keywords: atmosphere, energy balance, Great Barrier Reef, Gulf of Eilat, cloud, boundary layers

INTRODUCTION

Coral reefs represent pronounced transitions in water temperature, roughness and humidity in coastal and oceanic settings. These changes propagate vertically into the atmosphere leading to formation of convective internal atmospheric boundary-layers (CIBL) within the marine atmospheric boundary layer (MBL) (Garratt, 1990; Garratt, 1994). The magnitude of coral reef coupling to the atmosphere through air-sea exchanges of sensible (Qh) and latent heat flux (Qe),

and momentum flux (τ) is dependent on time of day, season, and prevailing synoptic meteorology as observed over land in CIBLs (Garratt, 1990; Mahrt, 2000). Additionally, over coral reefs, tides influence water temperature with midday to afternoon low tides typically coinciding with higher daytime water temperatures, while high tides bring cooler ocean water over coral reefs. In oceanic settings, the shallower water of coral reefs results in reduced wave height and surface roughness, potentially causing higher windspeeds. For example, MacKellar et al. (2012a) reported roughness lengths for Heron Reef on the southern Great Barrier Reef (GBR), Australia of 0.00018 to 0.00038 m compared to values often quoted for deeper ocean water which may range from 0.0002 to 0.006 m (Golbazi and Archer, 2019; He et al., 2021). Fringing coral reefs bordering coasts may also experience acceleration of wind as air moves from the aerodynamically rough land to the smoother water surface during offshore flow (Garratt, 1990; Vickers et al., 2001). At low tide, exposed reef rims and reef flats where coral bommies and debris from tropical storms surmount the reef, the frictional effects of the reefs surface on the lower atmosphere are greatest causing turbulence. Collectively, such surface heterogeneity over coral reefs is likely to influence the vertical diffusion of heat, water vapour, aerosols, and gases such as CO_2 and Dimethyl sulphide (DMS).

DMS is a naturally occurring aerosol precursor gas, which can be produced by corals and their symbionts. DMS affects the global sulphur budget and aerosol formation which it has been claimed may modify climate through direct and indirect forcing of the surface radiation budget (Charlson et al., 1987). Cropp et al. (2018) considered such bioclimatic feedback as a potential defence mechanism against thermal stress induced coral bleaching. Observations from One Tree Reef on the southern GBR by Broadbent and Jones (2006) found the highest concentrations were recorded during summer, while Swan et al. (2016) at nearby Heron Reef observed DMS peaks coincided with low tides and low wind speeds as did Cropp et al. (2018). However, recent numerical modelling by Fiddes et al. (2021a) using the coupled climate–chemistry model ACCESS-UKCA, found no clear evidence that coral reef derived DMS has any significant impact on the meteorology of coral reefs. A subsequent study by Fiddes et al. (2022) using the WRF-Chem model also found no impact by local DMS over the GBR. They suggested air contaminants from terrestrial sources where more influential in addition to aerosolised sea salt emissions and their impact on atmospheric turbidity and cloud microphysics.

The influence coral reefs exert on the overlying atmosphere is dependent on exchanges of energy, aerosol, and gases across their air-sea interfacial boundary, and then through the CIBL. CIBL formation above coral reefs which MacKellar et al. (2013) named the convective reef layer (CRL) occurs within the marine boundary layer (MBL) in response to air-sea turbulent flux exchanges. MacKellar et al. (2013) observed the CRL to develop in response to positive surface turbulent energy fluxes, particularly heat (Qh) causing the near surface reef atmospheric boundary layer to transition from a stable nocturnal early morning profile to an unstable daytime profile from mid-morning. Clayson and Edson (2019) using satellite and buoy data from the Gulf Stream and Kuroshio Extension found a diurnal cycle in mean wind speeds which were faster and more humid over warmer SSTs. They hypothesised this was the result of greater latent heat (Qe) exchange caused by winds entraining moisture. Accordingly, CRL development can be considered analogous to a terrestrial CIBL, where following sunrise downwelling shortwave (solar) radiation increases the surface temperature resulting in an increase in Qh. Resulting convective diffusion of Qh and Qe, as well as entrained gases and aerosols subsequently occur as wind speeds increase causing additional turbulent mixing.

Here we present observations from the humid tropical/subtropical Heron Reef on the southern GBR, Australia and the fringing coral reef bordering the hyper-arid desert of the northern Gulf of Eilat (GoE), Israel of air – sea exchanges of turbulent energy fluxes, associated meteorology and atmospheric boundary layers. These rare observations begin to shed light on the meteorology of coral reefs in different climatic zones and their influence on the overlying atmosphere. They are essential to inform debate on the role of coral reefs in marine and coastal meteorology and possible bioclimatic feedback processes such as cloud development. Recommendations for future research priorities are then made to advance understanding of the role of coral reefs in local to mesoscale meteorology.

RESEARCH SETTINGS – HERON REEF AND GULF OF EILAT

Heron Reef is located on the southern GBR, Australia (**Figure 1D**) and the desert fringing coral reef in the northern GoE, Israel (**Figure 1A**). The contrasting meteorology of these two locations being a humid marine tropical/subtropical environment and coastal hyper-arid location respectively, represent extremes in heat and moisture experienced by coral reefs and their air-sea exchanges of sensible and latent heat fluxes.

Heron Reef

Heron Reef is one of more than 2,900 coral reefs that make up the GBR, the world's largest emergent reef system covering ~345,950 km^2 (Woodroffe, 2003). It is located on the southern GBR around 80 km northeast of the township Gladstone on the northeast coast of Australia. The reef is a typical lagoonal platform reef covering ~27 km^2, as it extends south-eastward from Heron Island, which is located on the northwest margin of the reef (**Figure 1D**). Annual rainfall at Heron Reef is ~1,050 mm, with the majority of precipitation occurring during summer (December to February) coinciding with the Australian monsoon, and in autumn (March to May). June to September is the driest period of the year when anticyclones track east across the Australian continent and bring mostly calm and settled conditions to the area. The wind regime of Heron Reef is dominated by the south-easterly trade winds, while wind direction becomes more variable in summer with the

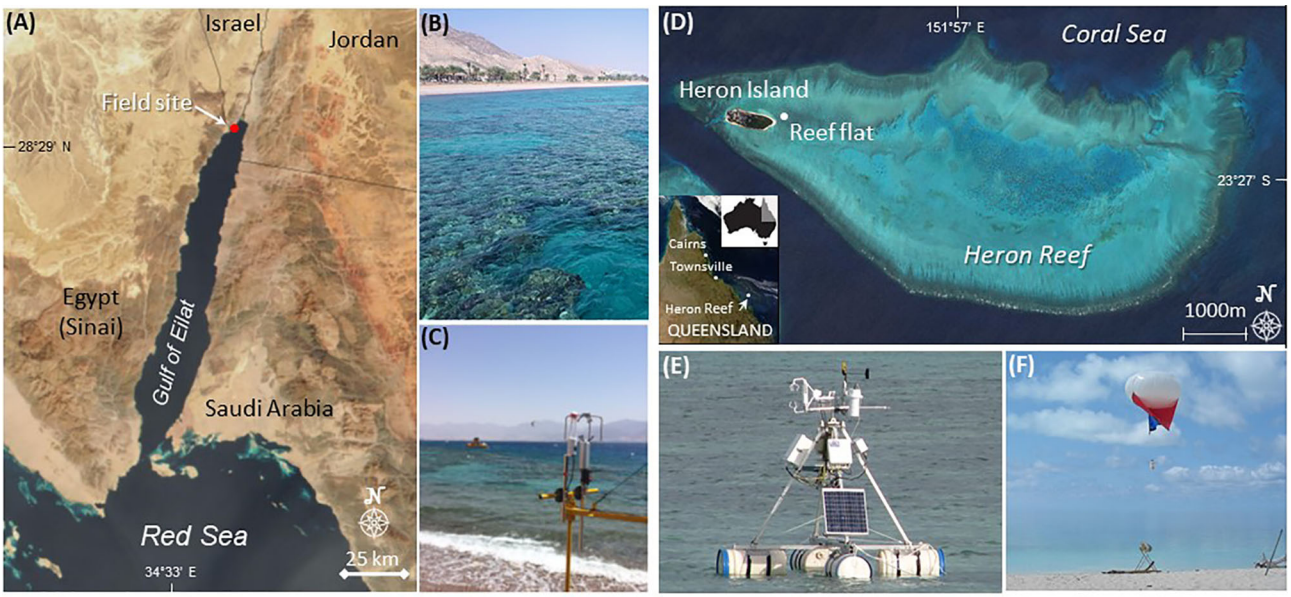

FIGURE 1 | Gulf of Eilat location map (*Google Earth*, earth.google.com/web/) and eddy covariance field site **(A)**; desert fringing coral reef, Eilat **(B)**; shoreline eddy covariance system, Eilat **(C)**; Heron Reef location map (Satellite image from the Ikonos satellite provided by DigitalGlobe and Centre for Spatial Environmental Research) with reef flat eddy covariance site indicated **(D)**; pontoon eddy covariance system, reef flat, Heron Reef **(E)**, helikite sounding system on shore of Heron Reef **(F)**.

occurrence of occasional strong northeasterlies, although south-easterly winds still dominate. The strongest winds are associated with the passage of tropical cyclones during the summer. The highest mean daily maximum air temperature occurs in January at 29.8°C, with the lowest mean daily minimum air temperature in July at 16.7°C (McGowan et al., 2010; MacKellar et al., 2012a).

The major geomorphic zones on Heron Reef are the reef flat, shallow, and deep lagoons which, respectively, cover 32%, 16%, and 12% of the total reef surface. The remaining area of Heron Reef is composed of the outer reef flat, reef slope, reef crest and the coral cay, which cover 20%, 13%, 6%, and 1%, respectively. The coral *Acropora* spp. is prevalent in the deeper waters of the reef system along with the massive corals *Porites* spp. on the reef flat. Heron Reef experiences semidiurnal tides with a spring and neap tidal range of 2.28 and 1.09 m (Chen and Krol, 1997). Wave height on the reef flat is typically <0.5 m under a mean wind speed of 5 ms^{-1}, and wave heights are <0.6 times the maximum water level (Gourlay, 1988). When the tide is higher than the reef rim, oceanic waves may travel across the reef flat, resulting in the regional wave climate being the key control of wave action. Occasionally, wind waves are superimposed on low to moderate sea swell produced by the prevailing south-easterly trade winds. Cyclonic storms during late summer that are concurrent with king tides may cause large waves to travel over the reef.

Gulf of Eilat

The GoE is an almost rectangular region roughly 6 × 10 km with steep lateral boundaries with a maximum depth of nearly 800 m (Carlson et al., 2012) in the northern Red Sea (**Figure 1A**). During the summer months, June-September, the lower level atmosphere in the region is dominated by the Persian Trough, which extends from the Asian monsoon region through the Persian Gulf (Alpert et al., 1990; Bitan and Sa'Aroni, 1992), generating winds from the northwest. Desert mountains located around the Ha'Arava Rift valley channel winds onto the northeast GoE with an average daytime speed of 5-7 m s^{-1} bringing hot and dry air.

The highest mean daily maximum air temperature occurs in July at 40°C with the lowest mean daily minimum air temperature occurring in January at 5.9°C. Annual mean total rainfall is 24 mm while >3350 hrs of sunshine occur highlighting the hyper-arid desert climate of the region. Mean daily water surface temperature (1988 to 2020) varies from around ~21°C during February to March (Shaked and Genin, 2020) peaking at ~28°C from July to September. Mean water depth at the field site from which measurements are discussed here on the northwest shoreline of the GoE over the reef table is 0.5 m. Mean tidal range during the observation period was 0.35 m, with a semi-diurnal cycle.

Coral coverage area is 28%, rock 15%, dead coral 10% and the remainder being substrate comprised of sand and shell fragments (Shaked and Genin, 2019). Coral taxa along the coast is highly diverse with the back-reef lagoon dominated by *Stylophora pistillata*, while in the forereef more than 40 coral genera are regularly identified, with the most common comprising of *Stylophora*, *Acropora*, *Montipora*, *Echinopora*, *Cyphastrea*, *Goniastrea*, *Porites* and *Dipsastrea*. Coral coverage averages approximately 25% with rock making up around 20%, dead coral 5% and the remaining being loose substrate of sand and shell fragments (Shaked and Genin, 2020) (**Figure 1B**). The shoreline current is predominantly from north to south in

response to prevailing northerly winds, with a semidiurnal and diurnal barotropic tide range of around 1 m (Shaked and Genin, 2019).

CORAL REEF – ATMOSPHERE FORCINGS

Reefs in the Humid Tropics/Subtropics: Case Study Heron Reef

Direct measurements air-sea energy exchanges over Heron Reef were made using an eddy covariance (EC) system mounted on a pontoon (MacKellar et al., 2013; McGowan et al., 2019) (**Figure 1E**). The EC included a Campbell Scientific CSAT-3 sonic anemometer, Li-Cor CS7500 open-path H_2O and CO_2 analyzer, a Kipp and Zonen CNR1 net radiometer (NR-Lite net radiometer by Kipp & Zonen) with additional sensors measuring water and air temperature, atmospheric pressure and relative humidity (MacKellar et al., 2012a; MacKellar et al., 2013). The EC instruments were controlled by a Campbell Scientific CR23X data logger with measurements made at 10 Hz with 15 minutes block averages recorded. Vertical profiles up to ~500 m asl. of air temperature, humidity, wind speed and direction were obtained using a Kestrel 4500 weather monitor tethered to a kite when wind speeds exceeded 5 ms^{-1}, or to a helium-inflated Helikite (**Figure 1F**) at lower wind speeds with measurements logged every 10 s (MacKellar et al., 2013). In 2009 a Vaisala ceilometer CL31 was also deployed at Heron Island to monitor cloud, aerosol and boundary layer height (Kotthaus et al., 2016) with a vertical measurement resolution of approximately 10 m.

Fair Weather Air-Sea Exchanges

Measurements of the daytime surface energy balance by EC over the reef flat on Heron Reef (151°55.203 E, 23°26.573 S) were made on the 4 February 2008 under settled fair weather conditions associated with a ridge of high pressure extending along the east Australian coast (**Figure 2A**). Winds were light ranging from 2 to 5 ms^{-1} with cloud cover varying throughout the day from 4/8 to 8/8 consisting of stratocumulus, cirrostratus in the morning with embedded cumulus in the prevailing easterly airstream. Review of available satellite imagery showed

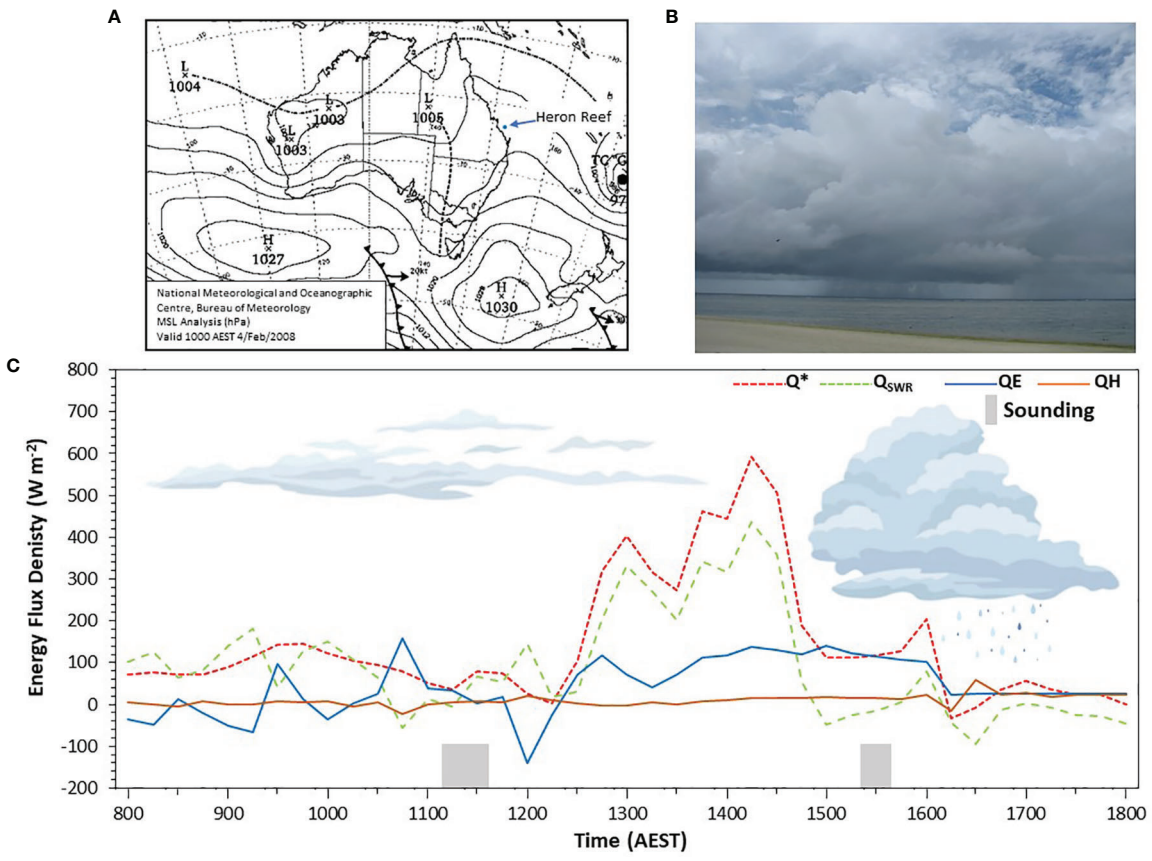

FIGURE 2 | Mean Sea Level Analysis 1000 AEST, 4 February 2008 **(A)**; photograph of convective shower approaching Heron Reef, 1524 AEST, 4 Feb 2008 **(B)**; daytime eddy covariance energy flux measurements made over the reef flat, Heron Reef with timing of tethersonde soundings shown with major cloud types **(C)**.

the cumulus cloud field becoming more significant in proximity to the southern GBR resulting in isolated convective showers in the afternoon at Heron Reef (**Figure 2B**).

The surface energy balance measured on the 4 February 2008 reflected the impact of mid-level cloud cover in the morning from 0800 AEST [Australian Eastern Standard Time (UTC +10 hrs)] to 1200 AEST with net radiation (Q*) ranging from ~10 to ~145 Wm^{-2} before increasing after midday (**Figure 2C**). Sensible heat flux (Qh) remained mostly constant throughout the day within the range of ~ -23 to ~59 Wm^{-2}, while Qe varied from positive to negative values during the morning before becoming mainly positive (evaporation) from midday to late afternoon (**Figure 2C**). Heat flux into the water and benthos (Q_{SWR}) was mostly positive averaging 351 Wm^{-2} hr between 0800 AEST to 1200 AEST, then 838 Wm^{-2} hr between 1215 to 1500 AEST before becoming negative between 1515 AEST to 1800 AEST averaging -69 Wm^{-2} hr. There was a net gain of energy to the reef flat between 0800 AEST to 1800 AEST on the 4 February 2008 of 371 Wm^{-2} hr. This caused water temperature to increase from 26.1°C at 0800EST to a maximum of 28.6°C at 1515 AEST and contributed to an increase in air temperature as shown in the tethersonde profiles in **Figure 3**.

Tethersonde profiles of wind speed, virtual potential temperature (θ_v) and mixing ratio were collected from 1110 to 1136 AEST (**Figures 3A–C**) and 1525 to 1536 AEST (**Figures 3D–F**). The late morning sounding displayed a well-mixed θ_v profile indicating a statically neutral lower atmosphere (**Figure 3A**) with a mixing ratio profile showing a moist surface layer ~70 m deep which we infer was the CRL caused by Heron Reef (positive Qe) below drier air above (**Figure 3B**). Wind speed was relatively constant in the CRL layer at ~5 ms^{-1} before gradually increasing through to the top of the profile at around 250 m (**Figure 3C**). In the second sounding from mid-afternoon the entire profile (~ 250 m) had warmed by 1 to 1.5°K and become weakly statically stable (**Figure 3D**). The mixing ratio profile showed an increase in moisture above the CRL (**Figure 3E**), while wind speed was very similar to that measured in the late morning profile (**Figure 3F**). The CRL was still evident in the mixing ratio profile with a maximum height of ~70 m. The photo of a convective shower moving onto Heron Reef at 1534 AEST (**Figure 2B**), highlights the change in conditions that occurred following maximum heating of the reef around 1300 to 1400 AEST with evaporation from the reef and adjacent ocean contributing to increased boundary layer

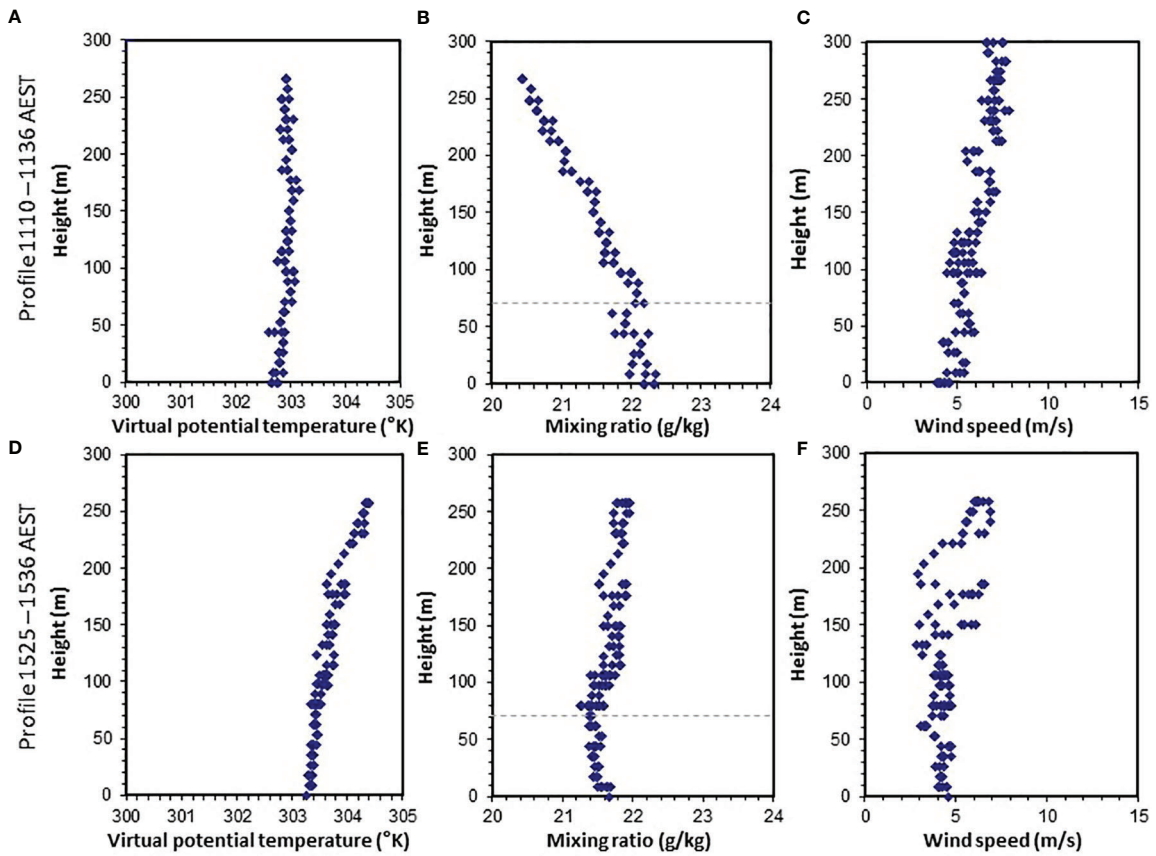

FIGURE 3 | Profiles of virtual potential temperature, mixing ratio and wind speed collected over Heron Reef, 4 Feb 2008 from 1110 – 1136 AEST **(A-C)** and 1525 – 1536 AEST **(D-F)**. Wind direction was consistent at around 95° giving a fetch of 7.64 km over the reef from the reef rim to the sounding site.

moisture and positive buoyancy with associated liberation of Qe following condensation resulting in convective showers.

Air-Sea Exchanges Under Monsoon Influences

The period 20 - 23 February 2009 was characterised by onset of monsoonal conditions at Heron Reef. Clear and settled weather with light winds prevailed on the 20 February due to a weak synoptic pressure gradient (**Figure 4A**). An inland surface trough was located over central Queensland, while the monsoon trough and weak tropical low were over the north Australian coast (**Figure 4A**). By the 22 February Heron Reef was under the influence of the east-southeast extension of the monsoon trough which had moved south into the Coral Sea and was located northeast of Heron Reef (**Figure 4B**). A ridge of high pressure along the southeast coast of Australia directed a warm moist easterly airstream onto Heron Reef (**Figure 4B**).

Surface energy balance measurements made over the reef flat (151°55.154 E, 23°26.617 S) under the increasing influence the Australian monsoon (20 to 23 February 2009) are presented in **Figure 4C**. These reflect clear sky conditions on the 20 February with Q* reaching a maximum of ~ 831 Wm^{-2} at 1215 AEST. Between 0600 AEST to 1800 AEST ~76% of Q* went into Q_{SWR} heating the water overlying the reef and underlying benthos and substrate. As a result, the reef flat water temperature increased from 26.3°C at 0600 AEST to a maximum of 34.4°C at 1600 AEST before decreasing slightly to 33.3°C at 1800 AEST as energy from the water was transferred to the atmosphere *via* evaporation (increased Qe and negative Q_{SWR}) (**Figures 4C, D**) as wind speed increased to

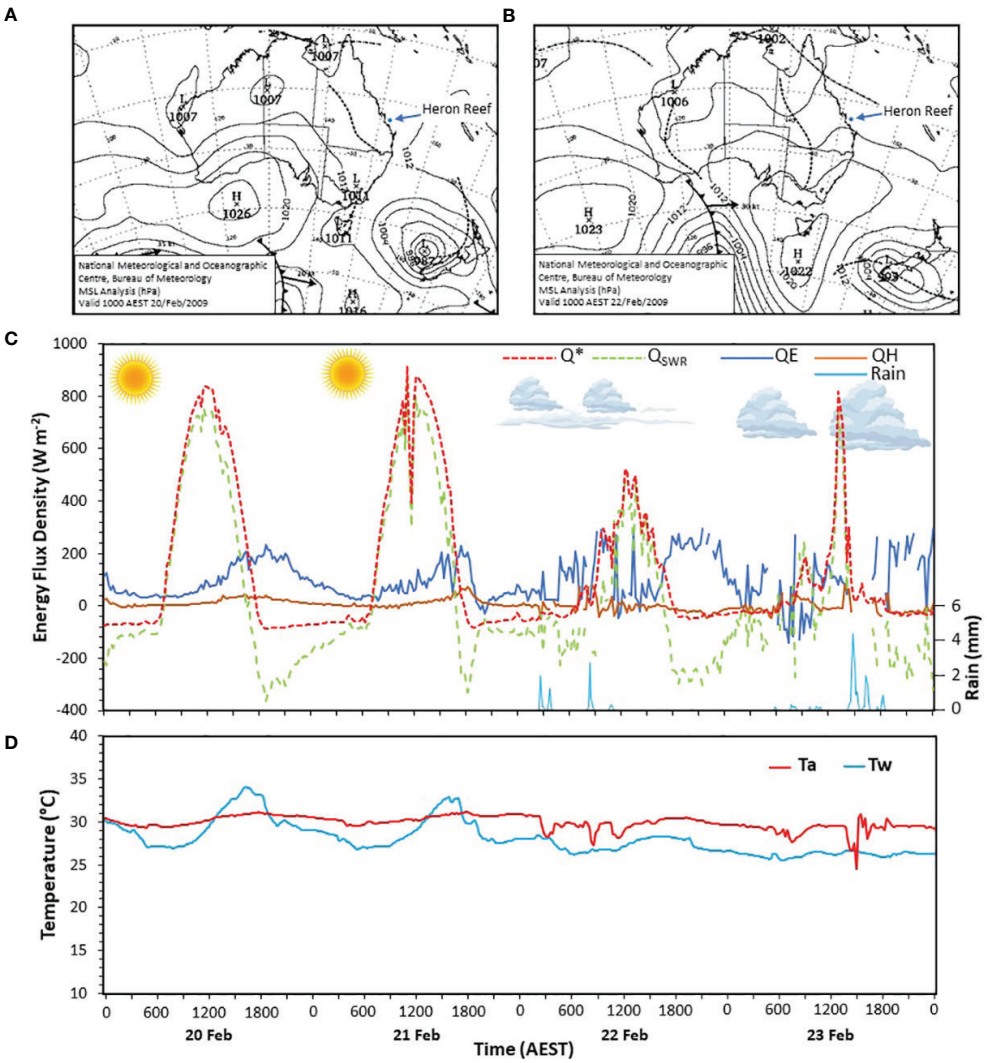

FIGURE 4 | Mean Sea Level Analysis 1000 AEST, 20 February 2009 **(A)** and 1000 AEST, 22 February 2009 **(B)**; with eddy covariance energy flux measurements (20 – 23 February 2009) made over the reef flat, Heron Reef and supporting meteorological observations **(C)**; and air and water temperature **(D)**.

around 4.5 ms^{-2}. Conditions on the 21 February were similar, but with cloud in the late morning causing a sharp decrease in Q* before it peaked in the early afternoon (**Figure 4C**). On the 22 February an increase in cloud cover reduced solar radiation receipt at the surface with Q* peaking at 512 Wm^{-2} at 1215 AEST. Showers affected Heron Reef throughout the morning as the monsoon trough moved south into the northern Coral Sea (**Figures 4B, C**). Water temperature decreased from 28.3°C in the early morning to around 26.6°C at 0600 AEST (**Figure 4D**) corresponding to onset of showers and an increase in wind speed to approximately 5 ms^{-2}. Water temperature then gradually increased to a maximum of 28.6° C at 1600 AEST before decreasing after 1800 AEST with 91% of Q_{SWR} lost *via* Qe and the residual to Qh (**Figures 4C, D**) as wind speeds peaked at 9.6 ms^{-2} in the late evening. Significant convective shower activity dominated the meteorology at Heron Reef on the 23 February with energy fluxes ranging between ~200 to -200 Wm^{-2} except for around 1330 AEST when Q* peaked briefly at 816 Wm^{-2} as skies cleared (**Figure 4C**). Wind speed reached a maximum of 10.4 ms^{-2} at 1600 AEST as convective showers passed over Heron Reef (**Figure 4C**) with Tw displaying a gradual decrease (**Figure 4D**). Air temperatures during the four-day period displayed a weak diurnal cycle on the 20 and 21 February reaching daytime maximums of around 30°C at 1800 AEST before trending down on the 22 and 23 February (**Figure 4D**). Down mixing of cooler air associated with the passage of convective showers over Heron Reef on the 22 and 23 February resulted in concurrent rapid decreases of Ta as shown in **Figure 4D**.

Figure 5 presents daily ceilometer backscatter plots for the 20 to 23 February 2009 from Heron Island (151°54'46.20" E, 23° 26'32.99" S). **Figure 5A** shows the backscatter plot for the 20

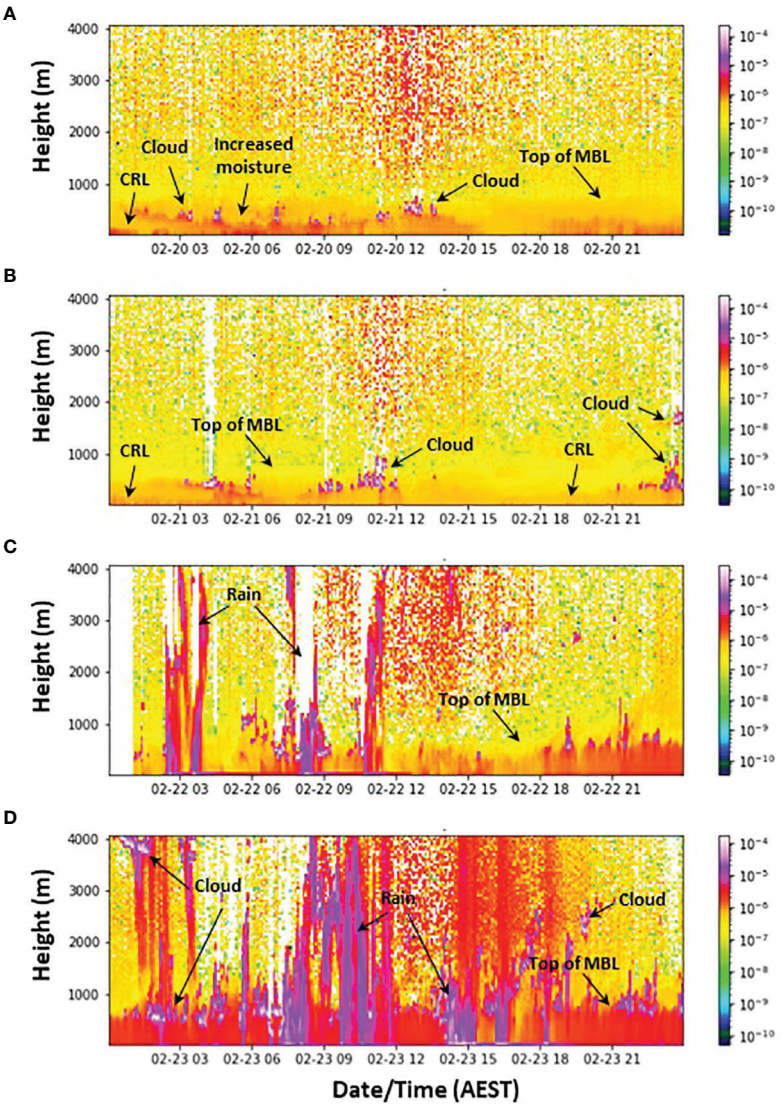

FIGURE 5 | Ceilometer reflectivity plots for the 20 **(A)**, 21 **(B)**, 22 **(C)** and 23 **(D)** February 2009. The ceilometer was installed on Heron Island (**Figure 1D**).

February when clear skies prevailed except for some isolated stratocumulus. A clear boundary in the reflectivity profile data at around 800 m asl we interpret as the top of the MBL. Below this, a layer of more humid air is evident, initially around 500 m asl. at 0100 AEST lowering to around 200 m asl. in depth at sunrise at 0600 AEST (**Figure 5A**). Isolated convective plume-initiated formation of cloud occurred during the day as highlighted in **Figure 5A**, while there was a very shallow surface layer of increased backscatter below 100 m asl which we interpret as the CRL. On the 21 February the top of the MBL lowered to ~600 to 700 m asl. (**Figure 5B**), while there was evidence of a shallow layer of increased backscatter in the lowest 100 m which we again interpret as the CRL. The presence of cloud can be seen in the ceilometer data before sunrise and then again through the morning to midday with a maximum height of approximately 1000 m asl. being mostly shallow cumulus. A layer of cirrostratus was also present but above 4000 m asl. (not shown). From mid-afternoon the top of the MBL becames less defined with the onset of cloud near 2400 hrs with a cloud base of 350 m, and cloud at 1800 m asl. (**Figure 5B**). The arrival of a more humid monsoon airmass on the 23 February resulted in convective showers affecting Heron Reef as previously discussed and seen in **Figure 5D**. The MBL ranged from ~700 to around 1000 m in depth, with increased moisture content into the evening as indicated by increased backscatter (**Figure 5D**). A lower cloud layer between ~600 to 1100m asl and other cloud layers between ~2000 m to > 4000m asl. were present on the 23 February with the ceilometer also identifying a layer of cirrostratus at around 6500 m asl (not shown).

Aerological profiles of temperature, humidity, wind speed and direction were obtained from the 20 – 23 February to maximum heights of around 500 m asl. (**Figure 6**). Vertical profiles of θ_v on the 20 February showed a warming through the morning and a transition to a statically unstable profile at 1445 AEST (**Figure 6A**). Subsequent cooling at the surface caused the lowest 100 m of the profile to cool by around 1°K by 1615 AEST

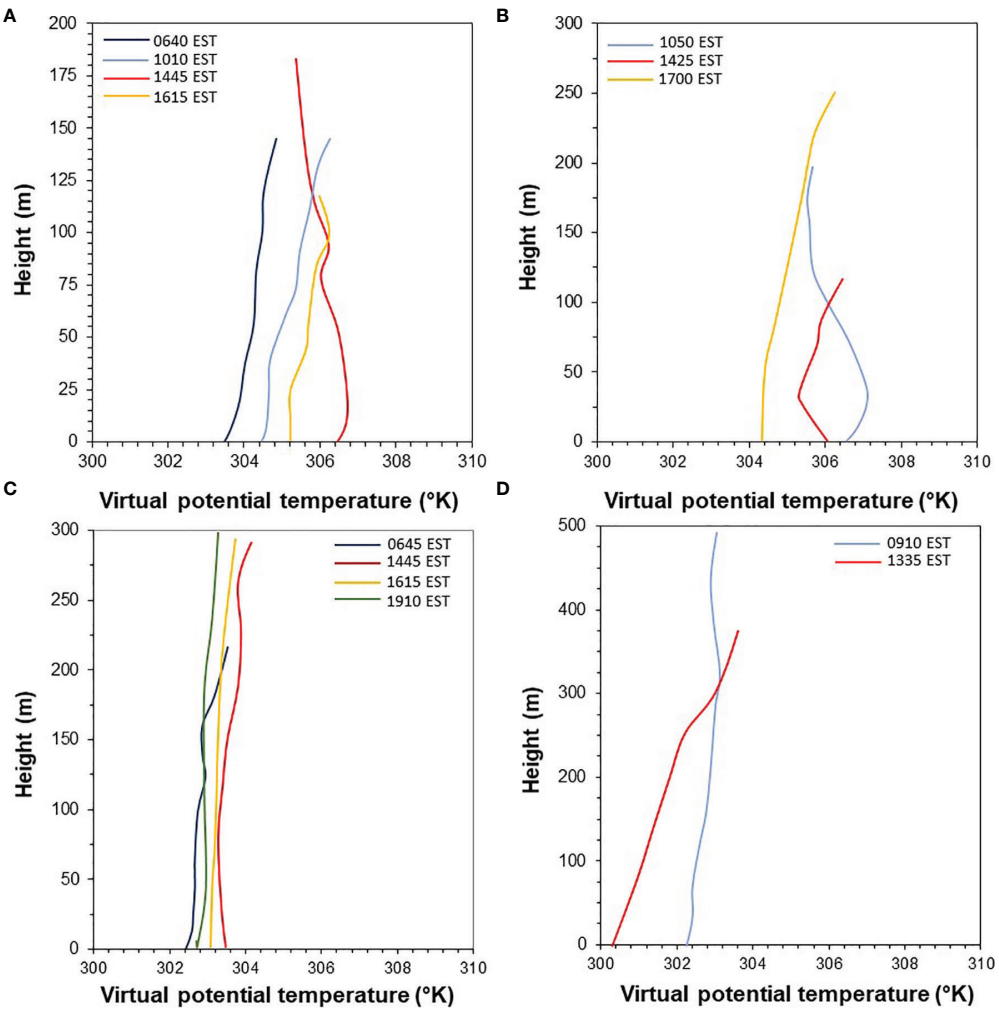

FIGURE 6 | Virtual potential temperature profiles collected over Heron Reef by tethersonde on the 20 **(A)**, 21 **(B)**, 22 **(C)** and 23 **(D)** February 2009.

leading to an increase in stability. This contributed to the absence of cloud as seen in the ceilometer data (**Figure 5A**). The θ_v profiles for the 21 February also display a cooling and increase in static stability from late morning through to late afternoon in the lowest 150 m (**Figure 6B**) which likely inhibited cloud development over Heron Reef also shown in **Figure 5B**. In contrast, the θ_v profiles for the 22 February indicate a statically neutral lower atmosphere in which the influence of Heron Reef is masked by the arrival of a monsoon airmass and associated increase in wind speed (**Figure 6C**). On the 23 February, the tethersonde profiles (**Figure 6D**) show the lower atmosphere became increasingly stable with cooling at the surface corresponding to increased cloud cover, reduced solar heating of the reef and down mixing of cooler air associated with convective showers. Satellite imagery from the 22 and 23 February 2009 show extensive high-level cirrus and cirrostratus cloud over the southern GBR with lower-level cumulus.

Desert Bordering Coral Reefs – Case Study Gulf of Eilat

EC measurements over the fringing coral reefs in the northwest GoE were made by instrumentation located on the shore as shown in **Figure 1C**. The EC system consisted of a RM Young 81000 3D sonic anemometer, Li-Cor 7500 open path gas analyser, Kipp and Zonen CNR1 radiometer, and ancillary sensors installed at the shoreline 2.5 m above mean sea level on the pier of Eilat's Coral World Underwater Observatory (29° 30'15.43" N, 34°55'6.68" E). Sensors were controlled by Campbell Scientific CR1000X dataloggers and regularly serviced with the Li-Cor 7500 open path gas analysers washed to ensure the optical sensors were free of salt and dust. The measurement footprint of the EC extended over corals in water depths from 0 m to 40 m. Simple linear interpolation was used to fill gaps where 1 data point was missing or where a data spike or unrealistic change in sign of energy flux had occurred. Longer gaps in data were filled using EC data from a nearby site (Abir et al., 2022) when that EC measurement footprint also extended over the fringing coral reef. A 3-point simple moving average was then applied to the EC data.

Air – Sea Exchanges During Hot and Dry Conditions

The 6 - 10 September 2020 was characterised by a broad area of lower atmospheric pressure and a weak synoptic pressure gradient over the Gulf of Eilat associated with the Persian Trough, while a ridge of high pressure was located over the western Mediterranean. This resulted in clear skies and northerly winds over the field site which peaked daily around 0900 IST (Israel Standard Time - UTC + 2 hrs) at 7 to 8 ms^{-1}.

The surface energy balance for this period shows Q* peaking daily under cloudless skies at around 800 W m^{-2} (**Figure 7A**). Latent heat flux peaked on the 6 and 7 September at ~500 W m^{-2} and then gradually trended lower toward the 10 September. Sensible heat flux was mostly negative associated with heat transfer from the air to the

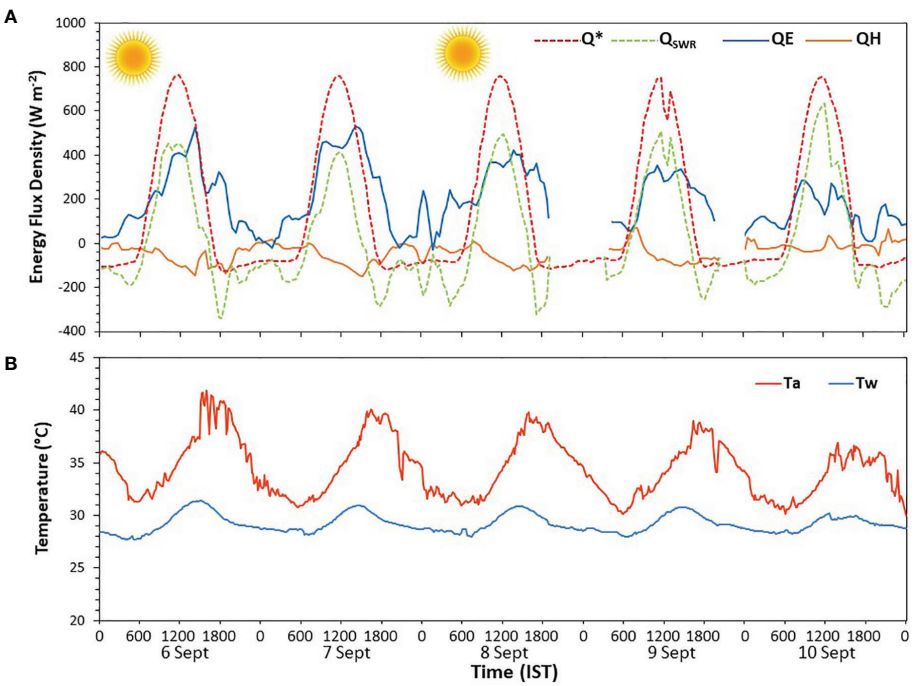

FIGURE 7 | Eddy covariance energy flux measurements (6 - 10 September 2020) made over the desert fringing coral reef at Eilat (**Figures 1A-C**) **(A)**; and corresponding water and air temperatures **(B)**.

water, while Q_{swr} peaked around midday, becoming more significant over the 5-day period (**Figure 7A**).

Throughout the 5-day period the temperature of the water overlying the fringing coral reef displayed a diurnal cycle ranging from a minimum of 27.8°C to a maximum of 31.2°C with no discernible warming/cooling trend (**Figure 7B**). Daily maximum Ta ranged from ~36°C to ~41°C with minimums of ~31°C (**Figure 7B**). These conditions resulted in a strong surface-based temperature inversion overlying the coral reef, while aerological profiles created using reanalysis data (NCEP operational Global Forecast System analysis data) displayed a stable layer over the GoE extending up to at least 800 m asl. As a result, the high positive daytime Qe flux transfers (evaporation) from the water to the air did not result in the formation of cloud, indicated in the Q* record (**Figure 7A**) as convection was supressed.

DISCUSSION

Coral reefs present distinct and typically abrupt changes in the thermal and dynamic properties of tropical and subtropical oceans. Direct measurements of air-sea exchanges of energy over coral reefs are essential to develop understanding of the influence coral reefs have on meteorology through exchanges of heat, moisture, and momentum with the atmosphere. Exchanges of Qe and Qh for example, influence thermodynamic processes in the atmospheric boundary-layer which may include winds, convection, cloud, and precipitation. The warmth of shallow waters overlying coral reefs and the formation of unstable CRLs may act to enhance vertical motion and dispersion of biogenic aerosols including the aerosol precursor gas DMS, salt, and moisture. However, direct measurements of air-sea energy exchanges over coral reefs and the local meteorology are rare, while the aerological profiles made at Heron Reef are unique (MacKellar et al., 2012b). Here we have presented selected new examples of summertime measurements of air-sea energy exchanges and profiles of the thermodynamic structure of the lower atmosphere over Heron Reef, GBR and, initial energy balance measurements from the desert fringing coral reefs in the GoE.

Humid Tropical/Subtropical Coral Reefs

EC measurements made during summer fair weather and monsoon conditions at Heron Reef showed the majority of available net radiant energy is partitioned into Q_{swr}. This raised the temperature of water overlying the reef resulting in the formation of a warm, humid, and unstable CRLs ~60 to ~100 m asl. (**Figures 3**–**6**) embedded within the MBL, which in case study 2 (20 - 23 February 2009) was ~600 to ~900 m in depth. The boundary at the top of the MBL, i.e., the entrainment zone, was clearly identified in ceilometer backscatter data indicating a sharp change in humidity (Flamant et al., 1997). As a result, under humid summer conditions coral reefs can modify the lower atmosphere resulting in the formation of an unstable CRL. This we believe contributed to formation of cumulus clouds following heating of the reef throughout late morning and early afternoon resulting in precipitation on the 4 February 2008. That is, the daily peak in radiative warming of reef SST and air–sea fluxes (early afternoon) invigorate convection leading to daily maximum cumulus in the late afternoon (Ruppert and Johnson, 2016).

While cloud height was only measured during 20 - 23 February 2009 and found to occur near the top of the MBL (and above), it's likely that the warmth of the reef and release of Qe associated with convective cloud formation may have contributed to onset of cumulus indicating more unstable conditions (**Figures 2B, C**). Cloud above the MBL as shown in **Figure 2B** and observed in case study 2 by ceilometer (**Figures 5B–D**) was likely caused by broader scale synoptic conditions. During case study 2, the MBL became more humid as seen in **Figure 5** indicated by the pronounced increase in reflectivity in **Figure 5D** (Dupont et al., 1994; Flamant et al., 1997). This increase in reflectivity may have also been in-part a result of increased biogenic aerosol concentrations (Schlosser et al., 2020) but without direct *in-situ* sampling this cannot be confirmed. Precipitation was identified by the ceilometer falling from cloud near the top of the MBL and from heights of 3000 to 4000 m asl (**Figure 5D**). Vertical profiles of $\theta_v$during case study 2 show on the 20 -21 February 2009 the CRL became more unstable through the morning and afternoon before onset of cooling in the late afternoon (**Figures 6A–C**). On the 23 Feb 2009 the $\theta_v$profiles show the lower atmosphere becoming stable with the lowest ~300 m cooling (**Figure 6D**) in response to likely down mixing of cooler air from aloft toward the surface with precipitation (**Figure 5D**). This sequence is like that reported by Ruppert and Johnson (2015) for days leading up to the onset of convection over warm SSTs in the Indian Ocean associated with the Madden Julian Oscillation. Namely, the diurnally forced convection that occurs in response to daytime peaks in SST and air–sea fluxes (Qe) over warm seas, initially under clear skies, increases humidity in the lower atmosphere and invigorates moist convection by reducing convective inhibition (Ruppert and Johnson, 2015). By the 23 Feb 2009 at Heron Reef such a sequence of events over the reef and adjacent sea led to periods of heavy convective rainfall (**Figure 6D**).

MacKellar et al. (2012b; 2013) presented results from the only other study that has made direct measurements of both air-sea energy exchanges over a coral reef (Heron Reef) and the CRL. They identified the CRL using vertical profiles of virtual potential temperature (θ_v) and mixing ratio (q) obtained from kite tethersonde soundings. Ceilometer data were used also to identify the mixed layer height with the addition of radiosonde soundings. The CRL was observed to reach a maximum height of approximately 135 m above sea level (asl.) in mid-afternoon (summer) with background mixed layer depths ranging from around 450 m to 2500 m depending on prevailing synoptic conditions. These observations are like those presented here for the summer case studies although MBL depths on occasions were greater. This likely reflects MacKellar's use of radiosondes providing direct measurements of temperature, and different prevailing synoptic meteorology. MacKellar et al. (2013)

highlighted similarities of the CRL observed at Heron Reef with CIBLs found downwind over the warm side of ocean fronts such as the Gulf Stream and Kuroshio extension, east of Japan. At such locations warmer SSTs initiate CIBL development within the mixed layer and cloud formation which on occasions may cause precipitation (Small et al., 2008). Over coral reefs such as Heron Reef, the CRL plume is likely to extend downwind similar to the CIBLs observed downwind of warm ocean currents (Hsu, 1984; Small et al., 2008).

Subtropical Desert Coral Reefs

In contrast to the warm humid setting of Heron Reef on the GBR, the EC measurements from over the desert fringing coral reefs in the GoE highlight the significant Qe fluxes associated with evaporation during the day and night. Q_{swr} is still very substantial in this arid location displaying a generally similar diurnal signal to Heron Reef. Accordingly, evaporation from water overlying the coral reefs at the GoE is the primary process by which energy is lost from the reef to the air (Abir et al., 2022). As a result, there was no net increase in water temperature from the 6 – 10 September 2020, although the diurnal range decreased slightly over the 5 days (**Figure 7A**). Notably, air temperature remained much higher than the water temperature, thereby causing a very stable layer of air over the coral reef. Stable internal boundary layers have been observed in other locations where warm air blows offshore over cool/cold sea surface as reported by Garratt and Ryan (1989) over the coast of southern Australia; Mahrt et al. (2016) Atlantic Ocean, Massachusetts and Grachev et al. (2018) on the North Carolina coast. Stable stratification generated in the GoE by warm-air advection and evaporation over coral reefs inhibit vertical motion at the surface. This stable layer was part of a deeper temperature inversion associated with the regional meteorology that was around 800 m deep.

Temperature inversions as observed in the GoE impede vertical motion in the atmosphere and cloud did not form. While no direct measurements of vertical profiles of temperature and humidity were made in the GoE we believe that in such a setting where water temperature remains well below air temperature, vertical dispersion of aerosols, moisture and DMS are unlikely. Instead, they will be advected downwind where they disperse in the dry atmosphere.

Coupling to the Atmospheric Boundary Layer

The case studies presented here show that coral reefs in humid climates may effectively couple to the overlying atmosphere influencing its thermodynamic properties impacting cloud and possibly precipitation. The coupling was observed to occur *via* convective exchange leading to formation of a CRL within the MBL. Leahy et al. (2013) using *in-situ* sea surface temperature measurements and satellite cloud field observations from the central GBR found cloud cover explaining up to 32.1% of variation in SST with the greatest effect during summer. Accordingly, our observations from Heron Reef begin to shed light on the possible role of coral reefs in this cloud formation over the GBR i.e., as coral reefs warm, they initiate convection triggering cloud formation under favourable synoptic conditions such as occur during the summer monsoon. In contrast, under settled summer El Niño conditions when the atmosphere is more stable over the GBR, cloud development may be suppressed resulting in extreme heating of water overlying coral reefs causing bleaching (McGowan and Theobald, 2017; Zhao et al., 2021).

In contrast, the case study from the GoE suggests that coral reefs in hot arid environments may remain decoupled from the overlying atmosphere as a result of strong surface-based temperature inversions. Such inversions inhibit vertical exchange of heat, moisture and aerosols and would contribute to inhibiting cloud development that would otherwise lower receipt of solar radiation over the reef. In these environments, observations from the fringing coral reefs in the GoE highlight the importance of Qe in protecting coral from heatwaves and associated coral bleaching (Abir et al., 2022).

CONCLUSION

Understanding exchanges of energy, moisture, momentum, and gases across the air-sea interfacial boundary on coral reefs and the influence on the atmosphere is critical to inform debate on future impacts of climate change on coral reefs. It is not scientific to assume that correlations are evidence enough of causality or to simplify complex cause – effect relationships because they align with socially and/or politically attractive narratives on the relationships between coral reefs – meteorology and climate. Direct measurements of the meteorology of coral reefs including energy exchanges across the air-sea interface and associated coupling to the lower atmosphere are therefore essential to inform such debate from which evidence-based policy to mitigate risks to coral reefs including from global warming can be developed.

Here we have presented through case study direct measurements of air-sea energy exchanges over coral reefs in two profoundly different climatic zones. These measurements show that under summertime conditions coral reefs in humid tropical/subtropical environments may couple to the lower atmosphere through exchange of heat, moisture, and momentum. This leads to the formation of CRLs within the lower levels of the MBL providing a mechanism for coral reefs to influence cloud, and possibly precipitation through convective exchange with the lower atmosphere. In contrast, our case study from the northern GoE in the Red Sea shows that where air overlying coral reefs is much warmer than the water temperature, stable stratification of the lower atmosphere will inhibit vertical motion and therefore, convective cloud development. In such different climatic regions, convection over coral reefs such as those in the GBR would be a possible mechanism by which aerosols and pre-curser aerosol gases such as DMS could be carried into the atmosphere, while in hot arid desert environments, a stable layer over corals reefs impedes such transport.

The research presented and cited in this article provides initial insights to coral reef meteorology and begins to shed

light on the interactions between coral reefs and broader scale meteorology. However, substantial knowledge gaps remain around seasonal variability in coral reef – atmosphere coupling and potential feedback mechanisms. While the works of Fiddes et al., 2022 question the role of coral reef bioclimatic links through coral reef emitted DMS in cloud microphysics, coral-reef forced convection may provide a possible mechanism for a DMS signal in cloud fields over reefs. Accordingly, future research is strongly recommended that combines direct measurement of the surface energy exchanges over coral reefs and atmospheric thermodynamics with aerosol profile sampling including within clouds. This should be combined with numerical modelling to provide data sets to nudge and validate model runs and to inform future direct measurement field research.

DATA AVAILABILITY STATEMENT

The raw data supporting the conclusions of this article will be made available by the authors, without undue reservation.

AUTHOR CONTRIBUTIONS

HM and MS conceived and conducted research at Heron Island. HM, NL, and SA conceived and conducted research at Eilat. All authors were involved with data analysis. HM wrote the manuscript with contributions from NL and SA. All authors contributed to the article and approved the submitted version.

ACKNOWLEDGMENTS

The authors acknowledge the support of their host institutions: The University of Queensland, Geological Survey of Israel, Hebrew University of Jerusalem, and The Inter-University Institute for Marine Sciences. We thank the Dead Sea Observatory team members Uri Malik, Guy Tau and Ziv Mor for their assist in the field, Adrien Guyot for processing the LiDAR data from Heron Island, and Yoni Shaked for assistance and discussions. The research was supported by funding from the Australia-Israel Cooperation in Science - Zelman Cowen Academic Initiatives (ZCAI), PIs – HM and NGL, and by the Israel Science Foundation (grant # ISF-2018/1471), PI – NGL.

REFERENCES

Abir, S., McGowan, H. A., Shaked, Y., and Lensky, N. G. (2022). Identifying an Evaporative Thermal Refugium for the Preservation of Coral Reefs in a Warming World - The Gulf of Eilat (Aqaba). *J. Geophys. Res. Atmos.*

Alpert, P., Abramsky, R., and Neeman, B. (1990). The Prevailing Summer Synoptic System in Israel–Subtropical High, Not Persian Trough. *Israel J. Earth Sci.* 39 (2), 93–102.

Bitan, A., and Sa'Aroni, H. (1992). The Horizontal and Vertical Extension of the Persian Gulf Pressure Trough. *Int. J. Climatol.* 12 (7), 733–747. doi: 10.1002/joc.3370120706

Broadbent, A., and Jones, G. (2006). Seasonal and Diurnal Cycles of Dimethylsulfide, Dimethylsulfoniopropionate and Dimethylsulfoxide at One Tree Reef Lagoon. *Environ. Chem.* 3, 260–267. doi: 10.1071/EN06011

Carlson, D. F., Fredj, E., Gildor, H., Biton, E., Steinbuck, J. V., Monismith, S. G., et al. (2012). Observations of Tidal Currents in the Northern Gulf of Eilat/Aqaba (Red Sea). *J. Marine Syst.* 102–104, 14–28. doi: 10.1016/j.jmarsys.2012.04.008

Charlson, R. J., Lovelock, J. E., Andreae, M. O., and Warren, S. G. (1987). Oceanic Phytoplankton, Atmospheric Sulphur, Cloud Albedo and Climate. *Nature* 326, 655–661. doi: 10.1038/326655a0

Chen, D., and Krol, A. (1997). "Hydrogeology of Heron Island, Great Barrier Reef, Australia", in Geology and Hydrogeology of Carbonate Islands. Developments in Sedimentology. *Eds. H. L. Vacher and T. Quinn* (New York: Elsevier Science), 867—884.

Clayson, C. A., and Edson, J. B. (2019). Diurnal Surface Flux Variability Over Western Boundary Currents. *Geophys. Res. Lett.* 46, 9174–9182. doi: 10.1029/2019GL082826

Cropp, R., Gabric, A., van Tran, D., Jones, G., Swan, H., and Butler, H. (2018). Coral Reef Aerosol Emissions in Response to Irradiance Stress in the Great Barrier Reef, Australia. *Ambio* 47 (6), 671–681. doi: 10.1007/s13280-018-1018-y

Dupont, E., Pelon, J., and Flamant, C. (1994). Study of the Moist Convective Boundary Layer Structure by Backscatter Lidar. *Bound Lay. Meteorol.* 69, 1–25. doi: 10.1007/BF00713292

Fiddes, S. L., Woodhouse, M. T., Lane, T. P., and Schofield, R. (2021a). Coral-Reef-Derived Dimethyl Sulfide and the Climatic Impact of the Loss of Coral Reefs. *Atmos. Chem. Phys.* 21, 5883–5903. doi: 10.5194/acp-21-5883-2021

Fiddes, S., Woodhouse, M., Utembe, S., Schofield, R., Alroe, J., Chambers, S., et al. (2022). The Contribution of Coral Reef-Derived Dimethyl Sulfide to Aerosol Burden Over the Great Barrier Reef: A Modelling Study. *Atmos. Chem. Phys. Discuss.* 22, 2419–2445. doi: 10.5194/acp-22-2419-2022

Flamant, C., Pelon, J., Flamant, P. H., and Durand, P. (1997). Lidar Determination of the Entrainment Zone Thickness at the Top of the Unstable Marine Atmospheric Boundary Layer. *Bound Lay. Meteorol.* 83, 247–284. doi: 10.1023/A:1000258318944

Garratt, J. R. (1990). The Internal Boundary Layer — A Review. *Bound Lay. Meteorol.* 50, 171–203. doi: 10.1007/BF00120524

Garratt, J. R. (1994). Review: The Atmospheric Boundary Layer. *Earth Sci. Rev.* 37, 89–134. doi: 10.1016/0012-8252(94)90026-4

Garratt, J. R., and Ryan, B. F. (1989). The Structure of the Stably Stratified Internal Boundary-Layer in Offshore Flow Over the Sea. *Bound Lay. Meteorol.* 47 (1), 17–40. doi: 10.1007/BF00122320

Golbazi, M., and Archer, C. L. (2019). Methods to Estimate Surface Roughness Length for Offshore Wind Energy. *Adv. Meteorol.* 2019, 5695481. doi: 10.1155/2019/5695481

Gourlay, M. R. (1988). "Coral Cays' Products of Wave Action and Geological Processes in a Biogenic Environment," in *Proc. 6th Int. Coral Reef Symposium, Great Barrier Reef Committee, Townsville, Australia*. 491–496.

Grachev, A. A., Leo, L. S., Fernando, H. J. S., Fairall, C. W., Creegan, E., Blomquist, B. W., et al. (2018). Air–Sea/Land Interaction in the Coastal Zone. *Bound Lay. Meteorol.* 167, 181–210. doi: 10.1007/s10546-017-0326-2

He, Y., Fu, J., Chan, P. W., Li, Q., Shu, Z., and Zhou, K. (2021). Reduced Sea-Surface Roughness Length at a Coastal Site. *Atmosphere* 12, 991. doi: 10.3390/atmos12080991

Hsu, S. A. (1984). Effect of Cold-Air Advection on Internal Boundary-Layer Development Over Warm Ocean Currents. *Dyn. Atmos. Oceans* 8, 307–319. doi: 10.1016/0377-0265(84)90015-0

Kotthaus, S., O'Connor, E., Münkel, C., Charlton-Perez, C., Haeffelin, M., Gabey, A. M., et al. (2016). Recommendations for Processing Atmospheric Attenuated Backscatter Profiles From Vaisala CL31 Ceilometers. *Atmos. Meas. Tech.* 9, 3769–3791. doi: 10.5194/amt-9-3769-2016

Leahy, S. M., Kingsford, M. J., and Steinberg, C. R. (2013). Do Clouds Save the Great Barrier Reef? Satellite Imagery Elucidates the Cloud-SST Relationship at the Local Scale. *PloS One* 8 (7), e70400. doi: 10.1371/journal.pone.0070400

MacKellar, M. C., McGowan, H. A., and Phinn, S. R. (2012a). Spatial Heterogeneity of Air-Sea Energy Fluxes Over a Coral Reef, Heron Reef, Australia. *J. Appl. Meteorol. Clim.* 51, 1353–1370. doi: 10.1175/JAMC-D-11-0120.1

MacKellar, M. C., McGowan, H. A., and Phinn, S. R. (2013). An Observational Heat Budget Analysis of a Coral Reef, Heron Reef, Great Barrier Reef, Australia. *J. Geophys. Res. Atmos.* 118 (6), 2547–2559. doi: 10.1002/jgrd.50270

MacKellar, M. C., McGowan, H. A., Phinn, S. R., and Soderholm, J. S. (2012b). Observations of Surface Energy Fluxes and Boundary-Layer Structure Over Heron Reef, Great Barrier Reef, Australia. *Bound Lay. Meteorol.* 146 (2), 319–340. doi: 10.1007/s10546-012-9767-9

Mahrt, L. (2000). Surface Heterogeneity and Vertical Structure of the Boundary Layer. *Bound Lay. Meteorol.* 96, 33–62. doi: 10.1023/A:1002482332477

Mahrt, L., Andreas, E. L., Edson, J. B., Vickers, D., Sun, J., and Patton, E. G. (2016). Coastal Zone Surface Stress With Stable Stratification. *J. Phys. Oceanogr.* 46 (1), 95–105. doi: 10.1175/JPO-D-15-0116.1

McGowan, H. A., Sturman, A. P., Mackellar, M. C., Weibe, A. H., and Neil, D. T. (2010). Measurements of the Surface Energy Balance Over a Coral Reef Flat, Heron Island, Southern Great Barrier Reef, Australia. *J. Geophys. Res. Atmos.* 15 (D19), D19124-1-D19124-12. doi: 10.1029/2010JD014218

McGowan, H., Sturman, P., Saunders, M., Theobald, A., and Wiebe, A. (2019). Insights From a Decade of Research on Coral Reef – Atmosphere Energetics. *J. Geophys. Res. Atmos.* 124 (8), 4269—4282. doi: 10.1029/2018JD029830

McGowan, H., and Theobald, A. (2017). ENSO Weather and Coral Bleaching on the Great Barrier Reef, Australia. *Geophys. Res. Lett.* 44 (20), 10,601—10,607. doi: 10.1002/2017GL074877

Ruppert, J. H.Jr., and Johnson, R. H. (2015). Diurnally Modulated Cumulus Moistening in the Pre-Onset Stage of the Madden–Julian Oscillation During DYNAMO. *J. Atmos. Sci.* 72 (4), 1622–1647. doi: 10.1175/JAS-D-14-0218.1

Ruppert, J. H. Jr., and Johnson, R. H. (2016). On the Cumulus Diurnal Cycle Over the Tropical Warm Pool. *J. Adv. Model. Earth Syst.* 8, 669–690. doi: 10.1002/2015MS000610

Schlosser, J. S., Dadashazar, H., Edwards, E.-L., Hossein Mardi, A., Prabhakar, G., Stahl, C., et al. (2020). Relationships Between Supermicrometer Sea Salt Aerosol and Marine Boundary Layer Conditions: Insights From Repeated Identical Flight Patterns. *J. Geophys. Res. Atmos.* 125, e2019JD032346. doi: 10.1029/2019JD032346

Shaked, Y., and Genin, A. (2019). *Gulf of Eilat National Monitoring Report 2017* (Eilat, Israel: Israel Ministry of Environmental Protection), 209p.

Shaked, Y., and Genin, A. (2020). *Gulf of Eilat National Monitoring Report 2019* (Eilat, Israel: Israel Ministry of Environmental Protection), 187p.

Small, R. J., DeSzoeke, S. P., Xie, S. P., O'Neill, L., Seo, H., Song, Q., et al. (2008). Air-Sea Interaction Over Ocean Fronts and Eddies 2008. *Dyn. Atmos. Oceans* 45 (3–4), 274–319. doi: 10.1016/j.dynatmoce.2008.01.001

Swan, H. B., Crough, R. W., Vaattovaara, P., Jones, G. B., Deschaseaux, E. S. M., Eyre, B. D., et al. (2016). Dimethyl Sulfide and Other Biogenic Volatile Organic Compound Emissions From Branching Coral and Reef Seawater: Potential Sources of Secondary Aerosol Over the Great Barrier Reef. *J. Atmos. Chem.* 73, 303–328. doi: 10.1007/s10874-016-9327-7

Vickers, D., Mahrt, L., Sun, J., and Crawford, T. (2001). Structure of Offshore Flow. *Mon. Weather Rev.* 129 (5), 1251–1258. doi: 10.1175/1520-0493(2001)129<1251:SOOF>2.0.CO;2

Woodroffe, C. D. (2003). *Coasts: Form, Process and Evolution* (New York.: Cambridge Univ. Press), 623p.

Zhao, W., Huang, Y., Siems, S., and Manton, M. (2021). The Role of Clouds in Coral Bleaching Events Over the Great Barrier Reef. *Geophys. Res. Lett.* 48, e2021GL093936. doi: 10.1029/2021GL093936

Conflict of Interest: The authors declare that the research was conducted in the absence of any commercial or financial relationships that could be construed as a potential conflict of interest.

frontiers | Frontiers in Marine Science

MINI REVIEW
published: 20 June 2022
doi: 10.3389/fmars.2022.869166

The Potential for Great Barrier Reef Regional Climate Regulation *via* Dimethylsulfide Atmospheric Oxidation Products

Hilton B. Swan *

Centre for Coastal Biogeochemistry, Faculty of Science and Engineering, Southern Cross University, Lismore, NSW, Australia

Research related to the potential for coral reef-derived dimethylsulfide (DMS) oxidation products to regulate the regional climate of the Great Barrier Reef (GBR) according to the CLAW hypothesis is summarized in this mini review. The GBR has been indicated as a region of high DMS production where atmospheric emissions may be increased when corals are subject to environmental stresses associated with low tide. During low wind speeds over aerially exposed coral reefs, plumes of atmospheric DMS and new sulfate-containing nano-particle production under photo-oxidative conditions have been detected on the GBR. Hygroscopic growth of these particles in combination with coagulation and condensation processes could potentially provide a coral-mediated mechanism of new aerosol for seeding low-level stratocumulus clouds. Fine mode aerosol optical depth over GBR coral reefs has been correlated with low wind speeds and a coral stress metric formulated as a function of irradiance, water clarity, and tide height. This correlation has been proposed as a possible mechanism by which the GBR might alter the optical properties of the overlying atmosphere to attenuate local insolation leading to regional climate regulation. However, recent regional-scale aerosol-climate modeling indicates that the potential for GBR regional climate regulation *via* DMS atmospheric oxidation products is weak under current anthropogenic conditions which have instigated mass coral bleaching events along the entire length of the GBR between 1998 and 2022. This increased bleaching indicates that DMS oxidation products are insufficient to regulate the regional climate of the GBR according to the CLAW hypothesis under current global warming conditions.

Keywords: dimethylsulfide (DMS), Great Barrier Reef (GBR), climate, oxidation, sulfate

OPEN ACCESS

Edited by:
Gabrielle Nevitt,
University of California, Davis,
United States

Reviewed by:
Stephen D. Archer,
Bigelow Laboratory For Ocean Sciences, United States
Mike Harvey,
National Institute of Water and Atmospheric Research (NIWA), New Zealand

****Correspondence:***
Hilton B. Swan
hilton.swan@scu.edu.au

Specialty section:
This article was submitted to Coral Reef Research, a section of the journal Frontiers in Marine Science

Received: *03 February 2022*
Accepted: *23 May 2022*
Published: *20 June 2022*

Citation:
Swan HB (2022) The Potential for Great Barrier Reef Regional Climate Regulation via Dimethylsulfide Atmospheric Oxidation Products. Front. Mar. Sci. 9:869166. doi: 10.3389/fmars.2022.869166

INTRODUCTION

It is now fifty years since Lovelock et al. (1972) proposed that dimethylsulfide (DMS) was the missing link in the natural biogeochemical sulfur cycle capable of annually cycling megatonnes of sulfur from the sea back onto the land. Later, in 1987, DMS was assigned as the driving force in a mechanism by which the ocean and the atmosphere were hypothesized to be dynamically coupled in a global system that had the potential to affect and possibly even regulate climate (Charlson et al.,

1987). This hypothesis, which was conceived almost by accident in 1985 during a visit by James Lovelock to Robert Charlson at the University of Washington in Seattle (Liss and Lovelock, 2007), has become known as the CLAW hypothesis, an acronym of the four contributing authors' surnames. CLAW hypothesized that the Earth's radiation balance may be modulated by reflection or absorption of solar radiation by clouds seeded by the oxidation products of the marine volatile DMS, an algal metabolic by-product that is constantly exchanged from the oceans to the atmosphere. Consequential changes in sea surface temperate (SST) could affect algal growth and hence DMS emissions, thereby providing a potential climate feedback loop where surface ocean primary productivity is dynamically linked to marine cloud production and albedo. Regarding this CLAW mechanism, it has more recently been stated by Liss and Lovelock (2007) that any climate feedback effect could be stabilizing (i.e. negative) or destabilizing (i.e. positive) and the extent, or even its existence, to play any part in the present day climate is in question. What makes the CLAW hypothesis so scientifically compelling is that it continues to be possible to provide empirical evidence for various processes in the proposed mechanism (**Figure 1**). For example, in Southern Ocean clean marine air sampled at Cape Grim in north-west Tasmania it has been possible to show coherence in the seasonal cycles of atmospheric DMS (DMS_a) and its major oxidation products methanesulfonic acid (MSA) and non-sea-salt sulfate (nss-SO_4) (Ayers et al., 1991). Additionally, cloud condensation nuclei (CCN) number concentrations, modeled cloud droplet concentrations, and mean cloud droplet effective radii were also shown to have the same seasonal phase cycles as DMS (Boers et al., 1994). These early data strongly indicated a connection between DMS emissions, aerosol particle chemistry, and CCN and cloud droplet concentrations (Ayers and Gillett, 2000). Other data have shown a strong relationship between DMS and solar radiation dose over the global surface ocean, providing support for a negative climate feedback (Vallina and Simó, 2007).

The CLAW hypothesis has been experimentally shown to be far more complex than first proposed, and despite much research it has not been possible to quantitatively demonstrate the relationship between the mass air-sea flux of DMS-derived sulfate and the number concentration of CCN (Ayers and Cainey, 2007). Failure to demonstrate this relationship led Quinn and Bates (2011) to suggest that it might be time to retire the CLAW hypothesis with over 20 years of collated evidence that DMS bio-regulation of climate is prevented by weak sensitivity to change in each step of the CLAW hypothesis feedback loop (**Figure 1**). DMS is, however, the major reduced sulfur-containing volatile emitted from the global oceans, currently estimated to be 27.1 Tg (as S) annually (Hulswar et al., 2021). This massive amount of biogenic sulfur is suspected to be the origin of the globally dominant nss-SO_4 contribution to CCN over the global oceans between 70°S and 80°N (Quinn et al., 2017); thus, signaling that DMS oxidation products and CCN are connected with the potential to influence Earth's energy budget, and ultimately climate. According to

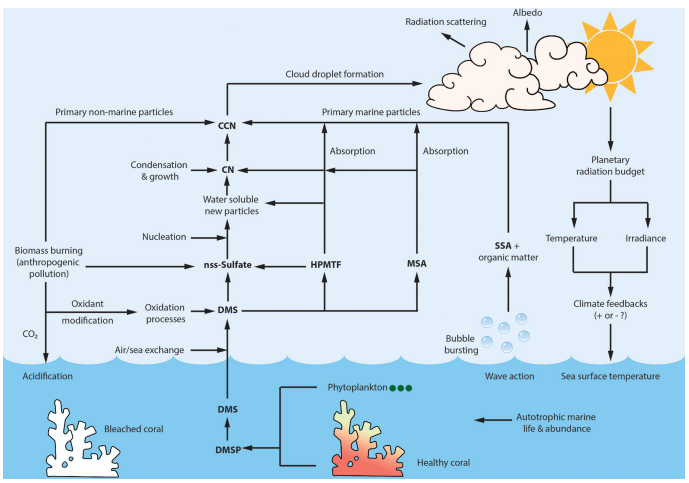

FIGURE 1 | Schematic of the proposed climate feedback loop according to the CLAW hypothesis (Charlson et al., 1987) adapted to the GBR with some updated information. DMSP, produced by coral and phytoplankton, is the dominant source of DMS which on exchange to the atmosphere can be oxidized to products such as nss-SO_4 and HPMTF which are involved in new particle production, while MSA primarily contributes to the growth of existing particles. CCN formed from these DMS oxidation products can generate marine clouds with increased albedo, which may alter the Earth's radiation budget leading to the hypothesized climatic feedback. The proposed biogenic feedback loop may be perturbed by primary marine sources of CCN such as SSA and organic matter released from surface waters by bubble bursting. Anthropogenic forcing over the GBR may contribute to recurrent coral bleaching and loss of DMS production to dampen the feedback loop. Additionally, regional biomass burning may contribute nss-sulfate and primary particles in the CCN size range (D_p ~50-100 nm) (Zaveri et al., 2022) as well as terrestrially-derived oxidants that may alter the background marine atmospheric oxidation processing capacity (Mauldin III et al., 2012; Zhu et al., 2021). Condensation nuclei (CN), Cloud condensation nuclei (CCN), Dimethylsulfide (DMS), Dimethylsulfoniopropionate (DMSP), Particle diameter (D_p), Great Barrier Reef (GBR), Hydroperoxymethyl thioformate (HPMTF), Methanesulfonic acid (MSA), non sea salt sulfate (nss-Sulfate), Sea spray aerosol (SSA).

James Lovelock, demonstration of climate regulation *via* cloud albedo control linked to DMS emissions is now only probable, if at all, in the southern hemisphere because of excessive anthropogenic sulfate pollution in the northern hemisphere (Lovelock, 2009). Given that global realization of CLAW is now most likely impossible, a relatively unpolluted location in the southern hemisphere such as the GBR remains a last marine frontier where research has been directed to possibly demonstrate regional climate regulation according to the CLAW hypothesis.

PRODUCTION OF DIMETHYLSULFIDE AND DIMETHYLSULFONIOPROPIONATE (DMS/P) BY SCLERACTINIAN CORALS

It has been known since the early 1990s that coral reef ecosystems can be significant sessile sources of dimethylsulfoniopropionate (DMSP), the major marine precursor of DMS (Jones et al., 1994; Hill et al., 1995). Initially, the algal zooxanthellae endosymbionts (*Symbiodium* sp.) were presumed and also indicated to be the coral's source of DMS/P because cellular or particulate DMSP was typically correlated with *Symbiodium* number (Broadbent and Jones, 2004; Jones et al., 2007; Van Alstyne et al., 2008); however, it is now recognized that the coral polyp also has the ability to produce DMSP (Raina et al., 2013). Just as the symbiotic union of the zooxanthellae and the polyp provides a very efficient metabolic system enabling coral to flourish in oligotrophic tropical waters, this union may also provide the basis for the very high concentrations of DMS/P that have been measured in coral and its products. For example, mucus ropes exuded from the staghorn coral *Acropora formosa* have been reported to contain 18.7 μM DMS and 54.4 μM DMSP (Broadbent and Jones, 2004), which are some of the highest concentrations of DMS/P measured in any natural marine material. Zooxanthellae DMSP cellular concentrations of up to 686 mmol L^{-1} (cell volume) (Yost and Mitchelmore, 2009) and 7590 mmol L^{-1} (cell volume) (Broadbent et al., 2002) are large by comparison with DMSP cellular concentrations reported in other marine dinoflagellates (Caruana and Malin, 2014). High zooxanthellae densities typically of 1-4 x 10^6 *Symbiodinium* cells cm^{-2} coral surface area in healthy *Acropora* sp. (Moothien-Pillay et al., 2005) make these abundant branching corals throughout the GBR highly concentrated sources of DMS/P. Consequently, the GBR has been described as a *DMS hotspot* (Jones et al., 2017; Jones et al., 2018); however, it is not identified as such among the 56 biogeochemical global ocean provinces defined by Hulswar et al. (2021), probably because the GBR is a relatively under-sampled location.

CONDITIONS THAT PROMOTE DMS TRANSFER FROM CORAL REEFS TO THE ATMOSPHERE

In chamber experiments with three Indo-Pacific coral species, it was shown that gas phase DMS increased by an order of magnitude when the corals were exposed to air, and this was followed by an additional rise in gas phase DMS on their re-submersion (Hopkins et al., 2016). In the environment, atmospheric DMS (DMS_a) was observed to peak over coral reefs in the northern GBR at, or shortly after, low tide when the reefs were exposed to the atmosphere (Jones and Trevena, 2005). This was also observed at Heron Island, a coral cay in the southern GBR, where it was possible to demonstrate that median DMS_a mixing ratios were a function of tide height, which controls the extent and duration of coral reef aerial exposure, **Figure 2** (Swan, 2017). A combination of DMS_a source signals are shown in **Figure 2**, where DMS_a derived from the coral reef is the tidally-induced contribution above the oceanic background DMS_a continuum. When a coral reef is aerially exposed, DMS can diffuse from the mucus covered coral surfaces directly to the atmosphere, a process that circumvents DMS air-sea exchange; hence, low-tide DMS emissions may result in rapidly released plumes. These were observed as intermittent DMS_a time-line spikes in the Heron Island datasets, which were in most instances detected under low wind speeds (WS < 2 m s^{-1}) when atmospheric mixing with oceanic air was least (Swan et al., 2017). Coral reefs emit DMS at low tide in response to environmental stresses when corals can be subject to elevated solar irradiance, heating and hypoxia in shallow pooled water, and dehydration due to air exposure (Deschaseaux et al., 2014).

DMS FLUX AND EMISSION ESTIMATES FROM THE GBR

Seasonally averaged DMS flux estimates for five coral reefs across the GBR, determined from spatially and temporally combined data, have been reported by Jones et al. (2018). These averaged fluxes, estimated from dissolved DMS (DMS_w) and WS using the gradient approach of Liss and Merlivat (1986), were 6.4 and 2.4 μmol m^{-2} d^{-1} for summer (Oct-Mar, n = 237) and winter (Apr-Sep, n = 156), respectively. Seasonal fluxes at Heron Island, estimated from DMS_a using the mass balance-photochemical box model of Ayers et al. (1995), were 5.0 and 1.4 μmol m^{-2} d^{-1} for the 2012 summer wet season (n = 651) and the 2013 winter dry season (n = 923), respectively (Swan et al., 2017). For those Heron Island field campaigns, the coral reef surrounding the island was estimated to contribute 4% during the summer and 14% during the winter to the background oceanic DMS flux sourced from the dominant south-easterly trade winds. A proxy for DMS_w across the GBR was derived by Jackson et al. (2021) using a multiple linear regression model, satellite-derived photosynthetically active radiation, SST data, and DMS_w field data compiled by Jones et al. (2018). Using that modeled DMS_w data, a climatology of DMS air-sea flux across the GBR was calculated using three gradient approach parameterizations. Average (± 1σ) seasonal DMS fluxes were 7.3 ± 1.6 and 3.1 ± 0.3 μmol m^{-2} d^{-1} in late summer and late winter, respectively, where inclusion of an estimate for DMS release from exposed corals at low tide increased the average flux by 1.5 μmol m^{-2} d^{-1}. DMS emission across the 347,000 km^2 area of the GBR is

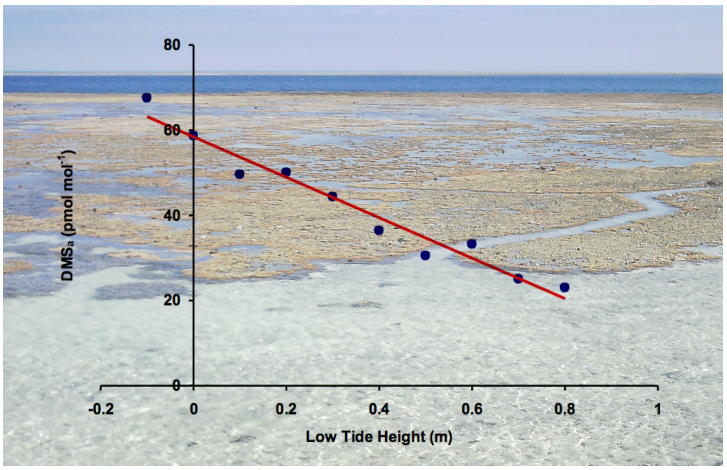

FIGURE 2 | Median atmospheric DMS mixing ratios plotted against low tide seawater height at Heron Island (23.44°S, 151.91°E) on the southern GBR, 18 Jul - 5 Aug 2013 (austral winter), derived from 30 min resolution measurements of DMS_a. The plotted median values are for measurements made in a time window approximately ± 1 h either side of the low tide height range that, to varying extents, aerially exposed the 27 km^2 lagoonal platform coral reef surrounding Heron Island shown in the photo (H.B. Swan). According to the dominant south-easterly trade winds at this location, the Heron Reef and the adjacent Wistari Reef, 1 km to the south, are expected to be the sources of DMS_a in excess of the approximately 20 pmol mol^{-1} DMS_a background wintertime mixing ratio.

estimated by Jackson et al. (2021) to be 0.03–0.05 Tg yr^{-1} of DMS (1,500–2,100 mol km^2 yr^{-1}), which represents 0.06-0.1% of the 52.5 Tg yr^{-1} of DMS estimated on average to be transferred from the global oceans to the atmosphere (Hulswar et al., 2021). Reported DMS fluxes from the GBR are not extraordinary; they are within the 0-10 µmol S m^{-2} d^{-1} range emitted from 93% of the world's oceans according to Hulswar et al. (2021).

AEROSOL OPTICAL DEPTH AND CLOUD COVER OVER THE GBR

The direct effect of marine aerosol to alter the extent that the atmosphere reflects and absorbs solar radiation can be evaluated by aerosol optical depth (AOD). A 16-year (2000-2015) satellite-derived record of fine mode AOD (0.1-0.25 µm radius) for an area of the GBR centred over Heron Island, was correlated with a coral reef stress metric formulated as a function of irradiance, water clarity, and tide height (Cropp et al., 2018). The correlation, which assumes that biogenic aerosol derived from the GBR was primarily linked to AOD, was strongest at low WS when biogenic aerosol is least advected away from its source point, and there is less sea spray aerosol generation. This correlation, which was consistent with field observations of DMS_a plumes at Heron Island at low-tide under low WS, was proposed as a possible mechanism by which coral reefs might alter the optical properties of the overlying atmosphere to attenuate local insolation (Cropp et al., 2018). This analysis was extended by Jackson et al. (2018) who analyzed fine mode AOD (2000-2017) over the entire 2,300 km length of the GBR and found AOD to be positively correlated with both SST and the coral reef stress metric. However, a thermal tipping point in the coral stress metric was identified where it became uncoupled from AOD, this being interpreted as a threshold for coral bleaching based on the assumption that bleaching leads to a reduction in emission of biogenic aerosol. The thermal threshold that leads to coral bleaching, separation of *Symbiodinium* from its polyp host and cessation of coral DMS production, has been reported to be when SST exceeds 30°C for an extended period (Fischer and Jones, 2012; Jones et al., 2017; Jones et al., 2018). Such marine heatwaves are increasing in frequency and, from a culmination of events in 1998, 2002, 2016, 2017 and 2020, have now resulted in mass coral bleaching along the entire GBR (Hughes et al., 2021). Increased summer cloud cover may alleviate coral bleaching by surface cooling, an effect that has been quantified over the GBR using satellite imagery and *in-situ* temperature and light loggers (Leahy et al., 2013). In that study, cloud cover alone was responsible for up to 32% of the variation in SST, although there was a 3-day lag between a change in cloud cover and a change in SST. Local-scale cloud cover over shallow GBR waters was recently reported to be more highly correlated with SST cooling than the larger-scale regional modulation of cloud cover linked to the El Niño–Southern Oscillation (Zhao et al., 2021). This cloud cover-SST relationship has been proposed to operate as an *ocean thermostat* in the western Pacific warm pool to the north of Australia where coral bleaching events have been relatively few in number despite the region having the highest average SST of all ocean regions (Kleypas et al., 2008). It has been proposed that DMS atmospheric oxidation products might promote a similar cloud cooling ocean thermostat effect over the GBR (Fischer and Jones, 2012), although this phenomenon may be explained by physical processes alone (Johnson et al., 2001; Takahashi et al., 2010).

MODELLING THE CLAW HYPOTHESIS GLOBALLY AND REGIONALLY ON THE GBR

Application of aerosol microphysics models to calculate the sensitivity of CCN, cloud fraction and surface incoming shortwave radiation to change due to varying DMS air-sea emissions over a wide range of climatologies have indicated the role of DMS in climate regulation to be globally weak (Woodhouse et al., 2010; Fiddes et al., 2018). These modeled outcomes are underpinned by observational evidence showing (i) gas-to-particle nucleation of DMS-derived H_2SO_4 does not commonly occur in the marine boundary layer (MBL) (Clarke et al., 1998; Gras et al., 2009; Kerminen et al., 2018); (ii) ultra-fine sea salt (Clarke et al., 2006; Smith, 2007; Xu et al., 2022) and other primary marine-derived materials (Leck and Bigg, 2007; Hawkins and Russell, 2010; Zelenyuk et al., 2010) can effectively act as CCN; and (iii) there are other marine-derived volatile organic compounds in addition to DMS that can form secondary organic aerosol (Meskhidze and Nenes, 2006; Exton et al., 2015; Swan et al., 2016). DMS may, however, have more importance regionally than globally to attenuate insolation according to large spatial and temporal differences in DMS_w concentrations and air-sea fluxes among the 56 global oceans provinces of Hulswar et al. (2021). Modelling of CCN production per unit mass of DMS emitted sulfur has been found to vary regionally by a factor of 20, suggesting that DMS emissions in some marine locations might provide regional climate regulation (Woodhouse et al., 2013). A recent GBR modeling study that added a coral-derived DMS surface emission of 0.3 Tg yr^{-1} S (1.7% of the global DMS sulfur emission) concluded that this superambient input of atmospheric sulfur into the model provided no robust effect on the regional climate of the GBR from direct and indirect aerosol effects (Fiddes et al., 2021). Another study that examined the effect of sub-daily changes in coral reef-derived DMS in a regional-scale climate model that was constrained using data gained from a recent field study (Sep-Oct 2016) on the GBR similarly found no significant changes in sulfate aerosol mass or total aerosol number to promote regional climate regulation (Fiddes et al., 2022). In that study, it was suggested that the close proximity of anthropogenic aerosol sources, such as power stations and other biomass burning sources, prevents the GBR from having any significant influence on the regional sulfate aerosol burden. The field study data used to constrain the model was collected following the 2016 summer of mass coral bleaching across the northern third of the GBR (Hughes et al., 2017). Although the field study was conducted on a section of the GBR that was less impacted by bleaching, uncertainty exists about the health of the GBR study zone at that time. Continuing bleaching of the GBR is closing the window of opportunity to research this topic (Jackson et al., 2020).

CONCLUDING COMMENTS

Periodic new sulfate-containing particle production (D_p < 20 nm) in the MBL has been indicated from the GBR (Modini et al., 2009) and on the GBR (Vaattovaara et al., 2013). These nano-particles can grow to the climatically active CCN size range (D_p ~50-100 nm) attenuating irradiance and contributing to marine cloud formation. However, aerosol contributions to CCN and cloud formation over the GBR have not been clearly identified and quantified, so it remains uncertain if the proposed ocean thermostat effect from low-level clouds to cool GBR SST is actually a negative feedback driven by coral-derived DMS oxidation products. Additionally, while clouds can reflect incoming sunlight leading to localized 3-day delayed temporal surface cooling, they also trap outgoing infrared radiation; hence, net radiative forcing by clouds over the GBR remains an uncertain complex component of the planetary greenhouse effect. While aerosol-climate models are important tools to assess the potential for DMS-facilitated climate regulation on the GBR, all are restricted by limited multiphase DMS chemistry, nucleation and nanoparticle growth mechanisms as well as other inherent short-comings and biases in meteorological, physical and chemical processes (Lee et al., 2019). DMS oxidation is far more complex than first imagined by Charlson et al. (1987) and continues to be elucidated (Von Glasow and Crutzen, 2004; Hoffmann et al., 2016). Notably, a previously unrecognized stable DMS oxidation product, hydroperoxymethyl thioformate (HPMTF, $HOOCH_2SCHO$) is currently not widely incorporated into atmospheric models. More than 30% of oceanic DMS emissions may form HPMTF, a major reservoir of sulfur in the MBL that is involved in new particle formation and growth (Veres et al., 2020). Mindful of these limitations, recent modeling (Fiddes et al., 2022; Jackson et al., 2022) indicates that DMS emissions from the GBR are currently insufficient, relative to background anthropogenic sulfur emissions, to significantly enhance sulfate aerosol and CCN number concentrations according to CLAW. Perhaps in pre-industrial times coral reef-derived DMS emissions may have exerted sufficient influence to regulate GBR regional climate (Fung et al., 2022). However, the GBR is no longer a pristine environment; it is impacted by regional pollution (Chen et al., 2019) and is also under immediate threat from global warming (Smith, 2019; Osman et al., 2021). Under current anthropogenic driven radiative forcing, the option to geo-engineer marine stratocumulus cloud albedo using ultra-fine sea salt, known as marine cloud brightening (MCB), has been proposed as a solution to protect the GBR. Modeling has indicated that MCB has the potential to sufficiently cool SST to limit coral bleaching on the GBR under a scenario of doubled atmospheric CO_2 levels (Latham et al., 2013). There are, however, logistical difficulties, uncertainties and risks of applying MCB (Stuart et al., 2013). Given that since 1998 only 2% of the GBR now remains untouched by bleaching (Hughes et al., 2021), which has again occurred in the 2021-22 summer during a La Niña year (GBRMPA et al., 2022), it is now apparent that it will not be DMS but an immediate coordinated global reduction of green house gas emissions that will save the GBR from continuing decline.

AUTHOR CONTRIBUTIONS

HS declares that he is the sole author of this mini review and has done his best to correctly summarize all cited research. The author agrees to be accountable for the content of this work and has approved the submitted version.

FUNDING

The Faculty of Science and Engineering, Southern Cross University, has provided financial support to publish this mini review. Australian Research Council grant DP150101649 for a Discovery Project titled, "The Great Barrier Reef as a significant source of climatically relevant aerosol particles" has assisted recent research cited in this mini review.

ACKNOWLEDGMENTS

I would like to thank the topic editors for facilitating the Frontiers Research Topic which led to this mini review. I would also like to thank Edith Olsen for assistance with preparation of **Figure 1** and the Faculty of Science and Engineering, Southern Cross University for an adjunct position that provides on-going association for work such as this to be published.

REFERENCES

Ayers, G. P., and Cainey, J. M. (2007). The CLAW Hypothesis: A Review of the Major Developments. *Environ. Chem.* 4, 366–374. doi: 10.1071/EN07080

Ayers, G. P., and Gillett, R. W. (2000). DMS and its Oxidation Products in the Remote Marine Atmosphere: Implications for Climate and Atmospheric Chemistry. *J. Sea Res.* 43, 275–286. doi: 10.1016/S1385-1101(00)00022-8

Ayers, G. P., Gillett, R. W., Ivey, J. P., Schäfer, B., and Gabric, A. (1995). Short-Term Variability in Marine Atmospheric Dimethylsulfide Concentration. *Geophysical Res. Lett.* 22, 2513–2516. doi: 10.1029/95GL02484

Ayers, G. P., Ivey, J. P., and Gillett, R. W. (1991). Coherence Between Seasonal Cycles of Dimethylsulphide, Methanesulphonate and Sulphate in Marine Air. *Nature* 329, 404–406. doi: 10.1038/349404a0

Boers, R., Ayres, G. P., and Gras, J. L. (1994). Coherence Between Seasonal Variation in Satellite-Derived Cloud Optical Depth and Boundary Layer CCN Concentrations at a Mid-Latitude Southern Hemisphere Station. *Tellus* 46B, 123–131. doi: 10.3402/tellusb.v46i2.15757

Broadbent, A. D., and Jones, G. B. (2004). DMS and DMSP in Mucus Ropes, Coral Mucus, Surface Films and Sediment Pore Waters From Coral Reefs in the Great Barrier Reef. *Mar. Freshw. Res.* 55, 849–855. doi: 10.1071/MF04114

Broadbent, A. D., Jones, G. B., and Jones, R. J. (2002). DMSP in Corals and Benthic Algae From the Great Barrier Reef. *Estuarine Coast. Shelf Sci.* 55, 547–555. doi: 10.1006/ecss.2002.1021

Caruana, A. M. N., and Malin, G. (2014). The Variability in DMSP Content and DMSP Lyase Activity in Marine Dinoflagellates. *Prog. Oceanography* 120, 410–424. doi: 10.1016/j.pocean.2013.10.014

Charlson, R. J., Lovelock, J. E., Andreae, M. O., and Warren, S. G. (1987). Oceanic Phytoplankton, Atmospheric Sulphur, Cloud Albedo and Climate. *Nature* 326, 655–661. doi: 10.1038/326655a0

Chen, Z., Schofield, R., Rayner, P., Zhang, T., Liu, C., Vincent, C., et al. (2019). Characterization of Aerosols Over the Great Barrier Reef: The Influence of Transported Continental Sources. *Sci. Total Environ.* 690, 426–437. doi: 10.1016/j.scitotenv.2019.07.007

Clarke, A. D., Owens, S. R., and Zhou, J. (2006). An Ultrafine Sea-Salt Flux From Breaking Waves: Implications for Cloud Condensation Nuclei in the Remote Marine Atmosphere. *J. Geophysical Res.* 111, D06202. doi: 10.1029/2005JD006565

Clarke, A. D., Varner, J. L., Eisele, F., Mauldin, R. L., Tanner, D., and Litchy, M. (1998). Particle Production in the Remote Marine Atmosphere: Cloud Outflow and Subsidence During Ace1. *J. Geophysical Res.* 103, 16397–16409. doi: 10.1029/97JD02987

Cropp, R., Gabric, A., Van Tran, D., Jones, G., Swan, H., and Butler, H. (2018). Coral Reef Aerosol Emissions in Response to Irradiance Stress in the Great Barrier Reef, Australia. *Ambio* 47, 671–681. doi: 10.1007/s13280-018-1018-y

Deschaseaux, E. S. M., Jones, G. B., Deseo, M. A., Shepherd, K. M., Kiene, R. P., Swan, H. B., et al. (2014). Effects of Environmental Factors on Dimethylated Sulfur Compounds and Their Potential Role in the Antioxidant System of the Coral Holobiont. *Limnology Oceanography* 59, 758–768. doi: 10.4319/lo.2014.59.3.0758

Exton, D. A., Mcgenity, T. J., Steinke, M., Smith, D. J., and Suggett, D. J. (2015). Uncovering the Volatile Nature of Tropical Coastal Marine Ecosystems in a Changing World. *Global Change Biol.* 21, 1383–1394. doi: 10.1111/gcb.12764

Fiddes, S. L., Woodhouse, M. T., Lane, T. P., and Schofield, R. (2021). Coral-Reef-Derived Dimethyl Sulfide and the Climatic Impact of the Loss of Coral Reefs. *Atmospheric Chem. Phys.* 21, 5883–5903. doi: 10.5194/acp-21-5883-2021

Fiddes, S. L., Woodhouse, M. T., Nicholls, Z., Lane, T. P., and Schofield, R. (2018). Cloud, Precipitation and Radiation Responses to Large Perturbations in Global Dimethyl Sulfide. *Atmospheric Chem. Phys.* 18, 10177–10198. doi: 10.5194/acp-18-10177-2018

Fiddes, S. L., Woodhouse, M. T., Utembe, S., Schofield, R., Alroe, J., Chambers, S. D., et al. (2022). The Contribution of Coral Reef-Derived Dimethyl Sulfide to Aerosol Burden Over the Great Barrier Reef: A Modelling Study. *Atmospheric Chem. Phys.* 22, 2419–2445. doi: 10.5194/acp-22-2419-2022

Fischer, E., and Jones, G. (2012). Atmospheric Dimethylsulphide Production From Corals in the Great Barrier Reef and Links to Solar Radiation, Climate and Coral Bleaching. *Biogeochemistry* 110, 31–46. doi: 10.1007/s10533-012-9719-y

Fung, K. M., Heald, C. L., Kroll, J. H., Wang, S., Jo, D. S., Gettelman, A., et al. (2022). Exploring Dimethyl Sulfide (DMS) Oxidation and Implications for Global Aerosol Radiative Forcing. *Atmospheric Chem. Phys.* 22, 1549–1573. doi: 10.5194/acp-22-1549-2022

Gras, J. L., Jimi, S. I., Siems, S. T., and Krummel, P. B. (2009). Postfrontal Nanoparticles at Cape Grim: Observations. *Environ. Chem.* 6, 508–514. doi: 10.1071/EN09075

Great Barrier Reef Marine Park Authority, Australian Institute of Marine Science and CSIRO. (2022). *Reef Snapshot: Summer 2021-22*. Available at: https://elibrary.gbrmpa.gov.au/jspui/bitstream/11017/3916/3/Reef-summer-snapshot-2021-22.pdf.

Hawkins, L. N., and Russell, L. M. (2010). Polysaccharides, Proteins, and Phytoplankton Fragments: Four Chemically Distinct Types of Marine Primary Organic Aerosol Classified by Single Particle Spectromicroscopy. *Adv. Meteorology* 612132, 1–14. doi: 10.1155/2010/612132

Hill, R. W., Dacey, J. W. H., and Krupp, D. A. (1995). Dimethylsulfoniopropionate in Reef Corals. *Bull. Mar. Sci.* 57, 489–494.

Hoffmann, E. H., Tilgner, A., Schrödner, R., Bräuer, P., Wolke, R., and Herrmann, H. (2016). An Advanced Modeling Study on the Impacts and Atmospheric Implications of Multiphase Dimethyl Sulfide Chemistry. *Proc. Natl. Acad. Sci.* 113, 11776–11781. doi: 10.1073/pnas.1606320113

Hopkins, F. E., Bell, T. G., Yang, M., Suggett, D. J., and Steinke, M. (2016). Air Exposure of Coral Is a Significant Source of Dimethylsulfide (DMS) to the Atmosphere. *Sci. Rep.* 6, 36031. doi: 10.1038/srep36031

Hughes, T. P., Kerry, J. T., Álvarez-Noriega, M., Álvarez-Romero, J. G., Anderson, K. D., Baird, A. H., et al. (2017). Global Warming and Recurrent Mass Bleaching of Corals. *Nature* 543, 373–377. doi: 10.1038/nature21707

Hughes, T. P., Kerry, J. T., Connolly, S. R., Álvarez-Romero, J. G., Eakin, M., Heron, S. F., et al. (2021). Emergent Properties in the Responses of Tropical Corals to Recurrent Climate Extremes. *Curr. Biol.* 31, p5393–5399. doi: 10.1016/j.cub.2021.10.046

Hulswar, S., Simo, R., Galí, M., Bell, T., Lana, A., Inamdar, S., et al. (2021). Third Revision of the Global Surface Seawater Dimethyl Sulfide Climatology (DMS-Rev3). *Earth System Sci. Data Discussions*. doi: 10.5194/essd-2021-236

Jackson, R., Gabric, A., and Cropp, R. (2018). Effects of Ocean Warming and Coral Bleaching on Aerosol Emissions in the Great Barrier Reef, Australia. *Sci. Rep.* 8, 14048. doi: 10.1038/s41598-018-32470-7

Jackson, R. L., Gabric, A. J., Cropp, R., and Woodhouse, M. T. (2020). Dimethylsulfide (DMS), Marine Biogenic Aerosols and the Ecophysiology of Coral Reefs. *Biogeosciences* 17, 2181–2204. doi: 10.5194/bg-17-2181-2020

Jackson, R. L., Gabric, A. J., Matrai, P. A., Woodhouse, M. T., Cropp, R., Jones, G. B., et al. (2021). Parameterizing the Impact of Seawater Temperature and Irradiance on Dimethylsulfide (DMS) in the Great Barrier Reef and the Contribution of Coral Reefs to the Global Sulfur Cycle. *J. Geophysical Research: Oceans* 126, e2020JC016783. doi: 10.1029/2020JC016783

Jackson, R. L., Woodhouse, M. T., Gabric, A. J., Cropp, R. A., Swan, H. B., Deschaseaux, E. S. M., et al. (2022). Modeling The Influence of Coral Reef-Derived Dimethylsulfide on the Atmosphere of the Great Barrier Reef, Australia. *Front. Mar. Sci.*

Johnson, R. H., Ciesielski, P. E., and Cotturone, J. A. (2001). Multiscale Variability of the Atmospheric Mixed Layer Over the Western Pacific Warm Pool. *J. Atmospheric Sci.* 58, 2729–2750. doi: 10.1175/1520-0469(2001)058<2729:MVOTAM>2.0.CO;2

Jones, G. B., Curran, M. A. J., and Broadbent, A. D. (1994). "Dimethylsulphide in the South Pacific," in *Recent Advances in Marine Science and Technology 1994*. Eds. O. Bellwood, H. Choat and N. Saxena (Queensland, Australia: Townsville: James Cook University Press), 183–190.

Jones, G., Curran, M., Broadbent, A., King, S., Fischer, E., and Jones, R. (2007). Factors Affecting the Cycling of Dimethylsulfide and Dimethylsulfoniopropionate in Coral Reef Waters of the Great Barrier Reef. *Environ. Chem.* 4, 310–322. doi: 10.1071/EN06065

Jones, G., Curran, M., Deschaseaux, E., Omori, Y., Tanimoto, H., Swan, H., et al. (2018). The Flux and Emission of Dimethylsulfide From the Great Barrier Reef Region and Potential Influence on the Climate of NE Australia. *J. Geophysical Research: Atmospheres* 123, 13835–13856. doi: 10.1029/2018JD029210

Jones, G., Curran, M., Swan, H., and Deschaseaux, E. (2017). Dimethylsulfide and Coral Bleaching: Links to Solar Radiation, Low Level Cloud and the Regulation of Seawater Temperatures and Climate in the Great Barrier Reef. *Am. J. Climate Change* 6, 328–359. doi: 10.4236/ajcc.2017.62017

Jones, G. B., and Trevena, A. J. (2005). The Influence of Coral Reefs on Atmospheric Dimethylsulphide Over the Great Barrier Reef, Coral Sea, Gulf of Papua and Solomon and Bismarck Seas. *Mar. Freshw. Res.* 56, 85–93. doi: 10.1071/MF04097

Kerminen, V.-M., Chen, X., Vakkari, V., Petäjä, T., Kulmala, M., and Bianchi, F. (2018). Atmospheric New Particle Formation and Growth: Review of Field Observations. *Environ. Res. Lett.* 13, 103003. doi: 10.1088/1748-9326/aadf3c

Kleypas, J. A., Danabasoglu, G., and Lough, J. M. (2008). Potential Role of the Ocean Thermostat in Determining Regional Differences in Coral Reef Bleaching Events. *Geophysical Res. Lett.* 35, L03613. doi: 10.1029/2007GL032257

Latham, J., Kleypas, J., Hauser, R., Parkes, B., and Gadian, A. (2013). Can Marine Cloud Brightening Reduce Coral Bleaching? *Atmospheric Sci. Lett.* 14, 214–219. doi: 10.1002/asl2.442

Leahy, S. M., Kingsford, M. J., and Steinberg, C. R. (2013). Do Clouds Save the Great Barrier Reef? Satellite Imagery Elucidates the Cloud-SST Relationship at the Local Scale. *PloS One* 8, e70400. doi: 10.1371/journal.pone.0070400

Leck, C., and Bigg, E. K. (2007). A Modified Aerosol-Cloud-Climate Feedback Hypothesis. *Environ. Chem.* 4, 400–403. doi: 10.1071/EN07061

Lee, S. H., Gordon, H., Yu, H., Lehtipalo, K., Haley, R., Li, Y., et al. (2019). New Particle Formation in the Atmosphere: From Molecular Clusters to Global Climate. *J. Geophysical Research: Atmospheres* 124, 7098–7146. doi: 10.1029/2018JD029356

Liss, P. S., and Lovelock, J. E. (2007). Climate Change: The Effect of DMS Emissions. *Environ. Chem.* 4, 377–378. doi: 10.1071/EN07072

Liss, P. S., Merlivat, L. Dordrecht, Netherlands: Reidel (1986). "Air-Sea Exchange Rates: Introduction and synthesis," in *The Role of Air-Sea Exchange in Geochemical Cycling*. Ed. P. Buat-Menard. (Dordrecht, Netherlands: Reidel Publishing Co.) 113–127.

Lovelock, J. E. (2009). *The Vanishing Face of Gaia: A Final Warning* (London, UK: Allen Lane, Penguin Group).

Lovelock, J. E., Maggs, R. J., and Rasmussen, R. A. (1972). Atmospheric Dimethylsulphide and the Natural Sulphur Cycle. *Nature* 237, 452–453. doi: 10.1038/237452a0

Mauldin, R. L.III, Berndt, T., Sipilä, M., Paasonen, P., Petäjä, T., Kim, S., et al. (2012). A New Atmospherically Relevant Oxidant of Sulfur Dioxide. *Nature* 488, 193–197. doi: 10.1038/nature11278

Meskhidze, N., and Nenes, A. (2006). Phytoplankton and Cloudiness in the Southern Ocean. *Science* 314, 1419–1423. doi: 10.1126/SCIENCE.1131779

Modini, R. L., Ristovski, Z. D., Johnson, G. R., He, C., Surawski, N., Morawska, L., et al. (2009). New Particle Formation and Growth at a Remote, Subtropical Coastal Location. *Atmospheric Chem. Phys.* 9, 7607–7621. doi: 10.5194/acp-9-7607-2009

Moothien-Pillay, R., Willis, B., and Terashima, H. (2005). Trends in the Density of Zooxanthellae in *Acropora Millepora* (Ehrenberg 1834) at the Palm Island Group, Great Barrier Reef, Australia. *Symbiosis* 38, 209–226. Available at: https://researchonline.jcu.edu.au/4563/1/4563_Pillay_et_al...2005.pdf

Osman, M. B., Tierney, J. E., Zhu, J., Tardif, R., Hakim, G. J., King, J., et al. (2021). Globally Resolved Surface Temperatures Since the Last Glacial Maximum. *Nature* 599, 239–244. doi: 10.1038/s41586-021-03984-4

Quinn, P. K., and Bates, T. S. (2011). The Case Against Climate Regulation *via* Oceanic Phytoplankton Sulphur Emissions. *Nature* 480, 51–56. doi: 10.1038/nature10580

Quinn, P. K., Coffman, D. J., Johnson, J. E., Upchurch, L. M., and Bates, T. S. (2017). Small Fraction of Marine Cloud Condensation Nuclei Made Up of Sea Spray Aerosol. *Nat. Geosci.* 10, 674–679. doi: 10.1038/ngeo3003

Raina, J.-B., Tapiolas, D. M., Foret, S., Lutz, A., Abrego, D., Ceh, J., et al. (2013). DMSP Biosynthesis by an Animal and its Role in Coral Thermal Stress Response. *Nature* 502, 677–680. doi: 10.1038/nature12677

Smith, M. H. (2007). Sea-Salt Particles and the CLAW Hypothesis. *Environ. Chem.* 4, 391–395. doi: 10.1071/EN07071

Smith, G. A. (2019). Seasonal Climate Summary for the Southern Hemisphere (Autumn 2017): The Great Barrier Reef Experiences Coral Bleaching During El Niño–Southern Oscillation Neutral Conditions. *J. South. Hemisphere Earth Syst. Sci.* 69, 310–330. doi: 10.1071/ES19006

Stuart, G. S., Stevens, R. G., Partanen, A. I., Jenkins, A. K. L., Korhonen, H., Forster, P. M., et al. (2013). Reduced Efficacy of Marne Cloud Brightening Geoengineering Due to in-Plume Aerosol Coagulation: Parameterization and Global Implications. *Atmospheric Chem. Phys.* 13, 10385–10396. doi: 10.5194/acp-13-10385-2013

Swan, H. B. (2017). *Investigation of Dimethylsulfide Biogeochemistry Relevant to the CLAW Hypothesis at Heron Island, Southern Great Barrier Reef* (Southern Cross University: Doctor of Philosophy (PhD) Dissertation).

Swan, H. B., Crough, R. W., Vaattovaara, P., Jones, G. B., Deschaseaux, E. S. M., Eyre, B. D., et al. (2016). Dimethyl Sulfide and Other Biogenic Organic Compound Emissions From Branching Coral and Reef Seawater: Potential Sources of Secondary Aerosol Over the Great Barrier Reef. *J. Atmospheric Chem.* 73, 303–328. doi: 10.1007/s10874-016-9327-7

Swan, H. B., Jones, G. B., Deschaseaux, E. S. M., and Eyre, B. D. (2017). Coral Reef Origins of Atmospheric Dimethylsulfide at Heron Island, Southern Great Barrier Reef, Australia. *Biogeosciences* 14, 229–239. doi: 10.5194/bg-14-229-2017

Takahashi, Y., Okazaki, Y., Sato, M., Miyahara, H., Sakanoi, K., Hong, P. K., et al. (2010). 27-Day Variation in Cloud Amount in the Western Pacific Warm Pool Region and Relationship to the Solar Cycle. *Atmospheric Chem. Phys.* 10, 1577–1584. doi: 10.5194/acp-10-1577-2010

Vaattovaara, P., Swan, H. B., Jones, G. B., Deschaseaux, E., Miljevic, B., Laaksonen, A., et al. (2013). The Contribution of Sulfate and Oxidized Organics in Climatically Important Ultrafine Particles at a Coral Reef Environment. *Int. J. Mar. Environ. Sci.* 7, 720–724. Available at: https://publications.waset.org/9998064/pdf

Vallina, S. M., and Simó, R. (2007). Strong Relationship Between DMS and the Solar Radiation Dose Over the Global Ocean. *Science* 315, 506. doi: 10.1126/science.1133680

Van Alstyne, K. L., Dominique, V. J., and Muller-Parker, G. (2008). Is Dimethylsulfoniopropionate (DMSP) Produced by the Symbionts or the Host in an Anemone-Zooxanthella Symbiosis? *Coral Reefs* 28, 167–176. doi: 10.1007/s00338-008-0443-y

Veres, P. R., Neuman, J. A., Bertram, T. H., Assaf, E., Wolfe, G. M., Williamson, C. J., et al. (2020). Global Airborne Sampling Reveals a Previously Unobserved Dimethyl Sulfide Oxidation Mechanism in the Marine Atmosphere. *Proc. Natl. Acad. Sci.* 117, 4505–4510. doi: 10.1073/pnas.1919344117

Von Glasow, R., and Crutzen, P. J. (2004). Model Study of Multiphase DMS Oxidation With a Focus on Halogens. *Atmospheric Chem. Phys.* 4, 589–608. doi: 10.5194/acp-4-589-2004

Woodhouse, M. T., Carslaw, K. S., Mann, G. W., Vallina, S. M., Vogt, M., Halloran, P. R., et al. (2010). Low Sensitivity of Cloud Condensation Nuclei to Changes in the Sea-Air Flux of Dimethyl-Sulphide. *Atmospheric Chem. Phys.* 10, 7545–7559. doi: 10.5194/acp-10-7545-2010

Woodhouse, M. T., Mann, G. W., Carslaw, K. S., and Boucher, O. (2013). Sensitivity of Cloud Condensation Nuclei to Regional Changes in Dimethyl-Sulphide Emissions. *Atmospheric Chem. Phys.* 13, 2723–2733. doi: 10.5194/acp-13-2723-2013

Xu, W., Ovadnevaite, J., Fossum, K. N., Lin, C., Huang, R.-J., Ceburnis, D., et al. (2022). Sea Spray as an Obscured Source for Marine Cloud Nuclei. *Nat. Geosci.* 15, 282–286. doi: 10.1038/s41561-022-00917-2

Yost, D. M., and Mitchelmore, C. L. (2009). Dimethylsulfoniopropionate (DMSP) Lyase Activity in Different Strains of the Symbiotic Alga *Symbiodinium Microadriaticum*. *Mar. Ecol. Prog. Ser.* 386, 61–70. doi: 10.3354/meps08031

Zaveri, R. A., Wang, J., Fan, J., Zhang, Y., Shilling, J. E., Zelenyuk, A., et al. (2022). Rapid Growth of Anthropogenic Organic Nanoparticles Greatly Alters Cloud Life Cycle in the Amazon Rainforest. *Sci. Adv.* 8, eabj0329. doi: 10.1126/sciadv.abj0329

Zelenyuk, A., Imre, D., Earle, M., Easter, R., Korolev, A., Leaitch, R., et al. (2010). *In Situ* Characterization of Cloud Condensation Nuclei, Interstitial, and Background Particles Using the Single Particle Mass Spectrometer, SPLAT II. *Analytical Chem.* 82, 7943–7951. doi: 10.1021/ac1013892

Zhao, W., Huang, Y., Siems, S., and Manton, M. (2021). The Role of Clouds in Coral Bleaching Events Over the Great Barrier Reef. *Geophysical Res. Lett.* 48, e2021GL093936. doi: 10.1029/2021GL093936

Zhu, B., Huang, X.-F., Xia, S.-Y., Lin, L.-L., Cheng, Y., and He, L.-Y. (2021). Biomass-Burning Emissions Could Significantly Enhance the Atmospheric Oxidizing Capacity in Continental Air Pollution. *Environ. pollut.* 285, 117523. doi: 10.1016/j.envpol.2021.117523

Conflict of Interest: The author declares that the research was conducted in the absence of any commercial or financial relationships that could be construed as a potential conflict of interest.

Publisher's Note: All claims expressed in this article are solely those of the authors and do not necessarily represent those of their affiliated organizations, or those of the publisher, the editors and the reviewers. Any product that may be evaluated in this article, or claim that may be made by its manufacturer, is not guaranteed or endorsed by the publisher.

frontiers | Frontiers in Marine Science

ORIGINAL RESEARCH
published: 20 June 2022
doi: 10.3389/fmars.2022.910441

The Interplay Between Dimethyl Sulfide (DMS) and Methane (CH_4) in a Coral Reef Ecosystem

Elisabeth S. M. Deschaseaux[1,2], Hilton B. Swan[1,2], Damien T. Maher[1,3], Graham B. Jones[1], Kai G. Schulz[1,2], Edwin P. Koveke[4], Kei Toda[4,5] and Bradley D. Eyre[1,2]*

[1] Faculty of Science and Engineering, Southern Cross University, Lismore, NSW, Australia, [2] Centre for Coastal Biogeochemistry, Faculty of Science and Engineering, Southern Cross University, Lismore, NSW, Australia, [3] Southern Cross GeoScience, Faculty of Science and Engineering, Southern Cross University, Lismore, NSW, Australia, [4] Department of Chemistry, Kumamoto University, Kumamoto, Japan, [5] International Research Organization for Advanced Science and Technology (IROAST), Kumamoto University, Kumamoto, Japan

OPEN ACCESS

Edited by:
Cliff Ross, University of North Florida, United States

Reviewed by:
Gael John Lecellier, Université de Versailles Saint-Quentin-en-Yvelines, France
Sohiko Kameyama, Hokkaido University, Japan

***Correspondence:**
Elisabeth S. M. Deschaseaux
elisabeth.deschaseaux@gmail.com

Specialty section:
This article was submitted to Coral Reef Research, a section of the journal Frontiers in Marine Science

Received: *01 April 2022*
Accepted: *04 May 2022*
Published: *20 June 2022*

Citation:
Deschaseaux ESM, Swan HB, Maher DT, Jones GB, Schulz KG, Koveke EP, Toda K and Eyre BD (2022) The Interplay Between Dimethyl Sulfide (DMS) and Methane (CH_4) in a Coral Reef Ecosystem. Front. Mar. Sci. 9:910441. doi: 10.3389/fmars.2022.910441

Earth's Radiation Budget is partly dictated by the fragile and complex balance between biogenic volatile organic compounds (BVOCs) and greenhouse gases (GHGs), which have the potential to impose cooling or warming once emitted to the atmosphere. Whilst methane (CH_4) is strictly associated with global warming due to its solar-radiation absorbing properties, dimethyl sulfide (DMS) is generally considered a cooling gas through the light scattering properties of its atmospheric oxidation products. However, DMS may also partially contribute to the Earth's warming through a small portion of it being degraded to CH_4 in the water column. Coral reefs emit both DMS and CH_4 but they have not previously been simultaneously measured. Here, we report DMS and CH_4 fluxes as well as aerosol particle counts at Heron Island, southern Great Barrier Reef, during the austral summer of 2016. Sea-to-air DMS and CH_4 fluxes were on average 24.9 ± 1.81 and 1.36 ± 0.11 μmol m^{-2} d^{-1}, whilst intermediate (< 0.5-2.5 um) and large (> 2.5 um) particle number concentrations averaged 5.51 x 10^6 ± 1.73 x 10^5 m^{-3} and 1.15 x 10^6 ± 4.63 x 10^4 m^{-3}, respectively. Positive correlations were found between DMS emissions and the abundance of intermediate (R^2 = 0.1669, $p < 0.001$, n = 93) and large (R^2 = 0.0869, p = 0.004, n = 93) aerosol particles, suggesting that DMS sea-to-air emissions significantly contribute to the growth of existing particles to the measured size ranges at the Heron Island lagoon. Additionally, a strong positive correlation was found between DMS and CH_4 fluxes (R^2 = 0.7526, $p < 0.00001$, n = 93), suggesting that the emission of these volatile compounds from coral reefs is closely linked. The slope of the regression between DMS and CH_4 suggests that CH_4 emissions at the Heron Island lagoon represent 5% of that of DMS, which is consistent with the average sea-to-air fluxes reported in this study (i.e. 24.9 ± 1.81 μmol m^{-2} d^{-1} for DMS and 1.36 ± 0.11 for CH_4). These findings provide new insights on the complexity of BVOC and GHG emissions in coral reef systems and their potential role in climate regulation.

Keywords: fluxes, great barrier reef, biogenic volatile organic compounds (BVOCs), greenhouse gases (GHGs), aerosol particles, Heron Island

1 INTRODUCTION

Dimethyl sulfide (DMS) and methane (CH_4) are key biogenic compounds in climate change processes (Carpenter et al., 2012). DMS is often associated with a cooling effect through contributing to aerosol formation that increase Earth's radiative properties (Charlson et al., 1987). In contrast, CH_4 is responsible for a warming effect with a short-term greenhouse potential that is 23 to 69 times greater than that of CO_2 (Shine et al., 2005). The bulk of DMS is produced through the algal and bacterial enzymatic cleavage of dimethylsulfoniopropionate (DMSP) (Simó, 2001), a biogenic sulfur compound that is synthesised by a wide range of marine algae (Stefels, 2000), bacteria (Curson et al., 2017) and invertebrate corals (Raina et al., 2013). In contrast, the bulk of biogenic CH_4 is mainly produced by anaerobic methanogenic bacterial activity through the reduction of either CO_2, acetate or methyl-group containing compounds (Liu and Whitman, 2008), although recent studies show that CH_4 can also be produced by plants, fungi, algae and cyanobacteria from methylated nitrogen- and sulfur-containing compounds in the presence of oxygen (Ernst et al., 2022). Thus, a small portion of CH_4 can originate from the hydrolysis of DMS according to the following equation (Kiene et al., 1986; Liu and Whitman, 2008):

$$2(CH_3)_2S + 2H_2O \rightarrow 3CH_4 + CO_2 + 2H_2S \quad (1)$$

The link between DMS degradation and CH_4 production has now been reported across several studies on anoxic marine sediments (Kiene and Visscher, 1987; Kiene, 1988; Wang et al., 2009), where methanogenic bacteria are particularly abundant (Mechalas, 1974; Barnes and Goldberg, 1976). Indeed, it seems that the DMS-to-CH_4 conversion can also be mediated by methanogenic bacteria (Kiene and Visscher, 1987) but also by methylotrophic bacteria belonging to the order Methanosarcinales and Methanobacteriales (Liu and Whitman, 2008). More recently, the role of DMS as a precursor of CH_4 was clearly demonstrated in upwelling waters as addition of ^{13}C enriched-DMS led to a significant increase in ^{13}C enriched-CH_4 (Florez-Leiva et al., 2013). Interestingly, DMS was estimated to contribute to about 28% of CH_4 production in both anoxic sediments (Kiene, 1988) and upwelling waters (Florez-Leiva et al., 2013), although these two marine habitats are likely to host very different bacterial communities. DMS as a potential precursor of CH_4 across various marine ecosystems adds a level of complexity to the role of DMS as a climate cooling agent (Charlson et al., 1987; Quinn and Bates, 2011; Jones, 2013).

DMS is expected to be particularly concentrated in coral reef ecosystems due to the high DMSP content in corals, coral-associated symbionts and a wide range of coral reef invertebrates (Deschaseaux et al., 2016; Haydon et al., 2018). However, although coral reef sea-to-air DMS fluxes contribute to atmospheric sulfur emissions (Swan et al., 2017), a recent modelling study suggested that coral-reef-derived DMS emissions most likely have a negligible effect on the local climate of the Great Barrier Reef (Fiddes et al., 2021). Coral reef frameworks are also sites of active anoxic and suboxic organic matter oxidation, making coral reef pore waters particularly rich in CH_4 and coral reef ecosystems ideal platforms for the release of CH_4 to the water column and atmosphere (Sansone et al., 1993; O'Reilly et al., 2015), which could be counteracting the cooling effect of DMS emissions. A recent study showed that permeable coral reef carbonate sediments were a source of DMS and CH_4 into the water column and that CH_4 production could be a sink for DMS in coral reef systems (Deschaseaux et al., 2019). Since sea-to-air DMS and CH_4 fluxes from coral reef systems have been independently reported by previous studies, the focus of this study was to simultaneously quantify and report sea-to-air DMS and CH_4 fluxes from the Heron Island reef lagoon, southern Great Barrier Reef, to assess the interplay of atmospheric DMS and CH_4 emissions.

We hypothesised that coral-reef DMS emissions would contribute to the growth of aerosol nanoparticles and that coral-reef DMS and CH_4 emissions are linked due to a small portion of DMS being hydrolysed to CH_4 in coral reef waters.

2 MATERIAL AND METHODS

2.1 Study Site and Sampling

A field campaign was conducted on Heron Island, southern Great Barrier Reef (23.44°S, 151.91°E), in the austral summer of 2016 (4^{th} to the 17^{th} of February) where dissolved CH_4 and CO_2 were measured alongside dissolved DMS (DMS_w) using a cavity-ring-down spectrometer (Picarro G2201-*i*) (Maher et al., 2013) and a Vapor Generation – Chemiluminescence (VG-CL) device (Nagahata et al., 2013), respectively. A Gas Chromatograph (Varian CP3800 GC) equipped with a pulsed flame photometric detector (GC-PFPD) was used to measure atmospheric DMS (DMS_a) (Swan et al., 2015; Swan et al., 2017).

A water pump and a 60 m suction-rated pipe were used to pump seawater from the Heron Island reef flat to the Heron Island Research Station (HIRS), where all instruments were operated. The seawater inlet was attached to a cinder block 50 cm above the sediment bed and about 50 cm below the low-tide mark. A non-return valve and a 1 mm mesh net were placed around the suction pipe inlet to prevent large pieces of sediment and seaweed getting through the suction line. The mesh was cleaned every 2-3 days to prevent biofouling. Part of the pumped seawater was diverted into a showerhead exchanger that was connected in line with the cavity-ring-down spectrometer for CH_4 and CO_2 measurements, while the remainder was diverted to the HIRS' flow-through seawater recycling system. The recycling water outlet was used to manually sample seawater at a low flow rate using a 50 mL syringe for DMS_w analysis. A HYDROLAB HL4 sonde was placed within 1 m of the water intake to record seawater temperature, salinity, dissolved oxygen (DO), and depth, every 15 min. Tide predictions were sourced from the Bureau of Meteorology (BoM) with low tide times locally adjusted +1.25 h for the Heron Island reef flat according to Swan et al. (2017).

An air intake consisting of ~10 m Teflon™ tubing was fixed to the roof of the HIRS, within ~100 m in line of sight to the reef flat location where seawater was continuously pumped from. The air intake was shielded from rain. A wireless automated weather station (AWS, model XC0348, Electus Distribution) mounted within 1 m of the air intake provided data for wind speed (WS, ± 1 m s^{-1} for WS < 10 m s^{-1} and ± 10% for WS > 10 m s^{-1}), wind direction (WD), rainfall, air temperature (± 1°C), humidity (± 5%) and barometric pressure (± 3hPa), at 5-min intervals. Meteorological data at 5 min intervals was used to match to the 15 min interval chemical measurements. Solar irradiance at the proximity of the air intake was recorded using a HOBO (Onset Co., USA) light logger (upper limit ~6000 μE m^{-2} s^{-1}). Light intensity HOBO Lux units were adjusted to a maximum light intensity of 2000 μEm^{-2} s^{-1}. First and last daytime lights were at 5:14 and 18:57 respectively on average over the sampling period. An air quality monitor laser particle counter (Dylos DC1700, Dylos Corp, CA, USA) was used to record 1-min averaged particle number concentrations at ambient humidity in the two size range fractions 0.5-2.5 μm and > 2.5 μm every 15 min. The air quality monitor was placed in a shielded location near the air intake.

2.2 DMS_w and DMS_a Measurements

DMS_w concentrations were determined in triplicate every 15 min by placing 10 mL of seawater into a 50 mL sample tube that was manually shaken for 1 min, then pressurised with 30 mL of air and injected onto the chemiluminescence device (VG-CL) (Nagahata et al., 2013). When DMS_w mixes with ozone in the VG-CL, it generates an instant chemiluminescent emission where the light intensity is converted into a quantifiable electrical signal. The injection tube was rinsed with deionised water in between each injection to prevent analyte carry-over. A 6-point calibration was run at the beginning of the field campaign, and either a 4 nM or 10 nM DMSP standard was randomly run each day to monitor the reproducibility and stability of the system over time. Because these measurements are labour-intensive and could not be automated, sampling occurred at random times of the day and night over the 2-week field campaign.

DMS_a concentrations were determined on the GC-PFPD using an automated cryogenic trapping system that collected ~4L of air for analysis, providing a 0.1 nmol m^{-3} (0.002 ppb) limit of detection. The expanded relative measurement uncertainty of the automated GC-PFPD was 13% (k = 2, for a 95% CI). A complete description of the configuration, operation, calibration, and uncertainty analysis of the automated GC-PFPD is described by Swan et al. (2015).

2.3 Flux Calculations

Sea-to-air DMS fluxes were estimated based on the different parameterisations proposed by Liss and Merlivat (1986) (LM86), Nightingale et al. (2000) (N00) and Wanninkhof (2014) (W14) and by applying the approach of Lana et al. (2011) (L11) (see details in **Supplementary Table 1**). The sea-to-air DMS fluxes and uncertainties presented here correspond to the median and standard error of these combined fluxes.

Briefly, sea-to-air fluxes of DMS (F_{DMS}) (in μmol m^{-2} d^{-1}) were estimated based on the following equation:

$$F_{DMS} = K_T(C_w - \alpha C_g) \quad (2)$$

Where K_T is the gas transfer velocity constant (in m d^{-1}), α is the dimensionless Henry's Law constant and C_w and C_g are DMS concentrations (in μmol m^{-3}) in the water and gas phase, respectively, with each parameterisation using a different approach to estimate K_T.

The dimensionless Henry's Law Constant (α) for DMS solubility in seawater was calculated using the following equation:

$$\alpha = 1/H_K \text{ x } RT \quad (3)$$

Where H_K (atm L mol^{-1}) is the Henry's Law Constant for DMS, R is the universal gas constant (0.082 L atm K^{-1} mol^{-1}) and T is the seawater temperature in Kelvin. H_K was calculated based on the following equation by Dacey et al. (1984):

$$H_K = e^{(-3547/T + 12.64)} \quad (4)$$

Sea-to-air CH_4, CO_2 and O_2 fluxes were calculated based on the parameterisation approaches proposed by Ho et al. (2006) and Wanninkhof (2014). Atmospheric concentrations were assumed to be constant (CH_4 1.8 ppm, CO_2 400 ppm and O_2 21000 ppm). Solubility coefficients for CH_4 (Wiesenburg and Guinasso Jr, 1979), CO_2 (Weiss, 1974) and O_2 (Benson and Krause Jr, 1984) were calculated based on temperature and salinity.

2.4 Reef Production

Reef DMS, CH_4, CO_2 and O_2 production (RP, mol m^{-2} h^{-1}) were calculated around each low tide using the following equation:

$$RP = \frac{\Delta Cw}{\Delta T} x \ D + \frac{MeanFlux}{24} \quad (5)$$

Where ΔC_W is the difference in dissolved concentrations between the highest point following low tide and the actual low tide, ΔT is the time difference between these 2 points, D is the average depth for that time period and MeanFlux is the average sea-to-air flux for that period.

2.5 Statistical Analysis

The significance of the correlations between DMS, CH_4, CO_2 and O_2 were evaluated using the Pearson correlation method. Given that DMS and CH_4 showed the strongest correlation (R^2 = 0.7526, p <0.00001, n = 93), we specifically assessed what drives DMS and CH_4 fluxes by carrying out stepwise multiple linear regressions (MLRs) against seven potential predictors and their interactions (salinity, pH, depth, wind direction, dewpoint, windchill and solar irradiance). In order to avoid over-fitting and find a balance between model complexity and explanatory power, we followed a backward elimination process based on the Akaike Information Criterion (AIC, details in **Supplementary Figure 1**) starting with all seven potential measured predictors. Note that we opted not to include

temperature and wind speed, which are covariates in flux calculations. Windchill and dewpoint are influenced by air temperature, which is not a covariate in flux calculations, and wind direction is not correlated to wind speed. Calculations were performed using the functions "boxplot", "stepwisefit", and "plotEffects" in MATLAB.

3 RESULTS

3.1 Environmental Data

Sea surface temperature (SST) within the Heron Island reef lagoon fluctuated between 25.0 and 29.2°C over the course of the campaign with an average SST of 27.3 ± 0.94°C. Salinity and pH were on average 37.0 ± 0.25 ppt and 8.18 ± 0.19, respectively. Seawater depth ranged from 0.46 to 1.38 m, 10 m wind speed from 0 to 9.20 m s^{-1}, windchill from 21.3 to 29.9°C, dewpoint from 20.0 to 23.4°C and light intensity from 0 to 2000 µE m^{-2} s^{-1}.

3.2 Sea-to-Air Fluxes and Relationships

Sea-to-air DMS fluxes varied from not-detectable to 69.5 µmol m^{-2} d^{-1} with an average flux of 24.9 ± 1.81 µmol m^{-2} d^{-1} (mean± SE, n = 93; **Figure 1A**). Sea-to-air CH_4 fluxes varied from -0.12 to 3.91 µmol m^{-2} d^{-1} with an average flux of 1.36 ± 0.11 µmol m^{-2} d^{-1} (**Figure 1B**). Atmospheric CO_2 and O_2 fluxes varied from -15.4 to 30.7 mmol m^{-2} d^{-1} and from -188 to 403 mmol m^{-2} d^{-1}, with mean CO_2 and O_2 fluxes of 0.30 ± 0.71 and 70.5 ± 12.3 mmol m^{-2} d^{-1}, respectively (**Figures 1C, D**).

All 24h-integrated sea-to-air fluxes showed a diurnal trend with DMS, CO_2 and CH_4 fluxes being generally greater at night than during the day while O_2 fluxes showed the opposite trend (**Figure 1**). Sea-to-air CO_2 fluxes showed the most variability during the first hours of sunlight while DMS and O_2 fluxes showed the most variability between dusk and midnight. CH_4 fluxes showed the most variability both at night and during the first hours of sunlight.

Sea-to-air O_2 fluxes negatively correlated with DMS (R^2 = 0.0569, n = 93, p = 0.02), CH_4 (R^2 = 0.1476, n = 93, p < 0.001) and CO_2 (R^2 = 0.346, n = 93, p <0.00001), although the negative relationship between O_2 and CO_2 was clearly the strongest (**Figure 2**). Sea-to-air CO_2 and CH_4 fluxes were weakly positively correlated (R^2 = 0.1709, n = 93, p <0.001) while CO_2 and DMS fluxes were not significantly correlated (R^2 = 0.0242, n = 93, p > 0.05). Sea-to-air DMS and CH_4 fluxes showed the strongest positive correlation (R^2 = 0.7526, n = 93; p < 0.00001).

Dissolved DMS, CH_4, CO_2 and O_2 concentrations are presented in the supplementary material (**Supplementary Figure 2**). Because fluxes are calculated based on concentrations and transfer velocity, and the transfer velocity is shared across fluxes, the relationships between dissolved DMS and dissolved CH_4, CO_2 and O_2 concentrations were also plotted. Dissolved DMS concentrations positively correlated with dissolved CH_4 (R^2 = 0.7706, n = 93) and CO_2 (R^2 = 0.2273, n = 93) concentrations and negatively correlated with dissolved O_2 concentrations (R^2 = 0.3847, n = 93) (**Supplementary Figure 3**, p < 0.00001).

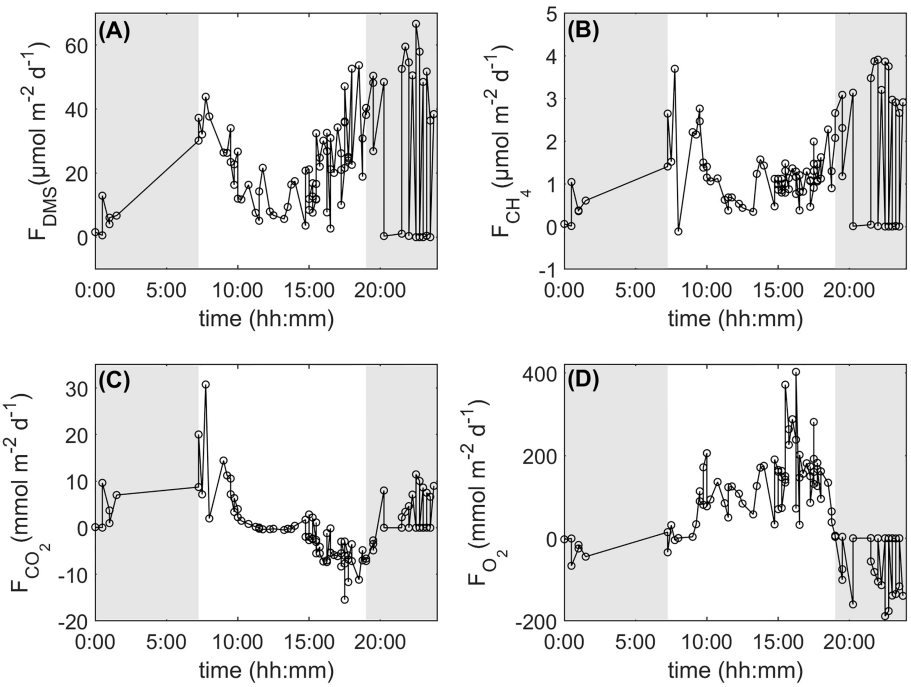

FIGURE 1 | 24-h integrated DMS **(A)**, CH_4 **(B)**, CO_2 **(C)** and O_2 **(D)** fluxes from the Heron Island reef, southern Great Barrier Reef, for the period 4-17 February, 2016. Shaded areas represent hours of darkness.

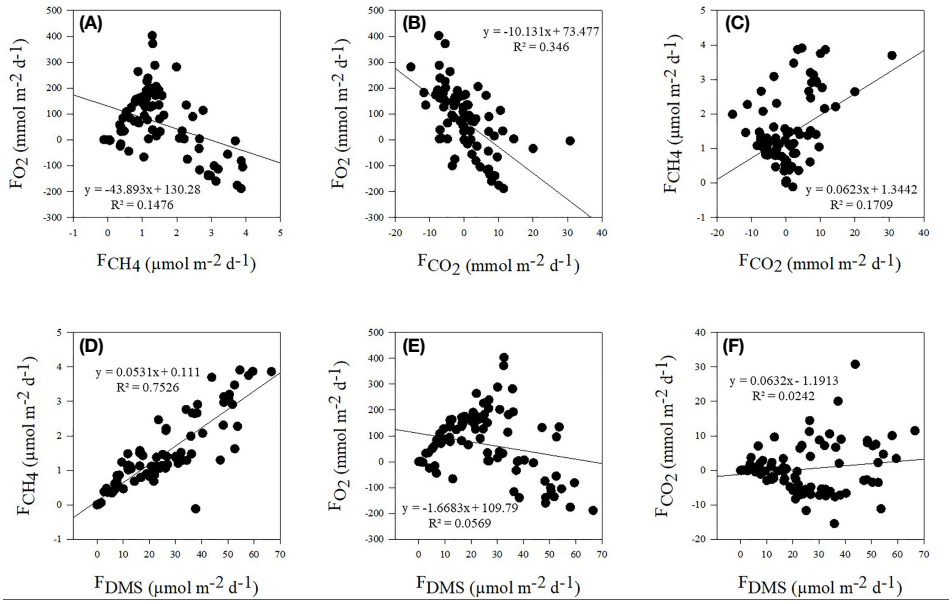

FIGURE 2 | Correlations between sea-to-air fluxes of CH_4 and O_2 **(A)**, CO_2 and O_2 **(B)** and CO_2 and CH_4 **(C)** as well as between fluxes of DMS and CH_4 **(D)**, O_2 **(E)** and CO_2 **(F)**. Trendlines, regression equation and R^2 values are displayed for each correlation.

3.3 Multiple Linear Regressions

The backward elimination process used in the stepwise Multiple Linear Regressions (MLRs) revealed that salinity, pH, depth, wind direction, dewpoint and wind chill were the six main drivers of sea-to-air DMS fluxes and that pH, depth, wind direction, dewpoint, wind chill and light were the six main drivers of CH_4 fluxes (**Table 1**). The linear fit between measured and predicted DMS and CH_4 fluxes exhibited an R^2 of 0.717 and 0.631 (n = 93, p <0.00001), respectively (**Figures 3A, B**). The most negative drivers of DMS emissions were wind chill and pH whereas the most positive driver was wind direction (**Figure 3C**). Similarly, the main negative and positive drivers of CH_4 emissions were pH and wind direction, respectively (**Figure 3D**). When plotting wind direction (in azimuth degrees) against DMS and CH_4 fluxes (**Supplementary Figure 4**), it appeared that the wind direction leading to the greatest DMS and CH_4 emissions was predominantly at 180°, which corresponds to the direction of the dominant southerly trade winds at Heron Island.

3.4 Reef Production

The DMS reef production exhibited positive values at all times, with a few sporadic spikes around peak hours of sunlight (~ 11:00) and in the middle of the night (~23:00) (**Figure 4A**). Although an order of magnitude lower, the CH_4 reef production was also positive at all times but with greater values recorded at night (**Figure 4B**). The CO_2 reef production was positive at night and for the first half of the day but negative from about 12:00 to 20:00 (**Figure 4C**). As expected, the O_2 reef production was

TABLE 1 | Multiple Linear Regression (MLR) statistics (estimated coefficient, standard error – SE; t and p values), describing sea-to-air DMS and CH_4 fluxes in response to various environmental variables (salinity, pH, depth, wind direction – WD, dewpoint – DP, windchill – WC and light) with interactions, for the best six-variable model using the Akaike Information Criterion (AIC, Supp. Mat.), i.e. lowest number (compare to **Figure 3**).

DMS	Estimate	SE	t	p	CH_4	Estimate	SE	t	p
(Intercept)	19054	2785	6.841	**<0.001**	(Intercept)	999.7	174.9	5.717	**<0.001**
salinity	22.42	5.333	4.203	**<0.001**	pH	-122.9	21.27	-5.778	**<0.001**
pH	-2419	348.3	-6.944	**<0.001**	depth	19.07	5.476	3.483	**0.001**
depth	211.4	88.35	2.393	**0.019**	WD	0.025	0.005	4.679	**<0.001**
WD	0.321	0.078	4.132	**<0.001**	DP	-44.22	7.805	-5.666	**<0.001**
DP	-651.5	121.1	-5.382	**<0.001**	WC	0.371	0.199	1.868	0.065
WC	-203.1	56.71	-3.581	**0.001**	light	-0.024	0.010	-2.476	**0.015**
pH:DP	79.02	14.73	5.366	**<0.001**	pH:DP	5.371	0.948	5.664	**<0.001**
pH:WC	24.78	7.047	3.517	**0.001**	pH:light	0.003	0.001	2.462	**0.016**
depth:WD	-0.312	0.090	-3.474	**0.001**	depth:WD	-0.027	0.006	-4.507	**<0.001**
depth:WC	-6.458	3.482	-1.854	0.067	depth:WC	-0.579	0.212	-2.734	**0.008**

Significant p *values appear in bold for a level of significance of ≤ 0.05.*

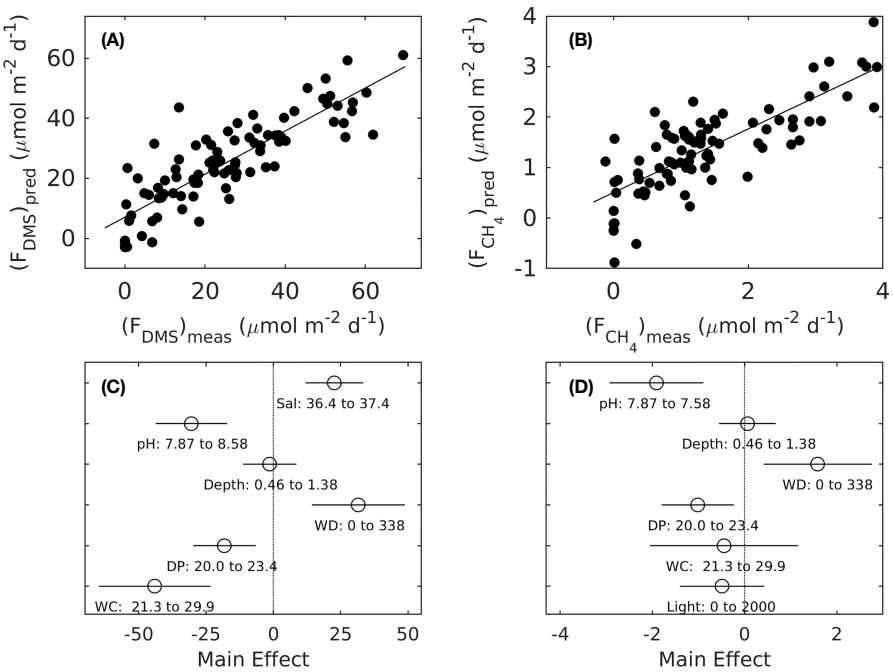

FIGURE 3 | Linear fits through *in situ* and predicted sea-to-air DMS (**A**, R^2 = 0.717) and CH_4 (**B**, R^2 = 0.631) fluxes by the stepwise Multiple Linear Regression (MLR) model with the lowest Akaike Information Criterion (AIC) with six main variables, and resulting main effect sizes of salinity, pH, depth, wind direction (WD), Dewpoint (DP) and Wind Chill (WC) for DMS fluxes **(C)** and of pH, depth, WD, DP and WC and light for CH_4 fluxes **(D)** (compare to **Table 1**).

essentially positive during the day until dusk, and negative at night (**Figure 4D**).

3.5 Particle Number Concentrations and Their Relationship With Wind Speed and DMS Exchange

Over the course of the study, intermediate (< 0.5-2.5 µm) and large (> 2.5 µm) aerosol particle number concentrations averaged 5.51 x 10^6 ± 1.73 x 10^5 m^{-3} and 1.15 x 10^6 ± 4.63 x 10^4 m^{-3}, respectively (**Figures 5A, B**). Particle numbers in the 0.5µm-2.5 µm portion size fraction were highest in the early morning (7:00 and 11:00) and again at the end of the day around and following sunset (from 18:30 to 20:00). Particle numbers in the > 2.5 µm size fraction occurred slightly later in the morning (~11:00), early afternoon (11:00 to 15:00) and in the evening between 18:30 and 20:00.

Wind speed positively correlated with the abundance of intermediate (R^2 = 0.3337, n = 93, p < 0.0001) and large (R^2 = 0.1424, n = 93, p = 0.0002) aerosol particles (**Figures 5C, D**). Sea-to-air DMS fluxes also positively correlated with the abundance of intermediate (R^2 = 0.1669, n = 93, p = 0.0001) and large (R^2 = 0.0869, n = 93, p = 0.004) aerosol particles (**Figures 5E, F**).

4 DISCUSSION

4.1 Flux Estimations

DMS fluxes reported in this study (Min = not-detectable, Max = 69.5 µmol m^{-2} d^{-1}, Mean = 24.9 ± 1.81 µmol m^{-2} d^{-1}, n = 93) fell within the range of previously reported sea-to-air DMS fluxes for 5 coral reef systems across the Great Barrier Reef, which varied from not-detectable to 153 µmol m^{-2} d^{-1} in the austral summer wet season (Jones et al., 2018). However, seasonal DMS fluxes recorded in the current study were about five and four times greater on average than the 2012 summer wet season study conducted on Heron Island (5.0 µmol m^{-2} d^{-1}, n = 651) (Swan et al., 2017) and the average DMS fluxes reported by Jones et al. (2018) (6.4 µmol m^{-2} d^{-1}, n = 237), respectively. Since DMS_a (mean ± SD) at Heron Island in the 2012 and 2016 summers were similar (i.e. 3.9 ± 1.5, n = 651, and 3.7 ± 0.8, n = 761 nmol m^{-3}, respectively, data not shown), the high fluxes in this study most likely result from temporally elevated DMS production in the Heron Island reef lagoon in the year 2016 or on the section of the Heron Island reef flat where seawater samples were collected. The significant differences in the average DMS fluxes for the summers of 2012 and 2016 at Heron Island might also reflect differences in the employed flux calculation (photochemical ambient mass balance approach used by Swan et al. (2017) as opposed to the gradient method flux calculation used in this study). Similarly, Jones et al. (2018) used the LM86 gradient method flux parameterisation, which was shown to give much lower flux estimates than the other gradient method flux parameterisations used in the current study (see **Supplementary Table 1**), hence indicating that the approach employed can lead to significantly different values. The estimated flux difference might also reflect the limitations of the non-automated VG-CL instrument used in this study, which ultimately led to

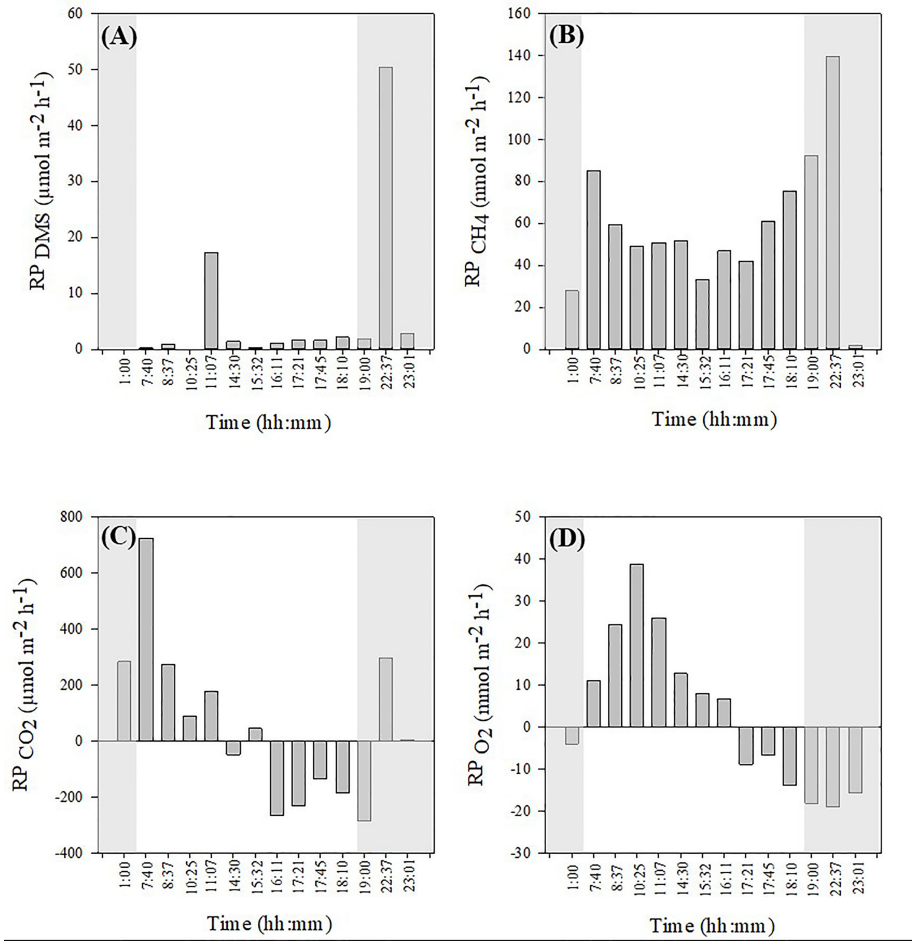

FIGURE 4 | 24h-integrated reef production (RP) for DMS **(A)**, CH_4 **(B)**, CO_2 **(C)** and O_2 **(D)** calculated around each low-tide period. Shaded areas represent hours of darkness.

preferential DMS_w sampling during the day and evenings, with a lack of night-time measurements to match with the continuous DMS_a measurements.

Sea-to-air fluxes for CH_4 (Min = −0.12 µmol m^{-2} d^{-1}, Max = 3.91 µmol m^{-2} d^{-1}, mean = 1.36 ± 1.03 mmol m^{-2} d^{-1}) and CO_2 (Min = −15.4, Max = 30.7 mmol m^{-2} d^{-1}, mean = 0.30 mmol m^{-2} d^{-1}) were consistent with previously reported water-air fluxes for the Great Barrier Reef (3.4 ± 0.1 µmol m^{-2} d^{-1} (O'Reilly et al., 2015) and 2.2 ± 0.5 µmol m^{-2} d^{-1} (Reading et al., 2021) for CH_4; −5.4 ± 0.8 mmol m^{-2} d^{-1} (O'Reilly et al., 2015), 1.44 ± 0.15 mmol m^{-2} d^{-1} (Lønborg et al., 2019) and 1.9 ± 0.4 mmol m^{-2} d^{-1} (Reading et al., 2021) for CO_2).

Sea-to-air O_2 fluxes in this study (Min = −188 mmol m^{-2} d^{-1}, Max = 403 mmol m^{-2} d^{-1}, mean = 70 ± 12 mmol m^{-2} d^{-1}) were similar to water-air fluxes reported for a Puerto Rican coral reef, with rates varying between −285 and 329 mmol m^{-2} d^{-1} (McGillis et al., 2011). However, they were rather low compared to O_2 fluxes reported for another coral reef system in the Florida Keys, (Min = −450 mmol m^{-2} d^{-1}, Max = 4500 mmol m^{-2} d^{-1}) (Long et al., 2013), which most likely reflects differences between the phototrophic communities of different reef systems (e.g. algal versus coral cover, phytoplankton composition).

4.2 The Interplay Between DMS and CH_4

The strong positive correlation between water-air DMS and CH_4 fluxes (R^2 = 0.7526) suggests that DMS and CH_4 emissions from the Heron Island reef lagoon are closely linked. Further to this observation, the MLR analysis revealed that sea-to-air DMS and CH_4 fluxes were both driven by pH, depth, wind direction, dewpoint and wind chill. This indicates that DMS and CH_4 fluxes are driven by very similar environmental factors, thus potentially explaining part of the correlation between DMS and CH_4 emissions at the Heron Island reef lagoon. Dissolved concentrations of DMS and CH_4 were also strongly correlated (**Supplementary Figure 3**), which indicates that the production of DMS and CH_4 in this reef system is also intimately linked. In contrast there was no clear correlation between the RPs of DMS

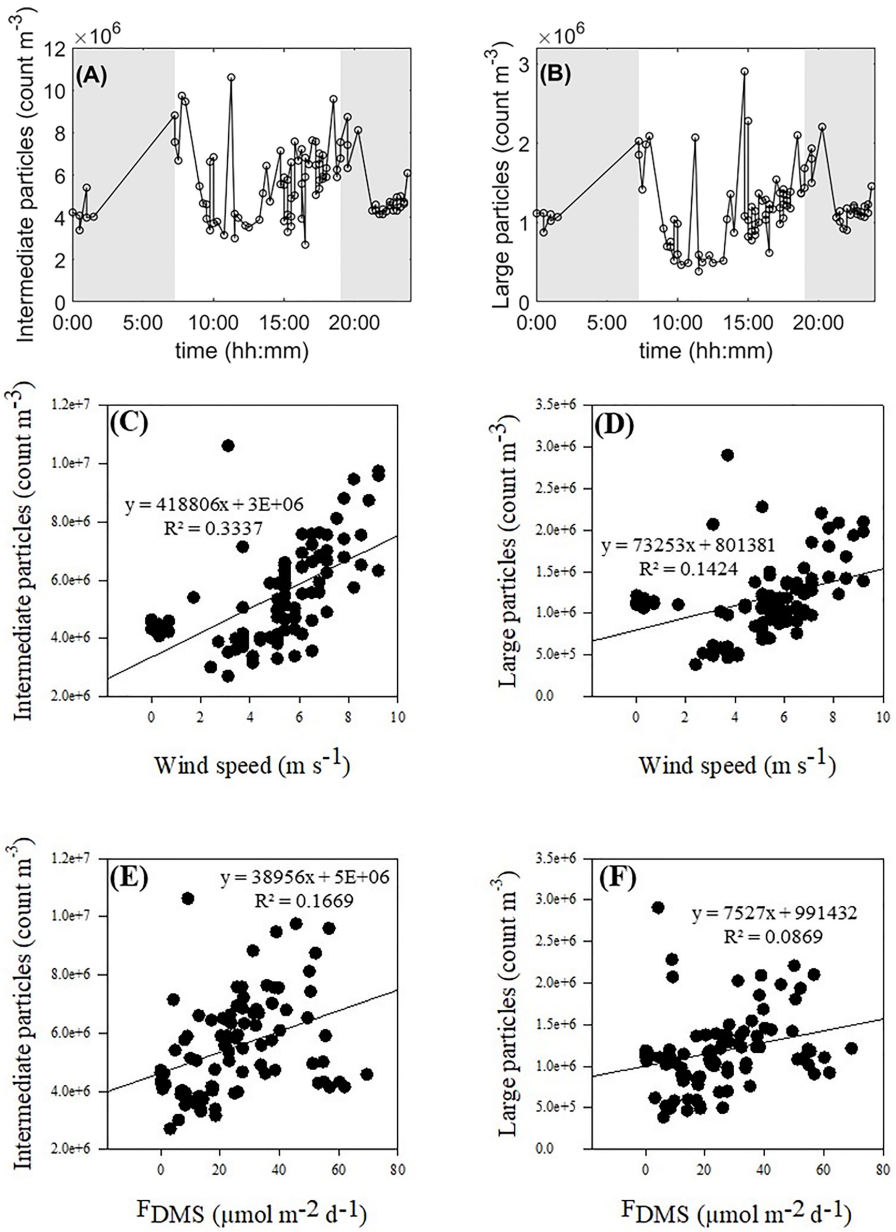

FIGURE 5 | 24h-integrated abundance of intermediate (0.5-2.5 μm) **(A)** and large (>2.5 μm) **(B)** aerosol particles and their relationships with wind speed **(C, D)** and sea-to-air DMS fluxes **(E, F)**, respectively. Shaded areas represent hours of darkness.

and CH_4, which suggests that DMS and CH_4 were subject to different accumulation rates and thus to different production and/or degradation processes.

DMS production mainly relies on the enzymatic cleavage of DMSP in the water column (Simó, 2001) while methanogenesis mainly depends on the conversion of CO_2 and acetate into CH_4 under anaerobic conditions (Liu and Whitman, 2008), which most likely occurs in marine sediments in coral reef ecosystems (Deschaseaux et al., 2019; Reading et al., 2021). The main sinks of dissolved DMS are expected to be biological and photochemical oxidation (del Valle et al., 2009) as well as emission fluxes from the water column to the atmosphere (Lana et al., 2011). Similarly, oceanic emissions (Weber et al., 2019) and microbial oxidation to CO_2 through both aerobic and anaerobic pathways (Pain et al., 2019) are considered the main sinks of dissolved CH_4 in marine systems. However, the rate and magnitude of DMS and CH_4 sinks rely on different degradation processes (e.g. microbial communities, vertical distribution in the water column). For instance, the magnitude of the aerobic and anaerobic CH_4 oxidation sinks is dictated by oxygen gradients and

groundwater residence time, respectively (Pain et al., 2019). The different sources and sinks of DMS and CH_4 in coral reef systems thus most likely explain the divergence in correlation between DMS and CH_4 sea-to-air emissions on one hand and the RPs of DMS and CH_4 on the other hand.

At the Heron Island reef lagoon, negative correlations were found between dark DMS and CH_4 fluxes from permeable carbonate coral reef sediments to the water column (Deschaseaux et al., 2019), suggesting that part of the DMS produced in coral reef sediments was degraded to CH_4 under dark anoxic conditions, most likely by anaerobic methanogens (Kiene and Visscher, 1987). However, CH_4 production can also occur under aerobic conditions and across all living organisms, including marine phytoplankton (Klintzsch et al., 2019; Ernst et al., 2022). As such, DMS-to-CH_4 hydrolysis may not only occurs in permeable carbonate coral reef sediments, but also in reef waters through phytoplankton activity and possibly within the coral tissue, where DMS plays a major role in structuring coral-associated bacterial communities (Raina et al., 2010).

Growing evidence shows that organic compounds containing sulfur- bonded methyl groups such as DMS are a source of CH_4 under both anaerobic and aerobic conditions (Liu and Whitman, 2008; Ernst et al., 2022), with CH_4 production by certain bacteria being enhanced in the presence of reactive oxygen species under oxidative stress (Ernst et al., 2022). DMS concentrations in marine algae and corals also increase under oxidative stress due to DMS being used as an antioxidant (Sunda et al., 2002; Deschaseaux et al., 2014). This suggests that the increase in CH_4 production might be due to more sulfur-methylated compounds made readily available to methylotrophs in various types of organisms.

It was estimated that DMS contributes up to 28% of CH_4 production in various marine systems (Kiene, 1988; Florez-Leiva et al., 2013), which could well be the case for coral reef ecosystems. At the Heron Island reef lagoon, it was estimated that a small portion (~6.5%) of the CH_4 produced in coral reef sediments under dark anoxic conditions might originate from DMS (Deschaseaux et al., 2019). Here, the slope of the regression between DMS and CH_4 indicates that 0.05 mole of CH_4 is emitted for each mole of DMS being emitted to the atmosphere. This shows that sea-to-air CH_4 emissions from the Heron Island reef lagoon represents 5% of that of DMS, which is consistent with the average sea-to-air DMS (24.9 ± 1.81 μmol m^{-2} d^{-1}) and CH_4 (1.36 ± 0.11 μmol m^{-2} d^{-1}) fluxes reported in this study. However, without using isotopic tracers, we cannot draw conclusions on the actual portion of CH_4 emissions from coral reef systems that actually originate from DMS hydrolysis.

4.3 Drivers of DMS and CH_4 in Coral Reef Systems

In addition to pH, depth, wind direction, dewpoint and wind chill, DMS emissions were also positively driven by salinity. These findings could be counter intuitive given that the most intense plume of DMS measured over the Heron Island reef occurred in the winter of 2013 at low tide when rainfall on the aerially exposed reef apparently caused a combined hypo-salinity osmotic and hypo-thermic temperature shock to the coral (Swan et al., 2017). However, salinity in this study only ranged from 36.4 to 37.4 ppt, and thus DMS emissions under rainfall at low tide was not captured. Nevertheless, it could also be that it was not only low salinity that led to high DMS emissions reported by Swan et al. (2017), but also temperature stress and/or other rain-induced environmental conditions. For instance, rain increases transfer velocity (Ho et al., 1997), which could explain the higher emissions in Swan et al. (2017) under rainfall at low tide.

Similarly, in addition to pH, depth, wind direction, dewpoint and wind chill, CH_4 emissions were also negatively affected by light whereas previous studies show that CH_4 production by phytoplankton was accentuated under increased light conditions (Klintzsch et al., 2020). Given that light mainly influences photosynthesis and O_2 production in biological systems, this data suggests that light-driven O_2 production might negatively impact CH_4 production or lead to enhanced CH_4 oxidation in coral reefs. This is consistent with sea-to-air O_2 fluxes being negatively correlated with both CH_4 and CO_2 in this study, with CO_2 being a precursor of CH_4 production (Liu and Whitman, 2008). Although CH_4 can originate from various biogenic sources in the presence of oxygen (Ernst et al., 2022), it could be that the main source of CH_4 in coral reef systems are methanogen-rich permeable carbonate sediments (Deschaseaux et al., 2019), which are productive under dark anoxic conditions.

Maximum dissolved DMS and DMSP concentrations in coral reef systems coincide with low pH, especially over areas dominated by seagrass and macroalgae (Burdett et al., 2013), which is consistent with pH negatively affecting DMS emissions in the current study. Coral-reef DMS emissions are thus expected to increase under low pH conditions, possibly due to macroalgae using DMSP to maintain metabolic functions during periods of low carbonate saturation state (Burdett et al., 2013). Sea-to-air CH_4 fluxes at Heron Island were also negatively correlated with pH, which suggests that ocean acidification may increase CH_4 emissions in coral reef systems, possibly due to low pH enhancing organic matter degradation in coral reefs like it is the case in seagrass sediments (Ravaglioli et al., 2020).

Spikes in DMS emissions at the Heron Island reef lagoon were previously detected at low tide generally under low wind speeds < 2 m s^{-1} (Swan et al., 2017), which agrees with depth being a negative driver of DMS emissions in this study. On the other hand, it is unknown whether dewpoint and windchill have ever been considered as environmental factors driving DMS and CH_4 emissions in marine systems, although it seems that low dewpoint and air temperatures coincided with high DMS and CH_4 emissions at the Heron Island reef system. This suggests that air temperature also plays a role in the gas transfer velocity of DMS and CH_4, most likely as it influences water temperature and thus the temperature-dependent gas solubility of these two compounds.

DMS and CH_4 emissions were highest under southerly winds, which travelled over the Heron Island's reef and the adjacent large Wistari reef, directly south of our sampling site. This indicates that Wistari reef is possibly the major source of coral-reef-derived DMS_a measured at Heron Island and that

coral reefs are a more predominant source of DMS and CH_4 than the surrounding ocean.

4.4 DMS and Climate in Coral Reef Systems

Although there is insufficient information to attribute the particle counts in this study to new particle formation, because the measured size ranges are far above that of new nanoparticles (Clarke et al., 2006), it was interesting to see that sea-to-air DMS fluxes positively correlated with intermediate (0.5-2.5 μm) and large (> 2.5 μm) particles, and that a stronger correlation occurred between DMS emissions and the abundance of particles in the intermediate size range. This likely indicates that DMS oxidation products possibly contributed to the growth of existing particles within the 0.5-2.5 μm measured size range, which are suspected to be predominantly sea spray aerosols (SSA) (Quinn et al., 2015). Given that number concentrations of intermediate size particles were correlated with wind speed (R^2 = 0.3337, **Figure 5C**) and that wind speed is a covariate in DMS flux, the observed correlation is expected to be linked to wind speed, which exchanges more DMS and SSA from the ocean. Given that coral-reef derived DMS and CH_4 emissions could be linked, with a small portion of DMS being hydrolysed to CH_4 in the water column, and that CH_4 is a GHG with a stronger greenhouse potential than that of CO_2 (Shine et al., 2005), it is important to consider both dissolved DMS and CH_4 when predicting BVOC and GHG emissions from marine systems.

5 CONCLUSION

To our knowledge, this study is the first to simultaneously measure and report sea-to-air DMS fluxes alongside sea-to-air CH_4 fluxes in a coral reef ecosystem. Depth, pH, wind direction, dewpoint and wind chill were common drivers of DMS and CH_4 emissions at Heron Island, a coral reef system on the southern Great Barrier Reef. Additionally, salinity was a positive driver of DMS emissions while light negatively affected sea-to-air CH_4 fluxes. This research also showed the strong correlation that exists between DMS and CH_4 emissions at Heron Island. Although it is not possible at this stage to estimate the portion of CH_4 that derives from DMS hydrolysis, it is clear that DMS and CH_4 emissions from the Heron Island reef are intimately linked, with potential consequences on ocean warming. DMS emissions were well correlated with the abundance of intermediate size particles (0.5-2.5 μm), which indicates that DMS contributes to the growth of existing aerosol particles, which could eventually form cloud condensation nuclei and induce cloud-mediated cooling on a local scale. This study highlights the complexity of BVOC and GHG co-emissions and the potential impact they may have on the regional climate of the Great Barrier Reef.

DATA AVAILABILITY STATEMENT

The data collected for this study has been made publicly available from the Southern Cross University online repository at: https://doi.org/https://doi.org/10.4226/47/59c460fbe8322 and https://doi.org/10.25918/data.193.

AUTHOR CONTRIBUTIONS

ED, BE, GJ, HS and DM conceptualised the experimental design. ED conducted the DMS_w analysis, DMS_w data processing, all data compiling, and manuscript writing. HS conducted the analysis and processing of DMS_a and particle number concentrations. DM conducted the analysis and processing of CH_4 and CO_2 data. ED and DM conducted the flux calculations for DMS and CH_4, CO_2 and O_2, respectively. KS conducted the MLR analysis and data processing on MATLAB. EK and KT designed the VG-CL and provided analytical support in the field. BE and GJ funded this research. All authors contributed to the article and approved the submitted version.

FUNDING

This research was funded by the ARC Discovery Project grants DP150102092 (recipient BE), "Dissolution of calcium carbonate in sediments in an acidifying ocean" and DP150101649 (recipient GJ), "The Great Barrier Reef as a significant source of climatically relevant aerosol particles".

ACKNOWLEDGMENTS

We would like to thank the staff at the Heron Island Research Station for their assistance.

SUPPLEMENTARY MATERIAL

The Supplementary Material for this article can be found online at: https://www.frontiersin.org/articles/10.3389/fmars.2022.910441/full#supplementary-material

REFERENCES

Barnes, R., and Goldberg, E. (1976). Methane Production and Consumption in Anoxic Marine Sediments. *Geology* 4, 297–300. doi: 10.1130/0091-7613(1976)4<297:MPACIA>2.0.CO;2

Benson, B. B., and Krause, D.Jr (1984). The Concentration and Isotopic Fractionation of Oxygen Dissolved in Freshwater and Seawater in Equilibrium With the Atmosphere 1. *Limnol. Oceanogr.* 29, 620–632. doi: 10.4319/lo.1984.29.3.0620

Burdett, H. L., Donohue, P. J. C., Hatton, A. D., Alwany, M. A., and Kamenos, N. A. (2013). Spatiotemporal Variability of Dimethylsulphoniopropionate on a Fringing Coral Reef: The Role of Reefal Carbonate Chemistry and Environmental Variability. *PloS One* 8, e64651. doi: 10.1371/journal.pone.0064651

Carpenter, L. J., Archer, S. D., and Beale, R. (2012). Ocean-Atmosphere Trace Gas Exchange. *Chem. Soc. Rev.* 41, 6473–6506. doi: 10.1039/c2cs35121h

Charlson, R. J., Lovelock, J. E., Andreae, M. O., and Warren, S. G. (1987). Oceanic Phytoplankton, Atmospheric Sulfur, Cloud Albedo and Climate. *Nature* 326, 655–661. doi: 10.1038/326655a0

Clarke, A. D., Owens, S. R., and Zhou, J. (2006). An Ultrafine Sea-Salt Flux From Breaking Waves: Implications for Cloud Condensation Nuclei in the Remote Marine Atmosphere. *J. Geophys. Res.: Atmosph.* 111, 1–14. doi: 10.1029/2005JD006565

Curson, A. R., Liu, J., Martínez, A. B., Green, R. T., Chan, Y., Carrión, O., et al. (2017). Dimethylsulfoniopropionate Biosynthesis in Marine Bacteria and Identification of the Key Gene in This Process. *Nat. Microbiol.* 2, 17001–17009. doi: 10.1038/nmicrobiol.2017.9

Dacey, J. W., Wakeham, S. G., and Howes, B. L. (1984). Henry's Law Constants for Dimethylsulfide in Freshwater and Seawater. *Geophys. Res. Lett.* 11, 991–994. doi: 10.1029/GL011i010p00991

del Valle, D. A., Kieber, D. J., Toole, D. A., Bisgrove, J., and Kiene, R. P. (2009). Dissolved DMSO Production *via* Biological and Photochemical Oxidation of Dissolved DMS in the Ross Sea, Antarctica. *Deep. Sea. Res. Part I.: Oceanogr. Res. Paper.* 56, 166–177. doi: 10.1016/j.dsr.2008.09.005

Deschaseaux, E. S., Jones, G. B., Deseo, M. A., Shepherd, K. M., Kiene, R., Swan, H., et al. (2014). Effects of Environmental Factors on Dimethylated Sulfur Compounds and Their Potential Role in the Antioxidant System of the Coral Holobiont. *Limnol. Oceanogr.* 59, 758–768. doi: 10.4319/lo.2014.59.3.0758

Deschaseaux, E., Jones, G., and Swan, H. (2016). Dimethylated Sulfur Compounds in Coral-Reef Ecosystems. *Environ. Chem.* 13, 239–251. doi: 10.1071/EN14258

Deschaseaux, E., Stoltenberg, L., Hrebien, V., Koveke, E. P., Toda, K., and Eyre, B. D. (2019). Dimethylsulfide (DMS) Fluxes From Permeable Coral Reef Carbonate Sediments. *Mar. Chem.* 208, 1–10. doi: 10.1016/j.marchem.2018.11.008

Ernst, L., Steinfeld, B., Barayeu, U., Klintzsch, T., Kurth, M., Grimm, D., et al. (2022). Methane Formation Driven by Reactive Oxygen Species Across All Living Organisms. *Nature* 603 (7901), 482–487. doi: 10.1038/s41586-022-04511-9

Fiddes, S., Woodhouse, M., Utembe, S., Schofield, R., Alroe, J., Chambers, S., et al. (2021). The Contribution of Coral Reef-Derived Dimethyl Sulfide to Aerosol Burden Over the Great Barrier Reef: A Modelling Study. *Atmosph. Chem. Phys. Discuss.* 22 (4), 2419–2445. doi: 10.5194/acp-2021-507

Florez-Leiva, L., Damm, E., and Farías, L. (2013). Methane Production Induced by Dimethylsulfide in Surface Water of an Upwelling Ecosystem. *Prog. Oceanogr.* 112, 38–48. doi: 10.1016/j.pocean.2013.03.005

Haydon, T. D., Seymour, J. R., and Suggett, D. J. (2018). Soft Corals Are Significant DMSP Producers in Tropical and Temperate Reefs. *Mar. Biol.* 165, 1–7. doi: 10.1007/s00227-018-3367-2

Ho, D. T., Bliven, L. F., Wanninkhof, R., and Schlosser, P. (1997). The Effect of Rain on Air-Water Gas Exchange. *Tellus. B.* 49, 149–158. doi: 10.3402/tellusb.v49i2.15957

Ho, D. T., Law, C. S., Smith, M. J., Schlosser, P., Harvey, M., and Hill, P. (2006). Measurements of Air-Sea Gas Exchange at High Wind Speeds in the Southern Ocean: Implications for Global Parameterizations. *Geophys. Res. Lett.* 33, 1–6. doi: 10.1029/2006GL026817

Jones, G. (2013). Coral Animals Combat Stress With Sulphur. *Nature* 502, 634–635. doi: 10.1038/nature12698

Jones, G., Curran, M., Deschaseaux, E., Omori, Y., Tanimoto, H., Swan, H., et al. (2018). The Flux and Emission of Dimethylsulfide From the Great Barrier Reef Region and Potential Influence on the Climate of NE Australia. *J. Geophys. Res.: Atmosph.* 123, 13,835–813,856. doi: 10.1029/2018JD029210

Kiene, R. P. (1988). Dimethyl Sulfide Metabolism in Salt Marsh Sediments. *FEMS Microbiol. Lett.* 53, 71–78. doi: 10.1111/j.1574-6968.1988.tb02649.x

Kiene, R. P., Oremland, R. S., Catena, A., Miller, L. G., and Capone, D. G. (1986). Metabolim of Reduced Methylated Sulfur Compounds in Anaerobic Sediments and by a Pure Culture of an Estuarine Methanogen. *Appl. Environ. Microbiol.* 52, 1037–1045. doi: 10.1128/aem.52.5.1037-1045.1986

Kiene, R. P., and Visscher, P. T. (1987). Production and Fate of Methylated Sulfur-Compounds From Methionine and Dimethylsulfoniopropionate in Anoxic Salt-Marsh Sediments. *Appl. Environ. Microbiol.* 53, 2426–2434. doi: 10.1128/aem.53.10.2426-2434.1987

Klintzsch, T., Langer, G., Nehrke, G., Wieland, A., Lenhart, K., and Keppler, F. (2019). Methane Production by Three Widespread Marine Phytoplankton Species: Release Rates, Precursor Compounds, and Potential Relevance for the Environment. *Biogeosciences* 16, 4129–4144. doi: 10.5194/bg-16-4129-2019

Klintzsch, T., Langer, G., Wieland, A., Geisinger, H., Lenhart, K., Nehrke, G., et al. (2020). Effects of Temperature and Light on Methane Production of Widespread Marine Phytoplankton. *J. Geophys. Res.: Biogeosci.* 125, e2020JG005793. doi: 10.1029/2020JG005793

Lønborg, C., Calleja, M. L., Fabricius, K. E., Smith, J. N., and Achterberg, E. P. (2019). The Great Barrier Reef: A Source of CO2 to the Atmosphere. *Mar. Chem.* 210, 24–33. doi: 10.1016/j.marchem.2019.02.003

Lana, A., Bell, T. G., Simó, R., Vallina, S. M., Ballabrera-Poy, J., Kettle, A. J., et al. (2011). An Updated Climatology of Surface Dimethlysulfide Concentrations and Emission Fluxes in the Global Ocean. *Global Biogeochem. Cycle.* 25, 1–17. doi: 10.1029/2010GB003850

Liss, P. S., and Merlivat, L. (1986). "Air-Sea Gas Exchange Rates: Introduction and Synthesis," in *The Role of Air-Sea Exchange in Geochemical Cycling*. Ed. P. Buat-Ménard (Dordrecht/Boston/Lancaster/Tokyo: D. Reidel publishing company), 113–127.

Liu, Y., and Whitman, W. B. (2008). Metabolic, Phylogenetic, and Ecological Diversity of the Methanogenic Archaea. *Ann. New York. Acad. Sci.* 1125, 171–189. doi: 10.1196/annals.1419.019

Long, M. H., Berg, P., De Beer, D., and Zieman, J. C. (2013). *In Situ* Coral Reef Oxygen Metabolism: An Eddy Correlation Study. *PloS One* 8, e58581. doi: 10.1371/journal.pone.0058581

Maher, D. T., Santos, I. R., Leuven, J. R., Oakes, J. M., Erler, D. V., Carvalho, M. C., et al. (2013). Novel Use of Cavity Ring-Down Spectroscopy to Investigate Aquatic Carbon Cycling From Microbial to Ecosystem Scales. *Environ. Sci. Technol.* 47, 12938–12945. doi: 10.1021/es4027776

McGillis, W. R., Langdon, C., Loose, B., Yates, K. K., and Corredor, J. (2011). Productivity of a Coral Reef Using Boundary Layer and Enclosure Methods. *Geophys. Res. Lett.* 38, 1–5. doi: 10.1029/2010GL046179

Mechalas, B. J. (1974). "Pathways and Environmental Requirements for Biogenic Gas Production in the Ocean", in *Natural Gases in Marine Sediments* (Boston, MA: Springer), 11–25.

Nagahata, T., Kajiwara, H., Ohira, S. I., and Toda, K. (2013). Simple Field Device for Measurement of Dimethyl Sulfide and Dimethylsulfoniopropionate in Natural Waters, Based on Vapor Generation and Chemiluminescence Detection. *Analyt. Chem.* 85, 4461–4467. doi: 10.1021/ac303803w

Nightingale, P. D., Malin, G., Law, C. S., Watson, A. J., Liss, P. S., Liddicoat, M. I., et al. (2000). *In Situ* Evaluation of Air-Sea Gas Exchange Parameterizations Using Novel Conservative and Volatile Tracers. *Global Biogeochem. Cycle.* 14, 373–387. doi: 10.1029/1999GB900091

O'Reilly, C., Santos, I. R., Cyronak, T., Mcmahon, A., and Maher, D. T. (2015). Nitrous Oxide and Methane Dynamics in a Coral Reef Lagoon Driven by Pore Water Exchange: Insights From Automated High-Frequency Observations. *Geophys. Res. Lett.* 42, 2885–2892. doi: 10.1002/2015GL063126

Pain, A. J., Martin, J. B., and Young, C. R. (2019). Sources and Sinks of CO2 and CH4 in Siliciclastic Subterranean Estuaries. *Limnol. Oceanogr.* 64, 1500–1514. doi: 10.1002/lno.11131

Quinn, P. K., and Bates, T. S. (2011). The Case Against Climate Regulation *via* Oceanic Phytoplankton Sulphur Emissions. *Nature* 480, 51–56. doi: 10.1038/nature10580

Quinn, P. K., Collins, D. B., Grassian, V. H., Prather, K. A., and Bates, T. S. (2015). Chemistry and Related Properties of Freshly Emitted Sea Spray Aerosol. *Chem. Rev.* 115, 4383–4399. doi: 10.1021/cr500713g

Raina, J. B., Dinsdale, E. A., Willis, B. L., and Bourne, D. G. (2010). Do the Organic Sulfur Compounds DMSP and DMS Drive Coral Microbial Associations? *Trends Microbiol.* 18, 101–108. doi: 10.1016/j.tim.2009.12.002

Raina, J.-B., Tapiolas, D. M., Foret, S., Lutz, A., Abrego, D., Ceh, J., et al. (2013). DMSP Biosynthesis by an Animal and its Role in Coral Thermal Stress Response. *Nature* 502, 677–680. doi: 10.1038/nature12677

Ravaglioli, C., Lardicci, C., Pusceddu, A., Arpe, E., Bianchelli, S., Buschi, E., et al. (2020). Ocean Acidification Alters Meiobenthic Assemblage Composition and Organic Matter Degradation Rates in Seagrass Sediments. *Limnol. Oceanogr.* 65, 37–50. doi: 10.1002/lno.11246

Reading, M. J., Maher, D. T., Santos, I. R., Jeffrey, L. C., Cyronak, T. J., Mcmahon, A., et al. (2021). Spatial Distribution of CO2, CH4, and N2O in the Great Barrier Reef Revealed Through High Resolution Sampling and Isotopic Analysis. *Geophys. Res. Lett.* 48, e2021GL092534. doi: 10.1029/2021GL092534

Sansone, F., Chanton, J., Haberstroh, P., and Bozeat, R. (1993). "Methane Cycling in Coral Reef Frameworks," in *Trends in Microbial Ecology*. Eds. R. Guerrero and C. Pedr6s-Ali6 (Barcelona: Span-ish Society for Microbiology), 157–162.

Shine, K. P., Fuglestvedt, J. S., Hailemariam, K., and Stuber, N. (2005). Alternatives to the Global Warming Potential for Comparing Climate Impacts of Emissions

of Greenhouse Gases. *Climatic. Change* 68, 281–302. doi: 10.1007/s10584-005-1146-9

Simó, R. (2001). Production of Atmospheric Sulfur by Oceanic Plankton: Biogeochemical, Ecological and Evolutionary Links. *Trends Ecol. Evol.* 16, 287–294. doi: 10.1016/S0169-5347(01)02152-8

Stefels, J. (2000). Physiological Aspects of the Production and Conversion of DMSP in Marine Algae and Higher Plants. *J. Sea. Res.* 43, 183–197. doi: 10.1016/S1385-1101(00)00030-7

Sunda, W., Kieber, D. J., Kiene, R. P., and Huntsman, S. (2002). An Antioxidant Function for DMSP and DMS in Marine Algae. *Nature* 418, 317–320. doi: 10.1038/nature00851

Swan, H. B., Ivey, J. P., Jones, G. B., and Eyre, B. D. (2015). The Validation and Measurement Uncertainty of an Automated Gas Chromatograph for Marine Studies of Atmospheric Dimethylsulfide. *Analyt. Methods* 7, 3893–3902. doi: 10.1039/C5AY00269A

Swan, H. B., Jones, G. B., Deschaseaux, E. S. M., and Eyre, B. D. (2017). Coral Reef Origins of Atmospheric Dimethylsulfide at Heron Island, Southern Great Barrier Reef, Australia. *Biogeosciences* 14, 229–239. doi: 10.5194/bg-14-229-2017

Wang, J., Sun, S., Qin, P., Wang, J., Zhong, C., and Xin, W. (2009). "DMS and CH4 Fluxes Along an Elevational Gradient of a Coastal Salt Marsh, East China: Positive Correlations", in *Bioinformatics and Biomedical Engineering* (IEEE, China: ICBBE 2009. 3rd International Conference on: IEEE), 1–6.

Wanninkhof, R. (2014). Relationship Between Wind Speed and Gas Exchange Over the Ocean Revisited. *Limnol. Oceanogr.: Methods* 12, 351–362. doi: 10.4319/lom.2014.12.351

Weber, T., Wiseman, N. A., and Kock, A. (2019). Global Ocean Methane Emissions Dominated by Shallow Coastal Waters. *Nat. Commun.* 10, 1–10. doi: 10.1038/s41467-019-12541-7

Weiss, R. F. (1974). Carbon Dioxide in Water and Seawater: The Solubility of a non-Ideal Gas. *Mar. Chem.* 2, 203–215. doi: 10.1016/0304-4203(74)90015-2

Wiesenburg, D. A., and Guinasso, (1979). Equilibrium Solubilities of Methane, Carbon Monoxide, and Hydrogen in Water and Sea Water. *J. Chem. Eng. Data* 24, 356–360. doi: 10.1021/je60083a006

Conflict of Interest: The authors declare that the research was conducted in the absence of any commercial or financial relationships that could be construed as a potential conflict of interest.

Publisher's Note: All claims expressed in this article are solely those of the authors and do not necessarily represent those of their affiliated organizations, or those of the publisher, the editors and the reviewers. Any product that may be evaluated in this article, or claim that may be made by its manufacturer, is not guaranteed or endorsed by the publisher.

frontiers | Frontiers in Marine Science

TYPE Original Research
PUBLISHED 12 August 2022
DOI 10.3389/fmars.2022.910423

OPEN ACCESS

EDITED BY
Rafel Simó,
Institut de Ciències del Mar (ICM-CSIC), Spain

REVIEWED BY
Michael Kingsford,
James Cook University, Australia
Zhenming Ji,
Sun Yat-sen University, China

*CORRESPONDENCE
Rebecca L. Jackson
rebecca.jackson@csiro.au

†PRESENT ADDRESS
Rebecca L. Jackson,
Coasts and Ocean Research, Oceans and Atmosphere, Commonwealth Scientific and Industrial Research Organisation, Canberra, ACT, Australia

SPECIALTY SECTION
This article was submitted to Coral Reef Research, a section of the journal Frontiers in Marine Science

RECEIVED 01 April 2022
ACCEPTED 19 July 2022
PUBLISHED 12 August 2022

CITATION
Jackson RL, Woodhouse MT, Gabric AJ, Cropp RA, Swan HB, Deschaseaux ESM and Trounce H (2022) Modelling the influence of coral-reef-derived dimethylsulfide on the atmosphere of the Great Barrier Reef, Australia.
Front. Mar. Sci. 9:910423.
doi: 10.3389/fmars.2022.910423

Modelling the influence of coral-reef-derived dimethylsulfide on the atmosphere of the Great Barrier Reef, Australia

Rebecca L. Jackson[1,2*†], Matthew T. Woodhouse[3], Albert J. Gabric[2], Roger A. Cropp[2], Hilton B. Swan[4], Elisabeth S. M. Deschaseaux[4] and Haydn Trounce[5]

[1]Coasts and Ocean Research, Oceans and Atmosphere, Commonwealth Scientific and Industrial Research Organisation, Canberra, ACT, Australia, [2]School of Environment and Science, Griffith University, Nathan, QLD, Australia, [3]Climate Science Centre, Oceans and Atmosphere, Commonwealth Scientific and Industrial Research Organisation, Aspendale, VIC, Australia, [4]Centre for Coastal Biogeochemistry, Faculty of Science and Engineering, Southern Cross University, Lismore, NSW, Australia, [5]International Laboratory for Air Quality and Health, School of Earth and Atmospheric Sciences, Queensland University of Technology, Brisbane, QLD, Australia

Marine dimethylsulfide (DMS) is an important source of natural sulfur to the atmosphere, with potential implications for the Earth's radiative balance. Coral reefs are important regional sources of DMS, yet their contribution is not accounted for in global DMS climatologies or in model simulations. This study accounts for coral-reef-derived DMS and investigates its influence on the atmosphere of the Great Barrier Reef (GBR), Australia, using the Australian Community Climate and Earth System Simulator Atmospheric Model version 2 (ACCESS-AM2). A climatology of seawater surface DMS (DMS_w) concentration in the GBR and an estimate of direct coral-to-air DMS flux during coral exposure to air at low tide are incorporated into the model, increasing DMS emissions from the GBR region by 0.02 Tg yr^{-1}. Inclusion of coral-reef-derived DMS increased annual mean atmospheric DMS concentration over north-eastern Australia by 29%, contributing to an increase in gas-phase sulfate aerosol precursors of up to 18% over the GBR. The findings suggest that the GBR is an important regional source of atmospheric sulfur, with the potential to influence local-scale aerosol-cloud processes. However, no influence on sulfate aerosol mass or number concentration was detected, even with a reduction in anthropogenic sulfur dioxide emissions, indicating that DMS may not significantly influence the regional atmosphere at monthly, annual or large spatial scales. Further research is needed to improve the representation of coral-reef-derived DMS in climate models and determine its influence on local, sub-daily aerosol-cloud processes, for which observational studies suggest that DMS may play a more important role.

KEYWORDS

coral reef, dimethylsulfide (DMS), sulfate, aerosol, ACCESS

1 Introduction

Aerosols and clouds play a key role in the Earth's radiative budget and climate by governing the amount of incoming and outgoing solar radiation and heat (Ramanathan et al., 1989; Andreae, 1995). Since the industrial revolution, anthropogenic greenhouse gas (GHG) emissions have exerted an average global radiative forcing of +2.72 (1.96 to 3.84) W m^{-2} (IPCC, 2021). Anthropogenic and natural aerosols have partially offset this warming effect through scattering of incoming short-wave radiation (aerosol-radiation interactions) (McCormick and Ludwig, 1967) and influencing the albedo, lifetime and cover of clouds (aerosol-cloud interactions) (Twomey et al., 1984).

In comparison to GHG emissions, the influence of aerosols on the climate is complex and less well quantified due to uncertainties in aerosol source strengths and their radiative effects (Twomey, 1974; Andreae and Rosenfeld, 2008). Consequently, estimates of aerosol radiative forcing range from -1.9 to -0.1 W m^{-2} (IPCC, 2013; IPCC, 2014). Approximately 45% of the variance in aerosol radiative forcing since the pre-industrial period is derived from uncertainties in natural aerosol sources, including marine dimethylsulfide (DMS) (Carslaw et al., 2013).

The precursor of DMS, dimethylsulfoniopropionate (DMSP), is produced throughout the ocean by a number of marine organisms including planktonic and benthic algae (Stefels, 2000; Sunda et al., 2002), corals and their endosymbiotic dinoflagellates (Raina et al., 2013), and marine bacteria (Curson et al., 2017). DMSP is produced for a range of physiological and ecological functions (Stefels, 2000; McParland and Levine, 2019). Catabolism of DMSP is mediated by the demethylation and cleavage pathways, with the latter producing DMS (Bullock et al., 2017). Seawater surface DMS (DMS_w) is ventilated to the marine boundary layer (MBL) where it is rapidly oxidized, primarily by hydroxyl radicals (OH), to sulfate aerosol precursor gases including sulfur dioxide (SO_2), methanesulfonic acid (MSA), hydroperoxymethyl thioformate (HPMTF) and sulfuric acid (H_2SO_4) (Andreae and Crutzen, 1997; Berndt et al., 2019; Hodshire et al., 2019; Veres et al., 2020).

Sulfuric acid, an aerosol precursor, may condense onto existing particles, facilitating growth to cloud condensation nuclei (CCN), or nucleate to form new non-sea salt sulfate (nss-SO_4) aerosol (Andreae and Crutzen, 1997; Woodhouse et al., 2013). The latter primarily occurs in the free troposphere, where background aerosol concentration and temperature are relatively low and conditions are optimal for the nucleation of trace gases (Korhonen et al., 2008; Sanchez et al., 2018). New nss-SO_4 particles may be entrained from the free troposphere to the MBL and increase the number of CCN and cloud droplets.

When high concentrations of fine aerosol grow rapidly to CCN, cloud droplet number increases and cloud droplet diameter decreases (assuming constant cloud liquid water content), enhancing the albedo and lifetime of clouds and suppressing precipitation (Rosenfeld et al., 2007; Dave et al., 2019). Conversely, when CCN activation size is not met, water vapor may remain in the atmosphere, suppressing local precipitation and increasing precipitation downwind if conditions for particle growth are more favorable (Andreae and Rosenfeld, 2008; Fan et al., 2018).

The influence of DMS on Earth's radiative balance is dependent on the efficiency of DMS oxidation and nucleation to secondary nss-SO_4, which ranges from 0.14-0.95 in the MBL (Von Glasow and Crutzen, 2004). The high range in efficiency is due to regional variability in pre-existing aerosols and the aerosol condensational sink (Woodhouse et al., 2013; Hoffmann et al., 2016). The annual mean contribution of DMS to CCN is estimated to be 3.3% in the Northern Hemisphere and 9.9% in the relatively cleaner Southern Hemisphere (Woodhouse et al., 2010). This response varies with season and location, with the greatest response occurring in pristine regions of high biological activity (Korhonen et al., 2008; Lana et al., 2012; Gabric et al., 2013; Woodhouse et al., 2013; Sanchez et al., 2018; Zavarsky et al., 2018). For example, when phytoplankton productivity (and DMS production) increases, DMS-derived sulfates contribute up to 46% of CCN over the Southern Ocean (30-45°S) in summer (Korhonen et al., 2008), and 33% of CCN over the North Atlantic in spring (Sanchez et al., 2018) *via* new particle nucleation and particle growth to CCN.

Coral reefs are identified as important regional sources of DMS (Broadbent and Jones, 2004; Swan et al., 2017; Jones et al., 2018). In the coral holobiont, DMS(P) production is upregulated in response to physiological stress caused by exposure to high sea surface temperature (SST), solar irradiance and changes in salinity (Raina et al., 2013; Deschaseaux et al., 2014; Gardner et al., 2016; Hopkins et al., 2016), all of which can be exacerbated during exposure to air at low tide (Buckee et al., 2020). This biogenic sulfur source could facilitate nss-SO_4 aerosol nucleation and growth to CCN, increasing the lifetime and albedo of low-level clouds (LLC) over coral reefs (similarly to Charlson et al., 1987). Evaporation over shallow, warm coral reef waters contributes to the formation of a convective boundary layer (~65-130 m), with relatively high humidity and temperature that is favourable for low-level cloud formation (McGowan et al., 2019). It has been hypothesized that DMS emissions facilitate the formation of a local or regional negative feedback within the coral reef boundary layer, shading and cooling the coral reef below (Fischer and Jones, 2012; Jones, 2015; Jones et al., 2017).

Global modelling studies have found that marine DMS is an important source of nss-SO_4 aerosol, influencing regional aerosol and cloud microphysical properties (Thomas et al., 2010; Woodhouse et al., 2010; Gabric et al., 2013; Mahajan et al., 2015) and providing a cooling effect of up to 0.45°C (Fiddes et al., 2018). However, with the exception of only two model studies (Fiddes et al., 2021, 2022), the coral reef source of

DMS is not currently accounted for in DMS climatologies or in climate models.

Global climate models typically prescribe DMS_w concentration using the Lana et al. (2011) monthly mean climatology. This climatology was derived from four decades of DMS_w observations over most of the global ocean (Kettle et al., 1999). However, very few observations were included for coral reef regions and extrapolation did not account for seasonal or spatial variability across coral reef flats and lagoon waters.

Only two model studies have investigated the importance of DMS flux from coral reefs on the climate (Fiddes et al., 2021; Fiddes et al., 2022). Both of these studies accounted for the coral reef source of DMS_w by adding a scaled laboratory-derived estimate of 50 nmol L^{-1} to the Lana et al. (2011) DMS_w climatology for coral reef regions. This method added 0.03 nmol L^{-1} to the global average seawater concentration and increased global sea-air emissions by 0.3 Tg yr^{-1} of DMS, representing 1.7% of global DMS emission estimates (Fiddes et al., 2021). This is higher than the estimate of 0.06-0.08 Tg yr^{-1} of DMS estimated to be released from tropical coral reefs based on field observations (Jones et al., 2018; Jackson et al., 2021).

Despite the relatively high coral reef DMS_w and DMS sea-air flux source, Fiddes et al. (2021) report only a small response in nucleation and Aitken mode aerosol number concentration and mass when the coral reef source of DMS was removed from the global ACCESS-UKCA (Australian Community Climate and Earth System Simulator-United Kingdom Chemistry and Aerosol) model. This suggests that tropical coral reef DMS emissions have no robust impact on contemporary global or regional climate, possibly due to confounding impacts of industrial sulfate emissions and other anthropogenic pollutants dominating the aerosol signal. Fiddes et al. (2022) demonstrated similar findings in the GBR region using the regional WRF-Chem (Weather Research and Forecasting model coupled with chemistry) model. However, observational studies suggest that the coral reef source of DMS may influence sulfate aerosol and LLC properties, at spatial or temporal scales that are perhaps not captured by global or regional climate models (Modini et al., 2009; Swan et al., 2016).

For example, positive correlations have been identified between the number concentration of atmospheric particles ranging from 0.5-2.5 µm (wet diameter) and both DMS sea-air flux (Deschaseaux et al., 2022) and DMS_a concentration (Jackson et al., 2020) at Heron Island in the southern GBR. The magnitude of the correlation between DMS_a and particle number concentration increased during daylight hours, when DMS oxidation rates over relatively clean oceans are highest (Gabric et al., 2008; Galí et al., 2013), and when wind speed was low (< 2 m s^{-1}) (Jackson et al., 2020). Although the observed size range was larger than newly nucleated particles, the positive correlation during calm, daylight hours may have reflected local condensational growth of existing fine particles (< 0.5 µm) to the larger, detectable size range (Jackson et al., 2020). Therefore, DMS-derived sulfates may play an important role in aerosol composition over the GBR.

A parameterization of DMS_w in the Great Barrier Reef (GBR), Australia, was recently derived from observational data obtained during Marine National Facility RV *Investigator* voyage IN2016_V05 (RVI). This parameterization was used to calculate a 19-year climatology of DMS_w and DMS flux from the GBR using remotely sensed observations (Jackson et al., 2021). The calculated DMS_w climatology reproduced observed seasonal and spatial variability well in the GBR (summarized in Jones et al., 2018) and estimates that the 347,000 km^2 of coral reefs and lagoon waters in the GBR release 0.03-0.05 Tg yr^{-1} DMS (0.015-0.026 Tg yr^{-1} S) (Jackson et al., 2021).

Here, we build on previous modelling work by investigating the influence of coral-reef-derived DMS on the contemporary and a relatively clean regional atmosphere. Coral-reef-derived DMS is accounted for by incorporating a climatology of DMS_w calculated from observational data in the GBR, and an estimate of direct coral-air DMS flux, into the Australian Community Climate and Earth-System Simulator Atmospheric Model version 2 (ACCESS-AM2). The accuracy of DMS sources in the model is evaluated by comparing model output with observations, and the influence of coral-reef-derived DMS on the regional atmosphere over north-eastern Australia is quantified.

2 Materials and methods

2.1 ACCESS-AM2 description

ACCESS-AM2 is a global physical climate model, which contributed to the World Climate Research Programme's Coupled Model Intercomparison Project Phase 6 (CMIP6). The physical atmospheric model in ACCESS is the Met Office Unified Model (UM) version 10.6 (Walters et al., 2019). This version uses the Global Atmosphere 7.1 (GA7.1) configuration and includes the Global Model of Aerosol Processes (GLOMAP) aerosol scheme (Mann et al., 2010; Mann et al., 2012).

GLOMAP-mode resolves aerosol mass, number concentration, size distribution, composition, and optical properties. Prognostic aerosol species included in GLOMAP-mode are sulfate, black carbon, organic carbon and sea salt, which are internally mixed within five modes corresponding to soluble nucleation (dry diameter < 5 nm), Aitken (dry diameter 5-50 nm), accumulation (dry diameter 50-500 nm), coarse (dry diameter > 500 nm) and insoluble Aitken mode. Processes simulated within GLOMAP-mode include primary emissions, new particle nucleation, particle growth *via* coagulation, condensation and cloud processes, particle removal by dry deposition, and in-cloud and below-cloud scavenging (Mann et al., 2010; Mann et al., 2012). Oxidant concentrations necessary for the sulfur cycle are prescribed from monthly varying inputs.

Atmospheric variables are resolved at a horizontal resolution of 1.25° latitude x 1.875° longitude (~135 km x ~200 km resolution in the low-latitudes), with 85 vertical levels (50 below 18 km and 35 above) reaching a model top of 85 km. Further details on the physical parameterizations in UM GA7.1 are described in detail in Walters et al. (2019). ACCESS-AM2 uses an identical implementation, of which a detailed description is provided in Bi et al. (2020). In this work, an atmosphere-only (ACCESS-AM2) configuration is used (Bodman et al., 2020).

2.2 Experimental design

2.2.1 Seawater surface DMS concentration

In ACCESS-AM2, DMS_w is prescribed from the global Lana et al. (2011) monthly mean climatology, henceforth L11 (Figure 1A). As discussed above, the L11 climatology was derived from DMS_w observations over most of the global ocean (Kettle et al., 1999). However, very few observations were included for coral reef regions and extrapolation did not account for seasonal or spatial variability across coral reef flats and lagoon waters. For this analysis, L11 is modified to include a climatology of DMS_w derived from an empirical relationship in the GBR (Jackson et al., 2021), henceforth referred to as the GBR climatology. The GBR climatology calculated in Jackson et al. (2021) (0.25-degree grid) was scaled up to the model grid by binning the values to a resolution of 1.25 x 1.875 degrees. L11 was then modified by substituting pixels within the GBR region (10.5-25°S; 142-154°E) with the GBR climatology, which added an average of 0.5 nmol to the GBR seawater surface concentration (Figure 1C).

The GBR climatology was derived from an empirical relationship between DMS_w, SST and PAR, measured during the RVI surveys from 28 September to 24 October 2016. The RVI surveys were undertaken as part of the 'Great Barrier Reef as a significant source of climatically relevant aerosol particles' project, known as the 'Reef to Rainforest' (R2R) campaign. The RVI path is shown in Figure 1A. The calculated GBR DMS climatology agrees with the range of observed seasonal and spatial (lagoon versus reef flat) seawater DMS concentrations at several locations in the GBR (summarized in Jones et al., 2018) and is considered to be a reasonable representation of DMS_w produced by corals and other marine organisms in GBR waters.

2.2.2 DMS sea-air and coral-air flux

DMS sea-air flux is calculated using the Liss and Merlivat (1986) parameterisation (Figure 1B). Current DMS sea-air flux parameterisations do not account for direct release of DMS from coral mucous when the reef is exposed to air during low tide. Coral aerial exposure is an important, albeit intermittent, source of atmospheric DMS (DMS_a) (Andreae et al., 1983), that can lead to rapidly released plumes of DMS_a over coral reefs (Jones et al., 2007; Swan et al., 2017). DMS_a plumes over aerially exposed coral reefs are significantly more concentrated than

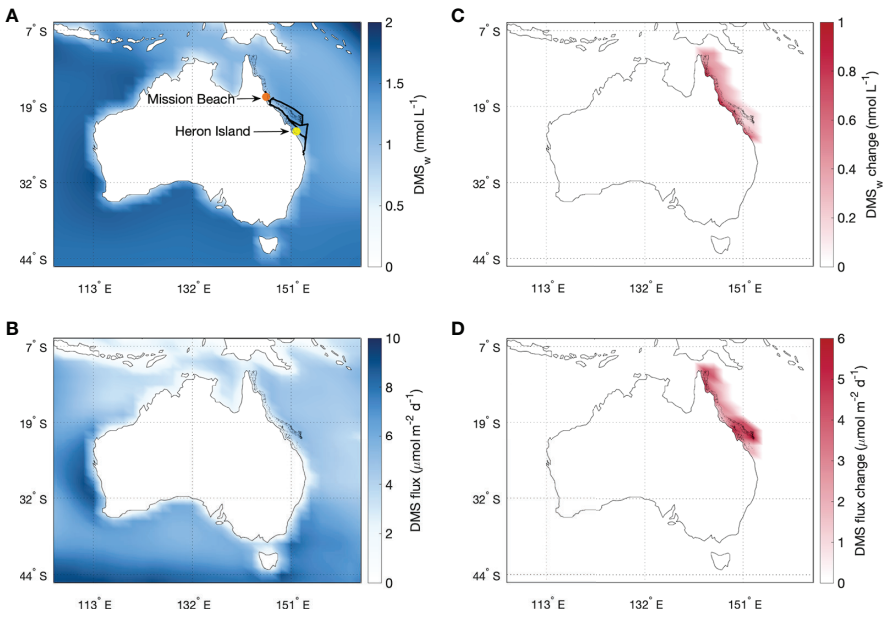

FIGURE 1
Annual mean **(A)** DMS_w and **(B)** DMS sea-air flux based on the L11 climatology, and the change in each variable due to the inclusion of **(C)** the GBR DMS climatology and **(D)** the GBR DMS climatology and coral-air DMS flux. The RVI path (black), Mission Beach (orange) and Heron Island (yellow) survey locations are shown in **(A)**.

the background DMS_a signal, for which the seasonal average ranges from approximately 1 nmol m^{-3} (~25 ppt) in winter to 4 nmol m^{-3} (~100 ppt) in summer over the GBR (Swan et al., 2017).

It has been estimated that *Acropora* corals exposed to air release 9-35 µmol m^{-2} d^{-1} (mean 22 µmol m^{-2} d^{-1}), according to measurements of gas-phase DMS_a in chamber experiments containing *Acropora* corals exposed to air (Hopkins et al., 2016). To account for direct coral-air DMS flux, the mean of the Hopkins et al. (2016) laboratory-derived estimate was added to the modelled DMS sea-air flux, scaled by the percentage of coral reef cover (i.e. coral-air flux = reef fraction x 22). The fraction of reef cover was calculated as the number of reef pixels within a 0.25-degree grid (as determined in Jackson et al., 2021), using a database of coral reef locations obtained from ReefBase (https://www.refbase.org) in MATLAB R2020a. The estimate of coral cover across the GBR ranged from 0.01-34% within the 0.25 degree-resolution grid.

The estimate of coral-air DMS flux used in Jackson et al. (2021) was scaled up to the model grid by binning the mean values to a resolution of 1.25 x 1.875 degrees. The resulting coral-air DMS flux estimate ranged from 0.2-2.6 µmol m^{-2} d^{-1} and added an average of 1.4 µmol m^{-2} d^{-1} of DMS to the regional sea-air flux. Our estimate may be a conservative representation of coral-air DMS flux, given that it is two orders of magnitude lower than the 0.01-0.02 Tg yr^{-1} estimate of Hopkins et al. (2016).

The approach used to estimate coral-air DMS flux is limited as it assumes that *Acropora* spp. are the sole source of DMS and it does not account for variability in the extent of coral exposure or the complexity of the reef environment (Hopkins et al., 2016). Further research is needed to reduce the uncertainty in coral-air DMS flux, to accurately scale laboratory-derived fluxes to the natural coral reef environment, and to account for diurnal variability in DMS coral-air flux and DMS_a concentration with variability in tidal cycles and photo-oxidation rates, respectively. Nevertheless, inclusion of the coral-air DMS flux estimate provides a more accurate estimate of total DMS flux from the GBR.

Incorporating both the GBR climatology and coral-air DMS flux into the model increased DMS flux from the GBR by an average of 3 µmol m^{-2} d^{-1} (Figure 1D); equivalent to 0.02 Tg yr^{-1} of DMS. In this study, coral-reef-derived DMS refers to the total contribution of DMS from corals and other organisms within the GBR, and includes the GBR DMS_w climatology and coral-air DMS flux estimates described above.

2.3 Analysis

Simulations were run for a 12-month period from January to December 2016, to coincide with three surveys undertaken as part of the R2R campaign in February and September-October 2016. Meteorology in the model was nudged to the ERA-5 data set (Hersbach et al., 2020). Although nudging dampens meteorological responses, this method allows simulated responses to be attributed to a change in an independent variable (e.g. DMS_w and coral-air DMS flux), while eliminating the need to run computationally expensive, long-term simulations to account for internal model variability. Nudging also allows the best comparison with field observations, by minimising uncertainty associated with meteorology.

As part of the R2R campaign, measurements were taken on board the RVI from 28 September to 24 October 2016. During the same period, shore-based measurements were made using the Atmospheric Integrated Research Facility for Boundaries and Oxidative Experiments (AIRBOX) mobile atmospheric chemistry laboratory at Mission Beach (17.82°S; 146.12°E) from 20 September to 16 October 2016. An overview paper describing these two field campaigns and datasets is currently in preparation (Trounce et al.,). A prior survey was undertaken at Heron Island (23.44°S; 151.91°E) on the southern GBR from 5 to 18 February 2016 (Swan and Jones, 2017; see also Deschaseaux et al., 2022). The RVI path, Mission Beach and Heron Island survey locations are shown in Figure 1A. A brief description of these surveys undertaken for the R2R campaign and methods used are provided in the Supplementary Information (SI).

To investigate whether the model output represents observations, modelled DMS_a (parts per trillion or pmol mol^{-1}) and wind speed (m s^{-1}) are compared with hourly mean observations for the RVI, Mission Beach and Heron Island survey periods and coordinates (± 0.05 degrees). Given the coarse model resolution, modelled DMS_a and wind speed were first interpolated to a 0.1-degree (~10 km) grid using a linear interpolation in MATLAB v2020a.

2.3.1 Experiment 1

For the control simulation, DMS_w was prescribed from the oceanic L11 climatology (Figure 1A). For the experimental simulation, DMS_w in the GBR region is prescribed from the GBR climatology and includes the estimate of coral-air DMS flux (henceforth GBR DMS). The change in annual mean DMS_a, gas-phase SO_2 and H_2SO_4 (ppt), sulfate aerosol mass (ppt), the number concentration of aerosol in the four soluble GLOMAP size modes (m^{-3}), aerosol with dry diameter greater than 3 nm (N3) (cm^{-3}), CCN with dry diameter greater than 70 nm (CCN70) (cm^{-3}) and cloud droplets (Nd) (m^{-3}), and surface downwelling short-wave radiation (SWR) (W m^{-2}) is then quantified between the control and experimental simulations over north-eastern Australia (9.5-26°S; 135-155°E). The analysis focused on this region to capture changes due to the inclusion of coral-reef-derived DMS.

2.3.2 Experiment 2

Given the global and Australian Government initiatives to shift towards renewable energy, anthropogenic sulfur emissions may decline in future. Therefore, it is important to understand the relative importance of biogenic and anthropogenic sulfate aerosol sources, and the effects of a change in emissions on the aerosol system. The influence of coral-reef-derived DMS in a relatively clean atmosphere is investigated by repeating the control and experimental simulations described above, with high level anthropogenic SO_2 emissions from north-eastern Australia removed from the model. 'High level' anthropogenic SO_2 in ACCESS-AM2 includes 100% of energy sector emissions, and 50% of industrial emissions. Given that the focus of this study is on atmospheric sulfate, other anthropogenic emissions (e.g. black carbon) were not modified, but could also have an impact.

3 Results

3.1 Comparison of observed and modelled data

Simulations using L11 and GBR DMS performed similarly in predicting observations of DMS_a at the local, hourly scale (Figures 2A–C). Both L11 and GBR DMS sources overestimated observed DMS_a during the R2R surveys (Table 1). Given that the nudged model simulations predicted observed wind speed moderately well ($r > 0.5$, $p < 0.001$) (Figures 2D–F), the differences between observed and modelled DMS_a are largely due to DMS_w and coral-air DMS flux sources in the model. Nevertheless, modelled DMS_a was within the range of concentrations previously reported for the GBR, which range from approximately 50-200 ppt (mean ~100

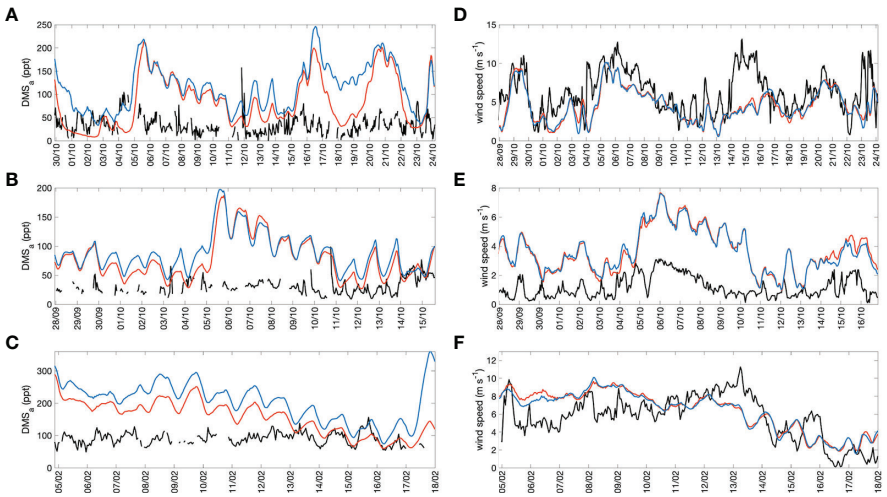

FIGURE 2
Time-series of observed (black) and modelled (left panels) DMS_a and (right panels) wind speed for the L11 (orange) and GBR DMS (blue) simulations during the **(A, D)** RVI, **(B, E)** Mission Beach and **(C, F)** Heron Island surveys.

TABLE 1 Mean and range of observed and modelled DMS_a (ppt or pmol mol^{-1}) during the RVI, Mission Beach and Heron Island surveys of the R2R campaign [concentration (deviation from observed mean)].

		Mean	Range
RVI	Observed	33	<1 – 158
(n = 456)	L11	86 (+ 53)	8 – 213
	GBR DMS	114 (+ 81)	33 – 245
Mission Beach	Observed	31	9 – 99
(n = 296)	L11	80 (+ 49)	27 – 187
	GBR DMS	89 (+ 58)	41 – 195
Heron Island	Observed	90	49 – 156
(n = 274)	L11	157 (+ 67)	60 – 289
	GBR DMS	199 (+ 109)	74 – 316

ppt) in summer (Jones et al., 2007; Swan et al., 2017; Swan and Jones, 2020; 2017) and can exceed 500 ppt over aerially exposed coral reefs (Jones et al., 2007; Swan et al., 2017). Therefore, the DMS_w climatologies in the model are assumed to represent the upper range of observed DMS in the GBR.

DMS_a concentration varies with the rate of DMS sea-air flux (which is primarily dependent on seawater surface DMS concentration, SST and wind speed) (Yang et al., 2011), coral-air DMS flux (Swan et al., 2017) and photochemical processes such as production of OH and subsequent oxidation of DMS_a to sulfate aerosol precursor compounds (Ayers and Gillett, 2000; Barnes et al., 2006). Consequently, observed and modelled DMS_a display a diel cycle (Figures 2A–C), decreasing around midday when solar radiation and the abundance of oxidative free radicals are highest (Gabric et al., 2008; Galí et al., 2013; Jackson et al., 2020). Increases in modelled DMS_a often aligned with modelled wind speed, reflecting wind-driven sea-air flux (Figure 2). Occasional pulses in modelled DMS_a occurred for the GBR DMS simulation during low wind speeds, reflecting the addition of coral-air flux (e.g. on 18 February 2016; Figure 2C). Conversely, observations of DMS_a and wind speed did not align well, possibly reflecting advection to and from the measurement platform.

Observations of DMS_a at Heron Island were approximately two-times higher than the RVI and Mission Beach observations, highlighting the variability in DMS concentrations in the GBR. It was expected that observed DMS_a would be highest at Heron Island, given that measurements were taken less than 100 m from the coral reef flat and were more likely to capture the high end of atmospheric concentrations over the reef. Further, the RVI and Mission Beach surveys took place six months after the March-April 2016 mass coral bleaching event on the GBR, which led to the loss of up to 40% of hard coral cover by November 2016 (Hughes et al., 2018). Observed DMS_w (not shown here) and DMS_a were lower during the RVI and Mission Beach surveys than previously reported for the GBR region (Swan and Jones, 2017; Jones et al., 2018, 2020), which may have been in part due to the loss of DMS-producing hard corals. Prior to the 2016 mass coral bleaching event, DMS_a measured at Heron Island ranged from 49-156 ppt (Table 1). However, with the exception of a pulse of DMS_a on 12 October 2016, DMS_a was below 100 ppt during the RVI and Mission Beach surveys (Figures 2A, B).

Considering that the L11 and GBR DMS sources are monthly mean climatologies (and fixed coral-air DMS flux) with no diurnal variation, a degree of variability was expected between the observed and coarse resolution modelled DMS_a. While modelled DMS_a represents the upper range of observations previously reported for the GBR region, simulations using L11 and GBR DMS sources still provide valuable insight into the influence of coral-reef-derived DMS on the regional atmosphere. Further research will improve our understanding of the complex coral reef sulfur cycle and will further improve the representation of coral-reef-derived DMS in climate models.

3.2 Influence of coral-reef-derived DMS over north-eastern Australia

Inclusion of coral-reef-derived DMS increased annual mean DMS_a concentration over the GBR by approximately 150% (Figures 3A, D), resulting in an area-averaged increase of 29% (29.4 ppt) over north-eastern Australia (Table 2). Similarly, annual mean gas-phase SO_2 and H_2SO_4 increased by a respective 1% and 3% over north-eastern Australia, in part due to the increase in DMS_a over the GBR, where the strongest increase in SO_2 (up to 17.6%) and H_2SO_4 (up to 14.9%) occurred (Figure 3). Regardless of the increase in SO_2 and H_2SO_4 (FigureS 3E, F), concentrations over marine areas are negligible in comparison to industrial regions of coastal and inland Australia (Figures 3B, C).

Changes for annual mean sulfate aerosol mass and number concentration over north-eastern Australia were small (≤ 2.4%), yet revealed some interesting results. Nucleation mode sulfate mass and number concentration decreased by a respective -1% and -0.6% over north-eastern Australia, while sulfate mass increased by similar magnitude for the Aitken mode (+0.8%) and to a lesser extent the accumulation mode (+0.01%) (Table 2). A small increase in sulfate mass (+2.4%) and number concentration (+0.5%) also occurred for coarse mode aerosols. The small increase in Aitken and accumulation mode mass without a corresponding increase in number suggests that additional sulfate contributed to the growth of these size modes *via* condensation or coagulation on existing particles.

Negligible changes occurred for N3, CCN70, Nd and surface SWR (≤ 0.1%) that were likely driven by internal model and meteorological variability. While meteorology in the model was nudged to the ERA-5 dataset, minor differences in meteorological fields can still occur between model runs (as occurred in this study for wind speed; see Table 2). A time-series of each variable area-averaged over north-eastern Australia is provided in SI Figure 1. Mapped changes for sulfate aerosol mass, particle number concentrations and SWR are provided in SI Figures 2–4.

Similarly to previous model studies (Fiddes et al., 2021; Fiddes et al.,2022), the weak response to the addition of coral-reef-derived DMS may be due to the dominant influence of anthropogenic sulfur and other emissions from north-eastern Australia (Chen et al., 2019). Anthropogenic sources can dominate aerosol emissions, particularly over coastal and inland regions. Consequently, the dominant pathway for biogenic trace gases in the marine boundary layer is condensation or coagulation onto existing particles, often resulting in aerosol growth rather than new particle nucleation (Woodhouse et al., 2013; Hoffmann et al., 2016).

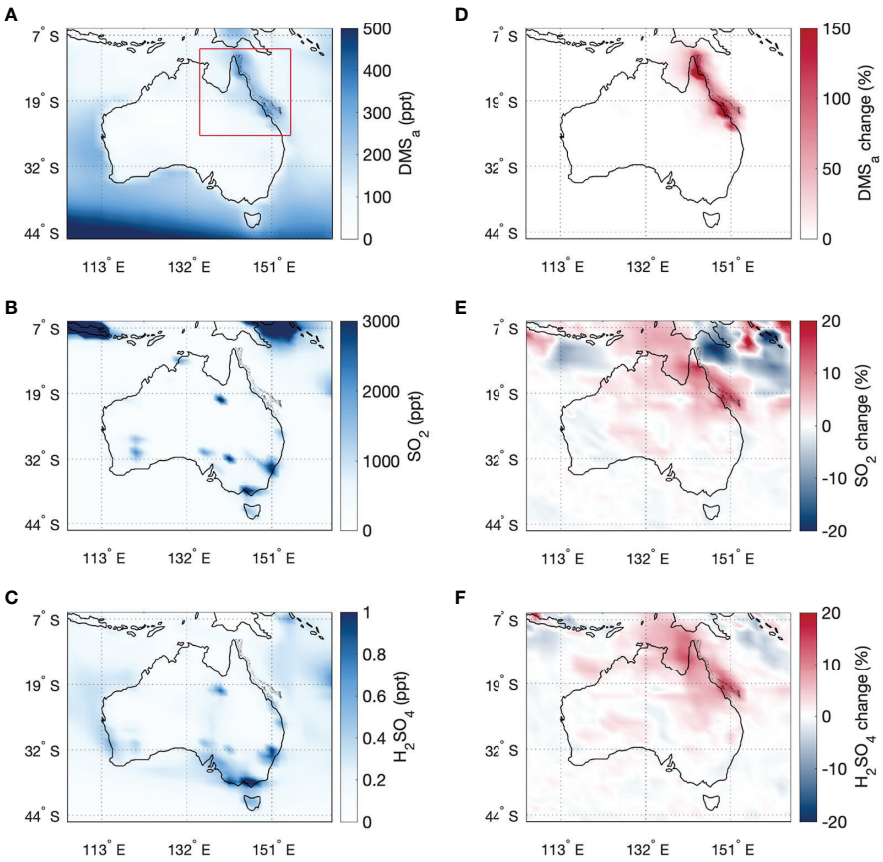

FIGURE 3
Annual mean **(A)** DMS_a, **(B)** SO_2 and **(C)** H_2SO_4 for the GBR DMS simulation, and **(D–F)** the percentage change in each variable between the GBR DMS and L11 simulations. The north-eastern Australian region (9.5-26°S; 135-155°E) for which the area-averaged changes are calculated for Table 2 is shown in red in panel **(A)**.

Given the response detected for DMS_a and gas-phase sulfate aerosol precursor compounds (SO_2 and H_2SO_4) at the annual mean time-scale, a stronger response in aerosol mass and number concentration may occur at local or sub-daily time scales as observational studies have suggested (Modini et al., 2009; Swan et al., 2016; Cropp et al., 2018), or with a reduction in anthropogenic pollutants. The latter is investigated below, where the influence of coral-reef-derived DMS is quantified when high-level anthropogenic SO_2 emissions (e.g. from industrial chimneys, shown as hotspots exceeding 2000 ppt in Figure 3B) are removed from north-eastern Australia.

3.3 Influence of coral-reef-derived DMS in a relatively clean atmosphere

After removing high level anthropogenic SO_2 emissions, the inclusion of coral-reef-derived DMS again increased DMS_a, SO_2 and H_2SO_4 concentrations over north-eastern Australia (Table 2). The increases are similar in space and magnitude to the results presented in section 3.2 above, however are stronger over the GBR (Figure 4). The stronger response is likely due to the addition of DMS-derived sulfur to a reduced pool of atmospheric SO_2 and H_2SO_4 concentrations.

The change in sulfate aerosol mass and particle number concentration between the L11 and GBR DMS simulations were small (≤ 3.6%) (Table 2; SI Figure 5). Sulfate aerosol mass and number concentration decreased for the nucleation and accumulation mode, yet increased for the Aitken mode. For coarse mode aerosols, there was an increase in sulfate mass, without a corresponding increase in number concentration (Table 2). As for section 3.2, the inconsistent changes in sulfate mass and number concentration between aerosol size modes suggests that DMS-derived sulfate may be a more important contributor to aerosol mass and growth of existing aerosols, rather than nucleation of new particles at the monthly and annual mean time-scale, even with a reduction in anthropogenic sulfur emissions.

TABLE 2 Annual mean change [actual (percentage)] between the GBR DMS and L11 simulations area-averaged over north-eastern Australia.

	Experiment 1	Experiment 2
DMS flux (µmol m^{-2} d^{-1})	+0.6 (25.1%)	+0.6 (25.9%)
DMS_a (ppt)	+29.4 (29.2%)	+29.5 (29.3%)
SO_2 (ppt)	+5.6 (1.4%)	+3.0 (0.9%)
H_2SO_4 (ppt)	+5.4 x10^{-3} (3.0%)	+6.2 x10^{-3} (4.0%)
Nuc. sul. mass (ppt)	-5.2 x10^{-5} (1.0%)	-4.9 x10^{-6} (0.1%)
Ait. sul. mass (ppt)	+0.3 (0.8%)	+0.4 (1.2%)
Acc. sul. mass (ppt)	+0.04 (0.01%)	-14.5 (3.6%)
Crs. sul. mass (ppt)	+0.2 (2.4%)	+0.05 (0.7%)
Nuc. no. (m^{-3})	-1.1 x10^{-21} (0.6%)	-1.1 x10^{-21} (0.6%)
Ait. no. (m^{-3})	-1.5 x10^{-20} (0.2%)	+1.1 x10^{-20} (0.2%)
Acc. no. (m^{-3})	-8.4 x10^{-21} (0.1%)	-1.1 x10^{-20} (0.1%)
Crs. no. (m^{-3})	+2.3 x10^{-22} (0.5%)	-8.6 x10^{-23} (0.2%)
N3 (cm^{-3})	-0.3 (0.1%)	+0.3 (0.1%)
CCN70 (cm^{-3})	-0.03 (0.01%)	-0.3 (0.1%)
Nd (m^{-3})	+0.07 (0.04%)	-0.3 (0.2%)
SWR (W m^{-2})	+0.07 (0.03%)	-0.2 (0.1%)
Wind (m s^{-1})	-7.3 x10^{-3} (0.1%)	+3.9 x10^{-3} (0.1%)

* Nuc., nucleation; Ait., Aitken; Acc., accumulation; Crs., coarse; sul., sulfate; no., number concentration; SWR, surface downwelling short-wave radiation; Wind, wind speed at 10 m.

4 Discussion

Inclusion of coral-reef-derived DMS added an average of 0.5 nmol L-1 to the sea surface DMS climatology and 3 µmol m^{-2} d^{-1} (0.02 Tg yr^{-1}) to the DMS sea-air flux for the GBR region. The additional DMS increased modelled annual mean DMS_a concentration by approximately 150% over the GBR and by 29% over north-eastern Australia. The concentration of gas-phase sulfate aerosol precursor compounds (SO_2 and H_2SO_4) increased by up to 17.6% over the GBR, supporting previous findings that the GBR is an important regional source of atmospheric sulfur (Broadbent and Jones, 2004; Jones et al., 2018; Jackson et al., 2021).

The increase in DMS_a and subsequent increase in sulfate aerosol precursors is primarily attributed to the inclusion of coral-to-air DMS flux. The GBR DMS_w climatology did not substantially increase seawater surface DMS concentration (< 1 nmol L^{-1}; Figure 1C), and likely had a minor contribution to the ~150% increase in DMS_a (Figure 3D). Previous field work has suggested that coral-air DMS flux is a stronger, although intermittent, contributor to DMS_a than sea-air flux in the GBR (Swan et al., 2017), leading to plumes of DMS_a above coral reefs that can exceed 500 ppt (Jones et al., 2007; Swan et al., 2017). This study supports this hypothesis, where an increase in DMS_a, SO_2 and H_2SO_4 was detected over the GBR (Figure 3), primarily due to the inclusion of coral-air DMS flux.

Gas-phase SO_2 may be further oxidised to H_2SO_4, which may condense onto existing particles as the dominant pathway within the marine boundary layer (Woodhouse et al., 2013;

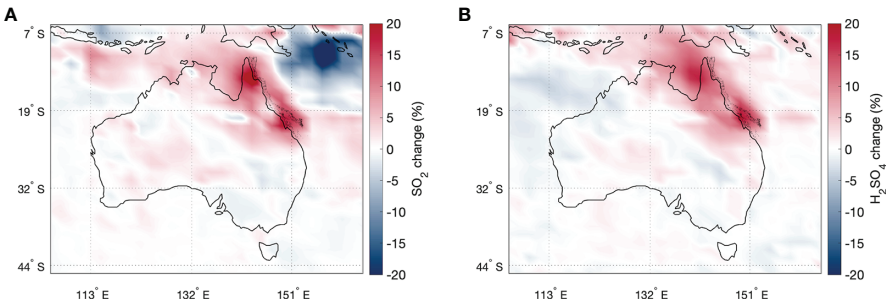

FIGURE 4
Change in annual mean **(A)** SO_2 and **(B)** H_2SO_4 between the GBR DMS and L11 simulations, when high anthropogenic SO_2 emissions from north-eastern Australia have been removed.

Hoffmann et al., 2016), or nucleate to form new nss-SO_4 particles (Andreae and Crutzen, 1997). Despite the increase in gas-phase sulfate aerosol precursors, coral-reef-derived DMS had no clear influence on modelled sulfate aerosol mass or number concentration at the monthly or annual mean time-scale, supporting previous model studies (Fiddes et al., 2021; Fiddes et al., 2022) which demonstrate that DMS-derived sulfates do not play an important role in aerosol formation or growth over large temporal and spatial scales. Fiddes et al. (2021) estimated that DMS_w derived from global tropical coral reefs contributed 0.3 Tg yr^{-1} S to the global sea-air flux in the global ACCESS-UKCA atmospheric model. Despite modelled DMS flux being an order of magnitude higher than the current study, Fiddes et al. (2021) found that coral-reef-derived DMS had only a minor influence on sulfate aerosol mass and number concentration for nucleation and Aitken mode aerosols, and no significant influence on cloud-relevant particles or the Earth's radiative balance. Fiddes et al. (2022) reported similar findings in the GBR region using the regional WRF-Chem model.

Small (≤ 2.4%) and inconsistent changes in sulfate aerosol mass and number concentration over north-eastern Australia in the present study are more likely due to internal model variability and minor changes in meteorology, than to coral-reef-derived DMS. While meteorology was nudged to the ERA-5 dataset, minor differences between model runs can occur. In this analysis, annual mean wind speed at 10 m differed by ± 0.1% between the control and experimental simulations (Table 2).

In comparison to the increase in gas-phase sulfate aerosol precursors, the negligible change in aerosol mass and number concentration may be due to the dominant influence of anthropogenic and other natural emissions (e.g. dust) from north-eastern Australia (Chen et al., 2019). To investigate whether the sensitivity of aerosol to DMS increased in a relatively less polluted atmosphere, we repeated the simulations with reduced anthropogenic SO_2 emissions from north-eastern Australia; representing an optimistic future scenario where a shift to renewable energy may reduce anthropogenic pollutants. It was hypothesised that by reducing emissions from industrial hotspots, such as Gladstone in south-east Queensland, a stronger response in aerosol mass and number concentration to DMS might be detected. However, the results presented in section 3.3 highlight the complexity and non-linearity of the aerosol system, where a change in aerosol sources does not necessarily result in a change in aerosol composition or concentration of the same direction or magnitude.

Addition of coral-reef-derived DMS to a simulated cleaner regional atmosphere did increase DMS_a, SO_2 and H_2SO_4. However, no clear influence was detected for sulfate aerosol mass or particle number concentration, suggesting that even with a reduction in anthropogenic sulfur emissions, coral-reef-derived DMS may not play a significant role in aerosol production and processing over the GBR. Again, negligible (≤ 3.6%) changes occurred that were not restricted to the GBR region. These changes are more likely due to model and meteorological variability than coral-reef-derived DMS and so are not discussed further here.

While this analysis provides further insight into the influence of coral-reef-derived DMS on the contemporary and relatively clean regional atmosphere, further research is needed to improve DMS sources in the model. Simulations using both L11 and GBR DMS overestimated observed DMS_a during the 2016 R2R campaign, yet modelled concentrations were still within the range previously reported for the GBR (Swan and Jones, 2017; Jones et al., 2018; Swan and Jones, 2020). As discussed above, the R2R surveys were taken approximately two weeks prior, and six months after the 2016 mass coral bleaching event, which led to the loss of up to 40% of hard coral cover in the GBR (Hughes et al., 2018). The loss of DMS-producing corals may be one reason why observed DMS_w and DMS_a during the RVI and Mission Beach surveys were low compared to previous surveys and modelled concentrations, highlighting the complexity in predicting coral-reef-derived DMS.

Further research is also required to understand the aerosol chemistry system and how it responds to changes in anthropogenic and natural emissions sources. While DMS emissions from the GBR did not influence aerosol mass or number concentration at the scales modelled in this study, observational studies suggest that DMS may be more important in local or sub-daily feedbacks. Nucleation events forming new particles that primarily consist of sulfates have been observed over the GBR (Modini et al., 2009), and coincided with elevated DMS_a concentrations on one occasion in the southern GBR (Swan et al., 2016). Further, DMS emissions and DMS_a concentration are positively correlated with atmospheric particle number concentration (>0.5 µm wet diameter) at Heron Island, likely reflecting condensational growth of smaller aerosols to the detectable size range (Jackson et al., 2020; Deschaseaux et al., 2022). Given that DMS emissions from the GBR are comparable to other highly productive regions such as the Southern Ocean or North Atlantic, where DMS-derived sulfates account for a significant portion of CCN (Korhonen et al., 2008; Sanchez et al., 2018), it is possible that DMS influences aerosol processes in the GBR at scales that are not captured by the coarse resolution global model.

5 Conclusions

This modelling study supports previous findings that the GBR is an important regional source of atmospheric sulfur. Inclusion of coral-reef-derived DMS increased the concentration of atmospheric DMS by 150% and sulfate aerosol precursor compounds by up to 18% over the GBR, with potential implications for local or sub-daily aerosol processes. However, no influence on modelled sulfate aerosol mass or particle

number concentration was detected in this study. While reducing anthropogenic SO_2 emissions did not strengthen the aerosol response to coral-reef-derived DMS, other anthropogenic and natural (e.g. dust) emissions from north-eastern Australia may confound the biogenic sulfur signal, particularly over large temporal and spatial scales. A stronger response to coral-reef-derived DMS may occur at local, sub-daily time-scales, that are perhaps not captured by global or regional climate models, or in the absence of anthropogenic emissions. However, further research is needed to disentangle the relative influence of natural and anthropogenic aerosol sources. Given the predicted rates of coral reef degradation and the global initiatives to shift towards renewable energy, it is important to understand how the complex aerosol-cloud system will respond to changes in natural and anthropogenic emissions.

Data availability statement

The ACCESS-AM2 atmospheric model used for this study is a licensed product of the UK Met Office and is available to specific users under a license agreement. The model output can be provided on request. The Heron Island DMS_a field data (Swan and Jones, 2017) are available from the Southern Cross University online repository (https://researchportal.scu.edu.au/). The RVI underway data (in2016_v05uwy5min_csv.zip) is available from the CSIRO Marine National Facility repository (https://marlin.csiro.au/) under a Creative Commons Attribution 4.0 License. The Heron Island wind speed data is available from H. B. Swan and E. S. M. Deschaseaux upon request. The RVI DMS_a data, and Mission Beach DMS_a and wind speed data are available from the relevant institutions upon request.

Author contributions

RJ completed the model simulations, data analysis and prepared the manuscript. MW provided guidance on the model setup, experimental design and analysis. HS, ED and HT provided field data. All authors contributed to the review and finalisation of the manuscript.

Funding

Research undertaken on Marine National Facility RV *Investigator* voyage IN2016_V05 (RVI) and the work of G. B. Jones, ED and HS at Heron Island was supported by Australian Research Council Discovery Project grant DP150101649 'The Great Barrier Reef as a significant source of climatically relevant aerosol particles'. RJ was supported by an Australian Government Research Training Program Scholarship, Commonwealth Scientific and Industrial Research Organisation post-graduate scholarship, and the Griffith University School of Environment and Science.

Acknowledgments

We acknowledge the use of the CSIRO Marine National Facility in undertaking this research. The authors gratefully acknowledge Professor Zoran Ristovski, Chief Scientist on the voyage IN2016_V05 'The Great Barrier Reef as a significant source of climatically relevant aerosol particles', the crew of the Marine National Facility RV *Investigator*, and all Mission Beach onsite personnel from CSIRO, Southern Cross University and Queensland University of Technology for the provision of DMS_a and wind speed measurements during the September-October 2016 field campaign. We also acknowledge the Australian Research Council for funding under the Discovery Project DP150101649. HS, ED and G. B. Jones are gratefully acknowledged for making available their Heron Island DMS_a and wind speed datasets. ED and HS would also like to thank the staff of the Heron Island Research Station for support during their field work. The modelling was undertaken using the National Computational Infrastructure facilities, supported by the Australian Government. The work forms part of RJ's PhD thesis, entitled 'Coral reefs as a source of dimethylsulfide (DMS) and the influence on the atmosphere of the Great Barrier Reef', which will be available on the Griffith University online repository (https://research-repository.griffith.edu.au) from 14 June 2023.

Conflict of interest

The authors declare that the research was conducted in the absence of any commercial or financial relationships that could be construed as a potential conflict of interest.

Publisher's note

Supplementary material

The Supplementary Material for this article can be found online at: https://www.frontiersin.org/articles/10.3389/fmars.2022.910423/full#supplementary-material

References

Andreae, M. O. (1995). "Climatic effects of changing atmospheric aerosol levels," in *In world survey of climatology* (Netherlands: Elsevier), vol. 16, 347–398. doi: 10.1016/S0168-6321(06)80033-7

Andreae, M. O., Barnard, W. R., and Ammons, J. M. (1983). The biological production of dimethylsulfide in the ocean and its role in the global atmospheric sulfur budget. *Ecol. Bulletins.* 35, 167–177.

Andreae, M. O., and Crutzen, P. J. (1997). Atmospheric aerosols: Biogeochemical sources and role in atmospheric chemistry. *Science* 276 (5315), 1052–1058. doi: 10.1126/science.276.5315.1052

Andreae, M. O., and Rosenfeld, D. (2008). Aerosol–cloud–precipitation interactions. part 1. the nature and sources of cloud-active aerosols. *Earth-Science. Rev.* 89 (1–2), 13–41. doi: 10.1016/j.earscirev.2008.03.001

Ayers, G. P., and Gillett, R. W. (2000). DMS and its oxidation products in the remote marine atmosphere: Implications for climate and atmospheric chemistry. *J. Sea. Res.* 43 (3–4), 275–286. doi: 10.1016/S1385-1101(00)00022-8

Barnes, I., Hjorth, J., and Mihalopoulos, N. (2006). Dimethyl sulfide and dimethyl sulfoxide and their oxidation in the atmosphere. *Chem. Rev.* 106 (3), 940–975. doi: 10.1021/cr020529+

Berndt, T., Scholz, W., Mentler, B., Fischer, L., Hoffmann, E. H., Tilgner, A., et al. (2019). Fast peroxy radical isomerization and OH recycling in the reaction of OH radicals with dimethyl sulfide. *J. Phys. Chem. Lett.* 10 (21), 6478–6483. doi: 10.1021/acs.jpclett.9b02567

Bi, D., Dix, M., Marsland, S., O'Farrell, S., Sullivan, A., Bodman, R., et al. (2020). Configuration and spin-up of ACCESS-CM2, the new generation Australian Community Climate and Earth System Simulator Coupled Model. *J. South. Hemisphere. Earth Syst. Sci.* 70 (1), 225–251. doi: 10.1071/ES19040

Bodman, R. W., Karoly, D. J., Dix, M. R., Harman, I. N., Srbinovsky, J., Dobrohotoff, P. B., et al. (2020). Evaluation of CMIP6 AMIP climate simulations with the ACCESS-AM2 model. *J. South. Hemisphere. Earth Syst. Sci.* 70 (1), 166–179. doi: 10.1071/ES19033

Broadbent, A. D., and Jones, G. B. (2004). DMS and DMSP in mucus ropes, coral mucus, surface films and sediment pore waters from coral reefs in the Great Barrier Reef. *Mar. Freshw. Res.* 55 (8), 849–855. doi: 10.1071/MF04114

Buckee, J., Pattiaratchi, C., and Verduin, J. (2020). Partial mortality of intertidal corals due to seasonal daytime low water levels at the Houtman Abrolhos Islands. *Coral. Reefs.* 39 (3), 537–543. doi: 10.1007/s00338-019-01887-5

Bullock, H. A., Luo, H., and Whitman, W. B. (2017). Evolution of dimethylsulfoniopropionate metabolism in marine phytoplankton and bacteria. *Front. Microbiol.* 8. doi: 10.3389/fmicb.2017.00637

Carslaw, K. S., Lee, L. A., Reddington, C. L., Pringle, K. J., Rap, A., Forster, P. M., et al. (2013). Large Contribution of natural aerosols to uncertainty in indirect forcing. *Nature* 503 (7474), 67–71. doi: 10.1038/nature12674

Charlson, R. J., Lovelock, J. E., Andreae, M. O., and Warren, S. G. (1987). Oceanic phytoplankton, atmospheric sulphur, cloud albedo and climate. *Nature* 326 (6114), 655–661. doi: 10.1038/326655a0

Chen, Z., Schofield, R., Rayner, P., Zhang, T., Liu, C., Vincent, C., et al. (2019). Characterization of aerosols over the Great Barrier Reef: The influence of transported continental sources. *Sci. Total. Environ.* 690, 426–437. doi: 10.1016/j.scitotenv.2019.07.007

Cropp, R. A., Gabric, A. J., van Tran, D., Jones, G., Swan, H., and Butler, H. (2018). Coral reef aerosol emissions in response to irradiance stress in the Great Barrier Reef, Australia. *Ambio* 47 (6), 671–681. doi: 10.1007/s13280-018-1018-y

Curson, A. R., Liu, J., Martínez, A. B., Green, R. T., Chan, Y., Carrión, O., et al. (2017). Dimethylsulfoniopropionate biosynthesis in marine bacteria and identification of the key gene in this process. *Nat. Microbiol.* 2, 17001–17009. doi: 10.1038/nmicrobiol.2017.9

Dave, P., Patil, N., Bhushan, M., and Venkataraman, C. (2019). "Aerosol influences on cloud modification and rainfall suppression in the south Asian monsoon region," in *Climate change signals and response*. Eds. C. Venkataraman, T. Mishra, S. Ghosh and S. Karmakar (Springer), 21–37. doi: 10.1007/978-981-13-0280-0_2

Deschaseaux, E. S. M., Jones, G. B., Deseo, M. A., Shepherd, K. M., Kiene, R. P., Swan, H. B., et al. (2014). Effects of environmental factors on dimethylated sulfur compounds and their potential role in the antioxidant system of the coral holobiont. *Limnol. Oceanography.* 59 (3), 758–768. doi: 10.4319/lo.2014.59.3.0758

Deschaseaux, E. S. M., Swan, H. B., Maher, D., Jones, G. B., Schulz, K., Koveke, E., et al. (2022). The interplay between dimethyl sulfide (DMS) and methane (CH_4) in a coral reef ecosystem. *Front. Mar. Science.: Coral. Reef. Res.* doi: 10.3389/fmars.2022.910441

Fan, J., Rosenfeld, D., Zhang, Y., Giangrande, S. E., Li, Z., Machado, L. A. T., et al. (2018). Substantial convection and precipitation enhancements by ultrafine aerosol particles. *Science* 359 (6374), 411–418. doi: 10.1126/science.aan8461

Fiddes, S. L., Woodhouse, M. T., Lane, T. P., and Schofield, R. (2021). Coral-reef-derived dimethyl sulfide and the climatic impact of the loss of coral reefs. *Atmospheric. Chem. Phys.* 21 (8), 5883–5903. doi: 10.5194/acp-21-5883-2021

Fiddes, S. L., Woodhouse, M. T., Nicholls, Z., Lane, T. P., and Schofield, R. (2018). Cloud, precipitation and radiation responses to large perturbations in global dimethyl sulfide. *Atmospheric. Chem. Phys.* 18 (14), 10177–10198. doi: 10.5194/acp-18-10177-2018

Fiddes, S. L., Woodhouse, M. T., Utembe, S., Schofield, R., Alexander, S. P., Alroe, J., et al. (2022). The contribution of coral-reef-derived dimethyl sulfide to aerosol burden over the Great Barrier Reef: A modelling study. *Atmospheric. Chem. Phys.* 22 (4), 2419–2445. doi: 10.5194/acp-22-2419-2022

Fischer, E., and Jones, G. (2012). Atmospheric dimethysulphide production from corals in the Great Barrier Reef and links to solar radiation, climate and coral bleaching. *Biogeochemistry* 110 (1), 31–46. doi: 10.1007/s10533-012-9719-y

Gabric, A. J., Matrai, P. A., Kiene, R. P., Cropp, R. A., Dacey, J. W. H., DiTullio, G. R., et al. (2008). Factors determining the vertical profile of dimethylsulfide in the Sargasso Sea during summer. *Deep. Sea. Res. Part II.: Topical Stud. Oceanography.* 55 (10–13), 1505–1518. doi: 10.1016/j.dsr2.2008.02.002

Gabric, A. J., Qu, B., Rotstayn, L., and Shephard, J. M. (2013). Global simulations of the impact on contemporary climate of a perturbation to the sea-to-air flux of dimethylsulfide. *Aust. Meteorolog. Oceanographic. J.* 63 (3), 365–376. doi: 10.22499/2.6303.002

Galí, M., Simó, R., Vila-Costa, M., Ruiz-González, C., Gasol, J. M., and Matrai, P. (2013). Diel patterns of oceanic dimethylsulfide (DMS) cycling: Microbial and physical drivers. *Global Biogeochem. Cycles.* 27 (3), 620–636. doi: 10.1002/gbc.20047

Gardner, S. G., Nielsen, D. A., Laczka, O., Shimmon, R., Beltran, V. H., Ralph, P. J., et al. (2016). Dimethylsulfoniopropionate, superoxide dismutase and glutathione as stress response indicators in three corals under short-term hyposalinity stress. *Proc. R. Soc. B.: Biol. Sci.* 283 (1824), 20152418. doi: 10.1098/rspb.2015.2418

Hersbach, H., Bell, B., Berrisford, P., Hirahara, S., Horányi, A., Muñoz-Sabater, J., et al. (2020). The ERA5 global reanalysis. *Q. J. R. Meteorolog. Soc.* 146 (730), 1999–2049. doi: 10.1002/qj.3803

Hodshire, A. L., Campuzano-Jost, P., Kodros, J. K., Croft, B., Nault, B. A., Schroder, J. C., et al. (2019). The potential role of methanesulfonic acid (MSA) in aerosol formation and growth and the associated radiative forcings. *Atmospheric. Chem. Phys.* 19 (5), 3137–3160. doi: 10.5194/acp-19-3137-2019

Hoffmann, E. H., Tilgner, A., Schroedner, R., Bräuer, P., Wolke, R., and Herrmann, H. (2016). An advanced modeling study on the impacts and atmospheric implications of multiphase dimethyl sulfide chemistry. *Proc. Natl. Acad. Sci.* 113 (42), 11776–11781. doi: 10.1073/pnas.1606320113

Hopkins, F. E., Bell, T. G., Yang, M., Suggett, D. J., and Steinke, M. (2016). Air exposure of coral is a significant source of dimethylsulfide (DMS) to the atmosphere. *Sci. Rep.* 6 (1), 1–11. doi: 10.1038/srep36031

Hughes, T. P., Kerry, J. T., Baird, A. H., Connolly, S. R., Dietzel, A., Eakin, C. M., et al. (2018). Global warming transforms coral reef assemblages. *Nature* 556 (7702), 492–496. doi: 10.1038/s41586-018-0041-2

IPCC (2013). *Climate change 2013: The physical science basis. contribution of working group I to the fifth assessment report of the intergivernmental panel on climate change*. Eds. T. Stocker, G. Qin, G. Plattner, M. Tignor, S. Allen, J. Boschung, et al (United Kingdom and NewYork, NY, USA: Cambridge University Press), pp. 1535.

IPCC (2021). "Summary for policymakers. in: Climate change 2021: The physical science basis," in *Contribution of working group I to the sixth assessment report of the intergovernmental panel on climate change*. Eds. V. Masson-Delmotte, P. Zhai, A. Pirani, S. L. Connors, C. Pean, S. Berger, N. Caud, Y. Chen, L. Goldfarb, M. I. Gomis, M. Huang, K. Leitzell, E. Lonnoy, J. B. R. Matthews, T. K. Maycock, T. Waterfield, O. Yelekci, R. Yu and B. Zhou (United Kingdom and New York, NY, USA: Cambridge University Press), pp. 3–32.

IPCC (2014). *Climate change 2014: Synthesis report. Contribution of working groups I, II and III to the fifth assessment report of the intergovernmental panel on climate change*. [Core Writing Team, R. K. Pachauri and L. A. Meyer (eds.)]. IPCC, Geneva, Switzerland, pp. 151.

Jackson, R. L., Gabric, A. J., Matrai, P. A., Woodhouse, M. T., Cropp, R. A., Jones, G. B., et al. (2021). Parameterizing the impact of seawater temperature and irradiance on dimethylsulfide (DMS) in the Great Barrier Reef and the contribution of coral reefs to the global sulfur cycle. *J. Geophysical. Research.: Oceans.* 126 (3), e2020JC016783. doi: 10.1029/2020JC016783

Jackson, R. L., Gabric, A. J., Woodhouse, M. T., Swan, H. B., Jones, G. B., Cropp, R. A., et al. (2020). Coral reef emissions of atmospheric dimethylsulfide and the influence on marine aerosols in the southern Great Barrier Reef, Australia. *J. Geophysical. Research.: Atmospheres.* 125 (7), e2019JD031837. doi: 10.1029/2019JD031837

Jones, G. B. (2015). "The reef sulphur cycle: Influence on climate and ecosystem services," in *In ethnobiology of corals and coral reefs* (Switzerland: Springer), 27–57. doi: 10.1007/978-3-319-23763-3_3

Jones, G. B., Curran, M., Broadbent, A., King, S., Fischer, E., and Jones, R. (2007). Factors affecting the cycling of dimethylsulfide and dimethylsulfoniopropionate in coral reef waters of the Great Barrier Reef. *Environ. Chem.* 4 (5), 310–322. doi: 10.1071/EN06065

Jones, G. B., Curran, M., Deschaseaux, E. S. M., Omori, Y., Tanimoto, H., Swan, H. B., et al. (2018). The flux and emission of dimethylsulfide from the Great Barrier Reef region and potential influence on the climate of NE Australia. *J. Geophysical. Research.: Atmospheres.* 123 (24), 13835–13856. doi: 10.1029/2018JD029210

Jones, G. B., Curran, M., Swan, H. B., and Deschaseaux, E. S. M. (2017). Dimethylsulfide and coral bleaching: Links to solar radiation, low level cloud and the regulation of seawater temperatures and climate in the Great Barrier Reef. *Am. J. Climate Change* 6 (02), 328. doi: 10.4236/ajcc.2017.62017

Kettle, A. J., Andreae, M. O., Amouroux, D., Andreae, T. W., Bates, T. S., Berresheim, H., et al. (1999). A global database of sea surface dimethylsulfide (DMS) measurements and a procedure to predict sea surface DMS as a function of latitude, longitude, and month. *Global Biogeochem. Cycles.* 13 (2), 399–444. doi: 10.1029/1999GB900004

Korhonen, H., Carslaw, K. S., Spracklen, D. V., Mann, G. W., and Woodhouse, M. T. (2008). Influence of oceanic dimethyl sulfide emissions on cloud condensation nuclei concentrations and seasonality over the remote southern hemisphere oceans: A global model study. *J. Geophysical. Research.: Atmospheres.* 113 (D15). doi: 10.1029/2007JD009718

Lana, A., Bell, T. G., Simó, R., Vallina, S. M., Ballabrera-Poy, J., Kettle, A. J., et al. (2011). An updated climatology of surface dimethlysulfide concentrations and emission fluxes in the global ocean. *Global Biogeochem. Cycles.* 25 (1). doi: 10.1029/2010GB003850

Lana, A., Simó, R., Vallina, S. M., and Dachs, J. (2012). Potential for a biogenic influence on cloud microphysics over the ocean: A correlation study with satellite-derived data. *Atmospheric. Chem. Phys.* 12 (17), 7977–7993. doi: 10.5194/acp-12-7977-2012

Liss, P. S., and Merlivat, L. (1986). Air-sea gas exchange rates: Introduction and synthesis. in. *Role. air-sea. exchange. geochem. cycling.* (Dordrecht: Springer) 185, 113–127. doi: 10.1007/978-94-009-4738-2_5

Mahajan, A. S., Fadnavis, S., Thomas, M. A., Pozzoli, L., Gupta, S., Royer, S., et al. (2015). Quantifying the impacts of an updated global dimethyl sulfide climatology on cloud microphysics and aerosol radiative forcing. *J. Geophysical. Research.: Atmospheres.* 120 (6), 2524–2536. doi: 10.1002/2014JD022687

Mann, G. W., Carslaw, K. S., Ridley, D. A., Spracklen, D. V., Pringle, K. J., Merikanto, J., et al. (2012). Intercomparison of modal and sectional aerosol microphysics representations within the same 3-d global chemical transport model. *Atmospheric. Chem. Phys.* 12 (10), 4449–4476. doi: 10.5194/acp-12-4449-2012

Mann, G. W., Carslaw, K. S., Spracklen, D. V., Ridley, D. A., Manktelow, P. T., Chipperfield, M. P., et al. (2010). Description and evaluation of GLOMAP-mode: A modal global aerosol microphysics model for the UKCA composition-climate model. *Geoscientific. Model. Dev.* 3 (2), 519–551. doi: 10.5194/gmd-3-519-2010

McCormick, R. A., and Ludwig, J. H. (1967). Climate modification by atmospheric aerosols. *Science* 156 (3780), 1358–1359. doi: 10.1126/science.156.3780.1358

McGowan, H., Sturman, A., Saunders, M., Theobald, A., and Wiebe, A. (2019). Insights from a decade of research on coral reef–atmosphere energetics. *J. Geophysical. Research.: Atmospheres.* 124 (8), 4269–4282. doi: 10.1029/2018JD029830

McParland, E. L., and Levine, N. M. (2019). The role of differential DMSP production and community composition in predicting variability of global surface DMSP concentrations. *Limnol. Oceanography.* 64 (2), 757–773. doi: 10.1002/lno.11076

Modini, R. L., Ristovski, Z. D., Johnson, G. R., He, C., Surawski, N., Morawska, L., et al. (2009). New particle formation and growth at a remote, sub-tropical coastal location. *Atmospheric. Chem. Phys.* 9 (19), 7607–7621. doi: 10.5194/acp-9-7607-2009

Raina, J. B., Tapiolas, D. M., Forêt, S., Lutz, A., Abrego, D., Ceh, J., et al. (2013). DMSP biosynthesis by an animal and its role in coral thermal stress response. *Nature* 502 (7473), 677–680. doi: 10.1038/nature12677

Ramanathan, V., Cess, R. D., Harrison, E. F., Minnis, P., Barkstrom, B. R., Ahmad, E., et al. (1989). Cloud-radiative forcing and climate: Results from the earth radiation budget experiment. *Science* 243 (4887), 57–63. doi: 10.1126/science.243.4887.57

Rosenfeld, D., Dai, J., Yu, X., Yao, Z., Xu, X., Yang, X., et al. (2007). Inverse relations between amounts of air pollution and orographic precipitation. *Science* 315 (5817), 1396–1398. doi: 10.1126/10.1126/science.1137949

Sanchez, K. J., Chen, C. L., Russell, L. M., Betha, R., Liu, J., Price, D. J., et al. (2018). Substantial seasonal contribution of observed biogenic sulfate particles to cloud condensation nuclei. *Sci. Rep.* 8 (1), 1–14. doi: 10.1038/s41598-018-21590-9

Stefels, J. (2000). Physiological aspects of the production and conversion of DMSP in marine algae and higher plants. *J. Sea. Res.* 43 (3–4), 183–197. doi: 10.1016/S1385-1101(00)00030-7

Sunda, W., Kieber, D. J., Kiene, R. P., and Huntsman, S. (2002). An antioxidant function for DMSP and DMS in marine algae. *Nature* 418 (6895), 317–320. doi: 10.1038/nature00851

Swan, H. B., Crough, R. W., Vaattovaara, P., Jones, G. B., Deschaseaux, E. S. M., Eyre, B. D., et al. (2016). Dimethyl sulfide and other biogenic volatile organic compound emissions from branching coral and reef seawater: Potential sources of secondary aerosol over the Great Barrier Reef. *J. Atmospheric. Chem.* 73 (3), 303–328. doi: 10.1007/s10874-016-9327-7

Swan, H. B., and Jones, G. B. (2017). *Atmospheric dimethylsulfide surface concentrations and supermicron particle number concentrations at heron island (23.44° s, 151.91° e) February 2016* (Southern Cross University). doi: 10.4226/47/59c460fbe8322

Swan, H. B., and Jones, G. B. (2020). *Database of surface level atmospheric dimethylsulfide (DMS) collected for the project "The Great Barrier Reef as a significant source of climatically relevant aerosol particles."* (Southern Cross University). doi: 10.25918/5c772187f39b6

Swan, H. B., Jones, G. B., Deschaseaux, E. S. M., and Eyre, B. D. (2017). Coral reef origins of atmospheric dimethylsulfide at Heron Island, Southern Great Barrier Reef, Australia. *Biogeosciences* 14 (1), 229–239. doi: 10.5194/bg-14-229-2017

Thomas, M. A., Suntharalingam, P., Pozzoli, L., Rast, S., Devasthale, A., Kloster, S., et al. (2010). Quantification of DMS aerosol-cloud-climate interactions using the ECHAM5-HAMMOZ model in a current climate scenario. *Atmospheric. Chem. Phys.* 10 (15), 7425–7438. doi: 10.5194/acp-10-7425-2010

Trounce, H., Ristovsky, Z., Miljevic, B., Cravigan, L., Alroe, J., Osuagwa, C., et al. (in preparation) Great Barrier Reef aerosol and cloud data from the reef to rainforest campaign. *Earth System. Sci. Data Discussions.*

Twomey, S. (1974). Pollution and the planetary albedo. *Atmospheric. Environ. (1967).* 8 (12), 1251–1256. doi: 10.1016/0004-6981(74)90004-3

Twomey, S., Piepgrass, M., and Wolfe, T. L. (1984). An assessment of the impact of pollution on global cloud albedo. *Tellus. B.* 36 (5), 356–366. doi: 10.1111/j.1600-0889.1984.tb00254.x

Veres, P. R., Neuman, J. A., Bertram, T. H., Assaf, E., Wolfe, G. M., Williamson, C. J., et al. (2020). Global airborne sampling reveals a previously unobserved dimethyl sulfide oxidation mechanism in the marine atmosphere. *Proc. Natl. Acad. Sci.* 117 (9), 4505–4510. doi: 10.1073/pnas.1919344117

Von Glasow, R., and Crutzen, P. J. (2004). Model study of multiphase DMS oxidation with a focus on halogens. *Atmospheric. Chem. Phys.* 4 (3), 589–608. doi: 10.5194/acp-4-589-2004

Walters, D., Baran, A. J., Boutle, I., Brooks, M., Earnshaw, P., Edwards, J., et al. (2019). The met office unified model global atmosphere 7.0/7.1 and JULES global land 7.0 configurations. *Geoscientific. Model. Dev.* 12 (5), 1909–1963. doi: 10.5194/gmd-12-1909-2019

Woodhouse, M. T., Carslaw, K. S., Mann, G. W., Vallina, S. M., Vogt, M., Halloran, P. R., et al. (2010). Low sensitivity of cloud condensation nuclei to changes in the sea-air flux of dimethyl-sulphide. *Atmospheric. Chem. Phys.* 10 (16), 7545–7559. doi: 10.5194/acp-10-7545-2010

Woodhouse, M. T., Mann, G. W., Carslaw, K. S., and Boucher, O. (2013). Sensitivity of cloud condensation nuclei to regional changes in dimethyl-sulphide emissions. *Atmospheric. Chem. Phys.* 13 (5), 2723–2733. doi: 10.5194/acp-13-2723-2013

Yang, M., Blomquist, B., Fairall, C., Archer, S., and Huebert, B. (2011). Air-sea exchange of dimethylsulfide in the Southern Ocean: Measurements from SO GasEx compared to temperate and tropical regions. *J. Geophysical. Research.: Oceans.* 116, C00F05. doi: 10.1029/2010JC006526

Zavarsky, A., Booge, D., Fiehn, A., Krüger, K., Atlas, E., and Marandino, C. (2018). The influence of air-sea fluxes on atmospheric aerosols during the summer monsoon over the tropical Indian ocean. *Geophysical. Res. Lett.* 45 (1), 418–426. doi: 10.1002/2017GL076410

frontiers | Frontiers in Marine Science

TYPE Original Research
PUBLISHED 09 September 2022
DOI 10.3389/fmars.2022.912862

OPEN ACCESS

EDITED BY
Graham Barry Jones,
Southern Cross University, Australia

REVIEWED BY
Stephen D. Archer,
Bigelow Laboratory For Ocean Sciences, United States
John Bythell,
Newcastle University, United Kingdom

*CORRESPONDENCE
Stephanie G. Gardner
stephanie.gardner@sydney.edu.au

SPECIALTY SECTION
This article was submitted to Coral Reef Research, a section of the journal Frontiers in Marine Science

RECEIVED 05 April 2022
ACCEPTED 15 August 2022
PUBLISHED 09 September 2022

CITATION
Gardner SG, Nitschke MR, O'Brien J, Motti CA, Seymour JR, Ralph PJ, Petrou K and Raina J-B (2022) Increased DMSP availability during thermal stress influences DMSP-degrading bacteria in coral mucus. *Front. Mar. Sci.* 9:912862. doi: 10.3389/fmars.2022.912862

Increased DMSP availability during thermal stress influences DMSP-degrading bacteria in coral mucus

Stephanie G. Gardner[1,2,3]*, Matthew R. Nitschke[1,4], James O'Brien[1], Cherie A. Motti[4], Justin R. Seymour[1], Peter J. Ralph[1], Katherina Petrou[4] and Jean-Baptiste Raina[1]

[1]Climate Change Cluster, University of Technology Sydney, Ultimo, NSW, Australia, [2]Centre for Marine Science and Innovation, University of New South Wales Sydney, Kensington, NSW, Australia, [3]School of Life Sciences, University of Technology Sydney, Ultimo, NSW, Australia, [4]Australian Institute of Marine Science, Townsville, QLD, Australia

Reef-building corals are among the largest producers of dimethylsulfoniopropionate (DMSP), an essential compound in marine biogeochemical cycles. DMSP can be catabolised in coral mucus by a wide diversity of coral-associated bacteria, where it can either be demethylated, leading to the incorporation of sulfur and carbon into bacterial biomass – or cleaved by lyases, releasing the climatically-active gas dimethyl sulfide (DMS). It has been demonstrated that thermal stress increases DMSP concentrations in many coral species, however the effect of increased DMSP availability on coral-associated bacteria has not been explored. Here we performed thermal stress experiments to examine how changes in DMSP availability impact bacterial degradation pathways in the mucus of *Acropora millepora*. DMSP concentrations increased with temperature, reaching a maximum of 177.3 μM after 10 days of heat stress, which represents the highest concentration of DMSP recorded in any environment to date. Bacterial communities in coral mucus were significantly different from the surrounding seawater, yet they did not vary significantly between temperature or time. However, during thermal stress, when DMSP concentrations increased, a significant increase in the abundance of both the demethylation gene *dmdA* and the cleavage gene *dddP* were recorded. Importantly, our results show that for the highest DMSP concentrations recorded (above 30 μM), the cleavage pathway became more abundant than the demethylation pathway. This suggests that under high DMSP concentrations characteristic of heat stress, a larger fraction of the DMSP pool in the coral mucus is likely catabolised through the DMS-producing cleavage pathway.

KEYWORDS

microbiome, coral mucus associated bacteria, DMSP-degrading genes, thermal stress, *Acropora millepora*, dimethylsulfoniopropionate (DMSP)

Introduction

Dimethylsulfoniopropionate (DMSP) is a critical compound in the marine sulfur and carbon cycles (Sievert et al., 2007) and an essential chemical currency in microbial interactions (Kiene et al., 2000). Global DMSP production is likely to exceed one billion tons of sulfur per year (Howard et al., 2006), but the distribution of this compound in the ocean is not homogenous. Although DMSP is present in seawater at low nanomolar concentrations (oceanic average: 16.91 ± 22.17 nM; see Kettle et al., 1999), specific marine environments have been identified as hotspots, such as highly productive polar waters (Trevena et al., 2003), or coral reefs (Hill et al., 1995). Within tropical coral reefs, large concentrations of DMSP have been recorded in many benthic organisms, including macroalgae (Van Alstyne et al., 2007), giant clams (Hill et al., 2000), soft corals (Haydon et al., 2018) and reef-building corals (Broadbent et al., 2002), and their microalgal symbionts (phylum Dinoflagellata; Caruana and Malin, 2014). DMSP concentrations in these different benthic organisms can vary by more than two orders of magnitude (Broadbent et al., 2002; Tapiolas et al., 2013), but to date the highest concentration ever measured (54 μM; or more than three orders of magnitude higher than the global seawater average) was recorded from the mucus of corals from the genus *Acropora* (Broadbent and Jones, 2004).

Coral mucus is a viscous mixture secreted by specialised epithelial cells, forming a coating over the polyps that is important for many aspects of coral biology (Meikle et al., 1988; Bythell and Wild, 2011). The surface mucus layer protects corals against desiccation at low tide (Brown and Bythell, 2005), as well as sudden changes in environmental conditions (e.g., temperature, salinity) (Piggot et al., 2009), while allowing gas and metabolite exchanges (Bythell and Wild, 2011), it is key to feeding and cleansing processes (Brown and Bythell, 2005) and acts as a significant input of carbon to reef waters that sustains other benthic organisms (Wild et al., 2004). The chemical composition of the mucus is variable between coral species (Ducklow and Mitchell, 1979; Meikle et al., 1988), but one commonality is the presence of large glycoproteins giving the mucus its gel-like texture (Bythell and Wild, 2011). Coral mucus has also been described as the first line of defence against pathogens (Ritchie, 2006a; Shnit-Orland and Kushmaro, 2009), as it is densely populated by specific bacterial communities (Garren and Azam, 2010), some of which can degrade DMSP (Raina et al., 2009; Frade et al., 2015).

DMSP is an important nutrient source for marine bacteria, contributing significantly to their sulfur (up to 95%; Zubkov et al., 2004) and carbon (up to 15%; Simó et al., 2002) requirements. Degradation of DMSP by bacteria occurs through two major pathways producing either methanethiol (MeSH; demethylation) or dimethyl sulfide (DMS; cleavage) as end products (Reisch et al., 2011; Sun et al., 2016). The demethylation pathway is estimated to catabolise approximately 70% of dissolved DMSP (Reisch et al., 2011), leading to the assimilation of both carbon and sulfur into bacterial biomass (Kieber et al., 1996; Kiene et al., 1999; Simó, 2001). The gene encoding the first enzymatic step of this pathway was discovered in an *Alphaproteobacterium* from the *Roseobacter* clade and termed *dmdA* (Howard et al., 2006). The second degradation route is the cleavage pathway which leads to the release of DMS and is suspected to degrade the remaining 30% of dissolved DMSP. Eight different DMSP lyases, termed *ddd*+ have been identified so far (Zhang et al., 2019), among which *dddP* (Todd et al., 2009) is one of the most prevalent in the marine environment. Many marine bacteria harbour both degradation pathways; however, the environmental factors that dictate which pathway is used have remained hypothetical for more than 20 years (Kiene et al., 2000; Simó, 2001). Understanding which pathway marine bacteria preferentially use under specific conditions is critical because it directly affects how much DMS is produced and ultimately released into the atmosphere.

A long standing hypothesis in the DMSP field proposed that external DMSP concentrations regulate which degradation pathway is usedby bacteria (Kiene et al., 2000; Simó, 2001). According to this hypothesis, when DMSP availability is low (or if there is a high bacterial sulfur demand), most DMSP is expected to be catabolised through demethylation. On the other hand, when DMSP availability is high, the less costly cleavage pathway is likely used (Reisch et al., 2011). Recent experimental evidence confirmed that external DMSP concentrations dictate the relative expression of the two pathways with an increase in DMSP cleavage (leading to DMS formation) measured near the surface of coral-associated microalgae, where DMSP concentrations are the highest (Gao et al., 2020). A previous study comparing different coral species also revealed that when DMSP concentrations were high, a lower relative abundance of the gene encoding the first step of the demethylation pathway (*dmdA*) was present in bacterial communities (Frade et al., 2015). Environmental stressors, such as heat, are known to cause an increase in DMSP concentrations in some corals (e.g., members of the *Acropora* genus; see Raina et al., 2013; Deschaseaux et al., 2014; Gardner et al., 2017). However, we do not know the effect that a sudden rise in DMSP availability may have on coral-associated bacterial communities and on the pathways they use to catabolise this compound.

Here we investigated how variations in DMSP concentrations caused by heat stress affect the abundance of bacterial genes involved in the demethylation and cleavage pathways in *Acropora millepora*, a reef building coral widespread throughout the Indo Pacific. To achieve this goal, we simultaneously measured: i) DMSP concentrations; ii) bacterial community structure; and iii) prevalence of DMSP-degrading genes during thermal stress in the mucus of *A. millepora*.

Methods

Coral collection and experimental set-up

Five colonies of *Acropora millepora* were collected from Heron Island lagoon in the southern Great Barrier Reef, Australia (151°55´E, 23°26´S) and acclimatised at ambient seawater temperature (27°C) in a flow-through aquaria system under 50% shaded sunlight (daily average of 600 µmol photons m^{-2} s^{-1}) for 3 days at 27 ± 0.5°C. Each colony was then split in half and divided between the control and the treatment tanks (1 tank per colony). Experimental tanks (30 L) were set up in a shaded flow-through aquaria with constant flow (5 L min^{-1}) of lagoon seawater (approx. 27 ± 0.5°C). The ambient light intensity was measured every 5 min using PAR loggers (Odyssey) and temperature was recorded every 10 min (Thermochron, Australia). For the thermal stress treatment tanks (n = 5), temperature was increased 1°C per day over 5 days from the ambient temperature of 27°C to reach the target temperature of 32°C and then held for a further 2 days. Physiological parameters (F_V/F_M and $\Delta F/F_M'$; see below) were recorded daily for the duration of the experiment. Coral mucus, coral host and seawater samples were collected over 4 time points; T0 (day 3), T1 (day 6), T2 (day 8) and T3 (day 10) (Figure 1), for chlorophyll *a*, cell density, surface area, quantification of DMSP/DMSO, 16S rRNA gene sequencing and identification of *dmdA* and *dddP* degradation genes.

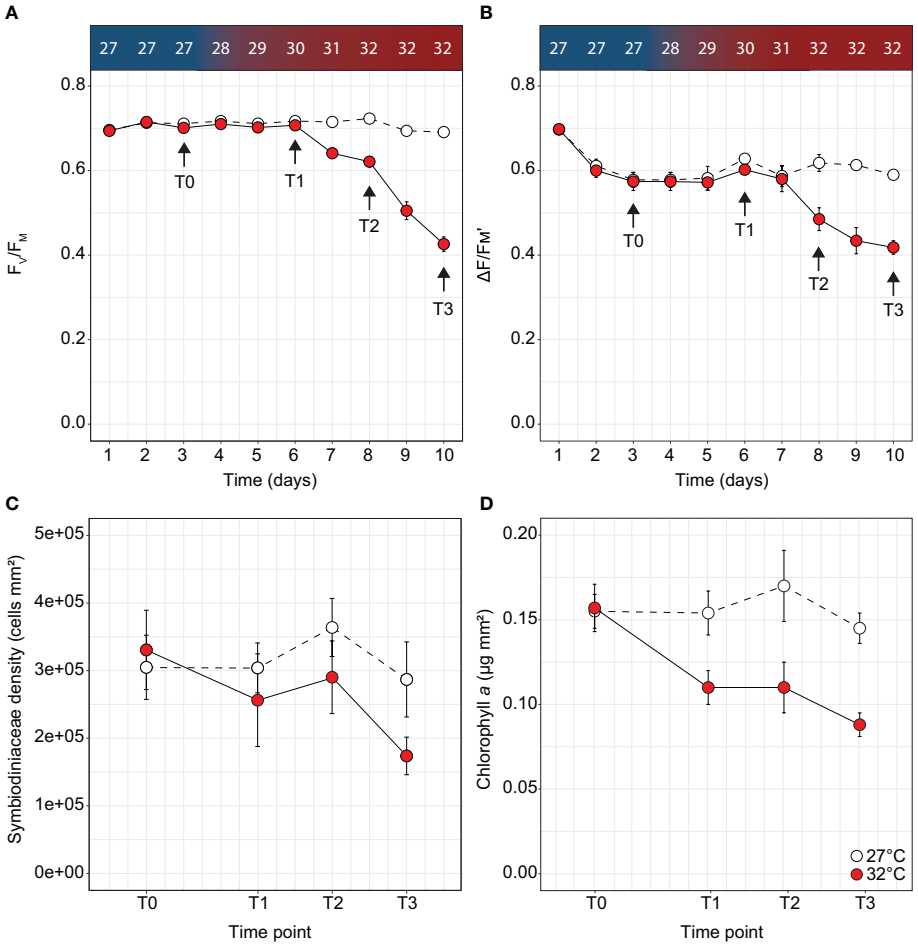

FIGURE 1
Physiological parameters measured over time for *Acropora millepora* under thermal stress including **(A)** maximum quantum yield of photosystem II (F_V/F_M), **(B)** effective quantum yield of photosystem II ($\Delta F/F_M'$), **(C)** Symbiodiniaceae density and **(D)** chlorophyll *a* for the control (white circles) and treatments (red circles). Letters indicate significant differences between timepoints for the treatment. Temperature increases indicated along the top panel for corresponding days and sampling timepoints. Averages (± SE) are shown (n = 4-5).

Photochemical efficiency of PSII

Using a MiniPAM (Walz GmbH, Effeltrich, Germany; MI: 8, Gain: 5, SI: 10, SW: 0.8s) chlorophyll *a* fluorescence was measured daily at midday (effective quantum yield of PSII; $\Delta F/F_M'$) and just after sunset (maximum quantum yield of PSII; F_V/F_M) to monitor photo-physiological stress of each colony, with 2 technical replicate measurements from distinct branches. At T3, a DivingPAM (Walz GmbH, Effeltrich, Germany; MI: 8 Gain: 7 SI: 8 SW: 0.8s) was used to conduct rapid light curves (RLC; see Ralph and Gademann, 2005) in the first hour of daylight, using the same settings as above. The RLC protocol consisted of a low-light acclimated (c.a. 5 µmol photons m^{-2} s^{-1}) F_V/F_M measurement to initiate the RLC, followed by $\Delta F/F_M'$ measurements under actinic light at eight 30 second intervals of increasing intensity (98, 162, 240, 325, 480, 610, 971, and 1,359 µmol photons m^{-2} s^{-1}). The saturating irradiance (E_K), an estimate of the irradiance where PSII transitions from a light-limited to a light-saturated state, and the maximum photochemical efficiency of PSII ($F_Q/F_{M(max)}$) were described using equation 1 (Hennige et al., 2008) where E = irradiance.

$$F_q'/F_m' = [(F_Q/F_{M(max)}E_K)(1 - \exp(-E/E_K))]/E \quad (1)$$

To detect whether utilisation of alternative pathways of excitation energy dissipation differed across temperature treatments, the extent of light dependant photochemical quenching ([1 – C], equation 2) and non-photochemical quenching ([1 – Q], equation 3) were calculated at each step of the RLC (Suggett et al., 2015; Nitschke et al., 2018).

$$[1 - C] = (F_m' - F)/(F_m' - F_o') \quad (2)$$

$$[1 - Q] = (F_v'/F_m')/(F_v/F_m) \quad (3)$$

Cell density, chlorophyll *a* and surface area

Coral tissue was removed from the skeleton of coral fragments using an airgun in 5 mL FSW (0.2 µm). The tissue slurry was concentrated *via* centrifugation at 3000 g for 10 min. The algal pellets were resuspended in 5 mL FSW (0.2 µm), and homogenised. A 3 mL subsample was then centrifuged at ~3,600 g for 4 min and resuspended in 3 mL of 90% acetone and left at 4°C in the dark for 24 h before spectrophotometric chlorophyll determination. Concentrations of chlorophyll *a* were calculated using the equations from Ritchie (2006b). The remaining 2 mL subsample was used for cell density measurements using a haemocytometer (n = 8). The bare coral skeletons were dried, and the surface area of each coral fragment was calculated using the paraffin wax technique (Stimson and Kinzie, 1991; Veal et al., 2010).

Sample collection

Coral mucus was collected by exposing the colony to air for 2 min (prompting mucus production from the epithelial cells and the gastrovascular cavity; see Sweet et al., 2011). Coral colonies were held inverted to allow excess seawater and mucus to drip off the branches. After 2 min air exposure, each colony was dipped back into the water for 1 min, removed from the seawater, and then held inverted in the air for a further 15 s to allow excess water to drip from the branches. The resulting mucus secreted during air exposure was then collected from the branch tips using a sterile 10 mL syringe with a 21″G sterile needle. For each colony, 4-5 mL mucus was collected in a falcon tube, of which 2 mL was immediately added to 4 mL analytical grade methanol (95%), sealed with parafilm and stored at -20°C in the dark for nuclear magnetic resonance (NMR) spectroscopy. An additional 2 mL of coral mucus was filtered using a glass filter tower (Cole-Parmer Instrument Company, USA) onto membrane filter (Whatman; 25 mm × 0.2 µm pore size), then the filter was snap frozen in liquid nitrogen and stored in cryovials at -80°C for 16S rRNA gene amplicon sequencing and quantitative PCR (qPCR) analyses. To sample the coral host, a 3 cm fragment was removed from each colony using sterile bone cutters; the fragment tip was discarded, and the middle section added to 3 mL methanol in a falcon tube, sealed with parafilm and stored in the dark at -20°C for NMR analysis. Water samples were also taken at each time-point (n = 3), where 1 L was collected from each tank in a large glass Schott bottle at 20 cm distances from the coral colony and filtered using a vacuum pump (Capex 8C, Charles Austen Pumps Ltd, Surrey, UK) onto 45 mm × 0.45 µm filters (Whatman). The filters were snap frozen and stored in cryovials at -80°C.

Quantification of DMSP and DMSO

Coral host fragments and mucus samples in methanol were stored at -20°C until processing at the Australian Institute of Marine Science, Townsville, Australia (AIMS). Coral fragments were further extracted using sonication on ice (bath at 40 kHz) in 1 mL of HPLC-grade methanol for 5 min. The two extracts from the coral host were pooled and dried overnight (8 h) using a concentrator (Savant SpeedVac SC210A, Thermo Scientific, USA). The coral mucus samples were also dried overnight (14 h) in the concentrator, then in a freeze drier (Dynavac FD12 Perogon Technologies, Australia) for a further 4 h to ensure complete dryness. The dried extracts from the host and mucus were resuspended in a mixture of deuterated methanol (CD_3OD; 750 µL) and deuterium oxide (D_2O; 250 µL), vortexed to solubilise the compounds and then centrifuged for 10 min to pellet the debris. An 800 µL aliquot of the particulate free extract was transferred into a 5 mm NMR tube (Norell 509-UP) and

analysed immediately by ^{1}H NMR following the method described in Tapiolas et al. (2013). Spectra were recorded on a 600 MHz NMR spectrometer (Bruker Avance, Germany) with a TXI cryoprobe, using the Bruker TOPSPIN 2.1 software, and referenced using CD_3OD (δ_H 3.31). Concentrations of DMSP and DMSO were quantified using the ERETIC method (electronic reference to access *in vivo* concentrations; Akoka and Trierweiler, 2002), which electronically generates an external reference signal that was calibrated using a 2 mM stock solution of acrylate. After calibration, the concentration of each target compound was determined by comparing the signal intensities of well resolved non-exchangeable protons: $(CH_3)_2SCH_2CH_2CO_2$ at δ2.95 ppm for DMSP and $(CH_3)_2SO$ at δ2.73 ppm for DMSO (in the coral host and mucus samples) in a 0.20 ppm window against the intensity of the reference signal through signal integration (Akoka and Trierweiler, 2002). Coral skeletons remaining after extraction were soaked in 10% bleach overnight, dried at 60°C in an oven and used for surface area measurements using the paraffin wax technique (Stimson and Kinzie, 1991; Veal et al., 2010). The surface area of each fragment was then used to normalise NMR data. The coral mucus samples were normalised to the volume of mucus originally collected in methanol (2 mL).

DNA extraction, amplicon sequencing and processing

DNA was extracted from filters used to collect mucus and water samples using methods modified from Schauer et al. (2000). Briefly, lysis buffer (0.5 mL) and 75 µL lysozyme (100 mg/mL) were added to cryovials containing the filters and incubated for 1 h at 37°C. Subsequently, 100 µL SDS (25%) and 10 µL Proteinase K (20 mg/mL) were added and incubated for 1 hr at 55°C. The recovered lysate (600 µL) was extracted twice using equal volumes of phenol:chloroform:isoamyl alcohol (25:24:1, pH8), followed by chloroform:isoamyl alcohol (24:1) and centrifuged for 30 min at 4°C and 16,000g. DNA was precipitated from the recovered aqueous phase (top layer) with 500 µL ice cold isopropanol, left in the dark for 15 min and centrifuged at 16,000g for 30 min. The pellet was rinsed with 500 µL of 70% ethanol before being dried in a concentrator for 10 min to ensure all ethanol was removed. The remaining DNA pellet was resuspended in 40 µL sterile milliQ, and the purity of the DNA was assessed using a NanoDrop spectrophotometer (Thermo Scientific, USA). Aliquots were stored at -20°C until use.

To examine the composition of bacterial assemblages, the 16S rRNA gene was amplified using 27F/519R (V1-V3 region) primers. PCR was carried out using the HotStarTaq Plus Master Mix Kit (Qiagen, USA) using the following conditions: (i) 3 min at 94°C; (ii) 28 cycles, with each cycle consisting of 30 s at 94°C, 40 s at 53°C, and 1 min at 72°C; (iii) a final elongation step of 5 min at 72°C. PCR products were checked in 2% agarose gels, and samples were pooled in equal proportions based on molecular weight and DNA concentrations. Pooled samples were purified using Ampure XP beads (Beckman-Coulter, USA) and processed using the Illumina TruSeq DNA library protocol. Sequencing was performed on an Illumina MiSeq platform (2 × 300 cycles; Molecular Research LP; Shallowater, TX, USA).

Raw data was demultiplexed and primers were removed using cutadapt (Martin, 2011). The open-source software package DADA2 (Callahan et al., 2016) was used to produce a table of chimera-free amplicon sequence variants (ASVs). ASVs were taxonomically classified using the RDP Classifier against the SILVA v.138 (August, 2020) reference database (Quast et al., 2013). A phylogenetic tree was generated by sequence alignment with MAFFT (Katoh and Standley, 2013) and the tree was produced with FastTreeMP (Price et al., 2009) on the CIPRES v3.3 Science Gateway (Miller et al., 2010). ASV count and taxonomic data were imported using the phyloseq package v.1.28 (McMurdie and Holmes, 2013) for analysis in R v3.6.1. Sequences classified as chloroplast, mitochondria, eukaryota, and archaea, as well as known common reagent contaminants (Sheik et al., 2018), were removed before further analysis. Singleton ASVs, together with one seawater sample containing <1,000 reads, were removed from the dataset. Overall, the dataset comprised 17 samples (9 for mucus and 8 for seawater), resulting in 414,856 sequences with a mean length of 294 bp. After quality filtration, exclusion of chimeras, and specific retention of bacterial sequences, 1,873 ASVs (Supplementary Table 1) were obtained from the 17 samples. Samples were rarefied to 5,099 to account for the variability in sequencing depth between samples. The mean good's coverage score was 99.81% ± 0.38 for the dataset indicating the sequencing depth was adequate to capture the majority of diversity in the samples.

Statistical analyses of the 16S rRNA gene sequencing data

Amplicon sequence variants (ASVs) were analysed with Phyloseq v1.28 (McMurdie and Holmes, 2013), Vegan v2.5.6 (Oksanen et al., 2007) and rstatix v0.7.0 (Kassambara, 2021). Alpha diversity indices (chao1 richness and the observed number of ASVs) were computed and a one-way ANOVA was run through rstatix for each diversity index after checking for homogeneity and normality using Levene's and Shapiro's tests, respectively. A principal coordinates analysis (PCoA) was used to visualise dissimilarities in microbial communities between sample types (mucus and seawater) and treatments (27°C and 32°C) using weighted unifrac distances, which considers the relative abundance of each ASV and integrates phylogenetic distance (Lozupone et al., 2011).

To statistically analyse differences in microbial community structure, ASV counts were Hellinger transformed to reduce the effects of numerically large values from very abundant taxa and weighted unifrac distances were computed. Permutational multivariate analysis of variance (PERMANOVA; n = 9,999 permutations, *adonis/adonis2* function in Vegan) was performed to test for significant differences between mucus and seawater samples and homogeneity of dispersions around group centroids (i.e., variation) was assessed using PERMDISP (*betadisper* function in Vegan). Data were further analysed using a two-factor nested PERMANOVA to assess differences between temperature treatment as a fixed factor (two levels: 27°C and 32°C) and time point (two levels: T0 and T3) nested within sample type (mucus and seawater). Stacked bar graphs were plotted using ggplot2 v3.3.5 to phylum level and represent those bacterial taxa with a relative abundance above 1% across all samples.

DMSP degrading predictions of the bacterial communities

To determine if thermal stress induced an increase in the relative abundance of taxa harbouring the demethylation pathway (*dmdA*) or the cleavage pathway (*dddP*), we functionally predicted the abundance of these two genes in the bacterial communities from the mucus T3 samples. Briefly, the mucus samples were rarefied to 9,182 (lowest read depth for the mucus samples), and all ASVs were compared to genomes harbouring *dmdA* and *dddP* (Supplementary Table 2) derived from KEGG (Kyoto Encyclopedia of Genes and Genomes) and NCBI (National Center for Biotechnology Information). Each ASV with a query coverage ≥ 90% and a similarity ≥ 95% with the 16S rRNA gene of one of the *dmdA* or *dddP*-harbouring genomes was considered as a putative DMSP degrader.

Amplification and identification of *dmdA* and *dddP* genes

Quantitative PCR (qPCR) was used to determine the total abundance of bacterial 16S rRNA genes and genes involved in marine DMSP cycling. Gene abundance was quantified using an automated Liquid Handling robot (epMotion 5075l) on a Bio-Rad CFX Touch Real-Time PCR Detection System. A range of *dmdA* subclades were initially screened (A/1, A/2, B/4, C/2, D/1 and D/3, E/2; Varaljay et al., 2010) using qPCR, but only a few successfully amplified in the samples (A/1, D/3, E/2), the most successful being *dmdA* A/1. All sample plates included a triplicate, six-point calibration curve constructed from a known amount of amplicon DNA measured by Qubit (according to the manufacturer's instructions), followed by five successive 10-fold dilutions and negative template controls of nuclease-free water.

Absolute quantification of the bacterial 16S rRNA gene was performed using the 16S rRNA specific primers BACT1369F (5' – CGGTGAATACGTTCYCGG – 3') and PROK1492R (5' – GGWTACCTTGTTACGACTT – 3') and a TaqMan probe TM1389F (5' – CTTGTACACACCGCCCGTC – 3') (Suzuki et al., 2000; Supplementary Table 3) with following cycling conditions: 95°C for 3 minutes followed by 39 cycles of 95°C for 30 s and 56°C for 60 s with an extension at 72°C for 30 s. Each individual PCR reaction volume was 5 µL and contained 2.5 µL iTaq Universal probes SMX (Bio-Rad), 0.2 µL of each forward and reverse 16S rRNA gene specific primers (10 µM), 0.1 µL of Taqman Probe Mix, TM1389F (5' – CTTGTACACACCGCCCGTC – 3') (10 µM), 1 µL of nuclease-free water and 1 µL of template DNA. The relative abundance of bacterial DMSP-degrading genes was acquired by normalising their copy numbers to the copy number of bacterial 16S rRNA gene, however, it should be noted that some bacterial genomes have multiple copies of the 16S rRNA gene (Cui et al., 2015).

Absolute quantification of the genes encoding DMSP catabolism were performed using primers for the DMSP cleavage gene *dddP*_874F (5' – AAYGAAATWGTT GCCTTTGA – 3') and *dddP*_971R (5' – GCATDGCRTAA ATCATATC – 3') (Levine et al., 2012) and DMSP demethylation gene *dmdA* A/1-spFP (5' – ATGGTGATTTG CTTCAGTTTCT – 3') and A/1-spRP (5' – CCCTGCTTTGA CCAACC – 3') (Varaljay et al., 2010; Supplementary Table 3). Analysis of DMSP degradation genes were performed on three technical replicates of the following mixture: 2.5 µL of 2 × Sensifast SYBR Hi-ROX mastermix, 0.2 µL of forward primer (10 µM initial), 0.2 µL of reverse primer (10 µM initial), 0.1 µL nuclease-free water and 2 µL of DNA template (diluted between 1:1 and 1:20). Amplification of the DMSP cleavage gene *dddP* and demethylation gene *dmdA* A/1, consisted of an initial denaturation step of 95°C for 5 min, followed by 40 cycles of 95°C for 30 s, 41°C (*dddP*) and 53°C (*dmdA*) for 30 s and 72°C for 30 s. To differentiate target amplicons from non-specific products, a dissociation melt curve was generated after each reaction.

Statistical analyses of the qPCR data

Quantitative PCR data was analysed with rstatix v0.7.0 (Kassambara, 2021) in R v3.6.1. Two-way repeated measures ANOVAs were run for the mucus datasets to determine the interaction between temperature treatment (27°C and 32°C) and time point (T0, T1, T2 and T3) after checking for homogeneity and normality using Levene's and Shapiro's tests, respectively. Tukey's *post-hoc* tests were used to determine differences between groups. Pairwise comparisons, using t-tests, were then run for each timepoint, for the coral host and mucus samples.

Throughout the manuscript, all reported values are mean ± SE, unless mentioned otherwise.

Results

Thermal bleaching responses and a sharp increase in coral mucus DMSP concentrations

Measures of Symbiodiniaceae PSII photochemical efficiency, cell densities, and chlorophyll content indicate *A. millepora* corals subjected to 32°C were in the early stages of a thermal bleaching response. Ten days after the onset of thermal stress, dark-adapted maximum quantum yields decreased by 39% relative to controls (F_V/F_M; Two-way ANOVA; $F_{9,180}$ = 53.35, p < 0.001; Supplementary Table 4 and Figure 1A) from 0.694 ± 0.007 (day 1) to 0.426 ± 0.017 (day 10). In addition, a 38% decrease in effective quantum yield was also recorded ($\Delta F/F_M'$; $F_{8,162}$ = 5.67, p < 0.001; Supplementary Table 4 and Figure 1B) from 0.698 ± 0.005 (day 1) to 0.434 ± 0.031 (day 10). In RLCs performed at day 10, no difference in E_K was observed between treatments (Figure S1A), however $F_Q/F_{M(max)}$ was significantly different, with decreases from 0.72 ± 0.01 to 0.66 ± 0.01 in thermally stressed corals (One-way ANOVA; $F_{1,8}$ = 12.64, p < 0.05, Figure S1B and Supplementary Table 4). No differences were observed in [1 - C]; however, stressed corals exhibited significantly increased utilisation of [1 - Q] at all RLC irradiance steps (One-way ANOVA, p < 0.05 for all irradiances, Supplementary Table 4 and Figure S1C), indicating increased reliance on non-photochemical quenching. Although no difference in Symbiodiniaceae density was recorded between treatments (Figure 1C), chlorophyll *a* in thermally stressed corals decreased by 43% from 0.157 ± 0.014 µg chl *a* mm^{-2} to 0.088 ± 0.007 µg chl *a* mm^{-2} (Two-way ANOVA; $F_{3,19}$ = 5.72, p = 0.007, Supplementary Table 4 and Figure 1D).

At the beginning of the thermal stress experiment (T0), DMSP concentrations in the coral mucus secreted after air exposure averaged 4.24 ± 1.35 µM across both treatments but started to sharply increase when the temperature reached 32°C by T2 (Figure 2A) to 71.23 ± 12.12 µM. By T3 this value reached 83.15 ± 27.87 µM, corresponding to a 15.6-fold increase over the controls ($F_{3,32}$ = 7.031, p < 0.001, Supplementary Table 4 and Figure 2A). We also measured a 2.9-fold increase for DMSO ($F_{3,32}$ = 3.954, p < 0.02, Supplementary Table 4 and Figure 2B), from 0.79 ± 0.15 µM at T0 to 1.77 ± 0.34 µM at T3 under elevated temperature. Conversely, in the coral host, no difference was detected for DMSO (p = 0.570; Supplementary Table 4 and Figure 2D) between control and thermally-stressed samples, while DMSP concentrations significantly differed between control and treatment by T2, and were 2.7-fold higher in thermally-stressed samples by T3 ($F_{3,32}$ = 3.85, p = 0.018, Supplementary Table 4 and Figure 2C).

Bacterial community structure differs across mucus and seawater

Both the observed number of ASVs and their richness (Chao1) were significantly higher in the mucus samples (observed: 201.56 ± 45.97; Chao1: 206.24 ± 48.33) compared with the surrounding seawater (observed: 77.70 ± 15.21, [$F_{1,15}$ = 5.83, p = 0.029]; Chao1: 77.86 ± 15.19, [$F_{1,15}$ = 5.78, p = 0.030]; Figure 3A). The overall microbial community structure of the two environments (coral mucus and seawater) also showed limited overlap (principal coordinates analysis (PCoA); Figure 3B). Mucus samples were more tightly clustered than the seawater samples; however, group dispersion was not significantly different (PERMDISP, p = 0.959, Figures 3B, C). Microbial community composition significantly varied between sample types (PERMANOVA, F = 3.85, R^2 = 0.20, p < 0.005), and between sample types when partitioned between timepoints and temperature treatments (PERMANOVA, F = 2.49, R^2 = 0.21, p = 0.011). However, no differences in microbial community composition in mucus samples were detected between temperatures (PERMANOVA, F = 0.76, R^2 = 0.05, p = 0.613) or timepoints (PERMANOVA, F = 1.62, R^2 = 0.10, p = 0.115), and variance was similar between groups for both (PERMDISP, p = 0.590 and p = 0.415, respectively).

The mucus samples were dominated by Proteobacteria from the Gammaproteobacteria (40.08% ± 5.04%), Alphaproteobacteria (19.40% ± 2.67) and Bacteroidia (16.10% ± 3.66) classes (Figure 3C). More specifically, three families represented 34.35% of the communities: Rhodanobacteraceae (20.63% ± 2.71%), Flavobacteriaceae (8.49% ± 2.27) and Rhodobacteraceae (5.23% ± 1.51; Supplementary Table 5A and Figure 3C). Conversely, the seawater samples were dominated by Bacteroidia (47%), Alphaproteobacteria (26%), and Gammaproteobacteria (10%; Figure 3C and Supplementary Table 5B). A predictive analysis was carried out on the samples collected during the last time point of the experiment (T3; day 10) to determine the taxonomic composition of DMSP degraders in coral mucus, together with their relative abundance in response to the large increase in DMSP concentrations recorded in the thermally stressed colonies. According to our analysis, an average of 5% of the bacterial communities harboured the demethylation gene *dmdA* in the control samples, the most abundant genera belonging to the *Pelagibacter*, *Phaeobacter* and *Cognatishimia* (Supplementary Table 2 and Figure 4). Importantly, the relative abundance of the bacteria putatively harbouring *dmdA* significantly increased in the heat-stressed samples to reach an average of 6.7% of the communities (t-test; t = -2.86, df = 4, p = 0.045). In comparison, 5.4% of the communities putatively harboured the cleavage gene *dddP*, with the Gammaproteobacteria *Caballeronia*, *Acinetobacter* and the Alphaproteobacteria *Phaeobacter* being the most abundant. However, heat stress did not significantly affect the relative abundance of *dddP* in the communities (t-test; t = -1.18, df = 4, p = 0.302; Figure 4).

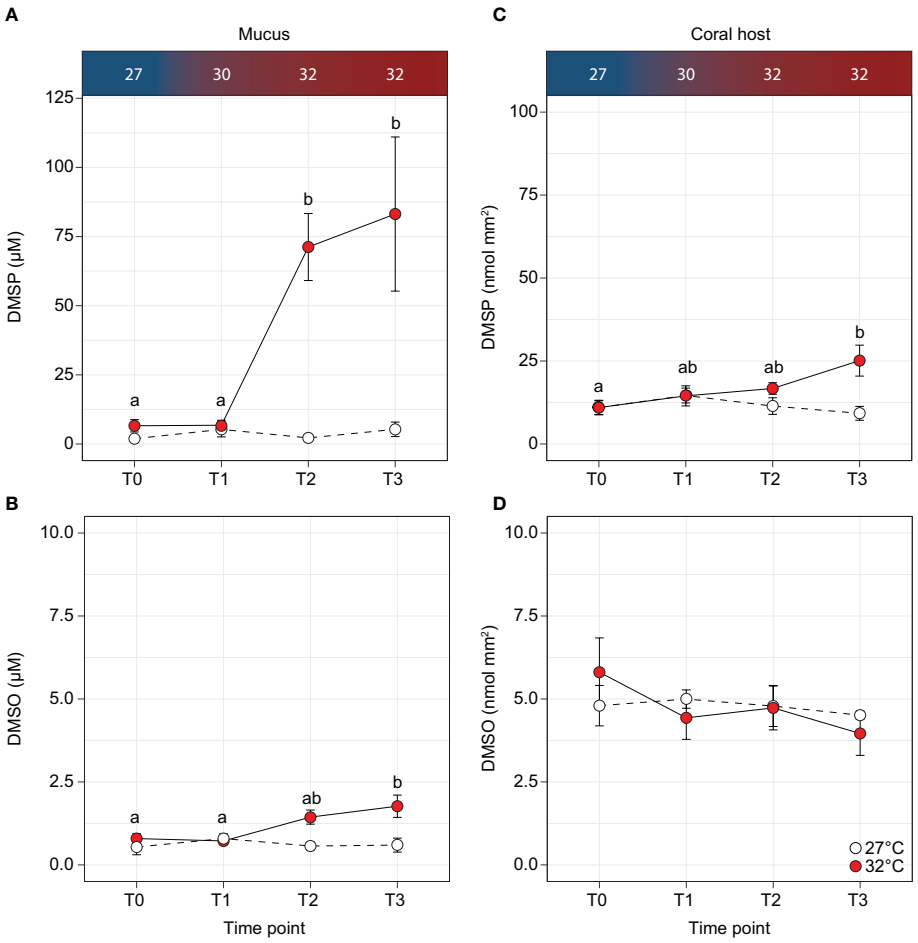

FIGURE 2
Concentrations of **(A, C)** dimethylsulphoniopropionate (DMSP) and **(B, D)** dimethylsulphoxide (DMSO) in the *Acropora millepora* mucus and coral host for the control (white circles) and temperature treatments (red circles). Letters indicate significant differences between timepoints for the treatments. Temperatures are indicated along the top panel for corresponding sampling time-points. Averages (± SE) are shown (n = 5).

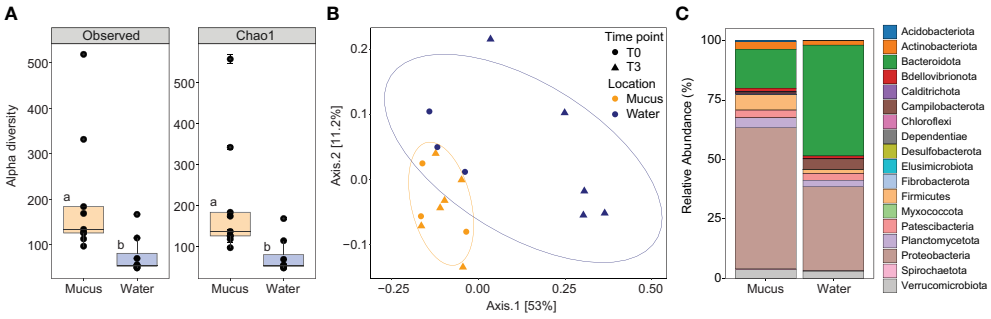

FIGURE 3
(A) Alpha diversity indices including the number of observed ASVs and species richness (Chao1) for the mucus (orange boxes), and seawater (blue boxes) samples. Data was rarefied to the smallest sample size depth of 5,099. Letters indicate *post-hoc* groupings. **(B)** Principal coordinate analysis (PCoA) based on weighted unifrac distance of the 16S rRNA gene amplicon sequences for the mucus (orange symbols) and seawater (dark blue symbols) at timepoint T0 (circle symbols) and T3 (triangle symbols). Ellipses show 80% confidence intervals. **(C)** Relative abundance of bacterial taxa plotted at the phylum level for the mucus and seawater samples, showing total relative abundance of each phylum >1%.

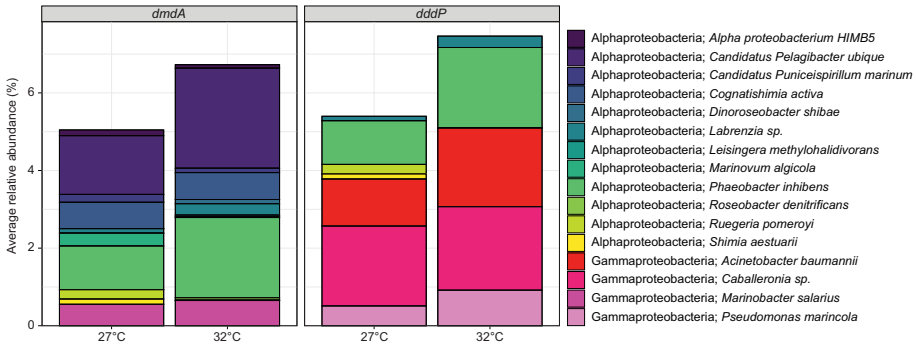

FIGURE 4
Average relative abundance (%) of ASVs that were taxonomically assigned to bacteria (>95% similarity) harbouring the DMSP-degrading genes *dmdA* and/or *dddP* for mucus samples at timepoint T3, for the control (27°C) and temperature (32°C) treatments. Data were rarefied to the smallest sample size depth of 9,182.

The abundance of DMSP degrading genes increase in coral mucus under thermal stress

To go beyond the functional predictions based on 16S rRNA gene similarities, we quantified the abundance of both *dmdA* A/1 and *dddP* in coral mucus throughout the experiment. The demethylation gene *dmdA* A/1 significantly increased in abundance in the thermally stressed fragments between T2 and T3 (ANOVA; $p = 0.0144$; Supplementary Table 2 and Figure 5A). At T3, the abundance of *dmdA* A/1 (per 16S rRNA gene copy) was 1.5-fold higher in the mucus from fragments exposed to 32°C compared to the controls ($F_{3,23} = 4.89$, $p = 0.009$; Supplementary Table 2 and Figure 5A). The abundance of the cleavage gene *dddP* in coral mucus exhibited a similar but more pronounced increase with temperature, with an 8.6-fold increase recorded between T1 and T2 (ANOVA; $p < 0.001$; Supplementary Table 2 and Figure 5B). At T2, the abundance of the *dddP* gene was 2.95-fold higher in the thermally stressed fragments than the controls. This difference slightly decreased by T3, with 2.3-fold more *dddP* gene copies in the thermally stressed fragments compared with the controls.

To determine if DMSP concentrations affected the prevalence of a specific pathway, we calculated the ratio of *dddP:dmdA* A/1 in each sample collected during the experiment (Figure 5C). For DMSP concentrations under 29.4 µM, the *dddP:dmdA* ratio was consistently less than 1, indicating that the demethylation pathway was more abundant in the mucus microbiome than the cleavage pathway. However, when DMSP concentrations were above 29.4 µM, 75% of the samples had a ratio larger than 1, which means that the cleavage pathway became more abundant than demethylation. Based on these data, a significant association was identified between DMSP concentrations and *dddP:dmdA* ratio (Fisher's exact test; $p = 0.002$; Figure 5C).

Discussion

DMSP is a key molecule in the marine sulfur cycle (Sievert et al., 2007), which is produced in large amounts by reef-building corals (Broadbent et al., 2002; Broadbent and Jones, 2004). Thermal stress is known to cause sudden increases in DMSP concentrations that have been linked to its antioxidant capabilities (Raina et al., 2013; Deschaseaux et al., 2014; Gardner et al., 2017), yet the subsequent response of coral-associated microbes that can catabolise this compound remains undefined. Our study aimed to identify how the increased availability of DMSP in *Acropora millepora* mucus during an ecologically relevant thermal stress affected the abundance of DMSP degrading bacteria and the genes they use to degrade this molecule. As predicted, elevated seawater temperature resulted in order of magnitude increase in DMSP concentration in the mucus layer of *A. millepora*. We subsequently identified putative DMSP degraders in the mucus secreted after air exposure and confirmed that the abundance of genes mediating the two DMSP degradation pathways increased with higher DMSP concentrations. Notably, at the highest DMSP concentrations recorded, the cleavage gene causing DMS production became more abundant than the demethylation gene, suggesting that a greater proportion of DMSP is catabolised through this route during heat stress, which has potentially significant implications given the climatic importance of DMS.

Elevated seawater temperature caused reductions in PSII photochemical efficiency (F_V/F_M) and chlorophyll content without a loss of Symbiodiniaceae cells. This, along with the increased reliance on non-photochemical quenching, indicates a nascent bleaching response where light energy is in excess and the integrity of the photosynthetic electron transport chain is compromised (Rochaix, 2011). A reduction in F_V/F_M is typical of thermally stressed *Acropora* symbionts at our sampling site (Heron Island) (Fisher et al., 2012; Gardner et al., 2017; Nitschke et al., 2018), which belong

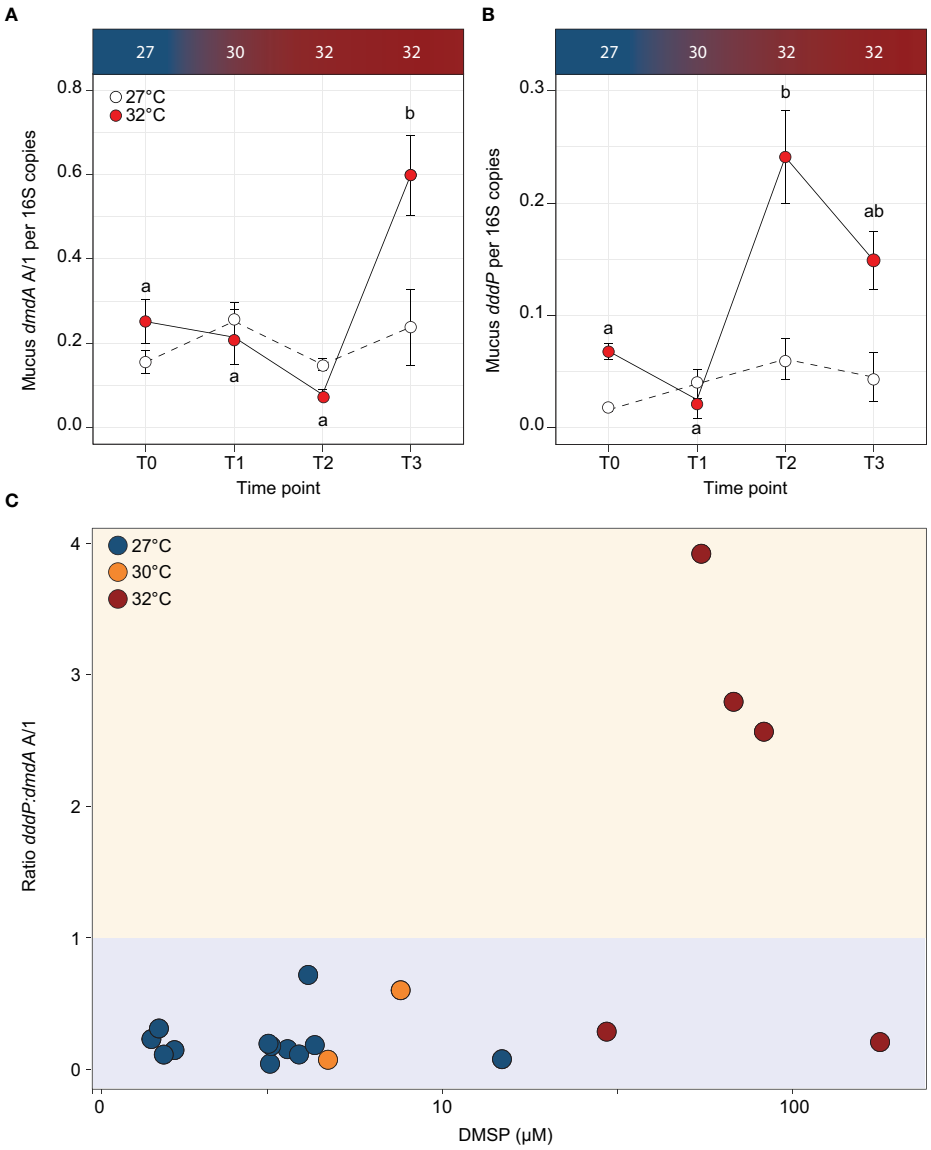

FIGURE 5
Abundance of DMSP degrading genes **(A)** *dmdA* A/1 and **(B)** *dddP* per 16S copies for each timepoint for the control (white circles) and temperature treatments (red circles) in the *Acropora millepora* mucus. Letters indicate significant differences between timepoints for the treatments. Averages (± SE) are shown (n = 3-5). **(C)** Ratio of *dddP:dmdA* A/1 (cleavage:demethylation pathway) to concentration of DMSP in *Acropora millepora* mucus for experimental temperatures 27°C (T0; blue circles), 30°C (T1; orange circles) and 32°C (T2 and T3; red circles). Ratio >1 (yellow shading) indicates when the cleavage pathway is higher than demethylation. When the ratio of *dddP:dmdA* is <1 (blue shading), the demethylation pathway is higher than the cleavage pathway. Temperature treatments are indicated along the top panel for corresponding sampling timepoints. DMSP concentration on the x-axis is on a log10 scale.

to *Cladocopium* of the C3 radiation (LaJeunesse et al., 2003; Fisher et al., 2012; Gardner et al., 2017). Cumulative thermal stress likely overwhelmed Symbiodiniaceae photosystem repair mechanisms (Takahashi et al., 2009), alternative electron flow pathways (e.g., the mehler reaction, see Roberty et al., 2014), and antioxidant systems (Gardner et al., 2017), leading to net production of reactive oxygen species (ROS) (Lesser, 2006; Lesser, 2011). Elevated cellular ROS emissions are characteristic of temperature sensitive Symbiodiniaceae cells (Suggett et al., 2008; Goyen et al., 2017; Buerger et al., 2020), and ROS leakage into host cells has been proposed as one of the mechanisms responsible for Cnidarian-Symbiodiniaceae dysbiosis (Lesser, 1997; Lesser, 2006; Lesser, 2011).

Coral mucus contains high concentrations of DMSP under normal conditions (Broadbent and Jones, 2004). In the present study, concentrations measured in the temperature treatments averaged 83 μM, more than 1.5-fold higher than previously reported for *Acropora*. In addition, increased temperature led to the highest concentrations yet reported in any environment (177 μM). Our observations of Symbiodiniaceae photosystem stress and concurrent increases in DMSP concentrations in the coral host aligns well with its putative role in photosystem repair (Archer et al., 2010) and also corroborate the ROS-detoxifying role of DMSP proposed for *Acropora* (Raina et al., 2013; Deschaseaux et al., 2014; Jones and King, 2015; Gardner et al., 2017) and demonstrated for other species (Sunda et al., 2002). Mucus has long been thought to play an essential role in a coral's ability to adapt to environmental change (Reshef et al., 2006). The exceptionally high concentrations of DMSP measured here, together with a nutrient-rich cocktail of proteins, polysaccharides and lipids, make coral mucus an ideal environment for microbial growth (Wild et al., 2004; Tremblay et al., 2011), and as such, the maintenance of a healthy coral microbiome.

We found little overlap in the identity of the taxonomy of the bacterial communities between mucus and seawater samples, consistent with previous work showing that mucus harbour specific taxa (Rohwer et al., 2001; Frias-Lopez et al., 2002; Rohwer et al., 2002). The two most abundant classes of bacteria present in mucus samples were Alphaproteobacteria and Gammaproteobacteria, known to harbour DMSP-degrading genes (Howard et al., 2008; Varaljay et al., 2010). We matched the 16S rRNA gene of bacteria present in the mucus samples to genomes that harbour *dmdA* and *dddP*, to identify and quantify putative DMSP degraders in the control and heat-stressed samples. The majority of the *dmdA*-harbouring bacteria identified in mucus belong to the Alphaproteobacteria class and include many representatives of the Roseobacter clade, such as *Phaeobacter*, *Ruegeria*, *Shimia*, or *Marinovum*. These Roseobacters are commonly associated with reef-building corals (Huggett and Apprill, 2019; Luo et al., 2021; Kuek et al., 2022), and akin to their interaction with phytoplankton (Seyedsayamdost et al., 2011), their relationships with corals can range from mutualistic (Sharp et al., 2015; Freire et al., 2019; Miura et al., 2019) to pathogenic under environmental stress (Casey et al., 2015; Pollock et al., 2017). In addition, the oligotrophic bacterium *Pelagibacter* was also present among the *dmdA*-harbouring bacteria identified in coral mucus. Given that this DMSP-degrading bacterium is the most abundant microorganism in seawater (Giovannoni, 2017), and mucus viscosity is known to trap particles from seawater (Wild et al., 2004), is it possible that some of these oligotrophs get also trapped in mucus. Conversely, the majority of *dddP*-harbouring bacteria belonged to the Gammaproteobacteria class, most notably members of the genus *Caballeronia*. The functional role of this genus is unknown in corals, but it is involved in mutualisms with plants (South et al., 2021) and insects (Mendiola et al., 2022). Although our approach enabled us to identify some of the DMSP degraders in coral mucus, our estimated proportion of DMSP degraders in the mucus (less than 10% of the total community) is most likely an underestimation, since our conservative functional assignment relies on a small number of genomes harbouring ratified or orthologous *dmdA*/*dddP* genes, but disregards the many homologous sequences that may be functional.

The abundance of the cleavage and demethylation genes in bacterial communities is an indicator of how DMSP is being catabolised. This is important because the demethylation pathway shunts the sulfur moiety towards the synthesis of amino acids (e.g., methionine; see Howard et al., 2006; Reisch et al., 2011), while the cleavage leads to the production of the climatically active DMS (Curson et al., 2011). Quantification of both *dmdA* and *dddP* genes using qPCR revealed that their abundance in coral mucus (per 16S rRNA gene copy) increased (1.5-fold and 3-fold increases, respectively) with DMSP concentrations during thermal stress. In addition, when DMSP concentrations increased beyond 30 μM in mucus, the cleavage gene *dddP* became more abundant than the demethylation gene *dmdA* (ratio of *dddP:dmdA* A/1 above 1). DMSP concentrations have long been hypothesised to be the key determinant of which of the two DMSP degradation pathways is preferentially used (Kiene et al., 2000; Simó, 2001). Recent laboratory results on a model bacterium confirmed that at low to medium concentrations, most of the DMSP is degraded *via* demethylation, but at elevated concentrations (>10 μM) a shift occurs toward cleavage (Gao et al., 2020). Although we did not investigate the expression of these pathways, we found that a similar threshold exists for the abundance of these genes in coral mucus. Therefore, our results suggest that under high DMSP concentrations, such as the ones recorded in coral mucus under thermal stress, a larger proportion of DMSP may be converted to DMS.

Here we measured the largest DMSP concentrations ever recorded in any environment in the mucus of the reef-building coral *Acropora millepora*. Thermal stress caused sharp increases in both DMSP, and the proportion of bacterial genes involved in its degradation. In addition, our results suggest that when DMSP concentrations are high, a greater proportion of DMSP is converted to DMS by bacteria, which corroborates the increase in DMS concentrations previously measured in corals under various environmental stressors (Deschaseaux et al., 2014). Stronger convection forces occurring in tropical regions result in fast transport of volatile gases, such as DMS (Randel and Jensen, 2013), which means that shifts in DMSP-degradation route used by coral-associated bacteria may have important effects on atmospheric chemistry.

Data availability statement

The raw sequencing data used in this study is available in the NCBI Sequence Read Archive under BioProject number

PRJNA816931. Scripts to reproduce these analyses are available on GitHub (https://github.com/StephGardner/Mucus-DMSP). Additional information is available in the supplementary information.

Ethics statement

Corals were collected under the Great Barrier Reef Marine Park Authority permit G14/36977.1 issued to KP.

Author contributions

SG, KP and J-BR designed the research. SG, MN, KP, and J-BR carried out the experiment. CM provided NMR expertise. JO'B performed qPCR. SG, MN and JB-R performed sample and data analysis. SG, J-BR and MN wrote the first draft of the manuscript. All authors edited the final manuscript. All authors contributed to the article and approved the submitted version.

Funding

SG was supported by an Australian Postgraduate Award, and research funding was provided by the Climate Change Cluster and the School of Life Sciences, University of Technology Sydney, a PADI Foundation Grant and a Danielle Simmons Research Award from the Australian Coral Reef Society. Corals were collected under the Great Barrier Reef Marine Park Authority permit G14/36977.1 issued to KP. J-BR was supported by an Australian Research Council Future Fellowship (FT210100100).

Conflict of interest

The authors declare that the research was conducted in the absence of any commercial or financial relationships that could be construed as a potential conflict of interest.

Publisher's note

Supplementary material

The Supplementary Material for this article can be found online at: https://www.frontiersin.org/articles/10.3389/fmars.2022.912862/full#supplementary-material

References

Akoka, S., and Trierweiler, M. (2002). Improvement of the ERETIC method by digital synthesis of the signal and addition of a broadband antenna inside the NMR probe. *Instrum. Sci. Technol.* 30 (1), 21–29. doi: 10.1081/CI-100108768

Archer, S. D., Ragni, M., Webster, R., Airs, R. L., and Geider, R. J. (2010). Dimethyl sulfoniopropionate and dimethyl sulfide production in response to photoinhibition in emiliania huxleyi. *Limnol. Oceanogr.* 55 (4), 1579–1589. doi: 10.4319/lo.2010.55.4.1579

Broadbent, A. D., and Jones, G. B. (2004). DMS and DMSP in mucus ropes, coral mucus, surface films and sediment pore waters from coral reefs in the great barrier reef. *Mar. Freshw. Res.* 55 (8), 849–855. doi: 10.1071/MF04114

Broadbent, A. D., Jones, G. B., and Jones, R. J. (2002). DMSP in corals and benthic algae from the great barrier reef. *Estuar. Coast. Shelf Sci.* 55 (4), 547–555. doi: 10.1006/ecss.2002.1021

Brown, B. E., and Bythell, J. C. (2005). Perspectives on mucus secretion in reef corals. *Mar. Ecol. Prog. Ser.* 296, 291–309. doi: 10.3354/meps296291

Buerger, P., Alvarez-Roa, C., Coppin, C. W., Pearce, S. L., Chakravarti, L. J., Oakeshott, J. G., et al. (2020). Heat-evolved microalgal symbionts increase coral bleaching tolerance. *Sci. Adv.* 6 (20), 2498. doi: 10.1126/sciadv.aba2498

Bythell, J. C., and Wild, C. (2011). Biology and ecology of coral mucus release. *J. Exp. Mar. Biol. Ecol.* 408 (1), 88–93. doi: 10.1016/j.jembe.2011.07.028

Callahan, B. J., McMurdie, P. J., Rosen, M. J., Han, A. W., Johnson, A. J. A., and Holmes, S. P. (2016). DADA2: High-resolution sample inference from illumina amplicon data. *Nat. Methods* 13, 581. doi: 10.1038/nmeth.3869

Caruana, A. M. N., and Malin, G. (2014). The variability in DMSP content and DMSP lyase activity in marine dinoflagellates. *Prog. Oceanogr.* 120, 410–424. doi: 10.1016/j.pocean.2013.10.014

Casey, J. M., Connolly, S. R., and Ainsworth, T. D. (2015). Coral transplantation triggers shift in microbiome and promotion of coral disease associated potential pathogens. *Sci. Rep.* 5 (1), 11903. doi: 10.1038/srep11903

Cui, Y., Suzuki, S., Omori, Y., Wong, S. K., Ijichi, M., Kaneko, R., et al. (2015). Abundance and distribution of dimethylsulfoniopropionate degradation genes and the corresponding bacterial community structure at dimethyl sulfide hot spots in the tropical and subtropical pacific ocean. *Appl. Environ. Microbiol.* 81 (12), 4184–4194. doi: 10.1128/aem.03873-14

Curson, A. R. J., Todd, J. D., Sullivan, M. J., and Johnston, A. W. B. (2011). Catabolism of dimethylsulphoniopropionate: microorganisms, enzymes and genes. *Nat. Rev. Microbiol.* 9 (12), 849–859. doi: 10.1038/nrmicro2653

Deschaseaux, E. S. M., Jones, G. B., Deseo, M. A., Shepherd, K. M., Kiene, R. P., Swan, H. B., et al. (2014). Effects of environmental factors on dimethylated sulfur compounds and their potential role in the antioxidant system of the coral holobiont. *Limnol. Oceanogr.* 59 (3), 758–768. doi: 10.4319/lo.2014.59.3.0758

Ducklow, H. W., and Mitchell, R. (1979). Composition of mucus released by coral reef coelenterates. *Limnol. Oceanogr.* 24 (4), 706–714. doi: 10.4319/lo.1979.24.4.0706

Fisher, P. L., Malme, M. K., and Dove, S. (2012). The effect of temperature stress on coral-symbiodinium associations containing distinct symbiont types. *Coral Reefs* 31, 473–485. doi: 10.1007/s00338-011-0853-0

Frade, P. R., Schwaninger, V., Glasl, B., Sintes, E., Hill, R. W., Simó, R., et al. (2015). Dimethylsulfoniopropionate in corals and its interrelations with bacterial assemblages in coral surface mucus. *Environ. Chem.* 13 (2), 252–265. doi: 10.1071/EN15023

Freire, I., Gutner-Hoch, E., Muras, A., Benayahu, Y., and Otero, A. (2019). The effect of bacteria on planula-larvae settlement and metamorphosis in the octocoral rhytisma fulvum fulvum. *PloS One* 14 (9), e0223214. doi: 10.1371/journal.pone.0223214

Frias-Lopez, J., Zerkle, A. L., Bonheyo, G. T., and Fouke, B. W. (2002). Partitioning of bacterial communities between seawater and healthy, black band diseased, and dead coral surfaces. *Appl. Environ. Microbiol.* 68 (5), 2214–2228. doi: 10.1128/AEM.68.5.2214-2228.2002

Gao, C., Fernandez, V. I., Lee, K. S., Fenizia, S., Pohnert, G., Seymour, J. R., et al. (2020). Single-cell bacterial transcription measurements reveal the importance of dimethylsulfoniopropionate (DMSP) hotspots in ocean sulfur cycling. *Nat. Commun.* 11 (1), 1942. doi: 10.1038/s41467-020-15693-z

Gardner, S. G., Raina, J.-B., Nitschke, M. R., Nielsen, D. A., Stat, M., Motti, C. A., et al. (2017). A multi-trait systems approach reveals a response cascade to bleaching in corals. *BMC Biol.* 15 (1), 117. doi: 10.1186/s12915-017-0459-2

Garren, M., and Azam, F. (2010). New method for counting bacteria associated with coral mucus. *Appl. Environ. Microbiol.* 76 (18), 6128–6133. doi: 10.1128/AEM.01100-10

Giovannoni, S. J. (2017). SAR11 bacteria: The most abundant plankton in the oceans. *Annu. Rev. Mar. Sci.* 9 (1), 231–255. doi: 10.1146/annurev-marine-010814-015934

Goyen, S., Pernice, M., Szabó, M., Warner, M. E., Ralph, P. J., and Suggett, D. J. (2017). A molecular physiology basis for functional diversity of hydrogen peroxide production amongst symbiodinium spp. (Dinophyceae). *Mar. Biol.* 164 (3), 46. doi: 10.1007/s00227-017-3073-5

Haydon, T. D., Seymour, J. R., and Suggett, D. J. (2018). Soft corals are significant DMSP producers in tropical and temperate reefs. *Mar Biol.* 165, 109. doi: 10.1007/s00227-018-3367-2

Hennige, S. J., Smith, D. J., Perkins, R., Consalvey, M., Paterson, D. M., and Suggett, D. J. (2008). Photoacclimation, growth and distribution of massive coral species in clear and turbid waters. *Mar. Ecol. Prog. Ser.* 369, 77–88. doi: 10.3354/meps07612

Hill, R. W., Dacey, J. W. H., and Edward, A. (2000). Dimethylsulfoniopropionate in giant clams (Tridacnidae). *Biol. Bull.* 199 (2), 108–115. doi: 10.2307/1542870

Hill, R. W., Dacey, J. W. H., and Krupp, D. A. (1995). Dimethylsulfoniopropionate in reef corals. *Bull. Mar. Sci.* 57 (2), 489–494.

Howard, E. C., Henriksen, J. R., Buchan, A., Reisch, C. R., Bürgmann, H., Welsh, R., et al. (2006). Bacterial taxa that limit sulfur flux from the ocean. *Science* 314 (5799), 649–652. doi: 10.1126/science.1130657

Howard, E. C., Sun, S., Biers, E. J., and Moran, M. A. (2008). Abundant and diverse bacteria involved in DMSP degradation in marine surface waters. *Environ. Microbiol.* 10 (9), 2397–2410. doi: 10.1111/j.1462-2920.2008.01665.x

Huggett, M. J., and Apprill, A. (2019). Coral microbiome database: Integration of sequences reveals high diversity and relatedness of coral-associated microbes. *Environ. Microbiol. Rep.* 11 (3), 372–385. doi: 10.1111/1758-2229.12686

Jones, G. B., and King, S. (2015). Dimethylsulphoniopropionate (DMSP) as an indicator of bleaching tolerance in scleractinian corals. *J. Mar. Sci. Eng.* 3 (2), 444–465. doi: 10.3390/jmse3020444

Kassambara, A. (2021). *"rstatix: Pipe-friendly framework for basic statistical tests"*. https://CRAN.R-project.org/package=rstatix

Katoh, K., and Standley, D. M. (2013). MAFFT multiple sequence alignment software version 7: improvements in performance and usability. *Mol. Biol. evol.* 30 (4), 772–780. doi: 10.1093/molbev/mst010

Kettle, A. J., Andreae, M. O., Amouroux, D., Andreae, T. W., Bates, T. S., Berresheim, H., et al. (1999). A global database of sea surface dimethylsulfide (DMS) measurements and a procedure to predict sea surface DMS as a function of latitude, longitude, and month. *Global Biogeochem. Cycles* 13 (2), 399–444. doi: 10.1029/1999GB900004

Kieber, D. J., Jiao, J., Kiene, R. P., and Bates, T. S. (1996). Impact of dimethylsulphide photochemistry on methyl sulphur cycling in the equatorial pacific ocean. *J. Geophys. Res.: Oceans* 101 (C2), 3715–3372. doi: 10.1029/95JC03624

Kiene, R. P., Linn, L. J., and Bruton, J. A. (2000). New and important roles for DMSP in marine microbial communities. *J. Sea Res.* 49 (3-4), 209–224. doi: 10.1016/S1385-1101(00)00023-X

Kiene, R. P., Linn, L. J., González, J., Moran, M., and Bruton, J. A. (1999). Dimethylsulfoniopropionate and methanethiol are important precursors of methionine and protein-sulfur in marine bacterioplankton. *Appl. Environ. Microbiol.* 65 (10), 4549–4558. doi: 10.1128/AEM.65.10.4549-4558.1999

Kuek, F. W. I., Motti, C. A., Zhang, J., Cooke, I. R., Todd, J. D., Miller, D. J., et al. (2022). DMSP production by coral-associated bacteria. *Front. Mar. Sci* 9. doi: 10.3389/fmars.2022.869574

LaJeunesse, T. C., Loh, W. K. W., van Woesik, R., Hoegh-Guldberg, O., Schmidt, G. W., and Fitt, W. K. (2003). Low symbiont diversity in southern great barrier reef corals, relative to those of the Caribbean. *Limnol. Oceanogr.* 48 (5), 2046–2054. doi: 10.4319/lo.2003.48.5.2046

Lesser, M. P. (1997). Oxidative stress causes coral bleaching during exposure to elevated temperatures. *Coral Reefs* 16, 187–192. doi: 10.1007/s003380050073

Lesser, M. P. (2006). Oxidative stress in marine environments: Biochemistry and physiological ecology. *Annu. Rev. Physiol.* 68, 253–278. doi: 10.1146/annurev.physiol.68.040104.110001

Lesser, M. P. (2011). "Coral bleaching: causes and mechanisms," in *Coral reefs: an ecosystem in transition*, *1st ed.* Eds. Z. Dubinsky and N. Stambler (New York: Springer), 405–419.

Levine, N. M., Varaljay, V. A., Toole, D. A., Dacey, J. W. H., Doney, S. C., and Moran, M. A. (2012). Environmental, biochemical and genetic drivers of DMSP degradation and DMS production in the Sargasso Sea. *Environ. Microbiol.* 14 (5), 1210–1223. doi: 10.1111/j.1462-2920.2012.02700.x

Lozupone, C., Lladser, M. E., Knights, D., Stombaugh, J., and Knight, R. (2011). UniFrac: an effective distance metric for microbial community comparison. *ISME J.: Multidiscip. J. Microb. Ecol.* 5 (2), 169–172. doi: 10.1038/ismej.2010.133

Luo, D., Wang, X., Feng, X., Tian, M., Wang, S., Tang, S.-L., et al. (2021). Population differentiation of rhodobacteraceae along with coral compartments. *ISME J.* 15 (11), 3286–3302. doi: 10.1038/s41396-021-01009-6

Martin, M. (2011). Cutadapt removes adapter sequences from high-throughput sequencing reads. *EMBnet.journal* 17(1), 10–12. doi: 10.14806/ej.17.1.200

McMurdie, P. J., and Holmes, S. (2013). Phyloseq: An r package for reproducible interactive analysis and graphics of microbiome census data. *PloS One* 8 (4), e61217. doi: 10.1371/journal.pone.0061217

Meikle, P., Richards, G. N., and Yellowlees, D. (1988). Structural investigations on the mucus from six species of coral. *Mar. Biol.* 99 (2), 187–193. doi: 10.1007/BF00391980

Mendiola, S. Y., Stoy, K. S., DiSalvo, S., Wynn, C. L., Civitello, D. J., and Gerardo, N. M. (2022). Competitive exclusion of phytopathogenic serratia marcescens from squash bug vectors by the gut endosymbiont caballeronia. *Appl. Environ. Microbiol.* 88 (1), e0155021. doi: 10.1128/aem.01550-21

Miller, M. A., Pfeiffer, W., and Schwartz, T. (2010). *"Creating the CIPRES science gateway for inference of large phylogenetic trees in proceedings of the gateway computing environments workshop (GCE)"* (New Orleans, Los Angeles), 1–8. doi: 10.1109/GCE.2010.5676129

Miura, N., Motone, K., Takagi, T., Aburaya, S., Watanabe, S., Aoki, W., et al. (2019). Ruegeria sp. strains isolated from the reef-building coral galaxea fascicularis inhibit growth of the temperature-dependent pathogen vibrio coralliilyticus. *Mar. Biotechnol.* 21 (1), 1–8. doi: 10.1007/s10126-018-9853-1

Nitschke, M. R., Gardner, S. G., Goyen, S., Fujise, L., Camp, E. F., Ralph, P. J., et al. (2018). Utility of photochemical traits as diagnostics of thermal tolerance amongst great barrier reef corals. *Front. Mar. Sci.* 5 (45). doi: 10.3389/fmars.2018.00045

Oksanen, J., Blanchet, F. G., Friendly, M., Kindt, R., Legendre, P., McGlinn, D., et al (2019). vegan: Community Ecology Package. R package version 2.5-6. https://CRAN.R-project.org/package=vegan

Piggot, A. M., Fouke, B. W., Sivaguru, M., Sanford, R. A., and Gaskins, H. R. (2009). Change in zooxanthellae and mucocyte tissue density as an adaptive response to environmental stress by the coral, montastraea annularis. *Mar. Biol.* 156 (11), 2379–2389. doi: 10.1007/s00227-009-1267-1

Pollock, F. J., Wada, N., Torda, G., Willis, B. L., Bourne, D. G., and Kostka, J. E. (2017). White syndrome-affected corals have a distinct microbiome at disease lesion fronts. *Appl. Environ. Microbiol.* 83 (2), e02799–e02716. doi: 10.1128/AEM.02799-16

Price, M. N., Dehal, P. S., and Arkin, A. P. (2009). FastTree: Computing Large minimum-evolution trees with profiles instead of a distance matrix. *Mol. Biol. Evol.* 26, 1641–1650. doi: 10.1093/molbev/msp077

Quast, C., Pruesse, E., Yilmaz, P., Gerken, J., Schweer, T., Yarza, P., et al. (2013). The SILVA ribosomal RNA gene database project: improved data processing and web-based tools. *Nucleic Acids Res.* 41 (Database issue), D590–D596. doi: 10.1093/nar/gks1219

Raina, J.-B., Tapiolas, D. M., Foret, S., Lutz, A., Abrego, D., Ceh, J., et al. (2013). DMSP biosynthesis by an animal and its role in coral thermal stress response. *Nature* 502 (7473), 677–680. doi: 10.1038/nature12677

Raina, J. B., Tapiolas, D., Willis, B. L., and Bourne, D. G. (2009). Coral-associated bacteria and their role in the biogeochemical cycling of sulfur. *Appl. Environ. Microbiol.* 75 (11), 3492–3501. doi: 10.1128/aem.02567-08

Ralph, P. J., and Gademann, R. (2005). Rapid light curves: A powerful tool to assess photosynthetic activity. *Aquat. Bot.* 82, 222–237. doi: 10.1016/j.aquabot.2005.02.006

Randel, W. J., and Jensen, E. J. (2013). Physical processes in the tropical tropopause layer and their roles in a changing climate. *Nat. Geosci.* 6 (3), 169–176. doi: 10.1038/ngeo1733

Reisch, C. R., Moran, M. A., and Whitman, W. B. (2011). Bacterial catabolism of dimethylsulfoniopropionate (DMSP). *Front. Microbiol.* 2. doi: 10.3389/fmicb.2011.00172

Reshef, L., Koren, O., Loya, Y., Zilber-Rosenberg, I., and Rosenberg, E. (2006). The coral probiotic hypothesis. *Environ. Microbiol.* 8 (12), 2068–2073. doi: 10.1111/j.1462-2920.2006.01148.x

Ritchie, K. B. (2006a). Regulation of microbial populations by coral surface mucus and mucus-associated bacteria. *Mar. Ecol. Prog. Ser.* 322, 1–14. doi: 10.3354/meps322001

Ritchie, R. J. (2006b). Consistent sets of spectrophotometric chlorophyll equations for acetone, methanol and ethanol solvents. *Photosyn. Res.*, 89 (1), 27–41. doi: 10.1007/s11120-006-9065-9

Roberty, S., Bailleul, B., Berne, N., Franck, F., and Cardol, P. (2014). PSI mehler reaction is the main alternative photosynthetic electron pathway in symbiodinium sp., symbiotic dinoflagellates of cnidarians. *New Phytol.* 204 (1), 81–91. doi: 10.1111/nph.12903

Rochaix, J.-D. (2011). Regulation of photosynthetic electron transport. *Biochim. Biophys. Acta (BBA) - Bioenerg.* 1807 (3), 375–383. doi: 10.1016/j.bbabio.2010.11.010

Rohwer, F., Breitbart, M., Jara, J., Azam, F., and Knowlton, N. (2001). Diversity of bacteria associated with the Caribbean coral montastraea franksi. *Coral Reefs* 20 (1), 85–91. doi: 10.1007/s003380100138

Rohwer, F., Seguritan, V., Azam, F., and Knowlton, N. (2002). Diversity and distribution of coral-associated bacteria. *Mar. Ecol. Prog. Ser.* 243, 1–10. doi: 10.3354/meps243001

Schauer, M., Massana, R., and Pedrós-Alió, C. (2000). Spatial differences in bacterioplankton composition along the Catalan coast (NW Mediterranean) assessed by molecular fingerprinting. *FEMS Microbiol. Ecol.* 33 (1), 51–59. doi: 10.1111/j.1574-6941.2000.tb00726.x

Seyedsayamdost, M. R., Case, R. J., Kolter, R., and Clardy, J. (2011). The Jekyll-and-Hyde chemistry of phaeobacter gallaeciensis. *Nat. Chem.* 3 (4), 331–335. doi: 10.1038/nchem.1002

Sharp, K. H., Sneed, J. M., Ritchie, K. B., McDaniel, L., and Paul, V. J. (2015). Induction of larval settlement in the reef coral porites astreoides by a cultivated marine roseobacter strain. *Biol. Bull.* 228 (2), 98–107. doi: 10.1086/BBLv228n2p98

Sheik, C. S., Reese, B. K., Twing, K. I., Sylvan, J. B., Grim, S. L., Schrenk, M. O., et al. (2018). Identification and removal of contaminant sequences from ribosomal gene databases: Lessons from the census of deep life. *Front. Microbiol.* 9. doi: 10.3389/fmicb.2018.00840

Shnit-Orland, M., and Kushmaro, A. (2009). Coral mucus-associated bacteria: a possible first line of defense. *FEMS Microbiol. Ecol.* 67 (3), 371–380. doi: 10.1111/j.1574-6941.2008.00644.x

Sievert, S. M., Kiene, R. P., and Schulz-Vogt, H. N. (2007). The sulfur cycle. *Oceanography* 20 (2), 117–123. doi: 10.5670/oceanog.2007.55

Simó, R. (2001). Production of atmospheric sulfur by oceanic plankton: biogeochemical, ecological and evolutionary links. *Trends Ecol. Evol.* 16 (6), 287–294. doi: 10.1016/S0169-5347(01)02152-8

Simó, R., Archer, S. D., Pedrós-Alió, C., Gilpin, L., and Stelfox-Widdicombe, C. E. (2002). Coupled dynamics of dimethylsulfoniopropionate and dimethylsulfide cycling and the microbial food web in surface waters of the north Atlantic. *Limnol. Oceanogr.* 47 (1), 53–61. doi: 10.4319/lo.2002.47.1.0053

South, K. A., Nordstedt, N. P., and Jones, M. L. (2021). Identification of plant growth promoting rhizobacteria that improve the performance of greenhouse-grown petunias under low fertility conditions. *Plants* 10 (7), 1410. doi: 10.3390/plants10071410

Stimson, J., and Kinzie, R. A. (1991). The temporal pattern and rate of release of zooxanthellae from the reef coral *Pocillopora damicornis* (Linnaeus) under nitrogen-enrichment and control conditions. *J. Exp. Mar. Biol. Ecol.* 153, 63–74. doi: 10.1016/S0022-0981(05)80006-1

Suggett, D. J., Goyen, S., Evenhuis, C., Szabo, M., Pettay, D. T., Warner, M. E., et al. (2015). Functional diversity of photobiological traits within the genus symbiodinium appears to be governed by the interaction of cell size with cladal designation. *New Phytol.* 208 (2), 370–381. doi: 10.1111/nph.13483

Suggett, D. J., Warner, M. E., Smith, D. J., Davey, P., Hennige, S., and Baker, N. R. (2008). Photosynthesis and production of hydrogen peroxide by *Symbiodinium* (pyrrhophyta) phylotypes with different thermal tolerances. *J. Phycol.* 44 (4), 948–956. doi: 10.1111/j.1529-8817.2008.00537.x

Sunda, W., Kieber, D. J., Kiene, R. P., and Huntsman, S. (2002). An antioxidant function for DMS and DMSP in marine algae. *Nature* 418, 317–320. doi: 10.1038/nature00851

Sun, J., Todd, J. D., Thrash, J. C., Qian, Y., Qian, M. C., Temperton, B., et al. (2016). The abundant marine bacterium pelagibacter simultaneously catabolizes dimethylsulfoniopropionate to the gases dimethyl sulfide and methanethiol. *Nat. Microbiol.* 1, 16065. doi: 10.1038/nmicrobiol.2016.65

Suzuki, M. T., Taylor, L. T., and DeLong, E. F. (2000). Quantitative analysis of small-subunit rRNA genes in mixed microbial populations *via* 5′-nuclease assays. *Appl. Environ. Microbiol.* 66 (11), 4605–4614. doi: 10.1128/AEM.66.11.4605-4614.2000

Sweet, M. J., Croquer, A., and Bythell, J. C. (2011). Bacterial assemblages differ between compartments within the coral holobiont. *Coral Reefs* 30 (1), 39–52. doi: 10.1007/s00338-010-0695-1

Takahashi, S., Whitney, S. M., and Badger, M. R. (2009). Different thermal sensitivity of the repair of photodamaged photosynthetic machinery in cultured symbiodinium species. *Proc. Natl. Acad. Sci.* 106 (9), 3237–3242. doi: 10.1073/pnas.0808363106

Tapiolas, D. M., Raina, J. B., Lutz, A., Willis, B. L., and Motti, C. A. (2013). Direct measurement of dimethylsulfoniopropionate (DMSP) in reef-building corals using quantitative nuclear magnetic resonance (qNMR) spectroscopy. *J. Exp. Mar. Biol. Ecol.* 443, 85–89. doi: 10.1016/j.jembe.2013.02.037

Todd, J. D., Curson, A. R. J., Dupont, C. L., Nicholson, P., and Johnston, A. W. B. (2009). The dddP gene, encoding a novel enzyme that converts dimethylsulfoniopropionate into dimethyl sulfide, is widespread in ocean metagenomes and marine bacteria and also occurs in some ascomycete fungi. *Environ. Microbiol.* 11 (6), 1376–1385. doi: 10.1111/j.1462-2920.2009.01864.x

Tremblay, P., Weinbauer, M. G., Rottier, C., Guérardel, Y., Nozais, C., and Ferrier-Pagès, C. (2011). Mucus composition and bacterial communities associated with the tissue and skeleton of three scleractinian corals maintained under culture conditions. *J. Mar. Biol. Assoc. United Kingdom.* 91 (03), 649–657. doi: 10.1017/S002531541000130X

Trevena, A. J., Jones, G., Wright, S., and Enden, R. (2003). Profiles of dimethylsulphoniopropionate (DMSP), algal pigments, nutrients, and salinity in the fast ice of prydz bay, Antarctica. *Sch. Environ. Sci. Manage. Pap.* 108, 3145. doi: 10.1029/2002JC001369

Van Alstyne, K. L., Koellermeier, L., and Nelson, T. A. (2007). Spatial variation in dimethylsulfoniopropionate (DMSP) production in ulva lactuca (Chlorophyta) from the northeast pacific. *Mar. Biol.* 150 (6), 1127–1135. doi: 10.1007/s00227-006-0448-4

Varaljay, V. A., Howard, E. C., Sun, S., and Moran, M. A. (2010). Deep sequencing of a dimethylsulfoniopropionate-degrading gene (dmdA) by using PCR primer pairs designed on the basis of marine metagenomic data. *Appl. Environ. Microbiol.* 76 (2), 609–617. doi: 10.1128/AEM.01258-09

Veal, C. J., Holmes, G., Nunez, M., Hoegh-Guldberg, O., and Osborn, J. (2010). A comparative study of methods for surface area and three dimensional shape measurement of coral skeletons. *Limnol. Oceanogr.* 8, 241–253. doi: 10.4319/lom.2010.8.241

Wild, C., Huettel, M., Klueter, A., Kremb, S. G., Rasheed, M. Y. M., and Jørgensen, B. B. (2004). Coral mucus functions as an energy carrier and particle trap in the reef ecosystem. *Nature* 428 (6978), 66–70. doi: 10.1038/nature02344

Zhang, X.-H., Liu, J., Liu, J., Yang, G., Xue, C.-X., Curson, A. R. J., et al. (2019). Biogenic production of DMSP and its degradation to DMS–their roles in the global sulfur cycle. *Sci. China Life Sci.* 62 (10), 1296–1319. doi: 10.1007/s11427-018-9524-y

Zubkov, M., Linn, L. J., Amann, R., and Kiene, R. P. (2004). Temporal patterns of biological dimethylsulphide (DMS) consumption during laboratory-induced phytoplankton bloom cycles. *Mar. Ecol. Prog. Ser.* 271, 77–86. doi: 10.3354/meps271077

frontiers | Frontiers in Marine Science

TYPE Original Research
PUBLISHED 29 September 2022
DOI 10.3389/fmars.2022.910420

OPEN ACCESS

EDITED BY
Rafel Simó,
Institut de Ciències del Mar (ICM-CSIC), Spain

REVIEWED BY
Hakase Hayashida,
Japan Agency for Marine-Earth Science and Technology, Japan
Tereza Jarnikova,
University of East Anglia, United Kingdom

*CORRESPONDENCE
Rebecca L. Jackson
rebecca.jackson@csiro.au

†PRESENT ADDRESS
Rebecca L. Jackson,
Coasts and Ocean Research, Oceans and Atmosphere, Commonwealth Scientific and Industrial Research Organisation, Canberra, ACT, Australia

SPECIALTY SECTION
This article was submitted to Coral Reef Research, a section of the journal Frontiers in Marine Science

RECEIVED 01 April 2022
ACCEPTED 31 August 2022
PUBLISHED 29 September 2022

CITATION
Jackson RL, Woodhouse MT, Gabric AJ and Cropp RA (2022) CMIP6 projections of ocean warming and the impact on dimethylsulfide emissions from the Great Barrier Reef, Australia. *Front. Mar. Sci.* 9:910420. doi: 10.3389/fmars.2022.910420

CMIP6 projections of ocean warming and the impact on dimethylsulfide emissions from the Great Barrier Reef, Australia

Rebecca L. Jackson[1*†], Matthew T. Woodhouse[2], Albert J. Gabric[1] and Roger A. Cropp[1]

[1]School of Environment and Science, Griffith University, Gold Coast, QLD, Australia, [2]Climate Science Centre, Oceans and Atmosphere, Commonwealth Scientific and Industrial Research Organisation, Aspendale, VIC, Australia

Coral reefs are important regional sources of biogenic sulfur to the tropical marine atmosphere, through stress-induced emissions of dimethylsulfide (DMS). Recent estimates suggest that the Great Barrier Reef (GBR), Australia emits 0.02-0.05 Tg yr^{-1} of DMS (equivalent to 0.010-0.026 Tg yr^{-1} S), with potential implications for local aerosol-cloud processes. However, the impact of ocean warming on DMS emissions from coral reefs remains uncertain, complicating efforts to improve the representation of coral reefs in DMS climatologies and climate models. We investigate the influence of predicted changes in sea surface temperature (SST), photosynthetically active radiation (PAR) and wind speed on contemporary DMS emissions from the GBR using model output from the Coupled Model Intercomparison Project Phase 6 (CMIP6). A multiple linear regression is used to calculate seawater surface DMS (DMS_w) concentration in the GBR in a contemporary (2001-2020) and end-of-century (2081-2100) scenario, as simulated by CMIP6 models under a SSP2-4.5 and SSP5-8.5 Shared Socioeconomic Pathway. By the end of this century, a 1.5-3.0°C rise in annual mean SST and a 1.1-1.7 mol m^{-2} d^{-1} increase in PAR could increase DMS_w concentration in the GBR by 9.2-14.5%, leading to an increase in DMS flux of 9.5-14.3%. Previous model studies have suggested that the aerosol system has a low sensitivity to relatively large changes in coral reef-derived DMS. Therefore, the predicted change in contemporary DMS emissions is unlikely to influence the regional atmosphere. Further research is needed to understand the combined effects of temperature, light, pH, salinity and ecosystem structure on DMS production in coral reefs to better predict potential changes in emissions. Nevertheless, the findings provide insight into how predicted ocean warming may affect present-day DMS emissions and the source-strength of the GBR to the atmospheric sulfur budget.

KEYWORDS

coral reef, dimethylsulfide (DMS), sea surface temperature, climate change, CMIP6

1 Introduction

Coral reefs are strong regional sources of biogenic sulfur through stress-induced emissions of dimethylsulfide (DMS). The atmospheric oxidation products of DMS are important sulfate aerosol precursor compound which can influence non-sea salt sulfate (nss-SO_4) aerosol properties (Gabric et al., 2013; Woodhouse et al., 2013; Fiddes et al., 2018; Sanchez et al., 2018; Jackson et al., 2020). It has been hypothesised that DMS emissions from coral reefs may facilitate aerosol nucleation and growth to cloud condensation nuclei (CCN), influencing the lifetime and albedo of low-level clouds (LLC) over coral reefs *via* aerosol direct and indirect effects on the radiation budget (Fischer & Jones, 2012; Jones, 2015; Jones et al., 2017). The potential for DMS-derived sulfates to influence aerosol-cloud processes over coral reefs is dependent on the rate of DMS emission, oxidation and subsequent atmospheric processing (such as nucleation, condensation or coagulation) (Andreae & Crutzen, 1997). However, the impact of ocean warming on the source-strength of coral reefs to the atmospheric sulfur budget remains uncertain.

The precursor of DMS, dimethylsulfoniopropionate (DMSP), is produced by a number of organisms including marine algae (Sunda et al., 2002), corals and endosymbiotic dinoflagellates (Raina et al., 2013). Catabolism of DMSP by endosymbiotic and free-living microbes occurs *via* the demethylation and cleavage pathways, with the latter producing DMS (Bullock et al., 2017).

When dissolved DMS is present in excess, seawater surface DMS (DMS_w) is ventilated to the marine boundary layer where it is rapidly oxidised to nss-SO_4 aerosol precursor compounds including sulfur dioxide (SO_2), methanesulfonic acid, hydroperoxymethyl thioformate and sulfuric acid (H_2SO_4) (Andreae & Crutzen, 1997; Berndt et al., 2019; Hodshire et al., 2019; Veres et al., 2020). These nss-SO_4 aerosol precursors may condense onto existing particles or nucleate to form new secondary marine aerosols (Andreae & Crutzen, 1997). Both processes can influence the number concentration and growth of aerosols to CCN and cloud droplets (Korhonen et al., 2008; Woodhouse et al., 2013; Sanchez et al., 2018). When high concentrations of fine-mode aerosol grow rapidly to CCN, cloud droplet number increases, cloud droplet size decreases (assuming constant cloud liquid water content) and the albedo and lifetime of LLC is enhanced (Andreae & Rosenfeld, 2008; Dave et al., 2019).

Various field studies, remotely sensed observations and model simulations have identified a significant link between atmospheric DMS (DMS_a), nss-SO_4 aerosol formation and growth, CCN and cloud droplet radius over the remote ocean (Korhonen et al., 2008; Woodhouse et al., 2013; Fiddes et al., 2018; Gabric et al., 2018; Sanchez et al., 2018). A mesocosm experiment found that submicron secondary marine aerosols primarily consisted of biogenic nss-SO_4 (> 50%) and organic species, and had a higher hygroscopicity and CCN potential than sea spray aerosols (Mayer et al., 2020). These findings suggest an important biogenic influence on cloud microphysical properties.

Globally, DMS emission estimates range from 17.6-34.4 Tg yr^{-1} S (Kettle & Andreae, 2000; Lana et al., 2011; Land et al., 2014). The total contribution of coral reefs to the atmospheric sulfur budget is not yet certain. However, it is estimated that the Great Barrier Reef (GBR), Australia, emits 0.02-0.05 Tg yr^{-1} of DMS (0.010-0.026 Tg yr^{-1} S) from approximately 347,000 km^2 of coral reefs and lagoon waters (Jones et al., 2018; Jackson et al., 2021). Assuming that DMS production and sea-air flux is consistent across coral reefs, tropical coral reefs and lagoon waters (~600,000 km^2) could emit 0.08 Tg yr^{-1} of DMS (0.041 Tg yr^{-1} S).

Estimates of DMS emissions from coral reefs are comparable to those from other highly productive regions. In polar waters, DMS production is closely related to phytoplankton productivity, particularly during seasonal sea ice melting which can induce ice algae blooms (Gabric et al., 2018; Gali et al., 2021). The Austral Polar biogeographic region (south of 59°S) is estimated to release 1.1 Tg yr^{-1} S (Webb et al., 2019), representing 3-6% of global emission estimates from ~3% of the ocean surface. Normalising the above estimates by area, the GBR and Antarctic waters release ~0.4 Tg yr^{-1} S per 1% of the ocean surface.

In corals, DMSP biosynthesis and cleavage to DMS is upregulated in response to oxidative stress caused by exposure to high sea surface temperature (SST), irradiance (Jones et al., 2007; Deschaseaux et al., 2014) and low salinity (Gardner et al., 2016). Oxidative stress is caused by the release of reactive oxygen compounds (ROS) by coral mitochondria and zooxanthellae photosystems (Weis, 2008; Lesser, 2011). The rate of photosynthesis in zooxanthellae increases linearly with photosynthetically active radiation (PAR) until Photosystem II (PS II) becomes saturated (Anderson et al., 1995; Gorbunov et al., 2001; Winters et al., 2003). Beyond this threshold, excess light energy is dissipated as heat *via* various photoprotective mechanisms (Melis, 1999; Gorbunov et al., 2001). However, when not all excess light energy is dissipated, photodamage can occur to PS II, inhibiting electron transport and damaging protein structure. High SST can exacerbate irradiance stress by lowering the PAR absorption capacity (Jones et al., 2000; Jones et al., 2002). Accumulating photodamage results in the release of ROS into coral tissues (Weis, 2008; Lesser, 2011) and if conditions persist, can result in corals expelling their zooxanthellae and becoming bleached (Downs et al., 2002; Yakovleva et al., 2009).

Irradiance stress can be exacerbated in corals when exposed to air at low tide (Buckee et al., 2020). During aerial exposure, corals produce a layer of mucous which has been reported to contain up to 54 µmol DMSP and 18 µmol DMS (Broadbent &

Jones, 2004). Given the strong concentration gradient between coral mucous and the atmosphere, large plumes of DMS can be exchanged directly from the coral surface to the atmosphere (Andreae et al., 1983; Jones et al., 2007; Hopkins et al., 2016; Swan et al., 2017). This mechanism of direct coral-air DMS flux distinguishes coral reefs from open ocean regions, where DMS flux is solely driven by diffusive mixing across the sea-air interface (Yang et al., 2011).

DMS_a concentrations above aerially exposed coral reefs can exceed 500 ppt (~23 nmol m^{-3}) (Jones et al., 2007), and on one occasion reached 1122 ppt (45.9 nmol m^{-3}). The latter was measured over Heron Island in the southern GBR in the winter of 2013, when the coral was apparently osmotically and thermally shocked by rainfall while exposed to air at low tide (Swan et al., 2017). These plumes of DMS_a can persist for around eight hours and are significantly more concentrated than the background DMS_a signal, which seasonally averages ~25 ppt (1 nmol m^{-3}) in winter to ~100 ppt (4 nmol m^{-3}) in summer (Swan et al., 2017).

DMS(P) can alleviate oxidative stress in corals by scavenging ROS and forming dimethyl sulfoxide (DMSO) (Deschaseaux et al., 2014; Jones & King, 2015). When oxidative stress exceeds coral thermal stress thresholds, DMS(P) oxidation increases and a decline in ambient DMS_w concentration occurs (Jones et al., 2007; Fischer & Jones, 2012; Deschaseaux et al., 2014). DMS(O) may also be formed *via* photoreactions at the sea surface (Gabric et al., 2008; Galí et al., 2013) and by algal and microbial metabolic processes (Spiese et al., 2009; Bourne et al., 2016), highlighting the complexity in the cycling of dimethylated sulfur compounds. The concentration of DMS in coral reef waters is therefore dependent on the rate of DMS(P)(O) biosynthesis, which is often related to coral oxidative stress.

Ocean warming poses one of the greatest threats to coral reefs (Ainsworth et al., 2016; Hughes et al., 2019). In addition to more frequent and severe coral bleaching events, warmer oceans may lead to a change in DMS production and emissions (Jackson et al., 2020). Given that DMS(P) production in the coral holobiont is upregulated in response to thermal stress (Raina et al., 2013), rising SST could increase coral DMS(P) biosynthesis. However, dissolved DMS concentrations have been found to decline when coral physiological stress thresholds are exceeded (Jones et al., 2007; Fischer and Jones, 2012), possibly due to a coral antioxidant response where DMS (P) scavenge reactive oxygen to form DMSO (Deschaseaux et al., 2014). Therefore, rising SST may increase stress-induced production of DMS(P), followed by oxidation to DMSO in temperature sensitive coral species, leading to a decline in ambient DMS concentrations and emissions. A decline in DMS emissions could be further exacerbated by increased coral bleaching and mortality. Conversely, if coral reefs are able to acclimate to rising ocean temperatures *via* natural or assisted means, such as the recruitment of temperature-tolerant zooxanthellae species (Berkelmans & Van Oppen, 2006; Bay et al., 2016), coral reef DMS emissions may not change significantly at all.

Here, we explore the impact of changes in SST, PAR and wind speed on DMS_w and DMS emissions from the GBR by the end of this century. A linear regression (described in Jackson et al., 2021) is used to calculate DMS_w, and the parameterisation of Liss and Slater (1974) is used to calculate DMS sea-air flux for a contemporary (2001-2020) and two end of century (2081-2100) scenarios, as simulated by Coupled Model Intercomparison Project Phase 6 (CMIP6) models under a SSP2-4.5 and SSP5-8.5 Shared Socioeconomic Pathway (SSP) (Moss et al., 2010; Gidden et al., 2019). The SSP2-4.5 scenario assumes a medium positive radiative forcing by 2100 (~4.5 W m^{-2}) (Fricko et al., 2017), while the SSP5-8.5 scenario assumes a high positive radiative forcing by 2100 (~8.5 W m^{-2}) (Kriegler et al., 2017). The influence of the predicted change in DMS emissions on the regional atmosphere is then discussed.

2 Methods

2.1 Calculation of seawater DMS concentration

The GBR spans 2,300 km of the north-eastern Australian coastline, with the Great Barrier Reef Marine Park (GBRMP) covering an area of approximately 347,000 km^2. DMS_w and DMS sea-air flux is calculated for the GBRMP region (10.5-25°S; 142-154°E) shown in Figure 1.

Jackson et al. (2021) used a multiple linear regression to predict DMS_w (Eq. 1.1) from measurements taken during Marine National Facility RV *Investigator* voyage IN2016_V06 (RVI) from September to October 2016 in the southern and central GBR. The RVI voyage was undertaken as part of the Australian Research Council Discovery Project 'The Great Barrier Reef as a significant source of climatically relevant aerosol particles'. The regression is used to calculate DMS_w (nmol L^{-1}) concentration from standardized SST and daily total PAR at 5 m (Eq. 1.1).

$$DMS_w = 0.10\ SST^2 + 0.34\ SST + 0.14\ PAR^2 + 0.12\ PAR + 1.28 \quad (1.1)$$

Water clarity affects the amount of solar irradiance which penetrates the sea surface and is accounted for by reducing surface PAR by the corresponding diffuse attenuation coefficient (k_{490}: m^{-1}) for a depth of 5 m (where PAR at 5 m=PAR×$e^{-5\ k_{490}}$). This depth was chosen because DMS_w samples were taken between 0-5 m during the RVI surveys. The regression derived in Jackson et al. (2021) explained 71% of the variance in observed DMS_w ($p<0.001$, n=24) and reproduced seasonal and spatial (reef flat versus lagoon) variability in observed concentrations moderately well for the GBR (summarised in

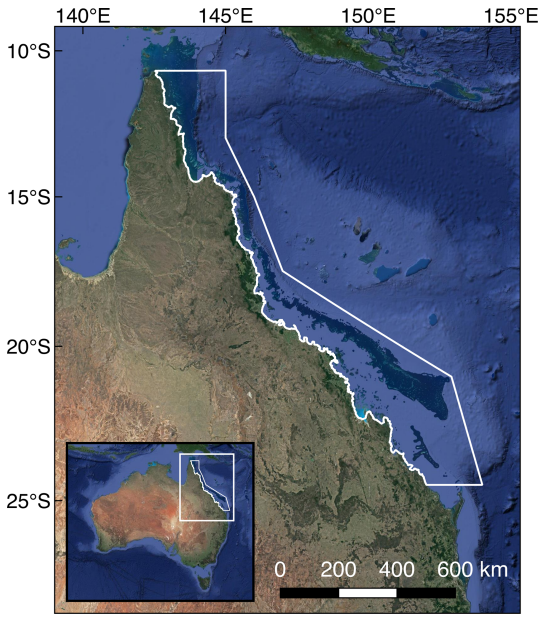

FIGURE 1
Map of north-eastern Australia, showing the boundary of the Great Barrier Reef Marine Park for which the change in each variable was investigated (white outline). Base map © Google Earth 2020.

Jones et al., 2018). The calculated DMS_w climatology represents average seawater surface DMS concentration derived from corals, algae and other DMS producing organisms in GBR waters.

DMS_w in coral reefs does not linearly increase with SST when corals experience high levels of thermal stress (Jones et al., 2007; Fischer & Jones, 2012). To account for this, a coral thermal stress threshold was calculated as 1°C above the local climatological maximum monthly mean (MMM) SST (i.e. the warmest monthly average SST) (Liu et al., 2006). SST anomalies above the MMM+1°C threshold can be used to calculate accumulated coral thermal stress and predict the risk of coral bleaching using metrics such as Degree Heating Weeks (DHW) (Liu et al., 2006) or the Light Stress Index (Skirving et al., 2018). Ecologically significant coral bleaching typically occurs when DHW > 4°C-weeks (where SST has remained 1°C above the MMM for four consecutive weeks, or 4°C above the MMM for 1 week). Several studies have shown that indices calculated from the MMM+1°C threshold can predict the extent and severity of coral bleaching well in the GBR (Bainbridge, 2017; Hughes et al., 2018; Skirving et al., 2018). Therefore, the MMM+1°C threshold can be used as a good indication of coral thermal stress.

Corals are assumed to be experiencing thermal stress (but not necessarily bleaching) when SST ≥ MMM+1°C (Liu et al., 2006). When corals are thermally stressed, reactive oxygen concentrations can increase (Lesser, 2011). DMS(P) scavenge ROS, forming DMSO (Deschaseaux et al., 2014), which can result in a decline in ambient DMS concentrations (Jones et al., 2007). We therefore assume that for days when SST ≥ MMM+1°C DMS_w no longer continues to increase with SST.

To avoid overestimating DMS_w on days when this threshold was exceeded, the SST terms in Eq. 1.1 were replaced with the calculated coral thermal stress threshold (MMM+1°C) (Eq. 1.2). Calculated DMS_w may still vary with PAR on these days. Capping the influence of SST on calculated DMS_w reduced daily mean concentration by less than 0.1 nmol L^{-1}.

$$DMS_w = 0.10\ \ threshold^2 + \ 0.34\ \ threshold + \ 0.14\ \ PAR^2 + 0.12\ \ PAR + 1.28 \qquad (1.2)$$

The coral thermal stress threshold was recalculated for the contemporary and each end of century climate scenario, making an optimistic assumption that corals will acclimate to rising ocean temperatures. The coral thermal stress threshold for the contemporary period ranged from 26.8°C in the southern GBR to 31.0°C in the northern GBR (mean 28.9°C), and was most commonly exceeded between late January to March. For the end of the century, the coral thermal stress threshold ranged from 28.7-32.6°C (mean 30.7°C) for the SSP2-4.5 scenario and from 30.2-34.1°C (mean 32.2°C) for the SSP5-8.5 scenario.

It is assumed that the empirical relationship derived between DMS_w, SST and PAR in the southern and central GBR can be used to estimate DMS_w beyond the region for which Eq. 1 was defined. We acknowledge that this may not be an accurate representation of DMS_w in the northern GBR or under future climate scenarios, however further research is needed to establish the validity of the observed relationship in other regions and time-periods. Further, the ability of corals to acclimate to rising SST, ocean acidification, sea-level rise, changes in water quality and ecosystem structure are uncertain, and we do not attempt to assume how corals will respond to such changes here. The purpose of this analysis is to investigate how predicted changes in SST, PAR and wind speed may affect contemporary DMS_w and sea-air flux from the GBR.

2.2 Calculation of DMS sea-air and coral-air flux

2.2.1 DMS sea-air flux

DMS sea-air flux was calculated as a function of wind speed at 10 m (U_{10}), SST and calculated DMS_w. DMS concentration is typically several orders of magnitude lower in the atmosphere than at the sea surface. Therefore, DMS sea-air flux is calculated as the product of the total gas transfer velocity (K_w: cm hr^{-1}) and the concentration of DMS at the sea surface (C_w: nmol L^{-1}) using Eq. 2 (Liss & Slater, 1974). Sea-air flux is then converted from units of µmol cm^{-2} hr^{-1} to µmol m^{-2} d^{-1}.

$$Flux = K_w C_w \quad (2)$$

DMS sea-air flux is calculated using two parameterisations for K_w. The water-side transfer velocity (k_w) parameterisation of Nightingale et al. (2000) was derived for carbon dioxide and is normalized to the SST-dependent Schmidt number of 660 for DMS (Sc_{DMS}), calculated as follows: Sc_{DMS}=2674−147.2 SST+ 3.726 SST^2−0.038 SST^3 (Saltzman et al., 1993). For this parameterisation, k_w increases with U_{10} (Eq. 3).

$$k_w = \left(0.222\ U_{10}^2 + 0.333\ U_{10}\right)\left(Sc_{DMS}/600\right)^{-0.5} \quad (3)$$

K_w is then calculated using Eq. 4 (McGillis et al., 2000; Nightingale et al., 2000). The atmospheric gradient fraction (γ_a) is defined by $\gamma_a = 1/(1+ k_a/\alpha k_{w,600})$ (McGillis et al., 2000), where α is the solubility coefficient for DMS (11.4 at 26°C) and k_a is the airside transfer velocity, calculated as a function of U_{10} and the molecular weight of DMS and water as follows: $k_a = 659\ U_{10}\ (62.13/18.02)^{-0.5}$ (Kondo, 1975)

$$K_w = k_w(1 - \gamma_a) \quad (4)$$

The second parameterization of k_w provides a more conservative estimate of K_w, by accounting for non-linearity in the DMS transfer velocity at high wind speeds (> 10 m s^{-1}). This is done by including an attenuation of the Henry's Law constant (H_{atten}) calculated using Eq. 5 (Vlahos & Monahan, 2009). H is the Henry's Law constant in seawater (0.089) (Przyjazny et al., 1983), ϕ_B is the surface area of bubbles under the sea surface given by ϕ_B=0.09 $(U_{10}/10)^3$ and C_{mix}/C_w is the solubility enhancement of DMS (~40) from Vlahos and Monahan (2009).

$$H_{atten} = H/1 + \phi_B(C_{mix}/C_w) \quad (5)$$

K_w is then calculated using Eq. 6 as a function of H_{atten}, $k_w = 4\times10^{-4} + 4\times10^{-5}(U_{10})^2$ and $k_a = 0.2\ U_{10}+0.3$ (Schwarzenbach et al., 2005; Vlahos & Monahan, 2009). The parameterizations of k_w and k_a are given in units of cm s^{-1} and are converted to cm hr^{-1} in order to calculate the total DMS transfer velocity (Eq. 6).

$$K_w = \left(\frac{1}{k_w} + \frac{1}{k_a H_{atten}}\right)^{-1} \quad (6)$$

2.2.2 DMS sea-air + coral-air flux

Current DMS sea-air flux parameterisations do not account for direct coral-air DMS flux from corals that are exposed to air at low tide. This is an important, albeit intermittent, source of DMS_a over coral reefs. Hopkins et al. (2016) estimate that *Acropora* corals exposed to air for an average of 12 hours per month release 9-35 µmol m^{-2} d^{-1} (mean 22 µmol m^{-2} d^{-1}). Given that *Acropora* are the dominant coral genus in the GBR, we add a fraction of the mean estimate to the DMS sea-air flux (Eq. 2), scaled by the percentage cover of coral reefs within each grid cell (where DMS flux= K_wC_w +[0.22×reef cover]). The fraction of reef cover was calculated as the number of reef pixels within a 0.25-degree grid (as determined in Jackson et al., 2021), using a database of coral reef locations obtained from ReefBase (https://www.reefbase.org) and MATLAB R2020a. Inclusion of the direct coral-air DMS flux estimate added 0.2-7.7 µmol m^{-2} d^{-1} (mean 1.6 µmol m^{-2} d^{-1}) to the calculated DMS sea-air flux from coral reefs in the GBR.

The approach used to estimate coral-air DMS flux is limited because it assumes that *Acropora* spp. are the sole source of direct coral-air DMS flux and it does not account for seasonal, diurnal or spatial variability in the extent of coral exposure, or the complexity of the reef environment (Hopkins et al., 2016). Further research is needed to reduce the uncertainty in this estimate and to accurately scale laboratory-derived fluxes to the natural coral reef environment. Nevertheless, inclusion of coral-air DMS flux improves the representation of coral reefs in DMS flux climatologies.

2.3 CMIP6 model output

CMIP6 model output was obtained from the Australian Community Climate and Earth-System Simulator Coupled Model (ACCESS-CM2) (Dix et al., 2019) and the ACCESS Earth System Model (ACCESS-ESM 1.5) (Ziehn et al., 2019) for the CMIP6 historical, SSP2-4.5 and SSP5-8.5 experiments. For the historical simulations, solar variability, volcanic aerosols and anthropogenic-driven changes in atmospheric composition (greenhouse gases and aerosol) are forced by datasets which are largely based on observations up to 2014 (Eyring et al., 2016). For the SSP scenario experiments, variables are simulated from 2015 onwards under the respective SSP trajectories. Model output from both models was used to ensure that data for all required physical and biological variables was available. These data are available from the Earth System Grid Federation (https://esfg-node.llnl.gov/search/cmip6/).

ACCESS-CM2 is a global physical climate model, consisting of the Met Office physical atmosphere Unified Model (UM) version 10.6 (Walters et al., 2019), the Modular Ocean Model version 5 (MOM5), the Community Atmosphere Biosphere Land Exchange version 2.5 (CABLE2.5) land surface model and the CICE5 sea ice model, coupled by the OASIS3-MCT numerical coupler. A detailed description of the ACCESS-CM2 configuration is provided in Bi et al. (2020). ACCESS-ESM 1.5 consists of a previous version of ACCESS (ACCESS 1.3), which uses the CABLE version 2.4 land surface model, along with coupled terrestrial (CASA-CNP) and ocean biogeochemistry (WOMBAT) models (Ziehn et al., 2020). ACCESS model output for CMIP6 historical simulations predicted spatial and interannual variability in observations and reanalysis data well for a range of variables, including over the Australian region (Bodman et al., 2020; Ziehn et al., 2020). Therefore, the ACCESS-CM2 and ACCESS-ESM1.5 model output was chosen for this analysis.

Atmospheric variables are resolved at a horizontal resolution of 1.25° latitude x 1.875° longitude, with 38 vertical levels for ACCESS-ESM1.5 and 85 vertical levels for ACCESS-CM2. Oceanic variables are resolved at a horizontal resolution of 1°, with 50 vertical levels. Each model provided various ensembles and model run variations. For this analysis, the most commonly available r1i1p1f1 ensemble is used for each scenario.

Model output was obtained for the GBRMP region (Figure 1) for the contemporary (2001-2020) and end of century (2081-2100) time periods. SST and wind speed at 10 m were downloaded at daily frequency. While using daily mean wind speed to calculate DMS sea-air flux can average out the influence of high wind speeds, daily mean wind speed was used to calculate flux consistently across all model scenarios, allowing the relative change in DMS sea-air flux to be determined. Downwelling shortwave radiation at the sea surface (SWR: W m^{-2}), chlorophyll-*a* at 5 m depth (CHL: mg m^{-3}) as a proxy for water clarity, and cloud cover (%) were downloaded at the provided monthly frequency. SWR was used to estimate total daily PAR (mol m^{-2} d^{-1}), using a conversion factor of 2.1 µmol m^{-2} s^{-1} PAR per W m^{-2} of total SWR (Howell et al., 1983). Monthly mean variables were linearly interpolated to a daily mean time-series at each pixel.

Data for k_{490} was not available from the two ACCESS models. Satellite-derived k_{490} products are derived from the normalized water-leaving radiance at 490 nm and 555 nm, calculated from top-of-atmosphere radiances in the absence of atmospheric perturbations (Wang et al., 2009). Given that k_{490} values in the GBR are typically less than 0.05 m^{-1}, the attenuation of PAR at 5 m is less than 10 mol m^{-2} d^{-1}. We derive a simple linear regression to predict k_{490} from CHL using a 20-year climatology of Moderate Resolution Imaging Spectroradiometer (MODIS) Aqua and Terra observations, area-averaged over the GBR (Eq. 7). The regression accounted for 73.5% ($p<0.001$, n=365) of the variance in MODIS k_{490} and is used to estimate k_{490} at each pixel for the contemporary and end of century CMIP6 model output. Calculated k_{490} is then used to derive daily total PAR at 5 m (henceforth PAR).

$$k_{490} = 0.07 \ \ CHL + 0.02 \tag{7}$$

The coarse resolution model output was linearly interpolated to a 0.25-degree grid (for consistency with Jackson et al., 2021) to enable spatiotemporal variability in each variable to be investigated, including along coastal regions. A multi-model average of each variable was then calculated and used to calculate a climatology of DMS_w (Eq. 1) and DMS flux (Eq. 2 + coral-air DMS flux) for the contemporary and end of century scenarios. The model source of each variable is listed in Table 1.

2.4 Remotely sensed observations

The historical CMIP6 model output was compared with a climatology of MODIS observations and ERA-5 reanalysis data (2001-2020) to evaluate how well the models predicted each variable for the GBR region. Daily mean SST, PAR, k_{490} and cloud cover were obtained from the MODIS sensor aboard the Aqua and Terra satellites, which both pass over the GBR at approximately noon local time (UTC+10 hr). A daily average at each pixel was calculated from the Aqua and Terra observations (n=7300). SST, PAR and k_{490} were downloaded at 0.04-degree resolution from NASA OceanColor (https://oceancolor.gsfc.nasa.gov). Cloud cover was downloaded at 1-degree resolution from the NASA Level-1 Atmosphere and Distribution System (http://laadsweb.modaps.eosdis.nasa.gov). Light attenuation at the surface was accounted for by reducing PAR by the corresponding k_{490} value for a depth of 5 m. Daily mean wind speed at 10 m was calculated from hourly ERA-5 100 m u- and v-wind vector components (Copernicus Climate Change Service, 2019). An area-average of each variable was calculated for the GBRMP region shown in Figure 1.

2.5 Analysis

The change in annual and seasonal mean SST, PAR, cloud cover (to investigate change in PAR), k_{490}, wind speed, K_w, DMS_w and DMS flux between the contemporary (2001-2020) and end of century (2081-2100) climatologies was investigated for the GBRMP (Figure 1). A contemporary climatology for each variable was calculated from CMIP6 historical model output from 2001 to 2014, extended to 2020 using an average of the SSP2-4.5 and SSP5-8.5 model output. Two end of century (2081-2100) climatologies were calculated for each variable under the respective SSP scenario.

3 Results

3.1 Comparison of model output and remotely sensed observations

To ensure the models adequately simulated contemporary conditions in the GBR, the CMIP6 contemporary climatology was

TABLE 1 CMIP6 models and output used in this analysis.

Institute	Model	Variable
Commonwealth Scientific and Industrial Research Organisation (CSIRO)	ACCESS-ESM 1.5	SST, SWR, Cloud, CHL, wind speed
CSIRO and Australian Research Council Centre of Excellence for Climate System Science	ACCESS-CM2	SST, SWR, Cloud, wind speed

compared with MODIS-derived SST, PAR at 5 m and cloud cover, and ERA-5 reanalysis wind speed data for the same time period (Figure 2). The CMIP6 model average overestimated MODIS-derived SST by approximately 1°C from February to September, underestimated PAR by up to 10 mol m^{-2} d^{-1} from October to May, and underestimated cloud cover by approximately 10% (Figure 2). The model average overestimated ERA-5 wind speed by approximately 1 m s^{-1} (Figure 2). The differences between the modelled and observed data are small in magnitude (< 20%), and are likely consistent between contemporary and future time periods. It is therefore assumed that the models simulated the relevant variables with enough confidence for this study.

3.2 Change in modelled SST, PAR, U_{10} and cloud cover

By the end of the century, annual mean SST increased by a respective 1.5°C (5.7%) and 3.0°C (11.4%) for the SSP2-4.5 and SSP5-8.5 scenarios (Table 2). The change in SST was relatively consistent year-round (Figure 3A), with minimal spatial variability (< 0.8°C) in the annual and seasonal mean change for the GBRMP (Supplementary Information Figure 1).

Annual mean PAR increased by a respective 1.1 mol m^{-2} d^{-1} (3.1%) and 1.7 mol m^{-2} d^{-1} (4.8%) for the SSP2-4.5 and SSP5- 8.5 scenarios (Table 2). The increase in PAR (Figure 3B) coincided with a decrease in cloud cover (Figure 3C) and k_{490} (Figure 3D). The change in annual and seasonal PAR was most pronounced in the southern half of the GBR (Supplementary Information Figure 2), following the zonal changes in cloud cover (Supplementary Information Figure 3) and k_{490} (Supplementary Information Figure 4). Annual mean cloud cover decreased by a respective 3.0% and 6.8% for the SSP2-4.5 and SSP5-8.5 scenarios (Table 2). Annual mean k_{490} decreased by < 0.015 m^{-1} by 2100 (Table 2; Figure 3D), which for a given depth of 5 m, contributed up to 7% of the predicted change in PAR.

The change in annual mean wind speed was minimal (<0.1 m s^{-1}) (Table 2; Figure 3E), but showed opposing seasonal trends. Wind speed increased throughout the GBR in winter, yet decreased in summer in the southern GBR under the SSP2-4.5 scenario, extending throughout the GBR under the SSP5-8.5 scenario (Supplementary Information Figure 5). The change in K_w was also minimal (<0.4 cm hr^{-1}) (Table 2; Figure 3F), with spatial changes (Supplementary Information Figure 6) that approximately correspond to those for wind speed.

In ACCESS, DMS sea-air flux is simulated using the Liss and Merlivat (1986) parameterisation, using monthly varying DMS_w concentrations prescribed by the Lana et al. (2011) climatology and evolving wind speed and SST. While DMS_w concentration does not change between model years, DMS sea-air flux can evolve with changes in SST and wind speed. Previous model studies have demonstrated that large perturbations in DMS sea-air flux do not substantially influence cloud cover or surface SWR in ACCESS (Fiddes et al., 2018). Therefore, we can assume that the influence of evolving DMS sea-air flux between the contemporary and end of century scenarios has a negligible influence on modelled cloud cover, PAR, SST and calculated DMS_w. While it has been hypothesised that DMS emissions can influence cloud properties (Fischer & Jones, 2012; Jones, 2015; Jones et al., 2017), the change in cloud cover is only reported here to investigate changes in surface PAR.

3.3 Change in calculated DMS_w

For the contemporary scenario, annual mean DMS_w area-averaged over the GBR was 1.52 ± 0.02 nmol L^{-1} (Table 2), ranging

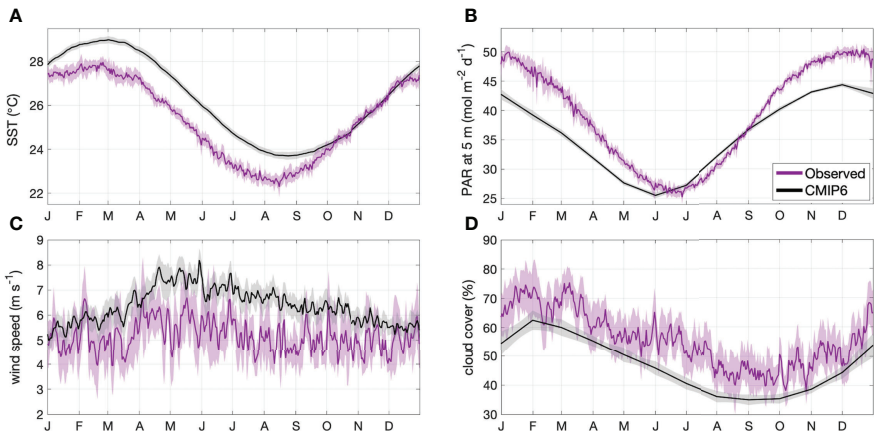

FIGURE 2
Area-averaged climatology ± 2 SE (shaded area) of contemporary (2001-2020) **(A)** SST, **(B)** PAR at 5 m, **(C)** wind speed and **(D)** cloud cover for the GBRMP. Climatologies are calculated from MODIS or ERA-5 reanalysis data (magenta) and CMIP6 model output (black).

TABLE 2 Climatological annual mean (± 2 standard errors) and range for variables area-averaged over the GBRMP for the contemporary (2001-2020) and end of century (2081-2100) scenarios.

	Annual mean			Annual range		
	Contemporary	**SSP2-4.5**	**SSP5-8.5**	**Contemporary**	**SSP2-4.5**	**SSP5-8.5**
SST	26.3 ± 0.1	27.8 ± 0.1	29.3 ± 0.1	23.7 – 29.0	25.2 – 30.8	26.6 – 32.3
PAR	35.6 ± 0.2	36.7 ± 0.2	37.3 ± 0.2	25.5 – 44.4	26.4 – 45.4	27.0 – 45.5
Cloud cover	46.5 ± 1.0	43.5 ± 1.0	39.7 ± 1.0	35.0 – 62.5	33.0 – 59.0	30.9 – 53.7
k_{490}	0.03 ±5.0x10^{-4}	0.03 ± 4.3x10^{-4}	0.03 ± 3.0x10^{-4}	0.02 – 0.05	0.02 – 0.04	0.02 – 0.04
wind speed	6.4 ± 0.2	6.4 ± 0.3	6.4 ± 0.3	5.0 – 8.2	5.2 – 8.0	4.8 – 8.3
K_w	9.2 ± 0.6	9.6 ± 0.6	9.6 ± 0.6	6.1 – 13.7	6.9 – 13.8	6.1 – 14.8
DMS_w	1.52 ± 0.02	1.66 ± 0.02	1.74 ± 0.02	0.99 – 2.03	1.05 – 2.29	1.13 – 2.34
DMS flux	4.2 ± 0.2	4.6 ± 0.2	4.8 ± 0.3	2.9 – 6.2	3.2 – 7.0	3.4 – 6.9

Units are as follows: SST (°C), PAR (mol m^{-2} d^{-1}), cloud cover (%), k_{490} (m^{-1}), wind speed (m s^{-1}), K_w (cm hr^{-1}), DMS_w (nmol L^{-1}) and DMS flux (µmol m^{-2} d^{-1}).

from 0.99 ± 0.003 nmol L^{-1} in winter to 2.03 ± 0.02 nmol L^{-1} in summer (Figure 4). By the end of the century, annual mean DMS_w increased by a respective 0.14 nmol L^{-1} (9.2%) and 0.22 nmol L^{-1} (14.5%) for the SSP2-4.5 and SSP5-8.5 scenarios. Seasonal changes ranged from a 6.1%-14.1% (SSP2-4.5 - SSP5-8.5) increase in the winter minimum, and a 12.8%-15.3% (SSP2-4.5 - SSP5-8.5) increase in the summer maximum concentration (Table 2; Figure 4). There was minimal spatial variability in the contemporary annual and seasonal mean DMS_w (<0.4 nmol L^{-1}), and in changes in DMS_w by the end of this century (<0.1 nmol L^{-1}) (Figure 5).

The sensitivity of calculated DMS_w to SST and PAR was 0.013 and 0.003, respectively, where a 1% increase in SST or PAR resulted in a respective 1.3% or 0.3% increase in DMS_w. Annual mean SST increased by 5.7-11.4% (Table 2), driving > 95% of the change in calculated DMS_w. Annual mean PAR increased by 3.1-4.8% (Table 2), contributing < 5% to the change in DMS_w. Calculated DMS_w was highest from February to March for all climate scenarios, when SST is highest and the calculated coral thermal stress threshold was most often exceeded. During days when this threshold was exceeded, the influence of SST was capped at the thermal stress threshold (Eq. 1.2), resulting in a plateau in the calculated summer DMS_w concentration.

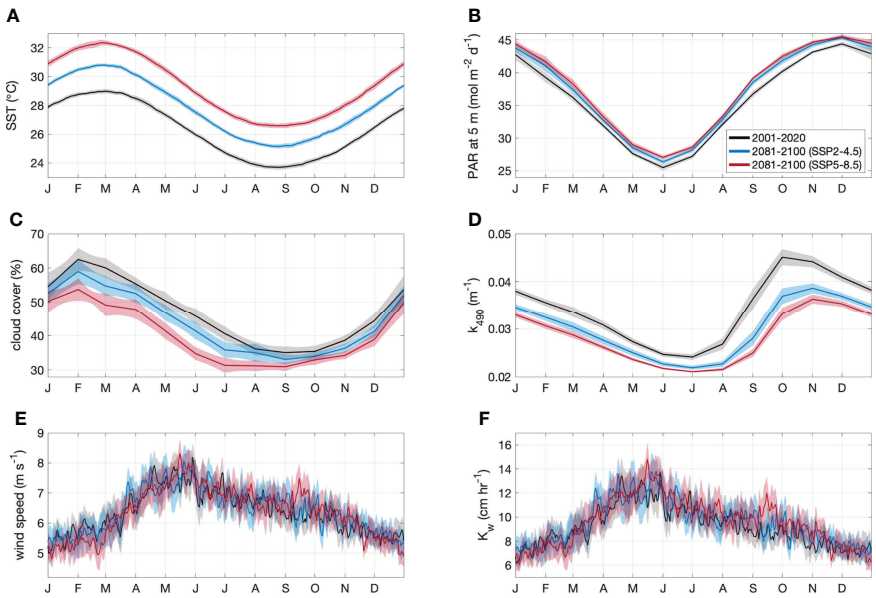

FIGURE 3
Area-averaged climatology ± 2 SE (shaded area) of **(A)** SST, **(B)** PAR at 5 m, **(C)** cloud cover, **(D)** k_{490}, **(E)** wind speed and **(F)** K_w for the GBRMP. Climatologies are derived from CMIP6 contemporary (black) and end of century model output for SSP2-4.5 (blue) and SSP5-8.5 (red) scenarios.

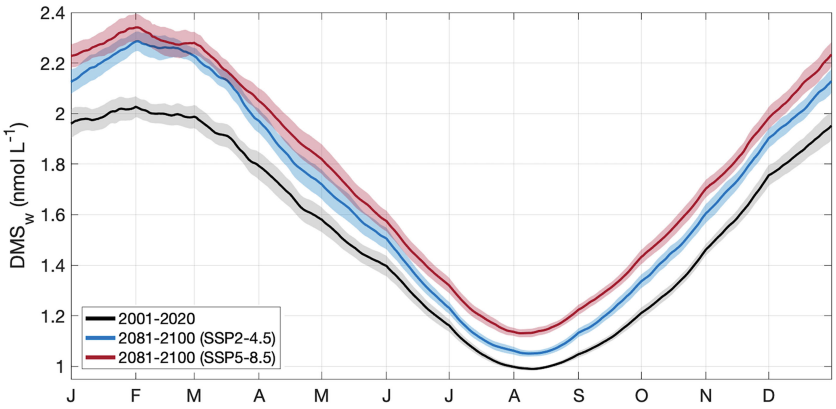

FIGURE 4
Area-averaged climatology ± 2 SE (shaded area) of DMS$_w$ in the GBRMP, derived from CMIP6 contemporary (black) and end of century model output for SSP2-4.5 (blue) and SSP5-8.5 (red) scenarios.

3.4 Change in calculated DMS sea-air flux

For the contemporary scenario, annual mean DMS flux was 4.2 ± 0.2 µmol m^{-2} d^{-1} (Table 2), ranging from 2.9 ± 0.1 µmol m^{-2} d^{-1} in winter to 6.2 ± 0.3 µmol m^{-2} d^{-1} in summer (Figure 6). Annual and seasonal mean DMS flux was consistently highest over coral reefs in the GBR (up to 12.6 mol m^{-2} d^{-1}) (Figure 7) due to the addition of direct coral-air DMS flux, which is an important source of emissions leading to significantly higher DMS$_a$ concentrations over coral reefs (Jones et al., 2007; Swan et al., 2017). By the end of the century, annual mean DMS flux increased by a respective 0.4 µmol m^{-2} d^{-1} (9.5%) and 0.6 µmol m^{-2} d^{-1} (14.3%) for the SSP2-4.5 and SSP5-8.5 scenarios (Table 2; Figure 6). Minimal spatial variability occurred for the change in DMS flux (<0.8 µmol m^{-2} d^{-1}) under these future scenarios (Figure 7).

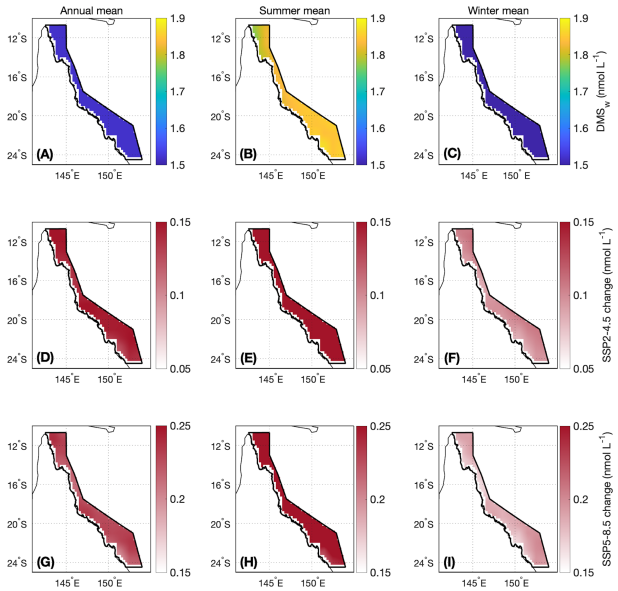

FIGURE 5
Contemporary **(A)** annual, **(B)** summer (November-April) and **(C)** winter (May-October) mean DMS$_w$ and the change in **(D, G)** annual, **(E, H)** summer and **(F, I)** winter mean DMS$_w$ by the end of this century modelled under a (middle panels) SSP2-4.5 and (lower panels) SSP5-8.5 scenario. The boundary of the GBRMP for which the area-averaged climatologies are calculated is shown as the bold black outline in each panel. Note that the colour scales differ between the SSP2-4.5 and SSP5-8.5 changes.

From the mean of the Nightingale et al. (2000) and Vlahos and Monahan (2009) parameterisations (Figure 6), contemporary DMS emissions from the GBR range from 0.028-0.038 Tg yr^{-1} of DMS (1297-1771 mol km^2 yr^{-1}). For the SSP2-4.5 and SSP5-8.5 end of century scenarios, DMS emissions are respectively estimated to be 0.030-0.043 Tg yr^{-1} of DMS (1403-1990 mol km^2 yr^{-1}) and 0.031-0.045 Tg yr^{-1} (1435-2086 mol km^2 yr^{-1}), representing a 7.1-13.2% and 10.7-18.4% increase in total annual DMS emissions.

DMS sea-air flux was calculated from DMS_w (Eq. 1) and K_w (a function of SST and wind speed, Eq. 4 and Eq. 6). The sensitivity of DMS flux to DMS_w, SST and wind speed was 0.008, 0.003 and 0.015, respectively, where a 1% change in DMS_w, SST or wind speed would result in a respective 0.8%, 0.3% or 1.5% change in DMS sea-air flux. Annual mean DMS_w increased by 9.2-14.5%, SST increased by 5.7-11.4% and wind speed changed by less than 0.1%. Therefore, the change in DMS_w, SST and wind speed contributed up to 77.5%, 23.9% and 1.0% of the change in annual mean DMS flux. Given that DMS_w is almost entirely dependent on SST (> 95%) and K_w is partially dependent on SST, more than 97.5% of the change in calculated DMS flux is driven by changes in SST, with the remaining 2.5% driven by changes in PAR (used to calculate DMS_w) and wind speed.

4 Discussion

Annual mean DMS_w in the GBR is estimated to be 1.52 nmol L^{-1}. The predicted rise in SST and PAR under an optimistic (SSP2-4.5) and worst-case (SSP5-8.5) end of century scenario may increase average DMS_w concentration in the GBR by a respective 9.2% and 14.5%. DMS_w was calculated as a function of SST and PAR, which respectively increased by 5.7-11.4% (SSP2-4.5 - SSP5-8.5), and 3.1-4.8% (SSP2-4.5 - SSP5-8.5). The increase in PAR was in part due to a decrease in and k_{490}, and a decrease in cloud cover which has been predicted to occur in the tropics and subtropics under future greenhouse gas warming (Schneider et al., 2019). The sensitivity of Eq. 1 to SST was greater than PAR and consequently, the increase in SST drove more than 95% of the change in calculated DMS_w.

Contemporary DMS emissions from the GBR ranged from 0.028-0.038 Tg yr^{-1}, equivalent to 0.015-0.020 Tg yr^{-1} of sulfur as DMS. By the end of this century, increased DMS_w concentration and predicted changes in wind speed could increase annual mean DMS emissions by a respective 9.5% and 14.3% under an optimistic (SSP2-4.5) and worst-case (SSP5-8.5) scenario.

In the Southern Hemisphere, the sensitivity of CCN to oceanic DMS sea-air flux is estimated to be 0.07 (Woodhouse

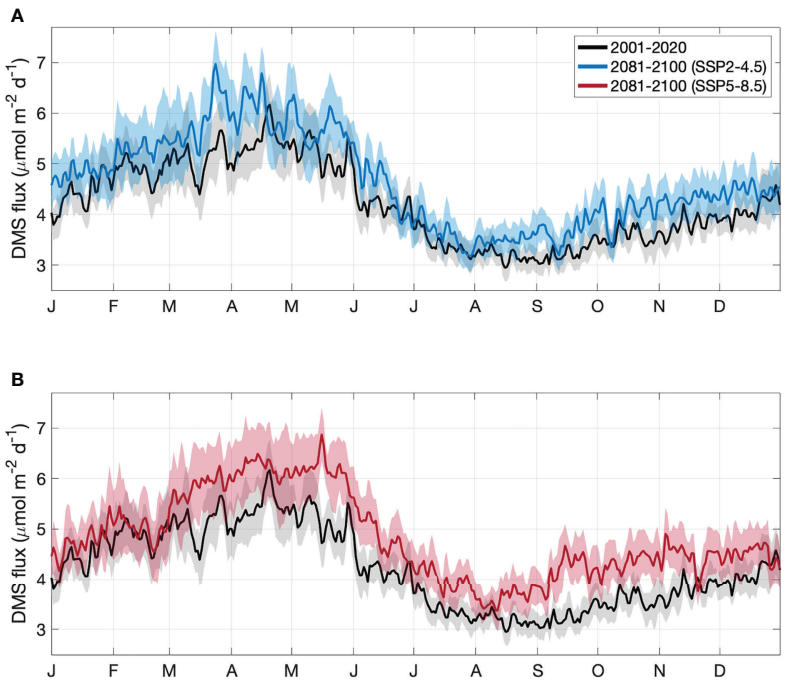

FIGURE 6
Area-averaged climatology of DMS sea-air flux in the GBR, derived from CMIP6 contemporary (black) and end of century model output for the **(A)** SSP2-4.5 (blue) and **(B)** SSP5-8.5 (red) climate.

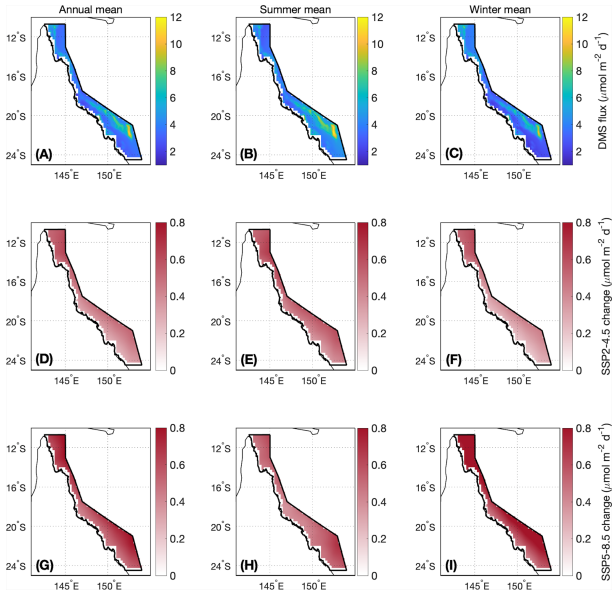

FIGURE 7
As for Figure 5, but for DMS flux.

et al., 2010). From this estimate, the predicted 9.5-14.3% increase in annual mean DMS flux from the GBR could result in only a 0.7-1.0% increase in annual mean CCN. Previous model studies have demonstrated that DMS emissions from coral reefs that are an order of magnitude larger than estimated in the current study (0.3 Tg yr^{-1}), do not significantly influence aerosol or cloud processes (Fiddes et al., 2021; Fiddes et al., 2022). Therefore, a 9.5-14.3% increase in DMS flux is unlikely to influence the regional atmosphere. However, observational studies suggest that local biogeophysical processes in the GBR could be more sensitive to changes in DMS emissions (Jones et al., 2007; Modini et al., 2009; Fischer & Jones, 2012; Jones et al., 2017; Cropp et al., 2018). This is an important question for future research.

Field and laboratory studies have observed an increase in DMS concentration in coral tissues and in reef seawaters with rising SST, until SST exceeds the coral thermal stress threshold (Jones et al., 2007; Fischer & Jones, 2012; Jones et al., 2017). For example, Jones et al. (2007) observed a ~50% decrease in DMS_w when SST exceeded 30°C and caused coral bleaching in the central GBR. The observed decrease in DMS_w may have been due to enhanced biochemical oxidation of DMS(P) to DMSO and a decline in DMS(P) biosynthesis as corals bleached (Jones et al., 2007; Fischer & Jones, 2012). To avoid overestimating calculated DMS_w concentration in this study, a coral thermal stress threshold was calculated and substituted into Eq. 1 for days when SST exceeded the threshold. Imposing an upper limit on the influence of SST on calculated DMS_w reduced calculated concentration by < 0.1 nmol L^{-1}.

Re-calculating the coral bleaching threshold for the end of the century assumes that living corals will be able to cope with rises in SST. This may occur through natural means such as the recruitment of temperature-tolerant zooxanthellae species (Berkelmans & Van Oppen, 2006; Bay et al., 2016), through assisted evolution (Van Oppen et al., 2015) or *via* solar radiation management strategies which can reduce surface irradiance and temperature (Kwiatkowski et al., 2015; Zhang et al., 2017).

If corals do not acclimate to the predicted increase in SST, the frequency of coral bleaching and mortality events will continue to reduce coral cover (Hughes et al., 2019), leading to a decline in coral-derived DMS_w. A decline in coral-derived DMS_w could be exacerbated by increased biochemical oxidation of DMS(P) to DMSO in surviving corals exposed to high temperatures (e.g. Fischer & Jones, 2012). While it is not possible to distinguish between coral and algal-derived DMS_w from observations of dissolved DMS concentration alone, increases in DMS-producing marine algae in degraded coral reef ecosystems (McCook and Diaz-Pilido, 2002; De'ath & Fabricius, 2010) could counteract a decline in coral-derived DMS_w (as discussed in Jackson et al., 2020). More research is required to determine whether corals can acclimate to rising SST and how DMS_w in coral reefs will be affected by changes in surface temperature, irradiance and coral-algal interactions.

Further research is also needed to determine the synergistic impacts of ocean acidification on DMS(P) biosynthesis. In comparison to coral DMS(P) biosynthesis, the impact of ocean acidification on algal DMS(P) production has been relatively well studied (Hopkins et al., 2020). Given that DMS

concentration in coral reef waters is partially driven by algal and microbial cycling of DMSP (Raina et al., 2009), changes in DMS concentration in the GBR may have similar responses to those reported for algal communities.

The impact of ocean acidification on algal DMS(P) production varies with location, season and community structure (Hopkins et al., 2020). In the subtropical North Atlantic, mesocosm experiments revealed a decrease in algal-derived DMS with lower pH due to reduced rates of microbial catabolism of DMSP (Archer et al., 2018). Conversely, the response of surface ocean micro-algae to acidification in the temperature north-western European shelf resulted in 110-225% increases in dissolved DMS concentrations in response to atmospheric CO_2 concentrations of 550-1,000 µatm, respectively (Hopkins & Archer, 2014). Other studies in the Artic and Southern Ocean have reported no significant impacts of short-term ocean acidification on micro-algal DMS production (Hopkins et al., 2020). Further complicating the matter, one study demonstrated that temperature had a stronger influence on DMS production in algae than pH, where increased production in response to temperature outweighed the decline in biosynthesis due to acidification (Arnold et al., 2013). Further research is needed to understand the influence of ocean acidification on DMS(P) biosynthesis in the global ocean and in coral reefs.

Sea level rise and the rate of coral reef vertical accretion is also likely to affect coral physiological stress and DMS emissions. Global mean sea level is predicted to rise by 40-80 cm under an end of century climate (Sanborn et al., 2020). In the late Holocene in the GBR, fast-growing branching corals (such as *Acropora* spp.) grew in relatively shallow, clear waters, which are representative of conditions which are still found in parts of the contemporary GBR. During this time, coral reef vertical accretion occurred at a rate of 0.2-1.1 cm yr^{-1} (mean 0.5 cm yr^{-1}) (Sanborn et al., 2020). Therefore, if sea level rise in the GBR remains below ~1 cm yr^{-1}, coral vertical accretion could keep pace with the rate of sea level rise.

Short-term processes such as El Nino Southern Oscillation (ENSO) can also influence regional sea level. During strong El Nino events, regional sea level in the tropical western Pacific can decline by up to 30 cm, leading to more frequent extreme low tides and coral air exposure (Becker et al., 2012; Widlansky et al., 2015). El Nino events are charactersied by a weakening or reversal of easterly trade winds and subsequent thermocline shoaling in the western Pacific and deepening in eastern Pacific. Regional sea level anomalies typically mirror these thermocline shifts (Widlansky et al., 2015). More frequent and prolonged coral exposure to air could increase direct coral-air DMS flux and concerningly, increase coral oxidative stress. In the western Pacific, El Nino events are associated with clear skies, high solar irradiance and high SST. When combined with increased aerial exposure of corals, these conditions could result in more frequent and severe coral bleaching (Buckee et al., 2020). Alternatively, rising sea levels could facilitate increased coral cover, due to reduced temperature, irradiance and coral physiological stress at depth, and less (if any) aerial exposure of corals at low tide (Brown et al., 2019).

The impacts of climate change on coral reef biogeochemical processes are complex and difficult to predict. This study assumes that corals will acclimate to rising ocean temperatures and predicts that DMS emissions from the GBR will increase as a result. However, further research is needed to understand the effects of temperature, light, ocean acidification, salinity, and changing sea level, water quality and ecosystem structure on DMS production and emissions in coral reefs before the change in DMS emissions by the end of this century can be more accurately determined. Nevertheless, we suggest that ocean warming could increase present-day DMS emissions and the source strength of the GBR to the atmospheric sulfur budget, if corals can acclimate to their changing environment.

5 Conclusions

Coral reefs are important regional sources of DMS, with potential implications for local aerosol and cloud processes. By the end of this century, a 1.5-3.0°C rise in annual mean SST and a 1.1-1.7 mol m^{-2} d^{-1} increase in PAR is predicted to increase calculated DMS_w by a respective 9.2% to 14.5%, leading to an increase in calculated DMS flux of 9.5% to 14.3% under an optimistic and worst-case emissions scenario, as simulated by ACCESS models for CMIP6. Previous model studies using ACCESS have demonstrated little to no sensitivity to larger fluctuations in coral reef DMS emissions. Therefore, a 9.5-14.3% increase in DMS emissions from the GBR is unlikely to significantly influence the regional atmosphere. However, anthropogenic aerosol emissions may decline in future with initiatives to shift towards renewable energy, in which case aerosol-cloud processes may become more sensitive to small changes in DMS flux, particularly at the local scale. Understanding the complex coral reef sulfur cycle and how the atmospheric aerosol system responds to changes in emission will require further research. The predicted increase in DMS_w and DMS flux from the GBR by the end of this century assumes that corals will acclimate to rising SST, and does not account for the impact of ocean acidification, changes to water quality, sea level or other factors associated with climate change. Nevertheless, the findings presented here provide insight into the effects of ocean warming on contemporary DMS emissions from the GBR and the contribution of the GBR to the atmospheric sulfur budget.

Data availability statement

The model output used in this analysis is available from the Earth System Grid Federation (https://esgf-node.llnl.gov/

projects/cmip6/). MODIS sensor observations are available from NASA's OceanColor (https://oceancolor.gsfc.nasa.gov) and Level-1 Atmosphere and Distribution System (https://ladsweb.modaps.eosdis.nasa.gov/). ERA5 u and v-wind vector components are available from the Copernicus Climate Change Service (https://cds.climate.copernicus.eu/).

Author contributions

RJ completed the data analysis and prepared the manuscript. All authors contributed to the interpretation of results, and review and finalisation of the manuscript.

Funding

RJ was supported by an Australian Government Research Training Program Scholarship, Commonwealth Scientific and Industrial Research Organisation post-graduate scholarship, and the Griffith University School of Environment and Science.

Acknowledgments

We gratefully acknowledge the World Climate Research Programme's Working Group on Coupled Modelling, which is responsible for CMIP, and we thank the climate modelling groups listed in Table 1 for producing and making available their model output (Dix et al., 2019; Ziehn et al., 2019). The U.S. Department of Energy's Program for Climate Model Diagnosis and Intercomparison provides coordinating support for CMIP and led development of software infrastructure in partnership with the Global Organization for Earth System Science Portals. We gratefully acknowledge the NASA Goddard Space Flight Center, Ocean Ecology Laboratory, Ocean Biology Processing Group, and associated MODIS mission scientists, for the provision of MODIS ocean color data, and the Copernicus Climate Change Service for wind speed reanalysis data used in this analysis. The work forms part of RJ's PhD thesis, entitled 'Coral reefs as a source of dimethylsulfide (DMS) and the influence on the atmosphere of the Great Barrier Reef', which will be available on the Griffith University online repository (https://research-repository.griffith.edu.au) from 14 June 2023.

Conflict of interest

The authors declare that the research was conducted in the absence of any commercial or financial relationships that could be construed as a potential conflict of interest.

Publisher's note

Supplementary material

The Supplementary Material for this article can be found online at: https://www.frontiersin.org/articles/10.3389/fmars.2022.910420/full#supplementary-material

References

Ainsworth, T. D., Heron, S. F., Ortiz, J. C., Mumby, P. J., Grech, A., Ogawa, D., et al. (2016). Climate change disables coral bleaching protection on the Great Barrier Reef. *Science* 352 (6283), 338–342. doi: 10.1126/science.aac7125

Anderson, J. M., Chow, W. S., and Park, Y.-I. (1995). The grand design of photosynthesis: acclimation of the photosynthetic apparatus to environmental cues. *Photosynthesis Res.* 46 (1), 129–139. doi: 10.1007/BF00020423

Andreae, M. O., Barnard, W. R., and Ammons, J. M. (1983). The biological production of dimethylsulfide in the ocean and its role in the global atmospheric sulfur budget. *Ecological Bulletins* 35, 167–177.

Andreae, M. O., and Crutzen, P. J. (1997). Atmospheric aerosols: Biogeochemical sources and role in atmospheric chemistry. *Science* 276 (5315), 1052–1058. doi: 10.1126/science.276.5315.1052

Andreae, M. O., and Rosenfeld, D. (2008). Aerosol–cloud–precipitation interactions. part 1. the nature and sources of cloud-active aerosols. *Earth-Science Rev.* 89 (1–2), 13–41. doi: 10.1016/j.earscirev.2008.03.001

Archer, S. D., Suffrian, K., Posman, K. M., Bach, L. T., Matrai, P. A., Countway, P. D., et al. (2018). Processes that contribute to decreased dimethyl sulfide production in response to ocean acidification in subtropical waters. *Front. Mar. Sci.* 5. doi: 10.3389/fmars.2018.00245

Arnold, H. E., Kerrison, P., and Steinke, M. (2013). Interacting effects of ocean acidification and warming on growth and DMS-production in the haptophyte coccolithophore E. miliania huxleyi. *Global Change Biol.* 19 (4), 1007–1016. doi: 10.1111/gcb.12105

Bainbridge, S. J. (2017). Temperature and light patterns at four reefs along the Great Barrier Reef during the 2015–2016 austral summer: understanding patterns of observed coral bleaching. *J. Operational Oceanography* 10 (1), 16–29. doi: 10.1080/1755876X.2017.1290863

Bay, L. K., Doyle, J., Logan, M., and Berkelmans, R. (2016). Recovery from bleaching is mediated by threshold densities of background thermo-tolerant symbiont types in a reef-building coral. *R. Soc. Open Sci.* 3 (6), 160322. doi: 10.1098/rsos.160322

Becker, M., Meyssignac, B., Letetrel, C., Llovel, W., Cazenave, A., and Delcroix, T. (2012). Sea Level variations at tropical pacific islands since 1950. *Global Planetary Change* 80, 85–98. doi: 10.1016/j.gloplacha.2011.09.004

Berkelmans, R., and Van Oppen, M. J. H. (2006). The role of zooxanthellae in the thermal tolerance of corals: a 'nugget of hope'for coral reefs in an era of climate change. *Proc. R. Soc. B: Biol. Sci.* 273 (1599), 2305–2312. doi: 10.1098/rspb.2006.3567

Berndt, T., Scholz, W., Mentler, B., Fischer, L., Hoffmann, E. H., Tilgner, A., et al. (2019). Fast peroxy radical isomerization and OH recycling in the reaction of OH

radicals with dimethyl sulfide. *J. Phys. Chem. Lett.* 10 (21), 6478–6483. doi: 10.1021/acs.jpclett.9b02567

Bi, D., Dix, M., Marsland, S., O'Farrell, S., Sullivan, A., Bodman, R., et al. (2020). Configuration and spin-up of ACCESS-CM2, the new generation Australian community climate and earth system simulator coupled model. *J. South. Hemisphere Earth Syst. Sci.* 70 (1), 225–251. doi: 10.1071/ES19040

Bodman, R. W., Karoly, D. J., Dix, M. R., Harman, I. N., Srbinovsky, J., Dobrohotoff, P. B., et al. (2020). Evaluation of CMIP6 AMIP climate simulations with the ACCESS-AM2 model. *J. South. Hemisphere Earth Syst. Sci.* 70, 166–179. doi: 10.1071/ES19033

Bourne, D. G., Morrow, K. M., and Webster, N. S. (2016). Insights into the coral microbiome: underpinning the health and resilience of reef ecosystems. *Annu. Rev. Microbiol.* 70, 317–340. doi: 10.1146/annurev-micro-102215-095440

Broadbent, A. D., and Jones, G. B. (2004). DMS and DMSP in mucus ropes, coral mucus, surface films and sediment pore waters from coral reefs in the Great Barrier Reef. *Mar. Freshw. Res.* 55 (8), 849–855. doi: 10.1071/MF04114

Brown, B. E., Dunne, R. P., Somerfield, P. J., Edwards, A. J., Simons, W. J. F., Phongsuwan, N., et al. (2019). Long-term impacts of rising sea temperature and sea level on shallow water coral communities over a~ 40 year period. *Sci. Rep.* 9 (1), 1–12. doi: 10.1038/s41598-019-45188-x

Buckee, J., Pattiaratchi, C., and Verduin, J. (2020). Partial mortality of intertidal corals due to seasonal daytime low water levels at the houtman abrolhos islands. *Coral Reefs* 39 (3), 537–543. doi: 10.1007/s00338-019-01887-5

Bullock, H. A., Luo, H., and Whitman, W. B. (2017). Evolution of dimethylsulfoniopropionate metabolism in marine phytoplankton and bacteria. *Front. Microbiol.* 8. doi: 10.3389/fmicb.2017.00637

Copernicus Climate Change Service (2019) *ERA5 fifth generation of ECMWF atmospheric reanalyses of the global climate: Hourly u and v-wind components on single levels from 1979 to present*. Available at: https://cds.climate.copernicus.eu/.

Cropp, R. A., Gabric, A. J., van Tran, D., Jones, G., Swan, H., and Butler, H. (2018). Coral reef aerosol emissions in response to irradiance stress in the Great Barrier Reef, Australia. *Ambio* 47 (6), 671–681. doi: 10.1007/s13280-018-1018-y

Dave, P., Patil, N., Bhushan, M., and Venkataraman, C. (2019). "Aerosol influences on cloud modification and rainfall suppression in the south Asian monsoon region," in *Climate change signals and response*. Eds. C. Venkataraman, T. Mishra, S. Ghosh and S. Karmakar (Singapore: Springer), 21–37. doi: 10.1007/978-981-13-0280-0_2

De'ath, G., and Fabricius, K. (2010). Water quality as a regional driver of coral biodiversity and macroalgae on the Great Barrier Reef. *Ecol. Appl.* 20 (3), 840–850. doi: 10.1890/08-2023.1

Deschaseaux, E. S. M., Beltran, V. H., Jones, G. B., Deseo, M. A., Swan, H. B., Harrison, P. L., et al. (2014). Comparative response of DMS and DMSP concentrations in symbiodinium clades C1 and D1 under thermal stress. *J. Exp. Mar. Biol. Ecol.* 459, 181–189. doi: 10.1016/j.jembe.2014.05.018

Deschaseaux, E. S. M., Jones, G. B., Deseo, M. A., Shepherd, K. M., Kiene, R. P., Swan, H. B., et al. (2014). Effects of environmental factors on dimethylated sulfur compounds and their potential role in the antioxidant system of the coral holobiont. *Limnology Oceanography* 59 (3), 758–768. doi: 10.4319/lo.2014.59.3.0758

Dix, M., Bi, D., Dobrohotoff, P., Fiedler, R., Harman, I., Law, R., et al. (2019). CSIRO-ARCCSS ACCESS-CM2 model output prepared for CMIP6. *Earth System Grid Federation*. doi: 10.22033/ESGF/CMIP6.4321

Downs, C. A., Fauth, J. E., Halas, J. C., Dustan, P., Bemiss, J., and Woodley, C. M. (2002). Oxidative stress and seasonal coral bleaching. *Free Radical Biol. Med.* 33 (4), 533–543. doi: 10.1016/S0891-5849(02)00907-3

Eyring, V., Bony, S., Meehl, G. A., Senior, C. A., Stevens, B., Stouffer, R. J., et al. (2016). Overview of the coupled model intercomparison project phase 6 (CMIP6) experimental design and organization. *Geoscientific Model. Dev.* 9, 1937–1958. doi: 10.5194/gmd-9-1937-2016

Fiddes, S. L., Woodhouse, M. T., Lane, T. P., and Schofield, R. (2021). Coral-reef-derived dimethyl sulfide and the climatic impact of the loss of coral reefs. *Atmospheric Chem. Phys.* 21 (8), 5883–5903. doi: 10.5194/acp-21-5883-2021

Fiddes, S. L., Woodhouse, M. T., Nicholls, Z., Lane, T. P., and Schofield, R. (2018). Cloud, precipitation and radiation responses to large perturbations in global dimethyl sulfide. *Atmospheric Chem. Phys.* 18 (14), 10177–10198. doi: 10.5194/acp-18-10177-2018

Fiddes, S. L., Woodhouse, M. T., Utembe, S., Schofield, R., Alexander, S. P., Alroe, J., et al. (2022). The contribution of coral-reef-derived dimethyl sulfide to aerosol burden over the Great Barrier Reef: A modelling study. *Atmospheric Chem. Phys.* 22 (4), 2419–2445. doi: 10.5194/acp-22-2419-2022

Fischer, E., and Jones, G. B. (2012). Atmospheric dimethysulphide production from corals in the Great Barrier Reef and links to solar radiation, climate and coral bleaching. *Biogeochemistry* 110 (1), 31–46. doi: 10.1007/s10533-012-9719-y

Fricko, O., Havlik, P., Rogelj, J., Klimont, Z., Gusti, M., Johnson, N., et al. (2017). The marker quantification of the shared socioeconomic pathway 2: A middle-of-the-road scenario for the 21st century. *Global Environ. Change* 42, 251–267. doi: 10.1016/j.gloenvcha.2016.06.004

Gabric, A. J., Matrai, P. A., Jones, G. B., and Middleton, J. (2018). The nexus between sea ice and polar emissions of marine biogenic aerosols. *Bull. Am. Meteorological Soc.* 99 (1), 61–81. doi: 10.1175/BAMS-D-16-0254.1

Gabric, A. J., Matrai, P. A., Kiene, R. P., Cropp, R. A., Dacey, J. W. H., DiTullio, G. R., et al. (2008). Factors determining the vertical profile of dimethylsulfide in the Sargasso Sea during summer. *Deep Sea Res. Part II: Topical Stud. Oceanography* 55 (10–13), 1505–1518. doi: 10.1016/j.dsr2.2008.02.002

Gabric, A. J., Qu, B., Rotstayn, L., and Shephard, J. M. (2013). Global simulations of the impact on contemporary climate of a perturbation to the sea-to-air flux of dimethylsulfide. *Aust. Meteorological Oceanographic J.* 63 (3), 365–376.

Galí, M., Lizotte, M., Kieber, D. J., Randelhoff, A., Hussherr, R., Xue, L., et al. (2021). DMS emissions from the Arctic marginal ice zone. *Elementa: Sci. Anthroposcene* 9 (1), 113. doi: 10.1525/elementa.2020.00113

Galí, M., Simó, R., Vila-Costa, M., Ruiz-González, C., Gasol, J. M., and Matrai, P. (2013). Diel patterns of oceanic dimethylsulfide (DMS) cycling: Microbial and physical drivers. *Global Biogeochemical Cycles* 27 (3), 620–636. doi: 10.1002/gbc.20047

Gardner, S. G., Nielsen, D. A., Laczka, O., Shimmon, R., Beltran, V. H., Ralph, P. J., et al. (2016). Dimethylsulfoniopropionate, superoxide dismutase and glutathione as stress response indicators in three corals under short-term hyposalinity stress. *Proc. R. Soc. B: Biol. Sci.* 283 (1824), 20152418. doi: 10.1098/rspb.2015.2418

Gidden, M. J., Riahi, K., Smith, S. J., Fujimori, S., Luderer, G., Kriegler, E., et al. (2019). Global emissions pathways under different socioeconomic scenarios for use in CMIP6: a dataset of harmonized emissions trajectories through the end of the century. *Geoscientific Model. Dev.* 12 (4), 1443–1475. doi: 10.5194/gmd-12-1443-2019

Gorbunov, M. Y., Kolber, Z. S., Lesser, M. P., and Falkowski, P. G. (2001). Photosynthesis and photoprotection in symbiotic corals. *Limnology Oceanography* 46 (1), 75–85. doi: 10.4319/lo.2001.46.1.0075

Hodshire, A. L., Campuzano-Jost, P., Kodros, J. K., Croft, B., Nault, B. A., Schroder, J. C., et al. (2019). The potential role of methanesulfonic acid (MSA) in aerosol formation and growth and the associated radiative forcings. *Atmospheric Chem. Phys.* 19 (5), 3137–3160. doi: 10.5194/acp-19-3137-2019

Hopkins, F. E., and Archer, S. (2014). Consistent increase in dimethyl sulfide (DMS) in response to high CO_2 in five shipboard bioassays from contrasting NW European waters. *Biogeosciences* 11 (18), 4925–4940. doi: 10.5194/bg-11/4925-2014

Hopkins, F. E., Bell, T. G., Yang, M., Suggett, D. J., and Steinke, M. (2016). Air exposure of coral is a significant source of dimethylsulfide (DMS) to the atmosphere. *Sci. Rep.* 6 (1), 1–11. doi: 10.1038/srep36031

Hopkins, F. E., Nightingale, P. D., Stephens, J. A., Moore, C. M., Richier, S., Cripps, G. L., et al. (2020). A meta-analysis of microcosm experiments shows that dimethyl sulfide (DMS) production in polar waters is insensitive to ocean acidification. *Biogeosciences* 17 (1), 163–186. doi: 10.5194/bg-17-163-2020

Howell, T. A., Meek, D. W., and Hatfield, J. L. (1983). Relationship of photosynthetically active radiation to shortwave radiation in the San Joaquin valley. *Agric. Meteorology* 28 (2), 157–175. doi: 10.1016/0002-1571(83)90005-5

Hughes, T. P., Kerry, J. T., Baird, A. H., Connolly, S. R., Chase, T. J., Dietzel, A., et al. (2019). Global warming impairs stock–recruitment dynamics of corals. *Nature* 568 (7752), 387–390. doi: 10.1038/s41586-019-1081-y

Hughes, T. P., Kerry, J. T., Baird, A. H., Connolly, S. R., Dietzel, A., Eakin, C. M., et al. (2018). Global warming transforms coral reef assemblages. *Nature* 556 (7702), 492–496. doi: 10.1038/s41586-018-0041-2

Jackson, R. L., Gabric, A. J., Cropp, R. A., and Woodhouse, M. T. (2020). Dimethylsulfide (DMS), marine biogenic aerosols and the ecophysiology of coral reefs. *Biogeosciences* 17 (8), 2181–2204. doi: 10.5194/bg-17-2181-2020

Jackson, R. L., Gabric, A. J., Matrai, P. A., Woodhouse, M. T., Cropp, R. A., Jones, G. B., et al. (2021). Parameterizing the impact of seawater temperature and irradiance on dimethylsulfide (DMS) in the Great Barrier Reef and the contribution of coral reefs to the global sulfur cycle. *J. Geophysical Research: Oceans* 126 (3), e2020JC016783. doi: 10.1029/2020JC016783

Jones, G. B. (2015). "The reef sulphur cycle: Influence on climate and ecosystem services," In N. Narchi and L. Price (Eds.), *Ethnobiology of corals and coral reefs* (Denmark: Springer), 27–57. doi: 10.1007/978-3-319-23763-3_3

Jones, G. B., Curran, M., Broadbent, A., King, S., Fischer, E., and Jones, R. (2007). Factors affecting the cycling of dimethylsulfide and dimethylsulfoniopropionate in coral reef waters of the Great Barrier Reef. *Environ. Chem.* 4 (5), 310–322. doi: 10.1071/EN06065

Jones, G. B., Curran, M., Deschaseaux, E. S. M., Omori, Y., Tanimoto, H., Swan, H. B., et al. (2018). The flux and emission of dimethylsulfide from the Great Barrier Reef region and potential influence on the climate of NE Australia. *J. Geophysical Research: Atmospheres* 123 (24), 13835–13856. doi: 10.1029/2018JD029210

Jones, G. B., Curran, M., Swan, H. B., and Deschaseaux, E. S. M. (2017). Dimethylsulfide and coral bleaching: Links to solar radiation, low level cloud and the regulation of seawater temperatures and climate in the Great Barrier Reef. *Am. J. Climate Change* 6 (02), 328. doi: 10.4236/ajcc.2017.62017

Jones, R., Hoegh-Guldberg, O., Larkum, A. W. D., and Schreiber, U. (2002). Temperature-induced bleaching of corals begins with impairment of the CO2 fixation mechanism in zooxanthellae. *Plant Cell Environ.* 21 (12), 1219–1230. doi: 10.1046/j.1365-3040.1998.00345.x

Jones, G. B., and King, S. (2015). Dimethylsulphoniopropionate (DMSP) as an indicator of bleaching tolerance in scleractinian corals. *J. Mar. Sci. Eng.* 3 (2), 444–465. doi: 10.3390/jmse3020444

Jones, R., Ward, S., Amri, A. Y., and Hoegh-Guldberg, O. (2000). Changes in quantum efficiency of photosystem II of symbiotic dinoflagellates of corals after heat stress, and of bleached corals sampled after the 1998 Great Barrier Reef mass bleaching event. *Mar. Freshw. Res.* 51 (1), 63–71. doi: 10.1071/MF99100

Kettle, A. J., and Andreae, M. O. (2000). Flux of dimethylsulfide from the oceans: A comparison of updated data sets and flux models. *J. Geophysical Research: Atmospheres* 105 (D22), 26793–26808. doi: 10.1029/2000JD900252

Kondo, J. (1975). Air-sea bulk transfer coefficients in diabatic conditions. *Boundary-Layer Meteorology* 9 (1), 91–112. doi: 10.1007/BF00232256

Korhonen, H., Carslaw, K. S., Spracklen, D. V., Mann, G. W., and Woodhouse, M. T. (2008). Influence of oceanic dimethyl sulfide emissions on cloud condensation nuclei concentrations and seasonality over the remote southern hemisphere oceans: A global model study. *J. Geophysical Res.: Atmospheres* 113 (D15), D15204. doi: 10.1029/2007JD009718

Kriegler, E., Bauer, N., Popp, A., Humpenöder, F., Leimbach, M., Strefler, J., et al. (2017). Fossil-fueled development (SSP5): an energy and resource intensive scenario for the 21st century. *Global Environ. Change* 42, 297–315. doi: 10.1016/j.gloenvcha.2016.05.015

Kwiatkowski, L., Cox, P., Halloran, P. R., Mumby, P. J., and Wiltshire, A. J. (2015). Coral bleaching under unconventional scenarios of climate warming and ocean acidification. *Nat. Climate Change* 5 (8), 777–781. doi: 10.1038/nclimate2655

Lana, A., Bell, T. G., Simó, R., Vallina, S. M., Ballabrera-Poy, J., Kettle, A. J., et al. (2011). An updated climatology of surface dimethlysulfide concentrations and emission fluxes in the global ocean. *Global Biogeochemical Cycles* 25 (1), GB1004. doi: 10.1029/2010GB003850

Land, P. E., Shutler, J. D., Bell, T. G., and Yang, M. (2014). Exploiting satellite earth observation to quantify current global oceanic DMS flux and its future climate sensitivity. *J. Geophysical Research: Oceans* 119 (11), 7725–7740. doi: 10.1002/2014JC010104

Lesser, M. P. (2011). "Coral bleaching: causes and mechanisms," in *Coral reefs: An ecosystem in transition*. (Dordrecht: Springer), 405–419.

Liss, P. S., and Merlivat, L. (1986). "Air-sea gas exchange rates: Introduction and synthesis," in *The role of air-sea exchange in geochemical cycling*. (Dordrecht: Springer) 113–127. doi: 10.1007/978-94-009-4738-2_5

Liss, P. S., and Slater, P. G. (1974). Flux of gases across the air-sea interface. *Nature* 247 (5438), 181–184.

Liu, G., Strong, A. E., Skirving, W., and Arzayus, L. F. (2006). Overview of NOAA coral reef watch program's near-real time satellite global coral bleaching monitoring activities. *Proc. 10th Int. Coral Reef Symposium* 1793, 1783–1793.

Mayer, K. J., Wang, X., Santander, M. V., Mitts, B. A., Sauer, J. S., Sultana, C. M., et al. (2020). Secondary marine aerosol plays a dominant role over primary sea spray aerosol in cloud formation. *ACS Cent. Sci.* 6 (12), 2259–2266. doi: 10.1021/acscentsci.0c00793

McCook, L. J., and Diaz-Pulido, G. (2002). The fate of bleached corals: patterns and dynamics of algal recruitment. *Mar. Ecol. Prog. Ser.* 232, 115–128. doi: 10.3354/meps232115

McGillis, W. R., Dacey, J. W. H., Frew, N. M., Bock, E. J., and Nelson, R. K. (2000). Water-air flux of dimethylsulfide. *J. Geophysical Research: Oceans* 105 (C1), 1187–1193. doi: 10.1029/1999JC900243

Melis, A. (1999). Photosystem-II damage and repair cycle in chloroplasts: what modulates the rate of photodamage *in vivo*? *Trends Plant Sci.* 4 (4), 130–135. doi: 10.1016/S1360-1385(99)01387-4

Modini, R. L., Ristovski, Z. D., Johnson, G. R., He, C., Surawski, N., Morawska, L., et al. (2009). New particle formation and growth at a remote, sub-tropical coastal location. *Atmospheric Chem. Phys.* 9 (19), 7607–7621. doi: 10.5194/acp-9-7607-2009

Moss, R. H., Edmonds, J. A., Hibbard, K. A., Manning, M. R., Rose, S. K., Van Vuuren, D. P., et al. (2010). The next generation of scenarios for climate change research and assessment. *Nature* 463 (7282), 747–756. doi: 10.1038/nature08823

Nightingale, P. D., Malin, G., Law, C. S., Watson, A. J., Liss, P. S., Liddicoat, M. I., et al. (2000). *In situ* evaluation of air-sea gas exchange parameterizations using novel conservative and volatile tracers. *Global Biogeochemical Cycles* 14 (1), 373–387. doi: 10.1029/1999GB900091

Przyjazny, A. W., Janicki, W., Chrzanowski, W., and Staszewki, R. (1983). Headspace gas chromatogroahpic determination coefficients of selected organosulphur compounds and their dependence of some parameters. *J. Chromatogr.* 280, 249–260. doi: 10.1016/S0021-9673(00)91567-X

Raina, J. B., Tapiolas, D. M., Forêt, S., Lutz, A., Abrego, D., Ceh, J., et al. (2013). DMSP biosynthesis by an animal and its role in coral thermal stress response. *Nature* 502 (7473), 677–680. doi: 10.1038/nature12677

Raina, J. B., Tapiolas, D., Willis, B. L., and Bourne, D. G. (2009). Coral-associated bacteria and their role in the biogeochemical cycling of sulfur. *Appl. Environ. Microbiol.* 75 (11), 3492–3501. doi: 10.1128/AEM.02567-08

Saltzman, E. S., King, D. B., Holmen, K., and Leck, C. (1993). Experimental determination of the diffusion coefficient of dimethylsulfide in water. *J. Geophysical Research: Oceans* 98 (C9), 16481–16486. doi: 10.1029/93JC01858

Sanborn, K. L., Webster, J. M., Webb, G. E., Braga, J. C., Humblet, M., Nothdurft, L., et al. (2020). A new model of Holocene reef initiation and growth in response to sea-level rise on the southern Great Barrier Reef. *Sediment. Geo.* 397, 105556. doi: 10.1016/j.sedgeo.2019.105556

Sanchez, K. J., Chen, C.-L., Russell, L. M., Betha, R., Liu, J., Price, D. J., et al. (2018). Substantial seasonal contribution of observed biogenic sulfate particles to cloud condensation nuclei. *Sci. Rep.* 8 (1), 1–14. doi: 10.1038/s41598-018-21590-9

Schneider, T., Kaul, C. M., and Pressel, K. G. (2019). Possible climate transitions from breakup of stratocumulus decks under greenhouse warming. *Nat. Geosci.* 12 (3), 163–167. doi: 10.1038/s41561-019-0310-1

Schwarzenbach, R. P., Gschwend, P. M., and Imboden, D. M. (2005). *Environmental organic chemistry* (New York: John Wiley & Sons).

Skirving, W., Enríquez, S., Hedley, J. D., Dove, S., Eakin, C. M., Mason, R. A. B., et al. (2018). Remote sensing of coral bleaching using temperature and light: progress towards an operational algorithm. *Remote Sens.* 10 (1), 18. doi: 10.3390/rs10010018

Spiese, C. E., Kieber, D. J., Nomura, C. T., and Kiene, R. P. (2009). Reduction of dimethylsulfoxide to dimethylsulfide by marine phytoplankton. *Limnology Oceanography* 54 (2), 560–570. doi: 10.4319/lo.2009.54.2.0560

Sunda, W., Kieber, D. J., Kiene, R. P., and Huntsman, S. (2002). An antioxidant function for DMSP and DMS in marine algae. *Nature* 418 (6895), 317–320. doi: 10.1038/nature00851

Swan, H. B., Jones, G. B., Deschaseaux, E. S. M., and Eyre, B. D. (2017). Coral reef origins of atmospheric dimethylsulfide at heron island, southern Great Barrier Reef, Australia. *Biogeosciences* 14 (1), 229–239. doi: 10.5194/bg-14-229-2017

Van Oppen, M. J. H., Oliver, J. K., Putnam, H. M., and Gates, R. D. (2015). Building coral reef resilience through assisted evolution. *Proc. Natl. Acad. Sci.* 112 (8), 2307–2313. doi: 10.1073/pnas.1422301112

Veres, P. R., Neuman, J. A., Bertram, T. H., Assaf, E., Wolfe, G. M., Williamson, C. J., et al. (2020). Global airborne sampling reveals a previously unobserved dimethyl sulfide oxidation mechanism in the marine atmosphere. *Proc. Natl. Acad. Sci.* 117 (9), 4505–4510. doi: 10.1073/pnas.1919344117

Vlahos, P., and Monahan, E. C. (2009). A generalized model for the air-sea transfer of dimethyl sulfide at high wind speeds. *Geophysical Res. Lett.* 36 (21), L21605. doi: 10.1029/2009GL040695

Walters, D., Baran, A. J., Boutle, I., Brooks, M., Earnshaw, P., Edwards, J., et al. (2019). The met office unified model global atmosphere 7.0/7.1 and JULES global land 7.0 configurations. *Geoscientific Model. Dev.* 12 (5), 1909–1963. doi: 10.5194/gmd-12-1909-2019

Wang, M., Son, S., and Harding, L. W.Jr. (2009). Retrieval of diffuse attenuation coefficient in the Chesapeake bay and turbid ocean regions for satellite ocean color applications. *J. Geophysical Research: Oceans* 114 (C10), C10011. doi: 10.1029/2009JC005286

Webb, A. L., van Leeuwe, M. A., den Os, D., Meredith, M. P., Venables, H. J., and Stefels, J. (2019). Extreme spikes in DMS flux double estimates of biogenic sulfur export from the Antarctic coastal zone to the atmosphere. *Sci. Rep.* 9 (2233), 2233. doi: 10.1038/s41598-019-38714-4

Weis, V. M. (2008). Cellular mechanisms of cnidarian bleaching: stress causes the collapse of symbiosis. *J. Exp. Biol.* 211 (19), 3059–3066. doi: 10.1242/jeb.009597

Widlansky, M. J., Timmermann, A., and Cai, W. (2015). Future extreme sea level seesaws in the tropical pacific. *Sci. Adv.* 1 (8), e1500560. doi: 10.1126/sciadv.1500560

Winters, G., Loya, Y., Röttgers, R., and Beer, S. (2003). Photoinhibition in shallow-water colonies of the coral stylophora pistillata as measured in situ. *Limnology Oceanography* 48 (4), 1388–1393. doi: 10.4319/lo.2003.48.4.1388

Woodhouse, M. T., Carslaw, K. S., Mann, G. W., Vallina, S. M., Vogt, M., Halloran, P. R., et al. (2010). Low sensitivity of cloud condensation nuclei to changes in the sea-air flux of dimethyl-sulphide. *Atmospheric Chem. Phys.* 10 (16), 7545–7559. doi: 10.5194/acp-10-7545-2010

Woodhouse, M. T., Mann, G. W., Carslaw, K. S., and Boucher, O. (2013). Sensitivity of cloud condensation nuclei to regional changes in dimethyl-sulphide

emissions. *Atmospheric Chem. Phys.* 13 (5), 2723–2733. doi: 10.5194/acp-13-2723-2013

Yakovleva, I. M., Baird, A. H., Yamamoto, H. H., Bhagooli, R., Nonaka, M., and Hidaka, M. (2009). Algal symbionts increase oxidative damage and death in coral larvae at high temperatures. *Mar. Ecol. Prog. Ser.* 378, 105–112. doi: 10.3354/meps07857

Yang, M., Blomquist, B. W., Fairall, C. W., Archer, S. D., and Huebert, B. J. (2011). Air-sea exchange of dimethylsulfide in the southern ocean: Measurements from SO GasEx compared to temperate and tropical regions. *J. Geophysical Res. Oceans* 116 (C4), C00F05. doi: 10.1029/2010JC006526

Zhang, Z., Jones, A., and Crabbe, M. J. C. (2017). Impacts of stratospheric aerosol geoengineering strategy on Caribbean coral reefs. *Int. J. Climate Change Strategies Manage* 10 (4), 523–532. doi: 10.1108/IJCCSM-05-2017-0104

Ziehn, T., Chamberlain, M. A., Law, R. M., Lenton, A., Bodman, R. W., Dix, M., et al. (2020). The Australian earth system model: ACCESS-ESM1. 5. *J. South. Hemisphere Earth Syst. Sci.* 70 (1), 193–214. doi: 10.1071/ES19035

Ziehn, T., Chamberlain, M., Lenton, A., Law, R., Bodman, R., Dix, M., et al. (2019) *CSIRO ACCESS-ESM1.5 model output prepared for CMIP6*. doi: 10.22033/ESGF/CMIP6.4322

frontiers | Frontiers in Marine Science

TYPE Original Research
PUBLISHED 13 October 2022
DOI 10.3389/fmars.2022.944141

OPEN ACCESS

EDITED BY
Nina Yasuda,
The University of Tokyo, Japan

REVIEWED BY
David Bourne,
James Cook University, Australia
Andrew WB Johnston,
University of East Anglia,
United Kingdom
Shinya Shikina,
National Taiwan Ocean University,
Taiwan

*CORRESPONDENCE
Rafel Simó
rsimo@icm.csic.es

†PRESENT ADDRESS
Stephanie G. Gardner,
Centre for Marine Science and Innovation, University of New South Wales Sydney, NSW, Australia

SPECIALTY SECTION
This article was submitted to Coral Reef Research, a section of the journal Frontiers in Marine Science

RECEIVED 14 May 2022
ACCEPTED 30 August 2022
PUBLISHED 13 October 2022

CITATION
Masdeu-Navarro M, Mangot J-F, Xue L, Cabrera-Brufau M, Gardner SG, Kieber DJ, González JM and Simó R (2022) Spatial and diel patterns of volatile organic compounds, DMSP-derived compounds, and planktonic microorganisms around a tropical scleractinian coral colony. *Front. Mar. Sci.* 9:944141. doi: 10.3389/fmars.2022.944141

Spatial and diel patterns of volatile organic compounds, DMSP-derived compounds, and planktonic microorganisms around a tropical scleractinian coral colony

Marta Masdeu-Navarro[1], Jean-François Mangot[1], Lei Xue[2], Miguel Cabrera-Brufau[1], Stephanie G. Gardner[1†], David J. Kieber[2], José M. González[3] and Rafel Simó[1*]

[1]Department of Marine Biology and Oceanography, Institut de Ciències del Mar (ICM-CSIC), Barcelona, Spain, [2]Department of Chemistry, State University of New York, College of Environmental Science and Forestry, Syracuse, NY, United States, [3]Department of Microbiology, University of La Laguna, La Laguna, Spain

Volatile organic compounds (VOCs) are constituents of marine ecosystems including coral reefs, where they are sources of atmospheric reactivity, indicators of ecosystem state, components of defense strategies, and infochemicals. Most VOCs result from sunlight-related processes; however, their light-driven dynamics are still poorly understood. We studied the spatial variability of a suite of VOCs, including dimethylsulfide (DMS), and the other dimethylsulfoniopropionate-derived compounds (DMSPCs), namely, DMSP, acrylate, and dimethylsulfoxide (DMSO), in waters around colonies of two scleractinian corals (*Acropora pulchra* and *Pocillopora* sp.) and the brown seaweed *Turbinaria ornata* in Mo'orean reefs, French Polynesia. Concentration gradients indicated that the corals were sources of DMSPCs, but less or null sources of VOCs other than DMS, while the seaweed was a source of DMSPCs, carbonyl sulfide (COS), and poly-halomethanes. A focused study was conducted around an *A. pulchra* colony where VOC and DMSPC concentrations and free-living microorganism abundances were monitored every 6 h over 30 h. DMSPC concentrations near the polyps paralleled sunlight intensity, with large diurnal increases and nocturnal decrease. rDNA metabarcoding and metagenomics allowed the determination of microbial diversity and the relative abundance of target functional genes. Seawater near coral polyps was enriched in DMS as the only VOC, plus DMSP, acrylate, and DMSO, with a large increase during the day, coinciding with high abundances of symbiodiniacean sequences. Only 10 cm below, near the coral skeleton colonized by a turf alga, DMSPC concentrations were much lower and the microbial community was significantly different. Two meters down current from the coral, DMSPCs decreased further and the microbial community was more similar to that near the polyps than that near the turf alga. Several DMSP cycling genes were enriched in near-polyp with respect to down-current waters, namely, the eukaryotic DMS production and

DMS oxidation encoding genes, attributed to the coral and the algal symbiont, and the prokaryotic DMS production gene *dddD*, harbored by coral-associated *Gammaproteobacteria*. Our results suggest that solar radiation-induced oxidative stress caused the release of DMSPCs by the coral holobiont, either directly or through symbiont expulsion. Strong chemical and biological gradients occurred in the water between the coral branches, which we attribute to layered hydrodynamics.

KEYWORDS

VOC, DMS, DMSP, acrylate, DMSO, coral, *Symbianodiciaea*, seaweed

Introduction

Coral reefs are highly diverse and productive ecosystems that thrive in oligotrophic waters of tropical and subtropical oceans (Hoegh-Guldberg et al., 2017). Reefs are built by calcifying scleractinian coral colonies that provide diverse and interdependent habitats to all kinds of organisms, including vertebrate and invertebrate animals, seaweeds, and microbes. The coral colony itself is a multi-organism consortium of the cnidarian, the symbiont microalgae, and a myriad of microorganisms associated with the coral tissues and exudates, with the whole entity being named the coral holobiont (Rohwer et al., 2002).

Coral reefs provide key ecosystem services: biodiversity, coastal protection, biogeochemical cycling, fisheries, provision of raw materials, and cultural benefits (Woodhead et al., 2019). Recently, an ecosystem service of short-term regulation of regional climate has been suggested too, at least for the large extending Great Barrier Reef (Jones, 2015; Jackson et al., 2020). This climate effect would operate from the observed capacity of coral reefs to emit volatile sulfur in the form of dimethylsulfide (DMS). In the atmosphere, emitted DMS oxidizes to form precursors of aerosols that enhance the formation, lifetime, and brightness of low-level clouds (Charlson et al., 1987; Simó, 2001), and thereby potentially reduce incident solar irradiance and temperature. Since the production and emission of DMS from coral reefs is triggered under higher irradiance and temperature, this reef–atmosphere interaction could potentially act as a regional thermostat (Jackson et al., 2020). This hypothesis is currently under scrutiny.

Sulfur emission for cloud seeding is not the only way coral reefs affect the overlying atmosphere. Tropical reefs are also suggested to be hot spots for the emission of biogenic volatile organic compounds (VOCs) beyond DMS (Exton et al., 2015). VOCs are sources of atmospheric reactivity, indicators of the ecosystem state, defense strategies, and chemical cues for organism–organism communication, e.g., to facilitate foraging. Ongoing studies are paving the road towards characterizing the volatilome at the reef ecosystem level, and they have revealed a diverse VOC composition (Lawson et al., 2020; 2021). While VOCs are being discovered that were unknown to marine systems, a look at the VOC whose production processes and ecological impacts are known will be informative of the physiological, ecosystem, and environmental functions they sustain.

Carbonyl sulfide (COS) is the most abundant and most stable sulfur gas in the atmosphere (Lennartz et al., 2020). Emitted by the biosphere and the oceans through the interaction of solar radiation and dissolved organic matter, it reaches the stratosphere where it influences ozone destruction and aerosol formation. Carbon disulfide (CS_2) is another sulfur volatile produced in the surface ocean by photochemistry and phytoplankton, and in sediments by microbial activity (Kim and Andreae, 1992). It further contributes to the atmospheric COS burden through oxidation (Lennartz et al., 2020). Whether coral reefs are significant producers of COS and CS_2 is unknown. Isoprene (C_5H_8) is another VOC that is best known for being the most abundantly produced by the global biosphere, one that affects the oxidative capacity of the troposphere owing to its reactivity with airborne oxidants. It is released by vascular plants and trees as a response to alleviate thermal stress; in the ocean, it is produced mainly by phytoplankton, but the mechanisms remain unclear (McGenity et al., 2018). Tropical coral holobionts also produce isoprene, but there is no consensus as to whether it arises from physiological stress (Swan et al., 2016; Dawson et al., 2021; Lawson et al., 2021). Halomethanes (halogenated C1 compounds) are commonly found in coastal ecosystems, where they are produced mainly by seaweeds, and to a lesser extent by phytoplankton, to combat oxidative stress (Carpenter et al., 2012). They have also been suggested to be involved in defense mechanisms. In the atmosphere,

halomethanes affect oxidant radicals and participate in tropospheric and stratospheric ozone destruction (Saiz-López and von Glasow, 2012). Whether coral holobionts are relevant sources of halomethanes is unknown.

Corals are known to undergo fundamental physiological changes in response to incident light during a diel cycle. They switch from autotrophic holobiont during the day, when the algal symbionts fix carbon and produce oxygen, to heterotrophs at night, when polyps prey on plankton and the animal respiration is higher due to digestion (Schneider et al., 2009). This physiological switch results in hyperoxic conditions in the holobiont during the day, and hypoxia at night. Among the suite of physiological responses to diurnal oxidative stress (Hemond and Vollmer, 2015), many hermatypic coral holobionts use dimethylsulfoniopropionate-derived compounds (DMSPCs) as antioxidants (e.g., Deschaseaux et al., 2014b). DMSP is an osmolyte in many algal taxa, including the coral symbionts *Symbiodiniaceae*. DMSP is such an abundant compound in the marine environment that it carries a large share of carbon and sulfur trophic transference in marine microbial food webs, and is a potent infochemical in foraging interactions, an antioxidant, and the source of climate-active DMS (Simó, 2001; Carpenter et al., 2012). In tropical coral holobionts, DMSP is synthesized not only by the algal symbionts (Deschaseaux et al., 2014a) but also by the cnidarian (Raina et al., 2013) and associated bacteria (Kuek et al., 2022). DMSP can be enzymatically cleaved to DMS and acrylate, a catabolic route that is thought to be the most instrumental for alleviating oxidative stress (Sunda et al., 2002), or it can be catabolized through demethylation and demethiolation, a route that leads to sulfur incorporation by the consumer (Howard et al., 2006).

We conducted a study in the shallow reefs of Mo'orea, in the French Polynesia, to describe the distributions of VOCs and DMSPCs around dominant reef-forming organisms and learn about their sources and drivers. To this aim, we studied the spatial variability of a suite of VOCs and DMSPCs in waters around colonies of two scleractinian corals (*Acropora pulchra* and *Pocillopora* sp.) and the brown seaweed *Turbinaria ornata*. We also conducted a dedicated study around an *A. pulchra* colony over a diel cycle. Taxonomic (rDNA metabarcoding) and functional (metagenomics) gene analyses helped to propose the most likely candidate organisms responsible for the diel DMSPC pattern observed. A companion paper reports the turnover of dissolved DMSP and acrylate in our study site (Xue et al., 2022).

Materials and methods

Study area

Fieldwork was conducted between 4 and 27 April 2018, on the north and northeast coast of the island of Mo'orea, French Polynesia (Figure 1A). On the inner side, the reef crest harbors large patches of *Acropora* spp. colonies and smaller patches of *Pocillopora* spp. and other corals, and there is an abundant population of the brown algal seaweed *T. ornata*. On the outer side, the forereef platform is mainly composed of the cauliflower coral *Pocillopora* spp.

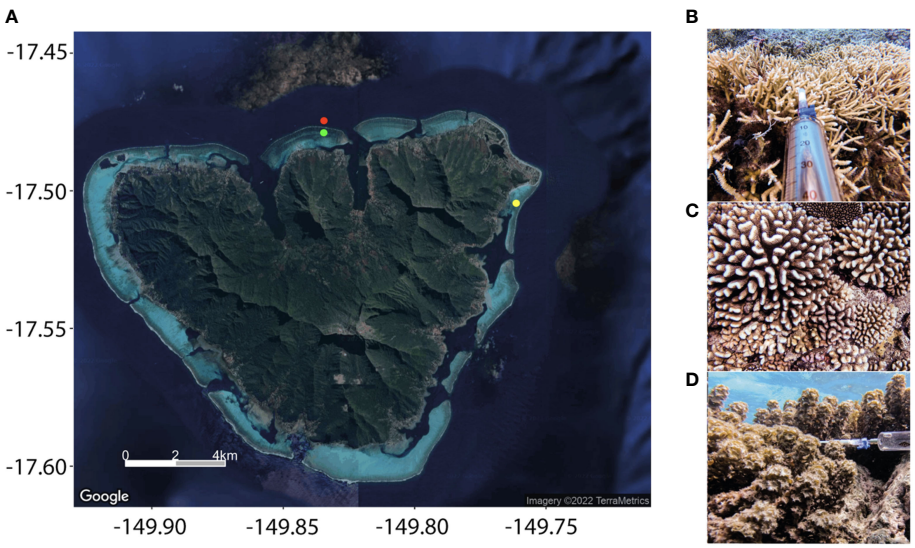

FIGURE 1
(A) Location of the sampling sites in Mo'orea. Zoom into the fore reef and back reef sampling sites in the northern coast, off Cook's Bay, and into the back reef sampling site in the Tema'e Beach reef, along the northwestern coast, where the diel study was conducted. Images of **(B)** *Acropora pulchra*, **(C)** *Pocillopora* sp., and **(D)** *Turbinaria ornata*, with the all-glass syringe used to collect seawater.

Sample collection and storage

Gradients around colonies. Water samples (0.5 L) for DMSPC and VOC measurements were taken from the interstitial space of, and nearby, two coral colonies and a seaweed patch (Figures 1B–D). One pair of seawater samples around the coral *Acropora pulchra* [AP(A)] was collected on 18 April; a second pair [AP(B)] was collected on 23 April, both at 1-m depth within the Tema'e Beach reef (17.501°S, 149.759°E), northeast coast (Figure 1A). The *A. pulchra* thicket had a diameter of several meters. In the same reef, another pair of seawater samples was collected around a 0.5-m-sized colony of the coral *Pocillopora* sp. [P(A)], at a depth of 2 m. Another pair of samples around a similar *Pocillopora* sp. colony [P(B)] was taken on 17 April at the forereef of the northern coast (17.475°S, 149.839°E), at a depth of about 3 m. Seawater samples around the brown seaweed *T. ornata* (TO) were collected on 16 April in the back reef of the northern coast (17.478°S, 149.839°E), approximately at 1 m depth. The seaweed thicket was 0.5–1 m large. In all cases, the pair of samples corresponded to a first sampling point as close as possible (~0.5 cm) to the organism without touching it, between the branches of *A. pulchra*, the verrucae of *Pocillopora* sp., or the thalli of *T. ornata* (IN), and a second sampling point 2 m away from the target organism (OUT).

Diel cycle. A diel study was conducted around an *A. pulchra* colony in the Tema'e Beach reef. Water samples were withdrawn from three different sampling points around the colony, at a depth of ~1 m (Figure 2): (IN) between the living branches, ~1 cm next to the polyps; (AL) deeper between the branches, ~0.5 cm next to the coral skeleton colonized by turf algae; and (OUT) 2 m down current from the patch over a sandy bottom ~2 m deep. Over 36 consecutive hours between 24 and 25 April, sampling was done at 07:00, 12:00, 17:00, 00:00, 07:00, and 12:00 local time. An adjacent coral colony was marked with flagging tape to facilitate location of the sampling site, so that samples were taken from the same branches at each time point. In the first five time points, 0.5 L of seawater was collected for the DMSP-derived compounds, VOC, and microbial abundance measurements. For the last time point only (12:00 on 25 April), 0.8 L was taken from IN and AL, and 2.5 L from OUT, to have enough volume for microbial DNA analysis.

Sampling protocol. All samples were collected using glass bottles that were rinsed three times with *in situ* seawater before sampling. For the IN and AL samples, water was withdrawn through 0.318-cm OD PTFE tubing attached to a 50-ml all-glass syringe *via* a three-way polycarbonate valve (Figure 1B), and transferred into the glass bottle avoiding bubble generation. The process was repeated until the bottle was full without headspace, so that approximately 10 individual samples were aggregated in a bottle. For the OUT samples, the bottle was filled directly without the syringe. Only one bottle was collected from IN, AL or OUT. Once all the bottles were filled and sealed with solid, ground-glass stoppers, the bottles were transported to the shore and driven to the lab for analysis within 1–2 h after collection.

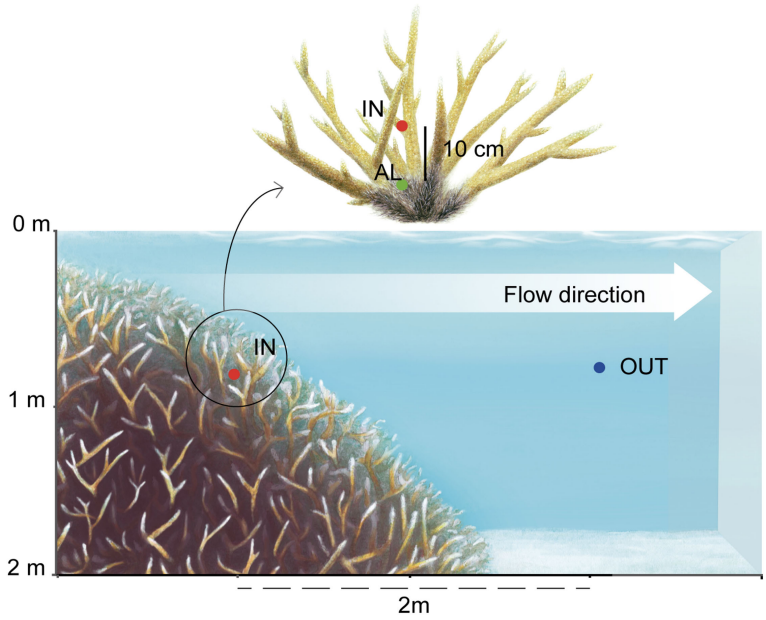

FIGURE 2
Scheme of sampling points in the diel study of *Acropora pulchra* in the Tema'e Beach reef. IN: between the living branches; AL: 10 cm deeper, next to the dead skeleton colonized by turf algae; OUT: 2 m down current from the patch. Artwork by J. Mir-Arguimbau.

Microbial abundances

For enumeration of heterotrophic prokaryotes (including bacteria and archaea) and pico- and nano-phytoplankton, 2- to 5-ml sample aliquots were fixed with glutaraldehyde (0.5%) and stored at −80°C until analysis based on size and fluorescence on a flow cytometer (CyFlow Cube 8, Sysmex Partec). Heterotrophic prokaryotes (including bacteria and archaea) were stained with SYBRgreen I (~20 µM final concentration) prior to quantification by green fluorescence. Prokaryotic and eukaryotic pico- and nano-phytoplankton were counted based on their red and orange autofluorescence.

VOC concentrations

For VOC analyses, we used an Agilent 5975T LTM gas chromatograph–mass spectrometer coupled to a Stratum (Teledyne Tekmar) purge and trap system. Seawater aliquots (25 ml) were taken from the sample bottles with an Artiglass syringe with a PTFE tube. After removal of air bubbles, the PTFE tube was replaced with a GF/F filter holder that was attached to the inlet of the sparge vessel *via* a Luer lock fitting, and the aliquot was filter injected. VOC were sparged at room temperature for 12 min with a flow rate of 40 ml/min of ultrapure He, trapped on a VOCARB 3000 absorption column held at room temperature, and desorbed by heating to 250°C. VOCs were separated in a capillary column LTM DB-VRX (Agilent; 20 m × 0.18 mm × 1 µm) held at 35°C for 4 min, then heated to 230°C at 30°C/min, and held at 230°C for 4 min, making a total analysis time of 14.5 min. The He carrier gas flow rate was 0.8 ml/min. Compounds were detected by an electron impact ionization mass spectrometer in selected ion monitoring mode. Target compounds [COS, C_2H_6S (DMS), CS_2, $C_2H_6S_2$ (DMDS), CH_3I, CH_2ClI, CH_2Br_2, and $CHBr_3$] were identified matching the retention times of their most characteristic (quantification) ions and their confirmation ions with those of pure standards (Table S1). Each sample was analyzed in duplicate.

DMSP, DMSO, and acrylate concentrations

For total DMSP (DMSPt, i.e., dissolved + particulate) analysis, we stored 40 ml of unfiltered seawater in crimped glass vials after adding two NaOH pellets (45 mg each, ~0.2 mol L^{-1} final concentration, pH >12). The DMSPt + DMS was determined as evolved DMS after undergoing alkaline hydrolysis for 1–2 months. Evolved DMS was analyzed back in the lab with a purge-and-trap system coupled to a gas chromatograph (Shimadzu GC14A) with flame photometric detection. The DMSPt concentration was calculated by subtraction of the on-site determined DMS concentration. All analyses were run in duplicate, and standard errors for both DMS and DMSP concentrations fell within 10% of the mean.

To determine dissolved DMSP (DMSPd), acrylate and DMSO concentrations, 15-ml sample aliquots were gravity filtered using precombusted, 25-mm-diameter GF/F filters into 20-ml scintillation vials using the small-volume drip filtration method described by Kiene and Slezak (2006). Filtered samples were microwaved to boiling, bubbled with high-purity nitrogen gas to remove DMS, and acidified with 150 µl of Ultrex HCl (Kinsey and Kieber, 2016). All samples were stored at room temperature in the dark until analysis in the lab. For DMSPd analysis, 200 µl of 5 M NaOH was added to 1 ml of seawater samples in precleaned, gas-tight borosilicate serum vials, which were reacted overnight at room temperature in the dark. Evolved DMS was analyzed using a cryogenic purge-and-trap system and a Shimadzu GC-14A gas chromatograph with a flame photometric detector (Kinsey et al., 2016). Acrylate concentrations were determined using a pre-column derivatization HPLC method that provided sufficient sensitivity for the analysis of sub-nanomolar acrylate concentrations in seawater (Tyssebotn et al., 2017). For derivatization, 300 µl of 20 mM TSA reagent in MeOH was pipetted into a 5-ml precleaned borosilicate vial containing 3 ml of a standard or seawater sample. Following pH adjustment to 4.0, each vial was tightly screw-capped and incubated in a 90°C water bath for 6 h. After cooling to room temperature, each derivatized sample was first filtered using a 0.2-µm Nylon syringe filter (Pall) followed by a 1-ml injection of each filtered sample on a reverse-phase Water HPLC column with UV detection at 257 nm to quantify the acrylate-TSA derivative. The limit of detection of this method was 0.2 nM for a 1-ml injection with a signal-to-noise ratio of 2.

For total and dissolved DMSO analysis, 1 ml of the same unfiltered or filtered seawater samples used for DMSP analysis were added 200 µl of 20% TiCl3 in precleaned borosilicate serum vials, which were incubated at 55°C in a water bath for 1 h. Evolved DMS was measured as above.

Solar radiation

The diel cycle of sunlight was provided by the meteorological station at the Gump Research Station (Washburn and Brooks, 2022), located 6 km away from our sampling site at Tema'e Beach. Meteorological data include air temperature, relative humidity, wind speed and direction, global solar radiation, atmospheric pressure, and integrated rainfall. Data are available every 5 min from August 2006 to the present day. Postprocessing of these data consisted of unit conversion and exclusion of corrupted data records.

DNA extraction, 16S/18S rRNA gene amplicon, and metagenomic sequencing

Samples for DNA collection from waters around the *A. pulchra* colony were taken from the remaining volumes [ca. 0.8 L (IN, AL) and 2.45 L (OUT)] of the samples collected at noon on the second day of the diel cycle. Samples were prefiltered through a 200-µm mesh, and the microbial biomass was collected on 0.2-µm pore-size, 47-mm-diameter polycarbonate filters using a peristaltic pump. The filters were flash frozen in liquid N_2 and stored at −80°C. Total DNA was extracted using the phenol-chloroform protocol as described in Massana et al. (1997). Prokaryotic and eukaryotic diversities were determined by amplicon sequencing of the V4/V5 and V4 regions of the 16S and 18S rDNA genes, respectively, using the Illumina MiSeq platform and paired-end reads (2 × 250 bp). PCR amplifications were done using (1) the prokaryotic universal primers 515F-Y (5'-GTGYCAGCMGCCGCGGTAA-3') and 926R (5'-CCGYCAATTYMTTTRAGTTT-3') (Parada et al., 2016), and (2) the eukaryotic universal primers V4F (5'-CCA GCA SCY GCG GTAATT CC-3') and V4R (5'-ACTTTC GTT CTT GAT YRR-3') (Balzano et al., 2015). All samples were sequenced at the Research and Testing Laboratories (RTL, Lubbock, TX, USA).

The presence and abundance of genes involved in the DMS/DMSP cycling were determined by metagenomics. Whole metagenome sequencing of DNA extracts from IN and OUT samples (attempt to sequence AL failed) was performed using a PCR-free protocol at the Centre Nacional d'Anàlisi Genòmica (CNAG, Barcelona, Spain; http://cnag.cat/). Short-insert paired-end libraries were prepared with the Illumina TruSeq Sample Preparation kit (Illumina Inc.) and sequenced on a NovaSeq 6000 Illumina platform (2 × 150 bp), yielding about 45 Gb of sequencing information per metagenome.

Amplicon data processing

Primers and spurious sequences from the amplicon sequencing data obtained from both prokaryotic and eukaryotic communities (16S and 18S rDNA sets, respectively) were trimmed from the forward and reverse reads using cutadapt v2.3 (Martin, 2011) with the default error tolerance and a minimum overlap equal to half the primer length. Trimmed reads were subsequently processed with DADA2 v1.4 (Callahan et al., 2016). On the basis of quality profiles, forward reads of the 16S and 18S rDNA sets were respectively truncated at 245 and 250 bp, respectively, and reverse reads were respectively truncated at 180 and 220 bp; reads with more than two expected errors [maxEE = c(2,2)], a quality score lower than two (truncQ = 2), and ambiguous nucleotides (Ns) were excluded.

Forward and reverse reads were then independently corrected using run-specific error-rate modeling and dereplicated. Corrected paired-end reads were subsequently merged to produce amplicon sequence variants (ASVs). Chimeric ASVs were identified and discarded from both datasets. Next, ASVs were taxonomically assigned using the Ribosomal Database Project naïve Bayesian classifier (Wang et al., 2007), as implemented in DADA2, and an 80% minimum bootstrap confidence threshold using SILVA (v132; Pruesse et al., 2007) and PR^2 (v4.11.1; Guillou et al., 2012) as reference databases for the 16S and 18S rDNA sets, respectively. For the 16S rDNA set, singletons and sequences affiliated to eukaryotes, organelles, or chloroplasts were removed prior to subsequent analyses. Singletons were also removed to build the 18S rDNA dataset. Since special attention was paid to the unicellular eukaryotic community members (i.e., protists), the sequences affiliated to metazoans, *Embryophyceae* (land plants), *Rhodophyta* (red algae), *Ulveophyceae* (*Chlorophyta*, green algae), and *Phaeophyceae* (brown algae) were removed, because their large 18S rRNA gene copy numbers and multicellularity would bias the data against the contribution of protistan taxa. To enable comparisons between samples, ASV tables were randomly subsampled down to the minimum number of reads per sample of both rDNA sets (18,510 and 6,952 reads for the 16S and 18S rDNA sets, respectively) using the *rarefy* function in the vegan v2.5.7 package (Oksanen et al., 2021) in R v4.0.2 (R Development Core Team, 2021). The final ASV tables contained 55,530 rDNA 16S sequences clustered into 1,496 prokaryotic ASVs and 22,485 rDNA 18S sequences clustered into 920 protistan ASVs.

Metagenomic sequence assembly, gene prediction, and generation of a reference gene/peptide catalog

Metagenomic raw reads were trimmed for TruSeq adapters with cutadapt v1.16 and quality-filtered with trimmomatic v0.38 (Bolger et al., 2014) using the following parameters: LEADING:3 TRAILING:3 SLIDINGWINDOW:4:15 MINLEN:50. Metagenomic samples were then assembled using megahit v1.2.8 (Li et al., 2016) with meta-large preset and a minimum contig length of 500 bp. For each obtained metagenome, gene-coding sequences were predicted on the assembled contigs using Prodigal v2.6.3 (Hyatt et al., 2010). All 5,670,580 predicted coding sequences larger than 100 bp from each assembled metagenome were pooled and clustered at 95% sequence similarity and 90% sequence overlap of the smaller sequence using cd-hit-est v.4.8.1 (Li and Godzik, 2006) using the following options: -c 0.95 -T 0 -M 0 -G 0 -aS 0.9 -g 1 -r 1 -d 0 to obtain 4,779,650 non-redundant gene clusters.

Abundance and functional annotation of the reference gene catalog

The quality-checked sequencing reads of metagenomic samples were back-mapped against the nucleotide sequences of each gene cluster using Bowtie2 v2.3.4.1 (Langmead and Salzberg, 2012) with default options, keeping only mapping hits with quality >10 with Samtools v.1.8 (options: -q 10 -F 4) (Li et al., 2009). Read counts were reported for each metagenome using the HTSeq v0.10.0 (Anders et al., 2015) and the function htseq-count (options: -t CDS -r pos –nonunique all) to get the abundance of each of the 4,779,650 non-redundant gene clusters.

Identification and quantification of predicted DMSPC cycling genes

The amino acid sequences of predicted prokaryotic and eukaryotic DMSPC cycling genes (*Alma1*, *dsyB*, *DSYB*, *dddD*, *dddK*, *dddP*, *dddQ*, *dddW*, *dddL*, *dddY*, *dddX*, *dmdA*, *acuI*, *dmsA*/*torA*, and *tmm*; Table S2; Figure 3) were identified in the newly generated gene catalog. Reference phylogenetic trees were used for each of the genes to quantify their abundance as described below.

First, a collection of prokaryotic genome sequences was retrieved from the MAR databases (Klemetsen et al., 2018), the OceanDNA MAG catalog (Nishimura and Yoshizawa, 2022), and genome sequences reported in Paoli et al. (2022). This genome set contained all 1,270 complete genomes in the MAR databases and 5,521 partial genomes that had the "high quality" status as described in Klemetsen et al. (2018). All 52,325 OceanDNA genomes were included since they had been quality filtered based on their completeness and degree of contamination with the formula: percent completeness − 5 × percent-contamination ≥50. Only the genomes that passed this same quality filter were considered (Paoli et al., 2022), yielding another 26,942 genomes. A taxonomy was assigned to the genomes with the GTDB Toolkit (GTDB-Tk; Chaumeil et al., 2020). A smaller database was constructed for the products of the eukaryotic genes (*Alma1* and *DSYB*) (Table S2) in addition to all other possible algal peptides retrieved by BLASTp v2.12.0+ against GenBank and with the same predicted function.

To obtain the sequences for constructing the reference trees, the corresponding peptide for each gene was retrieved from the genome database with HMMER3 v3.3.2 (Eddy, 2008). In the case of the DMSO reductase, the search was based on hits to TIGR00509, which included DMSO reductase (DmsA) and trimethylamine-*N*-oxide reductase (TorA). As for acrylate catabolism, the peptides were annotated as AcuI if the gene was adjacent to *dmdA*, as observed in *Rhodobacteraceae* (Todd et al., 2012a) and the gene product belonged to the putative quinone oxidoreductase, YhdH/YhfP family (TIGR02823). Only *Rhodobacteraceae* AcuI peptides were considered since there was not a clear boundary between orthologs (enzymes with the same function) and paralogs (enzymes with a different function within the same protein family) for other taxa in the phylogenetic

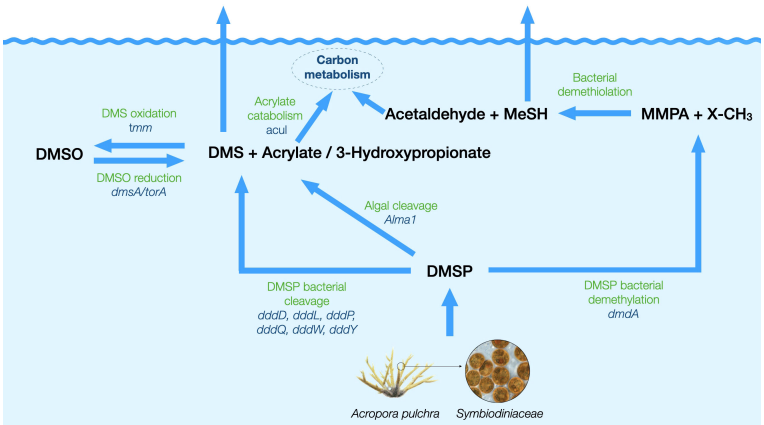

FIGURE 3
Schematic diagram of the putative pathways for the production and cycling of DMSP and derivatives around the studied *A. pulchra* colony, with the involved genes quantified in this study. DMSP is produced by the coral, the *Symbiodiniaceae*, and heterotrophic bacteria, and the target genes were *DSYB* for eukaryotes and *dsyB* for prokaryotes. DMSP is degraded into DMS and acrylate by its eukaryotic producers through the action of the *Alma1* gene, and also undergoes bacterial catabolism *via* multiple pathways: (i) bacterial demethylation into methylmercaptopropionate (MMPA), encoded by the gene *dmdA*, followed by demethiolation to methanethiol and acetaldehyde; (ii) bacterial cleavage into DMS and acrylate, targeted by the genes *dddP, dddL, dddQ, dddW*, and *dddY*; (iii) bacterial cleavage into DMS and 3-hydroxypropionate, encoded by the gene *dddD*. DMS oxidation to DMSO is encoded by *tmm*, and the reverse reduction is encoded by the DMSO/TMAO reductase gene (*dmsA/torA*). Acrylate is catabolized into the central carbon cycle, and one of the genes involved is *acuI*. Description and references of all these genes are given in Table S2.

reconstruction. For the remaining genes, since models (conserved domains in Table S2) retrieved the peptides of interest in addition to paralogs, hidden Markov models (HMMs) were designed to be specific for the gene products to quantify. Phylogenetic trees with peptides that shared the domains shown in Table S2 were used to select a subset with the predicted function. The selection of representative sequences for each gene as well as the boundary between orthologs and paralogs was based on the literature (Table S2). To select an HMM cutoff value, the highest e-value for the representative sequences for each gene when running the HMM profile was used as the highest e-value to do the searches in the peptides from the genome collection.

Reference phylogenetic trees were constructed with IQ-TREE v2.1.4-beta (Nguyen et al., 2015). The subclusters on each of the reference trees were labeled considering that their bootstrap values at the lowest nodes were above 70% and with a taxonomic rank common to all sequences within the subcluster. The reference trees were used to confirm that the taxonomy corresponded to the diversity described in the bibliography for each gene (Table S2).

To filter out most translated metagenome peptides that did not correspond to the function to quantify, first we did BLASTp searches of all metagenome peptides against each of the representative sets with a relaxed searching parameter (minimum bitscore of 50). The database to do the searches contained both the peptides from the reference trees for each gene and the rest of the peptides derived from the genome database, each with a proper label. Any metagenome peptide closer to the peptides on the reference trees was saved for the next annotation step. In case the reference sequences did not contain all diversity of peptides from each gene, an HMM search of the metagenome peptides was also carried out using the same HMM to retrieve the peptides to make the reference trees. Both hits with BLASTp and HMM searches were saved after removing duplicates between the two methods.

In a second step, the metagenome peptides that were retrieved before were placed on the reference trees. To do the placement, metagenome peptides were aligned with reference sequences using the package PaPaRa v2.5 (Berger and Stamatakis, 2011). A maximum likelihood placement was carried out with EPA-ng v0.3.8 (Barbera et al., 2019), with the amino acid substitution model predicted with IQ-TREE for the reference tree. Placed sequences with branch lengths longer than the longest distance between all pairs of sequences on the reference tree were removed (<1% of the sequences). Removed sequences were confirmed to correspond to a different function after performing BLASTp against the GenBank since closest sequences were classified with both Pfam or TIGRFAM in different protein families. At this step, <2% of the sequences had placements in subclusters with a different taxonomic label, although within the same higher rank in their taxonomy in most cases. From these multiple placements in the jplace files, for <1% of them, the sum of the "like weight ratio" that was shared with the best placement (highest "like weight ratio") was below 90%. Finally, the jplace file was converted into a newick text file using gappa v0.7.1 (Czech et al., 2020). The taxonomic assignments of the metagenome peptides in each group were confirmed after visualization of the placed sequences with iToL (Letunic and Bork, 2021).

For each DMSPC cycling gene, raw abundances of the identified peptide sequences were extracted from the gene abundance table previously obtained and normalized by gene size and sequencing depth using the transcripts per million (TPM) unit.

Results

Gradients of dissolved DMSPCs, VOCs, and microbes around reef-predominant organisms

Comparison of dissolved concentrations of DMSPCs and VOCs in the close vicinity of the organism colonies (0.5 cm, IN) and further away (2 m, OUT) was conducted to evaluate if three of the dominant organisms in the Mo'orea reefs were producers of these compounds (Figure 4).

A. pulchra *colonies*. Higher DMSPd concentrations (43–80 nM) were observed in seawater collected ~0.5 cm away from the coral (IN), 20- to 40-fold higher than OUT concentrations 2 m away (2 nM). A similar pattern was observed for DMS (12–50 nM *vs.* 1.3 nM), acrylate (18–65 nM *vs.* 2 nM), and DMSO (21–48 nM *vs.* 5 nM) (Figure 4). As for VOCs other than DMS, concentration gradients suggest that the *A. pulchra* holobiont produced the iodomethanes CH_3I (34–29 pM *vs.* 26–10 pM) and CH_2ClI (2.8 pM *vs.* 1.2 pM), yet the latter was only detectable around one of the colonies [AP(B)]. The only other VOC that showed some enrichment near the holobiont was COS (10–12 pM *vs.* 8–6 pM), whereas negligible differences were observed for dimethyl disulfide (DMDS), CS_2, isoprene, and bromomethanes (Figure 4). Likewise, no obvious differences were found in the prokaryotic and eukaryotic microbial abundances (Figure S1).

Pocillopora sp. *colonies*. Higher DMSPd concentrations were observed closest to this coral holobiont compared to 2 m away (2.2–6.8 nM IN *vs.* 0.8–1.3 nM OUT), although the concentration gradient was lower than observed for *A. pulchra* (Figure 4). However, the main difference from *A. pulchra* was the lack of a gradient for DMS (all approximately 1–2 nM) and DMSO (4.3–0.8 nM *vs.* 4.3–0.4 nM), and a weak gradient for

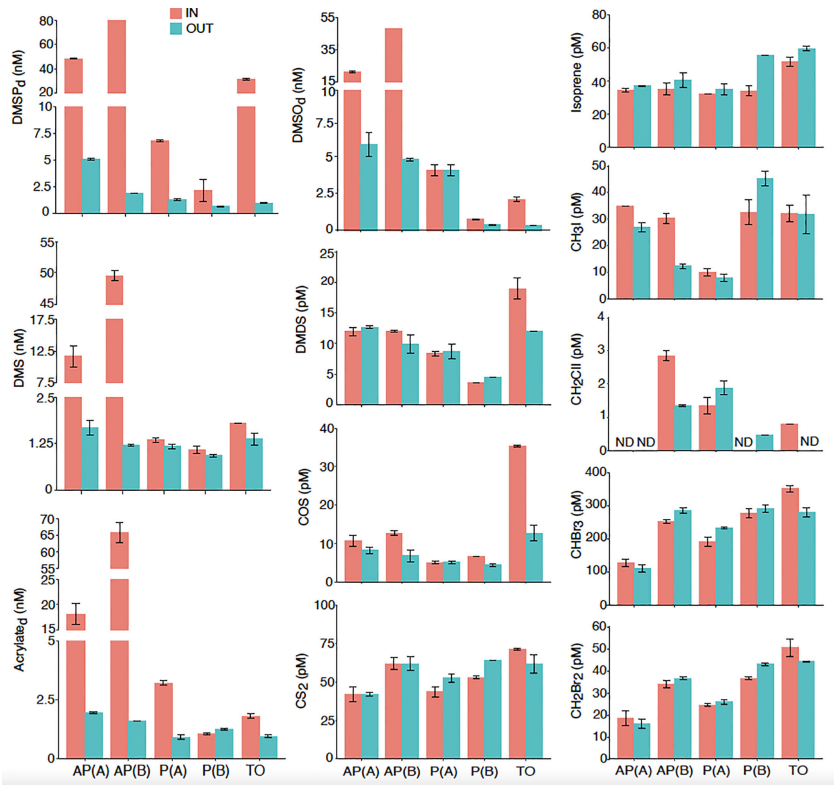

FIGURE 4
Dissolved DMSPC and VOC concentrations in the close vicinity (IN) and 2 m away (OUT) of two colonies of the coral *Acropora pulchra* [AP(A) and AP(B)], two colonies of the coral *Pocillopora* sp. [P(A) and P(B)], and a patch of the seaweed *Turbinaria ornata* (TO). Error bars denote the standard error of duplicate analyses. ND, not detected.

acrylate only observed on one occasion [3.3 nM *vs.* 1 nM in P(A), all ~1 nM in P(B)]. None of the measured VOCs, including DMS, showed enrichment in the inter-verrucae water of the *Pocillopora* sp. colonies, except for COS on one occasion [P(B)]. In most cases, the inter-verrucae water was slightly depleted in VOCs (Figure 4). As for microbial abundances, the only difference was with *Prochlorococcus*, which was more abundant close to the coral (Figure S1).

T. ornata *patch.* This seaweed showed enrichment in the closest sample for most sulfur compounds and halomethanes (Figure 4). The enrichment factor of DMSPd at 0.5 cm from the seaweed with respect to 2 m away was ~30 (31.5 nM IN *vs.* 1 nM OUT). Lower enrichments were observed for acrylate (1.8 nM *vs.* 1 nM), DMSO (2.3 nM *vs.* 0.4 nM), DMS (1.8 nM *vs.* 1.3 nM), and DMDS (19 pM *vs.* 12 pM). COS was the most enriched VOC near the seaweed (35 pM *vs.* 13 pM), and CS_2 was the least (70 pM *vs.* 60 pM). Higher concentrations closest to *T. ornata* were also observed for CH_2ClI (0.8 pM *vs.* not detected), $CHBr_3$ (352 pM *vs.* 280 pM), and CH_2Br_2 (50 pM *vs.* 44 pM). Isoprene and CH_3I showed no enrichment (Figure 4). Among microbes, only *Prochlorococcus* was more abundant close to the seaweed (Figure S1).

Diel cycle of DMSPCs, VOCs, and microorganisms around an *A. pulchra* colony

Here, an *A. pulchra* colony was sampled every 6 h throughout an entire day/night cycle, at three sampling points: between the living branches, ~0.5 cm next to the polyps (IN); deeper between the branches, ~0.5 cm next to the turf alga that colonizes the dead coral (AL); and 2 m down current from the colony patch in seawater overlaying a sandy bottom (OUT). DMSPC and VOC concentrations are shown in Figure 5.

DMSPCs. For the diel study, both the dissolved and total (dissolved + particulate) pools of non-volatile DMSPCs were measured (Figure 5). DMSP was 17%–65% dissolved in IN, 8%–50% in OUT, and 13%–29% in AL. Acrylate was 66%–90% dissolved in IN, 60%–94% in OUT, and 13%–57% in AL. DMSO was 88%–98% dissolved in IN, 93%–100% in OUT, and 29%–92% in AL. Again, DMSPC concentrations were much higher nearest the tips of the branches (IN), where live polyps were present, compared to the concentrations 2 m away (OUT). This was valid for both the dissolved and the total pools of DMSP, acrylate, and DMSO, as well as for DMS. The most salient

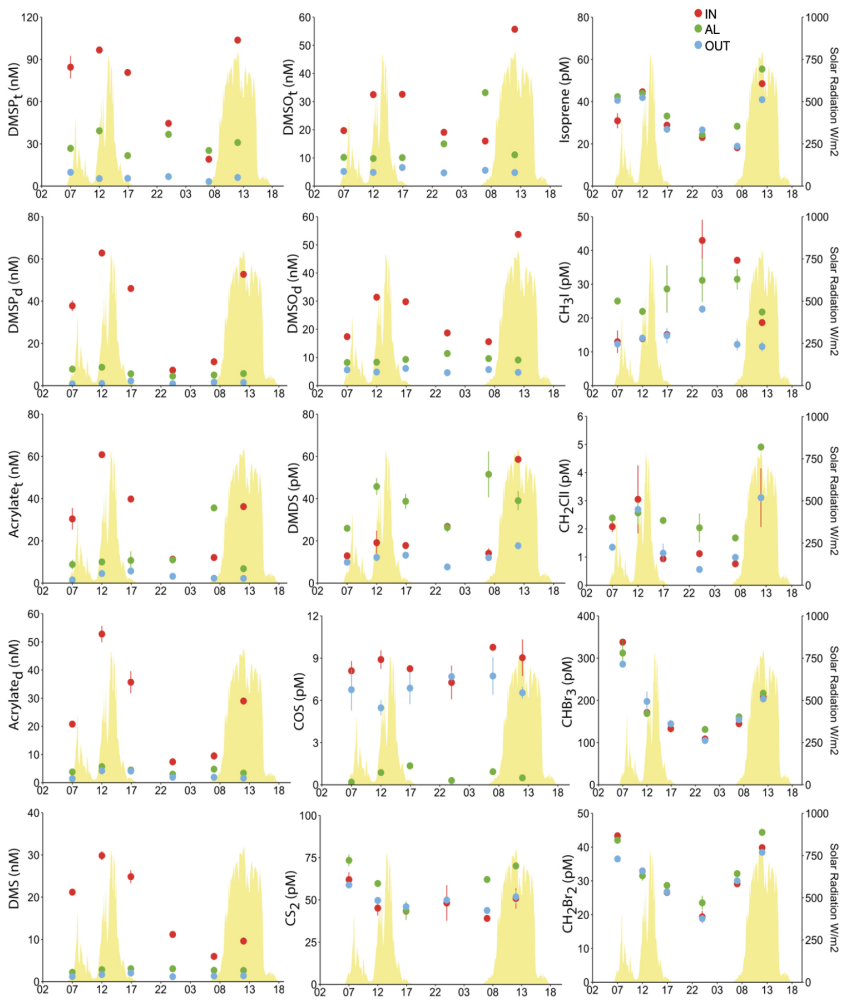

FIGURE 5
Total and dissolved DMSPC concentrations, and VOC concentrations around an *Acropora pulchra* colony over a diel cycle. Seawater samples were taken in the close vicinity of the living branch tips occupied by polyps (IN), the dead base of the branches, colonized by turf algae (AL), and 2 m away from the colony over a sandy bottom (OUT). Error bars denote the standard error of duplicate analyses. The yellow peaks in the background depict total solar radiation.

feature was the strong diel pattern in IN, with highest concentrations around local noon and lowest at late night (Figure 5). The pattern was very consistent across the four DMSPCs, pointing to common causes. Strikingly, in all cases and particularly at midday, concentrations dropped dramatically between IN and AL, which were only 10 cm apart (Figure 5). Not only were the concentrations lower, but no diel pattern was seen in AL. The lowest DMSPC concentrations were found in the seawater out of the coral patch, but it is noteworthy that there was greater similarity, in both concentrations and temporal trends, between AL and OUT (2 m) than between IN and AL (10 cm) (Figure 5). In other words, similarities were not related to distance.

VOCs. DMDS, which also has its putative origin in DMSP (see below), exhibited a diel pattern that roughly paralleled that of the DMSPC (increase at midday, decrease towards a minimum at late night), but its spatial distribution was totally distinct, with generally AL > IN > OUT (Figure 5). CS_2 concentration was also higher in AL during the day and indistinguishable among the three sampling points during the night (Figure 5). In contrast, the most volatile sulfur compound, COS, was similar in IN and OUT, without a clear diel pattern, but was greatly depleted in AL. Isoprene showed a very clear diurnal enhancement but without any spatial gradient. The pattern of CH_3I was opposite to those of most VOCs, with the maximum around midnight and the minimum at midday. The largest amplitude of this variation was observed in IN, and the smallest amplitude but generally higher concentrations were observed in AL. CH_2ClI concentrations clearly followed the sunlight cycle, and were generally higher in AL. Finally, the two

bromomethanes $CHBr_3$ and CH_2Br_2 did not exhibit spatial gradients but their diel cycle showed strong variability towards a minimum at midnight and increasing into the day (Figure 5).

Microbial abundances. In general, there were higher abundances of heterotrophic prokaryotes, *Prochlorococcus*, and autotrophic pico- and nanoeukaryotes in AL, while IN and OUT were only distinguishable because IN harbored higher densities of high nucleic acid containing bacteria (HNA-Bact) (Figure 6). The temporal variation was generally parallel across sampling points: bacteria showed a bimodal pattern with abundance maxima at midday and midnight. Phytoplankton showed a clear maximum, indicating concerted cell division, at midnight. The exception was *Synechococcus*, which showed no differences among sampling points and cell division in the afternoon towards the dusk (Figure 6).

Fine spatial distribution of microbial community composition and diversity around an *A. pulchra* colony

At noon of the second day of our diel survey, coinciding with maximum DMSPC concentrations around the coral colony, we collected extra water volume to investigate the microbial diversity by rDNA amplicon sequencing. A total of 1,496 prokaryotic and 920 eukaryotic ASVs were retrieved among the three sampling points IN, AL, and OUT (Figures 7A, B). Rarefaction curves leveled off for both 16S and 18S rDNA sets, suggesting that most microbial diversity was sequenced in each sample (Figure S2). For prokaryotes, the highest diversity was retrieved in AL: 924 ASVs (~62% of the total), 40% of which were specific to this sample (Figure 7A and Table S3). In the case of eukaryotes, the highest protistan diversity was retrieved in OUT, with a total of 735 ASVs (~80% of the total), of which up to half were only retrieved in this sample (Figure 7B and Table S3). Interestingly, the community richness of prokaryotes and protists, although relatively high in both cases, showed an opposite trend across samples, as indicated by the S_{Chao1} and Shannon diversity indices (Figure S2). Indeed, the most and least diverse prokaryotic communities occurred in AL (H' = 6) and OUT (H' = 4), respectively, while the opposite trend was seen for the protistan community (H' = 4.1 in AL and H' = 5.6 in OUT).

Overall, only small fractions of the prokaryotic (13%) and eukaryotic (5%) microbial diversities were shared between the three samples (Figures 7A, B). Pairwise comparisons of the community composition (Table S3) showed the highest similarity between IN and OUT for prokaryotes ($S_{Sørensen}$ = 0.58, S_{BC} = 0.68), and to a lesser extent also for protists ($S_{Sørensen}$ = 0.46, S_{BC} = 0.38). Both IN and OUT were relatively dissimilar to AL in their prokaryotic and eukaryotic composition ($S_{Sørensen}$ < 0.35, S_{BC} < 0.25). Consequently, the IN and OUT microbial communities shared up to 25% of their diversities despite being the most distant. The nearest communities (IN and AL, only 10 cm apart) had fewer taxa in common, only 7% of the protistan ASVs.

Given the low proportion of microbial diversity shared between samples and the singularity of AL, we explored if similar differences could be observed at the genus taxonomic level as a microbial food web descriptor (Figures 7C, D). We observed dissimilarities in cyanobacteria obtained by amplicon sequencing (Figure S3). As much as 32% and 44% of the prokaryotic community was constituted by cyanobacterial sequences in IN and OUT samples, respectively, while this proportion fell to <4% in AL. The two most abundant cyanobacteria genera were *Synechococcus*, predominant in OUT, and *Prochlorococcus*, with increased presence at IN (Figure 6). As

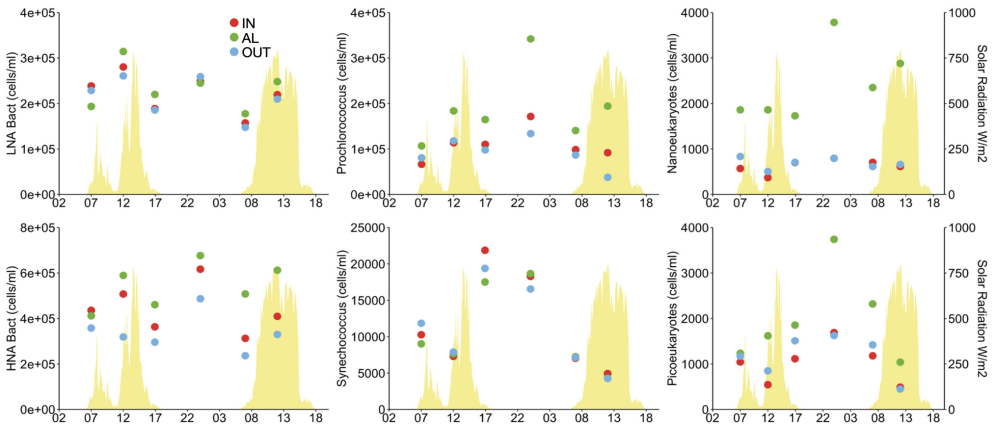

FIGURE 6
Microorganism abundances around an *Acropora pulchra* colony over a diel cycle as determined by flow cytometry. Details of where samples were collected are given in Figure 5. HNA, high nucleic acid containing heterotrophic prokaryotes; LNA, low nucleic acid containing heterotrophic prokaryotes.

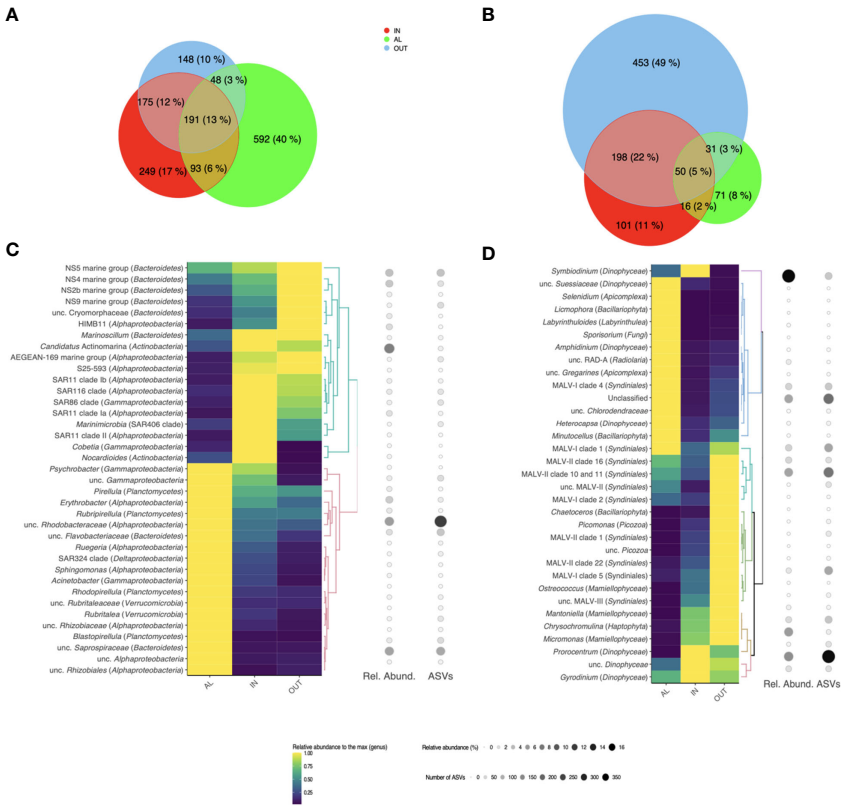

FIGURE 7
Microbial diversity and composition around an *Acropora pulchra* colony. Venn diagrams show the shared and unique amplicon sequencing variants (ASVs) between the heterotrophic bacterial **(A)** and protistan **(B)** communities in samples IN, AL and OUT collected on 25 April 2018 at local noon. Below the number of shared/unique ASVs, the percentages of the total richness they represent are indicated. Heatmaps display the distribution of the main bacterial **(C)** and protistan **(D)** genera in the samples. Only genera that are dominant in at least one of the three samples (representing more than 1% of the total reads in this sample) are showcased, and their relative abundances are scaled to the maximum relative abundance retrieved among the three samples. For each genus, its relative abundance (number of sequences) and richness (number of different ASVs) within the whole sequencing dataset are also indicated.

for the heterotrophic prokaryotic community (Figure 7C), the marine genera of the *Bacteroidetes* phylum (NS2b, NS4, NS5, and NS9 marine groups) and the alphaproteobacterial strain HIMB11 (*Rhodobacteraceae*) were dominant in OUT, while the bacterioplankton in IN were dominated by the ubiquitous alphaproteobacterial clades SAR11, SAR86, and SAR116, known oligotrophs, as well as coral reef characteristic bacteria such as *Candidatus* Actinomarina (Apprill et al., 2016) and *Marinoscillum* (Seo et al., 2009). The bacterioplankton composition in AL was indeed distinct, with abundant sequences affiliated to unclassified *Rhodobacteraceae* and *Flavobacteriaceae*, and to the gammaproteobacterial *Acinetobacter*, known to have copiotrophic lifestyle (Fuhrman et al., 2015). We also retrieved sequences affiliated to putative epiphytic bacteria, such as *Planctomycetes* (*Pirellula* spp. and *Rubripirellula* spp.) and *Verrucomicrobia*.

Regarding the protistan community (Figure 7D), there was a clear dominance of sequences affiliated to *Dinophyta* (i.e., *Dinophyceae* and *Syndiniales*) in the three samples. The overrepresentation of sequences affiliated to dinoflagellates in amplicon datasets is a well-known feature (e.g., Koid et al., 2012; Gong et al., 2015). It is mostly explained by the large variation in the ribosomal (r)DNA operon copy number across protist taxa, which can reach out several thousands in some dinoflagellates or ciliates (Zhu et al., 2005; Vd'acný et al., 2011). Yet, our results show a high prevalence of sequences affiliated to *Symbiodiniaceae* in IN, next to the polyps of *A. pulchra*, suggesting the release of algal symbionts to the surrounding environment, a process known to occur on a daily basis (Broadbent and Jones, 2006). Outside the colony patch (OUT), the eukaryotic community was dominated by sequences affiliated to *Mamiellales* (*Micromonas* spp. and *Mantoniella* spp.), *Haptophyta* (*Chysochromulina* spp.), and *Syndiniales* (parasitic dinoflagellates). Lastly, in AL, we retrieved sequences of *Labyrinthuloides*, organisms responsible for the decomposition of both allochthonous and autochthonous

organic matter (Collado-Mercado et al., 2010). This confirmed the unique environment around the turf alga at the base of the coral branches, where algal-derived organic matter favors the development of copiotrophs.

Quantification of functional genes for DMSPC cycling around an *A. pulchra* colony

At noon of the second day of the diel cycle, a number of target genes encoding for DMSPC transformations (Figure 3) were detected around the *A. pulchra* colony, including those encoding for DMSP biosynthesis (*dsyB* and *DSYB*), demethylation (*dmdA*), and cleavage (*Alma1* and *ddd*-), DMS oxidation (*tmm*), DMSO/TMAO reduction (*dmsA*/*torA*), and one of the possible routes of acrylate catabolism (*acuI*). When the IN and OUT samples were considered together, *dmdA* (widely distributed but mostly in SAR11, *Rhodobacteraceae*, and other *Alphaproteobacteria*) and *tmm* (also mostly in SAR11 and *Rhodobacteraceae*) were the most abundant among the target prokaryotic genes, followed by *dddP* (*Rhodobacteraceae* and SAR116) and *dddQ* (*Alphaproteobacteria*). No significant differences were apparent between IN and OUT except for the DMS production gene *dddD* (Figures 8A–C), which showed enrichment in IN by nearly a factor of 20 (Figure 8B). These sequences clustered with DddD peptides in *Endozoicomonas*, a genus of *Gammaproteobacteria* that dominates the coral microbiome across a wide range of coral species (Bourne et al., 2016) and can grow on DMSP as the sole carbon source (Tandon et al., 2020). Sequences of *dddD* in OUT were classified instead in the family *Litoricolaceae* (*Gammaproteobacteria*). Neither the gene for bacterial DMSP biosynthesis *dsyB* (alphaproteobacterial) nor the genes for DMSO reduction (alphaproteobacterial) and acrylate catabolism *acuI* (*Rhodobacteraceae*) showed any difference in relative abundance between IN and OUT (Figure 8B).

The gene encoding for the DSMP lyase, *Alma1*, was the most abundant of the three target eukaryotic genes, followed by the homolog to the prokaryotic *tmm*, and *DSYB* (Figures 8A, B). *Alma1* and *tmm*, likely associated with *Acropora* and *Symbiodiniaceae*, were found in IN and undetectable in OUT.

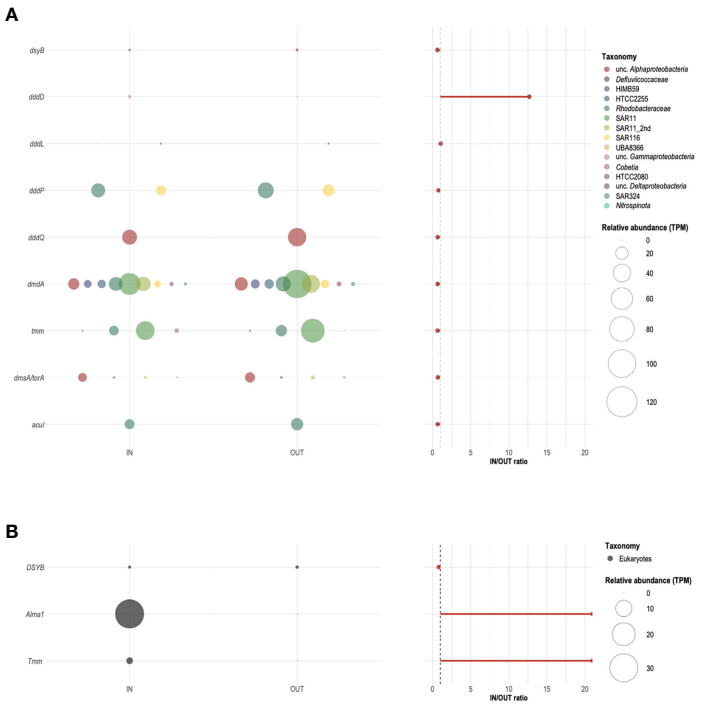

FIGURE 8
Relative abundance and taxonomic profiling of potential bacterial **(A)** and eukaryotic **(B)** DMSPC-cycling genes around an *Acropora pulchra* colony. Bubble plots on the left show the relative abundance, expressed in transcript per million (TPM) of target genes (*dsyB*, *DSYB*, *Alma1*, *dddD*, *dddL*, *dddP*, *dddQ*, *dmdA*, *tmm*, *dmsA*/*torA*, and *acuI*) identified in samples IN and OUT collected on 25 April 2018 at local noon. The colors of the bubbles indicate their taxonomic assignment. No sequences related to genes *dddK*, *dddW*, *dddY*, or *dddX* were detected in our metagenomes. The IN/OUT ratio of the relative abundance of each of the target genes is shown on the right. The dashed gray line corresponds to a ratio equal to 1.

Discussion

Sources of DMSPCs and VOCs

Concentration gradients in close proximity to three of the dominant benthic organisms in the reefs (Donovan et al., 2020) provided valuable information about the VOC and DMSPC sources (Figures 4, 5). *A. pulchra* was confirmed to be a strong source of all DMSPCs (DMSP, DMS, acrylate, and DMSO). Coral holobionts of the genus *Acropora* are well known for being DMSP producers and releasing products of DMSP catabolism (Tapiolas et al., 2010; Raina et al., 2013; Tandon et al., 2020; Guibert et al., 2020). DMS and acrylate were the only catabolic products that showed an increase near the polyps that paralleled the increase of DMSPd, indicating that DMSP-lyase-mediated DMSP cleavage was important, either by the coral itself, the algal symbiont (*Symbiodiniaceae*), or associated bacteria (see below). No significant gradient of DMDS was observed. This compound is very rarely measured in seawater; we interpret its occurrence in the Mo'orean reef sample chromatograms as a reflection of the presence of methanethiol (MeSH). It has been reported that high temperatures and activated carbon, two characteristics of our purge and trap system prior to GC injection and analysis, can oxidize MeSH to DMDS (Cheng et al., 2007). The absence of a gradient of DMDS from *A. pulchra* suggests that DMSP cleavage prevailed over the demethylation + demethiolation pathway (Figure 3; Landa et al., 2019) in DMSP catabolism. Much less is known about DMSO production and release by corals; our results point to DMSO resulting from DMS oxidation (photochemical or microbial) inside the coral holobiont. According to VOC gradients, *A. pulchra* was not a significant source of VOC other than DMS, except for a little COS, which might be related also to DMS photo-oxidation (Lennartz et al., 2020), and iodomethanes, which likely originated in the turf algae that covered the coral skeleton (see below).

Pocillopora sp. was also a source of DMSPd, yet the DMSPd concentrations between the verrucae were 6- to 40-fold lower than between the branches of *A. pulchra*. *Pocillopora* sp. corals are known to produce and release copious amounts of DMSP in connection to oxidative stress. Released DMSP, particularly when it accumulates in the mucus of stressed colonies, may elicit chemoattraction of pathogenic bacteria (Garren et al., 2014). Despite DMSP release, *Pocillopora* sp. was a weak source of DMS, acrylate, and DMSO (Figure 4). This is consistent with Exton et al. (2015) and Lawson et al. (2021), both of whom did not detect DMS in *Pocillopora* corals. We show that *Pocillopora* sp. does produce DMSP but probably does not harbor high DMSP-lyase activity for significant cleavage in the holobiont. This coral also did not produce any VOCs other than DMS, except for a little COS again, probably resulting from the photo-oxidation of DMS.

The seaweed *T. ornata* was a strong source of DMSP, but less so for DMS, acrylate, and DMSO. Burdett et al. (2013) already reported that intracellular DMSP makes up to 0.4% of the weight of a *Turbinaria* sp. from a tropical reef. Like *Pocillopora* sp., neither this seaweed nor its epiphytic bacteria seem to harbor DMSP lyases. This is further supported by the significant increase of DMDS (MeSH) towards the alga; instead of cleavage, released DMSP underwent degradation through demethylation (Figure 3). Since DMSP degradation with MeSH production is only known in prokaryotes, this process was probably conducted by epiphytic bacteria. The seaweed was also a strong source of COS; as with the corals, COS could result from DMS photo-oxidation, but it could also result from photochemical reactions on the seaweed-derived organic matter (Cutter et al., 2004). Other VOCs that were enriched near *T. ornata* were the halomethanes CH_2ClI, $CHBr_3$, and CH_2Br_2. Many macroalgae, including tropical seaweeds and including the genus *Turbinaria*, are known producers of halocarbons, particularly $CHBr_3$ (Leedham et al., 2013; Lim et al., 2017). Suggested physiological and ecological functions are oxidative-stress mitigation (Goodwin et al., 1997; Abrahamsson et al., 2003) and chemical defense against parasitic microbes (Ohsawa et al., 2001). Given that bromomethanes only showed positive gradients towards *T. ornata* and not to the corals, we suggest that the high levels of bromomethanes in the Mo'orean reefs are attributed to the large abundance of macroalgae, among which *T. ornata* dominates.

Are the Mo'orean reefs hotspots of VOC production?

Tropical coral reefs are suggested to be hotspots of VOC production (Exton et al., 2015) because of the high density and diversity of organisms, with presumably large needs for chemical interactions, and their exposure to natural physiological stressors such as high solar irradiance and temperature, water-column transparency to UV radiation, and low nutrient concentrations. Even though we did not characterize anything close to the entire volatilome in the Mo'orea coral reefs, our target VOCs were chemically diverse enough to provide insight into the "VOC hotspot" hypothesis.

In the two reef sites studied here, the OUT seawater samples taken 2 m away from reef-dominant organisms, generally over sandy floor, can be regarded as background waters from inside the reef lagoon that gather VOC contributions from all reef components (Figures 4, 5). Isoprene occurred in the 20–60 pM range, very similar to the range reported for ocean tropical waters outside the regions of equatorial upwelling (Dani and Loreto, 2017). COS ranged between 4 and 11 pM, a little lower than most of the measurements in the tropical ocean (10–20 pM; Lennartz et al., 2020). CS_2 was 40–60 pM, much higher than in most tropical ocean waters (5–15; Lennartz et al., 2020). The range of CH_3I concentrations in reef waters (8–45 pM) was higher than typical concentrations in tropical open waters (1–10 pM; Ziska et al., 2013). We measured very low concentrations of CH_2ClI (ND-3 pM), similar to the 1–3 pM reported by Ooki

et al. (2015) in non-upwelling tropical ocean waters. As for bromomethanes, concentrations in the Mo'orean reefs were 30- to 100-fold higher than those in non-coastal tropical waters in the case of $CHBr_3$ (100–300 pM *vs*. 1-8 pM), and 6- to 15-fold in the case of CH_2Br_2 (15–45 pM *vs*. 1–8 pM; Ziska et al., 2013). DMS concentrations were 1–1.3 nM, in the lower range of tropical open ocean levels (1–5 nM; Lana et al., 2011). We also detected DMDS at concentrations within the 5–15 pM range, which putatively correspond to MeSH concentrations of 10–30 pM, since 1 mol of DMDS corresponds to 2 mol of MeSH. Actually, very few measurements of oceanic MeSH exist because its high reactivity to surfaces makes its analysis challenging. From the few reported measurements, Kettle et al. (2001) estimated that the DMS : MeSH concentration ratio across the Atlantic was 1–30, with a mean of 5–6. We do not know if MeSH was totally converted to DMDS in our system, probably not because the average DMS : DMDS ratio was around 100 (i.e., the putative DMS : MeSH ratio was 50), but DMDS variability can be considered a good proxy of MeSH variability. Overall, the studied reef waters were rich only in CS_2, CH_3I, and particularly $CHBr_3$ and CH_2Br_2, when compared to the average tropical ocean.

DMSP-derived compounds (DMSPCs) other than DMS (namely, DMSP, acrylate, and DMSO) occurred at rather low dissolved concentrations 2 m away from the studied organisms. In the Mo'orean reef lagoon, DMSPd (1–5 nM) and DMSOd (0.5–6 nM) were four to six times lower than in the Great Barrier Reef. No similar data exist with which to compare our dissolved acrylate concentrations (1–3 nM). Plausible reasons for lower DMSPC in Mo'orea are as follows: (i) the fact that corals are not exposed to air and the consequent stress, (ii) differences in the dominant coral species, and (iii) differences in the filtration method (Xue et al., 2022). Furthermore, microbial consumption rates of DMSPd and acrylate in the Mo'orean reefs were faster than most reported rates from any site (Xue et al., 2022), yet there are no data from the Great Barrier Reef to compare with.

Are DMSPC and VOC patterns consistent with a role in coping with light-derived oxidative stress in *A. pulchra*?

Many studies have addressed how corals cope with environmental stress, including the exposure to high irradiance (e.g., Schrameyer et al., 2016; Nitschke et al., 2018). However, to our knowledge, only one study has looked at DMSPC production by a coral over an entire diel cycle (Broadbent and Jones, 2006), and no study has considered VOCs.

Over the diel cycle around the *A. pulchra* colony at the Tema'e Beach reef, both total and dissolved DMSPCs were much higher, closest to the coral polyps, where they largely increased towards noon and decreased towards midnight, following the pattern of solar radiation. Corals of the genus *Acropora* are known to increase their internal DMSP and/or DMSO concentrations in response to stress caused by high irradiance, risen temperatures, hyposaline events, or exposure to air at low tide (Raina et al., 2013; Deschaseaux et al., 2014b; Gardner et al., 2016; Hopkins et al., 2016). Upregulation of DMSP production and turnover can be contributed by the major holobiont components in which the capacity for DMSP biosynthesis has been described: the cnidarian host (Raina et al., 2013), the *Symbiodiniaceae* algal symbiont (Deschaseaux et al., 2014a), and the coral- and *Symbiodiniaceae*-associated bacteria (Curson et al., 2017; Lawson et al., 2020; Kuek et al., 2022). The breakdown of DMSP into DMS and acrylate is suggested to be a mechanism of the coral holobiont to alleviate oxidative stress (Raina et al., 2009), as indicated by previous studies of coral tissue and mucus (e.g., Hill et al., 1995; Broadbent et al., 2002; Raina et al., 2013; Swan et al., 2017; Haydon et al., 2018), since both DMS and acrylate may act as reactive oxygen species (ROS) scavengers (Tapiolas et al., 2010). The cnidarian *Acropora millepora* and several *Symbiodiniaceae* clades have been found to harbor the eukaryotic DMSP lyase Alma1 (Alcolombri et al., 2015), consistent with demonstrated DMSP cleavage activity (Yost and Mitchelmore, 2009). Coral-associated bacteria harbor prokaryotic DMSP lyases too (Raina et al., 2009).

Indeed, the data displayed in Figures 5, 7, and 8 support the light stress hypothesis. DMSPC concentrations in seawater next to the polyps (IN) increased with light, and the pools that increased the most were the dissolved forms. In the last time point of the diel series, at noon, the IN : OUT enrichment factors of 10–50 for dissolved DMSPCs contrasted with the fact that the prokaryotic microbial assemblage composition in IN and OUT was not that different (41% of shared ASVs), suggesting that the light-triggered DMSPCs were mainly released by the coral holobiont. All the target genes in the DMSPC cycle showed same specific abundances right next to the coral and 2-m down current, except for the eukaryotic DMSP cleavage gene (*Alma1*), the eukaryotic DMS oxidation gene (*tmm*), and the prokaryotic DMSP cleavage gene *dddD*. This points to a limited role of reef free-living bacteria to explain the diurnal pulses in DMS, acrylate, and DMSO near the coral. Even though free-living bacteria did not control these pulses, they were nonetheless tuned into daily inputs, as discussed in a companion paper (Xue et al., 2022). The diel trend in DMSPC concentrations paralleled the trend in the microbial uptake of dissolved acrylate and DMSP, with uptake rate constants higher during the day and lower at night, and turnover times on the order of hours. This suggests that the free-living microbial community was well attuned to diel changes in these substrates originating from the coral.

The observation that DMDS (MeSH) showed almost no gradient towards the coral is consistent with the observation that *dmdA* was not enriched in the bacteria closest to the coral tips, and confirms that the coral holobiont did not degrade most of its

DMSP through the sulfur-assimilative demethylation route but through cleavage. Non-cleaved DMSPd was dispersed by the flow and fed bacterial consumption along the reef lagoon (Xue et al., 2022). In contrast, DMDS (MeSH) concentrations were higher near the turf alga (AL) despite DMSPd concentrations that were much lower, indicating that a larger share of DMSP was demethylated. Unfortunately, we could not quantify functional genes in sample AL and hence we could not confirm that *dmdA* was enriched near the turf alga, but the presence of epiphytic and copiotrophic bacterial taxa (Figure 7) suggests higher bacterial activity, larger carbon and sulfur demands, and greater DMSP–sulfur assimilation.

Regarding VOCs other than DMS and DMDS, isoprene increased during the day and decreased at night. This pattern was expected, since isoprene is a photosynthesis-related compound proposed to be used by vascular plants and phytoplankton to combat thermal and oxidative stress (Meskhidze et al., 2015; Dani and Loreto, 2017; McGenity et al., 2018). In *Acropora* corals, Swan et al. (2016), Lawson et al. (2021) and Dawson et al. (2021) reported isoprene production by *A. aspera*, *A. intermedia*, and *A. horrida*, respectively. However, while *A. aspera* increased isoprene production when subject to stress and mucus release by shaking, and *A. horrida* behaved similarly upon temperature increase, no difference was observed in isoprene production by *A. intermedia* under heat stress. Since cultured *Symbiodiniaceae* produce isoprene (Exton et al., 2013), it is not known if the previously reported production by *Acropora* spp. holobionts is to be attributed only to the algal symbionts or to the cnidarian host as well. We did not find significant differences in the concentrations or diel pattern of isoprene concentration between the three sampling points, which indicates that the *A. pulchra* colony was not the source of this compound but rather the surrounding phytoplankton were responsible for sunlight-enhanced isoprene production in our reef.

Other VOCs that were expected to increase during daytime around *A. pulchra* were COS and CS_2, two products of amino acid, DMS, and organic matter photochemistry (Xie et al., 1998; Lennartz et al., 2020), with a release potential from the coral holobiont. The absence of a clear diel pattern of COS and the absence of a gradient with distance from the coral indicate that *A. pulchra* neither produced COS nor favored its production. The salient COS depletion near the turf alga on the dead coralline skeleton (AL), likely an organic matter-rich microhabitat, points to either enhanced hydrolysis (Elliott et al., 1987) or algal uptake (Blezinger et al., 2000) as local COS sinks. CS_2 showed the expected diel pattern but no gradient with distance from the coral tips, indicating no production by *A. pulchra*. Instead, it was higher near the turf alga, due to either organic matter photochemistry or production by increased phytoplankton numbers (Figure 6; Xie et al., 1999).

As for the iodomethanes, CH_3I concentration peaked at midnight. Therefore, the predominant CH_3I source around *A. pulchra* was not photochemical (Richter and Wallace, 2004) but biological (Yokouchi et al., 2014). Over most of the diel cycle, CH_3I was enriched near the turf alga on the dead branches, and only at midnight was it higher nearest to the coral tips. Thus, it is hard to say if CH_3I originated in the coral holobiont, the turf alga, or phytoplankton (which doubled at midnight, Figure 6). It was probably all of them. In contrast, the clear diel pattern of CH_2ClI points to light-related production. As a polyhalogenated compound, it could have resulted from the action of haloperoxidases (in this case, iodoperoxidases) used by organisms to alleviate hydrogen peroxide-induced stress under high sunlight (Moore et al., 1996). CH_2ClI concentrations were generally higher near the turf alga, with no clear evidence of production by the coral holobiont.

Similar to CH_2ClI, the two target poly-bromomethanes likely originated from the action of bromoperoxidases to scavenge harmful hydrogen peroxide (Moore et al., 1996). $CHBr_3$ and CH_2Br_2 exhibited parallel diel patterns with increasing concentrations during the day. The absence of spatial gradients towards the *A. pulchra* tips or the skeleton covered by the turf alga further supports that the main source was not the coral colony but the abundant seaweeds across the reef, particularly *T. ornata*.

Even though most of the target VOCs are regulated by sunlight-related chemical and biological processes, and several are likely involved in oxidative stress alleviation, no VOC except for DMS showed patterns consistent with being released by the *A. pulchra* holobiont to alleviate oxidative stress. In contrast to VOC, the distribution and diel pattern of DMSPC were compatible with their role as holobiont's antioxidants or, at least, their release as a consequence of oxidative stress.

DMSPC release and algal symbiont expulsion at high light

A detailed look at Figure 5 reveals that not only dissolved DMSPCs increased closest to *A. pulchra* during the day, but also particulate DMSP (DMSPp = DMSPt – DMSPd). The characteristics of the eukaryotic microbial assemblage (as defined by the 18S rDNA amplicons) near the coral at noon provided clues to the identity of the microorganisms this DMSPp belonged to: symbiodiniacean ASVs were heavily enriched in IN compared to OUT samples (Figure 7). The higher IN abundance of *Symbiodiniaceae* ASVs could explain the higher DMSPp concentrations near the polyps. Reinforcing this idea, two eukaryotic genes (*Alma1* and *tmm*) were among the few genes only found in IN. The closest archived sequences of these genes belong in *Acropora* and symbiodiniacean genomes (data not shown). The presence of *Acropora* genes can be explained by the release of DNA to the surrounding seawater as part of the extracellular DNA pool (eDNA; Kutti et al., 2020); the presence of symbiodiniacean genes can be explained by symbiont expulsion from the holobiont.

Expulsion of *Symbiodiniaceae* from the polyps into the surrounding seawater is a common process in corals (Hoegh-Guldberg et al., 1987). It occurs mostly around midday, typically associated with mucus release, and is thought to be a response to thermal and sunlight-derived oxidative stress when photo-inhibition and damage by ROS overcome protection in the algal symbiont (Weis, 2008; Curran and Barnard, 2021). We speculate that, in our study case in the shallow Tema'e Beach back reef, *A. pulchra* would expel symbionts as solar radiation increased, along with their associated high DMSPp content. As the expelled *Symbiodiniaceae* would be the most damaged by oxidative or thermal stress (Fujise et al., 2014), before and after expulsion they would transform part of their DMSP into DMS, acrylate, and DMSO (Sunda et al., 2002; Galí et al., 2013; Deschaseaux et al., 2014a). The absence of a thick mucus layer would facilitate the rapid dispersal and dilution of non-cleaved DMSPd by the fast flow, which made it available to reef lagoon bacteria and phytoplankton.

The higher relative abundance of the prokaryotic gene *dddD* near the polyps can also be explained by release from the coral holobiont. Interestingly, Raina et al. (2009) reported that bacteria isolated from coral tissue by enrichment with DMSP showed the presence of DddD and DddL as the only DMSP-degrading enzymes. In our metagenomes, *dddD* belonged entirely to *Gammaproteobacteria*, particularly to *Endozoicomonas* in the sample closest to the polyps. *Endozoicomonas* are ubiquitous endosymbionts in corals, predominant in coral tissues (Bourne et al., 2016). There is no evidence they are associated with *Symbiodiniaceae* (Maire et al., 2021) and can therefore be expelled together, but they are commonly found in the ecosphere around corals (Weber et al., 2019). Indeed, we detected *Endozoicomonas* ASVs only in sample IN, yet at relative abundance <1%.

What do VOCs, DMSPCs, microbial diversity, and gene abundances suggest about water flow, hydrodynamic layers, and connectivity in a branched-coral colony?

It has been long suggested that coral holobionts, by release of organics including DMSPCs, may shape the microbiome within and around them (Raina et al., 2010). This is clear inside the coral, as well as outside when there is a mucus layer, and since the mucus gets enriched in labile organics, symbiodiniacean cells, and associated bacteria, it is retained for a while next to the coral (as it offers viscous resistance to turbulent diffusion or advection by the flow), allowing local microbial growth, and may thus sustain a distinct microbial community. The mucus layer may also attract chemotactic microbes from the surrounding seawater (Garren et al., 2014). However, beyond the mucus layer, the strong flow across highly branched corals will prevent the buildup of a distinct microbiome in the waters next to the coral, except for those microbes released by the coral itself, which will rapidly dilute into the reef water.

In our *A. pulchra* colony, which was never exposed to the air and did not produce a visibly copious mucus, the taxonomic diversity of the microbial communities and their DMSPC-cycling gene inventory suggest a high connectivity between the coral tips and the surrounding waters (Figures 2, 7, 8). The chemical, taxonomic, and genetic differences between the waters next to the coral polyps (IN) and down current (OUT) can be explained by direct release from the coral holobiont. The most striking feature is that the sample AL, located only 10 cm below IN, was the most dissimilar of the three. Here, there could also be a constant release of epiphytic and endosymbiotic microbes from the turf alga, but the only explanation for the buildup of such a distinct community with respect to IN is that the connectivity between the two is dramatically reduced. This lack of connectivity can be explained by invoking the fine hydrodynamics of coral knolls (Shashar et al., 1996). While IN was located within the "outer benthic boundary layer", where the reef main current is modified by the overall shape of the coral colony and its neighboring structures, AL was probably located within the "inner benthic boundary layer", defined as the zone where water motion is reduced due to the coral height and internal structure. The existence of these two layers would have reduced intra-colony mixing. Inside each layer and looking even closer, both sampling points could have been within their own momentum boundary layer (a few centimeters thick, and note that we sampled 0.5 cm from the branches) that controls water movement in the close proximity to the coral surface. These thin local layers would have allowed measurable gradients of chemicals, microbes, and genes.

Conclusions

In comparison with the tropical oceans, the two Mo'orean back reef waters sampled showed elevated VOC concentrations only for CS_2, CH_3I, and particularly $CHBr_3$ and CH_2Br_2. Two of the dominant corals, *A. pulchra* and *Pocillopora* sp., were producers and releasers of DMSP, and the former accompanied DMSP with large production of its catabolites DMS, acrylate, and DMSO. However, these compounds were rapidly diluted and consumed in the reef (Xue et al., 2022). The two corals were not remarkable sources of VOC other than DMS. The abundant seaweed *T. ornata* also released DMSP and was directly or indirectly responsible for producing COS and poly-halomethanes, particularly $CHBr_3$ and CH_2Br_2.

Around a colony of *A. pulchra*, large diurnal increases in the concentrations of DMSP, DMS, acrylate, and DMSO closest to the polyps support the hypothesis that these compounds derive from sunlight-induced oxidative stress. rDNA metabarcoding and metagenome analyses of seawater samples around the

colony suggest that DMSP occurrence and its transformation into DMS, acrylate, and DMSO resulted mainly from coral symbionts and their shedding. Large differences in the chemical and microbial compositions next to the living branches and the deeper skeleton colonized by a turf alga, only 10 cm apart, illustrate the hydrodynamic complexity of branched coral colonies, where the coral structure affects the water flow and mixing.

Tropical coral reefs are threatened worldwide as a result of increased stress from global warming, clearer skies, ocean acidification, human uses, and nutrient and pollution dumping (Harborne et al., 2017). Protection and conservation strategies require the development of early reef health/damage indicators as well as a better knowledge of how these complex and ancient ecosystems have evolved fitness and resilience. Volatile and organosulfur compounds have been suggested to be both health indicators and shields against stress, and our work provides new insights into how they operate.

Data availability statement

The datasets presented in this study can be found in online repositories. DMSPC and VOC concentrations can be found at https://zenodo.org/badge/DOI/10.5281/zenodo.7043105.svg. Raw sequences are available at the European Nucleotide Archive (http://www.ebi.ac.uk/ena) under project numbers PRJEB54595 (16S rDNA metabarcoding), PRJEB54596 (18S rDNA metabarcoding) and PRJEB54597 (metagenomics).

Author contributions

MM-N and RS designed the study. MM-N and SG conducted the sample collection and filtration. MM-N, RS, LX, and DK performed the VOC, DMSP, DMSO, and acrylate analyses. MC-B determined microbial abundances by flow cytometry. MM-N isolated DNA and RNA for sequencing. J-FM and JG analyzed the sequencing data for microbial diversity and functional genes. RS, MM-N, J-FM, and JG wrote the manuscript with contributions from all co-authors. All authors contributed to the article and approved the submitted version.

Funding

This project has received funding from the European Research Council (ERC) under the European Union's Horizon 2020 research and innovation program (grant agreement #834162, SUMMIT Advanced Grant to RS). It was also funded by the Spanish Ministry of Science and Innovation (MCIN/AEI, doi: 10.13039/501100011033) through the BIOGAPS grant (CTM2016-81008-R) to RS, the TRAITS grant (PID2019-110011RB-C32) to JMG, the "Severo Ochoa Centre of Excellence" accreditation (CEX2019-000298-S) to the ICM, and predoctoral grants to MM-N (BES-2017-080048) and MC-B (FPU16-01925). LX and DK were supported by funding from the National Science Foundation Chemical Oceanography program (CO-1756907) to DK. SG was supported by an Australian Government Endeavour Research Fellowship.

Acknowledgments

We thank the UC Berkeley Richard Gump Research station staff for logistical support during the field study. Thanks are also extended to Cèlia Marrasé and Pablo Rodríguez-Ros for assistance during the fieldwork, and Yaiza M. Castillo for flow cytometry re-analyses. Computing analyses from both amplicon and metagenomic sequencing data were run at the Marine Bioinformatics Service of the ICM-CSC (http://marbits.icm.csic.es).

Conflict of interest

The authors declare that the research was conducted in the absence of any commercial or financial relationships that could be construed as a potential conflict of interest.

Publisher's note

Supplementary material

The Supplementary Material for this article can be found online at: https://www.frontiersin.org/articles/10.3389/fmars.2022.944141/full#supplementary-material

References

Abrahamsson, K., Choo, K.-S., Pedersеin, M., Johansson, G., and Snoeijs, P. (2003). Effects of temperature on the production of hydrogen peroxide and volatile halocarbons by brackish-water algae. *Phytochemistry* 64, 725–734. doi: 10.1016/S0031-9422(03)00419-9

Alcolombri, U., Ben-Dor, S., Feldmesser, E., Levin, Y., Tawfik, D. S., and Vardi, A. (2015). Identification of the algal dimethyl sulfide–releasing enzyme: A missing link in the marine sulfur cycle. *Science* 348, 1466–1469. doi: 10.1126/science.aab1586

Anders, S., Pyl, P. T., and Huber, W. (2015). HTSeq–a Python framework to work with high- throughput sequencing data. *Bioinformatics* 31, 166–169. doi: 10.1093/bioinformatics/btu638

Apprill, A., Weber, L. G., and Santoro, A. E. (2016). Distinguishing between microbial habitats unravels ecological complexity in coral microbiomes. *mSystems* 1, e00143-16. doi: 10.1128/mSystems.00143-16

Balzano, S., Abs, E., and Leterme, S. (2015). Protist diversity along a salinity gradient in a coastal lagoon. *Aquat. Microb. Ecol.* 74, 263–277. doi: 10.3354/ame01740

Barbera, P., Kozlov, A. M., Czech, L., Morel, B., Darriba, D., Flouri, T., et al. (2019). EPA-Ng: Massively parallel evolutionary placement of genetic sequences. *Systematic Biol.* 68, 365–369. doi: 10.1093/sysbio/syy054

Berger, S. A., and Stamatakis, A. (2011). Aligning short reads to reference alignments and trees. *Bioinformatics* 27, 2068–2075. doi: 10.1093/bioinformatics/btr320

Blezinger, S., Wilhelm, C., and Kesselmeier, J. (2000). Enzymatic consumption of carbonyl sulfide (COS) by marine algae. *Biogeochemistry* 48, 185–197. doi: 10.1023/A:1006134213995

Bolger, A. M., Lohse, M., and Usadel, B. (2014). Trimmomatic: a flexible trimmer for illumina sequence data. *Bioinformatics* 30, 2114–2120. doi: 10.1093/bioinformatics/btu170

Bourne, D. G., Morrow, K. M., and Webster, N. S. (2016). Insights into the coral microbiome: underpinning the health and resilience of reef ecosystems. *Ann. Rev. Microbiol.* 70, 317–340. doi: 10.1146/annurev-micro-102215-095440

Broadbent, A., and Jones, G. (2006). Seasonal and diurnal cycles of dimethylsulfide, dimethylsulfoniopropionate and dimethylsulfoxide at one tree reef lagoon. *Environ. Chem.* 3, 260. doi: 10.1071/EN06011

Broadbent, A. D., Jones, G. B., and Jones, R. J. (2002). DMSP in corals and benthic algae from the great barrier reef. *Est. Coast. Shelf Sci.* 55, 547–555. doi: 10.1006/ecss.2002.1021

Burdett, H. L., Donohue, P. J. C., Hatton, A. D., Alwany, M. A., and Kamenos, N. A. (2013). Spatiotemporal variability of dimethylsulphoniopropionate on a fringing coral reef: The role of reefal carbonate chemistry and environmental variability. *PloS One* 8 (5), e64651. doi: 10.1371/journal.pone.0064651

Callahan, B. J., McMurdie, P. J., Rosen, M. J., Han, A. W., Johnson, A. J. A., and Holmes, S. P. (2016). DADA2: High-resolution sample inference from illumina amplicon data. *Nat. Methods* 13, 581–583. doi: 10.1038/nmeth.3869

Carpenter, L. J., Archer, S. D., and Beale, R. (2012). Ocean-atmosphere trace gas exchange. *Chem. Soc Rev.* 41, 6473–6506. doi: 10.1039/c2cs35121h

Charlson, R. J., Lovelock, J. E., Andreae, M. O., and Warren, S. G. (1987). Oceanic phytoplankton, atmospheric sulfur, cloud albedo and climate. *Nature* 326, 655–661. doi: 10.1038/326655a0

Chaumeil, P.-A., Mussig, A. J., Hugenholtz, P., and Parks, D. H. (2020). GTDB-tk: a toolkit to classify genomes with the genome taxonomy database. *Bioinformatics* 36, 1925–1927. doi: 10.1093/bioinformatics/btz848

Cheng, X., Peterkin, E., and Narangajavana, K. (2007). Wastewater analysis for volatile organic sulfides using purge-and-trap with gas chromatography/mass spectrometry. *Water Environ. Res.* 79, 442–446. doi: 10.2175/106143006X111871

Collado-Mercado, E., Radway, J., and Collier, J. (2010). Novel uncultivated labyrinthulomycetes revealed by 18S rDNA sequences from seawater and sediment samples. *Aquat. Microb. Ecol.* 58, 215–228. doi: 10.3354/ame01361

Curran, A., and Barnard, S. (2021). What is the role of zooxanthellae during coral bleaching? review of zooxanthellae and their response to environmental stress. *S. Afr. J. Sci.* 117, 8639. doi: 10.17159/sajs.2021/8369

Curson, A. R. J., Liu, J., Bermejo Martiínez, A., Green, R. T., Chan, Y., Carrioín, O., et al. (2017). Dimethylsulfoniopropionate biosynthesis in marine bacteria and identification of the key gene in this process. *Nat. Microbiol.* 2, 17009. doi: 10.1038/nmicrobiol.2017.9

Cutter, G. A., Cutter, L. S., and Filippino, K. C. (2004). Sources and cycling of carbonyl sulfide in the Sargasso Sea. *Limnol. Oceanogr.* 49, 555–565. doi: 10.4319/lo.2004.49.2.0555

Czech, L., Barbera, P., and Stamatakis, A. (2020). Genesis and gappa: processing, analyzing and visualizing phylogenetic (placement) data. *Bioinformatics* 36, 3263–3265. doi: 10.1093/bioinformatics/btaa070

Dani, K. G. S., and Loreto, F. (2017). Trade-off between dimethyl sulfide and isoprene emissions from marine phytoplankton. *Trends Plant Sci.* 22, 361–372. doi: 10.1016/j.tplants.2017.01.006

Dawson, R. A., Crombie, A. T., Pichon, P., Steinke, M., McGenity, T. J., and Murrell, J. C. (2021). The microbiology of isoprene cycling in aquatic ecosystems. *Aquat. Microb. Ecol.* 87, 79–98. doi: 10.3354/ame01972

Deschaseaux, E. S. M., Beltran, V. H., Jones, G. B., Deseo, M. A., Swan, H. B., Harrison, P. L., et al. (2014a). Comparative response of DMS and DMSP concentrations in *Symbiodinium* clades C1 and D1 under thermal stress. *J. Exp. Mar. Biol. Ecol.* 459, 181–189. doi: 10.1016/j.jembe.2014.05.018

Deschaseaux, E. S. M., Jones, G. B., Deseo, M. A., Shepherd, K. M., Kiene, R. P., Swan, H. B., et al. (2014b). Effects of environmental factors on dimethylated sulfur compounds and their potential role in the antioxidant system of the coral holobiont. *Limnol. Oceanogr.* 59, 758–768. doi: 10.4319/lo.2014.59.3.0758

Donovan, M. K., Adam, T. C., Shantz, A. A., Speare, K. E., Munsterman, K. S., Rice, M. M., et al. (2020). Nitrogen pollution interacts with heat stress to increase coral bleaching across the seascape. *Proc. Natl. Acad. Sci. U.S.A.* 117, 5351–5357. doi: 10.1073/pnas.1915395117

Eddy, S. R. (2008). A probabilistic model of local sequence alignment that simplifies statistical significance estimation. *PloS Comput. Biol.* 4, e1000069. doi: 10.1371/journal.pcbi.1000069

Elliott, S., Lu, E., and Rowland, F. S. (1987). Carbonyl sulfide hydrolysis as a source of hydrogen sulfide in open ocean seawater. *Geophys. Res. Lett.* 14, 131–134. doi: 10.1029/GL014i002p00131

Exton, D. A., McGenity, T. J., Steinke, M., Smith, D. J., and Suggett, D. J. (2015). Uncovering the volatile nature of tropical coastal marine ecosystems in a changing world. *Glob. Change Biol.* 21, 1383–1394. doi: 10.1111/gcb.12764

Exton, D. A., Suggett, D. J., McGenity, T. J., and Steinke, M. (2013). Chlorophyll-normalized isoprene production in laboratory cultures of marine microalgae and implications for global models. *Limnol. Oceanogr.* 58, 1301–1311. doi: 10.4319/lo.2013.58.4.1301

Fuhrman, J. A., Cram, J. A., and Needham, D. M. (2015). Marine microbial community dynamics and their ecological interpretation. *Nat. Rev. Microbiol.* 13, 133–146. doi: 10.1038/nrmicro3417

Fujise, L., Yamashita, H., Suzuki, G., Sasaki, K., Liao, L. M., and Koike, K. (2014). Moderate thermal stress causes active and immediate expulsion of photosynthetically damaged zooxanthellae (*Symbiodinium*) from corals. *PloS One* 9 (12), e114321. doi: 10.1371/journal.pone.0114321

Galí, M., Ruiz-González, C., Lefort, T., Gasol, J. M., Cardelús, C., Romera-Castillo, C., et al. (2013). Spectral irradiance dependence of sunlight effects on plankton dimethylsulfide production. *Limnol. Oceanogr.* 58, 489–504. doi: 10.4319/lo.2013.58.2.0489

Gardner, S. G., Nielsen, D. A., Laczka, O., Shimmon, R., Beltran, V. H., Ralph, P. J., et al. (2016). Dimethylsulfoniopropionate, superoxide dismutase and glutathione as stress response indicators in three corals under short-term hyposalinity stress. *Proc. R. Soc B.* 283, 20152418. doi: 10.1098/rspb.2015.2418

Garren, M., Son, K., Raina, J.-B., Rusconi, R., Menolascina, F., Shapiro, O. H., et al. (2014). A bacterial pathogen uses dimethylsulfoniopropionate as a cue to target heat-stressed corals. *ISME J.* 8, 999–1007. doi: 10.1038/ismej.2013.210

Gong, J., Shi, F., Ma, B., Dong, J., Pachiadaki, M., Zhang, X., et al. (2015). Depth shapes α- and β-diversities of microbial eukaryotes in surficial sediments of coastal ecosystems: Diversity and biogeography of benthic microeukaryotes. *Environ. Microbiol.* 17, 3722–3737. doi: 10.1111/1462-2920.12763

Goodwin, K. D., North, W. J., and Lidstrom, M. E. (1997). Production of bromoform and dibromomethane by giant kelp: Factors affecting release and comparison to anthropogenic bromine sources. *Limnol. Oceanogr.* 42, 1725–1734. doi: 10.4319/lo.1997.42.8.1725

Guibert, I., Bourdreux, F., Bonnard, I., Pochon, X., Dubousquet, V., Raharivelomanana, P., et al. (2020). Dimethylsulfoniopropionate concentration in coral reef invertebrates varies according to species assemblages. *Sci. Rep.* 10, 9922. doi: 10.1038/s41598-020-66290-5

Guillou, L., Bachar, D., Audic, S., Bass, D., Berney, C., Bittner, L., et al. (2012). The protist ribosomal reference database (PR2): a catalog of unicellular eukaryote small sub-unit rRNA sequences with curated taxonomy. *Nucleic Acids Res.* 41, D597–D604. doi: 10.1093/nar/gks1160

Harborne, A. R., Rogers, A., Bozec, Y.-M., and Mumby, P. J. (2017). Multiple stressors and the functioning of coral reefs. *Annu. Rev. Mar. Sci.* 9, 445–468. doi: 10.1146/annurev-marine-010816-060551

Haydon, T. D., Seymour, J. R., and Suggett, D. J. (2018). Soft corals are significant DMSP producers in tropical and temperate reefs. *Mar. Biol.* 165, 109. doi: 10.1007/s00227-018-3367-2

Hemond, E. M., and Vollmer, S. V. (2015). Diurnal and nocturnal transcriptomic variation in the Caribbean staghorn coral, *Acropora cervicornis*. *Mol. Ecol.* 24, 4460–4473. doi: 10.1111/mec.13320

Hill, R. W., Dacey, W. H., and Krupp, D. A. (1995). Dimethylsulfoniopropionate in reef corals. *Bull. Mar. Sci.* 57, 489–494.

Hoegh-Guldberg, O., McCloskey, L. R., and Muscatine, L. (1987). Expulsion of zooxanthellae by symbiotic cnidarians from the red Sea. *Coral Reefs* 5, 201–204. doi: 10.1007/BF00300964

Hoegh-Guldberg, O., Poloczanska, E. S., Skirving, W., and Dove, S. (2017). Coral reef ecosystems under climate change and ocean acidification. *Front. Mar. Sci.* 29 doi: 10.3389/fmars.2017.00158

Hopkins, F. E., Bell, T. G., Yang, M., Suggett, D. J., and Steinke, M. (2016). Air exposure of coral is a significant source of dimethylsulfide (DMS) to the atmosphere. *Sci. Rep.* 6, 36031. doi: 10.1038/srep36031

Howard, E. C., Henriksen, J. R., Buchan, A., Reisch, C. R., Bürgmann, H., Welsh, R., et al. (2006). Bacterial taxa that limit sulfur flux from the ocean. *Science* 314, 649–652. doi: 10.1126/science.1130657

Hyatt, D., Chen, G.-L., LoCascio, P. F., Land, M. L., Larimer, F. W., and Hauser, L. J. (2010). Prodigal: prokaryotic gene recognition and translation initiation site identification. *BMC Bioinf.* 11, 119. doi: 10.1186/1471-2105-11-119

Jackson, R. L., Gabric, A. J., and Cropp, R. (2020). Coral reefs as a source of climate-active aerosols. *PeerJ.* 8, e10023. doi: 10.7717/peerj.10023

Jones, G. B. (2015). "The reef sulfur cycle: Influence on climate and ecosystem services," in *Ethnobiology of corals and coral reefs*. Eds. N. E. Narchi and L. L. Price (Switzerland: Springer International Publishing), 27–57. doi: 10.1007/978-3-319-23763-3_3

Kettle, A. J., Rhee, T. S., von Hobe, M., Poulton, A., Aiken, J., and Andreae, M. O. (2001). Assessing the flux of different volatile sulfur gases from the ocean to the atmosphere. *J. Geophys. Res.* 106, 12193–12209. doi: 10.1029/2000JD900630

Kiene, R. P., and Slezak, D. (2006). Low dissolved DMSP concentrations in seawater revealed by small-volume gravity filtration and dialysis sampling: Filtration and dialysis for dissolved DMSP. *Limnol. Oceanogr. Methods* 4, 80–95. doi: 10.4319/lom.2006.4.80

Kim, K. H., and Andreae, M. O. (1992). Carbon disulfide in the estuarine, coastal and oceanic environments. *Mar. Chem.* 40, 179–1971992. doi: 10.1016/0304-4203(92)90022-3

Kinsey, J. D., and Kieber, D. J. (2016). Microwave preservation method for DMSP, DMSO, and acrylate in unfiltered seawater and phytoplankton culture samples: Microwave sample preservation method. *Limnol. Oceanogr. Methods* 14, 196–209. doi: 10.1002/lom3.10081

Kinsey, J. D., Kieber, D. J., and Neale, P. J. (2016). Effects of iron limitation and UV radiation on *Phaeocystis antarctica* growth and dimethylsulfoniopropionate, dimethylsulfoxide and acrylate concentrations. *Environ. Chem.* 13, 195. doi: 10.1071/EN14275

Klemetsen, T., Raknes, I. A., Fu, J., Agafonov, A., Balasundaram, S. V., Tartari, G., et al. (2018). The MAR databases: development and implementation of databases specific for marine metagenomics. *Nucleic Acids Res.* 46, D692–D699. doi: 10.1093/nar/gkx1036

Koid, A., Nelson, W. C., Mraz, A., and Heidelberg, K. B. (2012). Comparative analysis of eukaryotic marine microbial assemblages from 18S rRNA gene and gene transcript clone libraries by using different methods of extraction. *Appl. Environ. Microbiol.* 78, 3958–3965. doi: 10.1128/AEM.06941-11

Kuek, F. W. I., Motti, C. A., Zhang, J., Cooke, I. R., Todd, J. D., Miller, D. J., et al. (2022). DMSP production by coral-associated bacteria. *Front. Mar. Sci* 9. doi: 10.3389/fmars.2022.869574

Kutti, T., Johnsen, I. A., Skaar, K. S., Ray, J. L., Husa, V., and Dahlgren, T. G. (2020). Quantification of eDNA to map the distribution of cold-water coral reefs. *Front. Mar. Sci.* 7. doi: 10.3389/fmars.2020.00446

Lana, A., Bell, T. G., Simoí, R., Vallina, S. M., Ballabrera-Poy, J., Kettle, A. J., et al. (2011). An updated climatology of surface dimethlysulfide concentrations and emission fluxes in the global ocean. *Global Biogeochem. Cycles* 25, GB1004. doi: 10.1029/2010GB003850

Landa, M., Burns, A. S., Durham, B. P., Esson, K., Nowinski, B., Sharma, S., et al. (2019). Sulfur metabolites that facilitate oceanic phytoplankton–bacteria carbon flux. *ISME J.* 13, 2536–2550. doi: 10.1038/s41396-019-0455-3

Langmead, B., and Salzberg, S. L. (2012). Fast gapped-read alignment with bowtie 2. *Nat. Methods* 9, 357–359. doi: 10.1038/nmeth.1923

Lawson, C. A., Raina, J.-B., Deschaseaux, E., Hrebien, V., Possell, M., Seymour, J. R., et al. (2021). Heat stress decreases the diversity, abundance and functional potential of coral gas emissions. *Global Change Biol.* 27, 879–891. doi: 10.1111/gcb.15446

Lawson, C. A., Seymour, J. R., Possell, M., Suggett, D. J., and Raina, J.-B. (2020). The volatilomes of symbiodiniaceae-associated bacteria are influenced by chemicals derived from their algal partner. *Front. Mar. Sci.* 7. doi: 10.3389/fmars.2020.00106

Leedham, E. C., Hughes, C., Keng, F. S. L., Phang, S.-M., Malin, G., and Sturges, W. T. (2013). Emission of atmospherically significant halocarbons by naturally occurring and farmed tropical macroalgae. *Biogeosciences* 10, 3615–3633. doi: 10.5194/bg-10-3615-2013

Lennartz, S. T., Marandino, C. A., von Hobe, M., Andreae, M. O., Aranami, K., Atlas, E., et al. (2020). Marine carbonyl sulfide (OCS) and carbon disulfide (CS_2): a compilation of measurements in seawater and the marine boundary layer. *Earth Syst. Sci. Data* 12, 591–609. doi: 10.5194/essd-12-591-2020

Letunic, I., and Bork, P. (2021). Interactive tree of life (iTOL) v5: an online tool for phylogenetic tree display and annotation. *Nucleic Acids Res.* 49, W293–W296. doi: 10.1093/nar/gkab301

Li, W., and Godzik, A. (2006). Cd-hit: a fast program for clustering and comparing large sets of protein or nucleotide sequences. *Bioinformatics* 22, 1658–1659. doi: 10.1093/bioinformatics/btl158

Li, H., Handsaker, B., Wysoker, A., Fennell, T., Ruan, J., Homer, N., et al. (2009). The sequence alignment/map format and SAMtools. *Bioinformatics* 25, 2078–2079. doi: 10.1093/bioinformatics/btp352

Li, D., Luo, R., Liu, C.-M., Leung, C.-M., Ting, H.-F., Sadakane, K., et al. (2016). MEGAHIT v1.0: A fast and scalable metagenome assembler driven by advanced methodologies and community practices. *Methods* 102, 3–11. doi: 10.1016/j.ymeth.2016.02.020

Lim, Y.-K., Phang, S.-M., Abdul Rahman, N., Sturges, W. T., and Malin, G. (2017). Halocarbon emissions from marine phytoplankton and climate change. *Int. J. Environ. Sci. Technol.* 14, 1355–1370. doi: 10.1007/s13762-016-1219-5

Maire, J., Girvan, S. K., Barkla, S. E., Perez-Gonzalez, A., Suggett, D. J., Blackall, L. L., et al. (2021). Intracellular bacteria are common and taxonomically diverse in cultured and in hospite algal endosymbionts of coral reefs. *ISME J.* 15, 2028–2042. doi: 10.1038/s41396-021-00902-4

Martin, M. (2011). Cutadapt removes adapter sequences from high-throughput sequencing reads. *EMBnet J.* 17, 10. doi: 10.14806/ej.17.1.200

Massana, R., Murray, A. E., Preston, C. M., and DeLong, E. F. (1997). Vertical distribution and phylogenetic characterization of marine planktonic archaea in the Santa Barbara channel. *Appl. Environ. Microbiol.* 63, 50–56. doi: 10.1128/aem.63.1.50-56.1997

McGenity, T. J., Crombie, A. T., and Murrell, J. C. (2018). Microbial cycling of isoprene, the most abundantly produced biological volatile organic compound on earth. *ISME J.* 12, 931–941. doi: 10.1038/s41396-018-0072-6

Meskhidze, N., Sabolis, A., Reed, R., and Kamykowski, D. (2015). Quantifying environmental stress-induced emissions of algal isoprene and monoterpenes using laboratory measurements. *Biogeosciences* 12, 637–651. doi: 10.5194/bg-12-637-2015

Moore, R. M., Webb, M., Tokarczyk, R., and Wever, R. (1996). Bromoperoxidase and iodoperoxidase enzymes and production of halogenated methanes in marine diatom cultures. *J. Geophys. Res.* 101, 20899–20908. doi: 10.1029/96JC01248

Nguyen, L.-T., Schmidt, H. A., von Haeseler, A., and Minh, B. Q. (2015). IQ-TREE: A fast and effective stochastic algorithm for estimating maximum-likelihood phylogenies. *Mol. Biol. Evol.* 32, 268–274. doi: 10.1093/molbev/msu300

Nishimura, Y., and Yoshizawa, S. (2022). The OceanDNA MAG catalog contains over 50,000 prokaryotic genomes originated from various marine environments. *Sci Data* 9, 305. doi: 10.1038/s41597-022-01392-5

Nitschke, M. R., Gardner, S. G., Goyen, S., Fujise, L., Camp, E. F., Ralph, P. J., et al. (2018). Utility of photochemical traits as diagnostics of thermal tolerance amongst great barrier reef corals. *Front. Mar. Sci.* 5 (45). doi: 10.3389/fmars.2018.00045

Ohsawa, N., Ogata, Y., Okada, N., and Itoh, N. (2001). Physiological function of bromoperoxidase in the red marine alga, *Corallina pilulifera*: production of bromoform as an allelochemical and the simultaneous elimination of hydrogen peroxide. *Phytochemistry* 58, 683–692. doi: 10.1016/S0031-9422(01)00259-X

Oksanen, J., Blanchet, F. G., Friendly, M., Kindt, R., Legendre, P., McGlinn, D., et al. (2021) *Vegan: Community ecology package*. Available at: https://CRAN.R-project.org/package=vegan.

Ooki, A., Nomura, D., Nishino, S., Kikuchi, T., and Yokouchi, Y. (2015). A global-scale map of isoprene and volatile organic iodine in surface seawater of the Arctic, Northwest pacific, Indian, and southern oceans. *J. Geophys. Res. Ocean.* 120, 4108–4128. doi: 10.1002/2014JC010519

Paoli, L., Ruscheweyh, H.-J., Forneris, C. C., Kautsar, S., Clayssen, Q., Salazar, G., et al. (2022). Uncharted biosynthetic potential of the ocean microbiome. *Nature* 607, 111–118 doi: 10.1038/s41586-022-04862-3

Parada, A. E., Needham, D. M., and Fuhrman, J. A. (2016). Every base matters: assessing small subunit rRNA primers for marine microbiomes with mock communities, time series and global field samples: Primers for marine microbiome studies. *Environ. Microbiol.* 18, 1403–1414. doi: 10.1111/1462-2920.13023

Pruesse, E., Quast, C., Knittel, K., Fuchs, B. M., Ludwig, W., Peplies, J., et al. (2007). SILVA: a comprehensive online resource for quality checked and aligned ribosomal RNA sequence data compatible with ARB. *Nucleic Acids Res.* 35, 7188–7196. doi: 10.1093/nar/gkm864

Raina, J.-B., Dinsdale, E. A., Willis, B. L., and Bourne, D. G. (2010). Do the organic sulfur compounds DMSP and DMS drive coral microbial associations? *Trends Microbiol.* 18, 101–108. doi: 10.1016/j.tim.2009.12.002

Raina, J.-B., Tapiolas, D. M., Foreêt, S., Lutz, A., Abrego, D., Ceh, J., et al. (2013). DMSP biosynthesis by an animal and its role in coral thermal stress response. *Nature* 502, 677–680. doi: 10.1038/nature12677

Raina, J.-B., Tapiolas, D., Willis, B. L., and Bourne, D. G. (2009). Coral-associated bacteria and their role in the biogeochemical cycling of sulfur. *Appl. Environ. Microbiol.* 75, 3492–3501. doi: 10.1128/AEM.02567-08

R Development Core Team (2021) *R: A language and environment for statistical computing*. Available at: http://www.r-project.org/.

Richter, U., and Wallace, D. W. R. (2004). Production of methyl iodide in the tropical Atlantic ocean. *Geophys. Res. Lett.* 31, L23S03. doi: 10.1029/2004GL020779

Rohwer, F., Segritan, V., Azam, F., and Knowlton, N. (2002). Diversity and distribution of coral-associated bacteria. *Mar. Ecol. Prog. Ser.* 243, 1–10. doi: 10.3354/meps243001

Saiz-López, A., and von Glasow, R. (2012). Reactive halogen chemistry in the troposphere. *Chem. Soc Rev.* 41, 6448–6472. doi: 10.1039/c2cs35208g

Schneider, K., Levy, O., Dubinsky, Z., and Ereza, J. (2009). *In situ* diel cycles of photosynthesis and calcification in hermatypic corals. *Limnol. Oceanogr.* 54, 1995–2002. doi: 10.4319/lo.2009.54.6.1995

Schrameyer, V., Krämer, W., Hill, R., Jeans, J., Larkum, A., Bischof, K., et al. (2016). Under high light stress two indo-pacific coral species display differential photodamage and photorepair dynamics. *Mar. Biol.* 163, 168. doi: 10.1007/s00227-016-2940-9

Seo, H.-S., Kwon, K. K., Yang, S.-H., Lee, H.-S., Bae, S. S., Lee, J.-H., et al. (2009). *Marinoscillum* gen. nov., a member of the family "Flexibacteraceae", with marinoscillum pacificum sp. nov. from a marine sponge and *Marinoscillum furvescens* nom. rev., comb. nov. *Int. J. Syst. Evol. Microbiol.* 59, 1204–1208. doi: 10.1099/ijs.0.004317-0

Shashar, N., Kinane, S., Jokiel, P. L., and Patterson, M. R. (1996). Hydromechanical boundary layers over a coral reef. *J. Exp. Mar. Biol. Ecol.* 199, 17–28. doi: 10.1016/0022-0981(95)00156-5

Simó, R. (2001). Production of atmospheric sulfur by oceanic plankton: biogeochemical, ecological and evolutionary links. *Trends Ecol. Evol.* 16, 287–294. doi: 10.1016/S0169-5347(01)02152-8

Sunda, W., Kieber, D. J., Kiene, R. P., and Huntsman, S. (2002). An antioxidant function for DMSP and DMS in marine algae. *Nature* 418, 317–320. doi: 10.1038/nature00851

Swan, H. B., Crough, R. W., Vaattovaara, P., Jones, G. B., Deschaseaux, E. S. M., Eyre, B. D., et al. (2016). Dimethyl sulfide and other biogenic volatile organic compound emissions from branching coral and reef seawater: potential sources of secondary aerosol over the great barrier reef. *J. Atmos. Chem.* 73, 303–328. doi: 10.1007/s10874-016-9327-7

Swan, H. B., Deschaseaux, E. S. M., Jones, G. B., and Eyre, B. D. (2017). Quantification of dimethylsulfoniopropionate (DMSP) in *Acropora* spp. of reef-building coral using mass spectrometry with deuterated internal standard. *Anal. Bioanal. Chem.* 409, 1929–1942. doi: 10.1007/s00216-016-0141-5

Tandon, K., Lu, C. Y., Chiang, P. W., Wada, N., Yang, S.-H-, Chan, Y.-H., et al. (2020). Comparative genomics: Dominant coral-bacterium *Endozoicomonas acroporae* metabolizes dimethylsulfoniopropionate (DMSP). *ISME J.* 14, 1290–1303. doi: 10.1038/s41396-020-0610-x

Tapiolas, D. M., Motti, C. A., Holloway, P., and Boyle, S. G. (2010). High levels of acrylate in the great barrier reef coral *Acropora millepora*. *Coral Reefs* 29, 621–625. doi: 10.1007/s00338-010-0608-3

Todd, J. D., Curson, A. R. J., Sullivan, M. J., Kirkwood, M., and Johnston, A. W. B. (2012a). The *Ruegeria pomeroyi* acuI gene has a role in DMSP catabolism and resembles yhdH of e. coli and other bacteria in conferring resistance to acrylate. *PloS One* 7 (4), e35947. doi: 10.1371/journal.pone.0035947

Tyssebotn, I. M. B., Kinsey, J. D., Kieber, D. J., Kiene, R. P., Rellinger, A. N., and Motard-Coêteí, J. (2017). Concentrations, biological uptake, and respiration of dissolved acrylate and dimethylsulfoxide in the northern gulf of Mexico. *Limnol. Oceanogr.* 62, 1198–1218. doi: 10.1002/lno.10495

Vd'ačnyí, P., Bourland, W. A., Orsi, W., Epstein, S. S., and Foissner, W. (2011). Phylogeny and classification of the litostomatea (Protista, ciliophora), with emphasis on free-living taxa and the 18S rRNA gene. *Mol. Phylogenet. Evol.* 59, 510–522. doi: 10.1016/j.ympev.2011.02.016

Wang, Q., Garrity, G. M., Tiedje, J. M., and Cole, J. R. (2007). Naiüve Bayesian classifier for rapid assignment of rRNA sequences into the new bacterial taxonomy. *Appl. Environ. Microbiol.* 73, 5261–5267. doi: 10.1128/AEM.00062-07

Washburn, L., and Brooks, A. (2022). "Gump station meteorological data". In: *Environmental data initiative*. MCR LTER: Coral Reef. knb-lter-mcr.9.46 doi: 10.6073/pasta/6d30349193252011bed853ae421d8b0d

Weber, L., Gonzalez-Díaz, P., Armenteros, M., and Apprill, A. (2019). The coral ecosphere: a unique coral reef habitat that fosters coral–microbial interactions. *Limnol. Oceanogr.* 64, 2373–2388. doi: 10.1002/lno.11190

Weis, V. M. (2008). Cellular mechanisms of cnidarian bleaching: stress causes the collapse of symbiosis. *J. Exp. Biol.* 211, 3059–3066. doi: 10.1242/jeb.009597

Woodhead, A. J., Hicks, C. C., Norström, A. V., Williams, G. J., and Graham, N. A. J. (2019). Coral reef ecosystem services in the anthropocene. *Funct. Ecol.* 33, 1023–1034. doi: 10.1111/1365-2435.13331

Xie, H., Moore, R. M., and Miller, W. L. (1998). Photochemical production of carbon disulphide in seawater. *J. Geophys. Res.* 103, 5635–5644. doi: 10.1029/97JC02885

Xie, H., Scarratt, M. G., and Moore, R. M. (1999). Carbon disulphide production in laboratory cultures of marine phytoplankton. *Atmos. Environ.* 33, 3445–3453. doi: 10.1016/S1352-2310(98)00430-0

Xue, L., Kieber, D. J., Masdeu-Navarro, M., Cabrera-Brufau, M., Rodríguez-Ros, P., Gardner, S. G., et al. (2022). Concentrations and biological consumption of acrylate and DMSP in the tropical pacific and coral reef ecosystem in mo'orea, French Polynesia. *Front. Mar. Sci.* 9, 911522. doi: 10.3389/fmars.2022.911522

Yokouchi, Y., Ooki, A., Hashimoto, S., and Itoh, N. (2014). "A study on the production and emission of marine-derived volatile halocarbons," in *Western Pacific air-Sea interaction study*. Eds. M. Uematsu, Y. Yokouchi, Y. Watanabe, S. Takeda and Y. Yamanaka (Tokyo: TERRAPUB), 1–25. doi: 10.5047/w-pass.a01.001

Yost, D., and Mitchelmore, C. (2009). Dimethylsulfoniopropionate (DMSP) lyase activity in different strains of the symbiotic alga *Symbiodinium microadriaticum*. *Mar. Ecol. Prog. Ser.* 386, 61–70. doi: 10.3354/meps08031

Zhu, F., Massana, R., Not, F., Marie, D., and Vaulot, D. (2005). Mapping of picoeucaryotes in marine ecosystems with quantitative PCR of the 18S rRNA gene. *FEMS Microbiol. Ecol.* 52, 79–92. doi: 10.1016/j.femsec.2004.10.006

Ziska, F., Quack, B., Abrahamsson, K., Archer, S. D., Atlas, E., Bell, T., et al. (2013). Global sea-to- air flux climatology for bromoform, dibromomethane and methyl iodide. *Atmos. Chem. Phys.* 13, 8915–8934. doi: 10.5194/acp-13-8915-2013

frontiers | Frontiers in Marine Science

TYPE Original Research
PUBLISHED 02 November 2022
DOI 10.3389/fmars.2022.911522

OPEN ACCESS

EDITED BY
Linda Wegley Kelly,
Scripps Institution of Oceanography, University of California, United States

REVIEWED BY
Wee Cheah,
University of Malaya, Malaysia
Ana Paula B. Moreira,
Federal University of Rio de Janeiro, Brazil

*CORRESPONDENCE
David J. Kieber
djkieber@esf.edu

†PRESENT ADDRESS
Stephanie G. Gardner,
Centre for Marine Science and Innovation, University of New South Wales Sydney, NSW, Australia

SPECIALTY SECTION
This article was submitted to Coral Reef Research, a section of the journal Frontiers in Marine Science

RECEIVED 02 April 2022
ACCEPTED 27 September 2022
PUBLISHED 02 November 2022

CITATION
Xue L, Kieber DJ, Masdeu-Navarro M, Cabrera-Brufau M, Rodríguez-Ros P, Gardner SG, Marrasé C and Simó R (2022) Concentrations, sources, and biological consumption of acrylate and DMSP in the tropical Pacific and coral reef ecosystem in Mo'orea, French Polynesia. *Front. Mar. Sci.* 9:911522. doi: 10.3389/fmars.2022.911522

Concentrations, sources, and biological consumption of acrylate and DMSP in the tropical Pacific and coral reef ecosystem in Mo'orea, French Polynesia

Lei Xue[1], David J. Kieber[1]*, Marta Masdeu-Navarro[2], Miguel Cabrera-Brufau[2], Pablo Rodríguez-Ros[2], Stephanie G. Gardner[2†], Cèlia Marrasé[2] and Rafel Simó[2]

[1]Department of Chemistry, State University of New York, College of Environmental Science and Forestry, Syracuse, NY, United States, [2]Department of Marine Biology and Oceanography, Institut de Ciències del Mar (ICM-CSIC), Barcelona, Spain

Shallow-water coral reefs hold large quantities of acrylate and its precursor dimethylsulfoniopropionate (DMSP), but production and removal processes for these compounds are poorly characterized. Here we determined the concentrations and cycling of acrylate and DMSP in a transect from a coral reef ecosystem to the open ocean, 2 km beyond the reef in Mo'orea, French Polynesia, during April 2018. Concentrations of dissolved acrylate and DMSP were low throughout the reef-ocean transect, ranging from 0.8–3.9 nM and 0.2–3.0 nM, respectively, with no difference observed between the coral reef and open ocean when comparing mean concentrations (± std dev) of dissolved acrylate (1.7 ± 0.7 vs 2.3 ± 0.8 nM) or DMSP (0.9 ± 0.7 vs 1.3 ± 0.6 nM). In the coral reef, dissolved acrylate was rapidly taken up by the heterotrophic community with a fast turnover time averaging ~ 6 h, six times faster than in the open ocean, and nearly as fast as the average turnover time of dissolved DMSP (~ 3 h). A clear diel trend was observed for the heterotrophic consumption of dissolved acrylate and DMSP in the coral reef, with higher uptake rate constants during daylight hours, synchronized with the larger daytime release of acrylate and DMSP from the coral compared to the nighttime release of these compounds. We also measured photochemical production rates of acrylate in Mo'orean waters, but rates were one to two orders of magnitude slower compared to its rates of biological consumption. Coral and macroalgae were the main sources of dissolved acrylate and DMSP to the reef ecosystem. Our results indicate there is rapid turnover of acrylate and DMSP in the coral reef with a tight coupling between production and removal pathways that maintain dissolved concentrations of these two

compounds at very low levels. These algal and coral-derived substrates serve as important chemical links between the coral and heterotrophic communities, two fundamental components in the ecological network in coral reefs.

KEYWORDS

acrylic acid, photochemistry, acropora, symbiodiniaceae, dimethylsulfoxide, DMSO, pocillopora, turbinaria

Introduction

Acrylate is produced through the enzymatic cleavage of DMSP, an organosulfur metabolite produced by many marine phytoplankton including the endosymbiotic dinoflagellates found in shallow reef-building coral. These dinoflagellates are some of the largest DMSP producers in the world's oceans (Keller, 1989; Caruana and Malin, 2014), with high cell densities in the coral host, rivaling those recorded for planktonic dinoflagellates during an algal bloom (Drew, 1972; Van Alstyne et al., 2006). DMSP is also detected in large quantities in the tissues and mucus of many coral species (Hill et al., 1995; Broadbent et al., 2002; Yost and Mitchelmore, 2010; Swan et al., 2017; Haydon et al., 2018) and giant clams (Hill et al., 2000; Van Alstyne et al., 2006; Guibert et al., 2020). Additionally, both the coral host (Raina et al., 2013) and its associated bacteria (Curson et al., 2017) can produce DMSP. Therefore, coral reef systems are prodigious producers of DMSP, with most of the DMSP production occurring in association with the coral and not in the water column.

DMSP lyases, which catalyze the conversion of DMSP to acrylate and dimethylsulfide (DMS) in equimolar quantities, has been detected in the coral endosymbiotic dinoflagellate Symbiodiniaceae (Yost and Mitchelmore, 2009; Caruana and Malin, 2014), suggesting that high concentrations of acrylate should also be present in the coral holobiont. Indeed, in a prevalent Great Barrier Reef coral, *Acropora millepora*, Tapiolas et al. (2010) determined that acrylate constituted 13–15% of the total carbon in the organic extract of the *A. millepora* holobiont. A subsequent survey observed high concentrations of acrylate in sixteen reef-building coral, with some of them showing acrylate concentrations comparable to or even higher than those of its precursor DMSP (Tapiolas et al., 2013).

Acrylate and DMSP are proposed to serve as antioxidants in coral (Yost et al., 2010; Raina et al., 2013; Deschaseaux et al., 2014; Gardner et al., 2016; Gardner et al., 2017), a function first proposed for these metabolites in microalgae (e.g., Sunda et al., 2002; Kinsey et al., 2016) and benthic macroalgae (Burdett et al., 2012; Kerrison et al., 2012; Rix et al., 2012). This function would not be surprising since corals are exposed to a diverse range of environmental stressors daily (e.g., high light, hypersalinity, air exposure) that can induce high levels of oxidative stress and the production of cell-damaging reactive oxygen species (ROS) including superoxide and hydroxyl radicals (Hoegh-Guldberg, 1999). When juveniles and adult colonies of *A. millepora* and *A. tenuis* were thermally stressed, Raina et al. (2013) observed a significant increase in DMSP and decrease in cellular acrylate concentrations. Gardner et al. (2016) observed a significant decrease in cellular DMSP and corresponding increase in the ratio of dimethylsulfoxide (DMSO) to DMSP in *A. millepora* under hyposaline conditions. While these studies showed different responses, both are consistent with acrylate and DMSP serving as de facto antioxidants in the coral holobiont during periods of low or high oxidative stress. In this capacity, cellular concentrations of acrylate and DMSP do not need to be actively controlled because their concentrations are many orders of magnitude higher than expected ROS levels. Instead, other physiological functions will control cellular concentrations of DMSP and acrylate including osmotic regulation or carbon overflow (Kinsey et al., 2016). In addition to the potential role in removing ROS in coral tissue or the mucus where acrylate concentrations are expected to be substantial (Broadbent and Jones, 2004; Tapiolas et al., 2010; Tapiolas et al., 2013), acrylate may play an antimicrobial role preventing the colonization of pathogenic bacteria (Raina et al., 2010), similar to the antiviral function proposed for acrylic acid in the microalgae *Emiliania huxleyi* (Evans et al., 2006; Evans et al., 2007).

Zooplankton grazing, cell lysis, algal exudation, and viral infection release particulate acrylate ($acrylate_p$) and DMSP ($DMSP_p$) from marine phytoplankton into the dissolved phase, where these compounds are largely consumed by the heterotrophic bacteria. Tyssebotn et al. (2017) determined that acrylate was readily consumed by microbes in the Gulf of Mexico at a rate between 0.07 and 1.8 nM d^{-1}, with a significant fraction of the acrylate assimilated into macromolecules or respired to CO_2. However, the contribution of acrylate to bacterial carbon demand in the Gulf of Mexico was negligible, ranging from 0.013 to 0.13% (Tyssebotn et al., 2017), and the turnover of acrylate was relatively slow (median 4.8 d) compared to the turnover of DMSP (median 3.1 h). In contrast to acrylate, the crucial role of DMSP as a source of reduced sulfur and carbon for marine bacteria is well documented (e.g., Kiene and Linn, 2000a; Simó

et al., 2002; Vila-Costa et al., 2007; Levine et al., 2016; Motard-Côté et al., 2016; Lizotte et al., 2017; Kiene et al., 2019). Corals can expel ~10% of their algal symbionts on a daily basis and even more when they are physically or chemically stressed (Broadbent and Jones, 2006), with the expelled Symbiodiniaceae exposed to stress and mortality similar to planktonic phytoplankton. This may result in releases of large quantities of DMSP and acrylate (Masdeu-Navarro et al., 2022) that will feed the fast microbial cycling of dissolved carbon and sulfur in the coral reef.

Acrylate and DMS are produced in equimolar quantities from the enzymatic lysis of DMSP by lyases. However, while DMS has been studied extensively in the global oceans including in coral reefs (Jones et al., 2018; Jackson et al., 2020) due to its potential role in regulating the Earth's radiation budget and climate (Charlson et al., 1987), only a few studies have examined the cycling and ecological impacts of acrylate in coral reefs beyond the impacts to the coral holobiont. In this study, we demonstrate that (1) both acrylate and DMSP are rapidly consumed by planktonic microbes once released into the dissolved phase, and (2) the consumption of dissolved acrylate and DMSP exhibit diel patterns in phase with their release from the coral holobiont.

Materials and methods

Study area

The main field study was conducted from April 4 to 27, 2018 in a coral reef offshore from the Richard Gump South Pacific Research Station located next to Cook's Bay (also known as Paopao Bay) on the northern shore of Mo'orea, French Polynesia (Figure 1). Mo'orea is a volcanic island surrounded by barrier reefs extending outward from the shoreline, creating an extensive semi-enclosed lagoonal system. The typical reef zonation consists of a shallow lagoon that includes a channel, fringing reef and a shallow back reef platform, and an outer fore reef that separates the lagoon from the open ocean (Leichter et al., 2013). The fore reef drops steeply from the near-sea surface to > 500 m over a distance of ~1 km. The shallow fore reef is nearly continuously covered by branching coral colonies of *Pocillopora* sp. and *Acropora* sp. (Adjeroud, 1997). The benthic community on the shallow back reef is composed of turf and fleshy macroalgae and patches of hermatypic corals surrounded by sandy-bottom open areas (http://mcr.lternet.edu/data), with an increasing proportion of

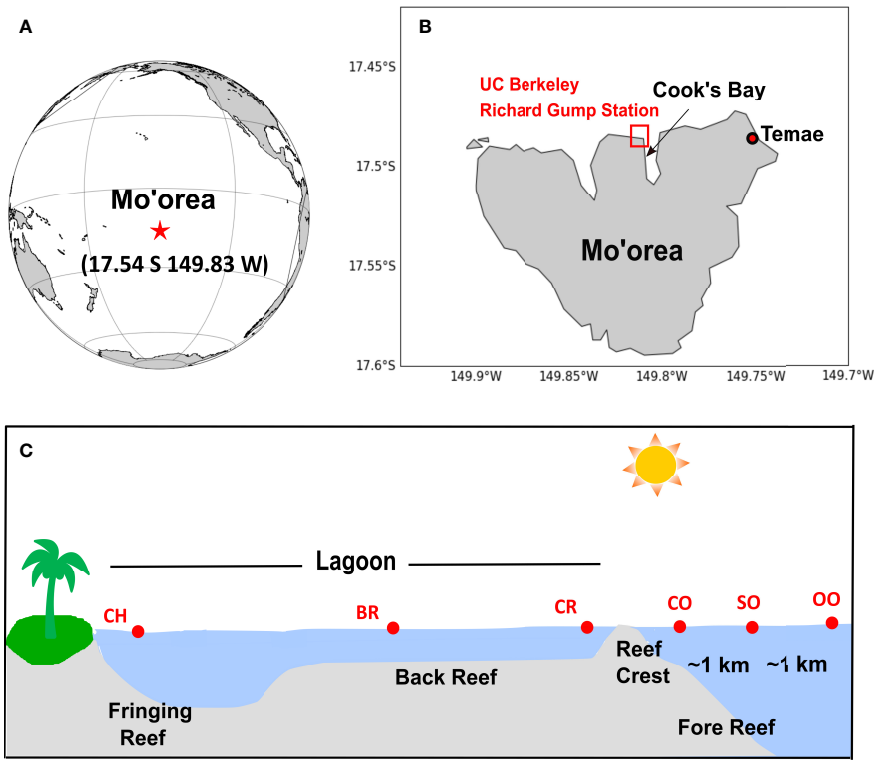

FIGURE 1
Locations of **(A)** the island of Mo'orea, in the South Pacific Ocean, **(B)** the Temae Park coral reef, and the UC Berkeley's Richard Gump Research Station and coral reef where most of the work reported here was conducted, and **(C)** schematic showing the Mo'orea coral reef and reef-ocean transect sampling stations: nearshore outflow channel (CH), back reef (BR), reef crest (reef side of the reef crest, CR), ocean crest (ocean side of the reef crest, CO, ~300 m away from station CR), shelf ocean (SO, ~1 km away from CO), and open ocean (OO, ~2 km away from CO). Note that distances between stations are not drawn to scale. Panel **(C)** was adapted with permission from Leichter et al. (2013).

sandy bottom as one moves shoreward towards the fringe reef and channel. Water movement in the back reef is relatively low from waves, and pass and lagoonal circulation, with flushing times of a few hours to more than day depending on winds and wave energy beyond the reef (Hench et al., 2008; Herdman et al., 2015). Although we did not measure wind speeds or wave heights, qualitatively conditions were calm in the lagoon with no storms or significant wave heights noted during the field study.

Six stations were sampled repeatedly over a three-week period as part of a coral reef-ocean transect study (Figure 1). The six stations included the nearshore outflow channel (CH), the back reef (BR), the reef crest (the reef side of the reef crest, CR), the ocean crest (the ocean side of the reef crest, CO), the shelf ocean (SO, ~1 km from CO), and the open ocean (OO, ~2 km away from CO); these stations correspond to some of the same sampling stations occupied by the Moorea Coral Reef Long Term Ecological Research (MCR LTER) project (Leichter et al., 2013). To assess potential sources of dissolved acrylate and DMSP to the coral reef, an ancillary study was conducted in a coral reef offshore of Temae Beach along the northeastern coast Mo'orea (17.501°S, 149.759°E, Figure 1). The Temae coral reef is a lagoonal system similar to our main study site off Cook's Bay. Two photos depicting typical intermittent reef patches surrounded by sandy bottom present in the Mo'orea coral reef lagoonal system at station BR and the Temae coral reef are shown in Figure S1. A google map showing an aerial overview of the island of Mo'orea and the study area is presented in our companion paper, along with photos showing our protocol used to collect samples close to the coral colonies (Masdeu-Navarro et al., 2022).

Sample collection and storage

Water samples from the near sea surface (~30 cm deep) were collected in precleaned 1, 2, or 8 L opaque (brown) polypropylene bottles from repeated sampling trips to the six stations along a reef-ocean transect (Figure 1). Diel sampling was carried out over a 30-hour period in the back reef (April 12–13) and open ocean stations (April 19–20). A surface microlayer sample was collected in the back reef on April 18 using a glass plate to preliminarily evaluate the potential enrichment and photochemical reactivity of the microlayer sample with respect to acrylate photoproduction compared to the underlying seawater. A bulk seawater sample from ~30 cm below the sea surface was collected in parallel with a precleaned air-tight, all-glass syringe (Hamilton) fitted with 0.32 cm OD Teflon tubing attached to the syringe using a polycarbonate luer-lock, 3-way valve fitting.

To collect samples for dissolved concentrations, each of the aforementioned samples was gravity filtered through a precombusted GF/F filter (25 mm diameter, Whatman) into a precleaned 20 mL scintillation vial following the procedure of small-volume drip filtration (Kiene and Slezak, 2006). Paired with each dissolved sample, another set of samples was collected for the measurement of total concentrations by pipetting 15 mL of unfiltered seawater into a 20 mL scintillation vial. All samples were microwaved to boiling (ca. ~12–15 sec; Kinsey and Kieber, 2016). After samples cooled to room temperature, both dissolved and total samples were bubbled for ~10 min using high-purity nitrogen gas followed by acidification with 150 µL of Ultrex HCl. Each sample was collected in duplicate and was stored at room temperature in the dark until analysis in Syracuse NY. Details regarding chemical sources and purity, and glassware cleaning procedures can be found in the Supplemental Material (SM).

Photochemical experiments

Experiments were performed to determine the photochemical production rate of acrylate in freshly collected 0.2 µm-filtered seawater. Photolysis experiments were conducted with seawater collected from the back reef (station BR), the sea surface microlayer in the back reef, and the open ocean (station OO). After a seawater sample was collected in an 8 L polypropylene bottle, it was gravity filtered through a precleaned 0.2 µm Polycap AS 75 Nylon filter (Whatman) into a precleaned 2.5 L Qorpak glass bottle.

In preparation for a photochemical experiment, the filtered seawater was slowly drawn from the 2.5 L glass bottle into several Teflon-sealed quartz tubes (with no headspace) according to the procedure outlined in Kieber et al. (1997). One set of four quartz tubes was submerged in a 3 cm-deep circulating water bath (28–30 °C) for exposure to sunlight, and a second set of four quartz tubes was wrapped in several layers of aluminum foil and placed in the water bath as dark controls. To obtain sufficient production of acrylate for HPLC analysis, samples from the coral reef and open ocean were exposed to solar radiation for a total of ~15 h and 20 h, respectively, over a two to three-day period. At the end of each experiment, a 10 mL sample was collected in triplicate from each quartz tube, and each 10 mL aliquot was dispensed into a precleaned 20 mL scintillation vial. Samples were subsequently acidified using 100 µL of Ultrex HCl and stored at room temperature in the dark until analysis in Syracuse, NY.

Samples were also collected from the quartz tubes at the beginning and end of each photochemical experiment to determine the absorption spectrum of chromophoric dissolved organic matter (CDOM) in the sunlight-exposed samples and dark controls. Details of the CDOM absorption measurements are given in section CDOM Absorbance.

Triplicate nitrate and nitrite actinometer solutions in 5 mL borosilicate vials were exposed to sunlight along with the quartz tubes to determine the photon exposure between 311 and 333 nm and 330 and 380 nm, respectively, using the methods outlined in

Jankowski et al. (1999) and Kieber et al. (2007). Borosilicate vials for both actinometers were enclosed in neutral-density screening with a percent transmission of 31%. The nitrite actinometer vials were also wrapped with Mylar D film (Jankowski et al., 2000). Dark actinometry controls were wrapped with several layers of aluminum foil, without screening or Mylar D film. Actinometry samples were analyzed at the Gump Research Station by batch fluorescence using a Horiba Aqualog Fluorometer calibrated with salicylic acid standards prepared in a pH 7.2, 2.5 mM sodium bicarbonate solution.

Biological consumption experiments

Time-course incubations were performed to determine biological consumption rates of dissolved acrylate ($acrylate_d$) and DMSP ($DMSP_d$) in unfiltered seawater samples collected from the back reef, station BR, and open ocean, station OO. To perform an incubation for acrylate consumption, 150 µL aliquots of an acrylate standard prepared from DMSP (Xue and Kieber, 2021) were added to unfiltered water samples in triplicate 250 mL polycarbonate (PC) bottles, yielding an initial concentration of ~15 nM for $acrylate_d$ in each bottle. Prior to filling the PC bottles with seawater, they were rinsed several times with Milli-Q water and the unfiltered seawater. The PC bottles were gently inverted several times to mix the added acrylate. Another set of three PC bottles received no added acrylate. Once samples were prepared, they were placed in a large, covered incubator with hosing to continually pump ambient surface seawater through the incubator to maintain the temperature at ~28 °C. All incubations were conducted in the dark. Subsamples were collected from each PC bottle at four separate times during an incubation. The total length of each incubation was 14 h for the coral reef waters and 18 h for the open ocean samples. For each time point, 15 mL subsamples were collected in triplicate from each bottle and processed as discussed below.

The biological consumption of $DMSP_d$ was determined using the glycine betaine (GBT) inhibition method outlined in Kiene and Gerard (1995). Briefly, six precleaned 250 mL PC bottles were filled with freshly collected, unfiltered seawater. Three bottles were treated with 10 µM GBT and three PC bottles were left untreated. All samples were incubated in the dark in the same incubator used for the acrylate incubations. At several time points during an incubation, subsamples from each bottle were collected and processed as outlined below. An additional time-course experiment was performed with a seawater sample from the coral reef BR station to determine if the added GBT caused the release of DMSP from the particulate phase into the dissolved phase. This incubation was conducted in the same manner as all other dark incubations, except that in this case subsamples were collected for the measurement of both dissolved and total DMSP ($DMSP_t$).

For each time point, 15 mL subsamples from the acrylate and DMSP incubations were gravity filtered using precombusted, 25 mm diameter GF/F filters into 20 mL scintillation vials using the small-volume drip filtration method outlined in Kiene and Slezak (2006). Filtered samples were microwaved to boiling, bubbled with high-purity nitrogen gas to remove DMS, and acidified with 150 µL of Ultrex HCl (Kinsey and Kieber, 2016). All samples were stored at room temperature in dark for analysis after they were transported back to Syracuse, NY.

Coral symbiont cultures

Non-axenic batch cultures of five coral dinoflagellate symbionts including *Breviolum aenigmaticum*, *Cladocopium* sp., *Durusdinium trenchii*, *Effrenium voratum*, and *Breviolum minutum* were grown at the State University of New York (SUNY), Buffalo Undersea Reef Research Culture Collection. Triplicate cultures were maintained in 30 mL f/2 medium under a 14:10 h light:dark cycle (70–90 µmol quanta m^{-2} s^{-1}, from 34 W fluorescent lights) at 26°C in 50 mL polycarbonate flasks (Bayliss et al., 2019). All cultures were sampled at their approximate exponential growth phase determined by the number of motile cells counted by microscopy.

A 2 mL aliquot of each culture was collected into a 5 mL Qorpak vial followed by immediate addition of 10 µL 50% glutaraldehyde solution (Fisher Scientific) to preserve the sample for cell volume and cell number measurements using a Beckman-Coulter Z2 Particle Counter and Size Analyzer. To collect dissolved samples, 15 mL of culture was gravity filtered through a 25 mm diameter A/E glass fiber filter (Pall) in a Gelman polysulfone filtration tower. For each filtration, the first 5–6 drops were discarded, and the filtrate was then collected in a 20 mL scintillation vial. To collect total samples, 10 mL of unfiltered sample was collected in a 20 mL scintillation vial. Both dissolved and total samples were microwaved until boiling in the SUNY Buffalo lab. After returning to the home laboratory approximately 3 h later, each sample was bubbled using ultrapure helium for 15 min followed by acidification using 150 µL of Ultrex HCl. Samples were stored at room temperature in dark until analyzed.

DMSP, DMSO and acrylate quantification

To measure concentrations of DMSP and DMSO, both compounds were first converted to dimethylsulfide (DMS). To convert DMSP or DMSO to DMS, 200 µL 5 M NaOH or 20% $TiCl_3$, respectively, was added to 1 mL of a standard or seawater sample in a precleaned borosilicate serum vial, which was immediately capped with a Teflon-lined butyl rubber stopper and sealed with an aluminum crimp cap. The DMSP samples

were incubated overnight at room temperature in dark; for the DMSO samples, serum vials were incubated at 55°C in a water bath for 1 h. DMS was analyzed using a cryogenic purge-and-trap system and a Shimadzu GC-14A with a flame photometric detector (Kinsey et al., 2016).

Acrylate concentrations were determined using a pre-column derivatization HPLC method that provided sufficient sensitivity for the analysis of low nM acrylate concentrations in seawater (Tyssebotn et al., 2017). For derivatization, 300 µL thiosalicylic acid (TSA, 20 mM) reagent in MeOH was pipetted into a 5 mL precleaned borosilicate vial containing 3 mL of a standard or seawater sample. Following pH adjustment to 4.0, each vial was tightly screw-capped and incubated at 90°C in a water bath for 6 h. After cooling to room temperature, each derivatized sample was first filtered using a 0.2 µm Nylon syringe filter (Pall) followed by injection of 1 mL into the Shimadzu HPLC system containing a reverse phase Waters HPLC column with UV detection at 257 nm to quantify the acrylate-TSA derivative. The limit of detection of this method is 0.2 nM for a 1 mL injection.

CDOM absorbance

The absorbance spectrum of 0.2 µm-filtered seawater was determined between 240 and 800 nm using a SD 2000 fiber optic spectrophotometer (Ocean Optics) equipped with a 101 cm pathlength capillary cell (World Precision Instruments) precleaned using MeOH and Milli-Q water. Each blank (Milli-Q water) or seawater sample was gently drawn into the capillary cell using a Rainin Rabbit-Plus peristaltic pump. All absorption spectra were baseline corrected by adjusting the absorbance between 630 and 640 nm to zero. The absorbance (A_λ) was converted to an absorption coefficient (a_λ, m^{-1}) using the equation $a_\lambda = 2.303A_\lambda/l$, where l is the cell pathlength determined according to the procedure in Cartisano et al. (2018).

Ancillary measurements

The sea-surface temperature was recorded using a SBE56 sensor (Sea-Bird Scientific) continuously flushed with pumped-in near surface seawater. For total organic carbon (TOC), 30 mL samples of unfiltered seawater were collected in acid-cleaned polycarbonate bottles and stored in the dark at −20°C until analysis. They were analyzed in triplicate with a Shimadzu TOC-LCSV, with Milli-Q water as a blank, potassium hydrogen phthalate as the calibration standard, and deep Sargasso Sea water as the reference. For particulate organic carbon (POC), 500–2000 mL of seawater was filtered through a pre-combusted (450°C, 4 h) 25 mm diameter GF/F glass fiber filter (Whatman), which was stored frozen at −20°C. Prior to analysis, the GF/F filters were thawed in an HCl-saturated atmosphere for 24 h to remove inorganic compounds. The filters were then dried and analyzed using an elemental analyzer (Perkin-Elmer 2400 CHN). For Chlorophyll *a* (Chl *a*), 250 mL seawater was filtered through a 25 mm diameter GF/C glass fiber filter (Whatman) that was subsequently stored frozen at −20°C. The pigments were extracted into 90% acetone at 4°C in the dark for 24 h. The fluorescence of the extracts was measured with a calibrated Turner Designs fluorometer. The abundance of micro-phytoplankton was determined under light microscopy using the Utermöhl technique (Utermöhl, 1958) on 100 mL of sedimented samples fixed with formalin-hexamine to a final concentration of 0.4%. For enumeration of heterotrophic prokaryotes (including bacteria and archaea) and pico- and nano-phytoplankton, samples were fixed with glutaraldehyde (0.5%) and analyzed by flow cytometry (CyFlow Cube 8, Sysmex Partec). For bacterioplankton quantification, samples were stained with SYBRgreen I (∼ 20 µM final concentration) prior to analysis following Gasol and Del Giorgio (2000). For pico- and nano-phytoplankton, forward scatter and red and orange autofluorescence was used to discriminate different populations following Olson et al. (2018). For nitrate, nitrite and phosphate, 10 mL aliquots of unfiltered seawater were collected in 12 mL polypropylene tubes and stored frozen at −20°C. These dissolved inorganic nutrients were quantified by standard, segmented flow analysis with colorimetric detection using a Bran & Luebe autoanalyzer and the procedure outlined in Hansen and Koroleff (1999).

Statistical analyses

Statistics including the Pearson correlation and t-test were performed using SigmaPlot software (version 11.0). Unless otherwise noted, t-tests were performed when data were normally distributed, as determined by the Shapiro–Wilk test. A Mann–Whitney Rank Sum test was used when normality tests failed. Minitab (version 21.2, Minitab LLC) was used to perform Principal Component Analysis (PCA) on a correlation matrix composed of 11 variables and 27 rows of data; an orthogonal regression analysis was used to compare total acrylate ($acrylate_t$) to total DMSP ($DMSP_t$), since measurement error was associated with both parameters. An α level of 0.05 was used for all statistical analyses. Standard deviations were used to report errors, unless otherwise noted.

Results and discussion

Biogeochemical properties along the transect

The daytime temperature in surface waters along the reef-ocean transect was nearly the same throughout the study, averaging 28.8 ±

0.01°C (Table 1). Chl *a* concentrations averaged between 0.18 ± 0.08 and 0.33 ± 0.10 μg L^{-1} among the transect stations, with slightly higher Chl *a* at CH and CO and the lowest Chl *a* observed at the open ocean station (Figure S2; Table 1). A drop in Chl *a* concentration occurred as the water flowed from the fore reef (CO) into the back reef (BR). Similar to prior studies in the Mo'orea coral reef (Nelson et al., 2011; Leichter et al., 2013), nitrate concentrations (and silicate, data not shown) in the coral reef were markedly higher than at the open-ocean sites at stations SO and OO (0.31 ± 0.03 vs 0.06 ± 0.02 μM; Table 1), which may be attributed to the elevated activity of nitrifying bacteria associated with corals (Beman et al., 2007; Wegley et al., 2007). Despite this elevated activity, overall the coral holobiont is expected to be a large sink for nitrate (Glaze et al., 2021). Therefore, there must be other nitrate sources to the coral reef to maintain the relatively high nitrate concentrations we observed. Potential sources include groundwater inputs (Nelson et al., 2015) or sediment resuspension (Erler et al., 2014). Similar trends of lower oceanic concentrations were seen for nitrite and phosphate, but differences were much smaller (Table 1). Nelson et al. (2011) observed a depletion of dissolved organic carbon (DOC) in the Mo'orea coral reef compared to the open ocean over a 4-year time period (68 vs 79 μM DOC). A similar difference was noted in our study, but observed differences (67.8 ± 5.2 in the open ocean vs 75.0 ± 5.7 μM in the coral reef) were not statistically significant ($p > 0.05$). The particulate organic carbon (POC) pool was small relative to DOC, ranging from 3.3 to 4.2 μM throughout the entire transect comprising less than 5% of the total organic carbon signal and with no differences noted between the coral reef and open-ocean sites.

During the main transect study, dinoflagellates and coccolithophores dominated the abundance of micro-phytoplankton, with relatively few diatoms present at the open-ocean stations or in the coral reef. The planktonic assemblage in the coral reef and open-ocean stations exhibited some marked differences, with dinoflagellate and coccolithophore cell numbers in near surface waters nearly double at the open-ocean stations SO and OO (~ 8×10^3 cells L^{-1}) compared to the back reef station (~ 4×10^3 cells L^{-1}). The summed abundances of pico- and nano-eukaryotic phytoplankton were lowest at the farthest open-ocean station OO (2.5×10^6 cells L^{-1}), increased to the highest cell numbers at SO and the fore reef (CO) ($4–5\times10^6$ cells L^{-1}), followed by a decrease to ca. 3×10^6 cells L^{-1} inside the coral reef. A similar yet clearer pattern of decrease into the reef was observed for *Synechococcus* (15×10^6 cells L^{-1} at OO, 50×10^6 cells L^{-1} at SO and CO, 25×10^6 cells L^{-1} at BR) and heterotrophic prokaryote abundances (ca. 0.9×10^9 cells L^{-1} at OO, SO and CO, and 0.5×10^9 cells L^{-1} at BR), but not for *Prochlorococcus* (gradual yet not significant decrease from 90×10^6 cells L^{-1} outside the reef to 70×10^6 cells L^{-1} inside the reef (Figure S2). Depletion of both autotrophic and heterotrophic microbial abundances was previously observed as the water crossed the reef crest into the back reef in this same northern Mo'orean coral reef (Payet et al., 2014), and this was attributed to top down control by coral filter feeding (Patten et al., 2011).

Transects of acrylate and organosulfur concentrations

The range of $acrylate_d$ (0.8–3.9 nM) and $acrylate_t$ concentrations (1.1–5.2 nM) in the transect are small (Figure 2A), and similar to those determined in the Gulf of Mexico in late fall, 0.8–2.1 nM for $acrylate_d$ and 1.4–3.4 nM for $acrylate_t$ (Tyssebotn et al., 2017), but one to three orders of magnitude lower than those previously observed off the coast of China in coastal and open ocean waters across different seasons. Concentrations in Chinese waters ranged from 60–578 nM in Jiaozhou Bay (Wu et al., 2015), 14–353 nM (Liu et al., 2016a) and 4.3–103 nM (Wu et al., 2020) in the Yellow and Bohai Seas, and 10–107 nM in the Changjiang Estuary and East China Sea (Wu et al., 2017). These high $acrylate_d$ concentrations are quite surprising since these waters are characterized by low algal biomass (Chl *a* < 0.5 μg L^{-1}), predominance of low DMSP producers (e.g., diatoms; Liu et al., 2016b), and fast photolysis

TABLE 1 Location of the sampling stations depicted in Figure 1, and the average temperature and concentrations of Chl *a*, nitrate, nitrite, ammonium, phosphate, dissolved organic carbon (DOC), particulate organic carbon (POC) and dissolved organic nitrogen (DON) in seawater samples collected from repeated sampling at each station over a two-week period.

Station	Lat. (°S)	Long. (°W)	Temp. (°C)	Chl *a* (μg L^{-1})	Nitrate	Nitrite	Ammonium	Phosphate (μM)	DOC	POC	DON
CH	17.484	149.839	28.7 (0.1)	0.31 (0.10)	0.30 (0.05)	0.05 (0.01)	0.29 (0.18)	0.16 (0.02)	63.9 (3.7)	4.2 (0.7)	4.2 (0.3)
BR	17.479	149.840	28.8 (0.2)	0.22 (0.06)	0.33 (0.06)	0.05 (0.01)	0.37 (0.12)	0.16 (0.02)	72.9 (8.8)	3.3 (0.3)	4.7 (0.6)
CR	17.477	149.839	28.8 (0.2)	0.25 (0.05)	0.29 (0.06)	0.05 (0.01)	0.29 (0.21)	0.16 (0.01)	66.5 (3.1)	4.0 (1.0)	3.9 (0.2)
CO	17.475	149.839	28.8 (0.2)	0.33 (0.10)	0.17 (0.07)	0.04 (0.01)	0.41 (0.32)	0.14 (0.02)	72.2 (8.5)	3.6 (0.3)	4.1 (1.1)
SO	17.467	149.839	28.8 (0.1)	0.28 (0.02)	0.08 (0.04)	0.05 (0.03)	0.88 (0.32)	0.13 (0.01)	74.5 (6.1)	4.4 (1.0)	4.9 (1.0)
OO	17.457	149.840	28.8 (0.4)	0.18 (0.08)	0.04 (0.01)	0.03 (0.03)	0.48 (0.36)	0.13 (0.02)	75.4 (5.3)	3.4 (0.6)	4.0 (1.2)

Values in parentheses denote the standard deviation (n = 4–5).

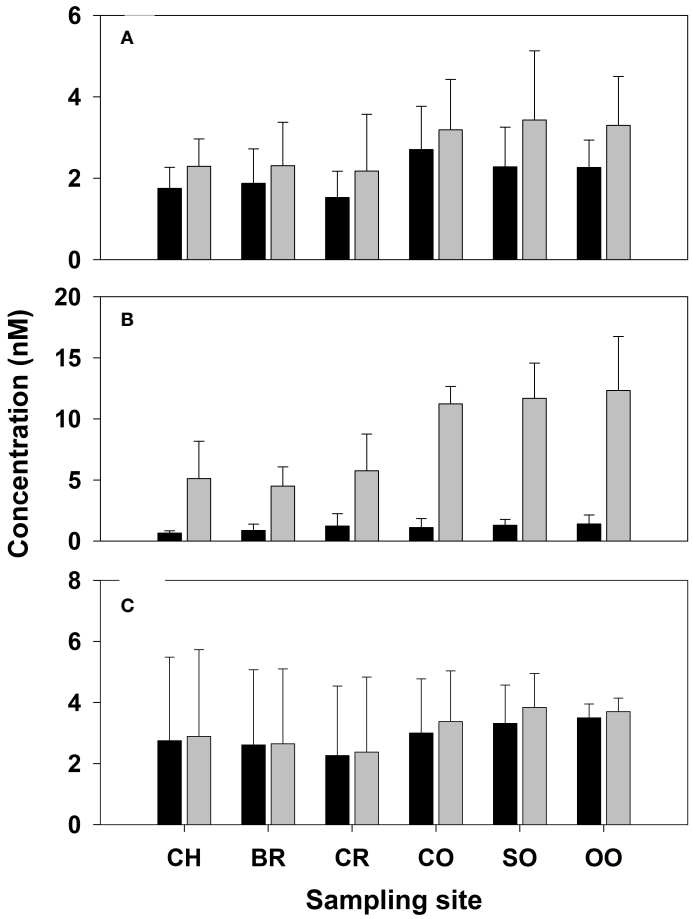

FIGURE 2
Mean dissolved (black-filled bars) and total (grey-filled bars) concentrations of **(A)** acrylate, **(B)** DMSP, and **(C)** DMSO in samples collected from repeated sampling at each sampling station between April 6 and 24, 2018. Error bars denote the standard deviation from the measurement of multiple samples collected over different days at each site (n = 4–5).

and biological consumption rates for $acrylate_d$. Additionally, $acrylate_d$ concentrations in these coastal waters were often substantially greater than its presumptive source DMSP (e.g., Wu et al., 2020). Wu et al. (2017) speculated that anthropogenic sources significantly contributed to the high $acrylate_d$ concentrations observed in their seawater samples, but they supplied no evidence to support this supposition and spatial distributions are inconsistent with an anthropogenic source. The basis for these large differences is not known, however, we speculate that their high acrylate concentrations were due to an artifact associated with co-eluting interferences in the direct HPLC–UV absorption method used to quantify acrylate (non-selective absorption detection at 210 nm).

DMSP concentrations in the Mo'orea coral reef transect study ranged from 0.3–2.8 nM and 2.8–11.1 nM for $DMSP_d$ and $DMSP_t$ (Figure 2B), respectively, slightly lower than $acrylate_d$ and higher than $acrylate_t$. $DMSP_d$ concentrations (1.1 ± 0.7 nM) were comparable to $DMSP_d$ concentrations reported in the literature using the same technique (< 2 nM) to filter samples collected under non-bloom conditions in the Atlantic (Lizotte et al., 2012; Levine et al., 2016), Pacific (Royer et al., 2010), Southern (Kiene et al., 2007), and Arctic Oceans (Motard-Côté et al., 2012). However, when compared to other coral-reef studies, $DMSP_d$ measured in Mo'orea was a factor of 3.5 to 6 lower than mean concentrations at three coral reefs in the Great Barrier Reef (Jones et al., 2007) including Pioneer Bay reef (3.2 nM), Nelly Bay reef (3.7 nM) and One Tree reef (5.5 nM). By comparison, $DMSP_p$ concentrations in the Mo'orea reef (4.2 ± 2.1 nM), determined by subtracting $DMSP_d$ from $DMSP_t$ and propogating the error, were similar to that in Pioneer Bay reef (3.3 nM) and Nelly Bay reef (2.2 nM) but 3.6 times lower than the mean concentration at One Tree reef (15.2 nM). Burdett et al. (2013) only reported $DMSP_t$ concentrations (range 14.7–23.9 nM, mean 19.5 nM) in waters collected along a transect across Suleman reef, Egypt, nearly four-fold higher than the mean $DMSP_t$ concentration in the Mo'orea coral reef (5.1 nM).

Differences between our DMSP results and prior coral-reef studies reflect dissimilarities in reef structure between the Mo'orea reef that was continuously submerged (only the reef crest was occasionally exposed to air) and several prior studies in the Great Barrier Reef where coral were periodically exposed to air and the associated physical stress. Deschaseaux et al. (2014) observed that increases in temperature, reduced salinity, air exposure, and high or low levels of sunlight resulted in greater oxidative stress and enhanced production of DMSP and DMSO in the coral holobiont. Likewise, Raina et al. (2013) determined higher levels of DMSP in thermally stressed *A. millepora* and *A. tenuis*. Higher particulate DMSP concentrations resulting from these physical stresses translate to higher fluxes of DMSP, DMSO (and presumably acrylate) into the dissolved phase. Differences in $DMSP_d$ will also arise from differences in the predominant corals present in the coral reef. In the Great Barrier Reef, *Acropora* sp. is a common reef-building coral (Dietzel et al., 2020) whereas *Pocillopora* sp. is an important coral in Mo'orea (Carlot et al., 2020), and, as will be discussed in the next section, *Acropora pulchra* is a much stronger source of $DMSP_d$ and $acrylate_d$ compared to *Pocillopora* sp. Differences in filtration techniques used to collect dissolved samples may also be at least partially responsible for the difference in $DMSP_d$ concentrations. The Great Barrier Reef samples were filtered using a 0.45-µm filter and peristaltic pump that may have ruptured cells and released DMSP from the particulate phase into dissolved phase. For Mo'orean waters, we collected dissolved samples using a small-volume drip filtration method using a GF/F filter (nominal pore size 0.7 µm), which has been showed to minimize the release of DMSP from algal cells (Kiene and Slezak, 2006).

Although not a main thrust of our study, DMSO concentrations were determined to provide context for the acrylate and DMSP results. In the transect, $DMSO_d$ fell within a wide range between 0.33–6.1 nM, but with no differences noted between the coral-reef stations and the open-ocean stations (Figure 2C). In all our samples, greater than 90% of the DMSO was detected in the dissolved phase (Figure 2C), with very little DMSO present in the particulate pool due to its rapid diffusion out of the cell into the dissolved phase (Spiese et al., 2016). Compared to $DMSP_d$ and DMS (DMS results presented in Masdeu-Navarro et al., 2022), $DMSO_d$ was the main contributor to the dissolved organic sulfur pool averaging nearly 3 nM throughout Mo'orea study. There are several potential sources of $DMSO_d$ in our study area including inputs from the particulate phase (e.g., from DMSO production in planktonic algae, macroalgae, the coral holobiont and subsequent diffusion into the dissolved phase), photochemical oxidation of DMS, or bacterial production from DMS (e.g., trimethylamine monooxygenase activity; Lidbury et al., 2016). These multiple sources, coupled with the chemical stability of DMSO, it's low volatility, and slow microbial consumption (Tyssebotn et al., 2017) likely led to its higher dissolved concentrations compared to dissolved DMS or DMSP, a finding that is consistently observed throughout the world's oceans and in coral reef ecosystems (e.g., Simó et al., 1997; Broadbent and Jones, 2004; del Valle et al., 2007; Kiene et al., 2007; Jones et al., 2007; Asher et al., 2017). Although DMSO was the main dissolved organosulfur compound detected in the Mo'orea coral reef, concentrations were nonetheless lower than found in other oceanic regions including, for example, the Western Mediterranean (Simó et al., 1997), Ross Sea (del Valle et al., 2007), Southern Ocean (Kiene et al., 2007), Gulf of Mexico (Tyssebotn et al., 2017), and Northeast Subarctic Pacific (Asher et al., 2017; Herr et al., 2021). Likewise, $DMSO_d$ concentrations reported here were much lower than $DMSO_d$ concentrations in two Great Barrier Reef studies including Nelly Bay reef (Broadbent and Jones, 2006) and One Tree reef (Jones et al., 2007). In these reefs, $DMSO_d$ ranged (mean) from 5.5–215 nM (17 nM) and 7.7–42 nM (17 nM), respectively. The low background $DMSO_d$ concentrations observed in our study compared to other oceanic regions suggest that production rates were lower and/or microbial consumption rates were faster in the Mo'orea coral reef than previously reported (Tyssebotn et al., 2017).

Acrylate and DMSP concentration data shown in Figure 2 were merged to compare the coral reef (CH, BR, and CR) and the open-ocean sites (SO, and OO), since the mean concentration of each compound was indistinguishable among the different stations in each ecosystem. Data from station CO were not included in the reef versus open ocean comparison due to its close proximity to the reef crest (ca. 150 m) and rapid water exchange with the back reef through the reef crest (ca. 36 min) (Hench et al., 2008; Herdman et al., 2015).

Merged $acrylate_d$ concentrations were 1.7 ± 0.7 nM in the coral reef (n = 15) and 2.3 ± 0.8 nM in the open-ocean sites (n = 8), with no significant difference between these two ecosystems ($p > 0.05$). In contrast, mean $acrylate_p$ concentrations (determined by subtracting $acrylate_d$ from $acrylate_t$ and propagating the error) were lower by a factor of two or more in the coral reef, 0.5 ± 0.5 nM, compared to concentrations at stations SO and OO (1.1 ± 0.7 nM). A large percentage of acrylate, ranging from 50 to 95%, was present in the dissolved phase in all surface waters, consistent with previous culture studies (Tyssebotn, 2015; Kinsey et al., 2016). Dissolved and particulate acrylate and DMSP concentrations reported in this section only include water samples more than a meter away from coral and do not include concentrations in the coral holobiont or in close proximity to the coral; concentrations in these environments are expected to be substantially higher as discussed below (also see Tapiolas et al., 2010; Raina et al., 2013; Tapiolas et al., 2013; Masdeu-Navarro et al., 2022).

Merged $DMSP_d$ concentrations ranged from 0.2–3.0 nM in the coral reef at stations CH, BR, and CR (n = 15) and 0.7–2.1 nM in oceanic waters at stations SO and OO (n = 8), with mean concentrations of 0.9 ± 0.7 nM and 1.3 ± 0.6 nM, respectively. No significant difference was observed between the coral reef

and the open ocean concentrations ($p > 0.05$). Unlike acrylate, $DMSP_d$ represented a small fraction of the total DMSP in surface seawater, generally comprising less than 10% throughout all surface samples. A pronouced reef-ocean difference was observed for $DMSP_p$, with concentrations on average ~2.5 times higher at the oceanic sites (SO and OO) compared to the reef sites (10.7 ± 3.1 nM and 4.2 ± 2.1 nM, respectively). Corresponding Chl *a* concentrations varied over a small range from 0.18–0.33 μg L^{-1} between the two ecosystems (Figure S2; Table 1), resulting in markedly higher $DMSP_p$: Chl *a* ratios (nmol:μg) at the oceanic sites compared to the reef sites (46.4 ± 18.8 vs. 15.2 ± 8.1). A similar pattern albeit with smaller differences between the two environments was observed for $acrylate_p$ concentrations (and ratios to Chl *a*), as discussed in the previous paragraph.

Large differences between coral-reef and open-ocean concentrations of $acrylate_p$ and $DMSP_p$ partly reflect differences in (1) the cell-abundance and composition of the oceanic and reef planktonic communities as previously discussed here (e.g., higher dinoflagellate and coccolithophore cell-number densities in the open-ocean stations) or in Leichter et al. (2013) and (2) top-down control of particulate concentrations by coral feeding on pico- and nano-phytoplankton. Differences may also arise from an upregulation of cellular DMSP production (and corresponding increase in DMSP lyase activity and acrylate production) in the algal community in response to oxidative stress in the oligotrophic open-ocean stations from nutrient limitation (Stefels and van Leeuwe, 1998; Spielmeyer and Pohnert, 2012; Bucciarelli et al., 2013; Kinsey et al., 2016). Nitrogen limitation is known to induce the replacement of N-containing osmolytes (e.g., proline or glycine betaine) by DMSP (Keller et al., 1999; Bucciarelli and Sunda, 2003). Nitrogen limitation has also been suggested to induce DMSP biosynthesis as an antioxidant in response to restricted synthesis of N-containing antioxidants such as ascorbate peroxidase (Sunda et al., 2007). However, even though we observed a large depletion in nitrate in the open ocean samples that were more than eight-fold lower than that in the coral reef (0.06 vs 0.33 μM nitrate, Table 1), inorganic N/P ratios remained low throughout the reef-ocean transect, in the 2.2–7.8 range, indicating pervasive inorganic nitrogen limitation throughout the region. Therefore, inorganic nitrogen stress cannot be invoked as the cause for observed differences in $DMSP_p$ and the $DMSP_p$: Chl *a* ratio along the transect, unless the phytoplankton in the reef relied more than the open-ocean phytoplankton on dissolved organic nitrogen (DON, Table 1) as an additional nitrogen source (e.g., Mulholland and Lee, 2009; Moneta et al., 2014). Consequently, the most likely rationale for the decrease in $DMSP_p$ from the open ocean to the coral reef was due to differences in the algal composition as well as the top-down control of $DMSP_p$ by coral feeding.

A significant positive correlation was found between $acrylate_t$ and $DMSP_t$ in surface waters from both the coral reef ($r = 0.63$, $p < 0.0001$, $n = 44$) and oceanic sites ($r = 0.75$, $p < 0.0001$, $n = 38$; Figure 3), which may be expected since $DMSP_p$ is the presumptive biological precursor of acrylate in seawater. However, the correlation was significantly weaker when only particulate concentrations were considered ($r = 0.37$ for the reef, $p > 0.05$; $r = 0.54$ for the oceanic sites, $p > 0.05$), which is not unexpected because an appreciable proportion of particulate-derived acrylate ends up in the dissolved phase whereas very little DMSP is dissolved. No significant correlation was observed in the coral reef or open-ocean sites between dissolved, particulate or total concentrations of acrylate and DMSO, acrylate and Chl *a*, or DMSP and Chl *a*. Principal component analysis (PCA) was performed to further explore these relationships in our study area (Figure S3). The two principal components accounted for 57.5% of the total variation, and the first axis of PCA showed a strong association between the dissolved or total acrylate and $DMSP_t$ and $DMSO_d$, indicating that these variables were highly correlated. However, PCA analysis also indicated that acrylate, DMSP and DMSO were all negatively aligned with Chl *a*, the nutrients nitrate and phosphate; and acrylate, DMSP and DMSO were all poorly correlated to nitrite and ammonium.

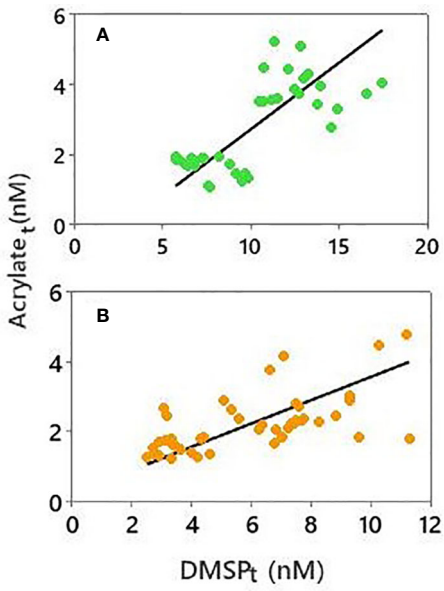

FIGURE 3
Correlation between $acrylate_t$ and $DMSP_t$ in samples collected between 4 and 27 April from the **(A)** oceanic stations (SO and OO) and **(B)** coral reef (CH, BR, CR). Solid lines denote the best-fit from orthogonal regression analysis: **(A)** slope = 0.38 ± 0.06, y-intercept = -1.08 ± 0.60 nM, r = 0.75; **(B)** slope = 0.33 ± 0.06, y-intercept = 0.24 ± 0.41 nM, r = 0.63.

Acrylate and DMSP sources

In the coral reef offshore from Cook's Bay, the main study site, higher $acrylate_d$ concentrations were observed in seawater collected ~0.5 cm away from the coral *A. pulchra* and decomposing seaweed, averaging 18.1 ± 2.9 and 16.5 ± 2.5 nM (Figure 4 and Table S1), respectively, aproximately ten-fold higher than the mean concentration of $acrylate_d$ in surface waters ~2 m from these sources (1.7 ± 0.6 nM). By contrast, no differences were noted in $acrylate_d$ concentrations in close proximity to *Turbinaria ornata* (1.8 ± 0.1 nM) or *Pocillopora* sp. (1.1 ± 0.9 nM) compared to $acrylate_d$ ~2 m from these sources. Although $acrylate_d$ concentrations were low, $acrylate_p$ concentrations (Figure 4 and Table S1) were substantially elevated in waters in close proximity to the macroalgae *T. ornata* (24.9 ± 1.3 nM) or the decomposing seaweed (34.1 ± 4.5 nM) relative to the low $acrylate_p$ concentrations in samples collected from nearby surface seawater (0.5 ± 0.5 nM). Likewise, substantial $DMSP_d$ was detected in close proximity to the coral and macroalgae, averaging 17.6 ± 1.0 nM for the decomposing seaweed, 31.5 ± 0.9 nM for *T. ornata*, and 43.2 ± 0.4 nM for *A. pulchra*, relative to the low average $DMSP_d$ concentration observed in coral reef surface waters (0.9 ± 0.7 nM). A more striking difference was observed for $DMSP_p$, which averaged 21.5 ± 5.3, 186.5 ± 17.3, and 256.5 ± 48.2 nM in waters near *A. pulchra*, *T. ornata*, or the decomposing seaweed (Figure 4 and Table S1), respectively, substantially higher than $DMSP_p$ in coral reef surface waters (4.2 ± 2.1 nM). Together with the large quantities of acrylate and DMSP previously measured in coral tissues and mucus (e.g., Broadbent et al., 2002; Tapiolas et al., 2010; Yost and Mitchelmore, 2010; Raina et al., 2013; Tapiolas et al., 2013; Haydon et al., 2018), it is reasonable to propose that shallow-water coral reefs represent a sizable reservoir of acrylate and organosulfur compounds in the coral-reef ecosystem that may play a disproportionally larger role in regional and global sulfur and carbon cycling than one would predict based on the relatively small areal coverage of coral reefs globally. However, a rigorous evaluation cannot be made here due to the small sample size.

In the Temae Park coral reef study, extremely high concentrations were observed for $acrylate_d$ (65.8 ± 4.2 nM), $DMSP_d$ (80.1 ± 8.9 nM), and $DMSO_d$ (48.4 ± 0.1 nM) in waters a ~0.5 cm away from the coral *A. pulchra*. These concentrations were on average ~30, 40 and 10 times higher than concentrations in waters ~10 cm and several meters away from the coral patch (Figure 5 and Table S2), revealing the large potential of *A. pulchra* as a source of these compounds to the coral reef. The gradients were much smaller for *Pocillopora* sp.; concentrations were 3.2 ± 0.1 nM $acrylate_d$, 6.8 ± 0.1 nM $DMSP_d$, and 4.3 ± 0.4 nM $DMSO_d$ approximately 0.5 cm from the surface of the coral polyps, which were ~3 and 6 times lower away from the *Pocillopora* sp. for $acrylate_d$ and $DMSP_d$ but nearly the same

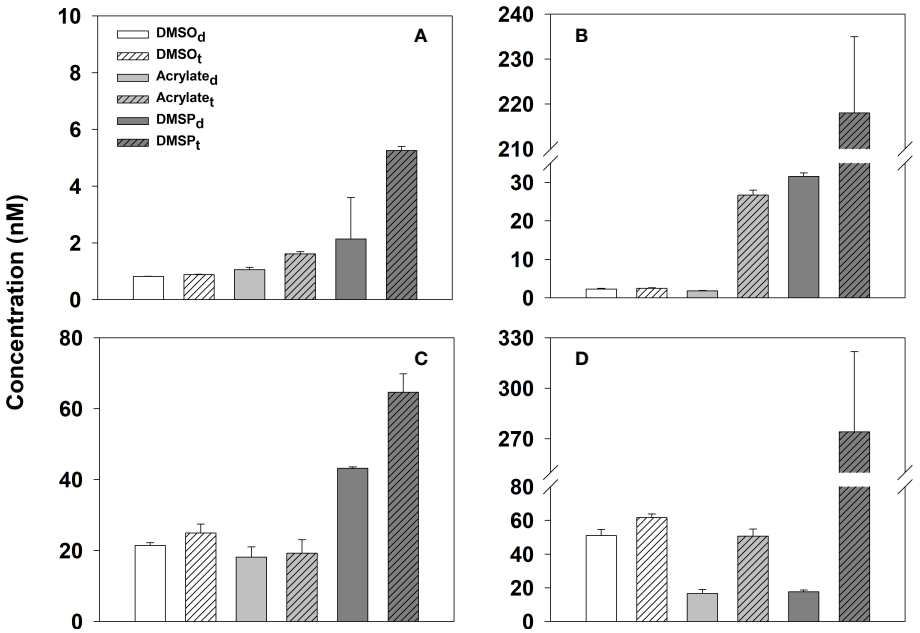

FIGURE 4
Dissolved and total concentrations of acrylate, DMSP and DMSO in samples collected at the CO site between April 15-18 in the vicinity of **(A)** *Pocillopora* sp., **(B)** a brown macroalgae, *Turbinaria ornata*, **(C)** *A. pulchra*, and **(D)** a decomposing seaweed raft. Error bars denote the standard deviation from the measurement of replicate samples. See Table S1 for the data used to generate this figure.

for $DMSO_d$ (Figure 5 and Table S2). Thus, this common coral may be a smaller source of dissolved acrylate and DMSP to the Mo'orea coral reef system compared to *A. pulchra* (also see Figure 4). Overall, *A. pluchara* was a strong source of dissolved acrylate, DMS (DMS data in Masdeu-Navarro et al., 2022), DMSP and DMSO, whereas *Pocillopora* sp. was a weak source for dissolved acrylate and DMSP and not a source of DMSO or DMS (Masdeu-Navarro et al., 2022). The lack of DMS production by *Pocillopora* sp. has been previously observed by Exton et al. (2015) and Lawson et al. (2020), and this likely resulted from low DMSP-lyase activity in *Pocillopora* sp., which would lead to low DMS production rates and low production rates of DMSO from DMS. This in turn likely resulted in no enhancement in $DMSO_d$ concentrations in the vicinity of *Pocillopora* sp. colonies.

Culture-based studies have shown that coral dinoflagellate symbionts contain large quantities of DMSP and DMS (e.g., Broadbent et al., 2002; Steinke et al., 2011; Deschaseaux et al., 2014) and presumably acrylate from the enzymatic lysis of DMSP. However, to date, acrylate concentrations have not been determined in coral algal symbionts although there is a large potential for its production based on the high lyase activity measured in some Symbiodiniaceae (Yost and Mitchelmore, 2009; Caruana and Malin, 2014). In the present study, acrylate and DMSP were detected in non-axenic cultures of five coral dinoflagellate symbionts during exponential growth under nutrient replete conditions (Table 2 and Figure 6). Cellular concentrations of acrylate and DMSP varied among the five species, ranging from 8.6–35.6 mM and 91.9–131.7 mM for acrylate and DMSP, respectively. These cellular acrylate and DMSP concentrations are comparable to those in axenic cultures of other dinoflagellates during early to mid exponential growth under nutrient replete conditions including *Karenia brevis* (2.5–14.5 mM acrylate and 23.0–36.0 mM DMSP; Tyssebotn, 2015) and *Prorocentrum minimum* (3.1–4.2 mM acrylate and 105–160 mM DMSP; Tyssebotn, 2015) or the prymnesiophyte *Phaeocystis antarctica* (3.7–5.2 mM acrylate and 261–275 mM DMSP; Kinsey et al., 2016), and one to two orders of magnitude higher than the diatom *Thalassiosira pseudonana* (0.02–0.25 mM acrylate and 1.8–4.0 mM DMSP; Tyssebotn, 2015). The mM concentrations of acrylate and DMSP observed here for the different coral symbionts suggests coral holobionts produce large quantities of acrylate and DMSP, and are therefore a large potential source of these compounds to the coral-reef ecosystem.

In all coral Symbiodiniaceae cultures, only a small percentage of the total DMSP (< 1%) was detected in dissolved phase, which can be attibuted to its low release from cells and rapid bacterial consumption of $DMSP_d$ in the non-axenic

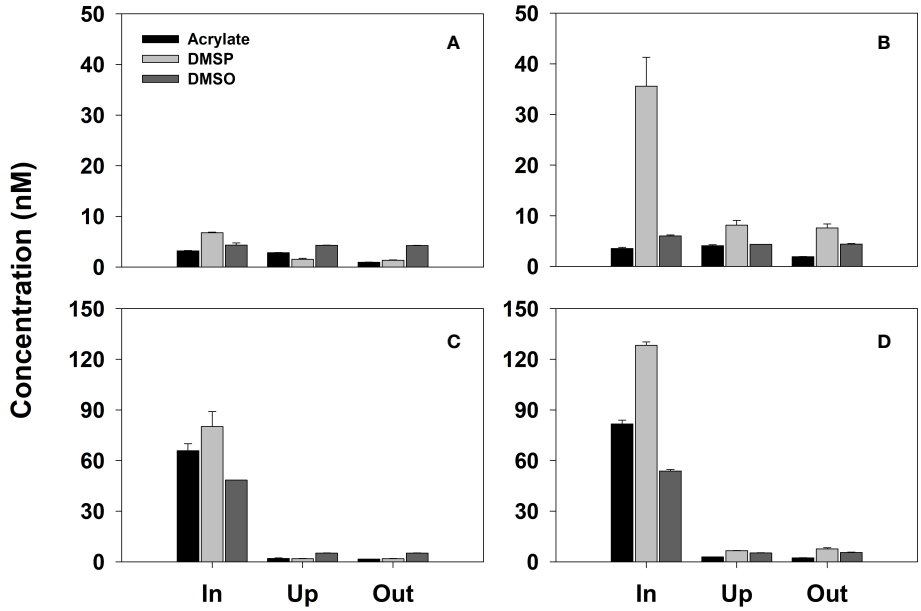

FIGURE 5
Dissolved (panels **A, C**) and total (panels **B, D**) acrylate, DMSP and DMSO in seawater samples collected at different distances from the coral *Pocillopora* sp. (panels **A, B**) and *A pulchra* (panels **C**, **D**) in a coral reef located offshore of Temae Park, Mo'orea at 7:00 am local time, April 23, 2018. x-axis label notation: In, a ~ 0.5 cm away from the tip of several coral polyps, Up, ~ 10 cm away from coral patch, and Out, several meters away from the coral overlying sandy sediment. See Table S2 for the data used to generate this figure.

TABLE 2 Cell size and mean abundance, cell volume (CV), dissolved and cellular concentrations of acrylate and DMSP in five non-axenic, batch cultures of known coral symbionts from the family Symbiodiniaceae.

Species	Cell size	Cell abundance	Cell volume	$Acrylate_d$	$DMSP_d$	$Acrylate_c$	$DMSP_c$
	(μm)	(cells mL^{-1}, $\times 10^6$)	(fL $cell^{-1}$)	(μM)		(mmol L^{-1} CV)	
Breviolum aenigmaticum	7.5	2.35 (0.25)	339 (15)	1.66 (0.54)	0.30 (0.10)	29.6 (10.5)	91.9 (8.6)
Cladocopium sp.	8.8	1.15 (0.16)	399 (27)	0.56 (0.11)	0.16 (0.02)	8.6 (2.5)	118.2 (22.1)
Durusdinium trenchii	9.5	0.82 (0.11)	462 (22)	0.57 (0.22)	0.008 (0.003)	35.6 (4.7)	121.3 (18.6)
Effrenium voratum	11.8	1.71 (0.19)	791 (96)	0.64 (0.17)	0.23 (0.04)	14.6 (3.5)	130.3 (27.9)
Breviolum minutum	6.8	2.10 (0.24)	310 (5)	1.36 (0.18)	0.37 (0.06)	14.7 (1.2)	131.7 (8.0)

Samples were collected for each culture during exponential growth. Values in parentheses denote the standard deviation from triplicate cultures.
The subscripts d and c denote dissolved and cellular, respectively. Cellular concentrations are mmol per liter cell volume.

cultures. Dissolved acrylate concentrations were higher than DMSP, ranging from 3.1 to 13% of the total acrylate; this percentage was significantly less than expected based on results from prior studies under similar growth conditions but with axenic cultures. In these prior studies, which included results from several different dinoflagellate species, from 50-95% of the total acrylate was present in the dissolved phase (Tyssebotn, 2015; Kinsey et al., 2016). The significantly lower percentage of $acrylate_d$ observed in our non-axenic Symbiodiniaceae cultures was likely due to the bacterial consumption of $acrylate_d$ in the culture medium.

Photochemical production of acrylate

Photochemical production of acrylate was consistently observed in the field using freshly collected, 0.2 μm-filtered seawater (Table 3), with no evidence for acrylate photolysis in

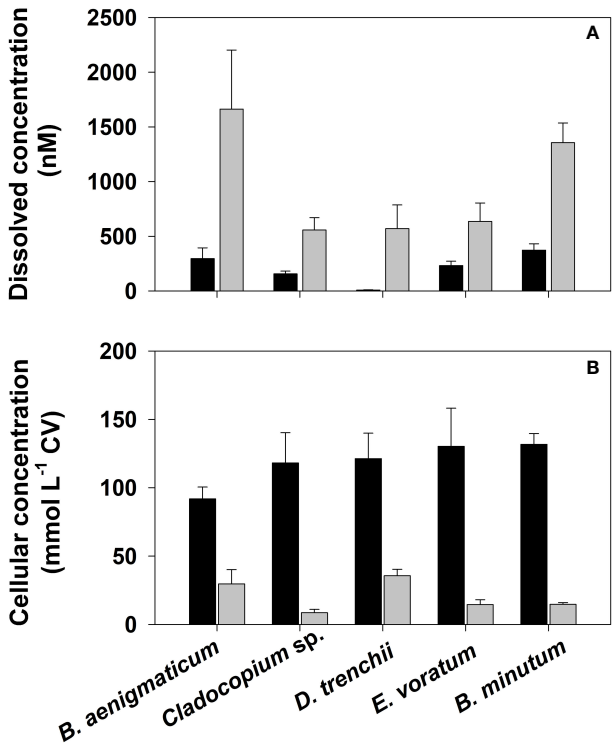

FIGURE 6
(A) Dissolved and **(B)** cell volume (CV) normalized cellular concentrations of acrylate (grey-filled bars) and DMSP (black-filled bars) in non-axenic batch cultures of five dinoflagellate coral symbionts during their exponential growth phase. Error bars represent the standard deviation determined from the analysis of three separate cultures. See Table S3 for culture collection and strain designations.

seawater at ambient concentrations (Xue and Kieber, 2021). To directly compare photochemical production results across different experiments, rates were expressed as a function of the photon exposure (instead of exposure time) between 330 and 380 nm as determined by nitrite actinometry. Photon-based production rates varied by approximately 55%, ranging from 1.6 to 2.9 pM (μmol quanta $cm^{-2})^{-1}$ in the back reef and open-ocean seawater samples (Table 3). Photochemical production rates of acrylate in the coral reef samples at station BR (mean, 2.3 pM (μmol quanta $cm^{-2})^{-1}$) were statistically the same as the oceanic rates at station OO (mean, 2.3 pM (μmol quanta $cm^{-2})^{-1}$) even though the CDOM absorbance coefficient at 330 nm in the back reef samples was on average 79% greater than in the open ocean samples (0.128 vs 0.0715 m^{-1}, respectively). Photochemical production rates would have been expected to be substantially higher in the coral reef if they were correlated to the CDOM absorption. Given that rates were not significantly different between these stations suggests that (1) specific precursors, not correlated to the CDOM absorbance, were responsible for the photochemical production of acrylate in these waters, and (2) these precursors were present at similar concentrations in the coral reef compared to the open ocean samples.

The photochemical production rate of acrylate in the sea-surface microlayer sample collected from the BR station was about a factor of two greater than the mean value in the subsurface samples (4.5 vs 2.3 nM (μmol quanta $cm^{-2})^{-1}$) (Table 3). Higher rates in the microlayer relative to the subsurface samples have been previously reported for the photochemical production of several LMW carbonyl compounds (e.g., by a factor of 1.2–25 for glyoxylic acid). This enhancement may arise from differences in DOM composition or the enrichment of organic matter in the microlayer compared to the underlying seawater (Zhou and Mopper, 1997). Although our microlayer photochemical experiment is not central to our coral reef study, our preliminary finding warrants further investigation given the magnitude of the rate enhancement for acrylate in the sea-surface microlayer.

To compare results obtained here with previous studies, acrylate production rates were also expressed in terms of exposure time assuming 10 h of solar radiation exposure per day (0700–1700). Hourly production rates ranged from 0.033 to 0.051 nM h^{-1}, comparable to that determined for glyoxal and methylglyoxal in Atlantic Ocean surface waters (0.06–0.2 and 0.02–0.07 nM h^{-1}, Zhu and Kieber, 2019) and one order of magnitude lower than the photoproduction rates of other carbonyl compounds including acetaldehyde (0.5 nM h^{-1}) and pyruvate (0.2 nM h^{-1}) in the Sargasso Sea (Mopper et al., 1991). The magnitude of this difference was even greater when compared to the photoproduction rates of acetaldehyde or pyruvate in coastal waters (Mopper and Stahovec, 1986; Kieber et al., 1990; de Bruyn et al., 2011; Takeda et al., 2014). Although hourly production rate comparisons are qualitatively useful to assess differences when light-based rate data are not available, it should be noted that hourly rates are not directly comparable (Kieber et al., 2007). Most published hourly production rates were determined during the summer on sunny days, whereas our acrylate hourly production rates were determined in April on days that were at times quite cloudy with periods of rain. The less than sunny condition was evident in the ratio of the nitrite actinometry to SMARTS clear-sky photon exposure that was significantly less than one, ranging from 0.66 to 0.87 (Xue and Kieber, 2021).

Acrylate$_d$ and DMSP$_d$ biological consumption

The biological consumption of acrylate$_d$ in waters from the Mo'orea back reef (BR) and the open ocean (OO) followed first-order decay kinetics (Figure 7). The slope of the best-fit line from linear regression analysis yielded the net biological consumption

TABLE 3 Acrylate concentration in dark controls (dark, n = 4) and light-exposed quartz tubes (light, n = 4), the temperature for each photochemical experiment (T), initial and final CDOM absorption coefficient at 330 nm (a_{330}), and the photon exposure between 311–333 nm and 330–380 nm determined using nitrate and nitrite actinometry, respectively.

Station	Sampling date 2018	Temperature (°C)[a]	a_{330} (m^{-1})		Photon exposure (μmol cm^{-2})		Acrylate (nM)		Production rate[b]
			Initial	Final	311-333 nm	330-380 nm	Dark	Light	
BR	Apr. 16	29.6	0.139	0.106	54.3 (2.6)	405.5 (13.5)	1.6 (0.29)	2.3 (0.31)	1.6 (0.4)
BR	Apr. 18	28.8	0.117	0.093	39.7 (0.2)	309.4 (5.4)	1.7 (0.53)	2.6 (0.40)	2.9 (0.7)
OO	Apr. 07	29.2	0.075	0.069	28.4 (0.5)	225.2 (7.6)	2.1 (0.20)	2.7 (0.17)	2.3 (0.8)
OO	Apr. 10	29.7	0.068	0.063	76.3 (3.5)	580.7 (21.5)	1.5 (0.34)	3.0 (0.50)	2.3 (0.6)
BR Microlayer	Apr. 18	28.8	0.228	0.164	39.7 (0.2)	309.4 (5.4)	4.2 (0.55)	5.6 (0.41)	4.5 (0.7)

[a]Water bath temperature; the temperature fluctuation in the water bath was < 0.5 °C for each experiment. [b]The production rate was calculated by dividing the acrylate production (light – dark) by the nitrite-based photon exposure. Units for production rate are pM (μmol quanta $cm^{-2})^{-1}$.
The sea-surface microlayer sample was collected from the back reef using a glass plate according to Cunliffe et al. (2013). All seawater samples were gravity filtered through a precleaned 0.2 μm Polycap AS 75 capsule filter (Toole et al., 2003). Values in parentheses denote the standard deviation.

rate constant ($k_{bio,acrylate}$). As shown in Table 4, acrylate$_d$ was rapidly consumed in waters from the back reef with $k_{bio,acrylate}$ ranging from 3.4 to 5.1 d^{-1} with a mean of 4.0 ± 0.7 d^{-1}, nearly six-fold faster than in the open ocean several km offshore from the coral reef (mean 0.7 ± 0.2 d^{-1}, range 0.3–1.1 d^{-1}). Rates were faster in the back reef even though heterotrophic prokaryotes in the coral reef surface waters were approximately 30% less abundant than in the open ocean (4.5×10^5 vs 6.6×10^5 cells mL^{-1}, Table 4). This depletion in heterotrophic prokaryotes in the Mo'orea coral reef agreed with that previously observed in these waters over a four-year period (Nelson et al., 2011). The larger consumption rate constants for acrylate$_d$ in the back reef habitat likely reflected differences in the bacterial community composition in reef waters compared to the open ocean (Leichter et al., 2013; Masdeu-Navarro et al., 2022), as well as differences in bacterial activity. Indeed, bacterial protein synthesis rates approached by bioorthogonal non-canonical amino acid tagging (BONCAT; Leizeaga et al., 2017) were ~ 4 times higher in BR than in OO (Masdeu-Navarro et al., unpublished results), likely because of the availability of nitrate and labile organic matter locally produced by the benthic community, including corals, seaweeds and microorganisms (Silveira et al., 2017). As discussed previously, *A. pulchra* and *T. ornata*, both important components of the Mo'orea reef system (Bulleri et al., 2013; Donovan et al., 2020), were important sources of DMSP and acrylate, which may be representative components of a pool of labile organic compounds to the coral reef.

The rapid consumption of acrylate$_d$ in the Mo'orea coral reef is striking when compared to results in the Gulf of Mexico. Tyssebotn et al. (2017) reported that acrylate$_d$ was consumed in unfiltered Gulf of Mexico water samples, with slow turnover times averaging 1.5 and 11 d at the coastal and open-ocean sites, respectively. These turnover times are 6 and 44 times slower than those observed in the Mo'orea coral reef (Figure 8). Although turnover times were faster, acrylate$_d$ concentrations in the coral reef (1.7 ± 0.7 nM) were not statistically different to concentrations in the Gulf of Mexico (1.5 ± 0.4 nM), indicating that in the coral reef there was a concurrent and rapid input of acrylate into the dissolved phase and fast microbial consumption of acrylate$_d$. In the Gulf of Mexico, inputs and removal rates were slow, and the consumption of acrylate$_d$ only contributed 0.013–0.13% to the bacterial carbon demand, suggesting that the role of acrylate$_d$ was negligible as a substrate for the entire heterotrophic community (Tyssebotn et al., 2017). In the Mo'orea coral reef, acrylate is expected to play a more substantial role in the microbial loop due to its extremely fast consumption and the large production from macroalgae and coral (see section Acrylate and DMSP Sources). Given its rapid turnover, further research is warranted to quantify the significance of acrylate as a substrate to the coral reef heterotrophic community.

The microbial consumption of acrylate$_d$ in the Mo'orea coral reef (mean turnover time 6 h, range 4.7–7.0 h) represents some of the fastest turnover times recorded when compared to the biological consumption of other low molecular weight carbon substrates in seawater. Acrylate turnover times are similar to or faster than some

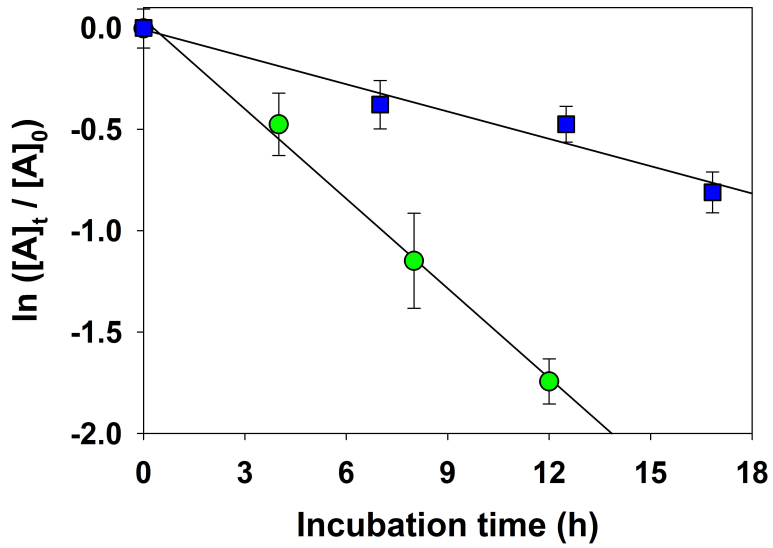

FIGURE 7
First-order kinetic plot for the net biological consumption of acrylate$_d$ in seawater samples collected from the back reef (green circles) and open ocean (blue squares). $[A]_0$ is the initial acrylate concentration and $[A]_t$ is the concentration of a subsample collected during each dark incubation at time t. Error bars denote the standard deviation from triplicate incubations. The biological consumption rate constant, $k_{bio,acrylate}$, was determined by taking the slope of the best-fit line from linear regression analysis.

TABLE 4 Ambient dissolved acrylate and DMSP concentrations, dissolved organic carbon (DOC), particulate organic carbon (POC), and biological rate constants and consumption rates of acrylate and DMSP in the coral-reef BR station and open-ocean OO station collected during diel sampling; local sampling times are reported in the sample column.

Sample	Acrylate$_d$ (nM)	[a]$k_{bio,\ acrylate}$	[b]Acrylate rate	DMSP$_d$ (nM)	[a]$k_{bio,\ DMSP}$	[b]DMSP rate	[c]Bacterial cell number	DOC (μM)	POC (μM)
Reef (BR)									
0400	2.0 (0.19)	3.4 (0.2)	6.8 (0.7)	1.2 (0.06)	5.5 (0.4)	6.4 (0.6)	4.7	76.7	2.8
1000	1.9 (0.12)	4.2 (0.3)	8.0 (0.8)	1.4 (0.05)	8.6 (0.8)	12.1 (1.2)	4.1	66.6	3.2
1600	2.2 (0.14)	4.3 (0.4)	9.4 (1.0)	1.4 (0.03)	8.3 (0.7)	11.6 (1.1)	3.5	64.0	3.5
2200	1.5 (0.16)	3.6 (0.3)	5.4 (0.7)	1.6 (0.05)	7.2 (1.1)	11.8 (1.8)	4.6	67.7	3.4
0400	2.0 (0.06)	3.5 (0.3)	7.0 (0.6)	1.4 (0.07)	7.1 (0.7)	10.2 (1.2)	4.7	68.3	2.8
1000	1.9 (0.11)	5.1 (0.2)	9.7 (0.7)	1.0 (0.05)	8.4 (0.3)	8.5 (0.5)	5.4	72.2	4.4
Mean	1.9 (0.33)	4.0 (0.7)	7.7 (1.9)	1.3 (0.13)	7.5 (1.7)	10.1 (2.7)	4.5 (0.6)	69.3 (4.5)	3.3 (0.6)
Ocean (OO)									
0400	1.4 (0.03)	1.1 (0.1)	1.5 (0.2)	1.3 (0.01)	4.2 (0.4)	5.6 (0.5)	6.6	73.2	2.8
1600	1.6 (0.30)	0.6 (0.1)	0.9 (0.2)	1.8 (0.09)	3.7 (0.6)	6.4 (1.1)	6.5	72.5	3.7
0400	1.7 (0.10)	0.3 (0.1)	0.6 (0.1)	2.1 (0.17)	1.9 (0.6)	3.9 (1.3)	6.4	75.2	3.0
1300	1.1 (0.11)	0.6 (0.1)	0.7 (0.1)	1.6 (0.08)	5.7 (0.3)	9.1 (0.6)	6.8	70.9	3.7
Mean	1.4 (0.33)	0.7 (0.2)	0.9 (0.3)	1.7 (0.21)	3.9 (1.0)	6.2 (1.9)	6.6 (0.2)	73.0 (1.8)	3.3 (0.5)

Values in parentheses denote the standard deviation. Units: [a]biological consumption rate constant (d^{-1}), [b]biological consumption rate (nM d^{-1}), and [c]bacterial cell number ($\times 10^5$ cells mL^{-1}).

of the most labile DOM detected in the oceans, including, for example, dissolved free amino acids (DFAA). Turnover times of DFAA range from 6–48 h in waters off Southern California (Carlucci et al., 1984), 5 and 18 h in high and low productivity Gulf of Mexico waters (Ferguson and Sunda, 1984), and 6.9–144 h (Suttle et al., 1991) and 0.4–7.0 h (Keil and Kirchman, 1999) in Sargasso Sea. Acrylate turnover rates were likely even faster than reported here since we could only determine the net loss of acrylate$_d$ in our study using the non-isotopic technique. If any processes had significantly contributed to the production of acrylate$_d$ during the dark incubation, this would have reduced the observed loss of acrylate and would have reduced the k_{bio} for the biological loss of acrylate. As such, the $k_{bio,acrylate}$ determined from our kinetic approach represent minimum estimates of the true $k_{bio,acrylate}$, which we suspect are faster than reported here. Also, no killed controls were incubated in parallel in our experiments. Therefore, we cannot say unequivocally that acrylate losses were solely due to its biological consumption. However, three lines of evidence suggest biological consumption likely controlled the loss of acrylate in our dark incubations. Acrylate is a highly polar and negatively charged

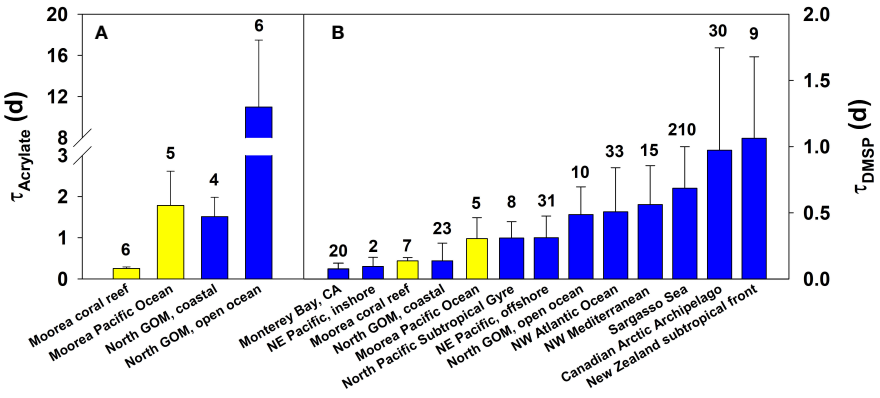

FIGURE 8
Turnover time (τ) of **(A)** acrylate$_d$ and **(B)** DMSP$_d$ from their biological consumption determined in our study (yellow-filled bars) and in previously published studies (blue-filled bars) from different marine environments across different seasons. The value above each bar depicts the number of samples from each study area, which may include multiple studies.

molecule at seawater pH, and therefore is unlikely to be removed from the dissolved phase through complexation or adsorption onto POC; no correlation was observed between POC and $k_{bio,acrylate}$ (Tables 1, 4). Likewise, acrylate is not expected to degrade thermally or by reactions with oxidants, since nM levels of acrylate in seawater were unchanged in filtered dark controls. Finally, biological consumption experiments conducted with unfiltered Gulf of Mexico seawater using nM additions of ^{14}C-labeled acrylate (labeled in the C2 and C3-carbon atoms) demonstrated that acrylate was respired to carbon dioxide and assimilated into macromolecules (Tyssebotn et al., 2017); it is highly unlikely that these products would be produced from abiotic thermal reactions in seawater.

The critical role of DMSP as a substrate for heterotrophic bacteria in seawater is well documented (Kiene et al., 2000; Simó et al., 2009; Buchan et al., 2014); however, its importance as a reduced sulfur and energy source in coral reefs has not been previously studied. Here, using the GBT inhibition technique, we for the first time determined biological consumption rates of $DMSP_d$ in coral-reef waters. The addition of 10 μM GBT in both back-reef and open-ocean waters led to an increase in $DMSP_d$ in the unfiltered samples during the time course of the incubation (Figure 9), resulting from the natural release of particulate DMSP into the seawater through processes such as exudation or grazing while consumption is blocked (Kiene and Gerard, 1995). This assumption is supported by the observation that the time-series decrease in $DMSP_p$ in samples with or without added GBT was the same (t-test, $p > 0.05$, data not shown), suggesting that the external addition of GBT did not artificially cause significant extra release of DMSP from the particulate phase into the dissolved phase in seawater. Therefore, a production rate (R_{prod}) was calculated based on the initial increase of $DMSP_d$ (≤ 3 h) in GBT experiments. In samples receiving no exogenous GBT, $DMSP_d$ decreased rapidly over time (Figure 9) allowing for the calculation of the net loss rate ($R_{loss,net}$). The total loss rate, R_{loss}, was calculated as the sum of R_{prod} and $R_{loss,net}$, and the rate constant for the total loss of $DMSP_d$ ($k_{bio,DMSP}$) was calculated assuming $DMSP_d$ total loss followed first-order kinetics.

Using the GBT approach, we determined that $DMSP_d$ was consumed extremely fast in waters overlying the reef, with $k_{bio,DMSP}$ ranging from 5.5 to 8.6 d^{-1}, nearly twice as fast as the open ocean rates (7.5 ± 1.7 vs 3.9 ± 1.0 d^{-1}, Table 4). Using the rate constants and *in situ* $DMSP_d$ concentrations reported in Table 4, corresponding rates of microbial consumption of $DMSP_d$ in the coral reef and open ocean ranged from 3.9–12 nM d^{-1} (Table 4). If we assume microbial DMS yields from DMSP enzymatic

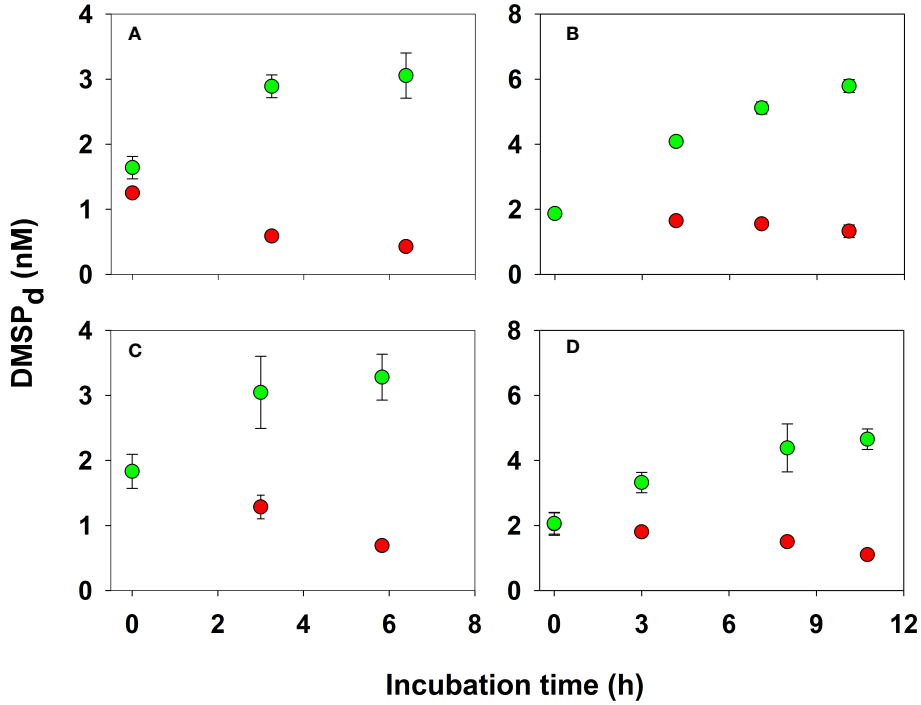

FIGURE 9
Time-course changes in the concentration of $DMSP_d$ in unfiltered seawater from the coral reef (panels **A**, **C**) and open ocean (panels **B**, **D**) incubated in the dark with (green circles) and without (red circles) added GBT (final concentration, 10 μM). Data points denote the mean of triplicate incubations with error bars showing the standard deviation; errors smaller than the symbol are not shown.

cleavage lie between 5–20% (Kiene and Linn, 2000b), then $DMSP_d$ consumption rates would have produced 0.20–2.4 nM DMS daily from this process in the Mo'orea coral reef and adjoining open ocean.

The biological consumption rate constant for $DMSP_d$ was on average nearly twice as fast as that for $acrylate_d$ in the back reef (7.5 ± 1.7 vs 4.0 ± 0.7 d^{-1}), and the difference in k_{bio} (± std dev) was even larger in the open ocean, 3.9 (± 1.0) d^{-1} for $DMSP_d$ and 0.7 (± 0.2) d^{-1} for $acrylate_d$. As shown in Figure 9, our $k_{bio,DMSP}$ in the Mo'orea coral reef was similar to values determined in inshore waters from the northern Gulf of Mexico (Kiene, 1996; Kiene and Linn, 2000a; Pinhassi et al., 2005; Motard-Côté et al., 2016), the northeast Pacific (Royer et al., 2010), and Monterey Bay (Kiene et al., 2019), and nearly 2–10 times faster than the consumption in the open Atlantic (Kiene and Linn, 2000a; Zubkov et al., 2002; Merzouk et al., 2008; Lizotte et al., 2012; Levine et al., 2016; Motard-Côté et al., 2016), Pacific (Merzouk et al., 2006; Royer et al., 2010; del Valle et al., 2012), Mediterranean Sea (Vila-Costa et al., 2008), and polar waters (Luce et al., 2011; Motard-Côté et al., 2012; Lizotte et al., 2017).

Diel study

The first-order rate constant, k_{bio}, for the biological consumption of $acrylate_d$ and $DMSP_d$ varied over the diel cycle in water samples collected from the Mo'orea coral reef and the open ocean (Figure 10). In the back reef (BR), k_{bio} values for both substrates were significantly greater ($p < 0.05$, two-sample t-test) during daylight hours (10:00 and 16:00) compared to nighttime (22:00 and 04:00), exhibiting a clear diel pattern. On average, k_{bio} was 4.5 ± 0.5 d^{-1} for $acrylate_d$ and 8.4 ± 1.1 d^{-1} for $DMSP_d$ in daylight samples, both nearly 30% greater than the mean k_{bio} in night samples. The diel maximum for each substrate was observed in the mid-morning, at 10:00 local time. k_{bio} was 5.1 ± 0.2 d^{-1} for $acrylate_d$ and 8.6 ± 0.8 d^{-1} for $DMSP_d$ at 10:00, both about 1.5-fold faster than the minima observed in the late-night sample at 04:00 on April 12. Even though consumption rate constants varied significantly, dissolved concentrations for both acrylate and DMSP varied very little in the back reef throughout the diel study (Table 4), indicating a tight balance between their production and removal.

In the open-ocean station (OO), several km offshore from the reef, k_{bio} for $acrylate_d$ consumption (0.7 ± 0.2 d^{-1}) was a factor of four or more slower than in the coral reef and no clear diel pattern was observed because of the slower rates and paucity of data (Table 4 and Figure 10). For $DMSP_d$, k_{bio} at the open-ocean site (3.9 ± 1.0 d^{-1}) was two to four times slower compared to the back reef, but, as with acrylate, the diel variation in the open ocean could not be detected due to the lack of sufficient data.

Very few studies have examined diel variations in the biological consumption of specific substrates in the oceans. Carlucci et al. (1984) reported a similar diel pattern for the microbial consumption of DFAA in waters off southern California, as we observed for $acrylate_d$ and $DMSP_d$ in the Mo'orea coral reef; DFAA turnover rates were always faster during daylight hours compared to night-time rates, ranging from 2.5 to 3.7 times and 1.7 to 1.9 times faster during the day compared to night in the spring and fall, respectively. Galí et al. (2013) reported higher rates of microbial consumption of DMS during the day in summer in the Sargasso and the Mediterranean Seas, but no differences in another summer Mediterranean Sea study. The faster biological turnover during the day may be attributed to the higher day time bacterial activity than at night, as has been previously observed from diverse marine locations (Fuhrman et al., 1985; Wheeler et al., 1989; Wikner et al., 1990; Zweifel et al., 1993; Gasol et al., 1998), including coral reef ecosystems (Moriarty et al., 1985; Linley and Koop, 1986), yet not in other studies (Galí et al., 2013). Over the reef flats at Lizard Island, Great Barrier Reef, Moriarty et al. (1985) observed that bacterial growth rates were significantly higher during the day than at night and early morning, and a large increase in growth rates was observed in the late afternoon. Moriarty et al. (1985) proposed that the bacterial growth was mainly stimulated by the release of coral-derived DOM or nutrients carried in the mucus, which also follows a strong diel pattern with maximal rates of release of mucus in the afternoon (Crossland et al., 1980; Wild et al., 2004). In the present study, a pronounced diel variation was observed for $acrylate_d$, $DMSO_d$ and $DMSP_d$ concentrations in waters within ~0.5 cm of the living *A. pulchra* coral host; dissolved concentrations were nearly one order of magnitude higher in samples collected at noon than at midnight (Masdeu-Navarro et al., 2022). This likely resulted from the combination of the expulsion of the algal symbionts during midday hours by the coral polyps (Hoegh-Guldberg et al., 1987) and UVR-induced oxidative stress (Galí et al., 2011). Production and release of organosulfur compounds and acrylate may markedly stimulate the activity of reef-associated bacteria after release into the surrounding water column, which would not be surprising since coral-derived DOC can indeed induce a rapid increase of bacterial abundance and growth rates (Nakajima et al., 2009; Taniguchi et al., 2014; Nakajima et al., 2017; Nakajima et al., 2018).

In contrast to its stimulating effect, studies have also shown that solar radiation, mainly UVR (290–400 nm), can inhibit the growth and activity of bacteria in seawater linked to DNA photodamage (Herndl et al., 1993; Aas et al., 1996; Jeffrey et al., 1996; Alonso-Sáez et al., 2006; Ruiz-González et al., 2013). The faster acrylate and DMSP turnover observed in our daylight samples was most likely a net result between the stimulation

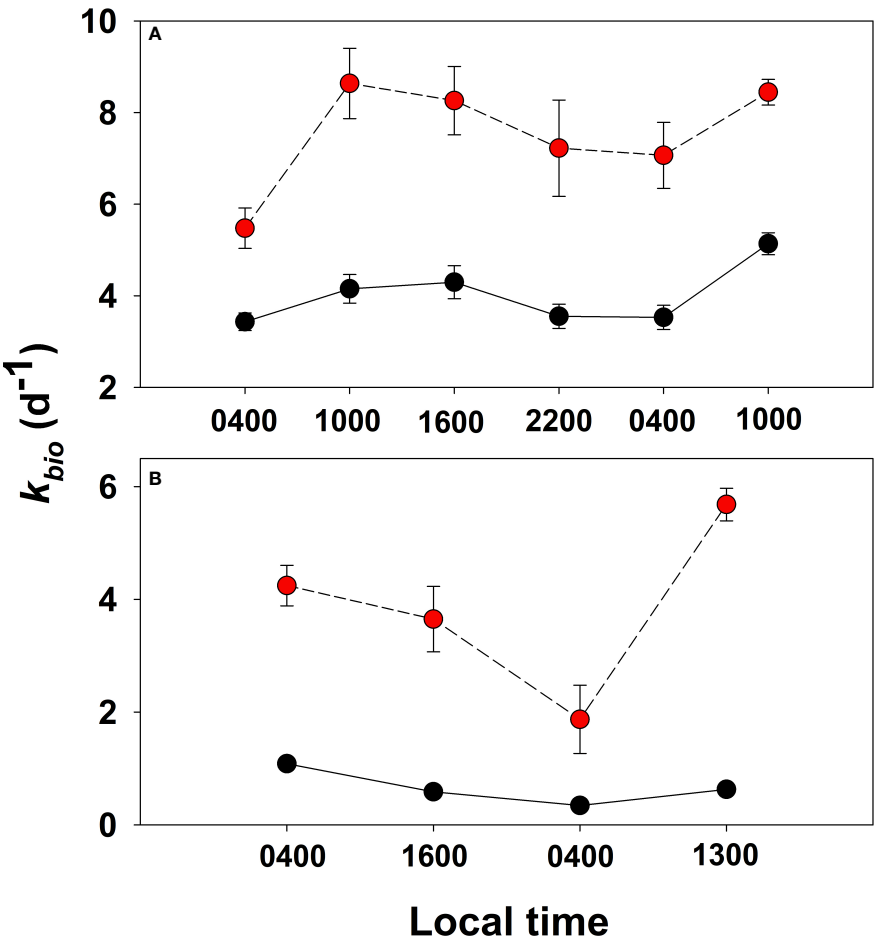

FIGURE 10
First-order rate constant (k_{bio}) for the biological consumption of acrylate$_d$ (black circles) and DMSP$_d$ (red circles) determined from dark incubations of unfiltered seawater collected from the coral reef BR station (panel **A**) and open ocean OO station (panel **B**) during the diel study. Error bars depict the standard deviation from triplicate incubations; errors smaller than the symbol are not shown.

from a larger supply of substrates and inhibition resulting from UVR-induced damage. However, one should note that our diel sampling strategy was to collect samples from a fixed location over time; the disadvantage of this sampling approach is that the same water mass was not followed. Consequently, care should be taken to interpret the diel pattern observed in our study, since it is possible that significantly different microbial populations may have been sampled over the course of the diel study.

Conclusions

Our study provides a novel data set on the distribution and cycling of acrylate and DMSP in a shallow-water coral reef, a severely understudied ecosystem despite its potential for large production and rapid turnover of these compounds in this ecosystem. We observed substantial levels of acrylate and DMSP in waters in the close proximity to important coral and a macroalgae present in the Mo'orea coral reef, as well as in cultures of symbiotic dinoflagellates. Collectively, these results indicate that quantitatively, coral reefs are an important source for acrylate and DMSP. The rapid biological consumption (on a time scale of hours) of dissolved acrylate and DMSP in coral reef waters indicates that these coral-derived substrates serve as efficient carbon, sulfur and energy sources for the growth of reef-associated heterotrophic communities and likely play a critical role in coral reef's ecological network (Figure 11). These new findings call for future studies to quantify the functional role of acrylate and organosulfur compounds in the

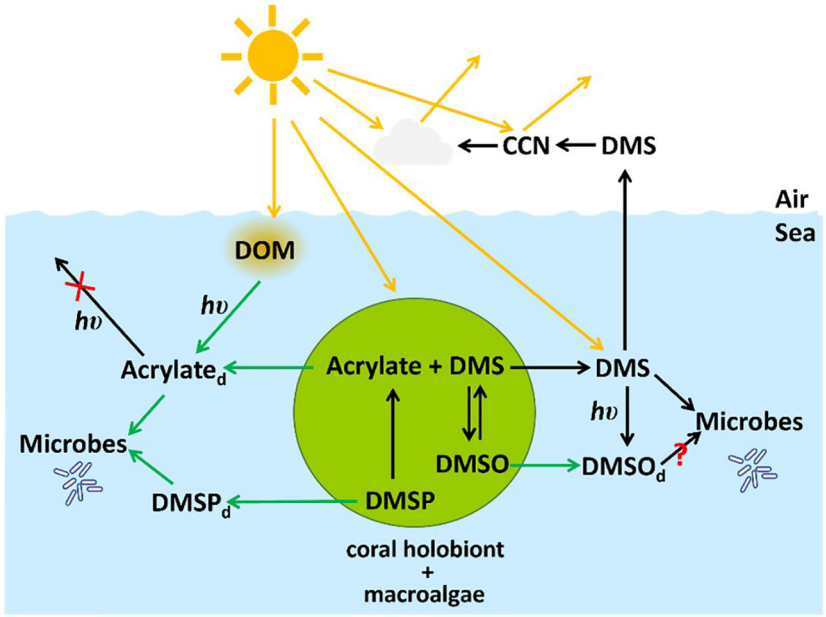

FIGURE 11
A simplified view of the marine organosulfur cycle (1) showing the link between the marine cycle and the atmosphere through DMS and the production of cloud condensation nuclei (CCN), and (2) depicting the main findings of our study highlighted by green arrows. Dissolved acrylate is photochemically produced from the interaction of sunlight (*hυ*) with dissolved organic matter (DOM), and macroalgae and the coral holobiont release acrylate and DMSP into the dissolved phase where they are rapidly consumed by microbes in the Mo'orea coral reef. Acrylate does not photolyze in seawater at ambient concentrations including seawater from the Mo'orea coral reef (Xue and Kieber, 2021) as denoted with a red X. Macroalgae and *A. pulchra* are important sources of dissolved acrylate, DMSP and DMSO. The microbial consumption of DMSO is the presumptive main loss, but this was not confirmed in our study as indicated by the red question mark.

coral holobiont and as microbial substrates in coral-reef environments. Together, this new knowledge will inform the integral role of coral reefs in regional and global carbon and sulfur budgets.

Data availability statement

The datasets used to generate the transect and biological turnover figures in this study are archived in the Biological and Chemical Oceanography-Data Management Office (BCO-DMO) for data management and can be accessed using the following two links doi: 10.26008/1912/bco-dmo.879142.1 and doi: 10.26008/1912/bco-dmo.879158.1. Data presented in this study that are not available from BCO-DMO are provided in Tables S1, S2 in the SM.

Author contributions

DK and LX designed the study. LX analyzed the acrylate, dimethylsulfoniopropionate and dimethylsulfoxide samples, and wrote the initial draft of the manuscript. DK provided review of results and their interpretation and manuscript editing. DK and RS led the field sampling with participation from MM-N, MC-B, PR-R, SG, and CM. MM-N, MC-B, CM and RS analyzed samples for ancillary data. All authors contributed to the article and approved the submitted version.

Funding

This work was supported by funding from the National Science Foundation Chemical Oceanography program (CO–1756907) to DK, from the Spanish Research Agency through the BIOGAPS project (CTM2016-81008-R) to RS, and from EU's Horizon H2020 research and innovation programme through a European Research Council Advanced Grant (ERC-2018-ADG-834162) to RS. The ICM-CSIC holds the 'Severo Ochoa Centre of Excellence' accreditation (CEX2019-000928-S). MC-B, MM-N and PR-R were supported by predoctoral grants from the Spanish government (FPU16-01925 and BES-2017-080048) and "La Caixa" Foundation, respectively. SG was supported by an Australian Government Endeavour Research Fellowship.

Acknowledgments

This work is dedicated to our friend and colleague, Ron Kiene, who's impact on our lives and our work goes well beyond his contributions to the marine-science community, and for that we

are eternally grateful and thankful. We also thank the UC Berkeley Richard Gump Research station staff for logistical support during the field study and Dr. Mary Alice Coffroth at the State University of New York at Buffalo for growing the coral symbiont cultures and sharing lab supplies for sampling. Thanks are also extended to Ms. Liang Chen in Dr. Kieber's laboratory for measuring cell numbers and cell volumes in culture samples, and to Dr. Kristin Bergauer for sharing unpublished BONCAT measurements of bacterial production obtained during our field study.

Conflict of interest

The authors declare that the research was conducted in the absence of any commercial or financial relationships that could be construed as a potential conflict of interest.

Publisher's note

Supplementary material

The Supplementary Material for this article can be found online at: https://www.frontiersin.org/articles/10.3389/fmars.2022.911522/full#supplementary-material

References

Aas, P., Lyons, M., Pledger, R., Mitchell, D. L., and Jeffrey, W. H. (1996). Inhibition of bacterial activities by solar radiation in nearshore waters and the gulf of Mexico. *Aquat. Microb. Ecol.* 11, 229–238. doi: 10.3354/ame011229

Adjeroud, M. (1997). Factors influencing spatial patterns on coral reefs around mo'orea, French Polynesia. *Mar. Ecol. Prog. Ser.* 159, 105–119. doi: 10.3354/meps159105

Alonso-Sáez, L., Gasol, J. M., Lefort, T., Hofer, J., and Sommaruga, R. (2006). Effect of natural sunlight on bacterial activity and differential sensitivity of natural bacterioplankton groups in northwestern Mediterranean coastal waters. *Appl. Environ. Microbiol.* 72, 5806–5813. doi: 10.1128/AEM.00597-06

Asher, E., Dacey, J. W., Ianson, D., Peña, A., and Tortell, P. D. (2017). Concentrations and cycling of DMS, DMSP, and DMSO in coastal and offshore waters of the subarctic pacific during summer 2010-2011. *J. Geophys. Res. C.* 122, 3269–3286. doi: 10.1002/2016JC012465

Bayliss, S. L. J., Scott, Z. R., Coffroth, M. A., and terHorst, C. P. (2019). Genetic variation in *Breviolum antillogorgium*, a coral reef symbiont, in response to temperature and nutrients. *Ecol. Evol.* 9, 2803–2813. doi: 10.1002/ece3.4959

Beman, J. M., Roberts, K. J., Wegley, L., Rohwer, F., and Francis, C. A. (2007). Distribution and diversity of archaeal ammonia monooxygenase genes associated with corals. *Appl. Environ. Microbiol.* 73, 5642–5647. doi: 10.1128/AEM.00461-07

Broadbent, A. D., and Jones, G. B. (2004). DMS and DMSP in mucus ropes, coral mucus, surface films and sediment pore water from coral reefs in the great barrier reef. *Mar. Freshw. Res.* 55, 849–855. doi: 10.1071/MF04114

Broadbent, A., and Jones, G. (2006). Seasonal and diurnal cycles of dimethylsulfide, dimethylsulfoniopropionate and dimethylsulfoxide at one tree reef lagoon. *Environ. Chem.* 3, 260–267. doi: 10.1071/EN06011

Broadbent, A. D., Jones, G. B., and Jones, R. J. (2002). DMSP in corals and benthic algae from the great barrier reef. *Estuar. Coast. Shelf Sci.* 55, 547–555. doi: 10.1006/ecss.2002.1021

Bucciarelli, E., Ridame, C., Sunda, W. G., Dimier-Hugueney, C., Cheize, M., and Belviso, S. (2013). Increased intracellular concentrations of DMSP and DMSO in iron-limited oceanic phytoplankton *Thalassiosira oceanica* and *Trichodesmium erythraeum*. *Limnol. Oceanogr.* 58, 1667–1679. doi: 10.4319/lo.2013.58.5.1667

Bucciarelli, E., and Sunda, W. G. (2003). Influence of CO_2, nitrate, phosphate, and silicate limitation on intracellular dimethylsulfoniopropionate in batch cultures of the coastal diatom *Thalassiosira pseudonana*. *Limnol. Oceanogr.* 48, 2256–2265. doi: 10.4319/lo.2003.48.6.2256

Buchan, A., LeCleir, G. R., Gulvik, C. A., and González, J. M. (2014). Master recyclers: Features and functions of bacteria associated with phytoplankton blooms. *Nat. Rev. Microbiol.* 12, 686–698. doi: 10.1038/nrmicro3326

Bulleri, F., Couraudon-Réale, M., Lison de Loma, T., and Claudet, J. (2013). Variability in the effects of macroalgae on the survival and growth of corals: The consumer connection. *PloS One* 8, e79712. doi: 10.1371/journal.pone.0079712

Burdett, H. L., Aloisio, E., Calosi, P., Findlay, H. S., Widdicombe, S., Hatton, A. D., et al. (2012). The effect of chronic and acute low pH on the intracellular DMSP production and epithelial cell morphology of red coralline algae. *Mar. Biol. Res.* 8, 756–763. doi: 10.1080/17451000.2012.676189

Burdett, H. L., Donohue, P. J. C., Hatton, A. D., Alwany, M. A., and Kamenos, N. A. (2013). Spatiotemporal variability of dimethylsulphoniopropionate on a fringing coral reef: The role of reefal carbonate chemistry and environmental variability. *PLoS One* 8, e64651. doi: 10.1371/journal.pone.0064651

Carlot, J., Rovère, A., Casella, E., Harris, D., Grellet-Muñoz, C., Chancerelle, Y., et al. (2020). Community composition predicts photogrammetry-based structural complexity on coral reefs. *Coral Reefs* 39, 967–975. doi: 10.1007/s00338-020-01916-8

Carlucci, A. F., Craven, D. B., and Henrichs, S. M. (1984). Diel production and microheterotrophic utilization of dissolved free amino acids in waters off southern California. *Appl. Environ. Microbiol.* 48, 165–170. doi: 10.1128/AEM.48.1.165-170.1984

Cartisano, C. M., Del Vecchio, R., and Blough, N. V. (2018). A calibration/validation protocol for long/multi-pathlength capillary waveguide spectrometers. *Limnol. Oceanogr.: Methods* 16, 773–786. doi: 10.1002/lom3.10282

Caruana, M. N., and Malin, G. (2014). The variability in DMSP content and DMSP lyase activity in marine dinoflagellates. *Prog. Oceanogr.* 120, 410–424. doi: 10.1016/j.pocean.2013.10.014

Charlson, R. J., Lovelock, J. E., Andreae, M. O., and Warren, S. G. (1987). Oceanic phytoplankton, atmospheric sulfur, cloud albedo and climate. *Nature* 326, 655–661. doi: 10.1038/326655a0

Crossland, C. J., Barnes, D. J., and Borowitzka, M. A. (1980). Diurnal lipid and mucus production in the staghorn coral. *Acropora acuminata*. *Mar. Biol.* 60, 81–90. doi: 10.1007/BF00389151

Cunliffe, M., Engel, A., Frka, S., Gašparović, B., Guitart, C., Murrell, J. C., et al. (2013). Sea Surface microlayers: A unified physicochemical and biological perspective of the air-ocean interface. *Prog. Oceanogr.* 109, 104–116. doi: 10.1016/j.pocean.2012.08.004

Curson, A. R. J., Liu, J., Bermejo Martínez, A., Green, R. T., Chan, Y., Carrión, O., et al. (2017). Dimethylsulfoniopropionate biosynthesis in marine bacteria and identification of the key gene in this process. *Nat. Microbiol.* 2, 1–9. doi: 10.1038/nmicrobiol.2017.9

de Bruyn, W. J., Clark, C. D., Pagel, L., and Takehara, C. (2011). Photochemical production of formaldehyde, acetaldehyde and acetone from chromophoric dissolved organic matter in coastal waters. *J. Photochem. Photobiol. A Chem.* 226, 16–22. doi: 10.1016/j.photochem.2011.10.002

del Valle, D. A., Kieber, D. J., John, B., and Kiene, R. P. (2007). Light-stimulated production of dissolved DMSO by a particle-associated process in the Ross Sea, Antarctica. *Limnol. Oceanogr.* 52, 2456–2466. doi: 10.4319/lo.2007.52.6.2456

del Valle, D. A., Kiene, R. P., and Karl, D. M. (2012). Effect of visible light on dimethylsulfoniopropionate assimilation and conversion to dimethylsulfide in the north pacific subtropical gyre. *Aquat. Microb. Ecol.* 66, 47–62. doi: 10.3354/ame01557

Deschaseaux, E. S. M., Jones, G. B., Deseo, M. A., Shepherd, K. M., Kiene, R. P., Swan, H. B., et al. (2014). Effects of environmental factors on dimethylated sulfur compounds and their potential role in the antioxidant system of the coral holobiont. *Limnol. Oceanogr.* 59, 758–768. doi: 10.4319/lo.2014.59.3.0758

Dietzel, A., Bode, M., Connolly, S. R., and Hughes, T. P. (2020). Long-term shifts in the colony size structure of coral populations along the great barrier reef. *Proc. R. Soc B.* 287, 20201432. doi: 10.1098/rspb.2020.1432

Donovan, M. K., Adam, T. C., Shantz, A. A., Speare, K. E., Munsterman, K. S., Rice, M. M., et al. (2020). Nitrogen pollution interacts with heat stress to increase coral bleaching across the seascape. *Proc. Nat. Acad. Sci.* 117, 5351–5357. doi: 10.1073/pnas.1915395117

Drew, E. A. (1972). The biology and physiology of algal-invertebrate symbiosis. II. the density of algal cells in a number of hermatypic hard corals and alcyonarians from various depths. *J. Exp. Mar. Biol. Ecol.* 9, 71–75. doi: 10.1016/0022-0981(72)90008-1

Erler, D. V., Santos, I. R., and Eyre, B. D. (2014). Inorganic nitrogen transformations within permeable carbonate sands. *Cont. Shelf Res.* 77, 69–80. doi: 10.1016/j.csr.2014.02.002

Evans, C., Kadner, S. V., Darroch, L. J., Wilson, W. H., Liss, P. S., and Malin, G. (2007). The relative significance of viral lysis and microzooplankton grazing as pathways of dimethylsulfoniopropionate (DMSP) cleavage: An *Emiliania huxleyi* culture study. *Limnol. Oceanogr.* 52, 1036–1045. doi: 10.4319/lo.2007.52.3.1036

Evans, C., Malin, G., Wilson, W. H., and Liss, P. S. (2006). Infectious titres of *Emiliania huxleyi* virus 86 are reduced by exposure to millimolar dimethylsulfide and acrylic acid. *Limnol. Oceanogr.* 51, 2468–2471. doi: 10.4319/lo.2006.51.5.2468

Exton, D. A., McGenity, T. J., Steinke, M., Smith, D. J., and Suggett, D. J. (2015). Uncovering the volatile nature of tropical coastal marine ecosystems in a changing world. *Glob. Change Biol.* 21, 1383–1394. doi: 10.1111/gcb.12764

Ferguson, R. L., and Sunda, W. G. (1984). Utilization of amino acids by planktonic marine bacteria: Importance of clean technique and low substrate additions. *Limnol. Oceanogr.* 29, 258–274. doi: 10.4319/lo.1984.29.2.0258

Fuhrman, J. A., Eppley, R. W., Hagström, Å., and Azam, F. (1985). Diel variations in bacterioplankton, phytoplankton, and related parameters in the southern California bight. *Mar. Ecol. Prog. Ser.* 27, 9–20. doi: 10.3354/meps027009

Galí, M., Saló, V., Almeda, R., Calbet, A., and Simó, R. (2011). Stimulation of gross dimethylsulfide (DMS) production by solar radiation. *Geophys. Res. Lett.* 38, L15612. doi: 10.1029/2011GL048051

Galí, M., Simó, R., Vila-Costa, M., Ruiz-González, C., Gasol, J. M., and Matrai, P. (2013). Diel patterns of oceanic dimethylsufide (DMS) cycling: Microbial and physical drivers. *Global Biogeochem. Cycles* 27, 1–17. doi: 10.1002/gbc.20047

Gardner, S. G., Nielsen, D. A., Laczka, O., Shimmon, R., Beltran, V. H., Ralph, P. J., et al. (2016). Dimethylsulfoniopropionate, superoxide dismutase and glutathione as stress response indicators in three corals under short-term hyposalinity stress. *Proc. R. Soc B* 283, 20152418. doi: 10.1098/rspb.2015.2418

Gardner, S. G., Raina, J.-B., Nitschke, M. R., Nielsen, D. A., Stat, M., Motti, C. A., et al. (2017). A multi-trait systems approach reveals a response cascade to bleaching in corals. *BMC Biol.* 15, 117. doi: 10.1186/s12915-017-0459-2

Gasol, J. M., and Del Giorgio, P. A. (2000). Using flow cytometry for counting natural planktonic bacteria and understanding the structure of planktonic bacterial communities. *Sci. Mar.* 64, 197–224. doi: 10.3989/scimar.2000.64n2197

Gasol, J. M., Doval, M. D., Pinhassi, J., Calderón-Paz, J. I., Guixa-Boixareu, N., Vaqué, D., et al. (1998). Diel variations in bacterial heterotrophic activity and growth in the northwest Mediterranean Sea. *Mar. Ecol. Prog. Ser.* 164, 107–124. doi: 10.3354/meps164107

Glaze, T. D., Erler, D. V., and Siljanen, H. M. P. (2021). Microbially facilitated nitrogen cycling in tropical corals. *ISME J.* 16, 68–77. doi: 10.1038/s41396-021-01038-1

Guibert, I., Bourdreux, F., Bonnard, I., Pochon, X., Dubousquet, V., Raharivelomanana, P., et al. (2020). Dimethylsulfoniopropionate concentration in coral reef invertebrates varies according to species assemblages. *Sci. Rep.* 10, 9922. doi: 10.1038/s41598-020-66290-5

Hansen, H. P., and Koroleff, F. (1999). "Determination of nutrients," in *Methods of seawater analysis*. Eds. K. Grasshoff, K. Kremling and M. Ehrhardt(WILEY-VCH Verlag GmbH), 159–228. doi: 10.1002/9783527613984.ch10

Haydon, T. D., Seymour, J. R., and Suggett, D. J. (2018). Soft corals are significant DMSP producers in tropical and temperate reefs. *Mar. Biol.* 165, 109. doi: 10.1007/s00227-018-3367-2

Hench, J. L., Leichter, J. J., and Monismith, S. G. (2008). Episodic circulation and exchange in a wave-driven coral reef and lagoon system. *Limnol. Oceanogr.* 53, 2681–2694. doi: 10.4319/lo.2008.53.6.2681

Herdman, L. M. M., Hench, J. L., and Monismith, S. G. (2015). Heat balances and thermally driven lagoon-ocean exchanges on a tropical coral reef system (Moorea, French Polynesia). *J. Geophys. Res. C.* 120, 1233–1252. doi: 10.1002/2014JC010145

Herndl, G. J., Müller-Niklas, G., and Frick, J. (1993). Major role of ultraviolet-b in controlling bacterioplankton growth in the surface layer of the ocean. *Nature* 361, 717–719. doi: 10.1038/361717a0

Herr, A. E., Dacey, J. W. H., Kiene, R. P., McCulloch, R. D., Schuback, N., and Tortell, P. D. (2021). Potential roles of dimethylsulfoxide in regional sulfur cycling and phytoplankton physiological ecology in the NE subarctic pacific. *Limnol. Oceanogr.* 66, 76–94. doi: 10.1002/lno.11589

Hill, R. W., Dacey, J. W. H., and Edward, A. (2000). Dimethylsulfoniopropionate in giant clams (Tridacnidae). *Biol. Bull.* 199, 108–115. doi: 10.2307/1542870

Hill, R. W., Dacey, J. W. H., and Krupp, D. A. (1995). Dimethylsulfoniopropionate in reef corals. *Bull. Mar. Sci.* 57, 489–494.

Hoegh-Guldberg, O. (1999). Climate change, coral bleaching and the future of the world's coral reefs. *Mar. Freshw. Res.* 50, 839–866. doi: 10.1071/MF99078

Hoegh-Guldberg, O., McCloskey, L. R., and Muscatine, L. (1987). Expulsion of zooxanthellae by symbiotic cnidarians from the red Sea. *Coral Reefs* 5, 201–204. doi: 10.1007/BF00300964

Jackson, R. L., Gabric, A. J., Woodhouse, M. T., Swan, H. B., Jones, G. B., Cropp, R. A., et al. (2020). Coral reef emissions of atmospheric dimethylsulfide and the influence on marine aerosols in the southern great barrier reef, Australia. *J. Geophys. Res. D.* 125, e2019JD031837. doi: 10.1029/2019JD031837

Jankowski, J. J., Kieber, D. J., and Mopper, K. (1999). Nitrate and nitrite ultraviolet actinometers. *Photochem. Photobiol.* 70, 319–328. doi: 10.1111/j.1751-1097.1999.tb08143.x

Jankowski, J. J., Kieber, D. J., Mopper, K., and Neale, P. J. (2000). Development and intercalibration of ultraviolet solar actinometers. *Photochem. Photobiol.* 71, 431–440. doi: 10.1562/0031-8655(2000)0710431DAIOUS2.0.CO2

Jeffrey, W. H., Pledger, R. J., Aas, P., Hager, S., Coffin, R. B., Von Haven, R., et al. (1996). Diel and depth profiles of DNA photodamage in bacterioplankton exposed to ambient solar ultraviolet radiation. *Mar. Ecol. Prog. Ser.* 137, 283–291. doi: 10.3354/meps137283

Jones, G., Curran, M., Broadbent, A., King, S., Fischer, E., and Jones, R. (2007). Factors affecting the cycling of dimethylsulfide and dimethylsulfoniopropionate in coral reef waters of the great barrier reef. *Environ. Chem.* 4, 310–322. doi: 10.1071/EN06065

Jones, G., Curran, M., Deschaseaux, E., Omori, Y., Tanimoto, H., Swan, H., et al. (2018). The flux and emission of dimethylsulfide from the great barrier reef region and potential influence on the climate of NE Australia. *J. Geophys. Res. D.* 123, 13,835–13,856. doi: 10.1029/2018JD029210

Keil, R. G., and Kirchman, D. L. (1999). Utilization of dissolved protein and amino acids in the northern Sargasso Sea. *Aquat. Microb. Ecol.* 18, 293–300. doi: 10.3354/ame018293

Keller, M. D. (1989). Dimethyl sulfide production and marine phytoplankton: The importance of species composition and cell size. *Biol. Oceanogr.* 6, 375–382. doi: 10.1080/01965581.1988.10749540

Keller, M. D., Kiene, R. P., Matrai, P. A., and Bellows, W. K. (1999). Production of glycine betaine and dimethylsulfoniopropionate in marine phytoplankton. II. n-limited chemostat cultures. *Mar. Biol.* 135, 249–257. doi: 10.1007/s002270050622

Kerrison, P., Suggett, D. J., Hepburn, L. J., and Steinke, M. (2012). Effect of elevated pCO_2 on the production of dimethylsulphoniopropionate (DMSP) and dimethylsulphide (DMS) in two species of ulva (Chlorophyceae). *Biogeochemistry* 110, 5–16. doi: 10.1007/s10533-012-9707-2

Kieber, D. J., Toole, D. A., Jankowski, J. J., Kiene, R. P., Westby, G. R., del Valle, D. A., et al. (2007). Chemical "light meters" for photochemical and photobiological studies. *Aquat. Sci.* 69, 360–376. doi: 10.1007/s00027-007-0895-0

Kieber, D. J., Yocis, B. H., and Mopper, K. (1997). Free-floating drifter for photochemical studies in the water column. *Limnol. Oceanogr.* 42, 1829–1833. doi: 10.4319/lo.1997.42.8.1829

Kieber, R. J., Zhou, X., and Mopper, K. (1990). Formation of carbonyl compounds from UV-induced photodegradation of humic substances in natural waters: Fate of riverine carbon in the sea. *Limnol. Oceanogr.* 35, 1503–1515. doi: 10.4319/lo.1990.35.7.1503

Kiene, R. P. (1996). "Turnover of dissolved DMSP in estuarine and shelf waters of the northern gulf of Mexico," in *Biological and environmental chemistry of DMSP and related sulfonium compounds*. Eds. R. P. Kiene, P. T. Visscher, M. D. Keller and G. O. Kirst (Plenum Press, Boston, MA), 337–349. doi: 10.1007/978-1-4613-0377-0_29

Kiene, R. P., and Gerard, G. (1995). Evaluation of glycine betaine as an inhibitor of dissolved dimethylsulfoniopropionate degradation in coastal waters. *Mar. Ecol. Prog. Ser.* 128, 121–131. doi: 10.3354/meps128121

Kiene, R. P., Kieber, D. J., Slezak, D., Toole, D. A., del Valle, D. A., Bisgrove, J., et al. (2007). Distribution and cycling of dimethylsulfide, dimethylsulfoniopropionate, and dimethylsulfoxide during spring and early summer in the southern ocean south of new Zealand. *Aquat. Sci.* 69, 305–319. doi: 10.1007/s00027-007-0892-3

Kiene, R. P., and Linn, L. J. (2000a). Distribution and turnover of dissolved DMSP and its relationship with bacterial production and dimethylsulfide in the gulf of Mexico. *Limnol. Oceanogr.* 45, 849–861. doi: 10.4319/lo.2000.45.4.0849

Kiene, R. P., and Linn, L. J. (2000b). The fate of dissolved dimethylsulfoniopropionate (DMSP) in seawater: Tracer studies using ^{35}S-DMSP. *Geochim. Cosmochim. Acta* 64, 2797–2810. doi: 10.1016/S0016-7037(00)00399-9

Kiene, R. P., Linn, L. J., and Bruton, J. A. (2000). New and important roles for DMSP in marine microbial communities. *J. Sea Res.* 43, 209–224. doi: 10.1016/S1385-1101(00)00023-X

Kiene, R. P., Nowinski, B., Esson, K., Preston, C., Marin, R., Birch, J., et al. (2019). Unprecedented DMSP concentrations in a massive dinoflagellate bloom in Monterey bay, CA. *Geophys. Res. Lett.* 46, 1–10. doi: 10.1029/2019GL085496

Kiene, R. P., and Slezak, D. (2006). Low dissolved DMSP concentrations in seawater revealed by small-volume gravity filtration and dialysis sampling. *Limnol. Oceanogr. Met.* 4, 80–95. doi: 10.4319/lom.2006.4.80

Kinsey, J. D., and Kieber, D. J. (2016). Microwave preservation method for DMSP, DMSO, and acrylate in unfiltered seawater and phytoplankton culture samples. *Limnol. oceanogr. Methods* 14, 196–209. doi: 10.1002/lom3.10081

Kinsey, J. D., Kieber, D. J., and Neale, P. J. (2016). Effects of iron limitation and UV radiation on *Phaeocystis antarctica* growth and DMSP, DMSO, and acrylate concentrations. *Environ. Chem.* 13, 195–211. doi: 10.1071/EN14275

Lawson, C. A., Seymour, J. R., Possell, M., Suggett, D. J., and Raina, J.-B. (2020). The volatilomes of symbiodiniaceae-associated bacteria are influenced by chemicals derived from their algal partner. *Front. Mar. Sci.* 7. doi: 10.3389/fmars.2020.00106

Leichter, J. J., Alldredge, A. L., Bernardi, G., Brooks, A. J., Carlson, C. A., Carpenter, R. C., et al. (2013). Biological and physical interactions on a tropical island coral reef: Transport and retention processes on moorea, French Polynesia. *Oceanography* 26, 52–63. doi: 10.5670/oceanog.2013.45

Leizeaga, A., Estrany, M., Forn, I., and Sebastián, M. (2017). Using click-chemistry for visualizing *in situ* changes of translational activity in planktonic marine bacteria. *Front. Microbiol.* 8. doi: 10.3389/fmicb.2017.02360

Levine, N. M., Toole, D. A., Neeley, A., Bates, N. R., Doney, S. C., and Dacey, J. W. H. (2016). Revising upper-ocean sulfur dynamics near Bermuda: New lessons from 3 years of concentration and rate measurements. *Environ. Chem.* 13, 302–313. doi: 10.1071/EN15045

Lidbury, I., Kröber, E., Zhang, Z., Zhu, Y., Murrell, J. C., Chen, Y., et al. (2016). A mechanism for bacterial transformations of DMS to DMSO: A missing link in the marine organic sulfur cycle. *Environ. Microbiol.* 18, 2754–2765. doi: 10.1111/1462-2920.13354

Linley, E. A. S., and Koop, K. (1986). Significance of pelagic bacteria as a trophic resource in a coral reef lagoon, one tree island, great barrier reef. *Mar. Biol.* 92, 457–464. doi: 10.1007/BF00392505

Liu, Y., Liu, C. Y., Yang, G. P., Zhang, H. H., and Zhang, S. H. (2016a). Biogeochemistry of dimethylsulfoniopropionate, dimethylsulfide and acrylic acid in the yellow Sea and the bohai Sea during autumn. *Environ. Chem.* 13, 127–139. doi: 10.1071/EN15025

Liu, X., Xiao, W. P., Landry, M. R., Chiang, K. P., Wang, L., and Huang, B. Q. (2016b). Responses of phytoplankton communities to environmental variability in the East China Sea. *Ecosystems* 19, 832–849. doi: 10.1007/s10021-016-9970-5

Lizotte, M., Levasseur, M., Law, C. S., Walker, C. F., Safi, K. A., Marriner, A., et al. (2017). Dimethylsulfoniopropionate (DMSP) and dimethylsulfide (DMS) cycling across contrasting biological hotspots of the new Zealand subtropical front. *Ocean Sci.* 13, 961–982. doi: 10.5194/os-13-961-2017

Lizotte, M., Levasseur, M., Michaud, S., Scarratt, M. G., Merzouk, A., Gosselin, M., et al. (2012). Macroscale patterns of the biological cycling of dimethylsulfoniopropionate (DMSP) and dimethylsulfide (DMS) in the Northwest Atlantic. *Biogeochemistry* 110, 183–200. doi: 10.1007/s10533-011-9698-4

Luce, M., Levasseur, M., Scarratt, M. G., Michaud, S., Royer, S.-J., Kiene, R., et al. (2011). Distribution and microbial metabolism of dimethylsulfoniopropionate and dimethylsulfide during the 2007 Arctic ice minimum. *J. Geophys. Res. C.* 116, C00G06. doi: 10.1029/2010JC006914

Masdeu-Navarro, M., Mangot, J.-F., Xue, L., Cabrera-Brufau, M., Gardner, S. G., Kieber, D. J., et al. (2022). Spatial and diel patterns of volatile organic compounds, DMSP-derived compounds, and planktonic microorganisms around a tropical scleractinian coral colony. *Front. Mar. Sci* 9, 944141. doi: 10.3389/fmars.2022.944141

Merzouk, A., Levasseur, M., Scarratt, M., Michaud, S., Lizotte, M., Rivkin, R. B., et al. (2008). Bacterial DMSP metabolism during the senescence of the spring diatom bloom in the Northwest Atlantic. *Mar. Ecol. Prog. Ser.* 369, 1–11. doi: 10.3354/meps07664

Merzouk, A., Levasseur, M., Scarratt, M. G., Michaud, S., Rivkin, R. B., Hale, M. S., et al. (2006). DMSP and DMS dynamics during a mesoscale iron fertilization experiment in the northeast pacific – part II: Biological cycling. *Deep-Sea Res. II* 53, 2370–2383. doi: 10.1016/j.dsr2.2006.05.022

Moneta, A., Veuger, B., van Rijswijk, P., Meysman, F., Soetaert, K., and Middelburg, J. J. (2014). Dissolved inorganic and organic nitrogen uptake in the coastal north Sea: A seasonal study. *Estuar. Coast. Shelf Sci.* 147, 78–86. doi: 10.1016/j.ecss.2014.05.022

Mopper, K., and Stahovec, W. L. (1986). Sources and sinks of low molecular weight organic carbonyl compounds in seawater. *Mar. Chem.* 19, 305–321. doi: 10.1016/0304-203(86)90052-6

Mopper, K., Zhou, X., Kieber, R. J., Kieber, D. J., Sikorski, R. J., and Jones, R. D. (1991). Photochemical degradation of dissolved organic carbon and its impact on the oceanic carbon cycle. *Nature* 353, 60–62. doi: 10.1038/353060a0

Moriarty, D. J. W., Pollard, P. C., and Hunt, W. G. (1985). Temporal and spatial variation in bacterial production in the water column over a coral reef. *Mar. Biol.* 85, 285–292. doi: 10.1007/BF00393249

Motard-Côté, J., Kieber, D. J., Rellinger, A., and Kiene, R. P. (2016). Influence of the Mississippi river plume and nonbioavailable DMSP on dissolved DMSP turnover in the northern gulf of Mexico. *Environ. Chem.* 13, 280–292. doi: 10.1071/EN15053

Motard-Côté, J., Levasseur, M., Scarratt, M. G., Michaud, S., Gratton, Y., Rivkin, R. B., et al. (2012). Distribution and metabolism of dimethylsulfoniopropionate (DMSP) and phylogenetic affiliation of DMSP-assimilating bacteria in northern Baffin Bay/Lancaster sound. *J. Geophys. Res. C.* 117, C00G11. doi: 10.1029/2011JC007330

Mulholland, M. R., and Lee, C. (2009). Peptide hydrolysis and the uptake of dipeptides by phytoplankton. *Limnol. Oceanogr.* 54, 856–868. doi: 10.4319/lo.2009.54.3.0856

Nakajima, R., Haas, A. F., Silveira, C. B., Kelly, E. L. A., Smith, J. E., Sandin, S., et al. (2018). Release of dissolved and particulate organic matter by the soft coral *Lobophytum* and subsequent microbial degradation. *J. Exp. Mar. Biol. Ecol.* 504, 53–60. doi: 10.1016/j.jembe.2018.02.008

Nakajima, R., Tanaka, Y., Guillemette, R., and Kurihara, H. (2017). Effects of coral-derived organic matter on the growth of bacterioplankton and heterotrophic nanoflagellates. *Coral Reefs* 36, 1171–1179. doi: 10.1007/s00338-017-1608-3

Nakajima, R., Yoshida, T., Azman, B. A. R., Zaleha, K., Othman, B. H. R., and Toda, T. (2009). *In situ* release of coral mucus by acropora and its influence on the heterotrophic bacteria. *Aquat. Ecol.* 43, 815–823. doi: 10.1007/s10452-008-9210-y

Nelson, C. E., Alldredge, A. L., McCliment, E. A., Amaral-Zettler, L. A., and Carlson, C. A. (2011). Depleted dissolved organic carbon and distinct planktonic bacterial communities in a rapid-flushing coral reef ecosystem. *ISME J.* 5, 1374–1387. doi: 10.1038/ismej.2011.12

Nelson, C. E., Donahue, M. J., Dulaiova, H., Goldberg, S. J., la Valle, F. F., Lubarsky, K., et al. (2015). Fluorescent dissolved organic matter as a multivariate biogeochemical tracer of submarine groundwater discharge in coral reef ecosystems. *Mar. Chem.* 177, 232–243. doi: 10.1016/j.marchem.2015.06.026

Olson, R. J., Zettler, E. R., and DuRand, M. D. (2018). "Phytoplankton analysis using flow cytometry," in *Handbook of methods in aquatic microbial ecology*. Eds. P. F. Kemp, B. F. Sherr, E. B. Sheer and J. J. Cole (Boca Raton, FL: Lewis Publishers), 175–186.

Patten, N. L., Wyatt, A. S. J., Lowe, R. J., and Waite, A. M. (2011). Uptake of picophytoplankton, bacterioplankton and virioplankton by a fringing coral reef community (Ningaloo reef, Australia). *Coral Reefs* 30, 555–567. doi: 10.1007/s00338-011-0777-8

Payet, J. P., McMinds, R., Burkepile, D. E., and Vega Thurber, R. L. (2014). Unprecedented evidence for high viral abundance and lytic activity in coral reef waters of the south pacific ocean. *Front. Microbiol.* 5. doi: 10.3389/fmicb.2014.00493

Pinhassi, J., Simó, R., González, J. M., Vila, M., Alonso-Sáez, L., Kiene, R. P., et al. (2005). Dimethylsulfoniopropionate turnover is linked to the composition and dynamics of the bacterioplankton assemblage during a microcosm phytoplankton bloom. *Appl. Environ. Microbiol.* 71, 7650–7660. doi: 10.1128/AEM.71.12.7650-7660.2005

Raina, J.-B., Dinsdale, E. A., Willis, B. L., and Bourne, D. G. (2010). Do the organic sulfur compounds DMSP and DMS drive coral microbial associations? *Trends Microbiol.* 18, 101–108. doi: 10.1016/j.tim.2009.12.002

Raina, J.-B., Tapiolas, D. M., Forêt, S., Lutz, A., Abrego, D., Ceh, J., et al. (2013). DMSP biosynthesis by an animal and its role in coral thermal stress response. *Nature* 502, 677–680. doi: 10.1038/nature12677

Rix, L. N., Burdett, H. L., and Kamenos, N. A. (2012). Irradiance-mediated dimethylsulphoniopropionate (DMSP) responses of red coralline algae. *Estuar. Coast. Shelf Sci.* 96, 268–272. doi: 10.1016/j.ecss.2011.11.022

Royer, S.-J., Levasseur, M., Lizotte, M., Arychuk, M., Scarratt, M. G., Wong, C. S., et al. (2010). Microbial dimethylsulfoniopropionate (DMSP) dynamics along a natural iron gradient in the northeast subarctic pacific. *Limnol. Oceanogr.* 55, 1614–1626. doi: 10.4319/lo.2010.55.4.1614

Ruiz-González, C., Simó, R., Sommaruga, R., and Gasol, J. M. (2013). Away from darkness: A review on the effects of solar radiation on heterotrophic bacterioplankton activity. *Front. Microbiol* 4, 131. doi: 10.3389/fmicb.2013.00131

Silveira, C. B., Cavalcanti, G. S., Walter, J. M., Silva-Lima, A. W., Dinsdale, E. A., Bourne, D. G., et al. (2017). Microbial processes driving coral reef organic carbon flow. *FEMS Microbiol. Rev.* 41, 575–595. doi: 10.1093/femsre/fux018

Simó, R., Archer, S. D., Pedrós-Alió, C., Gilpin, L., and Stelfox-Widdicombe, C. E. (2002). Coupled dynamics of dimethylsulfoniopropionate and dimethylsulfide cycling and the microbial food web in surface waters of the north Atlantic. *Limnol. Oceanogr.* 47, 53–61. doi: 10.4319/lo.2002.47.1.0053

Simó, R., Grimalt, J. O., and Albaigés, J. (1997). Dissolved dimethylsulphide, dimethylsulphoniopropionate and dimethylsulphoxide in western Mediterranean waters. *Deep Sea Res. II* 44, 929–950. doi: 10.1016/S0967-0645(96)00099-9

Simó, R., Vila-Costa, M., Alonso-Sáez, L., Cardelús, C., Guadayol, Ò., Vázquez-Domínguez, E., et al. (2009). Annual series of DMSP contribution to s and c fluxes through phytoplankton and bacterioplankton in a NW Mediterranean coastal site. *Aquat. Microb. Ecol.* 57, 43–55. doi: 10.3354/ame01325

Spielmeyer, A., and Pohnert, G. (2012). Daytime, growth phase and nitrate availability dependent variations of dimethylsulfoniopropionate in batch cultures of the diatom *Skeletonema marinoi*. *J. Exp. Mar. Biol. Ecol.* 413, 121–130. doi: 10.1016/j.jembe.2011.12.004

Spiese, C. E., Le, T., Zimmer, R. L., and Kieber, D. J. (2016). Dimethylsulfide membrane permeability, cellular concentrations and implications for physiological functions in marine algae. *J. Plankton Res.* 38, 41–54. doi: 10.1093/plankt/fbv106

Stefels, J., and van Leeuwe, M. A. (1998). Effects of iron and light stress on the biochemical composition of Antarctic *Phaeocystis* sp. (Prymnesiophyceae). i. intracellular DMSP concentrations. *J. Phycol.* 34, 486–495. doi: 10.1046/j.1529-8817.1998.340486.x

Steinke, M., Brading, P., Kerrison, P., Warner, M. E., and Suggett, D. J. (2011). Concentrations of dimethylsulfoniopropionate and dimethylsulfide are strain-specific in symbiotic dinoflagellates (*Symbiodinium* sp., *Dinophyceae*). *J. Phycol.* 47, 775–783. doi: 10.1111/j.1529-8817.2011.01011.x

Sunda, W. G., Hardison, R., Kiene, R. P., Bucciarelli, E., and Harada, H. (2007). The effect of nitrogen limitation on cellular DMSP and DMS release in marine phytoplankton: Climate feedback implications. *Aquat. Sci.* 69, 341–351. doi: 10.1007/s00027-007-0887-0

Sunda, W., Kieber, D. J., Kiene, R. P., and Huntsman, S. (2002). An antioxidant function for DMSP and DMS in marine algae. *Nature* 418, 317–320. doi: 10.1038/nature00851

Suttle, C. A., Chan, A. M., and Fuhrman, J. A. (1991). Dissolved free amino acids in the Sargasso Sea: Uptake and respiration rates, turnover times, and concentrations. *Mar. Ecol. Prog. Ser.* 70, 189–199. doi: 10.3354/meps070189

Swan, H. B., Deschaseaux, E. S. M., Jones, G. B., and Eyre, B. D. (2017). Quantification of dimethylsulphoniopropionate (DMSP) in *Acropora* spp. of reef building coral using mass spectrometry with deuterated internal standard. *Anal. Bioanal. Chem.* 409, 1929–1942. doi: 10.1007/s00216-016-0141-5

Takeda, K., Katoh, S., Mitsui, Y., Nakano, S., Nakatani, N., and Sakugawa, H. (2014). Spatial distributions of and diurnal variations in low molecular weight carbonyl compounds in coastal seawater, and the controlling factors. *Sci. Total Environ.* 493, 454–462. doi: 10.1016/j.scitotenv.2014.05.126

Taniguchi, A., Yoshida, T., and Eguchi, M. (2014). Bacterial production is enhanced by coral mucus in reef systems. *J. Exp. Mar. Bio. Ecol.* 461, 331–336. doi: 10.1016/j.jembe.2014.09.004

Tapiolas, D. M., Motti, C. A., Holloway, P., and Boyle, S. G. (2010). High levels of acrylate in the great barrier reef coral *Acropora millepora*. *Coral Reefs* 29, 621–625. doi: 10.1007/s00338-010-0608-3

Tapiolas, D. M., Raina, J.-B., Lutz, A., Willis, B. L., and Motti, C. A. (2013). Direct measurement of dimethysulfoniopropionate (DMSP) in reef-building corals using quantitative nuclear magnetic resonance (qNMR) spectroscopy. *J. Exp. Mar. Biol. Ecol.* 443, 85–89. doi: 10.1016/j.jembe.2013.02.037

Toole, D. A., Kieber, D. J., Kiene, R. P., Siegel, D. A., and Nelson, N. B. (2003). Photolysis and the dimethylsulfide (DMS) summer paradox in the Sargasso Sea. *Limnol. Oceanogr.* 48, 1088–1100. doi: 10.4319/lo.2003.48.3.1088

Tyssebotn, I. M. B. (2015). *An investigation of the marine acrylate cycle* (College of Environmental Science and Forestry. Syracuse, NY: Ph.D. thesis. State University of New York).

Tyssebotn, I. M. B., Kinsey, J. D., Kieber, D. J., Kiene, R. P., Rellinger, A. N., and Motard-Côté, J. (2017). Concentrations, biological uptake, and respiration of dissolved acrylate and dimethylsulfoxide in the northern gulf of Mexico. *Limnol. Oceanogr.* 62, 1198–1218. doi: 10.1002/lno.10495

Utermöhl, H. (1958). Zur vervollkommnung der quantitativen phytoplankton-methodik. *SIL Commun. 1953-1996* 9, 1–38. doi: 10.1080/05384680.1958.11904091

Van Alstyne, K. L., Schupp, P., and Slattery, M. (2006). The distribution of dimethylsulfoniopropionate in tropical pacific coral reef invertebrates. *Coral Reefs* 25, 321–327. doi: 10.1007/s00338-006-0114-9

Vila-Costa, M., Kiene, R. P., and Simó, R. (2008). Seasonal variability of the dynamics of dimethylated sulfur compounds in a coastal northwest Mediterranean site. *Limnol. Oceanogr.* 53, 198–211. doi: 10.4319/lo.2008.53.1.0198

Vila-Costa, M., Pinhassi, J., Alonso, C., Pernthaler, J., and Simó, R. (2007). An annual cycle of DMSP-sulfur assimilating bacterioplankton in the coastal NW Mediterranean. *Environ. Microbiol.* 9, 2451–2463. doi: 10.1111/j.1462-2920.2007.01363.x

Wegley, L., Edwards, R., Rodriguez-Brito, B., Liu, H., and Rohwer, F. (2007). Metagenomic analysis of the microbial community associated with the coral *Porites astreoides*. *Environ. Microbiol.* 9, 2707–2719. doi: 10.1111/j.1462-2920.2007.01383.x

Wheeler, P. A., Kirchman, D. L., Landry, M. R., and Kokklnakis, S. A. (1989). Diel periodicity in ammonium uptake and regeneration in the oceanic subarctic pacific: Implications for interactions in microbial food webs. *Limnol. Oceanogr.* 34, 1025–1033. doi: 10.4319/lo.1989.34.6.1025

Wikner, J., Rassoulzadegan, F., and Hagström, Å. (1990). Periodic bacterivore activity balances bacterial growth in the marine environment. *Limnol. Oceanogr.* 35, 313–324. doi: 10.4319/lo.1990.35.2.0313

Wild, C., Rasheed, M., Werner, U., Franke, U., Johnstone, R., and Huettel, M. (2004). Degradation and mineralization of coral mucus in reef environments. *Mar. Ecol. Prog. Ser.* 267, 159–171. doi: 10.3354/meps267159

Wu, X., Li, P.-F., Liu, C.-Y., Zhang, H.-H., Yang, G.-P., Zhang, S.-H., et al. (2017). Biogeochemistry of dimethylsulfide, dimethylsulfoniopropionate, and acrylic acid in the changjiang estuary and the East China Sea. *J. Geophys. Res. C.* 122, 10,245–10,261. doi: 10.1002/2017JC013265

Wu, X., Liu, C. Y., and Li, P. F. (2015). Photochemical transformation of acrylic acid in seawater. *Mar. Chem.* 170, 29–36. doi: 10.1016/j.marchem.2015.01.003

Wu, X., Li, P.-F., Zhang, H.-H., Zhu, M.-X., Liu, C.-Y., and Yang, G.-P. (2020). Acrylic acid and related dimethylated sulfur compounds in the bohai and yellow seas during summer and winter. *Biogeosci* 17, 1991–2008. doi: 10.5194/bg-17-1991-2020

Xue, L., and Kieber, D. J. (2021). Photochemical production and photolysis of acrylate in seawater. *Environ. Sci. Technol.* 55, 7135–7144. doi: 10.1021/acs.est.1c00327

Yost, D. M., Jones, R. J., and Mitchelmore, C. L. (2010). Alterations in dimethylsulphoniopropionate (DMSP) levels in the coral *Montastraea franksi* in response to copper exposure. *Aquat. Toxicol.* 98, 367–373. doi: 10.1016/j.aquatox.2010.03.005

Yost, D. M., and Mitchelmore, C. L. (2009). Dimethylsulphoniopropionate (DMSP) lyase activity in different strains of the symbiotic alga *Symbiodinium microadriaticum*. *Mar. Ecol. Prog. Ser.* 386, 61–70. doi: 10.3354/meps08031

Yost, D. M., and Mitchelmore, C. L. (2010). Determination of total and particulate dimethylsulphoniopropionate (DMSP) concentrations in four scleractinian coral species: A comparison of methods. *J. Exp. Mar. Biol. Ecol.* 395, 72–79. doi: 10.1016/j.jembe.2010.08.016

Zhou, X., and Mopper, K. (1997). Photochemical production of low-molecular-weight carbonyl compounds in seawater and surface microlayer and their air-sea exchange. *Mar. Chem.* 56, 201–213. doi: 10.1016/S0304-4203(96)00076-X

Zhu, Y., and Kieber, D. J. (2019). Concentrations and photochemistry of acetaldehyde, glyoxal, and methylglyoxal in the Northwest Atlantic ocean. *Environ. Sci. Technol.* 53, 9512–9521. doi: 10.1021/acs.est.9b01631

Zubkov, M. V., Fuchs, B. M., Archer, S. D., Kiene, R. P., Amann, R., and Burkill, P. H. (2002). Rapid turnover of dissolved DMS and DMSP by defined bacterioplankton communities in the stratified euphotic zone of the north Sea. *Deep-Sea Res. II* 49, 3017–3038. doi: 10.1016/S0967-0645(02)00069-3

Zweifel, U. L., Norrman, B., and Hagström, Å. (1993). Consumption of dissolved organic carbon by marine bacteria and demand for inorganic nutrients. *Mar. Ecol. Prog. Ser.* 101, 23–32. doi: 10.3354/meps101023

Frontiers in Marine Science

Explores ocean-based solutions for emerging global challenges

The third most-cited marine and freshwater biology journal, advancing our understanding of marine systems and addressing global challenges including overfishing, pollution, and climate change.

Discover the latest Research Topics

See more →

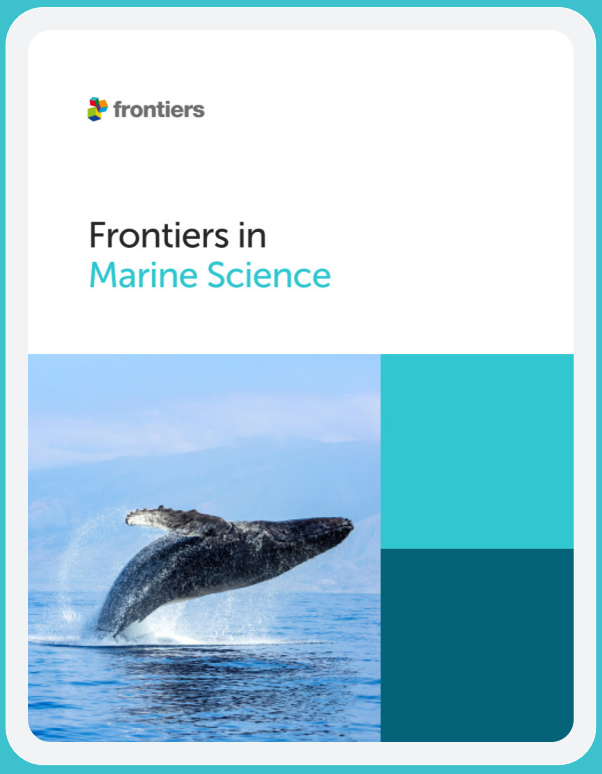

Frontiers

Avenue du Tribunal-Fédéral 34
1005 Lausanne, Switzerland
frontiersin.org

Contact us

+41 (0)21 510 17 00
frontiersin.org/about/contact